National Library
of Canada

Acquisitions and
Bibliographic Services Branch

395 Wellington Street
Ottawa, Ontario
K1A 0N4

Bibliothèque nationale
du Canada

Direction des acquisitions et
des services bibliographiques

395, rue Wellington
Ottawa (Ontario)
K1A 0N4

Your file Votre référence

Our file Notre référence

NOTICE

The quality of this microform is heavily dependent upon the quality of the original thesis submitted for microfilming. Every effort has been made to ensure the highest quality of reproduction possible.

If pages are missing, contact the university which granted the degree.

Some pages may have indistinct print especially if the original pages were typed with a poor typewriter ribbon or if the university sent us an inferior photocopy.

Reproduction in full or in part of this microform is governed by the Canadian Copyright Act, R.S.C. 1970, c. C-30, and subsequent amendments.

AVIS

La qualité de cette microforme dépend grandement de la qualité de la thèse soumise au microfilmage. Nous avons tout fait pour assurer une qualité supérieure de reproduction.

S'il manque des pages, veuillez communiquer avec l'université qui a conféré le grade.

La qualité d'impression de certaines pages peut laisser à désirer, surtout si les pages originales ont été dactylographiées à l'aide d'un ruban usé ou si l'université nous a fait parvenir une photocopie de qualité inférieure.

La reproduction, même partielle, de cette microforme est soumise à la Loi canadienne sur le droit d'auteur, SRC 1970, c. C-30, et ses amendements subséquents.

Canada

UNIVERSITY OF ALBERTA

ABSOLUTE INFRARED ABSORPTION INTENSITIES OF LIQUID BENZENE.

BY

CLIFFORD DALE KEEFE ©

A thesis submitted to the Faculty of Graduate Studies and Research in partial fulfilment of the requirements for the degree of DOCTOR OF PHILOSOPHY.

DEPARTMENT OF CHEMISTRY

Edmonton, Alberta

Fall 1994

National Library
of Canada

Acquisitions and
Bibliographic Services Branch

395 Wellington Street
Ottawa, Ontario
K1A 0N4

Bibliothèque nationale
du Canada

Direction des acquisitions et
des services bibliographiques

395, rue Wellington
Ottawa (Ontario)
K1A 0N4

Your file Votre référence

Our file Notre référence

The author has granted an irrevocable non-exclusive licence allowing the National Library of Canada to reproduce, loan, distribute or sell copies of his/her thesis by any means and in any form or format, making this thesis available to interested persons.

L'auteur a accordé une licence irrévocable et non exclusive permettant à la Bibliothèque nationale du Canada de reproduire, prêter, distribuer ou vendre des copies de sa thèse de quelque manière et sous quelque forme que ce soit pour mettre des exemplaires de cette thèse à la disposition des personnes intéressées.

The author retains ownership of the copyright in his/her thesis. Neither the thesis nor substantial extracts from it may be printed or otherwise reproduced without his/her permission.

L'auteur conserve la propriété du droit d'auteur qui protège sa thèse. Ni la thèse ni des extraits substantiels de celle-ci ne doivent être imprimés ou autrement reproduits sans son autorisation.

ISBN 0-315-95206-7

Canada

Name Clifford Dale Keefe.

Dissertation Abstracts International is arranged by broad, general subject categories. Please select the one subject which most nearly describes the content of your dissertation. Enter the corresponding four-digit code in the spaces provided.

0494 **U·M·I**

SUBJECT TERM

SUBJECT CODE

Subject Categories

THE HUMANITIES AND SOCIAL SCIENCES

COMMUNICATIONS AND THE ARTS

Architecture	0729
Art History	0377
Cinema	0900
Dance	0378
Fine Arts	0357
Information Science	0723
Journalism	0391
Library Science	0399
Mass Communications	0708
Music	0413
Speech Communication	0459
Theater	0465

EDUCATION

General	0515
Administration	0514
Adult and Continuing	0516
Agricultural	0517
Art	0273
Bilingual and Multicultural	0282
Business	0688
Community College	0275
Curriculum and Instruction	0727
Early Childhood	0518
Elementary	0524
Finance	0277
Guidance and Counseling	0519
Health	0680
Higher	0745
History of	0520
Home Economics	0278
Industrial	0521
Language and Literature	0279
Mathematics	0280
Music	0522
Philosophy of	0998
Physical	0523
Psychology	0525
Reading	0535
Religious	0527
Sciences	0714
Secondary	0533
Social Sciences	0534
Sociology of	0340
Special	0529
Teacher Training	0530
Technology	0710
Tests and Measurements	0288
Vocational	0747

LANGUAGE, LITERATURE AND LINGUISTICS

Language	
General	0679
Ancient	0289
Linguistics	0290
Modern	0291
Literature	
General	0401
Classical	0294
Comparative	0295
Medieval	0297
Modern	0298
African	0316
American	0591
Asian	0305
Canadian (English)	0352
Canadian (French)	0355
English	0593
Germanic	0311
Latin American	0312
Middle Eastern	0315
Romance	0313
Slavic and East European	0314

PHILOSOPHY, RELIGION AND THEOLOGY

Philosophy	0422
Religion	
General	0318
Biblical Studies	0321
Clergy	0319
History of	0320
Philosophy of	0322
Theology	0469

SOCIAL SCIENCES

American Studies	0323
Anthropology	
Archaeology	0324
Cultural	0326
Physical	0327
Business Administration	
General	0310
Accounting	0272
Banking	0770
Management	0454
Marketing	0338
Canadian Studies	0385
Economics	
General	0501
Agricultural	0503
Commerce-Business	0505
Finance	0508
History	0509
Labor	0510
Theory	0511
Folklore	0358
Geography	0366
Gerontology	0351
History	
General	0578
Ancient	0579
Medieval	0581
Modern	0582
Black	0328
African	0331
Asia, Australia and Oceania	0332
Canadian	0334
European	0335
Latin American	0336
Middle Eastern	0333
United States	0337
History of Science	0585
Law	0398
Political Science	
General	0615
International Law and Relations	0616
Public Administration	0617
Recreation	0814
Social Work	0452
Sociology	
General	0626
Criminology and Penology	0627
Demography	0938
Ethnic and Racial Studies	0631
Individual and Family Studies	0628
Industrial and Labor Relations	0629
Public and Social Welfare	0630
Social Structure and Development	0700
Theory and Methods	0344
Transportation	0709
Urban and Regional Planning	0999
Women's Studies	0453

THE SCIENCES AND ENGINEERING

BIOLOGICAL SCIENCES

Agriculture	
General	0473
Agronomy	0285
Animal Culture and Nutrition	0475
Animal Pathology	0476
Food Science and Technology	0359
Forestry and Wildlife	0478
Plant Culture	0479
Plant Pathology	0480
Plant Physiology	0817
Range Management	0777
Wood Technology	0746
Biology	
General	0306
Anatomy	0287
Biostatistics	0308
Botany	0309
Cell	0379
Ecology	0329
Entomology	0353
Genetics	0369
Limnology	0793
Microbiology	0410
Molecular	0307
Neuroscience	0317
Oceanography	0416
Physiology	0433
Radiation	0821
Veterinary Science	0778
Zoology	0472
Biophysics	
General	0786
Medical	0760

EARTH SCIENCES

Biogeochemistry	0425
Geochemistry	0996
Geodesy	0370
Geology	0372
Geophysics	0373
Hydrology	0388
Mineralogy	0411
Paleobotany	0345
Paleoecology	0426
Paleontology	0418
Paleozoology	0985
Palynology	0427
Physical Geography	0368
Physical Oceanography	0415

HEALTH AND ENVIRONMENTAL SCIENCES

Environmental Sciences	0768
Health Sciences	
General	0566
Audiology	0300
Chemotherapy	0992
Dentistry	0567
Education	0350
Hospital Management	0769
Human Development	0758
Immunology	0982
Medicine and Surgery	0564
Mental Health	0347
Nursing	0569
Nutrition	0570
Obstetrics and Gynecology	0380
Occupational Health and Therapy	0354
Ophthalmology	0381
Pathology	0571
Pharmacology	0419
Pharmacy	0572
Physical Therapy	0382
Public Health	0573
Radiology	0574
Recreation	0575
Speech Pathology	0460
Toxicology	0383
Home Economics	0386

PHYSICAL SCIENCES

Pure Sciences

Chemistry	
General	0485
Agricultural	0749
Analytical	0486
Biochemistry	0487
Inorganic	0488
Nuclear	0738
Organic	0490
Pharmaceutical	0491
Physical	0494
Polymer	0495
Radiation	0754
Mathematics	0405
Physics	
General	0605
Acoustics	0986
Astronomy and Astrophysics	0606
Atmospheric Science	0608
Atomic	0748
Electronics and Electricity	0607
Elementary Particles and High Energy	0798
Fluid and Plasma	0759
Molecular	0609
Nuclear	0610
Optics	0752
Radiation	0756
Solid State	0611
Statistics	0463

Applied Sciences

Applied Mechanics	0346
Computer Science	0984
Engineering	
General	0537
Aerospace	0538
Agricultural	0539
Automotive	0540
Biomedical	0541
Chemical	0542
Civil	0543
Electronics and Electrical	0544
Heat and Thermodynamics	0348
Hydraulic	0545
Industrial	0546
Marine	0547
Materials Science	0794
Mechanical	0548
Metallurgy	0743
Mining	0551
Nuclear	0552
Packaging	0549
Petroleum	0765
Sanitary and Municipal	0554
System Science	0790
Geotechnology	0428
Operations Research	0796
Plastics Technology	0795
Textile Technology	0994

PSYCHOLOGY

General	0621
Behavioral	0384
Clinical	0622
Developmental	0620
Experimental	0623
Industrial	0624
Personality	0625
Physiological	0989
Psychobiology	0349
Psychometrics	0632
Social	0451

Permission is hereby granted to C. Dale Keefe to use the material contained in the following publications in his thesis.

J.E. Bertie, S.L. Zhang, and C.D. Keefe "Infrared Intensities of Liquids XVI: Accurate Determination of Molecular Band Intensities from Infrared Refractive Index and Dielectric Constant Spectra" J. Mol. Struct., **354**, 157 (1994).

J.E. Bertie, S.L. Zhang, and C.D. Keefe "The measurement and use of absolute infrared absorption intensities of neat liquids." Vib. Spectrosc., In Press (1994).

John E. Bertie

Shuliang L. Zhang

Permission is hereby granted to C. Dale Keefe to use the material contained in the following publications in his thesis.

J.E. Bertie, C.D. Keefe, and R.N. Jones "Infrared intensities of liquids VIII. Accurate baseline correction of transmission spectra of liquids for computation of absolute intensities, and the 1036 cm^{-1} band of benzene as a potential intensity standard." Can. J. Chem., **69**, 1609 (1991).

J.E. Bertie, R.N. Jones, and C.D. Keefe "Infrared Intensities of Liquids XII: Optical Constants and Molar Absorption Coefficients of Benzene between 6200 and 500 cm^{-1} From Spectra Recorded in Several Laboratories." Appl. Spectrosc., **47**, 891 - 911 (1993).

J.E. Bertie, C.D. Keefe, and R.N. Jones, *Tables of Intensities for the Calibration of Infrared Spectroscopic Measurements in the Liquid Phase*. (Oxford, Blackwell Scientific Publications Ltd., 1994) In Press.

John E. Bertie

R Norman Jones

R. Norman Jones

Permission is hereby granted to C. Dale Keefe to use the material contained in the following publication in his thesis.

J.E. Bertie and C.D. Keefe "Comparison of Absolute Infrared Intensities of Benzene in the Liquid and Gas Phases." J. Chem. Phys., 101, (1994), In Press.

John E. Bertie

UNIVERSITY OF ALBERTA

RELEASE FORM

NAME OF AUTHOR: CLIFFORD DALE KEEFE

TITLE OF THESIS: ABSOLUTE INFRARED ABSORPTION INTENSITIES OF LIQUID BENZENE.

DEGREE: Ph.D.

YEAR THIS DEGREE GRANTED: 1994

Permission is hereby granted to the University of Alberta Library to reproduce single copies of this thesis and to lend or sell such copies for private, scholarly or scientific research purposes only.

The author reserves all other publication and other rights in association with the copyright in the thesis, and except as herein before provided neither the thesis nor any substantial portion thereof may be printed or otherwise reproduced in any material form whatever without the author's prior written permission.

Clifford Dale Keefe
3840 16A Avenue
Edmonton, Alberta
T6L 4C1

DATED: October 6, 1994

UNIVERSITY OF ALBERTA

FACULTY OF GRADUATE STUDIES AND RESEARCH

The undersigned certify that they have read, and recommend to the Faculty of Graduate Studies and Research for acceptance, a thesis entitled ABSOLUTE INFRARED ABSORPTION INTENSITIES OF LIQUID BENZENE submitted by CLIFFORD DALE KEEFE in partial fulfillment of the requirements for the degree of DOCTOR OF PHILOSOPHY.

J. E. Bertie, Supervisor

R. E. D. McClung

N. J. Dovichi

Monica Palcic

M. M. Palcic

Jim Franck

J. Franck

Mitsuo Tasumi

M. Tasumi, External Examiner

DATED: October 5, 1994

To Shelley

Abstract

The optical constants of liquid benzene-h_6, benzene-d_6, and binary mixtures of benzene-h_6 and benzene-d_6 were measured across the entire mid-infrared region at 25°C. The optical constants were used to calculate the molar absorption coefficient spectra and the molar polarizability spectra of these neat liquids and binary mixtures.

The optical constants and molar absorption coefficient spectrum of benzene-h_6 measured in this work and the optical constants and molar absorption coefficient spectra of toluene, chlorobenzene and dichloromethane measured separately, were used to establish secondary infrared intensity standards for liquids. These standards have been accepted by the International Union of Pure and Applied Chemistry.

The integrated intensities determined from the imaginary molar polarizability spectra were used to calculate the dipole moment derivatives with respect to normal coordinates for the fundamentals of both benzene-h_6 and benzene-d_6. The wavenumbers of the fundamentals of benzene-h_6 and benzene-d_6 were used to carry out normal coordinate and force field calculations for liquid benzene. The eigenvectors calculated from these normal coordinate calculations were used to calculate the dipole moment derivatives with respect to symmetry coordinates and with respect to internal coordinates.

The absorption intensities of benzene-h_6 and benzene-d_6 were compared to the literature absorption intensities for the gas phase, to determine the changes that occur upon condensation.

The molar polarizability spectra of binary mixtures of benzene-h_6 and benzene-d_6 were used to explore the extent to which the simple theory of the spectra

of solutions is valid when it concludes that for ideal solutions the molar polarizability spectrum is simply the sum of the molar polarizability spectra of the pure components weighted by their mole fraction in the mixture.

Acknowledgments

I would like to thank Dr. John E. Bertie for suggesting this project to me and for his help and guidance throughout the course of the project. It has been a pleasure to work with him for the past 4 years. Our many discussions have helped shape my scientific skills and attitudes that will remain with me throughout my career.

The contribution of Dr. R. Norman Jones to the Secondary Infrared Standards that have developed from this project is graciously acknowledged. Without his constant attention and drive the Secondary Infrared Standards would never have been submitted to the International Union of Pure and Applied Chemistry.

I express my appreciation to the following collaborators for supplying spectra that were used to estimate the accuracy of the results presented in this thesis; V. Behnam, R. Cain, W.O. George, K. Krishnan and M. Smith.

Without the help of the Spectral Services Laboratory, Microanalytical Laboratory, Electronics Shop, Glass Shop and Machine Shop this project would not have been possible, and for their help I am grateful. Thanks is also due to Mr. Barry Arnold of the Electrical Engineering Department for his help in polishing some of the salt windows for the transmission cells used in this study.

I would like to acknowledge the financial assistance of the Natural Sciences and Engineering Research Council of Canada, the Killam trust, the Faculty of Graduate Studies and Research and the Department of Chemistry. Without their support this research project would not have been possible. Lastly, thanks are due to my wife, Shelley, for her patience and understanding during the course of this work.

Table of Contents

Chapter 1 Introduction 1

1.1 Infrared Absorption Intensities 1

1.2 Overview of the Thesis 8

1.3 Electromagnetic Theory and Optical Properties 11

  1.3.1 Intensity Quantities 11

  1.3.2 Relation of Intensity Quantities to Theory 17

1.4 Previous Studies of the Vibrations and Infrared Absorption Intensities of Benzene 21

  1.4.1 Assignment of Fundamentals 21

  1.4.2 Infrared Absorption Intensities 23

    1.4.2a Infrared Absorption Intensities in the Liquid Phase 23

    1.4.2b Infrared Absorption Intensities in the Gas Phase 26

  1.4.3 Force Field Calculations 27

Chapter 2 The Determination of Real and Imaginary Refractive Index Spectra from an Experimental Absorbance Spectrum of a Cell Full of Liquid 29

2.1 Transmittance and Reflectance at an Interface Between Media; Fresnel's Equations 30

2.2 Reflectance and Transmittance of a Transmission Cell 33

  2.2.1 Transmittance and Reflectance of a Single Plate 34

  2.2.2 Transmittance and Reflectance of a Thin Absorbing Liquid Film 37

  2.2.3 Transmittance and Reflectance of the Complete Cell 38

2.3 The Kramers-Kronig Transformation 41

  2.3.1 The Finite KK Transform 43

2.3.2 Method of Calculating $n(\tilde{\nu}_{\mathrm{high}})$ 44

2.3.3 The Subtractive KK Transform 45

2.4 R. N. Jones' Procedure for Calculating Optical Constants from Transmission Spectra 47

2.5 Baseline Correction 48

2.5.1 The Detailed Solution 55

2.5.1a Calculation of The Ideal Apparent Absorbance 55

2.5.1b The Linear Absorption Coefficient of the Liquid in the Wings of the Band 59

2.5.1c Ideal Experimental Absorbance, Absorbance, and Imaginary Refractive Index Spectra 60

2.6 C. D. Keefe's Algorithm for Calculating Optical Constants of Liquids 67

Chapter 3 Measurement and Accuracy of the Optical Constants of Benzene-h_6 and Benzene-d_6 71

3.1 Optical Constants of Benzene-h_6 71

3.1.1 Measurement of Experimental Absorbance Spectra 72

3.1.2 Data Processing 75

3.1.3 Results 76

3.1.3a Imaginary Refractive Index from 6225 to 800 cm^{-1} 76

3.1.3b Imaginary Refractive index from 800 to 500 cm^{-1} 94

3.1.3c Imaginary Refractive index from 500 to 30 cm^{-1} 94

3.1.3d Real Refractive Index 97

3.1.4 Accuracy of the Results 97

3.1.4a Imaginary Refractive Index 101

3.1.4b Area Under the Imaginary Refractive Index 103

3.1.4c Real Refractive Index 104

3.2 Optical Constants of Benzene-d_6 105

3.2.1 Imaginary Refractive Index 105

3.2.2 Real Refractive Index 109

Chapter 4 Secondary Infrared Absorption Standards 116

4.1 Standard Band Groups 118

4.2 An Application to Quantitative Analysis 125

4.2.1 Program IRYTRUE 125

4.2.2 Reproducibility and Accuracy of Calibrated Cell Constants 127

Chapter 5 Integrated Intensities, Transition Moments and Dipole Moment Derivatives of Liquid Benzene-h_6 and Benzene-d_6 134

5.1 Dielectric Constants, Molar Polarizabilities and Molecular Properties 137

5.2 Integrated Intensities and Transition Moments of Benzene-h_6 and Benzene-d_6 from the Imaginary Molar Polarizability 149

5.2.1 The ν_{12} Band 173

5.2.2 The ν_{13} Band 175

5.2.3 The ν_{14} Band 176

5.2.4 The ν_4 Band 177

5.2.5 Other Peaks 177

5.3 Normal Coordinate Calculations 178

5.3.1 Principles 178

5.3.2 Geometry, Internal Coordinates and Symmetry Coordinates of Benzene 181

5.3.3 Reproducing Literature Calculations 181

5.3.4 Assignment and Wavenumbers of the Fundamentals of Liquid Benzene-h_6 and Benzene-d_6 186

5.3.5 Present Normal Coordinate Calculation for Liquid Benzene-h6 and Benzene-d_6 187

5.4 Dipole Moment Derivatives of Benzene-h_6 and Benzene-d_6 With Respect to Symmetry and Internal Coordinates 194

5.4.1 Dipole Moment Derivatives With Respect to Symmetry Coordinates for the Infrared Active Fundamentals 196

5.4.1a A_{2u} Vibrations 196

5.4.1b E_{1u} Vibrations 199

5.4.2 Dipole Moment Derivatives With Respect to Symmetry Coordinates for the Vibrations that are not Infrared Active Under D_{6h} 203

5.4.2a A_{1g} Vibrations 205

5.4.2b A_{2g} Vibrations 205

5.4.2c B_{1u} Vibrations 206

5.4.2d B_{2g} Vibrations 206

5.4.2e B_{2u} Vibrations 207

5.4.2f E_{1g} Vibrations 207

5.4.2g E_{2g} Vibrations 208

5.4.2h E_{2u} Vibrations 209

5.4.2i The Validity of the Parallel Dipole Approximation For Vibrations Inactive Under D_{6h} 209

5.4.2j Summary and Discussion of Vibrations Inactive Under D_{6h} 210

5.4.3 Dipole Moment Derivatives With Respect to the Internal Coordinates 211

5.4.3a Dipole Moment Derivatives With Respect to CH Stretch Coordinates 211

5.4.3b Dipole Moment Derivatives With Respect to CC Stretch Coordinates 212

5.4.3c Dipole Moment Derivatives With Respect to HCC Deformation Coordinates 213

5.4.3d Dipole Moment Derivatives With Respect to HCCC Out-Of-Plane Angle Coordinates 213

5.4.3e Summary of Dipole Moment Derivatives of Vibrations Active Under D_{6h} 214

Chapter 6 Comparison of Liquid and Gas Phase Intensities 215

6.1 Principles 216

6.2 Comparison of Experimental Gas Phase and Liquid Phase Intensities 218

6.2.1 Results 218

6.2.2 Discussion 230

6.2.3 Comparison of Transition Moments and Dipole Moment Derivatives of Liquid Benzene-h_6 and Benzene-d_6 With Those of Gaseous Benzene-h_6 and Benzene-d_6 235

6.3 Comparison of *Ab Initio* Intensities with Experimental Intensities 245

Chapter 7 Binary Mixtures of Liquid Benzene-h_6 and Liquid Benzene-d_6 249

7.1 Method and Experimental 249

7.2 Change in Intensity upon Isotopic Dilution 257

7.3 The Integrated Intensity of ν_4 of Benzene-d_6 273

7.4 Changes in Peak Wavenumber and Band Width Upon Isotopic Dilution 274

Chapter 8 Summary 290

References 294

Appendix I. Proof of the Hilbert and KK Transforms 309

Appendix II. Numerical Constants in Equations (1.3.37), (1.3.38), (1.3.44), (1.3.45), (1.3.47) and (1.3.48) 312

Appendix III. Numerical KK Transform 313

Appendix IV.Optical Constants of Benzene-h_6 315

Appendix V. Optical Constants of Benzene-d_6 321

Appendix VI. Optical Constants of Benzene-h_6 and Benzene-d_6 Mixtures 325

List of Tables

Table 2.1. Ideal apparent absorbance for KBr and NaCl windows. 58

Table 2.2. Calculation of ideal experimental absorbance for liquid benzene-h_6 63

Table 3.1. Linear absorption coefficients at anchor points for liquid benzene-h_6 at 25°C. 77

Table 3.2. Path lengths, high-wavenumber refractive index, and number of spectra from each spectroscopist, for the regions processed. 78

Table 3.3. Spectroscopist average areas under the imaginary refractive index band groups 80

Table 3.4. Spectroscopist average imaginary refractive index peak heights 81

Table 3.5. Overall average area under the imaginary refractive index bands. 85

Table 3.6. Overall average peak heights in the imaginary refractive index spectra. 92

Table 3.7. Linear absorption coefficients at anchor points for liquid benzene-d_6 at 25°C 107

Table 3.8. Path lengths and number of spectra recorded for the regions processed. 108

Table 4.1. Secondary infrared intensity standards. 120

Table 4.2. Benzene-h_6 Band 11 (1565 to 1420 cm^{-1}). 124

Table 4.3. Calibration of 11 μm KBr cell 130

Table 4.4. Calibration of 113 μm CaF_2 cell. 131

Table 4.5. Calibration of 532 μm KBr cell 132

Table 4.6. Comparison of cell constants and path lengths 133

Table 5.1. Benzene-h_6 and benzene-d_6 vibrations. 138

Table 5.2. Classical damped harmonic oscillator peaks used to fit the imaginary molar polarizability spectrum of benzene-h_6. 152

Table 5.3. Classical damped harmonic oscillator peaks used to fit the imaginary molar polarizability spectrum of benzene-d_6. 159

Table 5.4. Internal coordinates. ... 182

Table 5.5. Symmetry coordinates ... 184

Table 5.6. Anharmonic and harmonic wavenumbers of benzene-h_6 and benzene-d_6. ... 188

Table 5.7. Observed and calculated harmonic wavenumbers of benzene-h_6 and benzene-d_6. ... 189

Table 5.8. Internal coordinate force constants of benzene ... 190

Table 5.9. Eigenvectors of benzene-h_6 and benzene-d_6 ... 192

Table 5.10. Inverse eigenvectors of benzene-h_6 and benzene-d_6 ... 193

Table 5.11. Dipole moment derivative with respect to the normal coordinates. ... 197

Table 5.12. Dipole moment derivative with respect to symmetry coordinates ... 198

Table 6.1. Absorption intensities A_j of liquid benzene-h_6 and benzene-d_6 ... 220

Table 6.2. Absorption intensities A_j of gaseous benzene-h_6 and benzene-d_6. ... 223

Table 6.3. Absorption intensities C_j of liquid benzene compared with intensities A_j of gaseous benzene. ... 227

Table 6.4. Comparison of intensities A_j of liquid and gaseous benzene-h_6 and benzene-d_6. ... 229

Table 6.5. Ratios of integrated intensities of benzene-h_6 to integrated intensities benzene-d_6 for liquid and gas phases. ... 234

Table 6.6. Transition moments and dipole moment derivatives of liquid and gaseous benzene-h_6 and benzene-d_6. ... 237

Table 6.7. $\partial\bar{\mu}/\partial S_i$ of gaseous benzene-h_6 and benzene-d_6 from nonlinear least squares fit of experimental $\partial\bar{\mu}/\partial Q_j$ for E_{1u} vibrations. ... 239

Table 6.8. Dipole moment derivatives with respect to symmetry coordinates and internal coordinates for liquid and gaseous benzene-h_6 and benzene-d_6. ... 241

Table 6.9. Contribution of $\partial\bar{\mu}/\partial S_i$ to $\partial\bar{\mu}/\partial Q_j$ for liquid and gaseous benzene-h_6 and benzene-d_6 for E_{1u} vibrations. ... 242

Table 6.10. Calculated and experimental intensities of benzene-h_6. ... 246

Table 7.1. Linear absorption coefficients at anchor points for binary mixtures up to 52% benzene-h_6 in benzene-d_6 at 25°C. 251

Table 7.2. Linear absorption coefficients at anchor points for binary mixtures greater than 60% benzene-h_6 in benzene-d_6 at 25°C. 253

Table 7.3. Real refractive indices at 8000 cm^{-1} and molar volumes for binary mixtures of benzene-h_6 and benzene-d_6 at 25°C. 256

Table 7.4. Integrated intensities of mixtures of benzene-h_6 and benzene-d_6. 271

Table 7.5. Least squares equations for C_j versus mole fraction. 272

Table 7.6. Peak wavenumbers and FWHH's of the benzene-h_6 vibrations in the $\tilde{\nu}\alpha''_{\mathrm{m}}$ spectra of mixtures of benzene-h_6 and benzene-d_6. 276

Table 7.7. Peak wavenumbers and FWHH's of the benzene-d_6 vibrations in the $\tilde{\nu}\alpha''_{\mathrm{m}}$ spectra of mixtures of benzene-h_6 and benzene-d_6. 277

Table IV.1. Imaginary refractive indices between 6225 and 30 cm^{-1} of liquid benzene-h_6 at 25°C. 315

Table IV.2. Real refractive indices between 6225 and 30 cm^{-1} of liquid benzene-h_6 at 25°C. 318

Table V.1. Imaginary refractive indices between 5000 and 550 cm^{-1} of liquid benzene-d_6 at 25 °C 321

Table V.2. Real refractive indices between 5000 and 550 cm^{-1} of liquid benzene-d_6 at 25 °C. 323

Table VI.1. Imaginary refractive indices between 6500 and 450 cm^{-1} of 10.01% liquid benzene-h_6 in liquid benzene-d_6 at 25 °C 325

Table VI.2. Real refractive indices between 6500 and 450 cm^{-1} of 10.01% liquid benzene-h_6 in liquid benzene-d_6 at 25 °C 327

Table VI.3. Imaginary refractive indices between 6500 and 450 cm^{-1} of 25.38% liquid benzene-h_6 in liquid benzene-d_6 at 25 °C 329

Table VI.4. Real refractive indices between 6500 and 450 cm^{-1} of 25.38% liquid benzene-h_6 in liquid benzene-d_6 at 25 °C 331

Table VI.5. Imaginary refractive indices between 6500 and 450 cm^{-1} of 40.00% liquid benzene-h_6 in liquid benzene-d_6 at 25 °C 333

Table VI.6. Real refractive indices between 6500 and 450 cm^{-1} of 40.00% liquid benzene-h_6 in liquid benzene-d_6 at 25 °C 335

Table VI.7. Imaginary refractive indices between 6500 and 450 cm^{-1} of 51.95% liquid benzene-h_6 in liquid benzene-d_6 at 25 °C 337

Table VI.8. Real refractive indices between 6500 and 450 cm^{-1} of 51.95% liquid benzene-h_6 in liquid benzene-d_6 at 25 °C 339

Table VI.9. Imaginary refractive indices between 6500 and 450 cm^{-1} of 61.96% liquid benzene-h_6 in liquid benzene-d_6 at 25 °C 341

Table VI.10. Real refractive indices between 6500 and 450 cm^{-1} of 61.96% liquid benzene-h_6 in liquid benzene-d_6 at 25 °C 343

Table VI.11. Imaginary refractive indices between 6500 and 450 cm^{-1} of 70.08% liquid benzene-h_6 in liquid benzene-d_6 at 25 °C 345

Table VI.12. Real refractive indices between 6500 and 450 cm^{-1} of 70.08% liquid benzene-h_6 in liquid benzene-d_6 at 25 °C 347

Table VI.13. Imaginary refractive indices between 6500 and 450 cm^{-1} of 79.34% liquid benzene-h_6 in liquid benzene-d_6 at 25 °C 349

Table VI.14. Real refractive indices between 6500 and 450 cm^{-1} of 79.34% liquid benzene-h_6 in liquid benzene-d_6 at 25 °C 351

Table VI.15. Imaginary refractive indices between 6500 and 450 cm^{-1} of 94.26% liquid benzene-h_6 in liquid benzene-d_6 at 25 °C 353

Table VI.16. Real refractive indices between 6500 and 450 cm^{-1} of 94.26% liquid benzene-h_6 in liquid benzene-d_6 at 25 °C 355

List of Figures

Figure 2.1. Reflection and transmission of a plane wave at a plane boundary. 31

Figure 2.2. Schematic of a transmission cell. 34

Figure 2.3. Transmittance and reflectance of a single plate. 35

Figure 2.4. Experimental absorbance spectra of liquid benzene-h_6 50

Figure 2.5. Imaginary refractive index spectra of liquid benzene-h_6 51

Figure 2.6. Schematic of absorbance, ideal experimental absorbance and experimental absorbance. 54

Figure 2.7. Ideal apparent absorbance calculated by program BASELINE for cells full of benzene-h_6. 57

Figure 2.8. Experimental absorbance spectra of liquid benzene-h_6 61

Figure 2.9. Ideal experimental absorbance spectra of liquid benzene-h_6 64

Figure 2.10. Imaginary refractive index spectra of liquid benzene-h_6 65

Figure 2.11. Experimental absorbance, ideal experimental absorbance and absorbance spectra of liquid benzene-h_6 66

Figure 3.1. Average areas under the imaginary refractive index spectra. 83

Figure 3.2. Imaginary refractive index spectrum of benzene-h_6, 6200 - 3800 cm^{-1}. 86

Figure 3.3. Imaginary refractive index spectrum of benzene-h_6, 3800 - 2800 cm^{-1}. 87

Figure 3.4. Imaginary refractive index spectrum of benzene-h_6, 2800 - 1900 cm^{-1}. 88

Figure 3.5. Imaginary refractive index spectrum of benzene-h_6, 1900 - 1400 cm^{-1}. 89

Figure 3.6. Imaginary refractive index spectrum of benzene-h_6, 1400 - 800 cm^{-1}. 90

Figure 3.7. Imaginary refractive index spectrum of liquid benzene-h_6 at 25°C 96

Figure 3.8. Extrapolation of the real refractive index of benzene-h_6 in the visible to the infrared 98

Figure 3.9. Real refractive index spectrum of liquid benzene-h_6 at 25°C 99

Figure 3.10. Imaginary refractive index spectrum of liquid benzene-d_6 at 25°C 112

Figure 3.11. Real refractive index spectrum of liquid benzene-d_6 at 25°C 113

Figure 3.12. Molar absorption coefficient spectrum of liquid benzene-h_6 at 25°C 114

Figure 3.13. Molar absorption coefficient spectrum of liquid benzene-d_6 at 25°C 115

Figure 4.1. Molar absorption coefficient spectrum of Benzene-h_6 Band 11 (1565 to 1420 cm^{-1}). 122

Figure 4.2. Real refractive index spectrum of Benzene-h_6 Band 11 (1565 to 1420 cm^{-1}). 123

Figure 5.1. Imaginary dielectric constant spectrum of benzene-h_6. 139

Figure 5.2. Imaginary molar polarizability spectrum of benzene-h_6. 140

Figure 5.3. Imaginary dielectric constant spectrum of benzene-d_6. 141

Figure 5.4. Imaginary molar polarizability spectrum of benzene-d_6. 142

Figure 5.5. Real dielectric constant spectrum of benzene-h_6. 143

Figure 5.6. Real molar polarizability spectrum of benzene-h_6. 144

Figure 5.7. Real dielectric constant spectrum of benzene-d_6. 145

Figure 5.8. Real molar polarizability spectrum of benzene-d_6. 146

Figure 5.9. Imaginary molar polarizability, imaginary dielectric constant and imaginary refractive index spectra of ν_4 of benzene-h_6. 148

Figure 5.10. Experimental and fitted imaginary molar polarizability spectra of ν_{12} of benzene-h_6 165

Figure 5.11. Experimental and fitted imaginary molar polarizability spectra of ν_{13} of benzene-h_6 166

Figure 5.12. Experimental and fitted imaginary molar polarizability spectra of ν_{14} of benzene-h_6 167

Figure 5.13. Experimental and fitted imaginary molar polarizability spectra of ν_{12} of benzene-d_6 ... 168

Figure 5.14. Experimental and fitted imaginary molar polarizability spectra of ν_{13} of benzene-d_6 ... 169

Figure 5.15. Experimental and fitted imaginary molar polarizability spectra of ν_{14} of benzene-d_6 ... 170

Figure 5.16. Experimental and fitted imaginary molar polarizability spectra of benzene-h_6 between 3525 and 3340 cm^{-1} ... 171

Figure 5.17. Geometry and in-plane internal coordinates of benzene. ... 182

Figure 5.18. Out-of-plane internal coordinates of benzene. ... 183

Figure 6.1. Absorbance spectra of benzene-h_6 liquid and gas ... 224

Figure 6.2. Absorbance spectra of benzene-d_6 liquid and gas ... 225

Figure 6.3. The imaginary molar polarizability spectrum of ν_{14} (E_{1u}) of liquid benzene-h_6 ... 228

Figure 7.1. Real refractive index spectra for binary mixtures of benzene-h_6 and benzene-d_6 between 3200 and 800 cm^{-1}. ... 258

Figure 7.2. Real refractive index spectra for binary mixtures of benzene-h_6 and benzene-d_6 between 800 and 400 cm^{-1}. ... 259

Figure 7.3. Imaginary refractive index spectra for binary mixtures of benzene-h_6 and benzene-d_6 between 3200 and 800 cm^{-1}. ... 260

Figure 7.4. Imaginary refractive index spectra for binary mixtures of benzene-h_6 and benzene-d_6 between 800 and 400 cm^{-1}. ... 261

Figure 7.5. Wavenumber times the imaginary molar polarizability spectra for binary mixtures of benzene-h_6 and benzene-d_6 in the ν_{12} region of benzene-h_6. ... 262

Figure 7.6. Wavenumber times the imaginary molar polarizability spectra for binary mixtures of benzene-h_6 and benzene-d_6 in the ν_{13} region of benzene-h_6. ... 263

Figure 7.7. Wavenumber times the imaginary molar polarizability spectra for binary mixtures of benzene-h_6 and benzene-d_6 in the ν_{14} region of benzene-h_6. ... 264

Figure 7.8. Wavenumber times the imaginary molar polarizability spectra for binary mixtures of benzene-h_6 and benzene-d_6 in the ν_4 region of benzene-h_6. 265

Figure 7.9. Wavenumber times the imaginary molar polarizability spectra for binary mixtures of benzene-h_6 and benzene-d_6 in the ν_{12} region of benzene-d_6. 266

Figure 7.10. Wavenumber times the imaginary molar polarizability spectra for binary mixtures of benzene-h_6 and benzene-d_6 in the ν_{13} region of benzene-d_6. 267

Figure 7.11. Wavenumber times the imaginary molar polarizability spectra for binary mixtures of benzene-h_6 and benzene-d_6 in the ν_{14} region of benzene-d_6. 268

Figure 7.12. Wavenumber times the imaginary molar polarizability spectra for binary mixtures of benzene-h_6 and benzene-d_6 in the ν_4 region of benzene-d_6. 269

Figure 7.13. Integrated intensity versus mole fraction of benzene-h_6 for the infrared active fundamentals of benzene-h_6 and benzene-d_6. 270

Figure 7.14. Peak wavenumber versus mole fraction of benzene-h_6 for the infrared active fundamentals and related bands of benzene-h_6 and benzene-d_6. 279

Figure 7.15. Full width at half height versus mole fraction of benzene-h_6 for the infrared active fundamentals and related bands of benzene-h_6 and benzene-d_6. 281

Figure 7.16. Imaginary molar polarizability spectra of 0.25 mole fraction of benzene-h_6 in the regions of the infrared active fundamentals of benzene-h_6. 286

Figure 7.17. Imaginary molar polarizability spectra of 0.25 mole fraction of benzene-h_6 in the regions of the infrared active fundamentals of benzene-d_6. 287

Figure 7.18. Molar absorption coefficient spectra of 0.25 mole fraction of benzene-h_6 in the regions of the infrared active fundamentals of benzene-h_6. 288

Figure 7.19. Molar absorption coefficient spectra of 0.25 mole fraction of benzene-h_6 in the regions of the infrared active fundamentals of benzene-d_6. 289

Figure AI.1. Closed curve used to prove the Hilbert and Kramers-Kronig transforms. 309

List of Symbols

General

λ Vacuum wavelength.

ν Frequency; usual unit s^{-1}.

$\tilde{\nu}$ Vacuum wavenumber; usual unit cm^{-1}. $\tilde{\nu} = 1/\lambda$.

c Speed of light in vacuum.

C Molar concentration; usual unit mole L^{-1}.

V_m Molar volume; usual unit cm^3 $mole^{-1}$.

x_a Mole fraction of component a. For a binary solution $V_m = x_a/C_a$

$\boldsymbol{E}$ Electric field strength vector.

$\boldsymbol{D}$ Electric displacement vector.

$\boldsymbol{P}$ Electric polarization vector.

$\boldsymbol{H}$ Magnetic field strength vector.

$\boldsymbol{I}$ Poynting Vector. $\boldsymbol{I} = \boldsymbol{E} \times \boldsymbol{H}$.

σ conductivity.

ε_o Permittivity of vacuum.

μ_o Permeability of vacuum.

$\boldsymbol{x}, \boldsymbol{y}, \boldsymbol{z}$ units vectors in Cartesian coordinate system.

$$\nabla = \frac{\partial}{\partial x}\boldsymbol{x} + \frac{\partial}{\partial y}\boldsymbol{y} + \frac{\partial}{\partial z}\boldsymbol{z}$$

$\mathrm{i} = \sqrt{-1}$

^ used to indicate a complex quantity.

Wavenumber dependent Quantities

$\hat{n}(\tilde{\nu})$ Complex refractive index, $\hat{n}(\tilde{\nu}) = n(\tilde{\nu}) + \mathrm{i}k(\tilde{\nu})$

$n(\tilde{\nu})$ Real refractive index.

$k(\tilde{\nu})$ Imaginary refractive index, also called the absorption index.

$\hat{\varepsilon}(\tilde{\nu})$ Complex relative dielectric constant, $\hat{\varepsilon}(\tilde{\nu}) = \varepsilon'(\tilde{\nu}) + \mathrm{i}\varepsilon''(\tilde{\nu})$.

$\varepsilon'(\tilde{\nu})$ Real dielectric constant, usually called the dielectric constant.

$\varepsilon''(\tilde{\nu})$ Imaginary dielectric constant, also called the dielectric loss.

$\hat{\alpha}_{\mathrm{m}}(\tilde{\nu})$ Complex molar polarizability, $\hat{\alpha}_{\mathrm{m}}(\tilde{\nu}) = \alpha'_{\mathrm{m}}(\tilde{\nu}) + \mathrm{i}\alpha''_{\mathrm{m}}(\tilde{\nu})$; usual unit cm^3 mole^{-1}.

$\alpha'_{\mathrm{m}}(\tilde{\nu})$ Real molar polarizability.

$\alpha''_{\mathrm{m}}(\tilde{\nu})$ Imaginary molar polarizability.

$E_{\mathrm{m}}(\tilde{\nu})$ (Decadic) molar absorption coefficient; usual unit $\mathrm{cm}^2\ \mathrm{mole}^{-1} = 10^{-3}\ \mathrm{L}\ \mathrm{mole}^{-1}\ \mathrm{cm}^{-1}$.

$K(\tilde{\nu})$ - (Decadic) linear absorption coefficient; usual unit cm^{-1}.

Integrated Intensity Quantities

A_j - Area under band j in $2.303E_{\mathrm{m}}$ spectrum; usual unit km mole^{-1}.

B_j - Area under band j in the $V_{\mathrm{m}}\tilde{\nu}\varepsilon''$ spectrum divided by the Lorentz local field correction; usual unit km mole^{-1}.

C_j - Area under band j in $\tilde{\nu}\alpha''_{\mathrm{m}}$ spectrum; usual unit km mole^{-1}.

Molecular Properties

μ_j Magnitude of dipole moment derivative with respect to normal coordinate j; usual unit Debye Å^{-1} amu$^{-1/2}$.

$\vec{R}_j$ Dipole transition moment, $<f|\vec{\mu}|i>_j$, of the transitions that cause band j; usual unit Debye. 1 Debye = 3.3357×10^{-30} C m = 0.2082 electron Å.

Chapter 1

Introduction

1.1 Infrared Absorption Intensities

This thesis describes a study of the measurement and use of infrared intensities. Absolute absorption intensities were investigated, not relative intensities. The long-term goal of the research program of which this thesis forms a part is to make infrared spectra as quantitatively useful on their intensity axis as they have been for three decades on their wavenumber axis.

The three parameters characterizing vibrational bands are 1) wavenumber, 2) integrated intensity and 3) band shape[1]. The wavenumber is the easiest to measure and describe in terms of the basic molecular property it reflects, namely the difference between energy levels. The integrated intensity and band shape are much harder to measure accurately and their relation to theory is not as straightforward as for wavenumber. It is for these reasons that the intensity and band shape have been studied far less than the wavenumber. Integrated intensities have been measured since the late 1920's[2] and the integrated intensity has long been useful when used in conjunction with wavenumber[3]. A good review of the development of the measurement and use of integrated intensities from 1930 to 1980 has been given by Crawford[1].

Absolute infrared absorption intensities have been measured for over 40 years although largely on gaseous samples. But until the late 1970s there were two major impediments to advancement of the field. First, instrumentation was such that it was extremely time consuming to measure the absolute absorption intensity of even one band[4, 5]. It was an enormous task to do so for an entire spectrum. Second, the accuracy of the measurements was in serious doubt. The latter is not just a problem for the physics of the problem. It prevented major chemical advances because, for example, the relative intensities of OH and OD, or CH and CD, stretching vibrations could not be determined with sufficient accuracy to allow confidence in the result.

During this period the measurements were made largely on gases and solutes in inert solvents, and the additional difficulties introduced into the measurement of absolute absorption intensities of liquids by the size of the real refractive index of the liquid were well recognized[2]. Nevertheless, many significant studies of absorption intensities of neat liquids were made before the late 1970's[5-10].

There was much theoretical activity during this period, which is well summarized in a 1963 review by Overend[2] and in Person and Zerbi's 1982 monograph on vibrational intensities[11]. While, of course, it was recognized that infrared intensities reflect the change in the electron distribution in the molecule during atomic displacements, it was found difficult to develop a model that could relate intensities in different molecules. Because of these theoretical and experimental difficulties, several different parametric models were developed in the search for a chemically useful model[1]. Person and Zerbi's monograph is largely devoted to these different models, and contains rather little on experimental data and its measurement.

There were two major problems in the interpretation of absolute intensity data. First, intensities are proportional to the square of the transition moment, $\left|\vec{R}_{ul}\right|^2$, and the determination of the sign of $\vec{R}_{ul}$ was a challenge. Second, the eigenvectors from a normal coordinate analysis are required to obtain chemically transferable information from the intensities, and the reliability of normal coordinate calculations was suspect.

The 1970's saw a renewal of interest in intensity measurements due to improvements in the normal coordinate calculations as well as *ab initio* quantum-mechanical calculations to help determine the signs of the dipole moment derivatives[1].

The situation with respect to the measurement of absorption intensities of liquids also improved during the 1970s. Instrumentation improved markedly with the advent of FTIR spectrometers based on Michelson's interferometer and the use of computers to control the instruments. One of the pioneers of the use of computers in spectroscopy during the late 1960s and early 1970s was R. Norman Jones of the National Research Council of Canada. This led to his development[12-17] during the 1970s of methods to correct absorption spectra for experimental factors which inevitably accompany their measurement. This led to the publication in 1980 of the first extensive collection of infrared spectra whose intensities were calibrated against a primary standard[18]. The measurements were made with a dispersive, grating, spectrometer, and the spectra were reported graphically but only the peak heights were reported numerically.

FTIR spectrometers give far more precise (reproducible) spectra than dispersive spectrometers. In the middle 1980s, V. Behnam[19, 20] showed that uncalibrated FTIR spectra gave the same intensity values as were reported by Jones and co-workers[18], within their rather large evaluated uncertainties of about 6%, with 90% confidence limits much smaller than Jones' evaluated uncertainties. It seemed possible that FTIR spectra may be very accurate as well as very precise.

A further improvement was the remarkable development of inexpensive laboratory computers since 1980, along with an accompanying development of inexpensive and very powerful software. These improvements made it feasible to consider the possibility of measuring infrared spectra that are known quantitatively on both the intensity axis and the wavenumber axis over the entire infrared range.

The measurement of gas phase intensities of small molecules was improved enormously in the early 1980's when the instrumentation became capable of fully resolving each rotational line of a vibrational transition, so that the intensities of the lines could be measured directly[21]. This yields vibrational intensities of precisely known transitions, a marked improvement over the Wilson-Wells pressure broadening method[2] that had to be used previously.

In this same period, Gussoni and Zerbi and their co-workers were able to develop a parametric model that, even with data of questionable accuracy, enabled them to discuss the effective charge on atoms in a molecule and the charge flow when atomic displacements occur[22-24]. Currently, they are extending the same model to allow the calculation from vibrational intensities of the hyperpolarizabilities needed in non-linear optics.

With this background, this thesis forms part of a study to explore the accuracy with which infrared intensities can be measured with modern spectrometers and computers and, equally important, what information of chemical and physical interest can be obtained from accurate intensities.

The first goal of the work was to explore the accuracy of FTIR measurements of intensities. Two factors were explored and considered together with the discoveries of V. Behnam in 1985. First, errors that could be identified were corrected on the basis of sound physical principles. Second, the systematic errors associated with the operation or design of the instrument were explored by determining the agreement between the intensities measured by different workers using different instruments in different laboratories. This work led to the development and proposal of secondary standards for infrared absorption intensities of neat liquids. These standards have been accepted by the International Union of Pure and Applied Chemistry, and are in the process of publication as a monograph. The reliability and utility of these standards in practical use has been studied.

The second goal was to explore the physical and chemical information contained in these intensities. One of the liquids used as an intensity standard was benzene. This chemical is of such central importance in chemistry that it was chosen for study in this second phase of the work. It is rarely possible to obtain vibrational spectroscopic information from just one isotopic form of a chemical, and benzene-d_6 was also studied to complement the results obtained for benzene-h_6.

The primary measures of intensity calculated from the transmission spectra recorded in this work were spectra of the real and imaginary refractive indices of the liquid over the infrared region between 5000 and 450 cm^{-1}. These quantities are introduced in section 1.3. They are themselves of fundamental physical importance, but because over the wavenumber range in which they are known the real and imaginary refractive indices can also be used to calculate all other measures of absorption intensity, and indeed the result of any infrared absorption experiment which involves the liquid. Thus, the molar absorption coefficient widely used by chemists can be calculated from the refractive indices. Physicists regard the real and imaginary dielectric constants as the most fundamental property to describe vibrations in condensed phases, and these can be calculated from the refractive indices. These quantities have been calculated and are presented for liquid benzene-h_6 and benzene-d_6.

Several methods have been proposed[25-30] to calculate the transition moments and other theoretical spectroscopic molecular quantities from the absorption spectrum of a liquid. These methods have been explored as part of this work, with the conclusion that the most well-defined method is to invoke the Lorentz local field to relate the macroscopic electric field that acts on the liquid to the local electric field that acts on a molecule in the liquid, in order to allow the calculation of the mean molecular polarizability of molecules in the liquid. In fact the molar polarizability was calculated. The polarizability is again a complex quantity, to allow the description of absorption. The molar polarizability spectra of benzene-h_6 and benzene-d_6 are presented and were used to calculate the transition moments of the fundamental and overtone transitions of both isotopomers of benzene.

These results were used to examine experimentally the influence of intermolecular forces on the intensity of absorption by the fundamental vibrations. They were also used, with a normal coordinate calculation, to calculate the change in molecular dipole moment when a CH bond or a CC bond stretches or the HCC angle change in-plane or out-of-plane. This information relates to the electronic charge distribution in the molecule, which is of clear theoretical interest. Further, the intensities of the overtone and combination transitions of benzene-h_6 were compared with those calculated recently by *ab initio* quantum mechanics, a calculation that is at the forefront of current quantum chemistry.

Chemists are fundamentally interested in mixtures of chemicals. The simple theory that currently underlies the infrared spectra of liquids predicts that the imaginary molar polarizability spectrum of a binary mixture should be the sum of the imaginary molar polarizability spectra of the components weighted by their respective mole fractions. This was explored by studying the absorption intensities of mixtures of benzene-h_6 and benzene-d_6. These isotopomers mix to form an ideal solution. It is noteworthy, however, that the peak wavenumbers of each isotopomer are said to shift when mixed with each other. This was also explored in spectra of the different intensity quantities.

The purpose of this section has been to place the work of this thesis into its scientific context. To close the section it is appropriate to note that this thesis presents the absolute absorption intensities of 10 liquids to about 3% accuracy over the wide wavenumber range ~5000 to 450 cm^{-1}. In 1970, it was the work of one thesis to measure the intensities of one or two spectral bands of one liquid with quite uncertain accuracy.

Generally, infrared intensities have been presented in the literature only for selected bands and usually only as graphs, tables of peak wavenumbers and heights, and tables of areas[2, 5-8, 12, 18-20, 31-43]. In order for infrared intensities to be available to the scientific community to their full accuracy tables of intensity values need to be published across the entire mid-infrared region of the spectrum. A compact table and data compression method was recently published[44]. This method allows spectra with about 15000 data points to be presented in a two or three page table. This format is used to tabulate the refractive index spectra measured in this thesis.

The detailed structure of this thesis is described in section 1.2. Section 1.3 provides the connection of the experimental quantities to the fundamental molecular properties through electromagnetic theory. Section 1.4 gives a summary of the relevant literature on benzene and how it relates to what is done in this work.

1.2 Overview of the Thesis

Transmission spectra of liquid benzene-h_6 and benzene-d_6 and binary mixtures of benzene-h_6 and benzene-d_6 were measured. From the transmission spectra the refractive indices of the liquid were calculated. Once the refractive indices are known, other intensity quantities such as the molar absorption coefficients, dielectric constants and molar polarizabilities can be calculated, completely corrected for non-absorption effects. The equations relating the different intensity quantities are developed from electromagnetic theory in section 1.3.

Chapter 2 contains an account of the principles that underlie the determination of refractive indices from transmission spectra, and how these principles are implemented in practice. When dealing with absolute absorption intensities of liquids, it is necessary to correct for intensity lost due to reflection of the light by the cell and by the liquid. This can not be accounted for by ratioing the intensity of the light transmitted through the cell full of liquid to the intensity of the light transmitted through the cell full of air. This is because the refractive index of the liquid and air are sufficiently different that the intensity of light that is reflected is different in the two cases. The correction must be made by computation. Thus described in Chapter 2 is the iterative procedure developed by Jones[12-18, 45, 46] for calculating the refractive index spectra of liquids from transmission spectra. Later in the chapter it is demonstrated that previous experimental work has suffered from baseline variations of unknown origin, and a soundly based method for their removal from experimental absorbance spectra is described.

Several improvements were made to Jones' iterative procedure during this work. These improvements were in the amount of computer time required to calculate the refractive index spectra and the incorporation of the baseline correction procedure. Complete algorithms of the programs used to convert transmission spectra into refractive index spectra are presented in Chapter 2.

Chapter 3 describes the experimental determination of the refractive index spectra from transmission spectra of the liquids studied in this work. A study of the differences between the refractive index spectra of benzene-h_6 obtained from transmission spectra measured by different spectroscopists in different laboratories with different instruments is also presented. From this study, the accuracy of the average refractive index spectra of benzene-h_6 was estimated and the same accuracy was assumed for the refractive index spectra of benzene-d_6 and the binary mixtures of benzene-h_6 and benzene-d_6.

One of the uses of accurate absorption intensities, such as those measured from transmission spectra in this work is to calibrate other transmission measurements as well as measurements made by other techniques such as attenuated total reflection. Secondary infrared intensity standards were developed from the refractive index spectra of benzene-h_6 measured in this work and the refractive index spectra of toluene[47], chlorobenzene[48] and dichloromethane[49] measured separately. These standards were presented to and were accepted as secondary infrared intensity standards by the International Union of Pure and Applied Chemistry. These standards are discussed in Chapter 4, with their application to calibrate transmission cells.

Chapter 5 presents the results of the analysis of the liquid phase intensities of benzene-h_6 and benzene-d_6. The magnitudes of the dipole moment derivatives with respect to normal coordinates were calculated from the imaginary molar polarizability spectra. Curve fitting was used in this process to help separate the contributions of the different transitions and to ensure that intensity in the wings of the bands was included. Normal coordinates were calculated using the 40 wavenumbers of all fundamentals of benzene-h_6 and benzene-d_6. These normal coordinates were then used to calculate the dipole moment derivatives with respect to symmetry coordinates and internal coordinates.

In Chapter 6 the molar polarizability spectra of benzene-h_6 and benzene-d_6 are used to compare the integrated intensities of the infrared active fundamentals of these molecules in the liquid and gas phases. The intensities for the gas phase were taken from the literature. The experimental integrated intensities of the infrared active fundamentals of benzene-h_6 and benzene-d_6 in the two phases are compared in section 6.2. In section 6.3 the experimental integrated intensities of benzene-h_6 are compared with those[50] calculated by *ab initio* methods for the infrared active fundamentals and combinations.

Chapter 7 presents the refractive index spectra of binary mixtures of benzene-h_6 and benzene-d_6. The changes in peak positions and full widths at half height in the molar absorption coefficient spectra and in the spectra of the imaginary molar polarizability times wavenumber are compared with those for absorbance spectra given in the literature[51]. The change in integrated intensity with composition and the extent to which the molar polarizability spectra of the mixtures are simply the weighted sum of the molar polarizability spectra of the pure liquids are discussed.

Chapter 8 contains a summary of the results obtained in this work and a brief suggestion of how this work may be extended.

1.3 Electromagnetic Theory and Optical Properties

The response of a substance to an electric field is determined by the complex refractive index of the substance. The real and imaginary parts of the refractive index are collectively called the optical constants. Also related to the optical constants are the complex dielectric constant and the complex polarizability. These complex quantities are not independent and when one is known the others can be calculated from it. The results of any well defined infrared experiment can be calculated if the optical constants are known at the relevant wavenumbers.

In general, in an infrared experiment one measures the fraction of the incident light intensity transmitted (the transmittance) or reflected (the reflectance) by a substance. The transmittance and reflectance are related to the optical constants through Maxwell's equations.

1.3.1 Intensity Quantities

Maxwell's equations for an isotropic homogeneous neutral conducting medium are[52-54]

$$\nabla \bullet \boldsymbol{H} = 0 \tag{1.3.1}$$

$$\nabla \bullet \boldsymbol{E} = 0 \tag{1.3.2}$$

$$\nabla \times \boldsymbol{H} = \sigma \boldsymbol{E} + \varepsilon \varepsilon_0 \frac{\partial \boldsymbol{E}}{\partial t} \tag{1.3.3}$$

$$\nabla \times \boldsymbol{E} = -\mu \mu_0 \frac{\partial \boldsymbol{H}}{\partial t} \tag{1.3.4}$$

where $\boldsymbol{H}$ is the magnetic field vector, $\boldsymbol{E}$ is the electric field vector, μ is the relative magnetic dipole moment, μ_0 is the permeability of vacuum, ε is the relative dielectric constant of the medium (also called the permittivity), ε_0 is the permittivity of vacuum and σ is the conductivity of the medium. It should be emphasized that $\boldsymbol{E}$ and $\boldsymbol{H}$ are always orthogonal.

Through $\nabla \times (\nabla \times \boldsymbol{E})$, $\boldsymbol{A} \times (\boldsymbol{B} \times \boldsymbol{C}) = (\boldsymbol{A} \bullet \boldsymbol{C})\boldsymbol{B} - (\boldsymbol{A} \bullet \boldsymbol{B})\boldsymbol{C}$ and equations (1.3.2) and (1.3.3), equation (1.3.4) gives

$$-\nabla^2 \boldsymbol{E} = -\mu\mu_0 \frac{\partial}{\partial t}\left(\sigma \boldsymbol{E} + \varepsilon\varepsilon_0 \frac{\partial \boldsymbol{E}}{\partial t}\right) \tag{1.3.5}$$

The solution to equation (1.3.5) is

$$\boldsymbol{E} = \boldsymbol{E}_0 \mathrm{e}^{-\mathrm{i}2\pi\nu(t + x/\hat{\mathrm{v}})} \tag{1.3.6}$$

This represents a wave travelling in the $\boldsymbol{x}$ direction with speed $\hat{\mathrm{v}} = \mathrm{v}' + \mathrm{i}\mathrm{v}''$ and frequency ν. In general, the wave may propagate in any direction but for isotropic media $\boldsymbol{E}$ and $\boldsymbol{H}$ are orthogonal to this direction. Thus, it is convenient to use the Cartesian axis system with the wave propagating along $\boldsymbol{x}$, without loss of generality. Substitution of equation (1.3.6) into (1.3.5) leads to

$$\frac{1}{\hat{\mathrm{v}}^2} = \mu\mu_0\varepsilon\varepsilon_0 + \mathrm{i}\frac{\mu\mu_0\sigma}{2\pi\nu} \tag{1.3.7}$$

For a wave travelling in vacuum $\sigma = 0$, $\mu = \varepsilon = 1$ and its speed is defined[55] as $\mathrm{c} = 2.99792458 \times 10^{10}$ cm s^{-1}. Thus

$$\mathrm{v}' = (\mu_0\varepsilon_0)^{-1/2} = \mathrm{c} \tag{1.3.8}$$

and

$$\mathrm{v}'' = 0 \tag{1.3.9}$$

In a medium of complex refractive index $\hat{n} = n + \mathrm{i}k$, the speed is $\hat{\mathrm{v}} = \frac{\mathrm{c}}{\hat{n}}$. Thus equation (1.3.7) becomes

$$\hat{n}^2 = \mu\varepsilon + \mathrm{i}\frac{\mu\sigma}{2\pi\nu\varepsilon_\mathrm{o}} \tag{1.3.10}$$

$$\Rightarrow n^2 - k^2 = \mu\varepsilon \tag{1.3.11}$$

$$\text{and } 2nk = \frac{\mu\sigma}{2\pi\nu\varepsilon_\mathrm{o}} \tag{1.3.12}$$

Substitution for $\hat{\mathrm{v}}$ in terms of $\hat{n}$ and c in equation (1.3.6), gives

$$\boldsymbol{E} = \boldsymbol{E}_\mathrm{o}\mathrm{e}^{-\mathrm{i}2\pi\nu(t-\frac{n}{\mathrm{c}}x)}\mathrm{e}^{-\frac{2\pi\nu k}{\mathrm{c}}x} \tag{1.3.13}$$

Equation (1.3.13) shows that the real part of the refractive index controls the phase of the field, and the imaginary part controls the attenuation per unit distance travelled by the wave.

If $\nabla\times(\nabla\times\boldsymbol{H})$ is treated in the same manner, the resulting equation is

$$\boldsymbol{H} = \boldsymbol{H}_\mathrm{o}\mathrm{e}^{-\mathrm{i}2\pi\nu(t-\frac{n}{\mathrm{c}}x)}\mathrm{e}^{-\frac{2\pi\nu k}{\mathrm{c}}x} \tag{1.3.14}$$

The energy flux, $\boldsymbol{I}$, is $\boldsymbol{E}\times\boldsymbol{H}$ which is in the direction of propagation of the wave for isotropic media. For the collimated beam of light always assumed in spectroscopy, the energy flux, $\boldsymbol{I}$, is simply the intensity, i.e. the power crossing unit area. Thus

$$I = |\boldsymbol{I}| = E_\mathrm{o}H_\mathrm{o}\mathrm{e}^{-\mathrm{i}4\pi\nu(t-\frac{n}{\mathrm{c}}x)}\mathrm{e}^{-4\pi\frac{\nu k}{\mathrm{c}}x} \tag{1.3.15}$$

In a transmission experiment the reduction in the intensity per unit distance travelled by the wave is measured. This is

$$-\frac{dI}{dx} = K'I \tag{1.3.16}$$

$$\Rightarrow I = I_0 e^{-K'd} \tag{1.3.17}$$

where I_0 is the incident intensity and d is the path length.

Equation (1.3.17) is Lambert's law[56] where K' is the (Napierian) linear absorption coefficient. Comparison of equation (1.3.17) and equation (1.3.15) gives

$$K' = -\frac{1}{d}\ln\left(\frac{I}{I_0}\right) = \frac{4\pi\nu k}{c} = 4\pi\tilde{\nu}k \tag{1.3.18}$$

where $\tilde{\nu}$ is the vacuum wavenumber, $\tilde{\nu} = \frac{\nu}{c} = \frac{1}{\lambda}$ where λ is the vacuum wavelength.

Chemists usually prefer to use the Beer-Lambert Law, often called Beer's Law[56] and the decadic logarithm,

$$I = I_0 10^{-Kd} = I_0 10^{-E_m Cd} \tag{1.3.19}$$

instead of Lambert's Law. In equation (1.3.19), K is the (decadic) linear absorption coefficient, E_m is the (decadic) molar absorption coefficient and C is the molar concentration of the absorbing species. In this case

$$E_m = -\frac{1}{Cd}\log\left(\frac{I}{I_0}\right) = \frac{4\pi\tilde{\nu}k}{C\ln 10} = \frac{4\pi\tilde{\nu}k}{2.303C} \tag{1.3.20}$$

I/I_0 is referred to as the transmittance, T, and $-\log(I/I_0)$ is referred to as the (decadic) absorbance, A. Note that in equations (1.3.16) to (1.3.20) I differs from I_0 only by absorption of energy by the medium. Therefore, when the transmittance spectrum is measured for a liquid between two windows, it must be corrected for intensity lost by reflection and processes other than absorption.

Equation (1.3.7) is sometimes written in terms of the complex dielectric constant defined as

$$\hat{\varepsilon} = \varepsilon' + i\varepsilon'' = \varepsilon + i\frac{\sigma}{2\pi \nu \varepsilon_0} \quad (1.3.21)$$

ε' is the real part of the dielectric constant and is often referred to as the dielectric constant. ε'' is the imaginary dielectric constant and is frequently called the dielectric loss.

Thus from equations (1.3.21) and (1.3.10)

$$\hat{n}^2 = \mu\hat{\varepsilon} \quad (1.3.22)$$

For diamagnetic and paramagnetic materials $\mu \approx 1$ within $\pm 10^{-5}$ [53] and, therefore to good approximation

$$\hat{n}^2 = \hat{\varepsilon} \quad (1.3.23)$$

$$\Rightarrow \varepsilon' = n^2 - k^2 \quad (1.3.24)$$

$$\text{and } \varepsilon'' = 2nk \quad (1.3.25)$$

All of the compounds considered in this thesis are diamagnetic.

The optical constants and the dielectric constants are constants for constant frequency of the electromagnetic wave. All of them change with wavenumber, and in all of the above equations $\hat{n}$ and $\hat{\varepsilon}$ should be replaced by $\hat{n}(\tilde{\nu})$ and $\hat{\varepsilon}(\tilde{\nu})$, respectively.

For an isotropic homogeneous medium the electric displacement vector, ***D***, can be defined as the dielectric constant times the electric field vector or as the vector sum of the electric field vector and the electric polarization vector, ***P***[54, 57]. The appropriate equations are

$$\boldsymbol{D} = \hat{\varepsilon}\boldsymbol{E} \tag{1.3.26}$$

and

$$\boldsymbol{D} = \boldsymbol{E} + 4\pi\boldsymbol{P} \tag{1.3.27}$$

The electric polarization vector in a medium is proportional to the effective electric field[54], which is defined as the electric field which acts on a molecule of polarizability $\hat{\alpha}$ in the medium. Thus,

$$\boldsymbol{P} = N\hat{\alpha}\boldsymbol{E}_{\text{eff}} \tag{1.3.28}$$

where N is the number of molecules in unit volume and $\hat{\alpha}$ is the complex polarizability of the molecules. For an isotropic medium, the real and imaginary polarizabilities are scalar quantities, which are averaged over all molecules, and the effective field is given by[54]

$$\boldsymbol{E}_{\text{eff}} = \boldsymbol{E} + \frac{4\pi}{3}\boldsymbol{P} \tag{1.3.29}$$

Equations (1.3.26) to (1.3.29) provide a connection between the dielectric constant and the polarizability, namely

$$\frac{\hat{\varepsilon} - 1}{\hat{\varepsilon} + 2} = \frac{4\pi}{3} N\hat{\alpha} \tag{1.3.30}$$

This relation is called the Lorentz-Lorenz Formula[54].

The complex polarizability, $\hat{\alpha}$, is a molecular quantity and therefore its value is a very small number. To make the numbers a more convenient size, the complex molar polarizability is defined as

$$\hat{\alpha}_{\text{m}} = N_{\text{A}}\hat{\alpha} \tag{1.3.31}$$

where N_{A} is Avogadro's number. The complex molar polarizability is related by $\hat{\alpha}_{\text{m}} = V_{\text{m}}\,\hat{C}$, to the complex local susceptibility, $\hat{C}$, that was defined by Clifford and

Crawford[58] as $\frac{1}{\hat{C}} = \frac{1}{\hat{\chi}_e} - \frac{4\pi}{3}$, where $\hat{\chi}_e$ is the complex electric susceptibility. V_m is the molar volume and is equal to $\frac{N_A}{N}$.

Equations (1.3.30) and (1.3.31) yield the equations through which the real and imaginary molar polarizabilities are calculated from $\hat{\varepsilon}$, namely

$$\alpha'_m(\tilde{\nu}) = \frac{3V_m}{4\pi}\frac{\left(\varepsilon'(\tilde{\nu})-1\right)\left(\varepsilon'(\tilde{\nu})+2\right)+\varepsilon''(\tilde{\nu})^2}{\left[\varepsilon'(\tilde{\nu})+2\right]^2+\varepsilon''(\tilde{\nu})^2} \tag{1.3.32}$$

$$\alpha''_m(\tilde{\nu}) = \frac{9V_m}{4\pi}\frac{\varepsilon''(\tilde{\nu})}{\left[\varepsilon'(\tilde{\nu})+2\right]^2+\varepsilon''(\tilde{\nu})^2} \tag{1.3.33}$$

The integrated infrared absorption intensity of band *j* has been defined in terms of the area under the $E_m(\tilde{\nu})$ spectrum, the area under the $V_m\tilde{\nu}\varepsilon''(\tilde{\nu}))$ spectrum, and the area under the $\tilde{\nu}\alpha''_m(\tilde{\nu})$ spectrum. These integrated intensities have been called A_j [12, 59, 60], B_j [28, 29] and C_j [29, 30], respectively. The defining equations are

$$A_j = 2.303\int E_m(\tilde{\nu})\,d\tilde{\nu} \tag{1.3.34}$$

$$B_j = V_m\int \tilde{\nu}\,\varepsilon''(\tilde{\nu})\,d\tilde{\nu} + \left(\frac{\underline{\varepsilon}+2}{3}\right)^2 \tag{1.3.35}$$

$$C_j = \int \tilde{\nu}\,\alpha''_m(\tilde{\nu})\,d\tilde{\nu} \tag{1.3.36}$$

where the integrals are over band *j*. In equation (1.3.35), $\underline{\varepsilon}$ is the value the dielectric constant would have if the band were absent from the spectrum[61]. It is usually calculated as the mean value of the real dielectric constant through band *j*. The term $\frac{\underline{\varepsilon}+2}{3}$ is due to the Lorentz local field correction to the macroscopic electric field, ***E***.

1.3.2 Relation of Intensity Quantities to Theory

The quantities which can be derived from infrared experiments have been discussed above, and these quantities must be related to molecular properties through a molecular theory. Several authors[25-27] have discussed the calculation of the complex molar polarizability of randomly oriented molecules from quantum mechanics and from the classical damped harmonic oscillator model.

The quantum mechanical treatment gives, for the dipole transition moment (dipole matrix element between the initial, *i*, and final, *f*, states)

$$C_j = \int \tilde{\nu}\, \alpha''_{\mathrm{m}}(\tilde{\nu})\, \mathrm{d}\tilde{\nu} = \frac{N_{\mathrm{A}}\pi}{3hc}\, g_j\, \tilde{\nu}_j \left|\bar{R}_j\right|^2 \qquad (1.3.37)$$

where h is Planck's constant, c is the velocity of light in vacuum, g_j is the degeneracy, $\tilde{\nu}_j$ is the wavenumber and $\bar{R}_j$ is the dipole transition moment, $<f|\vec{\mu}|i>_j$, of the transitions that cause band j. Note that $\tilde{\nu}_j \left|\bar{R}_j\right|^2$ is really the average over all of the transitions that contribute to band j of the product of the transition wavenumber and the square of the transition moment.

For a fundamental band, with the assumption that all of the hot bands of the fundamental contribute to the band and with the expression for the transition moment[62], $<1|\vec{\mu}|0>$, of the fundamental transition of an electrically and mechanically harmonic oscillator, equation (1.3.37) yields the expression for the square of the dipole moment derivative with respect to the jth normal coordinate, $|\partial\vec{\mu}/\partial Q_j|^2$, which is designated μ_j^2 for brevity,

$$C_j = \int \tilde{\nu}\, \alpha''_{\mathrm{m}}(\tilde{\nu})\, \mathrm{d}\tilde{\nu} = \frac{N_{\mathrm{A}}\, g_i}{24\pi c^2}\, \mu_j^2 \qquad (1.3.38)$$

The same equation is obtained from the classical damped harmonic oscillator, CDHO, model[25-27].

The CDHO model also relates the complex molar polarizability spectra to the molecular properties[25-27] μ_j^2, Γ_j and $\tilde{\nu}_j$ through the equation

$$\hat{\alpha}_{\mathrm{m}}(\tilde{\nu}) = \frac{\varepsilon_\infty - 1}{\varepsilon_\infty + 2}\frac{3N_{\mathrm{A}}}{4\pi N} + \frac{N_{\mathrm{A}}}{4\pi^2 \mathrm{c}^2}\sum_j \frac{(\mu_j^2 / 3)}{\tilde{\nu}_j^2 - \tilde{\nu}^2 - \mathrm{i}\tilde{\nu}\Gamma_j} \tag{1.3.39}$$

Here Γ_j is essentially the full width at half height.

From this equation, the real and imaginary parts of the complex molar polarizability are given by

$$\alpha'_{\mathrm{m}}(\tilde{\nu}) = \frac{\varepsilon_\infty - 1}{\varepsilon_\infty + 2}\frac{3N_{\mathrm{A}}}{4\pi N} + \frac{N_{\mathrm{A}}}{4\pi^2 \mathrm{c}^2}\sum_j \frac{(\mu_j^2 / 3)(\tilde{\nu}_j^2 - \tilde{\nu}^2)}{(\tilde{\nu}_j^2 - \tilde{\nu}^2)^2 + \Gamma_j^2 \tilde{\nu}^2} \tag{1.3.40}$$

$$\begin{aligned} \alpha''_{\mathrm{m}}(\tilde{\nu}) &= \frac{N_{\mathrm{A}}}{4\pi^2 \mathrm{c}^2}\sum_j \frac{(\mu_j^2 / 3)\Gamma_j \tilde{\nu}}{(\tilde{\nu}_j^2 - \tilde{\nu}^2)^2 + \Gamma_j^2 \tilde{\nu}^2} \\ &= \sum_j \frac{S_j \Gamma_j \tilde{\nu}}{(\tilde{\nu}_j^2 - \tilde{\nu}^2)^2 + \Gamma_j^2 \tilde{\nu}^2} \end{aligned} \tag{1.3.41}$$

where

$$S_j = \frac{N_{\mathrm{A}}}{4\pi^2 \mathrm{c}^2}\frac{\mu_j^2}{3} \tag{1.3.42}$$

and is called the oscillator strength. It is straightforward to relate the oscillator strength, S_j, to the integrated intensity, C_j, through equation (1.3.38).

$$C_j = S_j g_j \frac{\pi}{2} \tag{1.3.43}$$

In these equations, ε_∞ is the real dielectric constant in the region below the electronic absorption and above the vibrational absorption where ε, and hence n, is essentially independent of the wavelength of the radiation. The factor of 3 in $\mu_j^2/3$ allows for the random orientation of the molecules.

To the extent that the absorption bands are sufficiently far apart, expressions for the complex dielectric constant can be deduced[25, 26, 30] from equation (1.3.39) for the polarizability. These equations lead to a second set of equations for obtaining $|\bar{R}_j|^2$ and μ_j^2 from optical data, this time from the molar conductivity, $V_\mathrm{m}\tilde{\nu}\varepsilon''$.

$$B_j = V_\mathrm{m} \int \tilde{\nu}\, \varepsilon''(\tilde{\nu})\, \mathrm{d}\tilde{\nu} \div \left(\frac{\underline{\varepsilon}+2}{3}\right)^2 = \frac{4\pi^2 N_\mathrm{A}}{3hc}\, g_j\, \tilde{\nu}_j\, |\bar{R}_j|^2 \qquad (1.3.44)$$

$$= \frac{N_\mathrm{A}}{6c^2}\, g_j\, \mu_j^2 \qquad (1.3.45)$$

Equations (1.3.20), (1.3.25) and (1.3.34) show that the area A_j can be related to $|\bar{R}_j|^2$ and μ_j^2 through equations (1.3.44) and (1.3.45) and the additional assumption that $n(\tilde{\nu})$ can be replaced by an average value across band j, $\underline{n}$: namely

$$\begin{aligned} V_\mathrm{m}\int \tilde{\nu}\varepsilon''\mathrm{d}\tilde{\nu} &= 2V_\mathrm{m}\int \tilde{\nu} n k\, \mathrm{d}\tilde{\nu} \\ &\approx \frac{V_\mathrm{m}\underline{n}}{2\pi}\int 4\pi\tilde{\nu} k\, \mathrm{d}\tilde{\nu} = \frac{2.303\underline{n}}{2\pi}\int E_\mathrm{m}\, \mathrm{d}\tilde{\nu} \end{aligned} \qquad (1.3.46)$$

Therefore

$$A_j = 2.303 \int E_\mathrm{m}(\tilde{\nu})\, \mathrm{d}\tilde{\nu} = \frac{8\pi^3 N_\mathrm{A}}{3hc}\, \frac{1}{\underline{n}} \left(\frac{\underline{n}^2+2}{3}\right)^2 g_j\, \tilde{\nu}_j\, |\bar{R}_j|^2 \qquad (1.3.47)$$

$$= \frac{\pi N_\mathrm{A}}{3c^2}\, \frac{1}{\underline{n}} \left(\frac{\underline{n}^2+2}{3}\right)^2 g_j\, \mu_j^2 \qquad (1.3.48)$$

where $\underline{\varepsilon}$ has been replaced by $\underline{n}^2$ in the Lorentz local field correction, as is often done[25, 26, 63].

Equations (1.3.37) and (1.3.38) relate the integrated intensity to the molecular properties through the fewest approximations. The numerical values of the constants for equations (1.3.37), (1.3.38), (1.3.44), (1.3.45), (1.3.47) and (1.3.48) are summarized in Appendix II.

Bertie *et al.* have shown[30] that the dipole moment derivatives obtained from A_j, B_j and C_j frequently agree to better than 1% in spectral regions of medium or weak absorption by liquids, if the value of ε is taken as the average of the maximum and minimum values of the real dielectric constant in the anomalous dispersion caused by band j. When bands overlap or when there are strong bands in the spectrum, Bertie *et al.* have shown[30] that the correct value of ε can not be determined and the dipole moments obtained from A_j and B_j can be in significant error. In these cases the dipole moment derivatives obtained from C_j are the most accurate.

1.4 Previous Studies of the Vibrations and Infrared Absorption Intensities of Benzene

In this section the previous studies of the vibrations of benzene and their infrared absorption intensities are reviewed briefly. In subsection 1.4.1 the assignment of the fundamentals is reviewed. In subsection 1.4.2 the infrared absorption intensities in the liquid and gas phases are reviewed. In the final subsection of this section, the normal coordinate calculations of benzene are reviewed.

1.4.1 Assignment of Fundamentals

The first extensive study of the vibrational spectrum of benzene was carried out by Ingold and co-workers in 1936 [64-69] and 1946 [70-76]. They measured the infrared and Raman spectra of C_6H_6, C_6D_6 and several other deuterium isotopomers of benzene in both the liquid and gas phases. Their assignment has remained essentially unchanged except for the wavenumbers of the infrared and Raman inactive fundamentals. Mair and Hornig[77] reassigned the infrared and Raman inactive B_{2u} fundamentals in 1949.

In 1956 [78] and 1959 [79] Brodersen and Langseth determined the wavenumbers of the fundamentals of C_6H_6 and its 12 deuterium isotopomers in both the liquid and gas phases. The samples they used had higher chemical and isotopic purity than those used in the previous studies[64-77], and they claimed a wavenumber accuracy of better than 0.5 cm^{-1} but reported the values only to the nearest 1 cm^{-1}. They did not change the assignment made by Ingold and by Mair and Hornig, but did assign most of the observed overtone and combination bands and assigned the spectra of several additional isotopomers.

Since the work of Brodersen and Langseth , the spectra of gaseous C_6H_6, C_6D_6 have been studied under very high resolution[80-99]. The vibrational-rotational analyses allowed by such studies have yielded much more accurate wavenumbers of the vibrational transitions. Goodman and co-workers[89, 100] summarize of the currently accepted wavenumbers of the fundamentals of benzene-h_6, benzene-d_6 and various other isotopomers in the gas phase.

Since the studies of Brodersen and Langseth, the only study of the vibrational assignment of the liquid was by Painter and Koenig[101]. They measured infrared and Raman spectra of $^{13}C_6H_6$ and $^{13}C^{12}C_5H_6$ which also contained $^{12}C^{13}C_5H_6$ and $^{12}C_6H_6$, respectively. They determined the wavenumbers of all fundamentals, including the infrared and Raman inactive ones which were determined from active combinations. Painter and Koenig's wavenumbers of the fundamentals of $^{12}C_6H_6$ agreed within 5 cm^{-1} with those reported by Brodersen and Langseth for natural C_6H_6, except ν_5 which they reassigned. It should be noted that the natural benzene-h_6 and benzene-d_6 used for this thesis is approximately 94% $^{12}C_6H_6$ or $^{12}C_6D_6$ and

6% $^{13}C^{12}C_5H_6$ or $^{13}C^{12}C_5D_6$. The bands due to the monocarbon-13 species at most cause asymmetry of the $^{12}C_6H_6$ or $^{12}C_6D_6$ bands.

1.4.2 Infrared Absorption Intensities

The infrared absorption intensities of benzene in the liquid[5-8, 12, 18-20, 32, 33, 36-38, 43] and the gas[2, 31, 34, 35, 39-42] phases have been measured by many workers. Two of the liquid studies[19, 20] only give tables of peak heights and another[18] gives only tables of peak heights and graphs of the complete spectra. The other liquid phase and gas phase studies give only integrated intensities of various bands.

The most recent summary of the results was made by Zelano and King in 1970[36]. Since 1970 the integrated intensities of the liquid were measured four times[12, 37, 38, 43] before this work and those of the gas have been measured four times[39-42]. Only the results since 1970 are summarized here, but in Chapter 6 the intensities determined in this work are compared with those in the literature for both the liquid and gas phases and all of the literature data is used.

1.4.2a Infrared Absorption Intensities in the Liquid Phase

In 1973, Tshmel and Vettegren[37] measured the real and imaginary refractive indices of benzene-h_6 between 1080 and 990 cm^{-1} from attenuated total reflection (ATR) spectra. They used single reflection ATR at 47° incidence in the KRS-6 (TlBrTlCl) element and perpendicular polarized light. They gave a table of the real and imaginary refractive indices over this range, and for example, found the peak of the band at 1036 cm^{-1} with $k_{max} = 0.070$.

In 1976, Zolotarev[38] measured the real and imaginary refractive indices of benzene-h_6 between 3100 and 3000, 1076 and 990, and 712 and 640 cm^{-1} from ATR spectra. He used a KRS-5 (TlBrTlI) element with perpendicular polarized light. For the two high-wavenumber regions he used 3 reflections at 44°10′ and between 712 and 640 cm^{-1} he used 1 reflection at 71°20′. He reported the refractive indices in a graph only for the 3100 to 3000 cm^{-1} and in tables only for the other two regions. He found k_{max} = ~0.045 at ~3036 cm^{-1}, 1.277 at 675 cm^{-1} and 0.0720 at 1035.5 cm^{-1}. The latter value is about 3% higher than that given by Tshmel and Vettegren[37].

In both of these studies the absorption was measured over very limited wavenumber ranges to which the KK transform was then applied to obtain the real refractive indices. It should be noted that for accurate values of the real refractive index the KK transform should be applied across the entire range of significant IR absorption (section 2.3).

Hawranek and Jones[12] measured the real and imaginary refractive index spectra of benzene-h_6 between 4200 and 550 cm^{-1} by their newly developed method from transmission spectra in 1976. Their grating spectrometer was checked against a primary intensity standard. Their spectra were presented as graphs of and a table of the peak wavenumbers and heights in the imaginary refractive index spectrum, the wavenumbers and values for the maxima and minima in the real refractive index spectrum and the integrated intensities of selected bands. This was the first determination of the refractive index spectra of benzene-h_6 over an extended range of the mid-infrared region (~4000 - 400 cm^{-1}). They found k_{max} = 0.0524 at 3036.7 cm^{-1}, 0.0678 at 1036.0 cm^{-1} and 1.29 at 673.0 cm^{-1}.

In 1980, Goplen, Cameron and Jones[18] measured the real and imaginary refractive indices of benzene-h_6 from transmission spectra over the range 4200 to 300 cm^{-1}. The method had been slightly refined since the work of Hawranek[12], particularly with regard to improving the accuracy of the real refractive indices. They tabulated peak heights in the molar absorption and imaginary refractive index spectra as well as the wavenumbers and values of the real refractive index at the maxima and minima in its spectrum. They also presented graphs of the real and imaginary refractive index spectra. This was the most complete study of the optical constants of benzene-h_6 until the present work and formed part of an extensive study of the optical constants of 13 organic liquids. Again, they used a dispersive spectrometer calibrated against a primary standard. The agreement of the present work with those of Jones and co-workers is discussed in Chapter 3. To compare with the earlier workers reported above they found, *inter al.*, that $k_{max} = 0.0520$ (13) at 3036.0 cm^{-1}, 0.0711 (14) at 1035.5 cm^{-1} and 1.22 (4) at 673.0 cm^{-1}.

Bertie, Jones and Behnam[19, 20] calculated the optical constants of benzene-h_6 from transmission spectra over the range 4400 - 800 cm^{-1}. They compared the peak imaginary refractive index values with those of Goplen, Cameron and Jones[18] for selected bands. Bertie *et al.* used an FTIR spectrometer that was not calibrated but they varied many of the instrumental parameters, such as beamsplitter, resolution, zero-filling, apodization function, and cells in order to try to determine the accuracy of their results rather than the precision. Their peak values generally agreed with those of Goplen, Cameron and Jones[18] but were far more precise (reproducible). From this study it was speculated[19, 20] that well-aligned FTIR spectrometers give accurate results even though they are not calibrated. The spectra used in this study were all recorded on one FTIR instrument by one spectroscopist. The results of the studies by Bertie *et al.* are discussed in Chapter 3 where an account is given of the extension of that study by comparing the measurements made by different spectroscopists on different instruments.

Son, Choi and Kim[43] measured the optical constants of benzene-h_6 between 3500 and 2500 cm^{-1} in 1993. They measured the transmission spectrum of benzene between two Ge plates 176 μm apart. They calculated the real refractive indices from the strong interference fringes observed, and calculated the imaginary refractive indices by a KK transform which made use of the classical damped harmonic oscillator model to compensate for the finite integration range. They presented the results as graphs of the real and imaginary refractive index spectra, a table of integrated intensities and a table of the real refractive index values at 15 wavenumbers between 3250 and 2850 cm^{-1}. They found $k_{\max} = \sim 0.053$ at 3035 cm^{-1}.

1.4.2b Infrared Absorption Intensities in the Gas Phase

Since 1970 the absorption intensities of gaseous benzene have been measured by Akiyama and co-workers[39, 40, 42] and by Goodman and co-workers[41]. Akiyama measured the integrated intensity of the 675 cm^{-1} band of benzene-h_6 and the 496 cm^{-1} band of benzene-d_6 in 1980[39] and of the 3048, 1484 and 1038 cm^{-1} bands of benzene-h_6 and the 2288, 1334 and 814 cm^{-1} bands of benzene-d_6 in 1982[40]. Akiyama, Shimizu, Itaya and Kakihana remeasured the intensity of the 675 cm^{-1} band of benzene-h_6 and the 496 cm^{-1} band of benzene-d_6 in 1989[42].

Goodman, Ozkabak and Wiberg measured the integrated intensities of the 3048, 1484 and 1038 cm^{-1} bands of benzene-h_6 and of the 2289, 1336 and 816 cm^{-1} bands of benzene-d_6 in 1989[41].

As noted in Chapter 6, there is fair agreement about the integrated intensity values, except for 1038 cm^{-1} band of benzene-h_6 and the 1336 and 816 cm^{-1} bands of benzene-d_6. In Chapter 6, these gas phase intensities and the earlier ones summarized by Zelano and King[36] are compared and are also compared with the liquid phase intensities determined in this work.

1.4.3 Force Field Calculations

The force field of benzene was first studied by Wilson in 1934[102]. He developed a potential surface using only the six diagonal force constants. Many different empirical[40, 100, 103-121] and theoretical[41, 50, 122-131] (semi-empirical and *ab initio*) force field calculations have been carried out since this first study. The most recent empirical force field calculation was in 1991 by Goodman *et al.*[100], who also thoroughly reviewed the previous calculations.

Goodman *et al.*[100] estimated the harmonic wavenumbers of 55 fundamentals of gaseous C_6H_6, C_6D_6, $^{13}C_6H_6$ and $^{13}C_6D_6$ from the observed anharmonic wavenumbers. They used these 55 harmonic wavenumbers to calculate the complete harmonic force field of benzene, requiring 34 distinct force constants[100]. They termed their result a "Benchmark Vibrational Potential Energy Surface". These force constants were used as the starting point to determine the force constants for the liquid phase presented in Chapter 5.

In 1981 Pulay, Fogarasi and Boggs[124] calculated the complete harmonic force field of gaseous benzene using systematically scaled *ab initio* quantum-mechanical calculations at the Hartree-Fock level using a double zeta basis set. They also calculated "the most important" cubic force constants. These force constants are compared with those determined for the liquid in Chapter 5. There have been many other theoretical calculations[50, 122, 123, 125-131] of the harmonic force field of benzene but none of these studies have given values significantly different from those of Pulay *et al.* Therefore, only the force constants calculated by Pulay *et al.* are compared to the force constants calculated for the liquid in the present work.

It should be particularly noted that Pulay[125] has investigated the effect of electron-correlation through a calculation that was said[125] to be equivalent to the Møller-Plesset perturbation theory using localized orbitals. Pulay concluded[125] that "the physical force field of benzene is close to our Set II", the "Set II" force constants of the 1981 paper[124].

Finally, it should be noted that all of the above calculations are for gaseous benzene. For liquid benzene, Painter and Koenig calculated[115] a force field from the wavenumbers of $^{12}C_6H_6$, $^{12}C_6D_6$, $^{13}C_6H_6$ and $^{13}C_6D_6$. Painter and Snyder[116] subsequently published a different force field that corrected errors in the first paper. The force field differs significantly from those of Goodman[100] and Pulay[124] for the gas, and contains only 22 force constants. The complete General Valence Force Field of Goodman[100] and Pulay[124] are preferred as a basis for a force field for liquid benzene.

Maslen *et al.*[50] have studied the anharmonic spectral effects in gaseous benzene via *ab initio* calculations. They calculated the quartic force field and the wavenumbers and intensities of the infrared active fundamentals and combinations. These intensities are compared with the observed intensities for the liquid phase in Chapter 6.

Chapter 2

The Determination of Real and Imaginary Refractive Index Spectra from an Experimental Absorbance Spectrum of a Cell Full of Liquid

An experimentalist obtains an absorbance spectrum of a cell full of liquid by measuring the transmission spectrum of the full cell relative to the empty sample compartment and taking the negative decadic logarithm of the transmittance. In FTIR spectroscopy, this is done by recording separate intensity spectra, which were traditionally called single beam spectra, of the full cell and of the empty sample compartment, ratioing them and taking the negative logarithm. On a double-beam dispersive instrument, it is done by recording the spectrum of the full cell relative to that of the empty reference beam, and taking the negative logarithm.

It is important to note that neither the FTIR nor the dispersive method yields the absorbance spectrum as it is currently defined by the International Union of Pure and Applied Chemistry (IUPAC). IUPAC defines[132, 133] absorbance to be a measure of the intensity loss due only to absorption by the sample. Absorbance does not include the intensity loss due to reflection effects at the inner and outer window surfaces, nor does it include intensity loss due to attenuation by the cell or other mechanism. For this reason, the term *experimental absorbance* spectrum is used here for the spectrum the experimentalist obtains by either of the above methods. The term absorbance spectrum is reserved for the spectrum that has been fully corrected for background effects and reflection losses so that it contains only the loss due to absorption. The term *apparent absorbance* is used for contributions to the experimental absorbance from effects other than absorption.

The experimental absorbance is, thus, the sum of the absorbance and the apparent absorbance due to reflection effects and other sources of energy loss. To calculate the absorbance spectrum from an experimental absorbance spectrum it is necessary to remove the apparent absorbance. This requires that the reflectance and transmittance of the cell be calculated.

Sections 2.1 and 2.2 develop the equations necessary to calculate the reflectance and transmittance of a cell. Also required before the optical constants can be calculated is the Kramers-Kronig transformation. This is discussed in section 2.3. The iterative procedure developed by Jones and co-workers to calculate the optical constants of a liquid from transmission spectra is based on the equations developed in sections 2.1 to 2.3. This iterative procedure is described in section 2.4.

In section 2.5 it is shown that transmission spectra, and the imaginary refractive index spectra obtained from them using the procedure developed by Jones and co-workers, typically suffer from baseline variations. A baseline correction procedure is presented in section 2.5 which removes baseline variations from transmission spectra and thus makes the imaginary refractive index spectra much more reproducible.

2.1 Transmittance and Reflectance at an Interface Between Media; Fresnel's Equations

In order to calculate the optical constants of a liquid from experimental absorbance spectra, it is necessary to correct the experimental absorbance spectra for reflection from and within the cell. To do this the reflectance and transmittance must be calculated at each interface. In this section Fresnel's equations for the reflection and transmission at a plane boundary are presented briefly to define the terminology

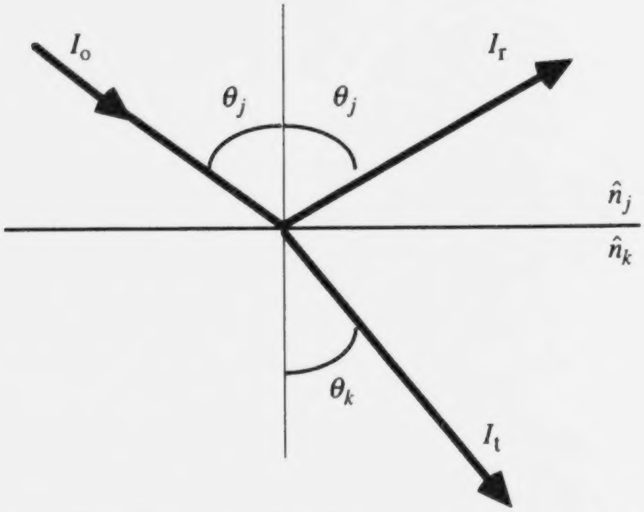

Figure 2.1. Reflection and transmission of a plane wave at a plane boundary. I_0 travels from medium j to medium k. The angle of incidence and reflection is θ_j and the angle of refraction is θ_k. The s and p polarizations of the electric field $\boldsymbol{E}$ are perpendicular to and in the plane of the paper, respectively.

and symbols. In section 2.2 these equations are applied to a transmission cell to develop the equations that form the basis of the iterative procedure for calculating optical constants from transmission spectra that is described in section 2.4.

Figure 2.1 shows the reflection and transmission of a plane wave at a plane boundary. The plane of incidence is assumed to be the plane of the paper. The electric field, $\boldsymbol{E}$, can either be parallel to the plane of incidence (termed p polarization) or perpendicular to the plane of incidence (termed s polarization). These two cases must be considered separately.

$\boldsymbol{I}_{\mathrm{o}}$, $\boldsymbol{I}_{\mathrm{r}}$ and $\boldsymbol{I}_{\mathrm{t}}$ are the incident, reflected and transmitted electric flux vectors, respectively. $\boldsymbol{E}_{\mathrm{o}}$, $\boldsymbol{E}_{\mathrm{r}}$ and $\boldsymbol{E}_{\mathrm{t}}$ are the corresponding electric field vectors. $\hat{n}_j$ and $\hat{n}_k$ are the complex refractive indices of media j and k, respectively. The directions of propagation of the incident and reflected rays make an angle θ_j with a vector normal to the plane boundary, while the transmitted ray makes an angle θ_k with the normal. Note that if the refractive index of the medium, $\hat{n}$, is a complex quantity then the angle θ in that medium is also complex.

The boundary conditions[52-54] are that the tangential components of the electric and magnetic field be continuous across the boundary. Thus for s polarization $\boldsymbol{E}$ must be continuous and for the p polarization $\boldsymbol{H}$ must be continuous. This results[52-54] in the following conditions for the ratio of the reflected or transmitted amplitude of the electric field vector, $\boldsymbol{E}$, to the incident amplitude.

$$r_{jk,\mathrm{s}} = \frac{E_{\mathrm{r,s}}}{E_{\mathrm{o,s}}} = \frac{\hat{n}_j \cos\theta_j - \hat{n}_k \cos\theta_k}{\hat{n}_j \cos\theta_j + \hat{n}_k \cos\theta_k} \tag{2.1.1}$$

$$r_{jk,\mathrm{p}} = \frac{E_{\mathrm{r,p}}}{E_{\mathrm{o,p}}} = \frac{\hat{n}_j \cos\theta_k - \hat{n}_k \cos\theta_j}{\hat{n}_j \cos\theta_k + \hat{n}_k \cos\theta_j} \tag{2.1.2}$$

$$t_{jk,\mathrm{s}} = \frac{E_{\mathrm{t,s}}}{E_{\mathrm{o,s}}} = \frac{2\hat{n}_j \cos\theta_j}{\hat{n}_j \cos\theta_j + \hat{n}_k \cos\theta_k} \tag{2.1.3}$$

$$t_{jk,\mathrm{p}} = \frac{E_{\mathrm{t,p}}}{E_{\mathrm{o,p}}} = \frac{2\hat{n}_j \cos\theta_j}{\hat{n}_j \cos\theta_k + \hat{n}_k \cos\theta_j} \tag{2.1.4}$$

where the subscript jk indicates that the wave is travelling from medium j to medium k.

These equations are known as Fresnel's equations. The reflectance, R, and transmittance, T, are defined as the fraction of the intensity of the incident light that is either reflected or transmitted, respectively. $I \propto E^2$, therefore the reflectance and transmittance can be calculated from Fresnel's equations as[53]

$$R_{jk,w} = |r_{jk,w}|^2 \tag{2.1.5}$$

$$T_{jk,w} = \left|t_{jk,w}\right|^2 \left|\frac{\hat{n}_k \cos\theta_k}{\hat{n}_j \cos\theta_j}\right| \tag{2.1.6}$$

where w = s or p.

2.2 Reflectance and Transmittance of a Transmission Cell

In a liquid transmission cell, the liquid of thickness d is placed between two transparent windows, as shown schematically in Figure 2.2. The cell is placed in the spectrometer which is either purged with dry nitrogen or evacuated. Thus n_0 can be taken as 1 in the following equations. It is included only to keep the equations general. The interfaces between the surroundings and the cell windows are labelled a and c, as indicated in Figure 2.2. Note that it is the liquid layer that is labelled b in Figure 2.2, not the interface between the cell windows and the liquid.

As light passes through the cell, some is reflected at each interface, i.e. by each window and the liquid layer. Also some of the light may be absorbed by the liquid. Throughout this thesis it is assumed that the windows are non absorbing in the infrared. Since the absorption is determined by the imaginary part of the refractive index of the substance, this means that the refractive index of the windows is assumed to be real while that of the liquid is complex.

The development of the calculation of the reflectance and transmittance of a transmission cell is presented in three stages. In subsection 2.2.1 the reflectance and transmittance by a single parallel-sided plate (solid or liquid) are calculated. In

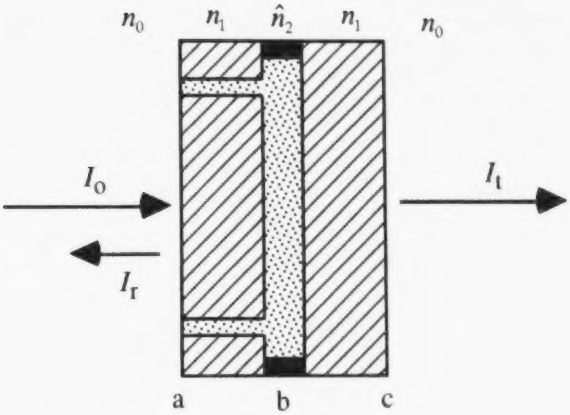

Figure 2.2. Schematic of a transmission cell. The medium surrounding the cell has refractive index n_0 which is real. The cell windows have refractive index n_1 which is also real. The liquid has thickness d and complex refractive index $\hat{n}_2$. I_0 is the incident energy flux, I_r is the reflected energy flux and I_t the transmitted energy flux. The letters a and c are used to indicate the interface between the surroundings and the cell windows. The letter b is used to indicate the liquid layer.

subsection 2.2.2 the reflectance and transmittance of a thin absorbing liquid film are calculated. In subsection 2.2.3 the reflectance and transmittance of the complete transmission cell are calculated. In subsection 2.2.4, the application of the equations given in subsections 2.2.1 to 2.2.3 to calculate the path length and reflectance of a transmission cell is discussed.

2.2.1 Transmittance and Reflectance of a Single Plate

Figure 2.3 shows schematically the transmission and reflection of a single plate. In the case shown, the refractive indices of all three media are considered complex to keep the resulting equations completely general. The electric field

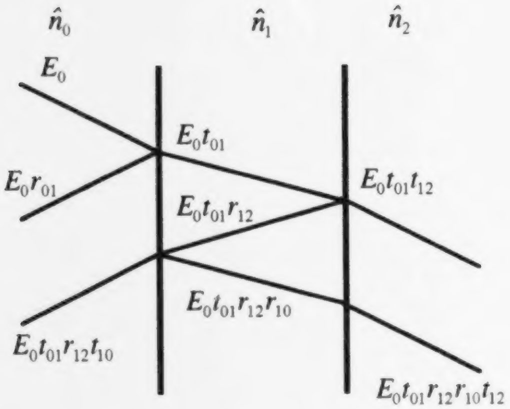

Figure 2.3. Transmittance and reflectance of a single plate.

incident upon the first interface is E_0. The electric field transmitted is $E_0 t_{01}$ and the electric field reflected is $E_0 r_{01}$, where the subscript indicating s or p polarization has been omitted. In practice all equations must be evaluated separately for s and p polarization.

Reflection and transmission occur at each interface. Thus, when the first transmitted ray reaches the second interface, $E_0 t_{01} t_{12}$ is transmitted and $E_0 t_{01} r_{12}$ is reflected back to the first interface where it is again reflected and transmitted as illustrated in Figure 2.3. Several rays thus reach surfaces 1-0 and 1-2. each ray having travelled a different distance in medium 1. Therefore when the rays are combined to get the total transmitted or reflected amplitude it is necessary to consider the phase difference between the different rays. The phase shift between successive rays is[53]

$$\delta = 4\pi \tilde{v} d \hat{n}_2 \cos\theta_2 \tag{2.2.1}$$

where d is the thickness of the plate. The sum over infinite reflections within the plate gives

$$\begin{aligned} E_t &= E_o(t_{01}t_{12} + t_{01}r_{12}r_{10}t_{12}e^{i\delta} + t_{01}r_{12}^2 r_{10}^2 t_{12}e^{i2\delta} + \cdots) \\ &= E_o \frac{t_{01}t_{12}}{1 - r_{10}r_{12}e^{i\delta}} \end{aligned} \tag{2.2.2}$$

$$\begin{aligned} E_r &= E_o(r_{01} + t_{01}r_{12}t_{10}e^{i\delta} + t_{01}r_{12}^2 r_{10}t_{10}e^{i2\delta} + \cdots) \\ &= E_o\left(r_{01} + \frac{t_{01}t_{10}r_{12}e^{i\delta}}{1 - r_{10}r_{12}e^{i\delta}} \right) \end{aligned} \tag{2.2.3}$$

The resulting equations for the transmittance and reflectance of a single plate surrounded by two semi-infinite media, i.e. by media that are continuous to infinity perpendicular to the plate, are (from equations 2.1.5 and 2.1.6)

$$T = \left| \frac{t_{01}t_{12}}{1 - r_{10}r_{12}e^{i\delta}} \right|^2 \left(\frac{\hat{n}_2 \cos\theta_2}{\hat{n}_0 \cos\theta_0} \right) \tag{2.2.4}$$

$$R = \left| r_{01} + \frac{t_{01}t_{10}r_{12}e^{i\delta}}{1 - r_{10}r_{12}e^{i\delta}} \right|^2 \tag{2.2.5}$$

The phase difference between successive rays varies between 0 and 2π for different wavenumbers. If the plate thickness is large compared with the wavelength of the radiation, the phase difference changes from 0 to 2π in such a small wavenumber range that the variations in T and R can not be observed. In such cases the phase difference between the different reflected and transmitted rays can be ignored and only the average of equations (2.2.4) and (2.2.5) needs to be calculated. However, this removes all knowledge of interference effects within the plate. For this case, the sum over infinite multiple reflections gives

$$T = \frac{T_{12}T_{01}}{1 - R_{10}R_{12}} \tag{2.2.6}$$

$$R = R_{01+} \frac{T_{01}^2 R_{12}}{1 - R_{10}R_{12}} \tag{2.2.7}$$

where R_{jk} and T_{jk} are defined by equations (2.1.5) and (2.1.6), respectively and the fact that $T_{10} = T_{01}$ has been used to simplify the equation for R.

2.2.2 Transmittance and Reflectance of a Thin Absorbing Liquid Film

The transmittance and reflectance for a liquid layer is treated exactly as the thick plate shown in Figure 2.3. When the thickness of the liquid layer is of the same order as the wavelength of the radiation one must take account of the phase shift between the different reflected and transmitted rays and equations (2.2.4) and (2.2.5) must be used. In Figure 2.2 the liquid layer is layer 2 and is between two identical windows which are termed layer 1. From equations (2.2.4) and (2.2.5), the resulting equations, taking account of this symmetry and renumbering of indices, are

$$T_b = \left| \frac{t_{12}t_{21}}{1 - r_{21}^2 e^{i\delta}} \right|^2 \tag{2.2.8}$$

$$R_b = \left| r_{12} + \frac{t_{12}t_{21}r_{21}e^{i\delta}}{1 - r_{21}^2 e^{i\delta}} \right|^2 \tag{2.2.9}$$

From equations (2.1.1) and (2.1.2), it can be shown that $r_{21} = -r_{12}$ and $r_{12}^2 + t_{12}t_{21} = 1$. Equations (2.2.8) and (2.2.9) can then be simplified to give

$$T_b = \left| \frac{t_{12}t_{21}}{1 - r_{12}^2 e^{i\delta}} \right|^2 \tag{2.2.10}$$

$$R_b = \left| \frac{r_{12}(1 - e^{i\delta})}{1 - r_{12}^2 e^{i\delta}} \right|^2 \qquad (2.2.11)$$

It is emphasized that this is the total transmittance or reflectance of the liquid layer between two semi-infinite cell windows. For a transmission cell the windows are finite and are assumed to be surrounded by semi-infinite media with refractive index n_0. This case is discussed in the next section.

2.2.3 Transmittance and Reflectance of the Complete Cell

The cell is shown schematically in Figure 2.2. a and c designate the interfaces between the surroundings and the cell windows. Thus, the reflectance and transmittance of a wave travelling from n_0 to n_1 are designated $R_a = R_{01}$ and $T_a = T_{01}$, respectively. Similarly, the reflectance and transmittance for a wave travelling from n_1 to n_0 is $R_c = R_{10}$ and $T_c = T_{10}$. For the present case, in which the surroundings and the cell windows have a real refractive index, the reflectance and transmittance at interfaces a and c are equal, i.e. $R_a = R_c$ and $T_a = T_c$.

In Figure 2.2, b designates the liquid layer, and the reflectance and transmittance of b are given by equations (2.2.10) and (2.2.11).

T_{ab} is the fraction of the intensity of a ray incident on the first window that is transmitted into the second window. It is obtained by substituting into equation (2.2.6) T_a for T_{01}, R_a for R_{01} and R_{10}, T_b from equation (2.2.10) for T_{12} and R_b from equation (2.2.11) for R_{12}.

$$T_{ab} = T_{ba} = \frac{T_a T_b}{1 - R_a R_b} \qquad (2.2.12)$$

R_{ab} is the fraction of the intensity of a ray incident on the first window that is reflected back to the surrounding due to the first window and the liquid. It is obtained by substituting into equation (2.2.7) T_a for T_{01}, R_a for R_{01} and R_{10}, and R_b from equation (2.2.11) for R_{12}. Because n_0 and n_1 are both real, $T_{01} = 1 - R_{01}$ and the resulting equation can be simplified to give

$$R_{ab} = \frac{R_a + R_b - 2R_a R_b}{1 - R_a R_b} \qquad (2.2.13)$$

R_{ba} is the fraction of the intensity of a ray incident upon the liquid layer from within the first window that is reflected back into the first window due to reflection in the liquid layer and the second window. It is obtained by substituting into equation (2.2.7) R_a for R_{12}, T_b from equation (2.2.10) for T_{01} and R_b from equation (2.2.11) for R_{01} and R_{10}.

$$R_{ba} = R_b + \frac{R_a T_b^2}{1 - R_a R_b} \qquad (2.2.14)$$

Note that $R_{ab} \neq R_{ba}$, if the liquid has a complex refractive index. If the liquid is non absorbing, $R_{ab} = R_{ba}$.

Summing for multiple reflections between the "reduced surface ab" and c one obtains the total reflectance and transmittance of the cell[15, 134] by substituting into equations (2.2.6) and (2.2.7) T_{ba} for T_{01}, R_{ab} for R_{01}, R_{ba} for R_{10}, T_a for T_{12} and R_a for R_{12}.

$$T_{abc} = \frac{I_t}{I_o} = \frac{T_a T_{ba}}{1 - R_a R_{ba}} \qquad (2.2.15)$$

and

$$R_{abc} = \frac{I_r}{I_o} = R_{ab} + \frac{R_a T_{ba}^2}{1 - R_a R_{ba}} \qquad (2.2.16)$$

T_{abc} is the fraction of the intensity incident upon the cell, I_0, that is transmitted by the cell and R_{abc} is the fraction that is reflected by the cell.

2.2.4 Calculation of the Path Length, Transmittance and Reflectance of a Transmission Cell

The phase shift, equation (2.2.1), provides a means to calculate the path length of a transmission cell. The transmission spectrum (and absorbance spectrum) of a transmission cell that is full of a non absorbing substance of refractive index n and has surfaces of the windows flat and parallel shows an interference fringe pattern. If two maxima (or minima) are at $\tilde{\nu}_1$ and $\tilde{\nu}_2$ then the phase shifts must be such that

$$\delta_1 = \delta_2 + 2\pi m \qquad (2.2.17)$$

where m is the number of maxima (or minima) from $\tilde{\nu}_1$ to $\tilde{\nu}_2$. Therefore

$$4\pi\tilde{\nu}_1 d\hat{n}_2\cos\theta_2 = 4\pi\tilde{\nu}_2 d\hat{n}_2\cos\theta_2 + 2\pi m$$

$$\Delta\tilde{\nu} = (\tilde{\nu}_1 - \tilde{\nu}_2) = \frac{m}{2d\hat{n}_2\cos\theta_2} \qquad (2.2.18)$$

At normal incidence this gives

$$d = \frac{m}{2\hat{n}_2\Delta\tilde{\nu}} \qquad (2.2.19)$$

For an empty cell $\hat{n}_2$ is real with $n_2 = 1$. A modified version, RNJ22A[135], of the program NRC program XXII written by Jones and co-workers[16] was used to calculate the path lengths of the cells used in this work from the transmission spectrum of the empty cell through equation (2.2.19).

It was noted above that the removal of reflection losses from the experimental absorbance spectrum of a liquid is necessary before the optical constants of the liquid can be obtained. Equation (2.2.15) provides a means to calculate the amount of light that is transmitted through the cell taking account of all reflection effects from within the cell. The only complication is that the reflectance calculated by equation (2.2.15) depends on the optical constants of the liquid which are not known initially. In order to use equation (2.2.15) an initial estimate of the optical constants of the liquid is needed and the optical constants of the liquid are refined by an iterative procedure.

Both the real and imaginary refractive index spectra of the liquid are needed to calculate the reflectance and transmittance of the cell, as outlined above. From the absorbance spectrum of the liquid only the imaginary refractive index spectrum can be calculated. Therefore it is also necessary to determine the real refractive index spectrum. The real and imaginary refractive index are not independent of each other. The connection between them is the Kramers-Kronig transformation. This transformation is discussed in the next section. The iterative procedure to calculate the optical constants of a liquid from an experimental absorbance spectrum of the liquid is discussed in Section 2.4.

2.3 The Kramers-Kronig Transformation

The real and imaginary components of the complex refractive index are not independent. They are related by the Hilbert and Kramers-Kronig (KK) transforms. This has the implication that once the complete spectrum of one of the components of the refractive index is known the other can be calculated from it.

It is shown in Appendix I that the Cauchy-Goursat integral theorem[136, 137] implies that the Hilbert transform relates the real and imaginary components of an analytic[136, 137] complex function that tends to a constant as the independent variable tends to infinity.

Toll[138] showed that the complex refractive index is analytic. Therefore, since the real refractive index tends to 1 and the imaginary refractive index tends to 0 as $\tilde{\nu}$ tends to ∞[139], the Hilbert transforms, equations (AI.3) and (AI.4), can be used to relate the real and imaginary components by

$$n(\tilde{\nu}_i) - 1 = \frac{1}{\pi} \mathrm{P} \int_{-\infty}^{\infty} \frac{k(\tilde{\nu})}{\tilde{\nu} - \tilde{\nu}_i} \mathrm{d}\tilde{\nu} \tag{2.3.1}$$

$$k(\tilde{\nu}_i) = \frac{-1}{\pi} \mathrm{P} \int_{-\infty}^{\infty} \frac{n(\tilde{\nu})}{\tilde{\nu} - \tilde{\nu}_i} \mathrm{d}\tilde{\nu} \tag{2.3.2}$$

It can also be shown[140] that $\hat{n}(\tilde{\nu}) = \hat{n}^*(-\tilde{\nu})$ which means that the KK transforms, equations (AI.5) and (AI.6), can also be used to the relate the real and imaginary refractive index.

$$n(\tilde{\nu}_i) - 1 = \frac{2}{\pi} \mathrm{P} \int_{0}^{\infty} \frac{\tilde{\nu} k(\tilde{\nu})}{\tilde{\nu}^2 - \tilde{\nu}_i^2} \mathrm{d}\tilde{\nu} \tag{2.3.3}$$

$$k(\tilde{\nu}_i) = \frac{-2\tilde{\nu}_i}{\pi} \mathrm{P} \int_{0}^{\infty} \frac{n(\tilde{\nu})}{\tilde{\nu}^2 - \tilde{\nu}_i^2} \mathrm{d}\tilde{\nu} \tag{2.3.4}$$

The Hilbert and KK transforms can also be applied to the complex dielectric constant in a completely analogous way. In this thesis only the KK transform from the imaginary refractive index to the real refractive index is used.

2.3.1 The Finite KK Transform

Equations (2.3.3) and (2.3.4) require that the integration be over the complete wavenumber range from 0 to ∞. To calculate $n(\tilde{\nu})$ thus requires knowledge of the $k(\tilde{\nu})$ spectrum at all wavenumbers. In practice the $k(\tilde{\nu})$ spectrum is only known over a limited range, say from $\tilde{\nu}_{\text{low}}$ to $\tilde{\nu}_{\text{high}}$. Therefore equation (2.3.3) must be broken into three integrals.

$$\begin{aligned} n(\tilde{\nu}_i) - 1 = {} & \frac{2}{\pi} \int_0^{\tilde{\nu}_{\text{low}}} \frac{\tilde{\nu} k(\tilde{\nu})}{\tilde{\nu}^2 - \tilde{\nu}_i^2} \mathrm{d}\tilde{\nu} + \frac{2}{\pi} \mathrm{P} \int_{\tilde{\nu}_{\text{low}}}^{\tilde{\nu}_{\text{high}}} \frac{\tilde{\nu} k(\tilde{\nu})}{\tilde{\nu}^2 - \tilde{\nu}_i^2} \mathrm{d}\tilde{\nu} \\ & + \frac{2}{\pi} \int_{\tilde{\nu}_{\text{high}}}^{\infty} \frac{\tilde{\nu} k(\tilde{\nu})}{\tilde{\nu}^2 - \tilde{\nu}_i^2} \mathrm{d}\tilde{\nu} \end{aligned} \qquad (2.3.5)$$

where it has been assumed that $\tilde{\nu}_i$ is in the range $\tilde{\nu}_{\text{low}}$ to $\tilde{\nu}_{\text{high}}$. In this thesis, $\tilde{\nu}_{\text{low}}$ is a wavenumber below strong infrared absorption and $\tilde{\nu}_{\text{high}}$ is a wavenumber far above strong infrared absorption and far below strong electronic absorption.

The three integrals in equation (2.3.5) must be considered separately. The first integral is the contribution from the region below the infrared and is neglected for benzene on the assumption that all significant absorption is above $\tilde{\nu}_{\text{low}}$. This is frequently not true and serious errors arise in the calculated $n(\tilde{\nu})$ spectrum if there is significant absorption in the region below $\tilde{\nu}_{\text{low}}$. Bertie and Zhang[141] have suggested several methods to improve the accuracy in these cases. For the liquids considered in this thesis, all of the significant absorption is above $\tilde{\nu}_{\text{low}}$.

The second integral in equation (2.3.5) can be integrated numerically since the $k(\tilde{\nu})$ spectrum is known in this region. The algorithm used to perform the numerical integration is presented in Appendix III.

The third integral in equation (2.3.5) is the contribution from the region above $\tilde{\nu}_{\text{high}}$. It is found experimentally that the refractive indices of colorless compounds are real and decline slowly in value with decreasing wavenumber in the visible region of the spectrum. It also is found that the contributions by the strong infrared absorption to the refractive index in the visible and near infrared (~20 000 to 8000 cm^{-1}) are extremely small. This allows the third integral in equation (2.3.5) to be replaced with $n(\tilde{\nu}_{\text{high}})$, where $n(\tilde{\nu}_{\text{high}})$ is calculated from several wavenumbers in the visible as show in section 2.3.2.

Equation (2.3.5) now becomes

$$n(\tilde{\nu}_i) = n(\tilde{\nu}_{\text{high}}) + \frac{2}{\pi}\mathrm{P}\int_{\tilde{\nu}_{\text{low}}}^{\tilde{\nu}_{\text{high}}} \frac{\tilde{\nu}k(\tilde{\nu})}{\tilde{\nu}^2 - \tilde{\nu}_i^2}\,\mathrm{d}\tilde{\nu} \qquad (2.3.6)$$

2.3.2 Method of Calculating $n(\tilde{\nu}_{\text{high}})$

In the visible region of the spectrum, it is found that for transparent substances the refractive index follows the form[54]

$$\varepsilon'(\tilde{\nu}) - 1 = n^2(\tilde{\nu}) - 1 = A + B\tilde{\nu}^2 + C\tilde{\nu}^4 + \ldots$$
$$- \frac{B'}{\tilde{\nu}^2} - \frac{C'}{\tilde{\nu}^4} - \ldots \qquad (2.3.7)$$

Recall, that from the definition of the complex dielectric constant, equations (1.3.24) and (1.3.25), $\varepsilon'(\tilde{\nu}) = n^2(\tilde{\nu})$ for $k(\tilde{\nu}) = 0$.

In this work, this equation was truncated at the $\tilde{\nu}^4$ term since the other terms generally do not have appreciable influence[142].

It is not always stated[54] that equation (2.3.7) is valid for liquids and can be obtained from the KK transform of the imaginary dielectric constant to the real dielectric constant[142]. This transform is completely analogous to equation (2.3.3) but with n replaced by ε' and k replaced by ε''.

$$\begin{aligned}\varepsilon'(\tilde{\nu}_i)-1&=\frac{2}{\pi}\mathrm{P}\int_0^\infty\frac{\tilde{\nu}\varepsilon''(\tilde{\nu})}{\tilde{\nu}^2-\tilde{\nu}_i^2}\mathrm{d}\tilde{\nu}\\&=\frac{2}{\pi}\int_{\tilde{\nu}_i}^\infty\frac{\tilde{\nu}\varepsilon''(\tilde{\nu})}{\tilde{\nu}^2-\tilde{\nu}_i^2}\mathrm{d}\tilde{\nu}+\frac{2}{\pi}\int_0^{\tilde{\nu}_i}\frac{\tilde{\nu}\varepsilon''(\tilde{\nu})}{\tilde{\nu}^2-\tilde{\nu}_i^2}\mathrm{d}\tilde{\nu}\end{aligned}\tag{2.3.8}$$

The integrals in equation (2.3.8) can be expanded using a Taylor expansion to give

$$\begin{aligned}\varepsilon'(\tilde{\nu}_i)-1&=\frac{2}{\pi}\int_{\tilde{\nu}_i}^{\infty}\frac{\varepsilon''(\tilde{\nu})}{\tilde{\nu}}\left[1+\left(\frac{\tilde{\nu}_i}{\tilde{\nu}}\right)^2+\left(\frac{\tilde{\nu}_i}{\tilde{\nu}}\right)^4+\ldots\right]\mathrm{d}\tilde{\nu}\\&\quad+\frac{2}{\pi}\int_0^{\tilde{\nu}_i}\frac{\tilde{\nu}\varepsilon''(\tilde{\nu})}{\tilde{\nu}_i^2}\left[1+\left(\frac{\tilde{\nu}}{\tilde{\nu}_i}\right)^2+\ldots\right]\mathrm{d}\tilde{\nu}\end{aligned}\tag{2.3.9}$$

The integrals over $\tilde{\nu}$ in equation (2.3.9) are simply numbers and can be replaced by constants, such as A, B, etc. to give equation (2.3.7). Note that equation (2.3.7) is as general as the KK transform but that it can only be truncated at the $\tilde{\nu}^4$ term in regions where there is very little absorption and ε' is essentially constant.

2.3.3 The Subtractive KK Transform

When the optical constants are calculated from transmission spectra it is not always possible to choose $\tilde{\nu}_{\mathrm{high}}$ at a wavenumber far above the strong infrared absorption. One method suggested[143] to improve on the KK transformation in such cases is the subtractive KK transform. This can be deduced from equation (2.3.6) in the following way.

Consider equation (2.3.6) at $\tilde{\nu}_r$

$$n(\tilde{\nu}_r) = n(\tilde{\nu}_{\mathrm{high}}) + \frac{2}{\pi} \mathrm{P} \int_{\tilde{\nu}_{\mathrm{low}}}^{\tilde{\nu}_{\mathrm{high}}} \frac{\tilde{\nu} k(\tilde{\nu})}{\tilde{\nu}^2 - \tilde{\nu}_r^2} \mathrm{d}\tilde{\nu} \qquad (2.3.10)$$

Equation (2.3.10) can be rearranged and substituted into equation (2.3.6) to give

$$n(\tilde{\nu}_i) = n(\tilde{\nu}_r) - \frac{2}{\pi} \mathrm{P} \int_{\tilde{\nu}_{\mathrm{low}}}^{\tilde{\nu}_{\mathrm{high}}} \frac{\tilde{\nu} k(\tilde{\nu})}{\tilde{\nu}^2 - \tilde{\nu}_r^2} \mathrm{d}\tilde{\nu} + \frac{2}{\pi} \mathrm{P} \int_{\tilde{\nu}_{\mathrm{low}}}^{\tilde{\nu}_{\mathrm{high}}} \frac{\tilde{\nu} k(\tilde{\nu})}{\tilde{\nu}^2 - \tilde{\nu}_i^2} \mathrm{d}\tilde{\nu} \qquad (2.3.11)$$

This is known as the subtractive KK transform. Note that the first integral need only be evaluated once. Only the second integral depends on $\tilde{\nu}_i$.

In equation (2.3.11), $\tilde{\nu}_r$ is inside the range $\tilde{\nu}_{\mathrm{low}}$ to $\tilde{\nu}_{\mathrm{high}}$, in contrast to equation (2.3.6) in which $\tilde{\nu}_{\mathrm{high}}$ is a wavenumber far above the strong infrared absorption. Equation (2.3.11) is most accurate when $\tilde{\nu}_i$ is close to $\tilde{\nu}_r$ and the probable error increases as $\tilde{\nu}_i$ gets further away from $\tilde{\nu}_r$.

The subtractive KK transform has been used by Jones and co-workers[13, 14, 17, 18] to calculate the optical constants of 13 organic liquids in the infrared. It has also been used by Bachrach and Brown[144] in the analysis of solid films of TlCl and TlBr in the visible, by Ahrenkiel[143, 145] in the analysis of reflection spectra in the visible and by Williams and co-workers[146] to compute the infrared real refractive index of solid ammonia. It is used in the conversion of transmission spectra to optical constant spectra in this thesis.

2.4 R. N. Jones' Procedure for Calculating Optical Constants from Transmission Spectra

This section describes the algorithm developed by R. Norman Jones and his co-workers in the 1970's[12-18, 45, 46] for calculating optical constants from transmission spectra. The algorithm consists of the following steps.

1) The transmittance of the cell, T_{abc}, is calculated from equation (2.2.15), under the approximation that the refractive index of the liquid is real and constant, i.e. assuming that the liquid does not absorb. $-\log_{10}(T_{abc})$ approximates the apparent absorbance by reflection losses in the cell full of liquid. It is subtracted from the experimental absorbance spectrum, *EAS*, to yield an approximate absorbance spectrum, *AS*.

2) The approximate absorbance spectrum is converted to an approximate imaginary refractive index spectrum of the liquid, $k(\tilde{\nu})$, through

$$k(\tilde{\nu}) = \frac{2.303AS(\tilde{\nu})}{4\pi d\tilde{\nu}} \qquad (2.4.1)$$

3) An approximate real refractive index spectrum of the liquid, $n(\tilde{\nu})$, is calculated from the approximate k spectrum by the Kramers-Kronig transform using equation (2.3.6) or (2.3.11).

4) The n and k spectra are used to calculate the transmittance, T_{abc}, spectrum of the cell full of liquid through equation (2.2.15) and thus the experimental absorbance spectrum, EAS_c, through $-\log_{10}(T_{abc})$.

5) The calculated experimental absorbance spectrum is compared with the measured one, EAS_m, and the k spectrum is adjusted by adding to it the correction

$$\Delta k(\tilde{\nu}) = k_{\text{new}}(\tilde{\nu}) - k_{\text{old}}(\tilde{\nu}) = \frac{2.303(EAS_{\text{m}}(\tilde{\nu}) - EAS_{\text{c}}(\tilde{\nu}))}{4\pi d\tilde{\nu}} \qquad (2.4.2)$$

6) A new *n* spectrum is calculated from this new *k* spectrum as in step 3.

7) Steps 4 to 6 are repeated until the magnitude of the correction in step 5 averaged over all spectral points is less than 2 x 10^{-5}.

Jones and co-workers have written a Fortran program, NRC program XLVI[17] based on the above algorithm to calculate the real and imaginary refractive indices from transmission spectra under certain ideal assumptions[15, 17] about the light beam, including the assumption of 0° incidence. NRC program XLVI requires as input a transmission spectrum of a cell full of a liquid, the cell window material, the cell path length and the refractive index of the liquid at a reference wavenumber, $\tilde{\nu}_r$. The refractive indices of 7 common window materials are build into the program so the user need not supply them[17].

2.5 Baseline Correction

The imaginary refractive index spectra obtained from NRC program XLVI are completely corrected for intensity losses due to reflection from and within the cell. However, the imaginary refractive index spectra computed from different experimental absorbance spectra of the same liquid show significant differences from one another in the position of the baseline. In this section a method is developed to remove these baseline variations from the experimental absorbance spectra. The resulting imaginary refractive index spectra are much more reproducible, so this correction was incorporated into the program used for the work of this thesis.

Experimental absorbance spectra of liquid benzene-h_6 and the imaginary refractive index spectra calculated from them are shown in Figures 2.4 and 2.5. These spectra were taken from earlier measurements made in this laboratory[19, 20]. Fifteen experimental absorbance spectra recorded in cells with four different path lengths are included in Figure 2.4. The inconsistencies in the baselines are clear, because the curves cross. In particular, two of the curves of set C obviously have very high baselines.

The NRC program XLVI[17], that transformed the experimental absorbance spectra to the imaginary refractive index spectra, corrects for reflection effects at the inner and outer window surfaces under certain ideal assumptions[15, 17] about the light beam, including the assumption of 0° incidence. All apparent absorbance due to reflection effects under these ideal assumptions should have been eliminated by the transformation of the experimental absorbance spectra to the imaginary refractive index spectra by the program, as should all effects of the different path lengths. Thus the 15 spectra in Figure 2.5 would be superimposed if the experimental absorbance spectra were recorded under the ideal conditions assumed by NRC program XLVI. *Ideal experimental absorbance* spectra are defined as experimental absorbance spectra recorded under the ideal conditions assumed by NRC program XLVI.

The imaginary refractive index spectra in Figure 2.5 show the magnitude of the error. There is a spread at the peak of 4% and a spread at the baseline of 5%, both percentages of the peak k value. The spread at the baseline must result from differences between the real experimental conditions and the ideal ones assumed by the program, i.e. from differences between the experimental absorbance spectra and the ideal experimental absorbance spectra.

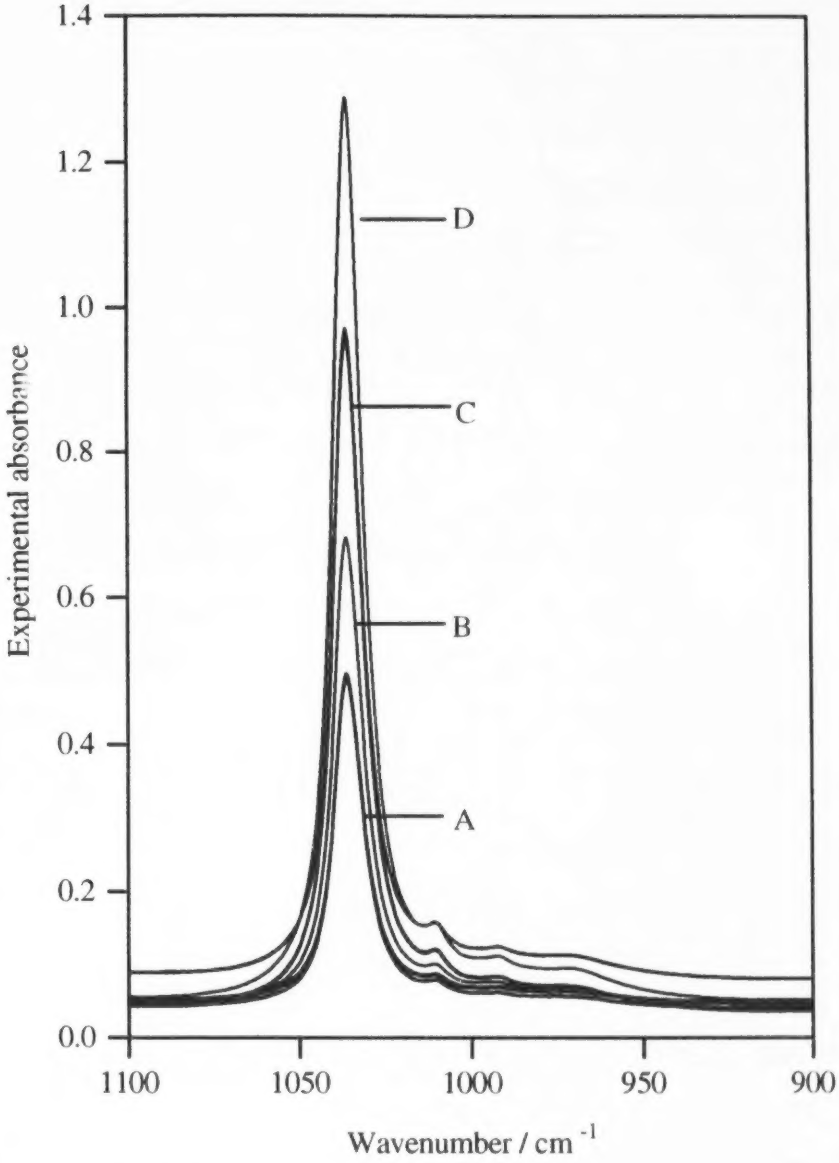

Figure 2.4. Experimental absorbance spectra of liquid benzene-h_6 in cells with KBr or NaCl windows. The number of spectra in each of the 4 groups of spectra labelled A to D and the approximate liquid layer thickness for each group are: Group A, 6 spectra, 11μm; Group B, 1 spectrum, 15μm; Group C, 7 spectra, 23 μm; Group D, 1 spectrum, 33 μm.

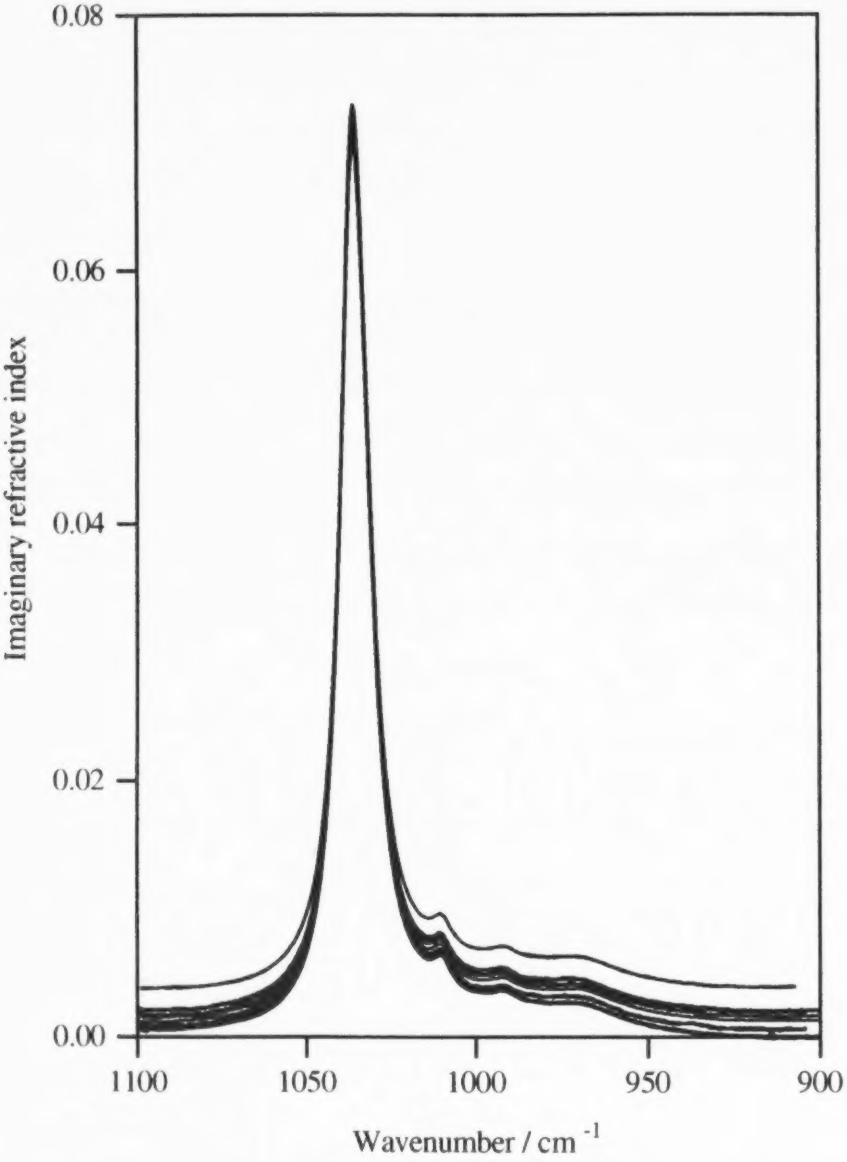

Figure 2.5. Imaginary refractive index spectra of liquid benzene-h$_6$. The 15 imaginary refractive index spectra were calculated from the 15 experimental absorbance spectra in Figure 2.4.

Differences in the baseline can arise from a variety of sources. A gross error occurs if the metal of the window holder blocks part of the beam. But even when, as usual, this is avoided, the angle of incidence of the infrared beam is very important, because marked variations are seen unless the cell is held very firmly in the infrared beam and its position is very reproducible each time it is placed in the beam.

The spectra in Figure 2.4 were measured in liquid cells that were held by a leaf-spring in a massive brass holder which was pinned into holes in the bottom of the sample compartment[19, 20]. This ensured that the position of the cell was very reproducible each time it was inserted, much more reproducible than is provided by the cell holders supplied by most manufacturers. This improved the reproducibility of the spectra immensely, but the baseline variations evident in Figures 2.4 and 2.5 resulted in spite of this. It was speculated[19] that they may arise from differences in the exact position of the infrared beam in the sample compartment each time the interferometer module is aligned which cause small differences in the angle of incidence.

Whatever be the source of the baseline variations, the correct position of the baseline in the ideal experimental absorbance spectrum can be calculated accurately. Thus the spurious, or non-ideal, apparent absorbance which contributes to the experimental baseline can be removed from the experimental absorbance spectrum with good accuracy by moving the baseline to where it ideally should be. The relations between the absorbance, the ideal experimental absorbance and the experimental absorbance are illustrated schematically in Figure 2.6.

The ideal experimental absorbance is simply the sum of the ideal apparent absorbance due to reflection and the absorbance of the sample. The ideal apparent absorbance due to reflection is the apparent absorbance due to reflection under the ideal conditions of NRC program XLVI. It can be calculated from Fresnel's equations, as described above. The programming of NRC XLVI was used.

The absorbance of the sample in a cell of known path length can be calculated for the baseline regions if the very small linear absorption coefficient, $K(\tilde{\nu})$, of the sample is known for these regions. The linear absorption coefficient can be found from measurements using long path length cells. In the resulting spectra, the absorbance of the sample in the baseline regions is sufficiently strong that the apparent absorbance due to non-ideal effects can be neglected.

The ideal experimental absorbances at wavenumbers in the wings of the band are thus calculated as the sum of the absorbance of the sample, determined from $K(\tilde{\nu})$ and the path length, and the ideal apparent absorbance due to reflection, calculated from Fresnel's equations and the refractive index. This is usually done at one wavenumber to each side of the band groups. The wavenumbers at which it is done are called anchor points.

The differences between the experimental absorbance and the ideal experimental absorbance at the anchor points are the desired corrections to the baseline at these two wavenumbers. The correction to the baseline at other wavenumbers is obtained as a straight line through these two points, yielding a linear correction spectrum.

The correction spectrum is subtracted from the experimental absorbance spectrum to yield the ideal experimental absorbance spectrum. The ideal experimental absorbance spectrum is then converted to the imaginary refractive index spectrum via NRC program XLVI.

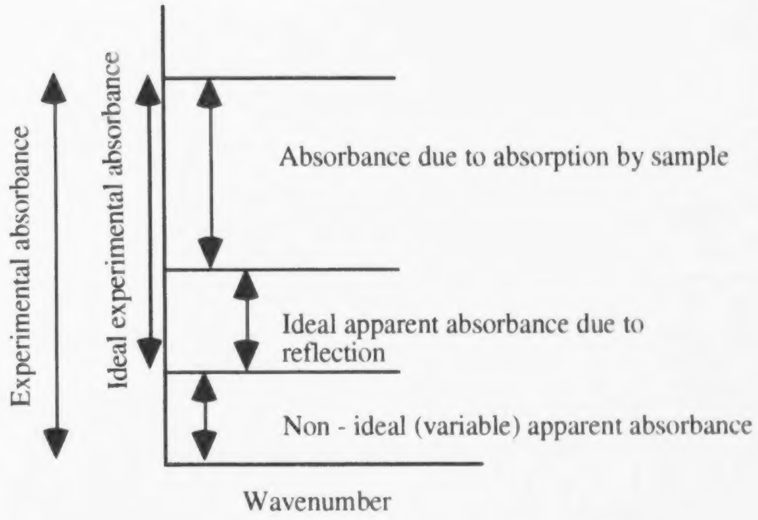
Experimental absorbance
Ideal experimental absorbance
Absorbance due to absorption by sample
Ideal apparent absorbance due to reflection
Non - ideal (variable) apparent absorbance
Wavenumber

Figure 2.6. Schematic of absorbance, ideal experimental absorbance and experimental absorbance.

2.5.1 The Detailed Solution

2.5.1a Calculation of The Ideal Apparent Absorbance

The ideal apparent absorbance is the absorbance due to reflection effects in a transmission cell full of liquid under the ideal assumptions described by Jones and colleagues[15] in equation 26 of their paper. These assumptions are normal incidence for the central ray, optically flat windows, and uniform intensity distribution across the beam.

It is noteworthy, in passing, that the intensity distribution across the beam is not an important factor. This is shown by using program XLVI to calculate the optical constants for different values of the half-cone angle of the convergent light in the focused beam. The calculated results are the same to better than 0.1% for half-angles of 0° and the 5.5°, of the Bruker 113V spectrometer. This could not be so if the spatial intensity distribution across the beam was important. A value of 5.5° was used for all the spectra processed in this work.

The Fortran programming to calculate the ideal apparent absorbance is provided as part of NRC program XLVI, and was copied into a program BASELINE. The programs use equations (2.2.10) to (2.2.15) along with the wavenumber-dependent real refractive index of the window material. They assume that the windows are sufficiently thick that interference fringes from within the windows are too closely spaced to be resolved, so that the effect of multiple reflection can be calculated by neglecting the phases of the multiple reflected rays in each window[15] as was developed in section 2.2.

The programs correctly calculate the interference fringes caused by multiple reflection within the thin liquid layer. For calculation of the baseline, absorption by the liquid was ignored, by assuming the imaginary refractive indices to be zero at all wavenumbers, and the real refractive index of the liquid was assumed constant at its value at the high wavenumber limit of the band. For the 1036 cm^{-1} band of benzene-h$_6$, the value at 1100 cm^{-1} was used, namely $n = 1.475$.

Figure 2.7 shows the spectral baselines, i.e. the ideal apparent absorbance spectra, calculated by program BASELINE for a nonabsorbing liquid with $n = 1.475$, as for benzene-h$_6$, in cells fitted with KBr windows or with NaCl windows. The refractive index discontinuity at the window-benzene-h$_6$ interface is so small that the amplitude of the interference fringes is small. It is clear that the baseline one would obtain by neglecting the fringes decreases in apparent absorbance from 1100 to 900 cm^{-1}. This is because the refractive indices of KBr[147, 148] and NaCl[149, 150] are larger at 1100 cm^{-1} than at 900 cm^{-1}, as is shown in Table 2.1. Table 2.1 also contains the numerical ideal apparent absorbance at 1100 and 900 cm^{-1} for the KBr and NaCl windows and cells 11, 23 and 33 mm thick.

Alternatively this information can be obtained, with slightly lower accuracy, without invoking program BASELINE. To an accuracy of better than 0.0005 the ideal apparent absorbances calculated at 1100 and 900 cm^{-1} equal those expected from a single window in air. Equation (2.2.6) gives the transmittance of a single thick plate with the interference fringes neglected. For the case consider here $\hat{n}_0 = \hat{n}_2 = 1$, $n_1 = n$, and $\theta_0 = \theta_1 = \theta_2 = 0$ and equation (2.2.6) becomes

$$T = \frac{T_{10}T_{01}}{1 - R_{01}R_{10}} \qquad (2.5.1)$$

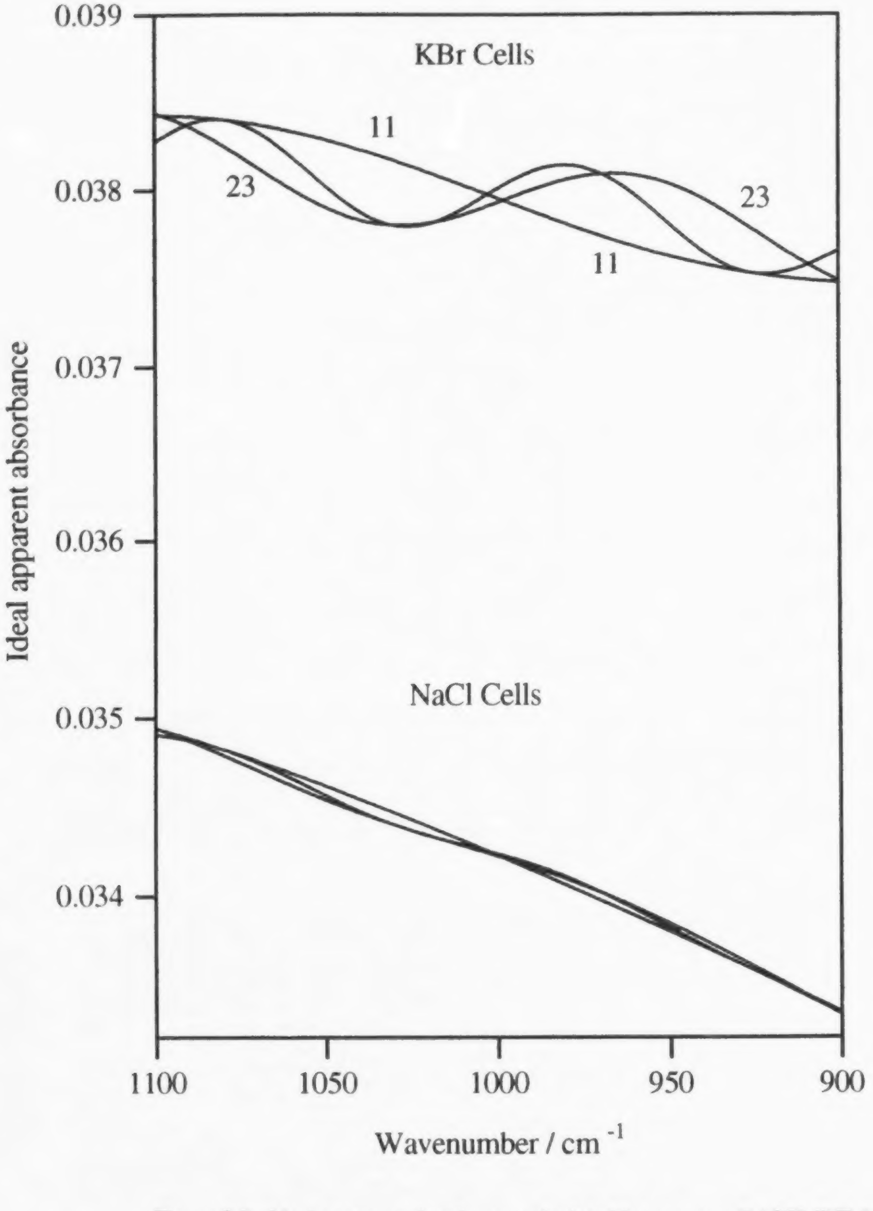

Figure 2.7. Ideal apparent absorbance calculated by program BASELINE for cells full of benzene-h_6. The window materials are shown and the path lengths 11, 23, and 33 μm were used for each window material.

Table 2.1. Ideal apparent absorbance for KBr and NaCl windows.

	Wavenumber / cm^{-1}			
	KBr Windows		NaCl Windows	
Path length / μm	1100	900	1100	900
	Refractive index of windows			
	1.5282	1.5239	1.5006	1.4870
	Ideal apparent absorbance			
(a) From Baseline				
11	0.0384	0.0375	0.0349	0.0333
23	0.0384	0.0375	0.0349	0.0333
33	0.0383	0.0377	0.0349	0.0333
(b) From equation (2.5.4)				
Any path length	0.0379	0.0374	0.0348	0.0333

From equations (2.1.1) to (2.1.6), it is easy to show that

$$R_{01} = R_{10} = \left(\frac{n_1 - n_0}{n_1 + n_0}\right)^2 = \left(\frac{n-1}{n+1}\right)^2 \qquad (2.5.2)$$

$$T_{01} = T_{10} = \frac{4n_0 n_1}{(n_1 + n_0)^2} = \frac{4n}{(n+1)^2} \qquad (2.5.3)$$

Substitution of equations (2.5.2) and (2.5.3) into equation (2.5.1) gives

$$T = \frac{2n_0 n_1}{n_1^2 + n_0^2} = \frac{2n}{n^2 + 1} \qquad (2.5.4)$$

The ideal apparent absorbance due to these reflection losses is $-\log_{10}(T)$.

The ideal apparent absorbances calculated from equation (2.5.4) are independent of the cell thickness. They are shown at the bottom of Table 2.1. The agreement between them and the more accurate values given by program BASELINE ranges from 0.0000 to 0.0005. In the remainder of this thesis, the ideal apparent absorbance was always calculated using program BASELINE.

2.5.1b The Linear Absorption Coefficient of the Liquid in the Wings of the Band

The absorbance of the liquid in the wings of a band is found from spectra of a liquid layer that is sufficiently thick to absorb so strongly that neglect of possible baseline inconsistencies has an acceptably small effect.

Figure 2.8 shows experimental absorbance spectra of benzene-h_6 in nominally 500 μm thick KBr cells. The second spectrum from the top, for example, was recorded in a 506.7 μm cell and shows experimental absorbances at 1095.8 and 912.2

cm^{-1} of 0.3430 and 0.3215. From program BASELINE, the ideal apparent absorbances are 0.0383 and 0.0376 at 1095.8 and 912.2 cm^{-1}. With the neglect of possible baseline inconsistencies, the difference between these two quantities at each wavenumber gives the absorbances of benzene-h_6 as 0.3047 and 0.2839, and the absorbances per unit path, i.e. the linear absorption coefficients, as 6.01 cm^{-1} and 5.60 cm^{-1}. In fact the average of 11 such spectra in 500 and 780 μm cells gave the linear absorption coefficients at 1095.8 and 912.2 cm^{-1} equal to 6.01 cm^{-1} and 5.57 cm^{-1} with 95% confidence limits of 0.09 cm^{-1}. Typically, the linear absorption coefficients at the anchor points can be determined with 95% confidence limits of about 1.5% below 4000 cm^{-1} and about 15% above 4000 cm^{-1}.

2.5.1c Ideal Experimental Absorbance, Absorbance, and Imaginary Refractive Index Spectra.

Table 2.2 summarizes the calculation of the ideal experimental absorbances at 1095.8 and 912.2 cm^{-1} of a KBr cell full of 23 μm thickness of liquid benzene-h_6. The absorbance at 1095.8 cm^{-1} of a benzene-h_6 layer 23.0 μm thick is $(6.01 \pm 0.09) \times 10^{-4}\ \mu m^{-1} \times 23.0 \mu m = 0.0138 \pm 0.0002$. The ideal apparent absorbance at 1095.8 cm^{-1} of a KBr cell filled with 23 μm thickness of benzene-h_6 is 0.0384 ± 0.0001 from program BASELINE. The ideal experimental absorbance at 1095.8 cm^{-1} of this cell is the sum of these two numbers, 0.0522 ± 0.0003. At 912.2 cm^{-1}, the corresponding numbers are $(5.57 \pm 0.09) \times 10^{-4}\ \mu m^{-1} \times 23.0\ \mu m = 0.0128 \pm 0.0002$, 0.0376 ± 0.0001 from BASELINE, and 0.0504 ± 0.0003.

Thus, the ideal experimental absorbance at the extreme of the band can be calculated with a precision of about 0.6%.

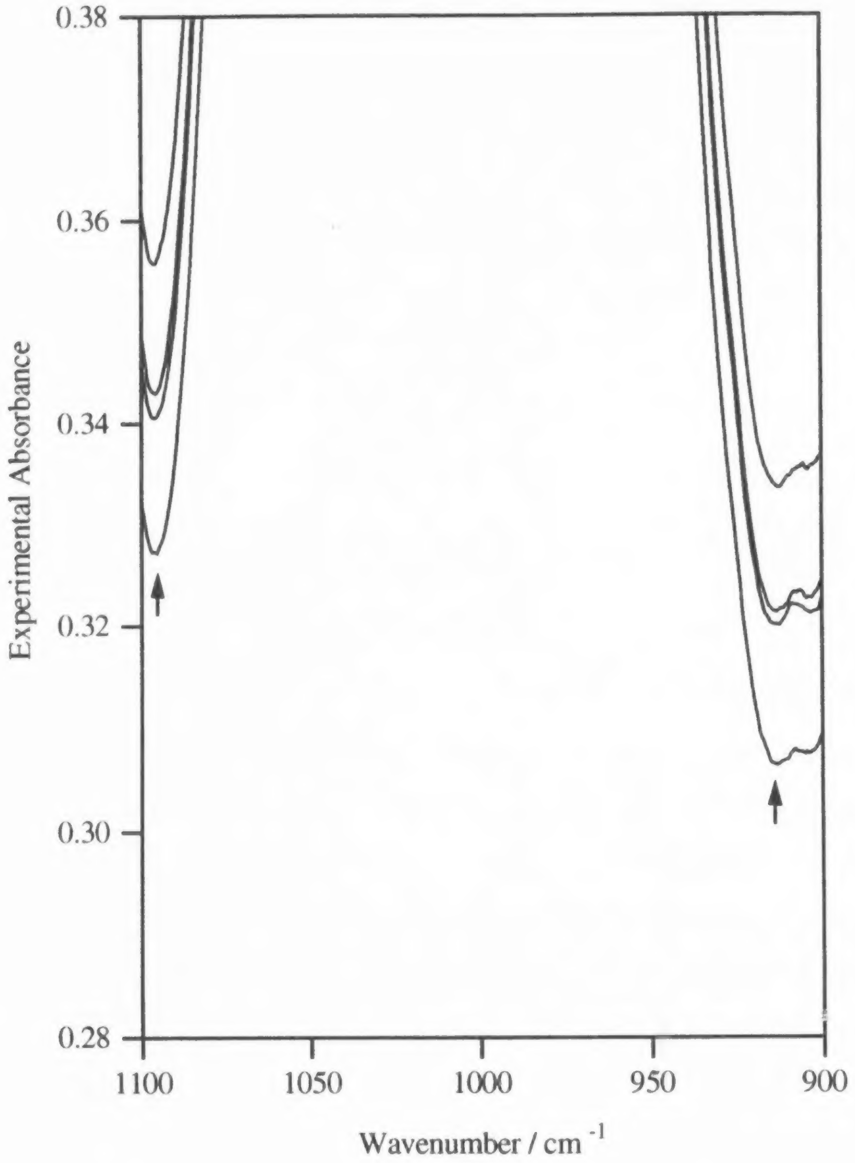

Figure 2.8. Experimental absorbance spectra of liquid benzene-h_6 in KBr and NaCl cells. Path lengths from top to bottom : 527.9 (KBr), 506.7 (KBr), 506.9 (NaCl) and 480.1 (KBr) μm, all ± 1 to 2 μm. The arrows are located at 1095.8 and 912.2 cm^{-1}.

The differences between these ideal experimental absorbances and the experimental absorbances must be removed before NRC program XLVI is used.

To correct the experimental absorbance spectra to ideal experimental absorbance spectra, a straight line was interpolated between the differences found at 1095.8 and 912.2 cm^{-1} and was subtracted from the experimental absorbance spectrum. Program BASECORR performed this correction. The fifteen ideal experimental absorbance spectra which resulted from application of this procedure to the fifteen experimental absorbance spectra of Figure 2.4 are shown in Figure 2.9. Comparison with Figure 2.4 shows that the baseline are much more consistent, in particular the curves no longer cross.

The ideal experimental absorbance spectra were processed to convert them to refractive index spectra, as outlined in section 2.4. The imaginary refractive index spectra which resulted for the 15 ideal experimental absorbance spectra of Figure 2.9 are shown in Figure 2.10. They should be compared with those in Figure 2.5 to see the marked improvement provided by this correction procedure. The spread of values at the peak is 2.5% of the peak value in Figure 2.10 and 4% of the peak value in Figure 2.5. At the edges of the band, the spread of values is 0.01% of the peak value in Figure 2.11 and 5% in Figure 2.5.

Once the imaginary refractive index spectrum is obtained, the absorbance spectrum can be calculated from it through

$$AS(\tilde{v}) = \frac{2\pi d\, \tilde{v}\, k(\tilde{v})}{2.303} \qquad (2.5.5)$$

Table 2.2. Calculation of ideal experimental absorbance for liquid benzene-h_6 in a 23 μm KBr cell at 1095.8 and 912.2 cm^{-1}.

Quantity	1095.8 cm^{-1}	912.2 cm^{-1}
Linear absorption coefficient[a]	$(6.01 \pm 0.09) \times 10^{-4}$	$(5.57 \pm 0.09) \times 10^{-4}$
Absorbance[b]	0.0138±0.0002	0.0128±0.0002
Ideal apparent absorbance[c]	0.0384±0.0001	0.0376±0.0001
Ideal experimental absorbance[d]	0.0522±0.0003	0.0504±0.0003

[a] Unit: μm^{-1}

[b] Absorbance = linear absorption coefficient multiplied by the path length.

[c] Calculated by BASELINE.

[d] Ideal experimental absorbance = ideal apparent absorbance + absorbance.

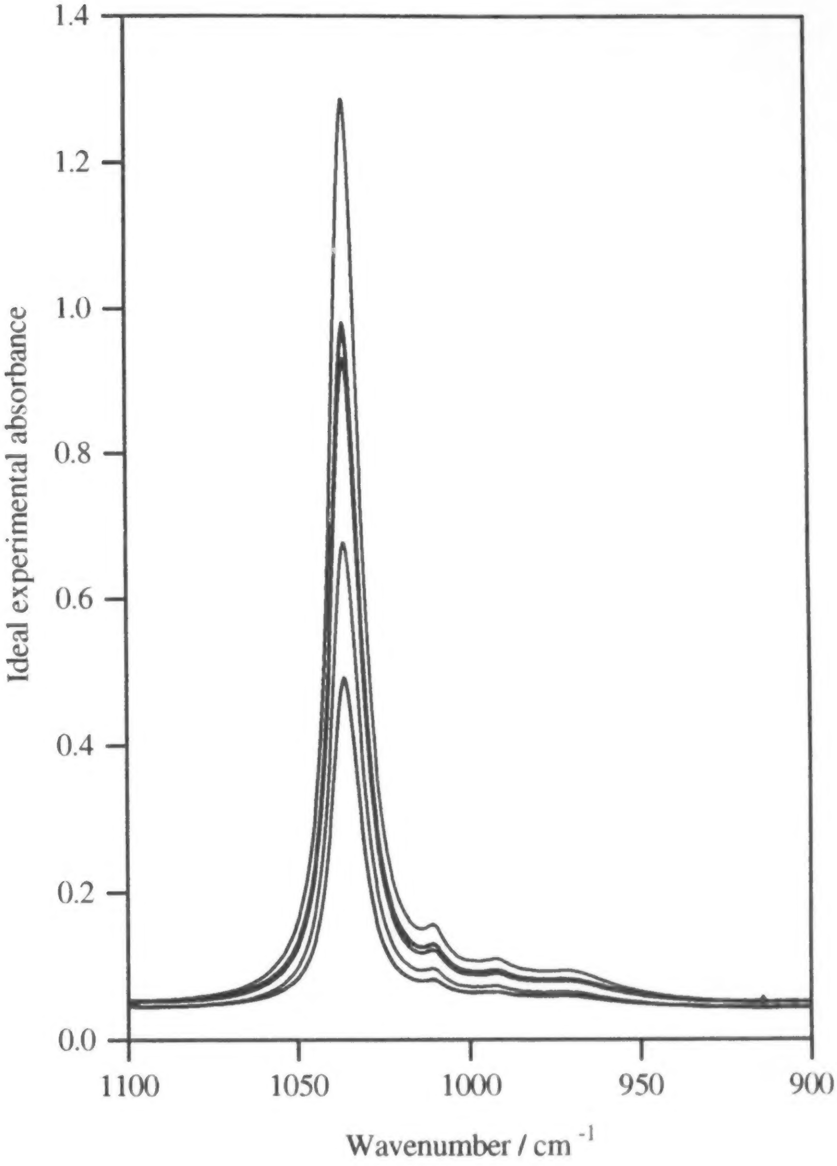

Figure 2.9. Ideal experimental absorbance spectra of liquid benzene-h_6 in KBr and NaCl cells. The 15 ideal experimental absorbance spectra were calculated from the experimental absorbance spectra in Figure 2.4.

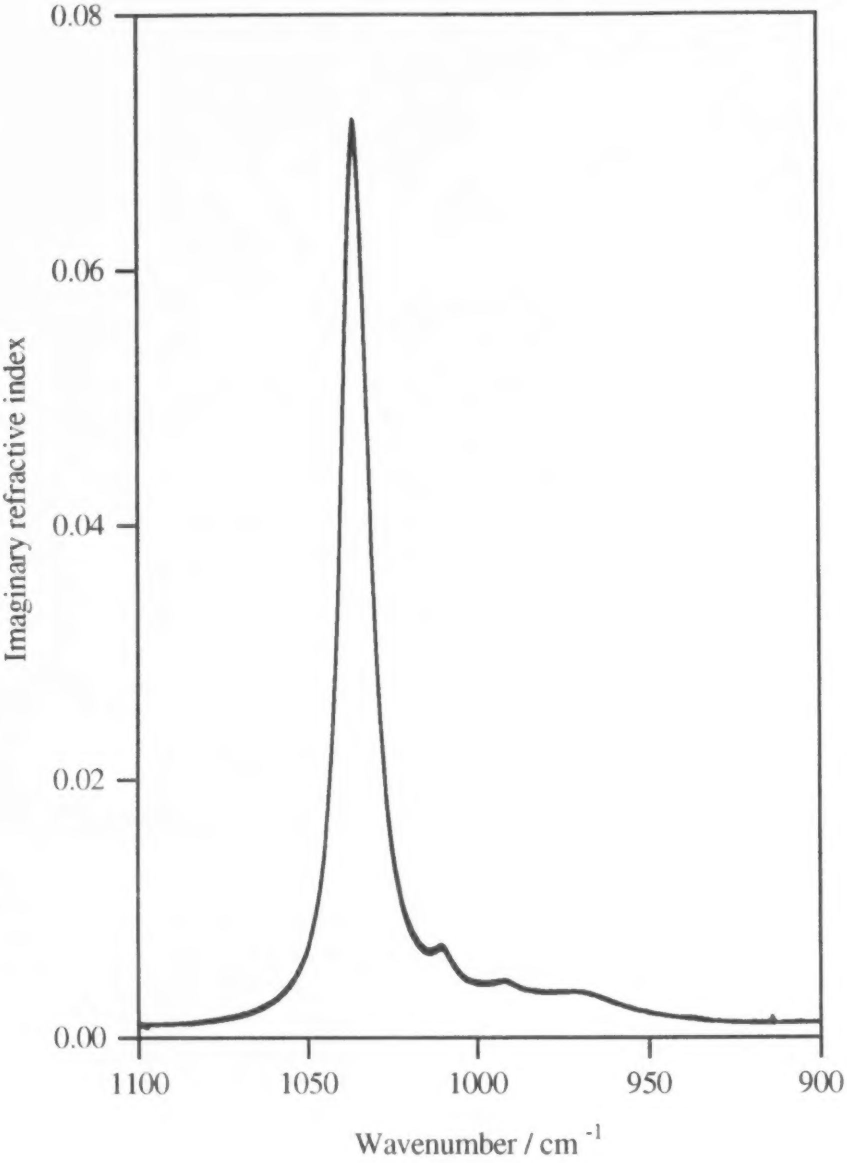

Figure 2.10. Imaginary refractive index spectra of liquid benzene-h_6. The 15 imaginary refractive index spectra of benzene-h_6 calculated from the spectra in Figure 2.9.

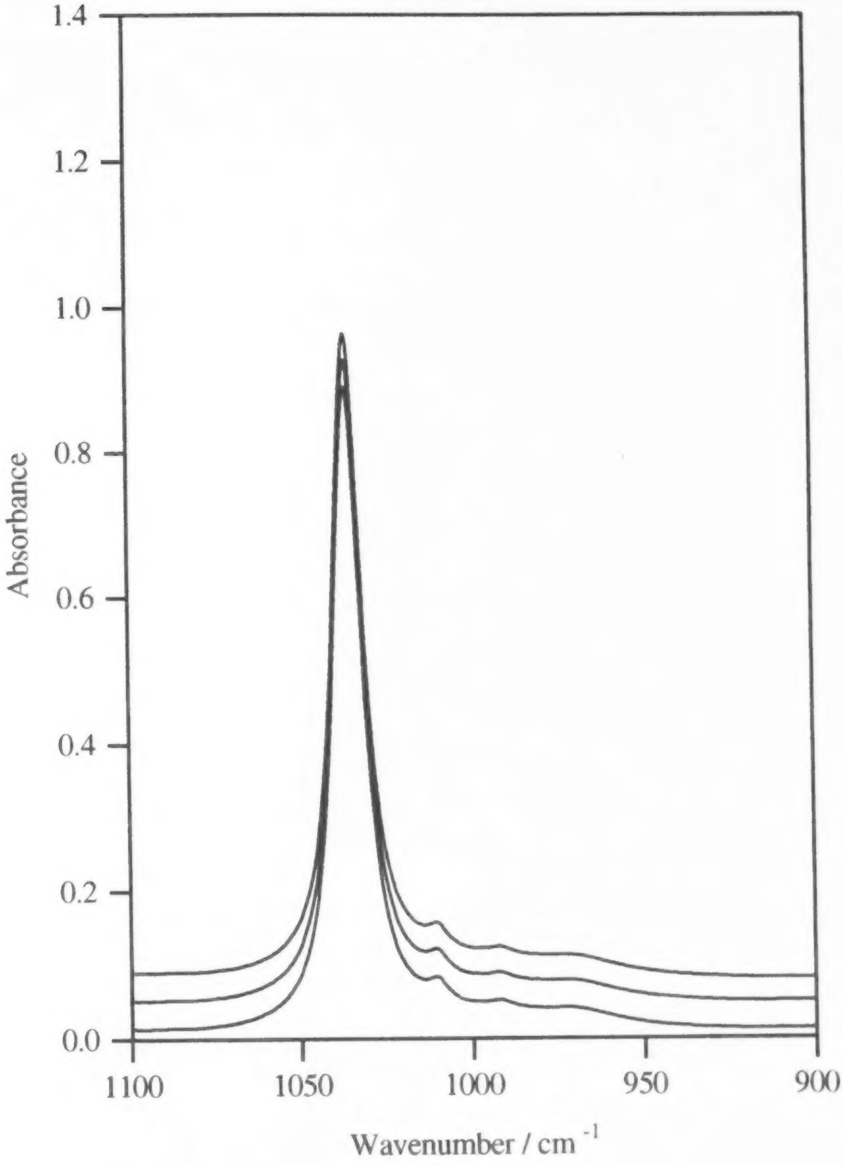

Figure 2.11. Experimental absorbance, ideal experimental absorbance and absorbance spectra of liquid benzene-h_6. From top to bottom, the experimental absorbance spectrum, the ideal experimental absorbance spectrum and the absorbance spectrum of one sample of benzene-h_6.

Figure 2.11 shows for one sample the experimental absorbance spectrum, the ideal experimental absorbance spectrum, and the absorbance spectrum of benzene-h_6, the latter showing only intensity loss due to absorption if the ideal assumptions described above are correct.

2.6 C. D. Keefe's Algorithm for Calculating Optical Constants of Liquids

The algorithm and computer program NRC XLVI developed by Jones[12-18, 45, 46] were modified in this work to incorporate the baseline correction procedure described above. The following programming changes were also made.

NRC program XLVI[17] was written in the mid 1970's and for speed considerations it was written to use integer data and perform integer calculations. The program was modified to read and use floating point experimental absorbance data. The program was modified to read and write files in both SpectraCalc (Galactic Industries Corporation, Salem New Hampshire, USA) .SPC format and ASCII .Y format. The latter consists of an ASCII file in which the first three entries are the starting wavenumber (XSP), ending wavenumber (XEP) and number of points (NP) and the remaining entries are the ordinate values at a constant spacing of DELX where

$$\mathrm{DELX} = \frac{\mathrm{XSP\text{-}XEP}}{\mathrm{NP\text{-}1}} \qquad (2.6.1)$$

NRC program XLVI[17] used complex variables in the algorithm to calculate the ideal experimental absorbance. This algorithm was converted to use real variables instead of complex variables, with a time saving of about 25% for this section of code. For small spectral files (<4000 data points) the calculation of the ideal experimental absorbance takes 40 to 75% of the computation time so using real variables in a savings 10 to 20% reduction in the total computation time. For larger spectral files (~12000 data points) the KK transformation from *k* to *n* takes about 75% of the computation time and using real variables results in only a 4% reduction in the total time.

The original code assumed that $R_{ab} = R_{ba}$, but, as was pointed out in subsection 2.2.3 and noted by Ohta and Ishida[151], this is not correct for an absorbing liquid. This error was corrected although it has a negligible effect on the resulting optical constant spectra for bands of normal intensity.

The KK transform in NRC XLVI[17] was replaced with Bertie and Zhang's[141] KK transform based on the MacLaurin algorithm[152]. The MacLaurin algorithm is given in Appendix III. Bertie and Zhang's KK transform is a factor of 16 faster than that in NRC XLVI.

This modified version of NRC program XLVI[17] was called RNJ46A.

The current algorithm is

1) The transmittance of the cell, T_{abc}, is calculated from equation (2.2.15), under the approximation that the refractive index of the liquid is real and constant, i.e. assuming that the liquid does not absorb. $-\log_{10}(T_{abc})$ is subtracted from the experimental absorbance spectrum, *EAS*, to yield an approximate absorbance spectrum, *AS*.

2) The baselines of the approximate absorbance spectrum and the experimental absorbance spectrum are corrected using the linear absorption

coefficients at two or more anchor points. This anchor point information has to be supplied by the user, if the baseline correction procedure is to be used. The program contains the option not to correct the baseline, but this is discouraged.

3) The corrected approximate absorbance spectrum is converted to an approximate imaginary refractive index spectrum of the liquid, $k(\tilde{\nu})$, through equation (2.4.1).

4) An approximate real refractive index spectrum of the liquid, $n(\tilde{\nu})$, is calculated from the k spectrum by the Kramers-Kronig transform using equation (2.3.6) or (2.3.11).

5) The n and k spectra are used to calculate the transmittance, T_{abc}, spectrum of the cell full of liquid through equation (2.2.15) and thus the experimental absorbance spectrum, EAS_{c}, through $-\log_{10}(T_{\mathrm{abc}})$.

6) The calculated experimental absorbance spectrum is compared with the baseline corrected measured one, EAS_{m}, and the k spectrum is adjusted by adding to it the correction

$$\Delta k(\tilde{\nu}) = k_{\mathrm{new}}(\tilde{\nu}) - k_{\mathrm{old}}(\tilde{\nu}) = \frac{2.303(EAS_{\mathrm{m}}(\tilde{\nu}) - EAS_{\mathrm{c}}(\tilde{\nu}))}{4\pi d\tilde{\nu}} \quad (2.6.1)$$

7) The experimental absorbance spectrum and the new k spectrum are baseline corrected using the linear absorption coefficients at the anchor points. For strong bands, the approximate T_{abc} calculated in Step 1 is not very accurate and the initial baseline correction needs to be adjusted. For weak or medium bands, this correction is negligible.

8) A new n spectrum is calculated from this new k spectrum as in step 4.

9) Steps 5 to 8 are repeated until the magnitude of the correction in step 6 averaged over all spectral points is less than 2 x 10^{-5}.

All of the experimental absorbance spectra measured in this work were converted to real and imaginary refractive index spectra using program RNJ46A.

Chapter 3

Measurement and Accuracy of the Optical Constants of Benzene-h_6 and Benzene-d_6

In this chapter, the experimental measurement of the optical constants of benzene-h_6 and benzene-d_6 is described and the results of the measurements are presented.

Spectroscopists in other laboratories were gracious enough to supply transmission spectra of benzene-h_6 and the empty cells. These spectra were used to study the agreement between the optical constants measured in different laboratories on different instruments. The agreement between the spectra along with the uncertainty in the baseline anchor points is used to estimate the accuracy of the optical constants. This estimated accuracy is assumed for the optical constants of benzene-d_6 and the mixtures of benzene-h_6 and benzene-d_6, since they were measured with the same method. The only difference is that the optical constants for these liquids were determined from transmission spectra measured by the author only.

3.1 Optical Constants of Benzene-h_6

The benzene-h_6 used in this laboratory was of spectroscopic or reagent grade. Samples were purified by fractional freezing one to three times and were checked by gas chromatography. Impurities were determined to be less than 0.05%. Samples were kept over 4A molecular sieve to ensure dryness. Mass spectrometry showed that there was ~6% $^{13}CC_5H_6$ in the benzene-h_6. No other isotopic impurities were detected.

3.1.1 Measurement of Experimental Absorbance Spectra

All of the spectra from this laboratory were measured with a Bruker IFS 113V spectrometer. Triangular apodization was used in the early work from this laboratory[19]. The present work in this laboratory used trapezoidal apodization, specifically a function which increases linearly from 0 to 1 through the central peak of the interferogram and declines linearly from 1 to 0 over the last 20% of the interferogram. A Globar source, 10 mm aperture and a deuterated triglycine sulfate, DTGS, detector were used for all spectra measured in this laboratory. 512 interferograms were recorded and averaged at nominal resolution of 1 cm^{-1} and one level of zero-filling was used in the Fourier transform. The actual resolution was 0.61 cm^{-1} below 4000 cm^{-1}, and was slightly poorer above 4000 cm^{-1} because of the 10 mm aperture. The maximum resolution, $\Delta\tilde{\nu}$, attainable at wavenumber $\tilde{\nu}$ is dependent upon the diameter of the aperture, l, and the focal length of the interferometer, F by[153]

$$\Delta\tilde{\nu} = \frac{\tilde{\nu} l^2}{8F^2} \tag{3.1.1}$$

For the Bruker 113V, the focal length is approximately 24 cm [153], and thus at 4000 cm^{-1}, the maximum resolution for a 10 mm aperture is 0.87 cm^{-1} and at 6500 cm^{-1}, the maximum resolution for a 10 mm aperture is 1.4 cm^{-1}.

To obtain one set of experimental absorbance spectra, FT spectra were recorded consecutively of the empty instrument, the empty cell, the empty instrument, the cell full of liquid, the empty instrument, and the empty cell. These FT spectra measure the intensity (power per unit area) of radiation which reaches the detector; they may be called single-beam spectra[154], following the practice with dispersive instruments, or may be called intensity spectra[155] if care is taken not to confuse this use of 'intensity' with 'absorption intensity'.

The experimental absorbance spectra of the empty cell and of the cell full of liquid were obtained by ratioing the corresponding intensity spectra against the intensity spectra of the empty instrument and taking the negative decadic logarithm of the resulting transmittance spectrum. The experimental absorbance spectrum of the empty cell was used only to determine the path length of the cell. It was found that the path length of the fixed path cells did not change with time, so the experimental absorbance spectrum of the empty fixed path cell was only measured once each day. The above procedure was always followed for variable path cells, in order to check that the path length did not change while the cell was filled, emptied and dried. It never did change.

In this way, experimental absorbance spectra of benzene-h_6 were obtained from fixed path length cells with KBr windows and path lengths between 12 and 1500 µm. To determine the linear absorption coefficients at the anchor points (section 2.5), spectra were also measured in KBr cells with path lengths of 500 and 1500 µm, and in variable path length NaCl and CaF_2 cells with path lengths up to 5 mm.

The path lengths of the cells were determined from the fringe patterns in the experimental absorbance spectra of the empty cells by program RNJ22A, which is NRC program XXII[16] modified to read files in SpectraCalc's ".SPC" format. For the variable path cells, which gave weaker fringe patterns than the cells with fixed path lengths, path lengths greater than 700 µm could not be determined in this way. They were found by calibrating the cell micrometer readings from the fringe patterns for path lengths up to 700 μm, and assuming the constant offset so found held for thicknesses above 700 μm.

In addition to the one hundred experimental absorbance spectra recorded in this work, spectra recorded in 1984 - 5 by V. Behnam and reported previously[19, 20] were also used. Further, four spectroscopists in other laboratories kindly recorded and supplied experimental absorbance spectra of benzene-h_6 under 1 or 2 cm^{-1} nominal resolution using normal conditions and "good analytical laboratory technique". They also supplied the experimental absorbance of the empty cells they used. It is worth noting that the relatively inexpensive polished KBr and NaCl windows supplied commercially are usually sufficiently flat to give the interference fringes needed for path length determination.

Benzene-h_6 used in other laboratories was generally of reagent, spectro- or HPLC grade, and spectra from other laboratories were taken to be acceptable if they showed no unexpected peaks. The spectra from other laboratories were recorded on Digilab, Nicolet, or Perkin-Elmer spectrometers. One spectroscopist used a mercury cadmium telluride detector at 77^{o}K, and the rest used room-temperature DTGS detectors. Either 1 or 2 cm^{-1} resolution was used, with Happ-Genzel apodization[154] in two cases, triangular apodization[154] in one case, and a medium Norton-Beer function[154] in one case.

In this way, spectra were obtained from this and four other laboratories recorded by six different workers on five different models of FT spectrometer by four different manufacturers.

3.1.2 Data Processing

All the spectra recorded in this laboratory were collected on a Bruker 113V FTIR spectrometer. The Aspect 2000 computer of the Bruker 113V communicates with a Dell system 220 80286 PC (IBM-compatible) computer through the parallel port on the PC and the ports for the high-speed-paper-tape punch and reader. A digital direct memory access interface card (model PDMA-16 from the Metrabyte Corporation, Taunton Massachusetts, USA) was fitted to the PC computer to allow it to communicate with the Aspect, and the two computers are linked by a 60' long, 40 conductor cable. The data transfer is controlled by the programs ASTOPC for the Dell and the Aspect computers. A data file of 6000 points transfers in about two seconds. This system was developed for the Aspect 2000 and Aspect 3000 computers in the Chemistry Department at the University of Alberta by R.E.D. McClung and G. Bigam.

The spectra are transferred as Bruker ".DATA" files in the "ATS" data format, and are imported into SpectraCalc as ".SPC" files via a data converter supplied by Galactic Industries Corporation. The programs that were used in this work can read and write the SpectraCalc ".SPC" files. They can also read and write ASCII Y files (section 2.6).

The experimental absorbance spectra from the other laboratories were supplied on PC readable disks and were converted to .SPC files using the data conversion routines supplied with SpectraCalc. All of the experimental absorbance spectra from this and other laboratories were converted to refractive index spectra by the author.

3.1.3 Results

3.1.3a Imaginary Refractive Index from 6225 to 800 cm^{-1}

In order to use the baseline correction procedure described in Chapter 2, the linear absorption coefficients of the liquid must be known at two or more anchor points in the region of the spectrum being studied. Table 3.1 summarizes the wavenumbers of the anchor points, the measured linear absorption coefficients and their 95% confidence limits, and the cell path lengths and approximate real refractive indices used to determine them. Table 3.1 includes the imaginary refractive indices and the 95% confidence limits in the imaginary refractive indices at the anchor points. The linear absorption coefficients at the anchor points were determined from experimental absorbance spectra in cells such that the experimental absorbance was in the range 0.1 to 1.5 for anchor points below 4000 cm^{-1} and in the range 0.03 to 1.5 for anchor points above 4000 cm^{-1}. The experimental absorbance spectra were converted to real and imaginary refractive index spectra by program RNJ46A, using this anchor point information.

Table 3.2 shows the spectral regions that were used in the computations, together with the cell thicknesses used, the value of n_{∞}, and the number of spectra from each spectroscopist, for each region. Each spectrum was only used in those regions in which the bands had peak absorbances between 0.2 and 2.5, which were found to be the absorbance limits of reliable measurement. The real refractive index at the highest wavenumber in each region, n_{∞}, is required by the Kramers-Kronig transform in program RNJ46A. It was read either from the graphs in reference 18 or, in most cases, from tables of $n(\tilde{\nu})$ in this laboratory which were calculated from the $k(\tilde{\nu})$ spectra in reference 19. The spectra recorded by the author are labelled with the

Table 3.1. Linear absorption coefficients at anchor points for liquid benzene-h_6 at 25°C.

Wavenumber / cm^{-1}	Path length / mm	$n(\tilde{\nu})$ [a]	$K(\tilde{\nu})$ / cm^{-1} [b]	$k(\tilde{\nu})$ [b,c]
6215.4	1 - 5	1.482	0.242 (±19)	0.0000071 (±6)
6052.4	1 - 5	1.482	0.736 (±144)	0.0000223 (±44)
5726.1	1 - 5	1.482	0.369 (±24)	0.0000118 (±8)
5559.2	1 - 5	1.482	0.422 (±63)	0.0000139 (±21)
5278.6	1 - 5	1.482	0.193 (±46)	0.0000067 (±16)
5005.8	1 - 5	1.482	0.309 (±44)	0.0000113 (±16)
4768.1	1 - 5	1.482	0.433 (±32)	0.0000166 (±12)
4492.8	1 - 5	1.482	0.625 (±18)	0.0000255 (±7)
4144.2	0.5 - 5	1.481	2.31 (±4)	0.000102 (±18)
3970.7	0.5 - 5	1.481	2.33 (±4)	0.000108 (±18)
3810.1	2 - 4	1.473	0.992 (±7)	0.0000477 (±3)
3559.9	2 - 4	1.473	0.579 (±16)	0.0000298 (±8)
3237.4	2 - 4	1.475	2.030 (±6)	0.0001149 (±3)
2918.7	0.5 - 0.8	1.475	6.19 (±29)	0.000389 (±18)
2699.8	2 - 4	1.473	0.922 (±3)	0.0000626 (±2)
2257.2	2 - 4	1.473	0.822 (±3)	0.0000667 (±2)
2127.1	2 - 4	1.474	0.595 (±2)	0.0000513 (±2)
1864.3	0.5 - 0.8	1.474	4.52 (±7)	0.000444 (±69)
1767.4	0.5 - 0.8	1.475	4.53 (±9)	0.000470 (±93)
1562.5	0.5 - 0.8	1.471	6.27 (±9)	0.000735 (±11)
1422.2	0.5 - 0.8	1.471	5.13 (±7)	0.000661 (±9)
1095.8	0.5 - 0.8	1.475	6.01 (±9)	0.00101 (±2)
912.2	0.5 - 0.8	1.481	5.57 (±9)	0.00112 (±2)
903.0	0.5 - 0.8	1.481	5.60 (±9)	0.00114 (±2)
802.7	0.5 - 0.8	1.481	5.29 (±13)	0.00121 (±3)

[a] Approximate value of $n(\tilde{\nu})$ used to calculated the ideal apparent absorbance when calculating $K(\tilde{\nu})$.

[b] The value in parentheses is the 95% confidence limit in the terminal digit, $\Delta K(\tilde{\nu})$ or $\Delta k(\tilde{\nu})$.

[c] The 95% confidence limit of $k(\tilde{\nu})$, $\Delta k(\tilde{\nu})$, was calculated by $\Delta k(\tilde{\nu}) = \frac{2.303\Delta K(\tilde{\nu})}{4\pi\tilde{\nu}}$.

Table 3.2. Path lengths, high-wavenumber refractive index, and number of spectra from each spectroscopist, for the regions processed.

Region / cm^{-1}	Path length / μm	n_∞ [a]	CDK	A	B	C	VB	D	Total
6225 - 4140	500 - 700	1.482	6	0	0	0	0	0	6
4150 - 3960	50 - 200	1.481	6	3	2	0	5	2	18
3980 - 3800	500 - 2500	1.481	22	1	0	0	4	0	27
3820 - 3525	50 - 500	1.473	2	2	1	0	3	2	10
3565 - 3215	200 - 500	1.473	2	1	1	0	4	0	8
3320 - 2915	10 - 25	1.475	6	1	0	0	12	1	20
2920 - 2250	20 - 500	1.481	2	7	0	0	12	0	21
2260 - 2125	30 - 500	1.473	2	2	2	2	13	0	21
2130 - 1860	10 - 200	1.474	10	6	2	2	15	2	37
1905 - 1720	10 - 125	1.475	10	6	1	1	20	2	40
1775 - 1560	50 - 500	1.479	2	3	1	0	12	1	19
1565 - 1335	10 - 20	1.471	6	1	0	0	11	0	18
1425 - 1090	10 - 500	1.487	6	6	2	2	6	2	24
1100 -905	10 - 60	1.475	4	5	0	2	23	0	34
915 - 800	50 - 500	1.481	2	4	2	2	8	1	19

[a] n_∞ is the real refractive index at the highest wavenumber in the region.

initials CDK. Spectra measured earlier in this laboratory by V. Behnam are labelled with the initials VB. The other spectroscopists who supplied spectra are identified by single letter A to D.

The experimental absorbance spectra in each region were converted to imaginary refractive index, $k(\tilde{\nu})$, spectra by program RNJ46A. The peak height for each band and the areas under the band groups were measured for each $k(\tilde{\nu})$ spectrum. For each spectroscopist the average area and peak height were calculated for each band, with the 95% confidence limits. For each spectroscopist an average $k(\tilde{\nu})$ spectrum was calculated and this has the average areas and peak heights. The average areas and peak heights of the bands obtained by the different spectroscopists are tabulated in Tables 3.3 and 3.4, respectively.

Table 3.4 includes the $k(\tilde{\nu})$ peak wavenumbers which were determined, with the peak heights, by fitting the top three points of the band to a parabola and determining the maximum of the parabola. The accuracy of the digitized wavenumbers was found to be ±0.1 cm^{-1} by calibration against standard gases[156, 157]. Using synthesized spectra, it was found that when spectra are digitized at 0.5 cm^{-1} intervals fitting the top three points of the band to a parabola results in an accuracy of ±0.2 cm^{-1} in the peak wavenumber. Therefore the peak wavenumbers given in Table 3.4 are estimated to be accurate with ±0.2 cm^{-1}.

The areas and peak heights from the different spectroscopists in Tables 3.3 and 3.4 are in excellent agreement. The agreement is not always within the precision of the data of each spectroscopist, suggesting that systematic errors, or inadequate statistics, of the order of 2% may still affect the results in some regions. The quality of the agreement is shown pictorially in Figure 3.1, which shows the average area for

Table 3.3. Spectroscopist average areas under the imaginary refractive index band groups[a].

Region / cm^{-1}	CDK	A	B	C	VB	D
6175.0 - 5814.3	0.0336 (8)					
4763.3 - 4493.3	0.0420 (6)					
4141.4 - 3971.7	0.0919 (15)	0.0912(10)	0.0923 (226)		0.0917 (8)	0.0923 (35)
3973.6 - 3864.6	0.00818 (6)	0.00808			0.00780 (12)	
3810.2 - 3560.4	0.0468	0.0442 (6)	0.0467		0.0449 (7)	0.0459 (25)
3528.6 - 3364.7	0.00993 (6)	0.00977	0.00988		0.00981(16)	
3237.9 - 2918.7	1.583 (14)	1.604			1.613 (8)	1.593
2919.2 - 2791.5	0.0516 (18)	0.0526 (21)			0.0542 (8)	
2724.4 - 2534.0	0.0298 (8)	0.0314 (32)			0.0340 (13)	
2441.4 - 2257.3	0.0549 (1)	0.0564 (11)			0.0557 (8)	
2257.3 - 2127.1	0.0236	0.0233 (13)	0.0237 (57)	0.0234 (25)	0.0236 (2)	
2070.2 - 1903.9	0.247 (1)	0.248 (1)	0.250 (40)	0.247 (5)	0.248 (1)	0.243 (2)
1864.8 - 1767.9	0.354 (2)	0.354 (1)	0.363	0.352	0.356 (1)	0.347 (14)
1768.4 - 1653.2	0.0594 (16)	0.0579 (1)	0.0578		0.0603 (10)	0.0575
1653.2 - 1564.9	0.0844 (4)	0.0828 (13)	0.0843		0.0835 (6)	0.0828
1562.5 - 1422.2	1.581(22)	1.597			1.590 (5)	
1422.2 - 1357.6	0.104 (2)	0.102 (1)	0.103(9)	0.101 (1)	0.101 (1)	0.103 (24)
1357.6 - 1096.3	0.428 (4)	0.420 (4)	0.416 (4)	0.422 (15)	0.416 (7)	0.423 (44)
1096.3 - 912.2	1.351 (24)	1.358 (17)		1.360 (36)	1.357 (7)	(1.321 (32))[b]
903.0 - 802.7	0.239 (3)	0.239 (2)	0.239 (12)	0.237 (6)	0.239 (1)	0.238

[a] The numbers in brackets are the 95% confidence limits in the last digit. In some cases there were too few spectra to yield the 95% confidence limit and in others no spectrum was available from that spectroscopist for that region.

[b] This value was not used in the final averages because the corresponding peak $k(\tilde{\nu})$ value is 10% lower than that of any other spectroscopist.

Table 3.4. Spectroscopist average imaginary refractive index peak heights[a].

$\tilde{\nu}$ / cm^{-1}	CDK	A	B	C	VB	D
5982.1	0.000329 (12)					
5929.5	0.000181 (3)					
5912.1	0.000234 (2)					
4689.6	0.000189 (2)					
4669.2	0.000528 (20)					
4642.4	0.000412 (6)					
4622.5	0.000388 (7)					
4604.2	0.000202 (2)					
4583.3	0.000473 (12)					
4543.7	0.000165 (1)					
4056.8	0.00334 (8)	0.00330 (4)	0.00336 (82)		0.00337 (4)	0.00340 (24)
3956.7	0.000185 (3)	0.000173			0.000174 (2)	
3935.4	0.000257 (4)	0.000249			0.000265 (2)	
3696.0	0.000829 (1)	0.000750 (33)	0.000804		0.000790 (22)	0.000791 (118)
3642.4	0.000955 (20)	0.000882 (62)	0.000911		0.000929 (11)	0.000925 (3)
3611.2	0.000377 (8)	0.000357 (8)	0.000365		0.000364 (3)	0.000373 (18)
3514.7	0.0000487 (11)	0.0000472	0.0000485		0.0000480 (7)	
3487.6	0.0000734 (8)	0.0000688	0.0000702		0.0000721 (7)	
3448.2	0.000167 (4)	0.000161	0.000165		0.000165 (2)	
3091.1	0.0305 (4)	0.0295			0.0307 (1)	0.0292
3071.7	0.0229 (1)	0.0220			0.0233 (1)	0.0211
3036.2	0.0508 (10)	0.0531			0.0543 (9)	0.0571
2906.3	0.000824 (10)	0.000795 (14)			0.000818 (7)	
2887.3	0.00160 (4)	0.00156 (18)			0.00164 (1)	
2852.5	0.000355 (8)	0.000354 (6)			0.000368 (4)	
2818.8	0.000697 (7)	0.000695 (21)			0.000729 (10)	
2653.0	0.000753 (6)	0.000728 (17)			0.000768 (8)	
2614.0	0.000422 (7)	.000412 (15)			0.000434 (8)	
2595.3	0.000818 (27)	0.000781 (15)			0.000826 (8)	
2382.2	0.000553 (10)	0.000552 (6)			0.000560 (6)	
2324.9	0.00231 (1)	0.00225 (1)			0.00229 (2)	

Table 3.4. Continued.

$\tilde{\nu}$ / cm^{-1}	CDK	A	B	C	VB	D
2282.4	0.000167 (6)	0.000165 (4)			0.000161 (4)	
2210.5	0.00142 (1)	0.00138 (1)	0.00141 (36)	0.00139 (35)	0.00142 (1)	
2004.7	0.00105 (1)	0.00104 (1)	0.00105 (16)	0.00104 (1)	0.00106 (1)	0.00098 (4)
1988.0	0.00114 (1)	0.00112 (7)	0.00112 (16)	0.00112 (9)	0.00114 (1)	0.00100 (30)
1960.2	0.0101 (1)	0.0101 (1)	0.0102 (18)	0.0101 (6)	0.0101 (1)	0.0097 (5)
1815.3	0.0156 (1)	0.0156 (1)	0.0160	0.0156	0.0157 (1)	0.0150 (17)
1754.4	0.00142 (5)	0.00137 (2)	0.00136		0.00141 (2)	0.00131
1713.1	0.000542 (26)	0.000510 (5)	0.000505		0.000538 (8)	0.000474
1671.0	0.00130 (3)	0.00127 (1)	0.00126		0.00130 (1)	0.00123
1617.8	0.00184 (4)	0.00179 (3)	0.00181		0.00183 (2)	0.00170
1586.3	0.00138 (2)	0.00136 (3)	0.00136		0.00137 (1)	0.00136
1528.1	0.00723 (4)	0.00729			0.00731 (4)	
1479.0	0.148 (5)	0.160			0.153 (1)	
1393.4	0.00532 (5)	0.00524 (6)	0.00525 (88)	0.00524 (52)	0.00524 (2)	0.00491 (58)
1309.8	0.000879 (41)	0.000892 (17)	0.000867 (43)	0.000894 (19)	0.000869 (43)	0.000894 (108)
1249.2	0.00178 (4)	0.00171 (2)	0.00169 (37)	0.00171 (10)	0.00171 (3)	0.00170 (9)
1176.7	0.00575 (4)	0.00562 (3)	0.00564 (58)	0.00568 (9)	0.00568 (3)	0.00566 (53)
1148.7	0.00349 (3)	0.00344 (1)	0.00346 (20)	0.00348 (4)	0.00344 (4)	0.00343 (6)
1035.9	0.0713 (11)	0.0703 (13)		0.0708 (92)	0.0712 (2)	(0.0643 (244))[b]
849.8	0.00556 (8)	0.00551 (5)	0.00553 (88)	0.00554 (18)	0.00558 (4)	0.00544

---

[a] The numbers in brackets are the 95% confidence limits in the last digit. In some cases there were too few spectra to yield the 95% confidence limit and in others no spectrum was available from that spectroscopist for that region.

[b] This value was not used in the final averages because it is 10% lower than that of any other spectroscopist.

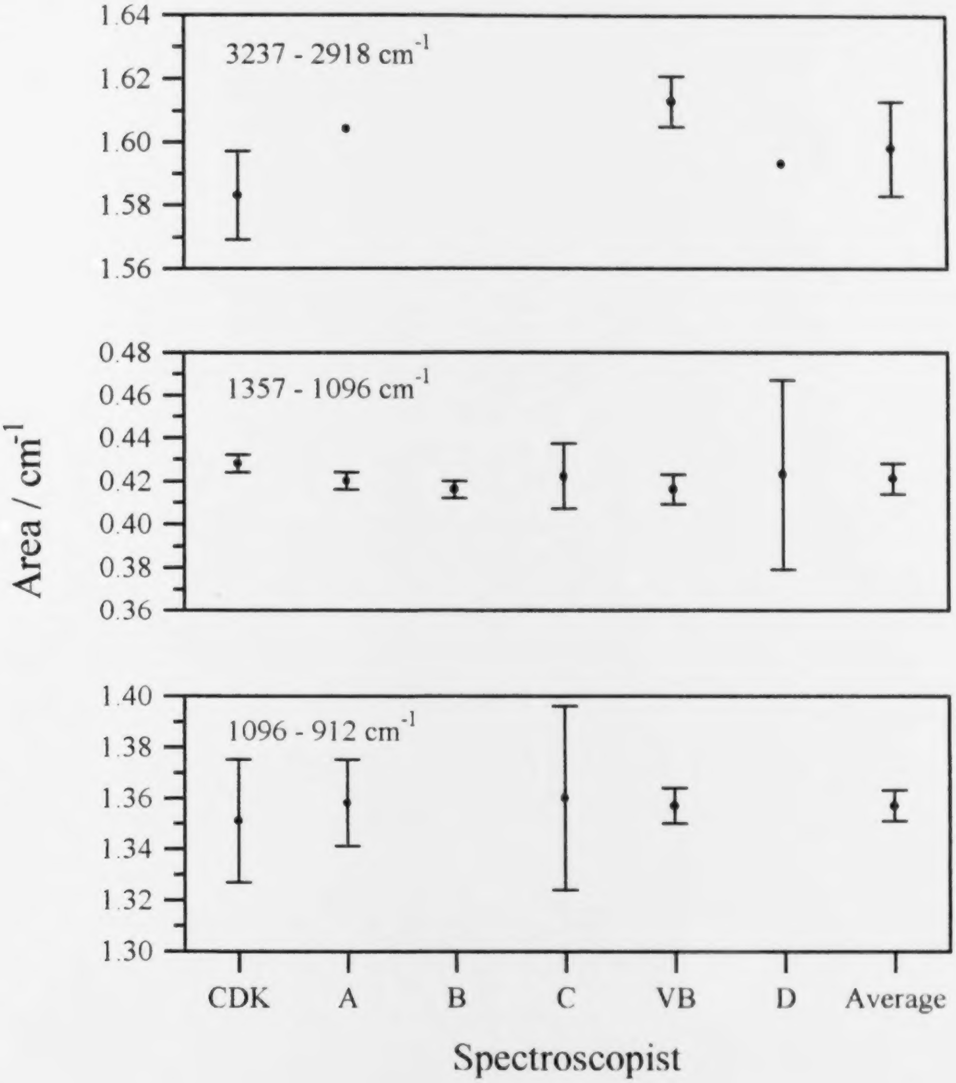

Figure 3.1. Average areas (dots) and 95% confidence limits (vertical error bars) under the imaginary refractive index spectra in the regions 3237 to 2918 cm^{-1} (upper), 1357 to 1096 cm^{-1} (middle) and 1096 to 912 cm^{-1} (bottom) for the six spectroscopists. The values are taken from Table 3.3. Also shown for each region above the label 'Average' is the unweighted average area from Table 3.5 with the maximum deviation from it indicated by a vertical error bar.

each spectroscopist for the regions 3237 to 2918 cm^{-1}, 1357 to 1096 cm^{-1}, and 1096 to 912 cm^{-1}, with the 95% confidence limits of each shown by the error bars.

For each region, the average spectra from the different spectroscopists were themselves averaged to yield a weighted average $k(\tilde{\nu})$ spectrum, with the weighting factor for each spectroscopist being the number of spectra which contributed to that spectroscopist's average. To check the influence of the fact that the two spectroscopists in this laboratory, CDK and VB, both used the same instrument and ran far more spectra than the other collaborators, an unweighted average $k(\tilde{\nu})$ spectrum was also calculated. The overall average area for each region, and the overall average peak heights, were measured from both the weighted and the unweighted average $k(\tilde{\nu})$ spectra.

The overall average areas under the $k(\tilde{\nu})$ band groups are presented in Table 3.5. Because the integration ranges have different widths for different band groups, Table 3.5 includes the height of the strongest peak in the group to give an indication of the prominence of the absorption. The $k(\tilde{\nu})$ spectrum is shown in Figures 3.2 to 3.6 over the integration ranges given in Table 3.5. Table 3.5 also gives for each band group the *maximum deviation of the average of any one spectroscopist from the unweighted average*, which shows the agreement between the different spectroscopists, and the estimated accuracy of the overall unweighted average areas, which is discussed later. Again, a good sense of the quality of these results can be obtained from Figure 3.1, which includes the unweighted average areas for the three regions and their maximum deviations.

Table 3.5. Overall average area under the imaginary refractive index bands.

		Area / cm^{-1}				
Region / cm^{-1}	k_{max}[a]	Weighted Average	Unweighted Average	Maximum Deviation[b]	Anchor point Uncertainty[c]	% Estimated accuracy [d]
6175.0 - 5814.3	0.000329	0.0336	0.0336	± 0.0008	± 0.0004	3.6
4763.3 - 4493.3	0.000528	0.0420	0.0420	± 0.0006	± 0.0003	2.1
4141.4 - 3971.7	0.00335	0.0918	0.0919	± 0.0007	± 0.0002	1.0
3973.6 - 3864.6	0.000257	0.00812	0.00802	±0.00022	± 0.00011	4.1
3810.2 - 3560.4	0.000903	0.0455	0.0457	± 0.0015	± 0.0001	3.5
3528.6 - 3364.7	0.000165	0.00984	0.00985	±0.00008	± 0.00010	1.8
3237.9 - 2918.7	0.0536	1.602	1.598	±0.015	± 0.003	1.1
2919.2 - 2791.5	0.00160	0.0536	0.0530	±0.0014	± 0.0012	4.9
2724.4 - 2534.0	0.000808	0.0327	0.0317	±0.0023	± 0.00004	7.2
2441.4 - 2257.3	0.00228	0.0559	0.0557	±0.0008	± 0.00004	1.5
2257.3 - 2127.1	0.00140	0.0236	0.0235	±0.0002	± 0.00003	1.0
2070.2 - 1903.9	0.0100	0.248	0.247	±0.004	± 0.0006	1.9
1864.8 - 1767.9	0.0155	0.354	0.354	±0.009	± 0.001	2.8
1768.4 - 1653.2	0.00136	0.0596	0.0585	±0.0018	± 0.0012	5.1
1653.2 - 1564.9	0.00178	0.0834	0.0835	±0.0009	± 0.0009	2.2
1562.5 - 1422.2	0.154	1.587	1.589	±0.008	± 0.001	0.6
1422.2 - 1357.6	0.00518	0.102	0.102	±0.002	± 0.0006	2.5
1357.6 - 1096.3	0.00566	0.421	0.421	±0.007	± 0.003	1.9
1096.3 - 912.2	0.0709	1.357	1.357	±0.006	± 0.003	0.7
903.0 - 802.7	0.00552	0.239	0.239	±0.002	± 0.002	1.7

[a] Height of the strongest peak in the region

[b] Maximum deviation from the unweighted average, except for regions 6175.0 - 5814.3, and 4763.3 - 4493.3 cm^{-1}. In these two cases the values listed are the 95% confidence limits of the areas under the average spectra for CDK, the only worker who measured spectra in these regions.

[c] The uncertainty due to the anchor points is the integration range multiplied by the average of the 95% confidence limits of $k(\tilde{\nu})$ (Table 3.1) at the two anchor points used for that range.

[d] The estimated accuracy is taken as the sum of the maximum deviation and the uncertainty due to the anchor points.

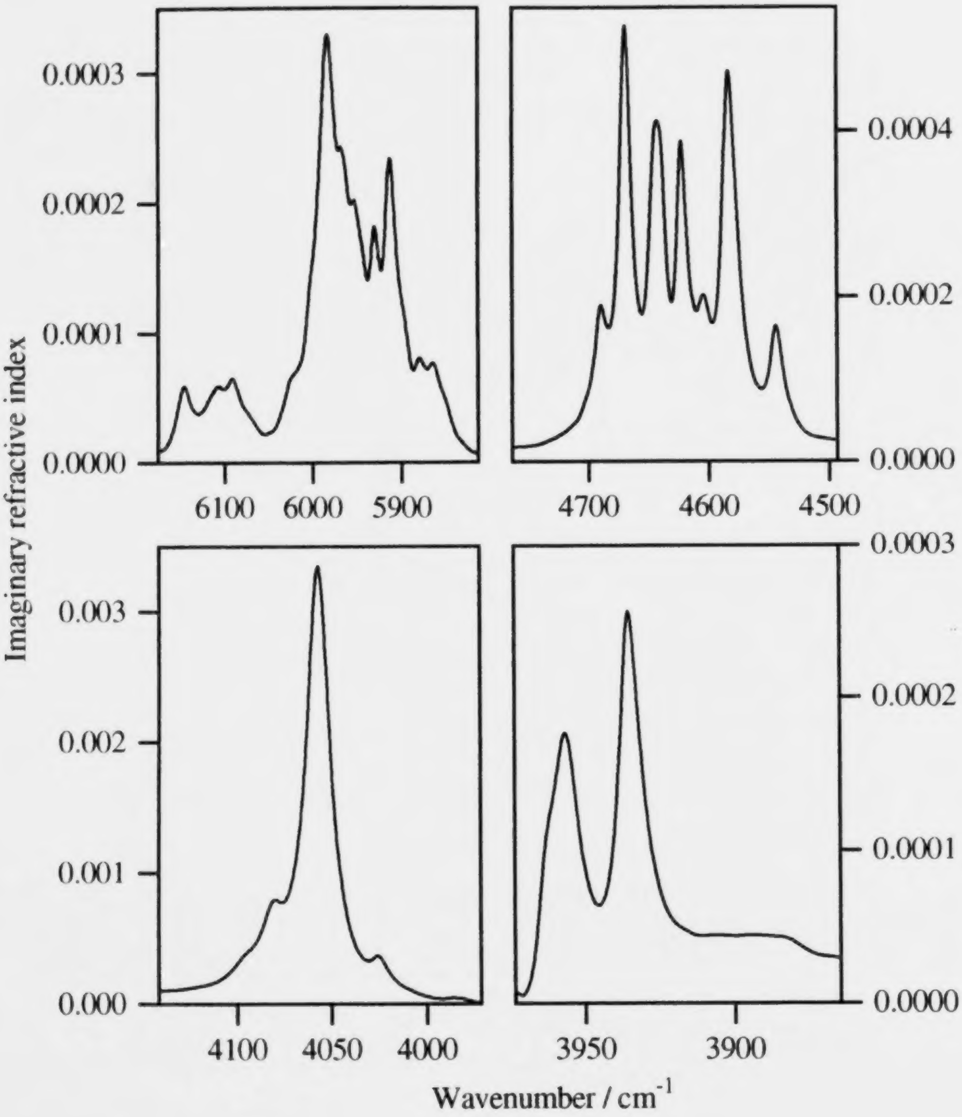

Figure 3.2. Imaginary refractive index spectrum of benzene-h$_6$, 6200 - 3800 cm^{-1}. The ranges shown are the integration ranges given in Table 3.5.

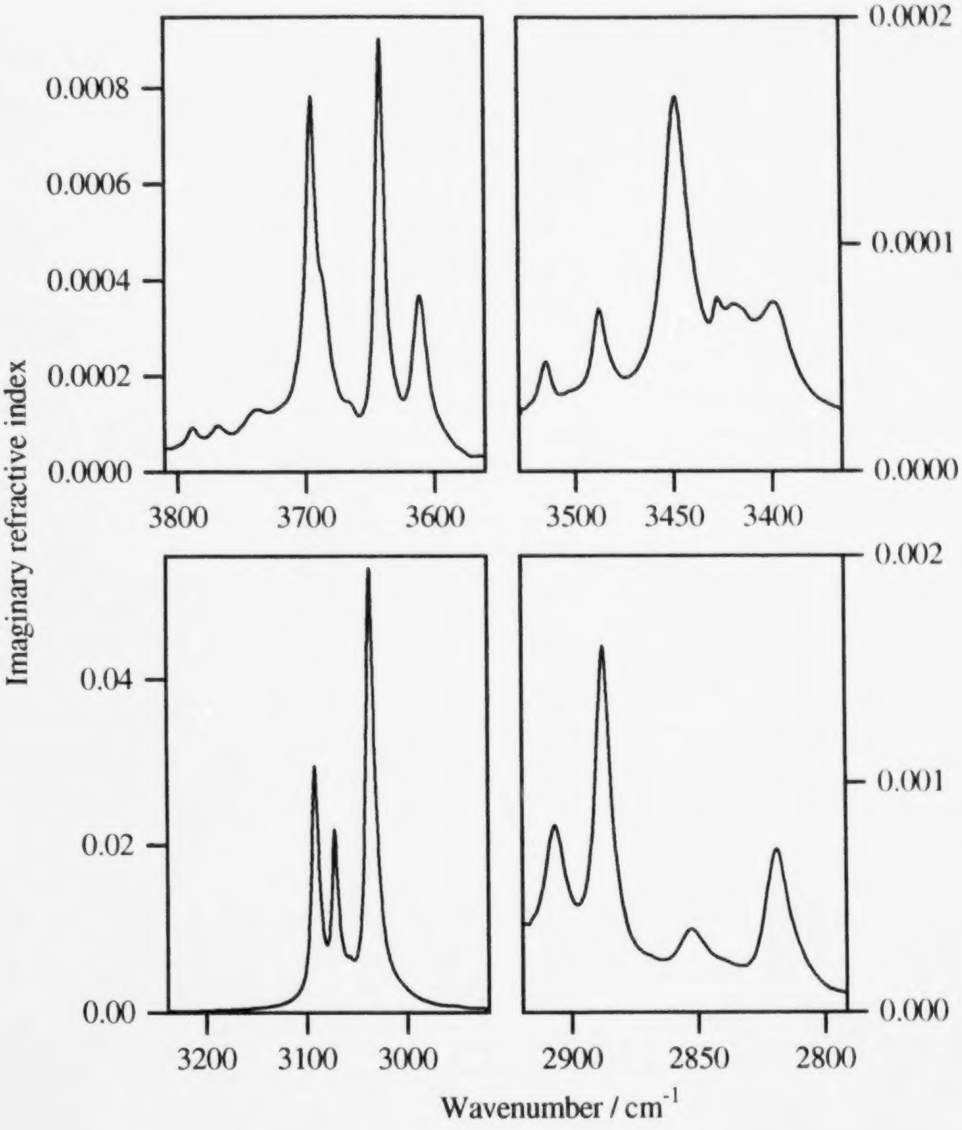

Figure 3.3. Imaginary refractive index spectrum of benzene-h$_6$, 3800 - 2800 cm^{-1}. The ranges shown are the integration ranges given in Table 3.5.

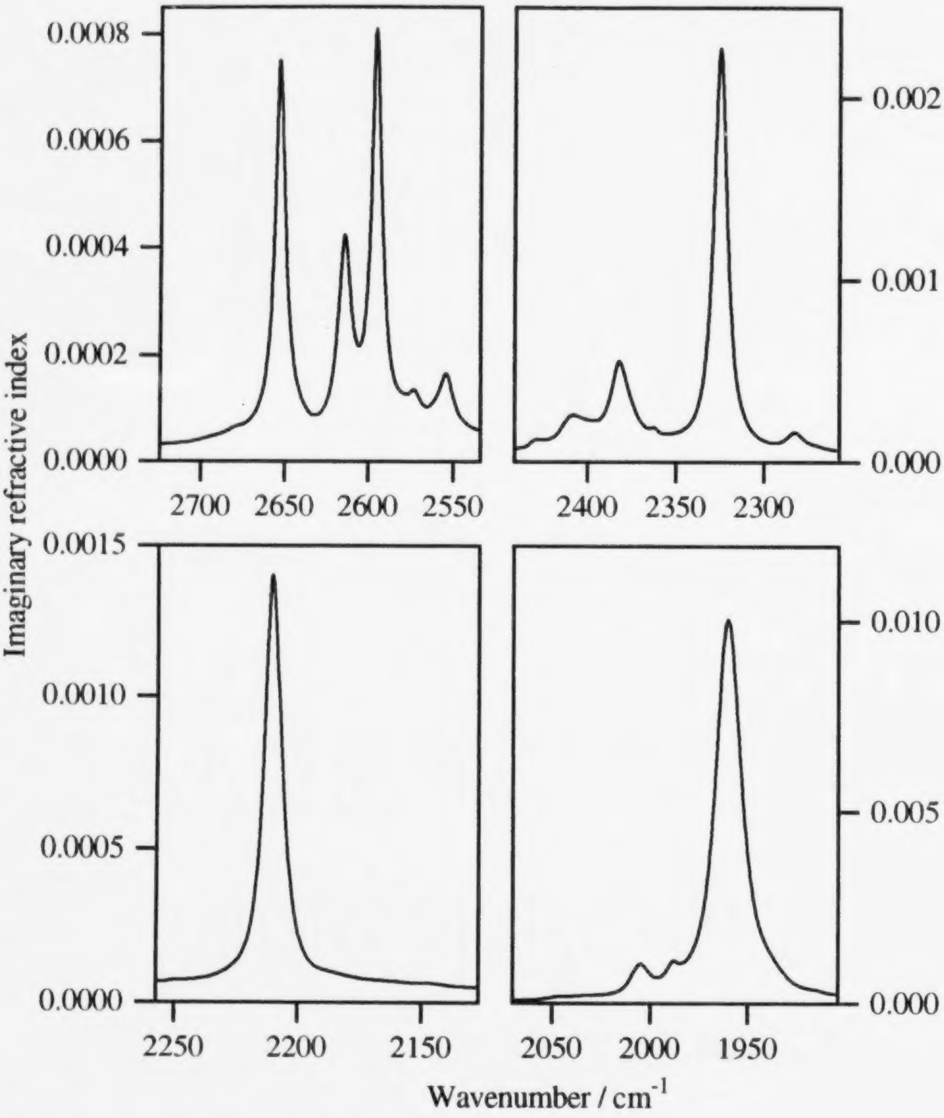

Figure 3.4. Imaginary refractive index spectrum of benzene-h_6, 2800 - 1900 cm^{-1}. The ranges shown are the integration ranges given in Table 3.5.

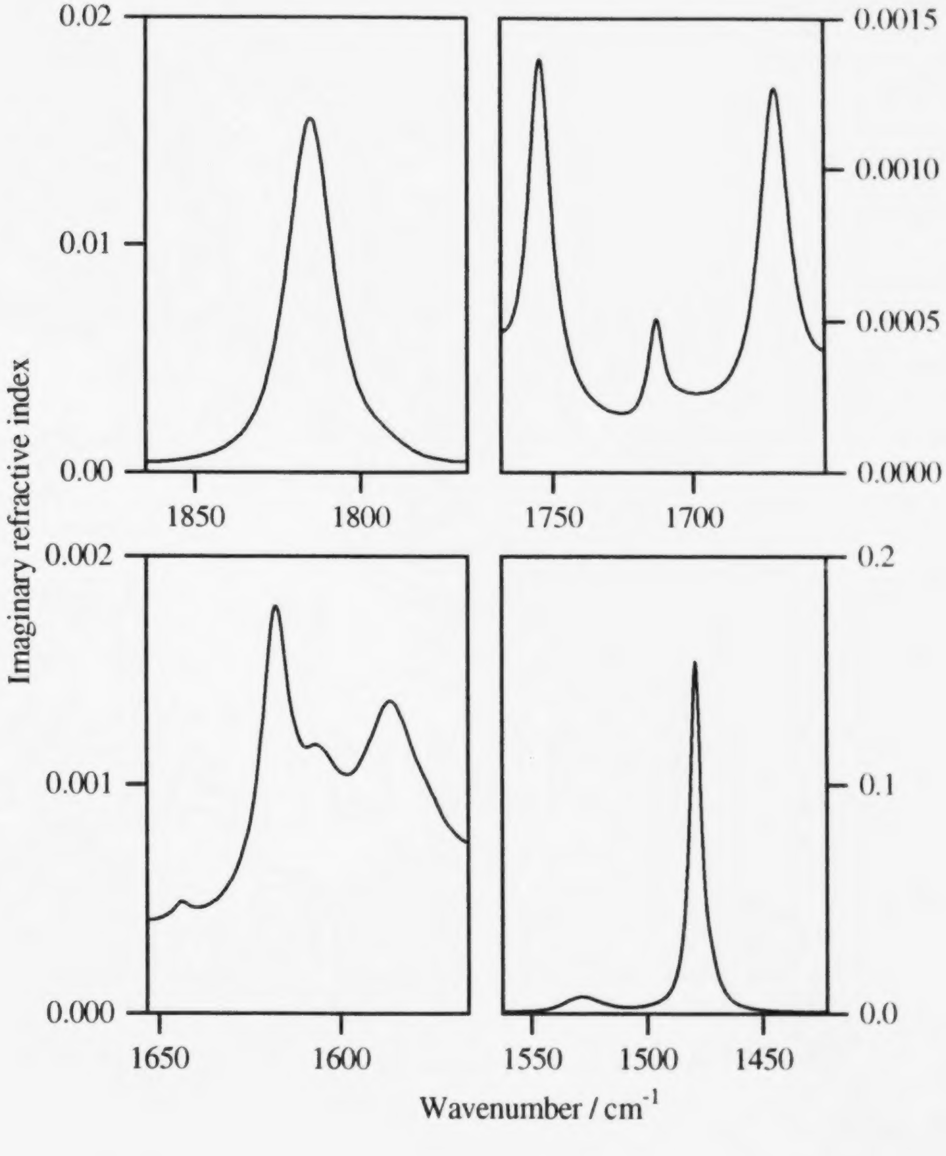

Figure 3.5. Imaginary refractive index spectrum of benzene-h$_6$, 1900 - 1400 cm^{-1}. The ranges shown are the integration ranges given in Table 3.5.

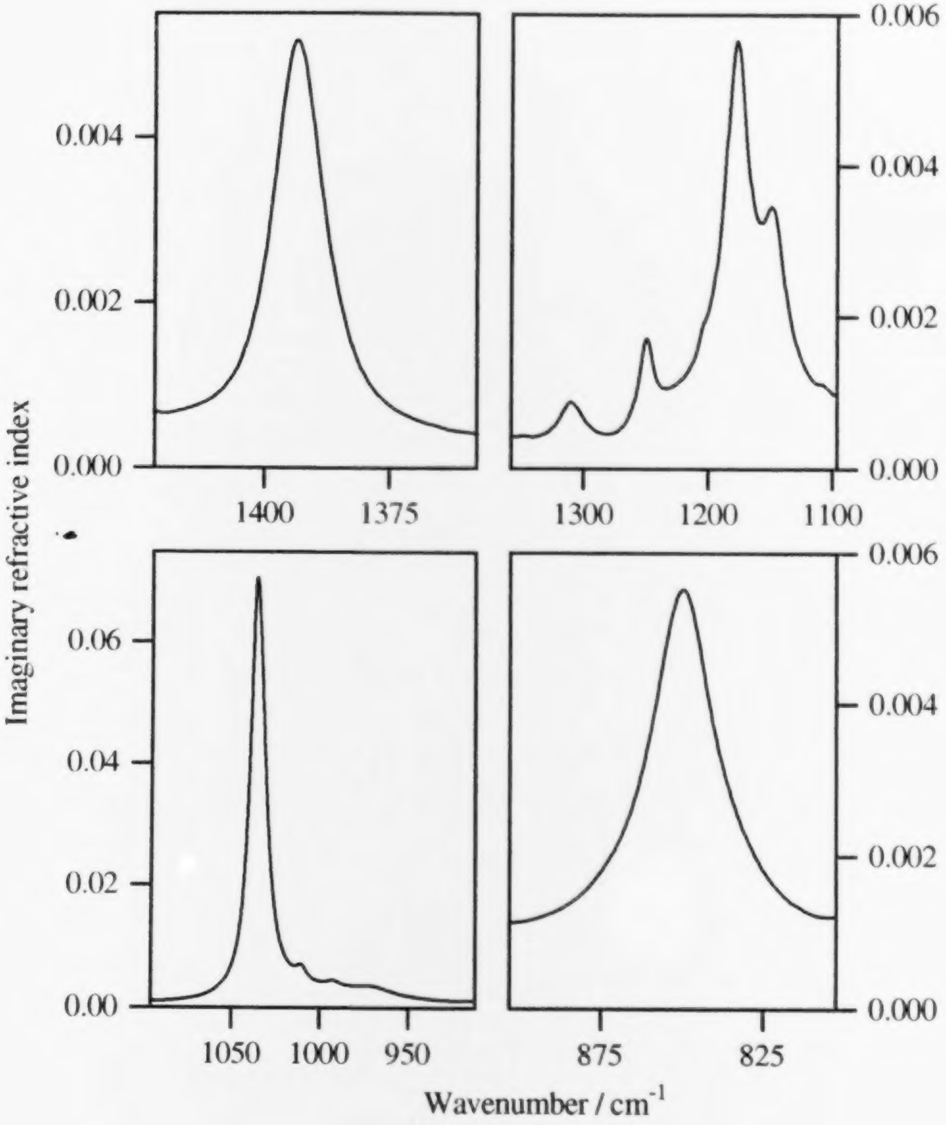

Figure 3.6. Imaginary refractive index spectrum of benzene-h_6, 1400 - 800 cm^{-1}. The ranges shown are the integration ranges given in Table 3.5.

For 19 of the 20 regions in Table 3.5 the agreement between spectroscopists ranges from 0.5% to 3.3%, with an average agreement of 1.7% over the nineteen band groups of varied intensities. For only one region is the agreement poor, the maximum deviation being 7.3% in the region of very weak absorption between 2724 and 2534 cm^{-1} . For the ten regions in which the maximum $k(\tilde{\nu})$ value exceeds 0.002, the agreement ranges from 0.5% to 2.5% with an average agreement of 1.25%. Such agreement between spectra measured in different laboratories on instruments by different manufacturers is very encouraging.

The weighted and unweighted average areas in Table 3.5 agree to well within the estimated accuracy of the unweighted averages, indicating that the much larger number of spectra from this laboratory did not significantly influence the averages.

The final imaginary refractive index spectrum is shown in Figure 3.7. The overall weighted and unweighted average peak heights in the $k(\tilde{\nu})$ spectra are given in Table 3.6 along with the maximum deviations from the unweighted averages of the averages of the different spectroscopists, the % estimated accuracies of the unweighted averages, which are discussed later, the previous values published from this laboratory[19] and the calibrated results of Jones and co-workers[18]. Again the weighted and unweighted averages agree within the estimated accuracies of the unweighted averages. Peak heights greater than 0.002 agreed between spectroscopists to 2% on average, and those less than 0.002 agreed to 3%.

Table 3.6. Overall average peak heights in the imaginary refractive index spectra.

$\tilde{\nu}$ / cm^{-1}	Unweighted Average[a]	% Estimated Accuracy[b]	Weighted Average	Ref. 19[c]	Ref. 18[d]
5982.1	0.000329 (12)	4.0	0.000329		
5929.5	0.000181 (3)	2.2	0.000181		
5912.1	0.000234 (2)	1.3	0.000234		
4689.6	0.000189 (2)	1.6	0.000189		
4669.2	0.000528 (20)	4.0	0.000528		
4642.4	0.000412 (6)	1.7	0.000412		
4622.5	0.000388 (7)	2.1	0.000388		
4604.2	0.000202 (2)	1.5	0.000202		
4583.3	0.000473 (12)	2.7	0.000473		
4543.7	0.000165 (1)	1.2	0.000165		
4056.8	0.00335 (5)	1.5	0.00335	0.00340 (8)	0.00334 (12)
3956.7	0.000177 (8)	5.1	0.000183		0.000270 (19)
3935.4	0.000257 (8)	3.5	0.000259		0.000349 (20)
3696.0	0.000782 (47)	6.1	0.000781	0.000793 (41)	0.000771 (52)
3642.4	0.000903 (52)	5.9	0.000907	0.000927 (38)	0.000961 (69)
3611.2	0.000365 (12)	3.6	0.000365		0.000375 (22)
3514.7	0.0000480 (8)	4.2	0.0000481		0.000051 (5)
3487.6	0.0000711(23)	4.2	0.0000718		0.000074 (6)
3448.2	0.000165 (4)	2.4	0.000165		0.000159 (11)
3091.1	0.0296 (11)	3.7	0.0304	0.0308 (4)	0.0301 (8)
3071.7	0.0218 (15)	6.9	0.0229	0.0234 (2)	0.0228 (6)
3036.2	0.0536 (35)	6.5	0.0532	0.0542 (7)	0.0520 (13)
2906.3	0.000812 (17)	4.6	0.000811		0.000828 (51)
2887.3	0.00160 (4)	2.5	0.00161		0.00171 (12)
2852.5	0.000359 (9)	5.6	0.000362		0.000350 (24)
2818.8	0.000707 (22)	2.8	0.000715		0.000746 (44)
2653.0	0.000750 (22)	2.7	0.000753		0.000783 (46)
2614.0	0.000423 (11)	2.4	0.000426		0.000447 (26)
2595.3	0.000808 (27)	3.7	0.000810		0.000838 (50)
2382.2	0.000555 (5)	0.9	0.000557		0.000568 (38)

Table 3.6. Continued.

$\tilde{\nu}$ / cm^{-1}	Unweighted Average[a]	% Estimated Accuracy[b]	Weighted Average	Ref. 19[c]	Ref. 18[d]
2324.9	0.00228 (3)	1.3	0.00227	0.00229 (5)	0.00231 (16)
2282.4	0.000164 (3)	1.8	0.000163		0.000166 (12)
2210.5	0.00140 (2)	1.4	0.00141	0.00142 (5)	0.00147 (11)
2004.7	0.00103 (5)	4.8	0.00104		0.00104 (6)
1988.0	0.00110 (10)	9.0	0.00113		0.00113 (4)
1960.2	0.0100 (3)	3.0	0.0100	0.01021 (9)	0.00992 (31)
1815.3	0.0155 (5)	3.2	0.0156	0.0157 (1)	0.0150 (4)
1754.4	0.00136 (6)	5.1	0.00139	0.00142 (4)	0.00141(5)
1713.1	0.000507 (35)	9.8	0.000526		0.000563 (20)
1671.0	0.00127 (4)	3.9	0.00129	0.00132 (5)	0.00129(5)
1617.8	0.00178 (8)	5.1	0.00181	0.00186 (4)	0.00182 (7)
1586.3	0.00136 (2)	2.2	0.00136		0.00139 (5)
1528.1	0.00728 (5)	0.8	0.00728		0.00734 (21)
1479.0	0.154 (6)	3.9	0.152	0.154 (1)	0.152 (3)
1393.4	0.00518 (27)	5.4	0.00522	0.00528(6)	0.00528 (17)
1309.8	0.000882 (15)	3.4	0.000881		0.000951 (34)
1249.2	0.00171 (7)	4.7	0.00172	0.00177 (7)	0.00176 (6)
1176.7	0.00566 (9)	1.8	0.00567	0.00584 (12)	0.00580 (19)
1148.7	0.00345 (4)	1.5	0.00345	0.00361 (12)	0.00342 (15)
1035.9	0.0709 (6)	0.8	0.0711	0.0718 (4)	0.0711 (14)
849.8	0.00552 (8)	1.8	0.00554	0.00583 (15)	0.00568 (21)

[a] The number in brackets in this column is the maximum deviation from the unweighted average, except for peaks above 4500 cm^{-1}. In these cases the values listed are the 95% confidence limits of the peaks in the average spectra for CDK, the only worker who measured spectra in these regions.

[b] The estimated accuracy is taken as the sum of the maximum deviation and the uncertainty due to the anchor points. The uncertainty due to the anchor points is taken as the average of the 95% confidence limits of $k(\tilde{\nu})$ (Table 3.1) for the two anchor points either side of the peak.

[c] The numbers in brackets in this column are the 90% confidence limits in the last digit[19].

[d] The numbers in brackets in this column are the evaluated uncertainties in the values[18].

3.1.3b Imaginary Refractive index from 800 to 500 cm^{-1}

The absorption band in this region is 10 times more intense than any other absorption band of benzene-h_6 and has a large influence on the $n(\tilde{\nu})$ values calculated over the whole wavenumber range. The band was too intense to be measured in this work, requiring cell path lengths as small as 2 μm. Accordingly, the $k(\tilde{\nu})$ spectrum between 800 and 500 cm^{-1} was taken from Jones and co-workers[18] by enlarging their graph of $k(\tilde{\nu})$ over this region and digitizing the spectrum by hand. The resulting imaginary refractive index band is included in Figure 3.7.

3.1.3c Imaginary Refractive index from 500 to 30 cm^{-1}

The absorption in this region is extremely weak and it is necessary to use cells with 3 to 5 mm path lengths. Spectra were recorded in 3 mm and 5mm polyethylene cells. The path length of each cell was found by measuring the thickness of the windows with a micrometer before the cell was assembled. The thickness of the windows varied by about 0.003 mm when the thickness was measured at different positions. After the cell was assembled and filled with liquid, the overall thickness between the outsides of the windows was measured at several positions with the same micrometer. This overall thickness varied by 0.05 to 0.10 mm, which is 1 to 3%. The path length was then found as the difference between the overall thickness and the thickness of the two windows. The path lengths found in this way are accurate to within 0.05 to 0.10 mm.

Spectra were recorded using 3, 12, 23 and 50 μm mylar beamsplitters for the regions 500 to 150 cm^{-1}, 215 to 30 cm^{-1}, 120 to 30 cm^{-1}, and 50 to 30 cm^{-1}, respectively.

The experimental absorbance spectra of the "3 mm" cell full of liquid were subtracted from those of the "5 mm" cell. Molar absorption coefficient spectra were calculated from these difference absorbance spectra using the difference between the path lengths of the two cells. The molar absorption coefficient spectra were averaged where the regions over lapped and merged to form the final molar absorption coefficient spectrum from 500 to 30 cm^{-1}. This method[158] eliminates the reflection of the cells, if both the 3 and 5 mm cells have the same apparent absorbance. This was checked for the empty cells and it was found that they agreed within the experimental error of 10 to 20%. From this molar absorption coefficient spectrum, the imaginary refractive index spectrum between 500 and 30 cm^{-1} was calculated via equation (1.3.20).

This method is much easier than the method used to determine the imaginary refractive index above 800 cm^{-1}. However, it is also much less accurate. The method neglects the fact that the reflectance and transmittance of the liquid layer depends on the thickness of the liquid layer, [equations (2.2.10) and (2.2.11)]. It can be used in this region because the absorption is extremely weak and the reproducibility of the experimental absorbance spectra of the cells full of liquid was only on the order of 10 to 20%.

The final imaginary refractive index spectrum between 6225 and 30 cm^{-1} is shown in Figure 3.7 and is tabulated in compact table format[44] in Table IV.1 in Appendix IV.

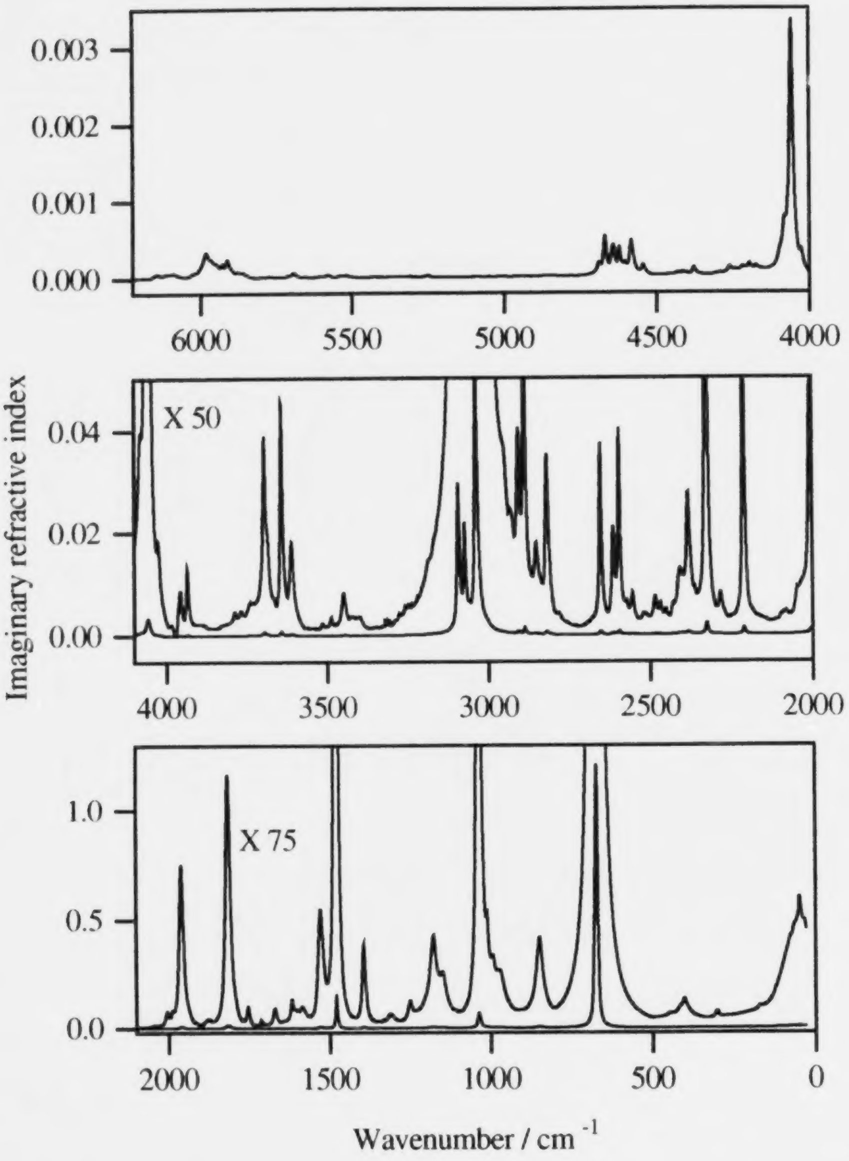

Figure 3.7. Imaginary refractive index spectrum between 6225 and 30 cm^{-1} of liquid benzene-h$_6$ at 25°C. The ordinate scale labels in the middle and bottom boxes are for the lower spectrum in the box; they must be divided by 50 and 75, as shown, for the upper spectrum in the box.

3.1.3d Real Refractive Index

The real refractive index spectrum, $n(\tilde{\nu})$, was calculated from the final $k(\tilde{\nu})$ spectrum by Kramers-Kronig transformation, equation (2.3.6), taking the real refractive index to be 1.4804 at 8000 cm^{-1} . This value was obtained by fitting the literature[159] values of the refractive index at seven wavelengths in the visible region to $n^2 = a\tilde{\nu}^4 + b\tilde{\nu}^2 + c$ and extrapolating to 8000 cm^{-1}, as discussed in section 2.3.2. The literature data and the fitted curve are shown in Figure 3.8. The equation of the fitted curve is

$$n^2 = 2.1784(\pm 0.0003) + 2.00(\pm 0.02)\times 10^{-10}\,\tilde{\nu}^2 + 9.2(\pm 0.2)\times 10^{-20}\,\tilde{\nu}^4$$

Further, it was assumed that the $k(\tilde{\nu})$ values are all zero between 6225 and 8000 cm^{-1}. The final real refractive index spectrum is shown in Figure 3.9 and the values are tabulated in compact table format[44] in Table IV.2 in appendix IV.

3.1.4 Accuracy of the Results

The purpose of this experimental study was to determine the accuracy of the measurements, rather than to obtain the highest possible precision. To obtain high precision, as many errors as possible are suppressed, by varying as few parameters as possible during the measurements, to obtain the greatest reproducibility. Every error that is suppressed introduces a potential systematic error into the measurement. The result may be very precise (reproducible) but may be very inaccurate (wrong in the sense of being different from "Nature's value".) Thus to reveal accuracy the errors in the measurements must be revealed, and to this end as few parameters as possible were kept constant in this work.

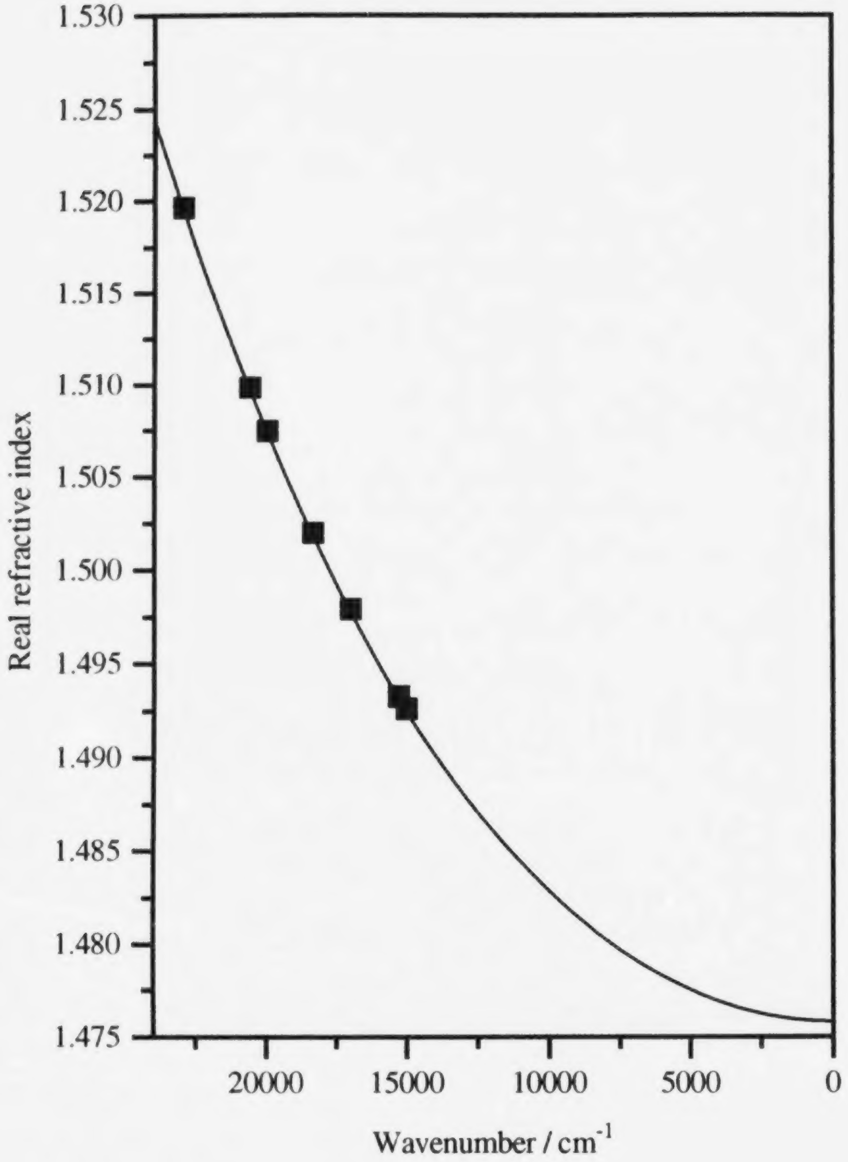

Figure 3.8. Extrapolation of the real refractive index of benzene-h_6 in the visible to the infrared. The squares are the real refractive index values given by Timmermans[159] and the curve is the least squares fit of this data to $n^2 = a\tilde{v}^4 + b\tilde{v}^2 + c$.

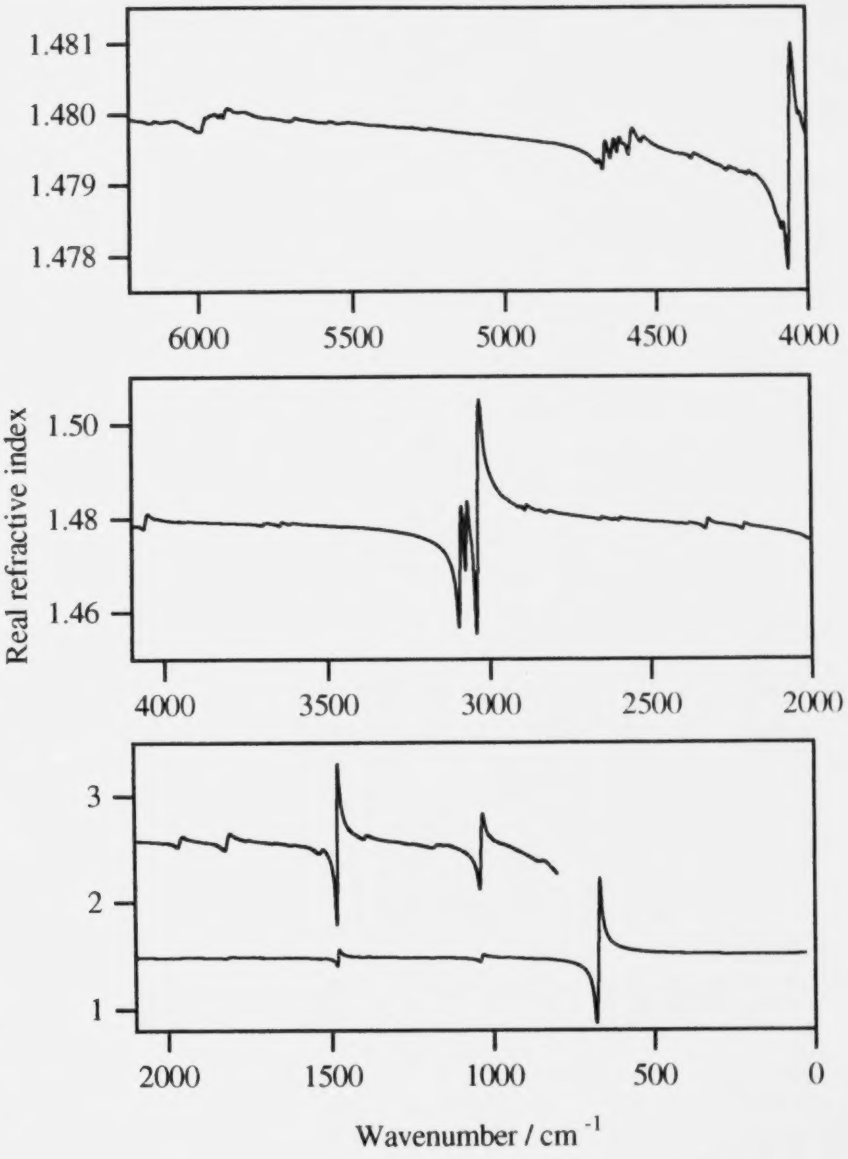

Figure 3.9. Real refractive index, $n(\tilde{\nu})$, spectrum between 6225 and 30 cm^{-1} of liquid benzene-h$_6$ at 25°C. In the bottom box, the partial spectrum shown by the upper curve is $(n(\tilde{\nu})) - 1.22) \times 10$, to offset the curve for clarity.

To achieve this, several practices were adopted for measurements in this laboratory. Several different transmission cells were used, and the cell was removed from the instrument and dried after each spectrum, to ensure that effects of different cells and their filling and positioning were revealed. Measurements were made with both Ge-on-KBr and Si-on-CaF_2 beam splitters, and the averages reported for CDK and VB include data from both beamsplitters. Measurements by both CDK and VB, were made over a period of a year, with other measurements made between the benzene-h_6 measurements, and measurements of benzene-h_6 in any one cell were generally made on different days. The source unit of the spectrometer was changed between the studies by CDK and VB, and the instrument was optically realigned at least twice between the two studies, as well as once during VB's work, and the detector has been realigned during each of these two studies. Instrumental factors like apodization were explored[19], and found to have negligible effect. Resolution also had negligible effect as long as it was 2 cm^{-1} or better.

The use of the 95% confidence limit to describe the precision of a measurement is technically based on the experimental error being random. The 95% confidence limits reported in this work can be challenged on the ground that the errors included may not all be random. The variation of many parameters and the use of different instruments by different spectroscopists should mean that the deviations from the average values include the effect of systematic errors, which can not technically be described by a 95% confidence limit. In particular, the measurements from the four spectroscopists in other laboratories on instruments made by different manufacturers may contain systematic errors associated with different instrument design, different laboratory, different environment, different cells, different samples and different operator.

Nevertheless it is believed that 95% confidence limits can usefully describe the variations observed, if it is recognized that the limits are probably larger than they would have been if only random errors had been included. In fact, the 95% confidence limits are believed to better reflect the accuracy of the measurements presented above than technically, and usually, is the case.

3.1.4a Imaginary Refractive Index

For the reasons discussed above, it is believed that the agreement between the average results of the different spectroscopists gives a valid indication of the accuracy of the results. For each region, the maximum deviation from the unweighted average is used to express this agreement.

The use of anchor points to eliminate the baseline variation replaces one clear source of variability and error by systematic errors, the errors in the value of $k(\tilde{\nu})$ at the anchor points. These errors are given in Table 3.1 as the 95% confidence limits of the linear absorption coefficient, $\Delta K(\tilde{\nu})$ and of the imaginary refractive index, $\Delta k(\tilde{\nu})$. The accuracy of the anchor point linear absorption coefficients causes an absolute uncertainty in $k(\tilde{\nu})$ that is approximately 1 $\times 10^{-6}$ above 3000 cm^{-1}, and approximately 1 $\times 10^{-5}$ below 3000 cm^{-1}.

To obtain the *% estimated accuracy* of the $k(\tilde{\nu})$ values, the average of the uncertainties in $k(\tilde{\nu})$ at the anchor points immediately to each side of the band group was added to the maximum deviation from the unweighted average and expressed as a percentage of the $k(\tilde{\nu})$ value. The accuracy of the $k(\tilde{\nu})$ values is discussed first for the peak values and then for values in the baseline.

The % estimated accuracies of the $k(\tilde{\nu})$ values at the peak heights are included in Table 3.6. There are four peaks for which the % estimated accuracies are abnormally high, at 3072, 3036, 1988, and 1713 cm^{-1}. These peaks are discussed below, and are excluded from the following general comments. The heights of the 12 peaks below 4100 cm^{-1} which have $k_{max} > 0.002$ have estimated accuracies of ±2% on average. The heights of the 25 peaks below 4100 cm^{-1} which have $k_{max} < 0.002$ have estimated accuracies of ±3.5% on average. The heights of the 10 peaks above 4100 cm^{-1} have estimated accuracies of ±2.5% on average, but were all obtained by one spectroscopist, CDK.

The heights of the peaks at 1988 and 1713 cm^{-1} (Figures 3.4 and 3.5) have estimated accuracies of 9 and 9.8%. No reason for the poor accuracy in these two cases is evident, except perhaps that the 1988 cm^{-1} peak is nearly a shoulder and forms part of the base of a much stronger band. Far more noteworthy is the poor accuracy of the heights of the two peaks at 3072 and 3036 cm^{-1} (Figure 3.3). These are only known to about 7% (Table 3.6) even though they are among the few relatively intense bands of benzene-h_6. While the highest-wavenumber band of benzene-h_6 in this region (3091 cm^{-1}) was satisfactorily reproducible, surprising variability was found in the line shapes and relative intensities of these two lower-wavenumber bands. The different spectra obtained by each worker agreed fairly well among themselves, but there was a surprising variation between the average spectra of the different workers, even between the averages of VB and CDK, both of whom used the same instrument. Possible causes of this behaviour have been explored without success. Spectra of toluene recorded by VB and CDK, and by other spectroscopists, show no such anomalous behaviour in this region or elsewhere[47].

The $k(\tilde{\nu})$ values at the peaks must be compared with the only calibrated results available, those of Jones and co-workers[18]. The only k_{max} values in Table 3.6 that lie outside the combined evaluated uncertainties of Jones and co-workers[18] and the estimated accuracy of the unweighted average are the three values at 3957, 3935, and 1310 cm^{-1}.

The $k(\tilde{\nu})$ values in the baseline are not known as accurately as those in regions of significant absorption, except at the anchor points. From the agreement between different workers and the uncertainties in the anchor point values, the accuracy of the baseline $k(\tilde{\nu})$ values is estimated to be approximately $\pm 2 \times 10^{-6}$ above 3000 cm^{-1}, between $\pm 1 \times 10^{-5}$ and $\pm 5 \times 10^{-5}$ below 3000 cm^{-1}. The latter correspond to ~±10% of the weakest $k(\tilde{\nu})$ values between 3000 and 1200 cm^{-1}, and between ±1 and ±5% of the weakest $k(\tilde{\nu})$ values below 1200 cm^{-1}.

Jones and co-workers evaluated the uncertainty of the 670 cm^{-1} band to be about 4%. The imaginary refractive index spectrum between 500 and 30 cm^{-1} is not known as accurately as the rest of the imaginary refractive index spectrum. From the experimental reproducibility (10 to 20%) and the agreement with Garg *et. al.*[158] and Asfar and co-workers[160, 161] it is estimated that the $k(\tilde{\nu})$ values are accurate to within ±10 to ±20% between 500 and 30 cm^{-1}.

3.1.4b Area Under the Imaginary Refractive Index

To calculate the % estimated accuracy of the areas under the $k(\tilde{\nu})$ band groups, the average of the uncertainties in $k(\tilde{\nu})$ at the anchor points immediately to the sides of the band group was multiplied by the integration range, this was added to the maximum deviation from the unweighted average, and expressed as a percentage of the area for each band. These percent estimated accuracies of the areas are included in Table 3.5. The weakly absorbing region between 2724 and 2534 cm^{-1} is anomalously inaccurate, and is omitted from further discussion. For the remaining nineteen regions the band areas are accurate to ±2.3% on average. For the ten regions which contain a band with $k_{\max}> 0.002$, the areas are accurate to ±1.6% on average. This accuracy is very encouraging.

It is noteworthy that the error in $k(\tilde{\nu})$ at the anchor points significantly influences the estimated accuracy of the areas. For band groups with $k_{\max} > 0.002$, the anchor point uncertainty causes ~0.3% of the total % estimated error in the area and for band groups with $k_{\max} < 0.002$, the anchor point uncertainty causes ~1.0% of the total % estimated error in the area. However, this error does not influence the accuracy of the areas for calibration reference if the area is measured above a baseline drawn between the anchor points, or above a baseline drawn between the integration limits. The use of the areas under these bands as calibration standards is discussed in Chapter 4.

3.1.4c Real Refractive Index

The real refractive index, $n(\tilde{\nu})$, was calculated by adding the value n=1.4804 at 8000 cm^{-1} to the value of $\Delta n(\tilde{\nu}) = n(\tilde{\nu}) - n(8000\ \text{cm}^{-1})$ that is calculated by the Kramers-Kronig transform. There are several factors which contribute to the accuracy of $n(\tilde{\nu})$. There is ~0.05% accuracy intrinsic[141] to the numerical Kramers-Kronig transform used in this work. The value of n at 8000 cm^{-1} has an accuracy of about 0.03%. The ~2.5% accuracy of $k(\tilde{\nu})$ results in ~2.5% accuracy in $\Delta n(\tilde{\nu})$, which is about 0.002% of $n(\tilde{\nu})$. Lastly, the ~4% evaluated uncertainty[18] in the $k(\tilde{\nu})$ values of the strong band at 673 cm^{-1}, affects the accuracy of $n(\tilde{\nu})$ by $\leq 0.1\%$. The overall estimated accuracy of the $n(\tilde{\nu})$ values is ~0.2%.

Similar measurements of the optical constants of toluene [47] chlorobenzene[48] and dichloromethane[49] gave similar accuracies for the real and imaginary refractive index spectra to those obtained for benzene-h_6 in this work. It is therefore assumed that the optical constants of the other liquids measured in this work have approximately the same accuracies.

3.2 Optical Constants of Benzene-d_6

The benzene-d_6 was obtained from General Intermediates of Canada and was used without further purification. Samples were kept over molecular sieve to ensure dryness. Samples were checked by gas chromatography. Impurities were determined to be less than 0.06%. Mass spectrometry showed that there was ~6% $^{13}CC_5D_6$ in the benzene-d_6. No other isotopic impurities were detected.

The experimental and instrumental details of these measurements were the same as those described in section 3.1 for benzene-h_6.

Experimental absorbance spectra of benzene-d_6 were measured in fixed path length cells with KBr windows and path lengths between 11 and 1500 μm, in fixed path length cells with CaF_2 windows and path lengths of 110 and 1180 μm, and in variable path length cells with NaCl and CaF_2 windows and path lengths up to 4 mm.

3.2.1 Imaginary Refractive Index

The values of $K(\tilde{\nu})$ needed at anchor points in the baseline in order to correct the baselines were determined from the experimental absorbance spectra in cells which gave the experimental absorbance at these anchor points in the range 0.1 - 2.0 for anchor points below 4000 cm^{-1} and in the range 0.03 - 0.04 for anchor points above 4000 cm^{-1}. The path lengths used for each anchor point are given in Table 3.7. In order to calculate $K(\tilde{\nu})$ at the anchor points, an approximate value of $n(\tilde{\nu})$ is required at these anchor points. The value of n_∞ is known, as described in section 3.2.2, but n at various wavenumbers in the infrared were required. This approximate $n(\tilde{\nu})$ was obtained by measuring the ATR spectrum of benzene-d_6 in the CIRCLE cell and calculating the real and imaginary refractive indices by the method previously published[155, 162] with $n_\infty = 1.4780$ (*vide infra*). The real refractive index values used to calculate the ideal apparent absorbance at the anchor points are given in Table 3.7.

Table 3.7 summarizes the wavenumbers of the anchor points, the measured linear absorption coefficients, $K(\tilde{\nu})$, and their 95% confidence limits, and the imaginary refractive indices at the anchor points and their 95% confidence limits.

The experimental absorbance spectra from all cells were converted to imaginary refractive index spectra by program RNJ46A, using this anchor point information. Again the imaginary refractive index spectra were only used in regions where the corresponding experimental absorbance peaks were between 0.2 and 2.0. The imaginary refractive index spectra from the appropriate cell thicknesses were averaged for each region. Table 3.8 shows the cell thicknesses as well as the number of spectra recorded and used for each spectral region.

The very strong band at 496 cm^{-1} was too intense to be measured in this work, requiring cell path lengths <11 μm (the thinnest cell available for this study). This absorption is 2 to 3 times more intense than any other absorption band of benzene-d_6[36] This band was approximated as follows. The imaginary refractive

Table 3.7. Linear absorption coefficients at anchor points for liquid benzene-d_6 at 25°C.

Wavenumber / cm^{-1}	Path length / mm	$n(\tilde{\nu})$ [a]	$K(\tilde{\nu})$ / cm^{-1} [b]	$k(\tilde{\nu})$ [b,c]
4761.8	3.2 - 3.8	1.478	0.042 (±17)	0.0000016 (±7)
4235.4	3.2 - 3.8	1.478	0.032 (±9)	0.0000014 (±4)
4000.1	2.8 - 3.8	1.478	0.120 (±8)	0.0000055 (±4)
3865.6	1.2 - 3.8	1.478	1.00 (±1)	0.0000474 (±5)
3755.6	1.2 - 3.8	1.478	0.526 (±10)	0.0000257 (±5)
3668.9	1.2 - 3.8	1.478	0.409 (±14)	0.0000204 (±7)
3482.8	1.8 - 3.8	1.477	0.182 (±8)	0.0000096 (±4)
3343.9	1.2 - 3.8	1.477	0.594 (±13)	0.0000326 (±7)
3178.5	1.2 - 3.8	1.478	1.03 (±1)	0.0000594 (±6)
2980.4	1.2 - 3.8	1.477	0.823 (±8)	0.0000506 (±5)
2803.5	1.2 - 3.8	1.477	0.922 (±7)	0.0000603 (±5)
2584.1	1.2 - 3.8	1.477	0.528 (±6)	0.0000374 (±4)
2016.2	1.2 - 3.8	1.479	0.218 (±6)	0.0000198 (±5)
1814.2	1.2 - 3.8	1.478	0.740 (±21)	0.0000748 (±21)
1646.4	1.2 - 3.8	1.476	3.51 (±1)	0.000391 (±1)
1580.8	1.2 - 3.8	1.478	3.87 (±2)	0.000449 (±2)
1508.5	1.2 - 3.8	1.477	1.980 (±4)	0.0002405 (±5)
1418.3	1.2 - 3.8	1.478	3.41 (±1)	0.000441 (±1)
1237.1	1.5 - 3.7	1.479	1.077 (±5)	0.0001595 (±7)
1090.5	3.2 - 3.7	1.478	0.898 (±2)	0.0001509 (±3)
908.8	1.5 - 3.7	1.475	5.10 (±2)	0.001029 (±4)
722.2	0.5 - 3.7	1.465	3.37 (±2)	0.000855 (±5)
511.5	0.01 - 0.05	1.285	199 (±1)	0.0713 (±4)

[a] Approximate value of $n(\tilde{\nu})$ used to calculated the ideal apparent absorbance when calculating $K(\tilde{\nu})$.

[b] The value in parentheses is the 95% confidence limit in the terminal digit, $\Delta K(\tilde{\nu})$ or $\Delta k(\tilde{\nu})$.

[c] The 95% confidence limit of $k(\tilde{\nu})$, $\Delta k(\tilde{\nu})$, is calculated by $\Delta k(\tilde{\nu}) = \dfrac{2.303\Delta K(\tilde{\nu})}{4\pi\tilde{\nu}}$.

Table 3.8. Path lengths and number of spectra recorded for the regions processed.

Region / cm^{-1}	Path lengths / μm	Number of spectra
5000 - 4545	3300 - 3800	6
4548 - 4415	~ 500	3
4416 - 3845	1500 - 3800	22
3846 - 3775	~ 500	8
3778 - 3290	1200 - 3800	24
3294 - 3246	1200 - 1800	7
3250 - 3200	50 - 100	9
3216 - 2890	1500 - 2800	10
2892 - 2800	~ 500	8
2807 - 2430	2800 - 3800	15
2432 - 2395	500 - 1800	18
2400 - 2380	35 - 100	15
2384 - 2300	~ 500	8
2303 - 2225	~ 11	4
2225 - 2155	500 - 1200	10
2157 - 1880	1500 - 3800	22
1885 - 1805	500 - 1800	17
1809 - 1700	1500 - 3800	22
1704 - 1630	500 - 1500	14
1635 - 1595	35 - 50	12
1580 - 1465	500 - 1200	9
1566 - 1415	35 - 50	12
1418 - 1350	~ 500	8
1360 - 1290	35 - 50	12
1292 - 1180	500 - 1500	8
1182 - 1125	35 - 50	10
1131 - 900	500 - 1500	8
903 - 820	~ 500	5
824 - 790	~11	4
793 - 550	~500	5

index values of the 673 cm^{-1} band of benzene-h_6 were multiplied by $(496/673)^2$ = 0.543 and the band was shifted to 496 cm^{-1}. It was assumed that there was no change in the full width at half height. The factor $(496/673)^2$ was obtained from the application of the isotope rule for infrared intensities. The isotope intensity rule states[62] that the sum of intensity divided by the square of the harmonic wavenumber for all vibrations in a symmetry species is isotopic invariant. The 673 and 496 cm^{-1} bands belong to the A_{2u} symmetry species for benzene-h_6 and benzene-d_6, respectively. Since there is only one A_{2u} vibration, the intensity of the two fundamentals is simply related by the ratio of the square of the harmonic wavenumbers. For these two bands there is very little difference between the experimental anharmonic wavenumbers and the harmonic wavenumbers, therefore the square of the ratio of the anharmonic wavenumbers was used to scale the intensity.

The average $k(\tilde{\nu})$ spectra for the different regions were merged to give a final $k(\tilde{\nu})$ spectrum from 5000 to 450 cm^{-1}. This $k(\tilde{\nu})$ spectrum is shown in Figure 3.10 and is tabulated in compact table format[44] in Table V.1 in Appendix V. The $k(\tilde{\nu})$ spectrum of benzene-d_6 is taken to have the same accuracy as that of benzene-h_6, ~±2 to ±3% for the areas under the bands and the peak heights.

3.2.2 Real Refractive Index

The real refractive index spectrum, $n(\tilde{\nu})$, was calculated from the final $k(\tilde{\nu})$ spectrum by Kramers-Kronig transformation, equation (2.3.6) . The Kramers-Kronig transform requires the value of the real refractive index at the high end of the spectrum. It was assumed that the $k(\tilde{\nu})$ values are all zero between 5000 and 8000 cm^{-1} and therefore the real refractive index of benzene-d_6 is required at 8000 cm^{-1}. The only value of the real refractive index of benzene-d_6 in the literature is at the Na D line where n = 1.4986 at 20°C [163]. The real refractive index of benzene-h_6 at 20°C at the Na D line is 1.5010 [159]. This is a difference of 0.0024 at 20°C. Assuming the difference between the real refractive index of benzene-h_6 and benzene-d_6 is the same at 8000 cm^{-1} and 25°C, 0.0024 must be subtracted from the real refractive index of benzene-h_6 at 8000 cm^{-1} to give the real refractive index of benzene-d_6. In section 3.1.3d, the real refractive index of benzene-h_6 was determined to be 1.4804 at 8000 cm^{-1} and 25°C. Therefore, the real refractive index of benzene-d_6 at 8000 cm^{-1} and 25°C is taken to be 1.4780.

The final real refractive index spectrum of benzene-d_6 is shown graphically in Figure 3.11 and is tabulated in compact table format[44] in Table V.2 in Appendix V. The $n(\tilde{\nu})$ values are believed accurate to ±0.2%, as was found for benzene-h_6.

From the optical constants of benzene-h_6 and benzene-d_6 the molar absorption coefficient spectra, the complex dielectric constant spectra and the imaginary molar polarizability spectra were calculated through the equations summarized in section 1.3. A molar volume of 89.41 cm^3 mole^{-1} was used for benzene-h_6 and a molar volume of 88.59 cm^3 mole^{-1} was used for benzene-d_6. These values were calculated from the density and molecular weight. For benzene-h_6 a density of 0.8737 g cm^{-3} [164] and a molecular weight of 78.12 g mole^{-1} were used. For benzene-d_6 a density of 0.950 g cm^{-3} [163] and a molecular weight of 84.16 g mole^{-1} were used. The molar absorption coefficient spectra of benzene-h_6 and benzene-d_6 are shown in Figures 3.12 and 3.13. The complex dielectric constant spectra and the complex molar polarizability spectra are shown in Chapter 5. The use of the molar absorption coefficient spectra and optical constants of benzene-h_6 as secondary infrared intensity standards is discussed in Chapter 4. In Chapter 5, the areas under the bands in the $\tilde{\nu}\alpha_m''$ spectra of liquid benzene-h_6 and liquid benzene-d_6 are used to determine the value of the dipole moment derivatives with respect to normal coordinates, symmetry coordinates and internal coordinates for the four infrared active fundamentals of both molecules in the liquid phase. In Chapter 6, these same areas are used to compare the intensities of the infrared active fundamentals in the liquid phase with those reported in the literature for the gas phase.

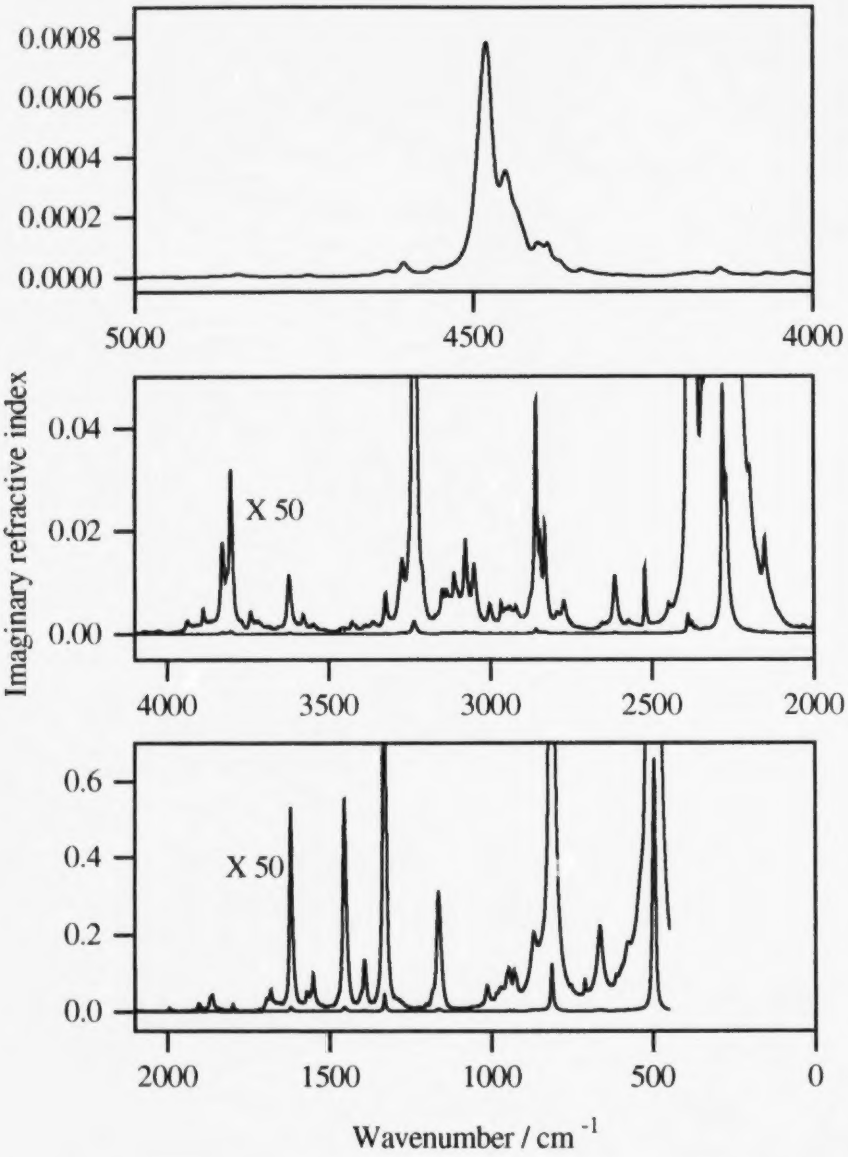

Figure 3.10. Imaginary refractive index, $k(\tilde{\nu})$, spectrum between 5000 and 450 cm^{-1} of benzene-d$_6$ at 25°C. The scale labels in the middle and bottom boxes are for the lower spectrum in the box; they must be divided by 50 for the upper spectrum in the box.

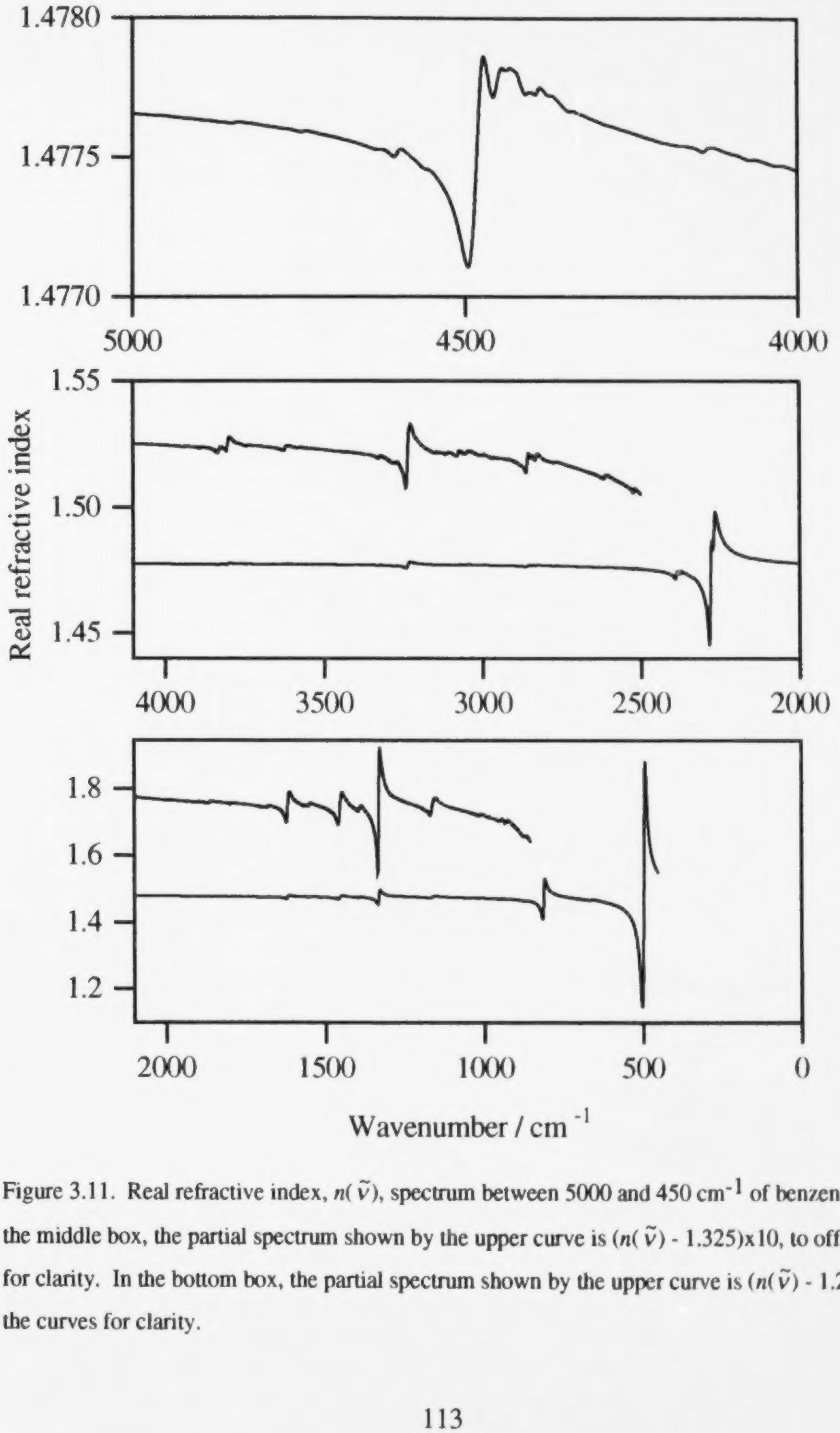

Figure 3.11. Real refractive index, $n(\tilde{\nu})$, spectrum between 5000 and 450 cm^{-1} of benzene-d_6 at 25°C. In the middle box, the partial spectrum shown by the upper curve is $(n(\tilde{\nu}) - 1.325)\mathrm{x}10$, to offset the curves for clarity. In the bottom box, the partial spectrum shown by the upper curve is $(n(\tilde{\nu}) - 1.27)\mathrm{x}8.5$, to offset the curves for clarity.

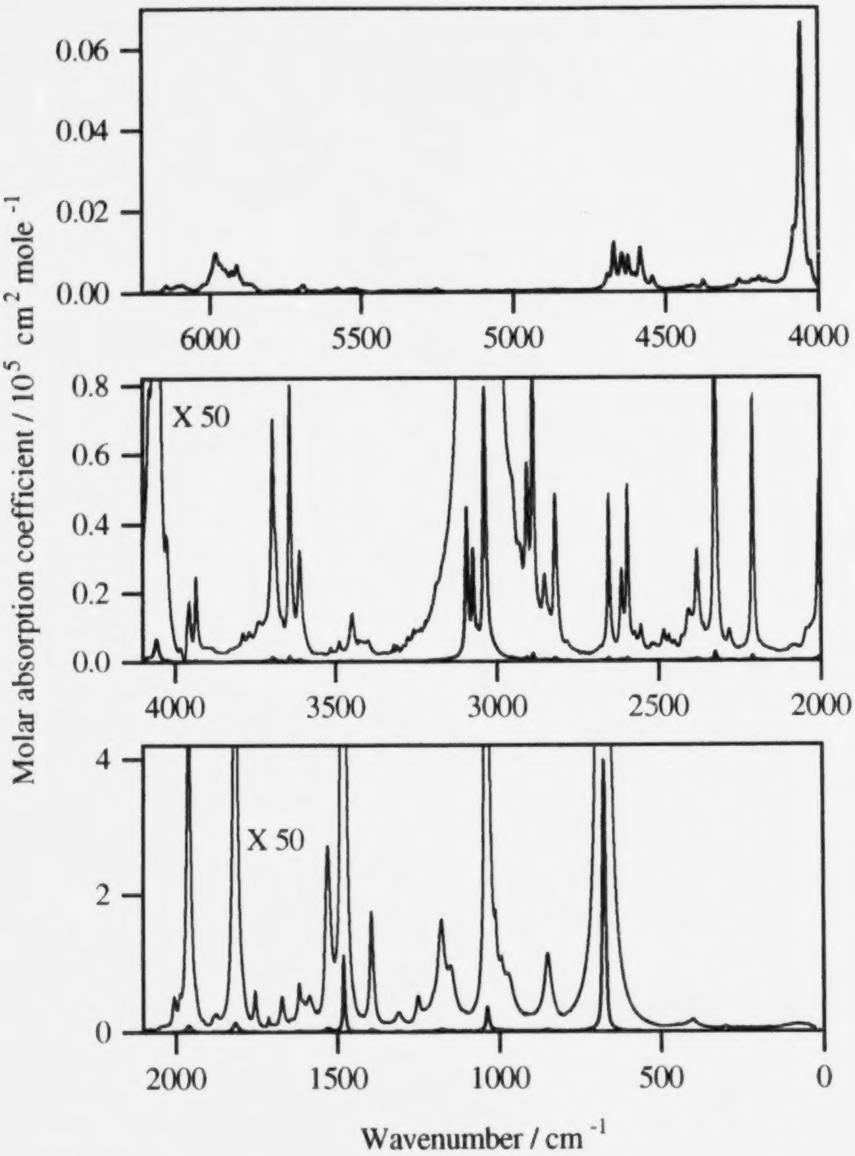

Figure 3.12. Molar absorption coefficient, $E_m(\tilde{\nu})$, spectrum between 6225 and 30 cm^{-1} of benzene-h$_6$ at 25°C. The ordinate scale labels in the middle and bottom boxes are for the lower spectrum in the box; they must be divided by 50 and 75, as shown, for the upper spectrum in the box.

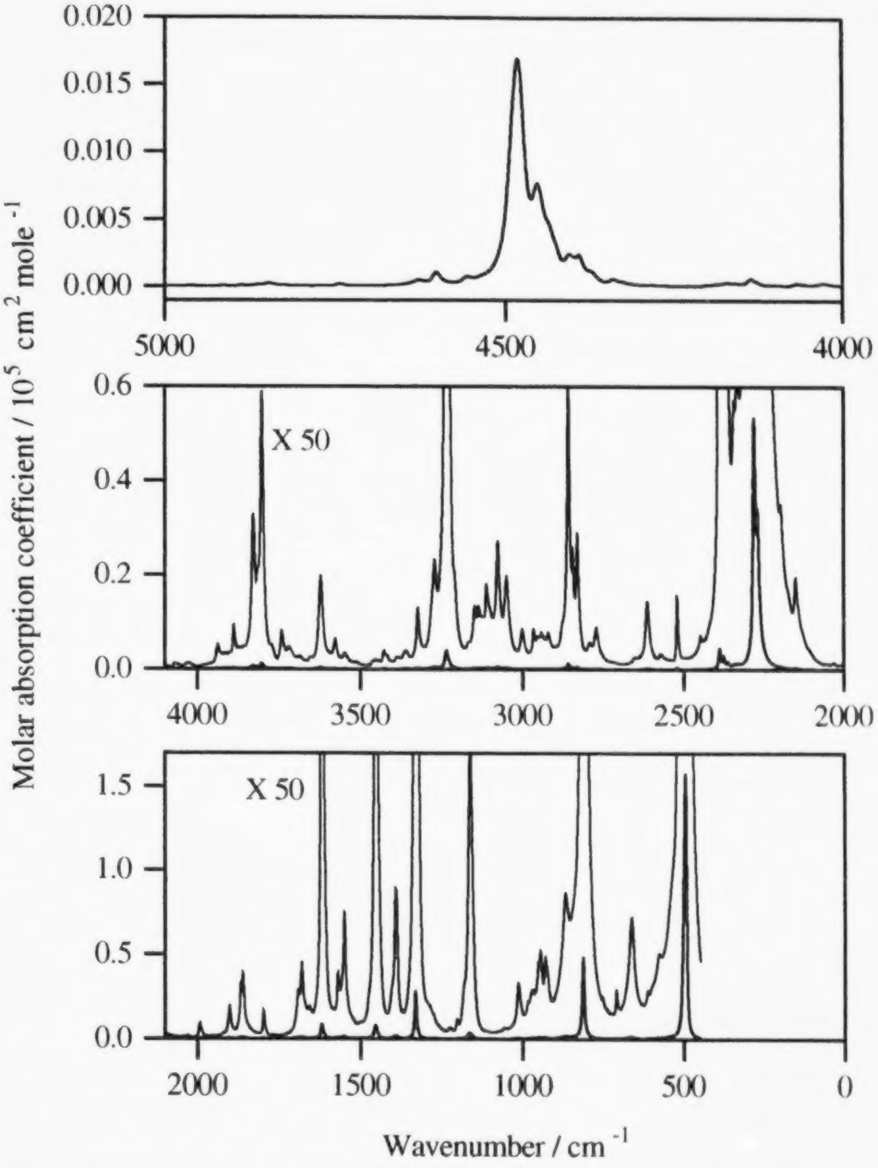

Figure 3.13. Molar absorption coefficient, $E_m(\tilde{\nu})$, spectrum between 5000 and 450 cm^{-1} of benzene-d$_6$ at 25°C. The ordinate scale labels in the middle and bottom boxes are for the lower spectrum in the box; they must be divided by 50 and 75, as shown, for the upper spectrum in the box.

Chapter 4

Secondary Infrared Absorption Standards

Infrared wavenumber calibration standards were first established in the late 1950's by the Commission on Molecular Structure and Spectroscopy of the International Union of Pure and Applied Chemistry (IUPAC)[156]. They were later extended into the far infrared[157, 165, 166] and were revised in a second edition of the *Tables of Wavenumbers for the Calibration of Infrared Spectrometers*[157].

The situation concerning infrared intensity standards is very different, and until the work described here, spectroscopists have not had any recognized intensity standards. It was mentioned in Chapters 1 and 3 that the optical constants of benzene-h_6 can be used as secondary infrared intensity standards. In this chapter the optical constants of benzene-h_6 presented in Chapter 3 are used, along with the optical constants of toluene, chlorobenzene and dichloromethane measured separately[47-49], to establish secondary infrared intensity standards. The work to establish these standards was done under the direction of a Working Party of the Commission on Molecular Structure and Spectroscopy of the Physical Chemistry Division of IUPAC. A brief outline of the steps taken by the Working Party to establish secondary infrared standards is next presented and then the standards themselves are discussed in section 4.1.

In 1983, the Commission on Molecular Structure and Spectroscopy of the Physical Chemistry Division of IUPAC created a Working Party to establish secondary infrared intensity standards, particularly standards to calibrate liquid phase measurements. Dr. R. Norman Jones of the National Research Council of Canada was chairman of the Working Party and Dr. John E. Bertie of the University of Alberta was secretary. The author joined the project in 1990 and it is since that time that most of the work of determining the standards was done.

The first step taken by the Working Party was to select a series of bands that would be suitable as possible standards. The four liquids benzene-h_6, toluene, chlorobenzene and dichloromethane were ultimately selected as the standard liquids. Once these liquids were selected, spectra of the standards had to be measured and a study of the accuracy of these spectra was necessary. For this purpose the Working Party solicited experimental absorbance spectra of the selected liquids from different spectroscopists. These experimental absorbance spectra were converted to complex refractive index spectra and molar absorption coefficient spectra by the procedures discussed in Chapter 2. The calculation and study of the accuracy of the complex refractive index spectra and the molar absorption coefficient spectra of benzene-h_6 was discussed in Chapter 3. An identical study of toluene[47] was carried out by Y. Apelblat and the author. Further, identical studies of chlorobenzene[48] and of dichloromethane[49] were carried out by Y. Apelblat and by Z. Lan and Y. Apelblat, respectively.

From these studies, standards were developed based on 43 band groups from the spectra of the four standard liquids. These standards were presented to and accepted by the Commission on Molecular Structure and Spectroscopy and the Physical Chemistry Division of IUPAC during the 37th General Assembly at Lisbon in August 1993. They are in press as the monograph *Tables of Intensities for the Calibration of Infrared Spectroscopic Measurements in the Liquid Phase*[167].

The standard band groups and their accuracy are discussed in section 4.1. An illustration of the use of these standards is presented in section 4.2.

4.1 Standard Band Groups

Benzene-h_6, toluene, chlorobenzene and dichloromethane were chosen as standard liquids on the basis of their chemical and spectroscopic suitability. In making the choice some considerations were their ready availability in high purity, their simple molecular structure, and the absence of conformational or hydrogen bonding equilibria which would have tended to accentuate temperature effects on the intensities and profiles. An additional consideration for including toluene, chlorobenzene and dichloromethane was their relatively low toxicity[168-170] which makes them more convenient for use in some industrial laboratories.

The band groups selected as standards derive from a data base of 786 bands of 13 organic liquids measured by Jones and co-workers[18, 45]. Initially 7 of these liquids (nitromethane, dichloromethane, dibromomethane, benzene-h_6, chlorobenzene, bromobenzene, and hexafluorobenzene) were selected as appropriate[171]. These were later reduced to the three liquids, benzene-h_6, chlorobenzene and dichloromethane. To these toluene was added during the course of the work.

Standards based on 15 band groups of benzene-h_6, 8 band groups of toluene, 12 band groups of chlorobenzene and 8 band groups of dichloromethane were developed. The spectral regions of the 43 standard band groups are shown in Table 4.1. Collectively, they are suitable for calibrations between 4800 and 600 cm^{-1}. For each standard band group the monograph contains a graph of the molar absorption coefficient spectrum, a graph of the real refractive index spectrum, a table of the real and imaginary refractive indices and molar absorption coefficient values, and a listing of the spectral range and standard areas under the band group in the molar absorption coefficient spectrum. To illustrate what is contained in the monograph, the first two pages presented for each band group and the first page of the table presented for each band group are shown in Figure 4.1 and 4.2 and Table 4.2 for Band 11 (1565 - 1420 cm^{-1}) of benzene-h_6. The real refractive index spectra are estimated to be accurate to ±0.2%. The imaginary refractive index spectra and the molar absorption coefficient spectra are estimated to be accurate to $\leq \pm 3\%$ in regions of absorption and $\leq \pm 10\%$ in the baseline. The areas are estimated to be accurate to within ±1 to ±2%, in general.

The intensity standards can be used to calibrate other transmission measurements as well as measurements by other techniques such as attenuated total reflection. The calibration of transmission cells is discussed in section 4.2. The path lengths of the transmission cells that can be calibrated by each band group is included in Table 4.1. Transmission cells with path lengths between 2 and 5000 μm can be calibrated. The calibration of ATR cells will not be discussed here, but recent measurements[28, 29, 155, 172-174] from this laboratory using the Circle cell were calibrated[155, 162] with benzene-h_6. The resulting optical constants agreed to within ±3% with those measured by transmission spectroscopy[29, 174].

Table 4.1. Secondary infrared intensity standards.

Standard Band	Spectral Range / cm^{-1}	Suitable Path lengths / μm
Benzene-h_6 Band 1	4765-4490	250 - 1000
Benzene-h_6 Band 2	4150-3965	25 - 100
Benzene-h_6 Band 3	3820-3525	100 - 500
Benzene-h_6 Band 4	3540-3360	1000 - 5000
Benzene-h_6 Band 5	3250-2915	2 - 10
Benzene-h_6 Band 6	2445-2250	100 - 500
Benzene-h_6 Band 7	2260-2125	250 - 1000
Benzene-h_6 Band 8	2075-1900	25 - 100
Benzene-h_6 Band 9	1905-1720	25 - 100
Benzene-h_6 Band 10	1660-1560	250 - 1000
Benzene-h_6 Band 11	1565-1420	2 - 10
Benzene-h_6 Band 12	1430-1350	100 - 250
Benzene-h_6 Band 13	1365-1090	100 - 250
Benzene-h_6 Band 14	1100-905	5 - 25
Benzene-h_6 Band 15	915-800	100 - 500
Toluene Band 1	3155-2765	5 - 25
Toluene Band 2	1980-1905	100 - 250
Toluene Band 3	1915-1835	100 - 250
Toluene Band 4	1840-1750	100 - 250
Toluene Band 5	1760-1710	100 - 500
Toluene Band 6	1655-1550	10 - 25
Toluene Band 7	1515-1395	2 - 10
Toluene Band 8	715-655	2 - 10
Chlorobenzene Band 1	3245-2925	25 - 100
Chlorobenzene Band 2	2005-1900	100 - 250
Chlorobenzene Band 3	1910-1830	100 - 250
Chlorobenzene Band 4	1840-1750	100 - 250
Chlorobenzene Band 5	1760-1685	100 - 500
Chlorobenzene Band 6	1610-1540	5 - 25
Chlorobenzene Band 7	1535-1405	2 - 5
Chlorobenzene Band 8	1350-1245	100 - 500
Chlorobenzene Band 9	1145-1045	2 - 10

Table 4.1. Continued.

Standard Band	Spectral Range / cm^{-1}	Suitable Path lengths / µm
Chlorobenzene Band 10	1050-965	2 - 10
Chlorobenzene Band 11	955 - 845	25 - 100
Chlorobenzene Band 12	725-645	2 - 10
Dichloromethane Band 1	4080-3850	250 - 1000
Dichloromethane Band 2	3335-2865	10 - 100
Dichloromethane Band 3	2755-2620	250 - 1000
Dichloromethane Band 4	2620-2475	1000 - 3000
Dichloromethane Band 5	2485-2375	250 - 1000
Dichloromethane Band 6	2385-2210	100 - 250
Dichloromethane Band 7	1360-1180	2 - 10
Dichloromethane Band 8	970-855	25 - 100

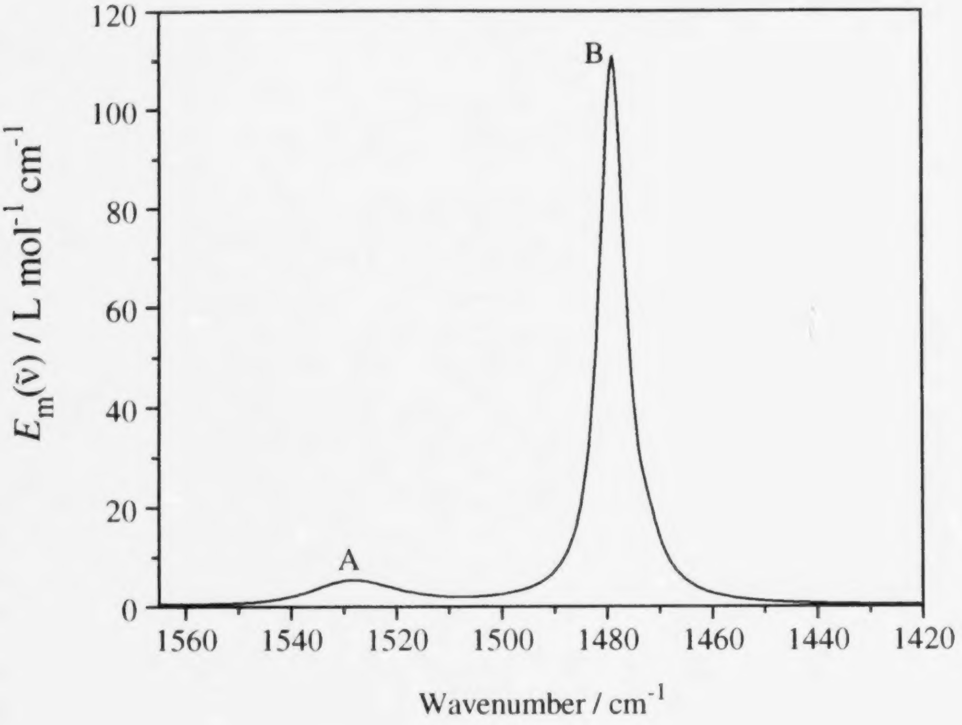

Maxima	$\tilde{\nu}$ (cm^{-1})	E_m	k
A	1528.0	5.420	0.007269
B	1479.0	110.8	0.1536

Total range (cm^{-1})	1565.0 - 1420.0
Integration range (cm^{-1})	1562.5 - 1422.0
Area above base (L mol^{-1}cm^{-2})	1079 ± 5
Total area (L mol^{-1}cm^{-2})	1151 ± 7
Total number of data points	291

Figure 4.1. Molar absorption coefficient spectrum of Benzene-h_6 Band 11 (1565 to 1420 cm^{-1}).

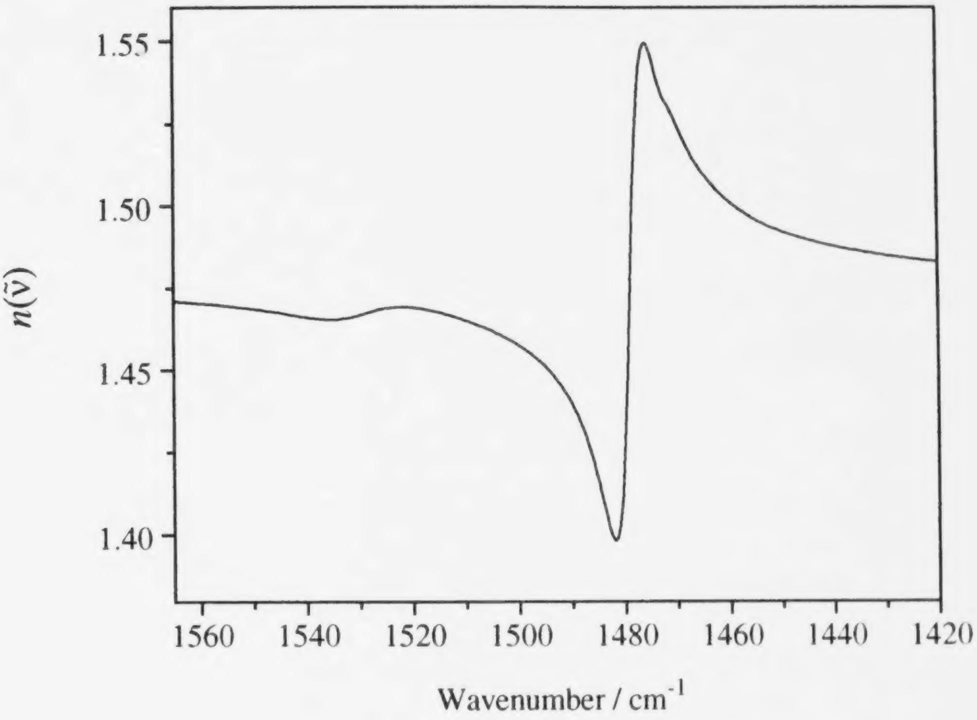

Real refractive index ($n(\tilde{\nu})$)

$\tilde{\nu}$ (cm^{-1})	Maxima		Minima
1535.0			1.46537
1522.0	1.46914		
1482.0			1.39810
1476.0	1.54959		
(1472.0)		(1.53149)	

Figure 4.2. Real refractive index spectrum of Benzene-h_6 Band 11 (1565 to 1420 cm^{-1}).

Table 4.2. Benzene-h_6 Band 11 (1565 to 1420 cm^{-1}).

$\tilde{\nu}$ (cm^{-1})	$n(\tilde{\nu})$	$k(\tilde{\nu})$	$E_m(\tilde{\nu})$ [a]	$\tilde{\nu}$ (cm^{-1})	$n(\tilde{\nu})$	$k(\tilde{\nu})$	$E_m(\tilde{\nu})$ [a]
1565.0	1.47104	0.0007475	0.5708	1539.5	1.46593	0.002934	2.204
1564.5	1.47099	0.0007433	0.5674	1539.0	1.46584	0.003116	2.340
1564.0	1.47092	0.0007353	0.5611	1538.5	1.46576	0.003286	2.467
1563.5	1.47085	0.0007294	0.5564	1538.0	1.46565	0.003483	2.614
1563.0	1.47078	0.0007295	0.5563	1537.5	1.46557	0.003690	2.768
1562.5	1.47071	0.0007323	0.5583	1537.0	1.46549	0.003928	2.946
1562.0	1.47064	0.0007286	0.5553	1536.5	1.46543	0.004157	3.117
1561.5	1.47056	0.0007321	0.5578	1536.0	1.46539	0.004393	3.293
1561.0	1.47048	0.0007472	0.5691	1535.5	1.46538	0.004658	3.490
1560.5	1.47041	0.0007700	0.5863	1535.0	1.46537	0.004906	3.674
1560.0	1.47035	0.0007842	0.5969	1534.5	1.46540	0.005161	3.864
1559.5	1.47029	0.0007793	0.5929	1534.0	1.46545	0.005439	4.071
1559.0	1.47021	0.0007886	0.5999	1533.5	1.46553	0.005686	4.254
1558.5	1.47014	0.0008076	0.6141	1533.0	1.46564	0.005938	4.441
1558.0	1.47009	0.0008059	0.6126	1532.5	1.46576	0.006154	4.601
1557.5	1.47002	0.0008002	0.6081	1532.0	1.46589	0.006365	4.758
1557.0	1.46993	0.0007976	0.6059	1531.5	1.46607	0.006578	4.915
1556.5	1.46985	0.0007965	0.6049	1531.0	1.46624	0.006749	5.041
1556.0	1.46976	0.0008067	0.6124	1530.5	1.46644	0.006903	5.155
1555.5	1.46966	0.0008214	0.6234	1530.0	1.46667	0.007043	5.257
1555.0	1.46957	0.0008442	0.6405	1529.5	1.46688	0.007141	5.329
1554.5	1.46949	0.0008682	0.6585	1529.0	1.46713	0.007222	5.387
1554.0	1.46942	0.0008768	0.6648	1528.5	1.46736	0.007262	5.416
1553.5	1.46933	0.0008830	0.6693	1528.0	1.46758	0.007269	5.420
1553.0	1.46923	0.0008955	0.6786	1527.5	1.46782	0.007252	5.405
1552.5	1.46913	0.0009146	0.6928	1527.0	1.46804	0.007207	5.370
1552.0	1.46904	0.0009309	0.7049	1526.5	1.46823	0.007131	5.311
1551.5	1.46893	0.0009542	0.7223	1526.0	1.46843	0.007027	5.232
1551.0	1.46883	0.0009808	0.7422	1525.5	1.46860	0.006912	5.145
1550.5	1.46871	0.001008	0.7624	1525.0	1.46874	0.006773	5.040
1550.0	1.46861	0.001042	0.7883	1524.5	1.46888	0.006598	4.908
1549.5	1.46851	0.001071	0.8095	1524.0	1.46897	0.006430	4.781
1549.0	1.46839	0.001101	0.8318	1523.5	1.46905	0.006244	4.642
1548.5	1.46828	0.001135	0.8573	1523.0	1.46910	0.006068	4.509
1548.0	1.46816	0.001175	0.8876	1522.5	1.46913	0.005886	4.372
1547.5	1.46803	0.001225	0.9246	1522.0	1.46914	0.005681	4.219
1547.0	1.46790	0.001273	0.9610	1521.5	1.46913	0.005498	4.082
1546.5	1.46777	0.001336	1.008	1521.0	1.46910	0.005316	3.945
1546.0	1.46764	0.001397	1.053	1520.5	1.46905	0.005102	3.785
1545.5	1.46752	0.001465	1.104	1520.0	1.46898	0.004913	3.643
1545.0	1.46738	0.001543	1.163	1519.5	1.46887	0.004715	3.495
1544.5	1.46725	0.001612	1.215	1519.0	1.46876	0.004542	3.366
1544.0	1.46711	0.001694	1.276	1518.5	1.46862	0.004390	3.253
1543.5	1.46696	0.001798	1.354	1518.0	1.46848	0.004233	3.135
1543.0	1.46683	0.001904	1.433	1517.5	1.46833	0.004092	3.030
1542.5	1.46668	0.002032	1.529	1517.0	1.46818	0.003958	2.929
1542.0	1.46656	0.002151	1.619	1516.5	1.46799	0.003809	2.818
1541.5	1.46643	0.002273	1.709	1516.0	1.46781	0.003687	2.727
1541.0	1.46628	0.002421	1.821	1515.5	1.46760	0.003566	2.637
1540.5	1.46616	0.002581	1.940	1515.0	1.46740	0.003463	2.560
1540.0	1.46605	0.002747	2.064	1514.5	1.46719	0.003368	2.489

[a] The unit of E_m is L $mole^{-1}$ cm^{-1}.

4.2 An Application to Quantitative Analysis

4.2.1 Program IRYTRUE

To encourage uniformity in the application of these standards in quantitative analysis, an algorithm was developed to calibrate transmission cells. The algorithm uses the area under the standard molar absorption coefficient band group above a linear baseline to calibrate transmission measurements. It is recommended that this area also be used when these standards are used to calibrate other techniques. This algorithm has been incorporated into a computer program IRYTRUE. This program is described in detail in two appendices to the monograph[167]. The program has been tested over the past 5 years in several laboratories on a wide range of IBM compatible personal computers with the MS-DOS and OS/2 operating systems.

The original version of IRYTRUE was written by D. J. Moffatt of the National Research Council of Canada in Ottawa. When the author joined the project to develop secondary standards in 1990, he assumed responsibility for the maintenance and improvement of the program. Since that time the program has been significantly improved and modified. The algorithm was modified so that transmission measurements are calibrated using the area above a linear baseline instead of the area above zero ordinate. This drastically reduced the number of iterations for the program to calibrate transmission measurements. Originally as many as 6 or more iterations were required for the calibration and now the calibration can usually be performed in 2 iterations. A graphical display of the standard and experimental molar absorption coefficient spectra and the option to perform calibrations on several different bands in the same experimental absorbance spectrum were added.

The objective of the program is to evaluate a "*cell constant*". This replaces the cell path length used in conventional infrared quantitative analysis of liquid samples. The principal contribution to the cell constant comes from the path length, but it also contains contributions from the disturbance of the optical beam, defocusing effects consequent on the insertion of the cell into the beam, and other systematic effects which distort the measurements.

To calibrate a transmission cell, IRYTRUE requires as input an experimental absorbance spectrum for at least one of the standard calibration band groups measured in the cell. This spectrum must be stored in an ASCII "Y" file (see section 2.6). This file can contain more than the wavenumber range of one standard band group, but IRYTRUE only uses the wavenumber range of one standard band group at a time. IRYTRUE provides the option of performing multiple calibrations using the same experimental absorbance spectrum but different standard band groups.

IRYTRUE first computes an estimate of the cell constant using the peak height of the experimental absorbance spectrum (EA_{max}) and the peak height of the standard molar absorption coefficient spectrum ($SE_{\mathrm{m,\,max}}$) via the equation:

$$CC = \frac{EA_{\mathrm{max}}}{Conc \times SE_{\mathrm{m,\,max}}} \qquad (4.1.1)$$

where CC is the cell constant and $Conc$ is the molar concentration of the liquid at 25°C. The value of $Conc$ is built into the program for the four standard liquids and thus the user does not need to supply it.

IRYTRUE then computes the experimental E_{m} spectrum based on this estimated cell constant. The program corrects the experimental E_{m} spectrum for reflection losses and non-ideal apparent absorbance across the band group by subtracting a linear correction so that the ordinate values at the integration limits are the same as the ordinate values at the integration limits in the standard E_m spectrum.

IRYTRUE calculates the area under this experimental E_m spectrum above a linear baseline between the ordinate values at the integration limits. This area is then ratioed to the corresponding area of the standard band to yield a correction factor. IRYTRUE next improves the first approximation to the cell constant, by multiplying the initial cell constant by this correction factor, and computes a new set of experimental E_m values using this cell constant in place of the previous value. The baseline of the experimental E_m spectrum is again set to be the same as the standard E_m spectrum as described above.

IRYTRUE next calculates a new correction factor by ratioing the new area above the baseline in the experimental E_m spectrum to that in the standard E_m spectrum. This procedure is iterated until a constant value for the cell constant is achieved. Because the area above the baseline is used to iterate the cell constant the final value is usually achieved after 1 or 2 iterations. This cell constant can then be used in place of the cell path length in subsequent analytical calculations.

If desired this procedure can be repeated using different calibration bands in different regions of the same experimental absorbance spectrum, to check the value of the cell constant. The final output from IRYTRUE tabulates all calibrations for a given calibration spectrum and calculates an average cell constant.

4.2.2 Reproducibility and Accuracy of Calibrated Cell Constants

IRYTRUE was used to calibrate 11, 113 and 532 μm transmission cells with several different standard band groups. For the 11 μm cell, 3 benzene-h_6 band groups, 4 toluene band groups, 6 chlorobenzene band groups and 2 dichloromethane band groups were used. For the 113 µm cell, 7 benzene-h_6 band groups, 4 toluene band groups, 4 chlorobenzene band groups and 2 dichloromethane band groups were used. For the 532 µm cell, 6 benzene-h_6 band groups, 1 toluene band group, 2 chlorobenzene band groups and 4 dichloromethane band groups were used. The results are shown in Tables 4.3 - 4.5.

For the 11 µm cell, the cell constants calculated from the different standard bands vary by ~0.9 µm. This is about an 8% variation. The cell constants calculated for the 3 standard bands of benzene-h_6 vary by 0.47 µm, those for the 4 standard bands of toluene vary by 0.73 µm, those for the 6 standard bands of chlorobenzene vary by 0.64 and those for the 2 standard bands of dichloromethane vary by 0.07 µm.

For the 113 µm CaF_2 cell, the cell constants vary by about 5 µm, a 5% variation. The cell constants calculated for the 7 standard bands of benzene-h_6 vary by 5.2 µm, those for the 4 standard bands of toluene vary by 1.0 µm, those for the 4 standard bands of chlorobenzene vary by 0.0 µm and those for the 2 standard bands of dichloromethane vary by 2.9 µm.

For the 532 µm cell the cell constants vary by 10.5 µm, a 2% variation. The cell constants calculated for the 6 standard bands of benzene-h_6 vary by 9.3 µm, those for the 2 standard bands of chlorobenzene vary by 0.6 and those for the 4 standard bands of dichloromethane vary by 4.4 µm.

The average cell constant and its 95% confidence limit for each cell were calculated from all the bands used in Tables 4.3 - 4.5. These values are given in Table 4.6 along with the average and 95% confidence limit for each standard liquid for each cell. The results from different standard bands vary by several percent, particularly for the 11 µm cell (Table 4.3), but the 95% confidence limit of the average over several bands is in the range 1.6% to 0.3% of the average cell constant. The average cell constants calculated by using only one standard calibration liquid agree with the overall average within 1 to 3%.

The path length of each cell was also calculated, via program RNJ22A[135], from the fringe pattern observed in the experimental absorbance spectrum of the empty cell. These path lengths and 95% confidence limits are included in Table 4.6. Each path length is an average of at least 10 independently measured experimental absorbance spectra of the empty cell. The cell constants calculated from the individual standard calibration liquids agree with the cell path lengths within 0.54, 1.5 and 5.8 µm for the 11, 113 and 532 µm cells, respectively. This is about a 1% difference for the 113 and 532 µm cells and a 5% difference for the 11 µm cell. The average cell constant over all standard liquids, agrees with the cell path length within 0.3, 0.5 and 1.0 µm, or 2.8, 0.4 and 0.2% respectively for the 11, 113 and 532 µm cells.

It is clear from the above that the standard calibration bands can be used to calculate cell constants that are accurate to better than 3% for very thin cells and better that 1% for thicker cells. This accuracy is useful for improving the comparability of results obtained from different instruments and in different laboratories. It is to be noted that such accuracy can only be obtained when more then one standard band is used to calibrate the cell. Preferably more than one standard liquid should be used to calibrate the cell, but acceptable results can be obtained even when only one standard liquid is used as long as several bands are used for that liquid.

Table 4.3. Calibration of 11 μm KBr cell.

Calibration Band	Cell Constant / μm
Benzene-h_6 5	10.63
Benzene-h_6 11	11.10
Benzene-h_6 14	10.99
Toluene 1	10.85
Toluene 6	11.10
Toluene 7	10.90
Toluene 8	10.37
Chlorobenzene 1	10.23
Chlorobenzene 6	10.39
Chlorobenzene 9	10.69
Chlorobenzene 10	10.87
Chlorobenzene 11	10.35
Chlorobenzene 12	10.52
Dichloromethane 2	11.03
Dichloromethane 7	11.10

Table 4.4. Calibration of 113 μm CaF_2 cell.

Calibration Band	Cell Constant / μm
Benzene-h_6 2	114.3
Benzene-h_6 3	113.6
Benzene-h_6 6	113.2
Benzene-h_6 7	114.9
Benzene-h_6 8	112.6
Benzene-h_6 10	116.4
Benzene-h_6 12	111.2
Toluene 2	113.7
Toluene 3	114.6
Toluene 4	114.6
Toluene 5	113.6
Chlorobenzene 2	113.4
Chlorobenzene 3	113.4
Chlorobenzene 4	113.4
Chlorobenzene 5	113.4
Dichloromethane 2	110.0
Dichloromethane 6	112.9

Table 4.5. Calibration of 532 μm KBr cell.

Calibration Band	Cell Constant / μm
Benzene-h_6 3	529.4
Benzene-h_6 4	531.8
Benzene-h_6 6	527.4
Benzene-h_6 7	534.2
Benzene-h_6 10	536.7
Benzene-h_6 15	527.8
Toluene 5	526.2
Chlorobenzene 5	532.6
Chlorobenzene 8	532.0
Dichloromethane 1	529.2
Dichloromethane 3	530.4
Dichloromethane 4	533.6
Dichloromethane 5	531.6

Table 4.6. Comparison of cell constants and path lengths.

	Cell Constant / μm		
	11 μm KBr	113 μm CaF_2	532 μm KBr
Benzene-h_6	10.91 ± 0.61	113.7 ± 1.5	531.2 ± 3.9
Toluene	10.81 ± 0.49	114.1 ± 0.9	526.2
Chlorobenzene	10.51 ± 0.25	113.4 ± 0.0	532.3 ± 3.8
Dichloromethane	11.07 ± 0.44	111.5 ± 18.4	531.2 ± 3.0
Average of all bands	10.74 ± 0.17	113.5 ± 0.7	531.0 ± 1.8
Cell path length from fringes	11.05 ± 0.05	113.0 ± 1.0	532.0 ± 0.2

Chapter 5

Integrated Intensities, Transition Moments and Dipole Moment Derivatives of Liquid Benzene-h_6 and Benzene-d_6

In Chapter 4, the optical constants of benzene-h_6 as secondary infrared intensity standards were discussed. In this chapter the imaginary molar polarizability spectra of benzene-h_6 and benzene-d_6 calculated from the optical constants presented in Chapter 3 are used to determine the transition moments and dipole moments derivatives for these molecules in the liquid phase.

The real and imaginary refractive index spectra of benzene-h_6 and benzene-d_6 from Chapter 3 were used to calculate the complex dielectric constant spectra and the complex molar polarizability spectra. These are presented in section 5.1, in which evidence is presented to show that the imaginary molar polarizability spectrum is a more reliable indicator of the molecular properties and behaviour of the liquid than either the imaginary refractive index or the imaginary dielectric constant spectra, provided that the Lorentz local field is accurate. Thus the integrated intensities are most reliably obtained from the imaginary polarizability spectrum, $\alpha''_m(\tilde{\nu})$.

Section 5.2 presents the methods used to determine the integrated intensities from the α''_m spectrum and the results obtained. To obtain the intensities, the molar polarizability spectrum has to be separated into contributions from the different transitions. This can be done by somewhat arbitrarily assigning integration limits to the bands and assuming the area between these limits is due to a specific transition. Another way to try and separate the contributions of the different transitions, is to fit the imaginary polarizability spectrum with bands of an appropriate shape and calculate the integrated intensity of the component bands. The general theory of infrared spectra of liquids[29, 30] indicates that the bands in the α_m'' spectrum have the CDHO bandshape of the Classical Damped Harmonic Oscillator (section 1.3). Thus, the molar polarizability spectra were fitted with CDHO bands. The integrated intensities C_j are the area under the $\tilde{\nu}\alpha_m''$ spectra of the bands required to fit the spectra, and these were calculated from the band parameters, effectively taking the integral from zero to infinity. Thus, curve fitting has the advantage that the total area due to a specific transition can be obtained free of error due to integration limits. The major disadvantage of curve fitting is that bands that are not obviously present in the spectrum often need to be added to obtain a good fit. This raises the question of whether these bands are real or are an artifact of the fitting procedure. It is shown in section 5.2 that the imaginary molar polarizability spectra of benzene-h_6 and benzene-d_6 were fitted very well and very few bands that were not obviously present in the experimental spectra were needed.

For a fundamental transition under the double harmonic approximation, the transition moment directly gives the dipole moment derivative with respect to the normal coordinate. Since the normal coordinates are mass weighted it is necessary to remove this mass weighting so that the dipole moment derivatives for different isotopic molecules refer to the same quantity and can be compared. This amounts to converting the dipole moments derivatives with respect to the normal coordinates to dipole moment derivatives with respect to symmetry coordinates or internal coordinates. This requires knowledge of the normal coordinates of the different isotopic molecules.

In section 5.3, the wavenumbers of the fundamental vibrations of liquid benzene-h_6 and benzene-d_6 are used to determine the normal coordinates. These normal coordinates are used in section 5.4 to calculate the dipole moments derivatives with respect to symmetry coordinates and internal coordinates from the dipole moment derivatives with respect to the normal coordinates.

Before going further, it is necessary to define the nomenclature used to describe the vibrations of benzene. Isolated benzene-h_6 and benzene-d_6 both have D_{6h} symmetry. Their vibrational representation is[62] $2A_{1g} + A_{2g} + A_{2u} + 2B_{1u} + 2B_{2g} + 2B_{2u} + E_{1g} + 3E_{1u} + 4E_{2g} + 2E_{2u}$. The infrared active vibrations are in $A_{2u} + 3E_{1u}$ and the Raman active vibrations are in $2A_{1g} + E_{1g} + 4E_{2g}$. These activities are strictly valid only for the gas phase but these vibrations also yield the strongest absorption in the spectra of the liquid. The intensities of the fundamentals that are infrared inactive in the gas phase but are observed in the liquid phase spectra are discussed in section 5.3.2.

Two numbering systems are used for the vibrations of benzene; Wilson's[102] and Herzberg's[175]. Wilson's system is only used for benzene but Herzberg's system is in general use. In both numbering systems the vibrations are numbered according to their symmetry and within each symmetry species Herzberg numbers in order of decreasing wavenumber but Wilson numbers in order of increasing wavenumber with one or two exceptions. The main difference between the two systems is the order in which the symmetry species are listed. Wilson's scheme uses the order of symmetry species in the Character Tables in Reference 62 and Herzberg's scheme uses the order in the Character Tables in Reference 175. Thus, for D_{6h} molecules like benzene, Herzberg's system numbers the A_{1g} vibrations first followed by the A_{1u}, A_{2g}, A_{2u}, B_{1g}, B_{1u}, B_{2g}, B_{2u}, E_{1g}, E_{1u}, E_{2g} and E_{2u} vibrations. For benzene the highest wavenumber A_{1g} vibration, the symmetric CH stretching mode, is ν_1 and the lowest wavenumber E_{2u} vibration, the ring deformation mode, is assigned the highest number, ν_{20}. Each component of a degenerate vibration is assigned the same number, but the two components are designated a or b, for example ν_{20a} and ν_{20b}. The fundamental vibrations of benzene are listed in Table 5.1 with their description in Herzberg's numbering scheme, with Wilson's included for convenient reference, and their gas-phase activity. Herzberg's numbering system is used in this thesis, following the suggestion of Miller[176].

5.1 Dielectric Constants, Molar Polarizabilities and Molecular Properties

From the complex refractive index spectra of benzene-h_6 and benzene-d_6 presented in Chapter 3, the molar absorption coefficient spectra, the complex dielectric constant spectra and the complex molar polarizability spectra were calculated by the equations summarized in section 1.3. The imaginary dielectric constant and molar polarizability spectra are shown in Figures 5.1 and 5.2 for benzene-h_6 and Figures 5.3 and 5.4 for benzene-d_6. The real dielectric constant and real molar polarizability spectra are shown in Figures 5.5 and 5.6 for benzene-h_6 and in Figures 5.7 and 5.8 for benzene-d_6.

From the graphs of the complex refractive index (Figures 3.7, 3.9, 3.10 and 3.11), the complex dielectric constant (Figures 5.1, 5.3, 5.5, and 5.7) and the complex molar polarizability (Figures 5.2, 5.4, 5.6 and 5.8) it is clear that the imaginary components of these complex quantities are qualitatively very similar as are the real components. This raises the questions of what differences exist between the quantities and whether each of the quantities can yield the same molecular information.

Table 5.1. Benzene-h_6 and benzene-d_6 vibrations.

Vibration	Herzberg Notation	Wilson Notation	Activity
A_{1g} CH stretch	ν_1	ν_2	Raman
A_{1g} CC stretch	ν_2	ν_1	Raman
A_{2g} HCC deformation	ν_3	ν_3	Inactive
A_{2u} CH out of plane bend	ν_4	ν_{11}	Infrared
B_{1u} CH stretch	ν_5	ν_{13}	Inactive
B_{1u} CCC deformation	ν_6	ν_{12}	Inactive
B_{2g} CH out of plane bend	ν_7	ν_5	Inactive
B_{2g} CCCC torsion	ν_8	ν_4	Inactive
B_{2u} CC stretch and HCC deformation	ν_9	ν_{14}	Inactive
B_{2u} CC stretch and HCC deformation	ν_{10}	ν_{15}	Inactive
E_{1g} CH out of plane bend	ν_{11}	ν_{10}	Raman
E_{1u} CH stretch	ν_{12}	ν_{20}	Infrared
E_{1u} CC stretch and HCC deformation	ν_{13}	ν_{19}	Infrared
E_{1u} CC stretch and HCC deformation	ν_{14}	ν_{18}	Infrared
E_{2g} CH stretch	ν_{15}	ν_7	Raman
E_{2g} CC stretch, HCC and CCC deformations	ν_{16}	ν_8	Raman
E_{2g} CC stretch, HCC and CCC deformations	ν_{17}	ν_9	Raman
E_{2g} CC stretch, HCC and CCC deformations	ν_{18}	ν_6	Raman
E_{2u} CH stretch	ν_{19}	ν_{17}	Inactive
E_{2u} CC stretch	ν_{20}	ν_{16}	Inactive

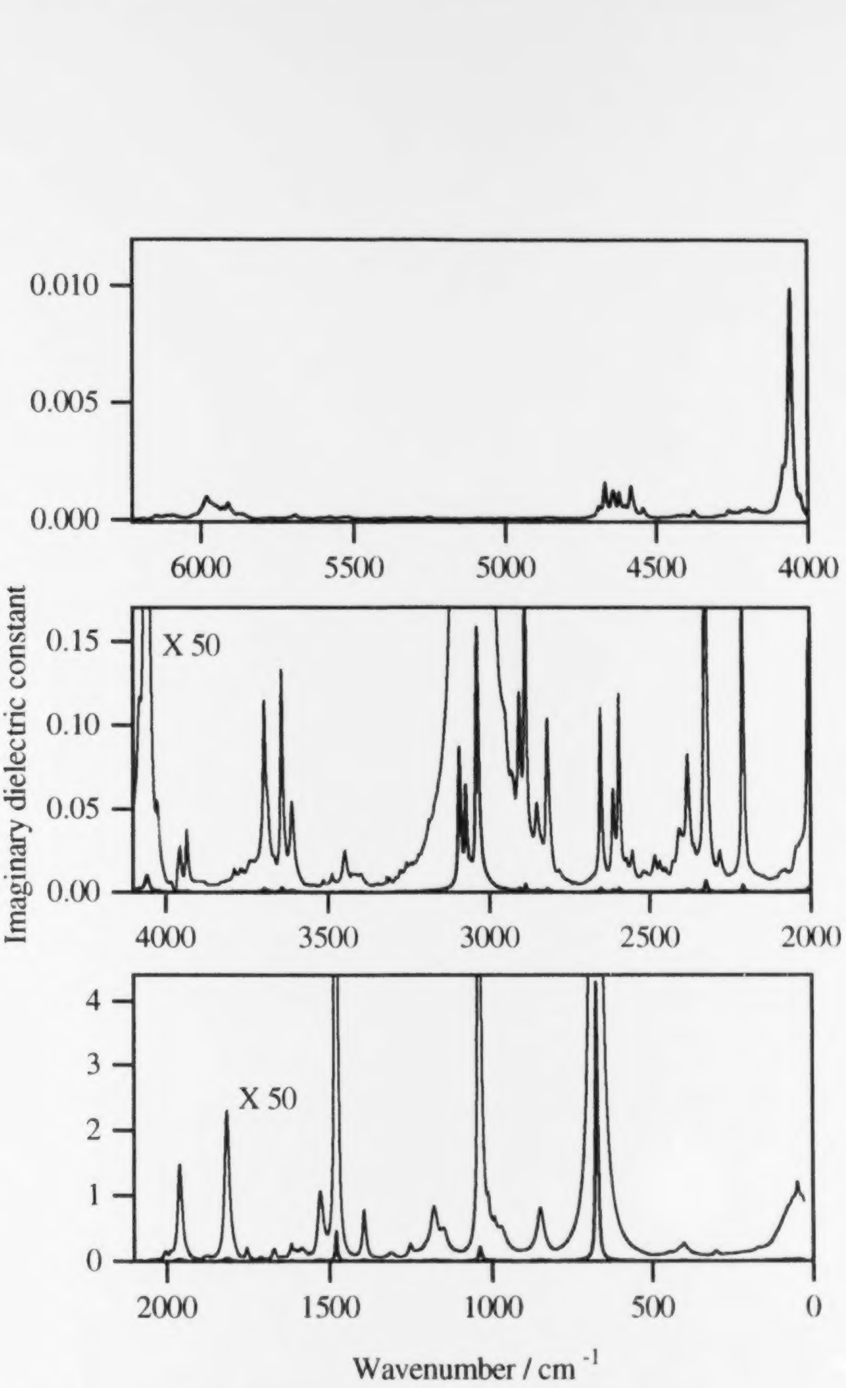

Figure 5.1. Imaginary dielectric constant spectrum of benzene-h$_6$. In the middle and bottom boxes, the ordinate scales are for the lower curves. They need to be divided by 50 for the upper curves.

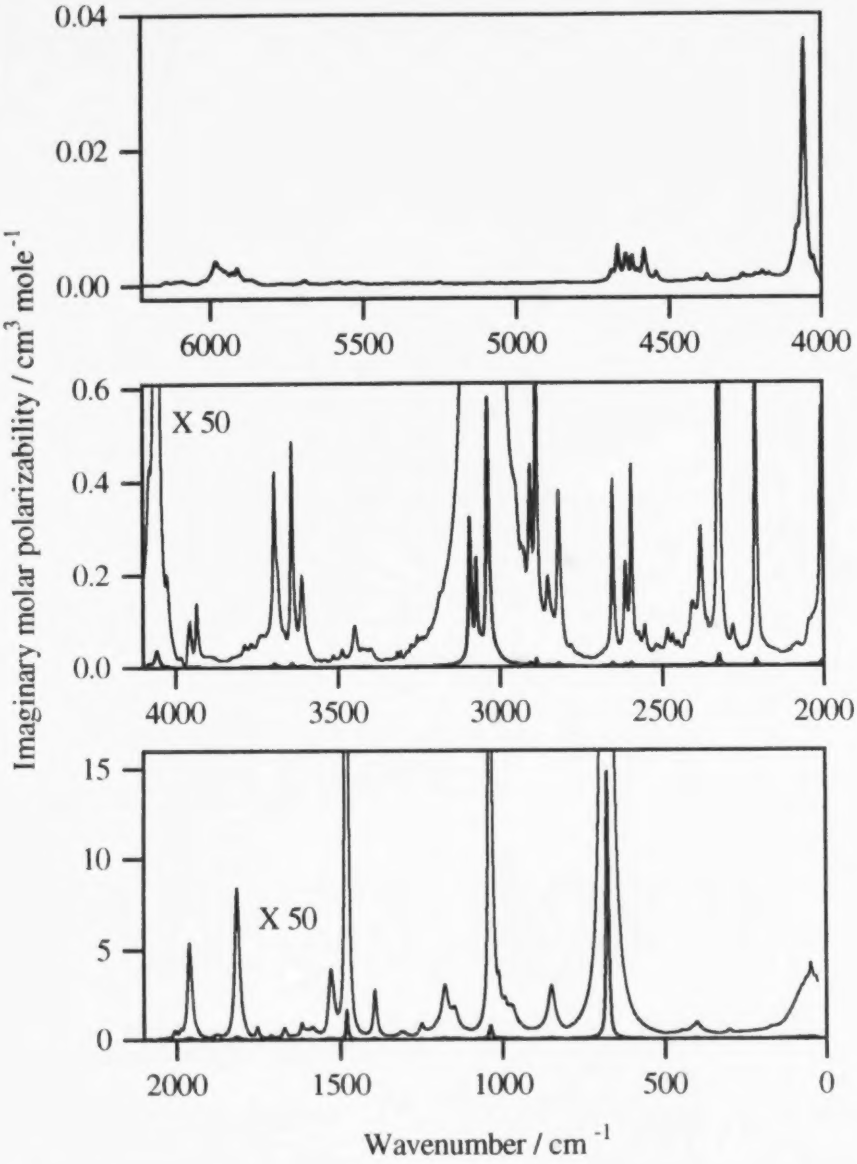

Figure 5.2. Imaginary molar polarizability spectrum of benzene-h$_6$. In the middle and bottom boxes, the ordinate scales are for the lower curves. They need to be divided by 50 for the upper curves.

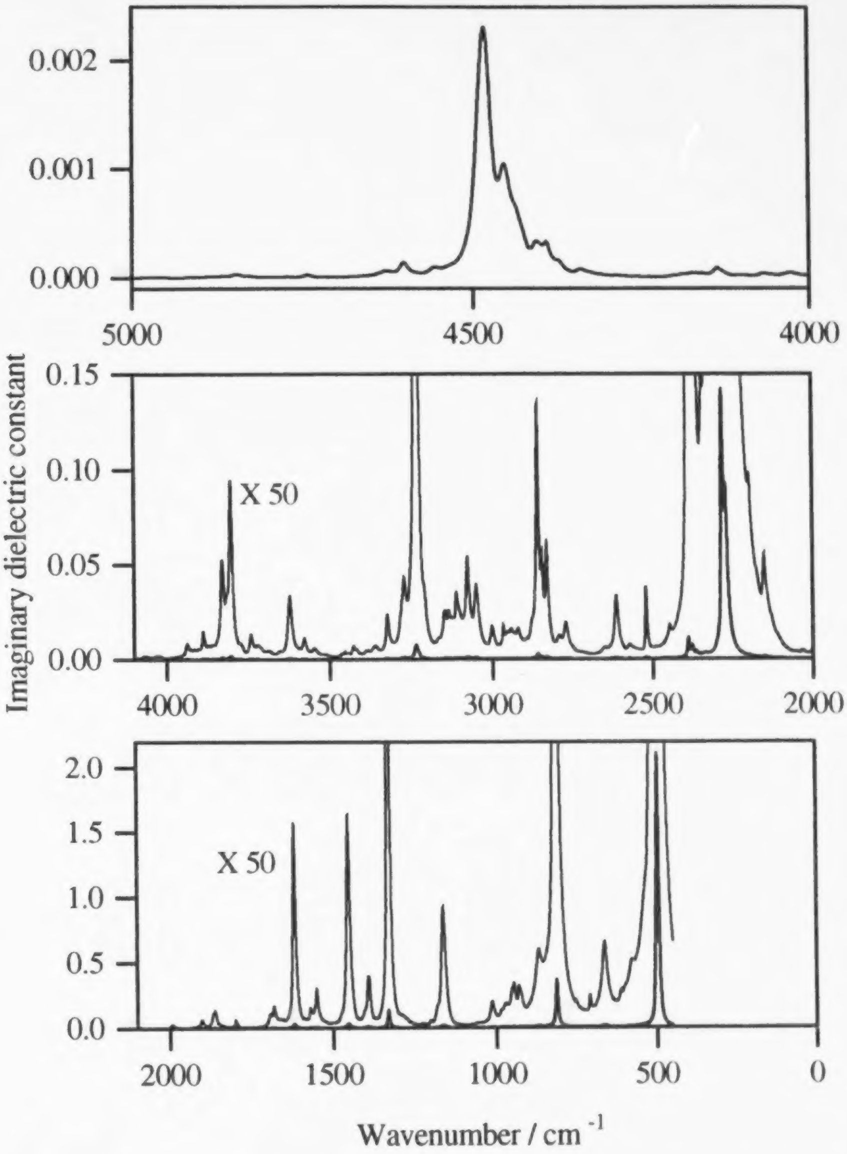

Figure 5.3. Imaginary dielectric constant spectrum of benzene-d_6. In the middle and bottom boxes, the ordinate scales are for the lower curves. They need to be divided by 50 for the upper curves.

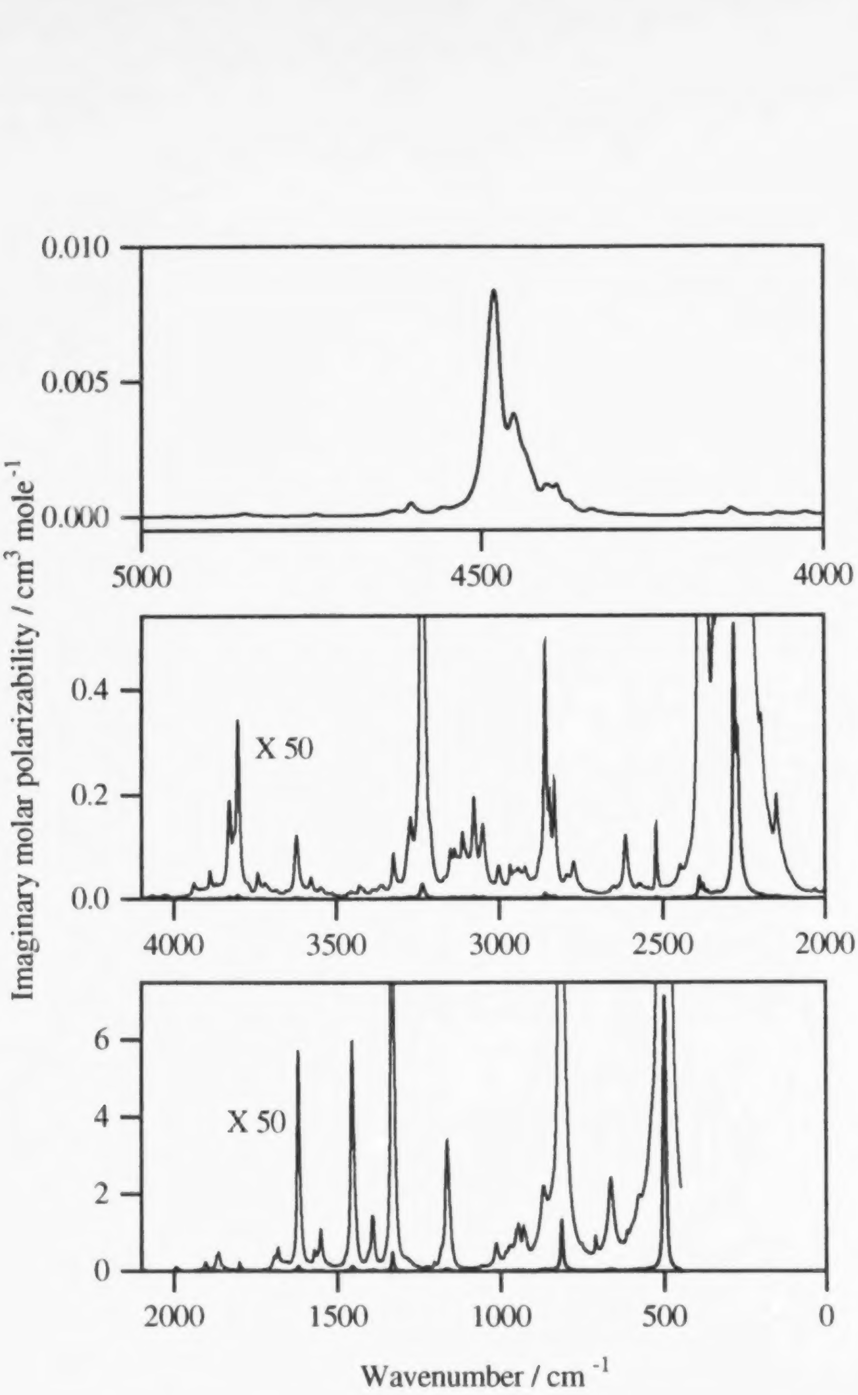

Figure 5.4. Imaginary molar polarizability spectrum of benzene-d_6. In the middle and bottom boxes, the ordinate scales are for the lower curves. They need to be divided by 50 for the upper curves.

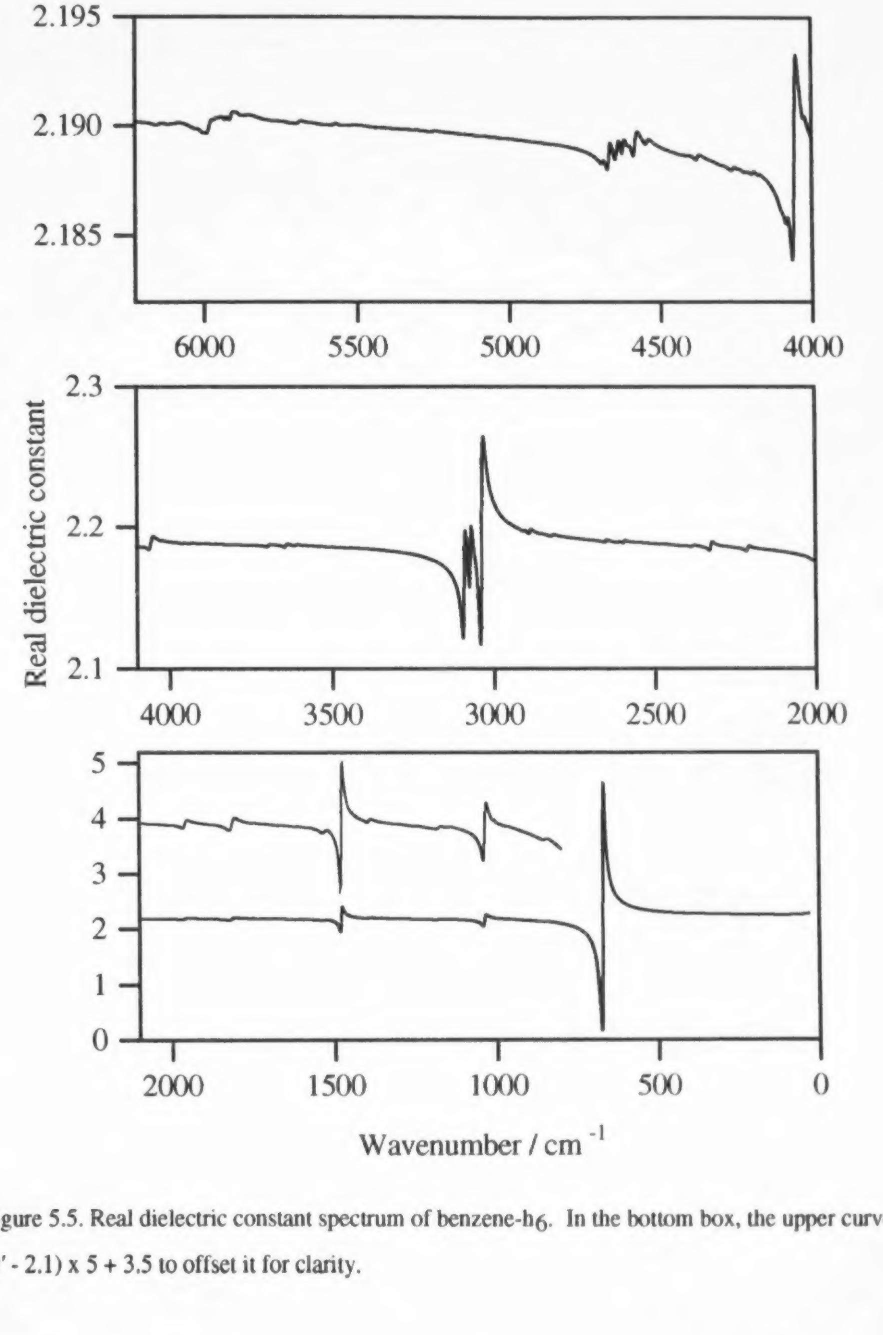

Figure 5.5. Real dielectric constant spectrum of benzene-h_6. In the bottom box, the upper curve is (ε' - 2.1) x 5 + 3.5 to offset it for clarity.

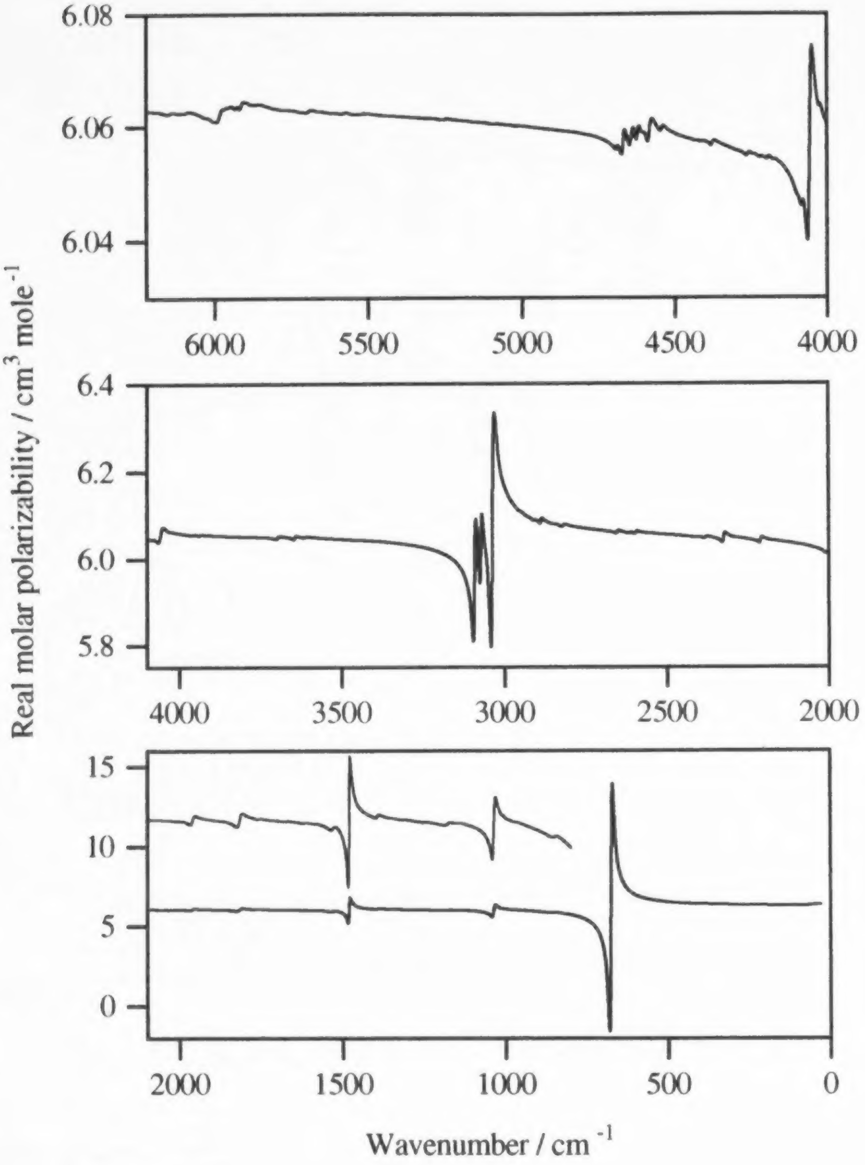

Figure 5.6. Real molar polarizability spectrum of benzene-h_6. In the bottom box, the upper curve is $(\alpha'_m - 6.5) \times 5 + 14.0$ to offset it for clarity.

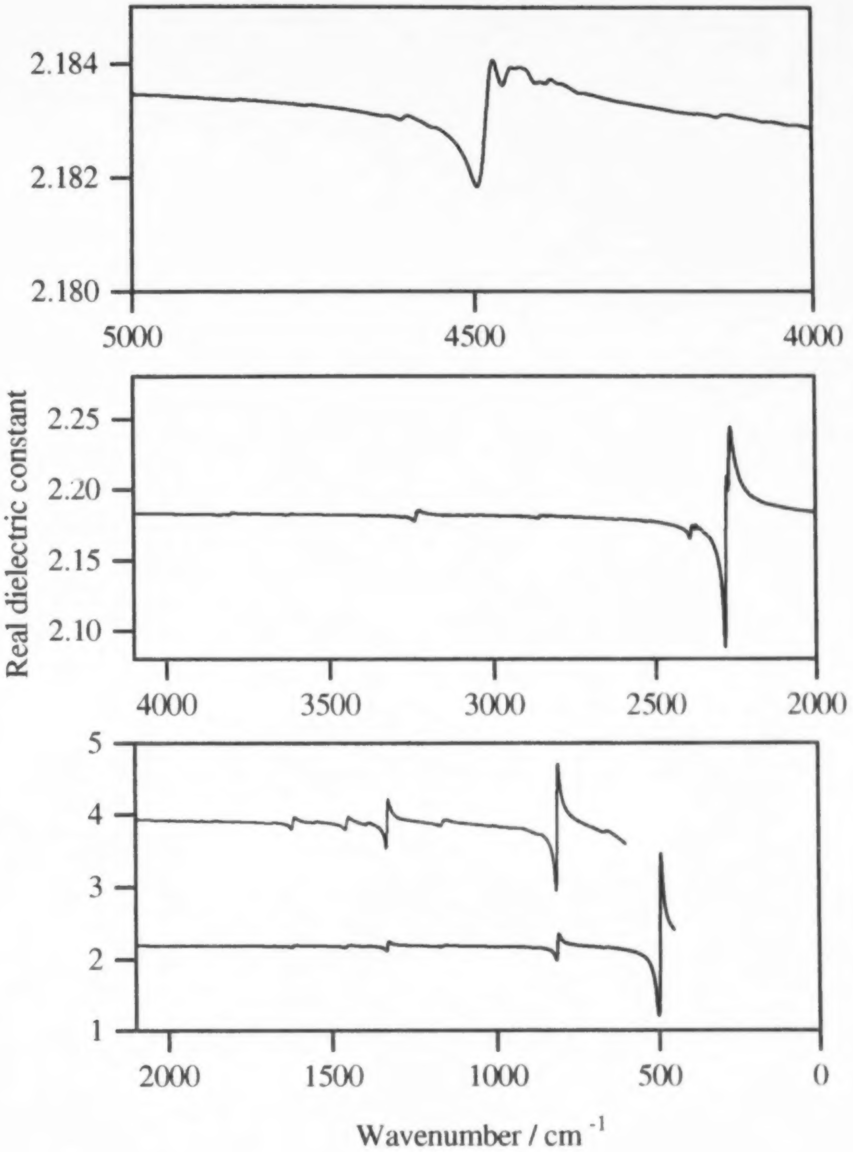

Figure 5.7. Real dielectric constant spectrum of benzene-d_6. In the bottom box, the upper curve is (ε' - 2.1) x 5 + 3.5 to offset it for clarity.

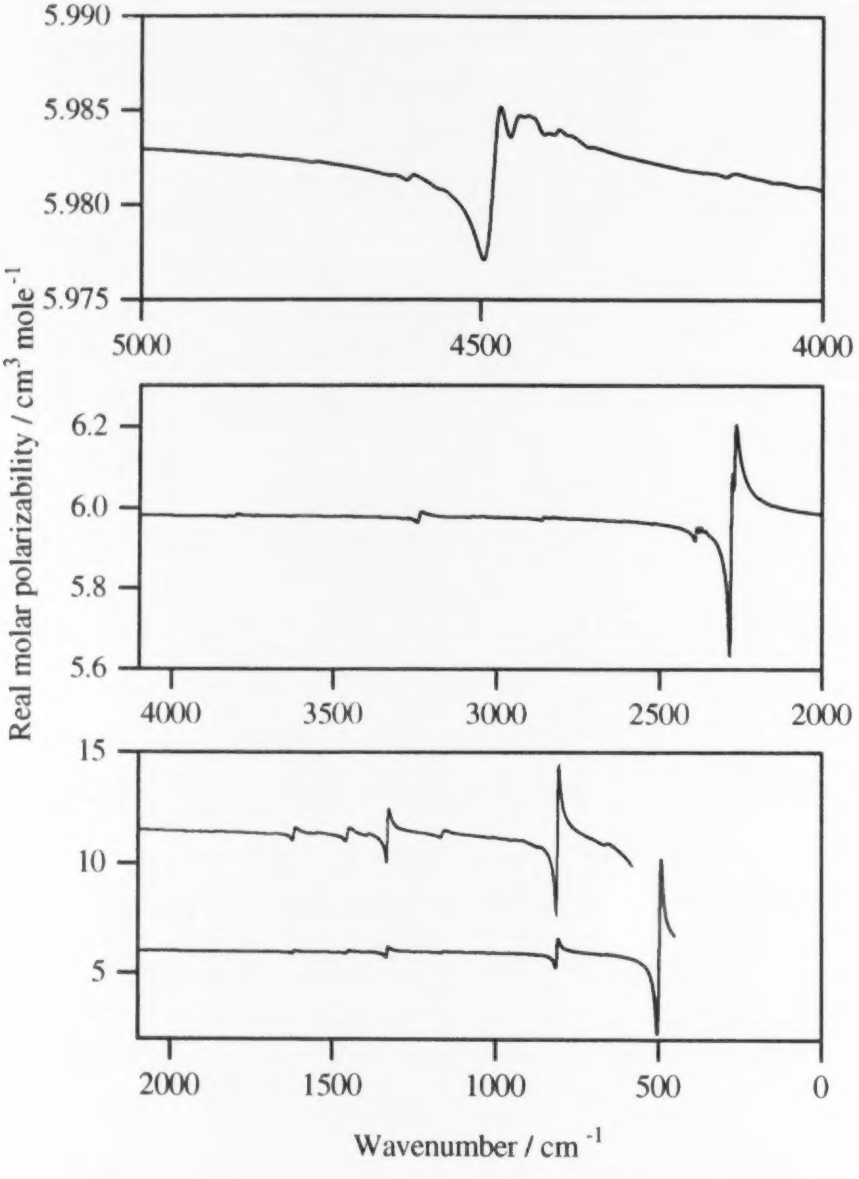

Figure 5.8. Real molar polarizability spectrum of benzene-d_6. In the bottom box, the upper curve is (α_m' - 6.5) x 5 + 14.0 to offset it for clarity.

The magnitude of the transition moment can be calculated from k, ε'' and α''_{m} through equations (1.3.46), (1.3.44) and (1.3.37), respectively. However, Bertie *et al.*[30] have shown that the imaginary molar polarizability spectra must be used to obtain accurate transition moments. If the transition moment is obtained from the imaginary refractive index or imaginary dielectric constant spectra, an error of 10% or greater can be introduced.

Bertie *et al.*[30] have also shown that the imaginary molar polarizability spectrum most clearly reveals the wavenumber, $\tilde{v}_j$, and damping constant, Γ_j, of the mechanical oscillator, and the bandshape of the oscillator, free from effects of the permittivity of the liquid, or its dispersion. This is illustrated in Figure 5.9 for ν_4, the most intense band of benzene-h_6. The top box in Figure 5.9 shows the imaginary molar polarizability spectrum and the middle and bottom boxes show the corresponding imaginary dielectric constant and imaginary refractive index spectra. It is clear that the peak position is not the same in the different spectra. The peak wavenumber in the imaginary molar polarizability spectrum is 673.1 $\mathrm{cm^{-1}}$. In the imaginary dielectric constant spectrum the peak wavenumber is 671.5 $\mathrm{cm^{-1}}$ and in the imaginary refractive index spectrum it is 676.1 $\mathrm{cm^{-1}}$. Bertie *et al.*[30] have shown that the peak position in the imaginary molar polarizability spectrum is essentially $\tilde{v}_j$ and in fact the peak position in the wavenumber times imaginary molar polarizability spectrum is exactly $\tilde{v}_j$.

It is also clear from Figure 5.9, that the full width at half height (FWHH) is different in the different spectra. In the imaginary molar polarizability spectrum the FWHH is 9.0 $\mathrm{cm^{-1}}$ and in the imaginary dielectric constant and imaginary refractive

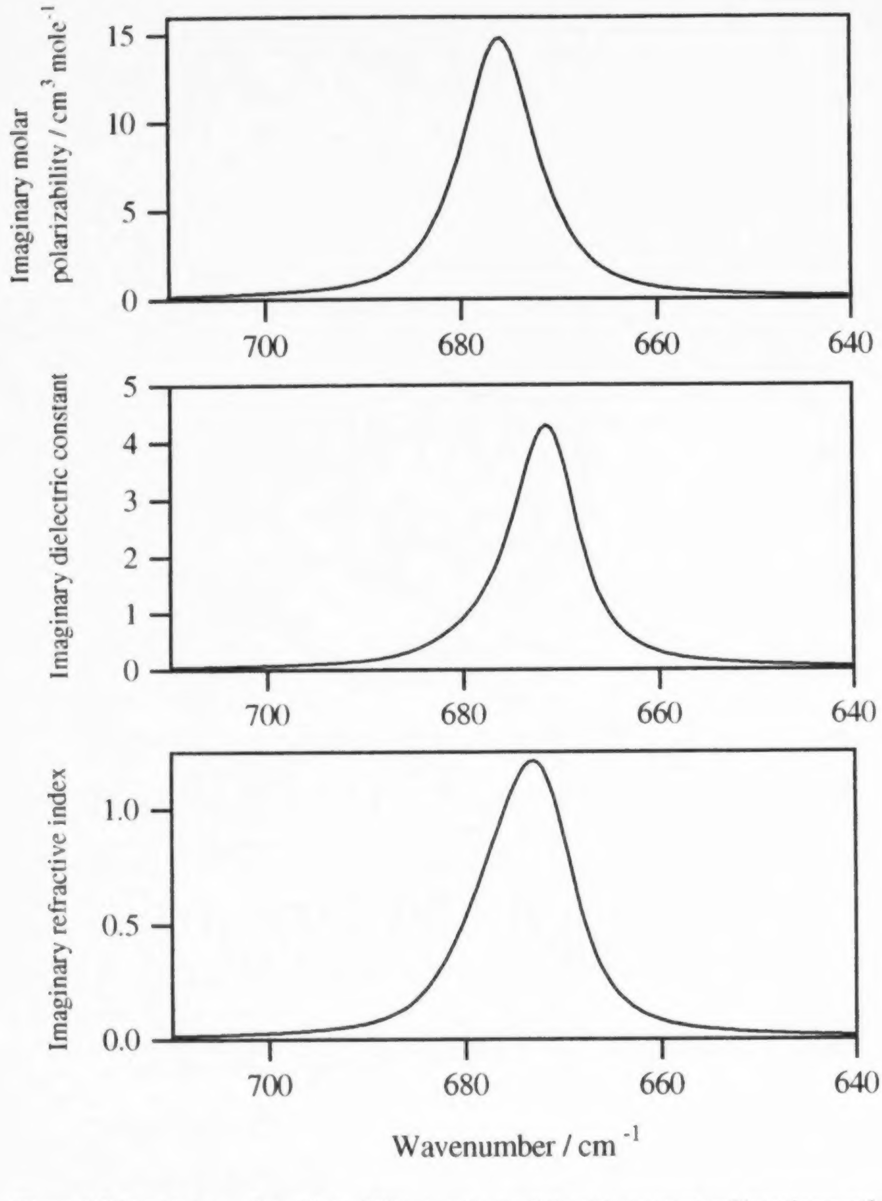

Figure 5.9. Imaginary molar polarizability, imaginary dielectric constant and imaginary refractive index spectra of ν_4 of benzene-h$_6$.

index spectra it is 8.3 and 10.8 cm^{-1}, respectively. The FWHH value in the imaginary molar polarizability spectrum is essentially Γ_j [30].

Finally, it should be noted that the band shapes are different in the different spectra. The imaginary molar polarizability band is symmetric while it is clear that the imaginary dielectric constant and imaginary refractive index bands are asymmetric, the latter markedly so. Theory predicts (section 1.3) that the α''_{m} band has the essentially symmetric CDHO shape. The shape of the ε'' band is also predicted[30] to be symmetric if the band is well separated from all other bands in the spectrum, but otherwise asymmetry is introduced into it by dispersion of the real molar polarizability. The imaginary refractive index band is heavily influenced by the dispersion of the real dielectric constant and is not expected to be symmetric except for weak bands[30]. The differences between the different intensity spectra are discussed again in Chapter 7 for the mixtures of benzene-h_6 and benzene-d_6. In the next section, the imaginary molar polarizability spectrum is used to obtain the integrated intensities and transition moments of benzene-h_6 and benzene-d_6.

5.2 Integrated Intensities and Transition Moments of Benzene-h_6 and Benzene-d_6 from the Imaginary Molar Polarizability

Following the result of theory, the α''_{m} spectrum was separated into contributions from the different transitions by fitting CDHO curves to fit it. The integrated intensities C_j (equation (1.3.36)) were then calculated from the fitted bands through equation (1.3.43).

Galactic Industries' program CURVEFIT was modified to use CDHO bands. This program was also written in Fortran and compiled with Microway's NDP Fortran under OS/2 2.1 in order to provide access to 16 Megabyte of memory and to obtain a tenfold increase in execution speed.

To fit the spectrum of benzene-h_6 some 200 CDHO bands were required and over 150 CDHO bands were needed to fit the spectrum of benzene-d_6. Very few of the required bands were not visible in the spectrum. No baseline was included in the fit.

The following fitting procedure was used. The spectra were split into approximately 10 to 15 regions. An initial fit was first obtained for each region by including the obvious bands and iterating to find the best fit. Once these initial bands were obtained the bands in each region were refined again including the effect of the wing of any band situated outside the region that contributed more than 10^{-6} cm^3 mole^{-1} to the α''_{m} spectrum in the region being fitted. These two steps were carried out until the bands were constant. Extra bands were added where the fit was not satisfactory. If a reasonable number of extra bands did not significantly improve the fit in a region, the extra bands were not included in the final fit.

The peaks required to fit the benzene-h_6 and benzene-d_6 spectra are given in Tables 5.2 and 5.3, respectively, with their assignment. In CH stretch region, and all regions to low wavenumber, practically all the peaks required to fit the spectrum could be assigned convincingly. The CDHO parameters (equation (1.3.41)) are given in Table 5.2 and 5.3 as Γ_j, the peak position , $\tilde{\nu}_j$ in cm^{-1}, and C_j in km mole^{-1} which was calculated from the parameter S_j, also in km mole^{-1}, of equation (1.3.41) through equation (1.3.43). The values of $\left|\vec{R}_j\right|$ were calculated from equation (1.3.37) and are included in Table 5.2 and 5.3 for all peaks that have a peak height >0.00015 cm^3 mole^{-1} in the $\tilde{\nu}\alpha''_{\mathrm{m}}$ spectrum.

The agreement between the experimental and fitted imaginary molar polarizability spectra was very good but not perfect. These spectra are shown for ν_{12}, ν_{13} and ν_{14} in Figures 5.10 to 5.15 for benzene-h_6 and benzene-d_6. For the other regions of weaker but still significant intensity, the fitted spectrum generally agreed to better than ±2%. This quality of curve fitting is very encouraging.

In regions where the absorption is very weak, compared to nearby peaks, the fit appeared to be very poor because of the far wings of the stronger band. This was found for benzene-d_6 in the regions 2700 - 2500 cm^{-1} and 2100 - 1700 cm^{-1}, where the absorption is very weak and next to the strong CD stretching region and for benzene-h_6 in the 5500 - 4700 cm^{-1} region, where the absorption is extremely weak, and between 3600 and 3200 cm^{-1} where it is very weak compared to the neighboring bands. The latter region is shown in Figure 5.16. The fitted spectrum is higher than the experimental spectrum and the fit certainly does not look very good. However, for the purpose of the fitting procedure, namely to obtain integrated intensities under individual bands in the spectrum, the fit is far better that it looks, and is definitely useful. The component bands in the lower box were fitted first to the small part of the spectrum shown, and reproduced the observed spectrum rather well. It was only when the wings of the neighboring bands were allowed to influence the region that the baseline was raised and the appearance of the fit deteriorated. The integrated intensities, C_j, of the bands in this region are believed known to better than ~±25%, which is certainly useful.

A second aspect of the poor fit shown in Figure 5.16 is that it is clear that the far wings of the bands are higher than they should be. Therefore the CDHO band does not fit the far wings of the observed bandshape very well, although it clearly fits the peaks rather well, and one must ask whether the integrated intensities of the strong

Table 5.2. Classical damped harmonic oscillator peaks used to fit the imaginary molar polarizability spectrum of benzene-h_6.

Peak Position / cm^{-1}	Assignment of wavenumber [a]	Γ_j / cm^{-1}	C_j / km mole^{-1}	$\lvert\vec{R}_j\rvert$ [b]	Assignment of intensity
6187.7		7.1	0.00006		
6145.5	1+13+16 *	18.5	0.00090		
6110.2		35.0	0.00151		
6089.4	1+12 *	20.4	0.00078		
6072.2	12+15 *	15.5	0.00018		
6023.5	12+13+13 *	20.2	0.00065	0.00184	
6001.7		15.4	0.00070	0.00192	
5993.5		6.7	0.00007	0.00061	
5982.4	5+15	22.9	0.00655	0.00587	
5976.3		4.1	0.00002	0.00032	
5964.4		16.6	0.00172	0.00301	
5952.7	1+2+13+18	6.8	0.00009	0.00069	
5948.2		24.8	0.00285	0.00388	
5929.1	1+13+16	11.6	0.00107	0.00238	
5911.8	1+12	15.4	0.00282	0.00388	
5898.1		17.8	0.00091	0.00220	
5878.7	not assigned	13.5	0.00040	0.00146	
5861.9		27.5	0.00153	0.00287	
5800.7		25.5	0.00017		
5770.0		30.0	0.00051		
5742.0		15.8	0.00012		
5711.5		18.4	0.00024		
5691.8		18.4	0.00106		
5655.8		20.8	0.00022		
5604.9		30.3	0.00048		
5577.8		17.0	0.00052		
5535.7		26.6	0.00054		
5517.5		14.0	0.00027		
5499.1		43.0	0.00042		

Table 5.2. Continued.

Peak Position / cm^{-1}	Assignment of wavenumber [a]	Γ_j / cm^{-1}	C_j / km mole^{-1}	$\left\|\vec{R}_j\right\|$ [b]	Assignment of intensity
5424.7		32.4	0.00034		
5400.4		11.4	0.00005		
5373.3		30.1	0.00024		
5346.0		20.8	0.00021		
5320.0		32.9	0.00024		
5306.0		9.2	0.00011		
5287.1		7.6	0.00006		
5250.1		20.1	0.00047		
5200.2		82.2	0.00021		
5150.5		20.0	0.00009		
5128.1		17.8	0.00007		
5094.9		17.6	0.00011		
5083.2		13.3	0.00012		
5050.2		28.4	0.00020		
5014.7		17.0	0.00019		
4995.4		10.9	0.00008		
4976.6		11.3	0.00002		
4959.5		28.3	0.00017		
4926.4		38.1	0.00027		
4900.4		29.0	0.00021		
4868.6		27.6	0.00022		
4843.9		45.1	0.00062		
4811.2		11.5	0.00003		
4778.7		50.3	0.00056		
4691.9	}2+13+16+18 *	74.6	0.00165	} 0.00302	
4690.0		11.8	0.00107		
4669.2		11.5	0.00425	0.00535	
4644.9	}12+16 *	11.6	0.00231	}0.00357	
4639.3		9.7	0.00144		
4622.9	}2+5+18 *	8.1	0.00151	} 0.00296	
4618.6		12.5	0.00106		
4604.3	not assigned	14.0	0.00119	0.00285	

Table 5.2. Continued.

Peak Position / cm^{-1}	Assignment of wavenumber [a]	Γ_j / cm^{-1}	C_j / km mole^{-1}	$\lvert\vec{R}_j\rvert$ [b]	Assignment of intensity
4584.1	}5+16 *	10.2	0.00221	} 0.00416	
4578.8		18.0	0.00283		
4543.1	}1+13; 13+15 *	14.0	0.00133	} 0.00313	
4538.1		127.1	0.00149		
4498.6		26.2	0.00023		
4488.7		15.0	0.00013		
4481.2		13.6	0.00010		
4457.3		43.5	0.00071		
4430.0	2+3+13+18	17.9	0.00042		
4413.8	3+13+16	7.7	0.00011		
4405.2		25.3	0.00062		
4377.8	3+12	9.2	0.00051		
4372.1	9+15 *	17.1	0.00046		
4344.0		71.8	0.00059		
4292.6		28.9	0.00052		
4274.0		8.2	0.00001		
4260.4	2+13+17+18	13.6	0.00085		
4241.3	13+16+17	26.8	0.00096		
4218.7	5+17	13.4	0.00052		
4208.7		13.7	0.00030		
4194.7	12+17	13.1	0.00084		
4173.2	10+15	10.6	0.00034		
4151.9		122.4	0.00817		
4096.8	1+14	25.6	0.00266	0.00320	
4081.1	14+15	15.7	0.00456	0.00420	
4056.8	6+15	15.0	0.0339	0.0115	
4024.2	2+12; 15+19 *	9.3	0.00117	0.00214	
3957.2	2+3+6+18	10.5	0.00115		
3934.8	3+6+16	8.7	0.00132		
3897.7		62.8	0.00144		
3819.7		44.2	0.00064		

Table 5.2. Continued.

Peak Position / cm^{-1}	Assignment of wavenumber [a]	Γ_j / cm^{-1}	C_j / km mole^{-1}	$\lvert\vec{R}_j\rvert$ [b]	Assignment of intensity
3801.9		18.9	0.00010		
3788.2	2+6+17+18	12.9	0.00042		
3769.1	6+16+17	15.8	0.00049		
3738.2	1+4	34.5	0.00194		
3705.1		31.3	0.00168		
3696.1	2+13+18+18	8.2	0.00308	0.00362	
3686.1	13+16+18	15.3	0.00228	0.00312	
3667.5		9.3	0.00027		
3642.3	12+18	8.3	0.00434	0.00433	
3611.5 3610.9	}5+18 *	41.8 11.9	0.00206 0.00190	}0.00588	
3574.2		61.8	0.00095		
3541.5		20.3	0.00011		
3515.1	not assigned	9.5	0.00014		
3502.7		7.5	0.00002		
3487.5	not assigned	7.9	0.00016		
3448.1	15+20	15.7	0.00129		
3427.3		3.4	0.00002		
3419.0		29.9	0.00077		
3397.4	not assigned	23.0	0.00061		
3362.2		40.2	0.00025		
3347.9	2+3+18+20	16.5	0.00012		
3331.5		18.1	0.00015		
3322.2	3+16+20	11.1	0.00013		

Table 5.2. Continued.

Peak Position / cm^{-1}	Assignment of wavenumber ^{a}	Γ_j / cm^{-1}	C_j / km mole^{-1}	$\lvert\bar{R}_j\rvert$ ^{b}	Assignment of intensity
3121.4		15.1	0.00178	0.0529	ν_{12}
3091.0	2+13+18	8.7	0.130		
3071.7	13+16	6.0	0.0456		
3069.4		15.2	0.0433		
3036.5	12	8.5	0.204		
3032.5		8.9	0.0360		
3020.1		17.7	0.0158		
3057.1	13+16 of ^{13}C **	7.0	0.00595		
3028.1	12 of ^{13}C **	9.9	0.0216		
3004.6		30.3	0.0217		
2963.5		70.0	0.0129		
2926.7		6.6	0.00021		
2906.2	2+9+18	8.6	0.00221	0.00346	
2887.3	9+16	7.2	0.00485	0.00514	
2851.5	not assigned	17.2	0.00176	0.00441	
2819.2	3+13	9.6	0.00256	0.00427	
2813.2		13.2	0.00071		
2653.6	13+17	44.0	0.00070	0.00416	
2652.9		7.3	0.00222		
2614.0	2+6+18	9.5	0.00148		
2595.2	6+16	7.6	0.00244	0.00385	
2573.9	2+18+19	20.0	0.00058		
2554.2	16+19	12.1	0.00058		
2516.3	not assigned	34.1	0.00074		
2484.6	9+17; 2+13+18-18	13.8	0.00057		
2468.6	2+13; 13+16-18	10.1	0.00026		
2455.0	not assigned	26.0	0.00024		
2451.6		10.5	0.00013		
2429.4	12-18	8.3	0.00014		
2407.5	not assigned	22.5	0.00175		
2381.9	3+14	12.6	0.00221	0.00382	
2367.5	not assigned	47.6	0.00167		
2324.9	10+17; 11+13	9.1	0.00799	0.0104	
2280.3	not assigned	25.9	0.00114		
2211.0	14+17	6.5	0.00216	0.00552	
2208.8		9.8	0.00212		

Table 5.2. Continued.

Peak Position / cm^{-1}	Assignment of wavenumber [a]	Γ_j / cm^{-1}	C_j / km mole^{-1}	$\lvert\bar{R}_j\rvert$ [b]	Assignment of intensity
2005.1	6+7; 2+18+20	11.3	0.00289	0.00674	
1988.4	16+20	6.5	0.00096	0.00390	
1961.2	7+19	13.3	0.0370	0.0200	
1955.8		12.4	0.0110		
1941.6		17.9	0.00191		
1882.8	11+14	8.2	0.00051		
1875.0	not assigned	7.1	0.00055		
1818.4	11+19	13.0	0.0267	0.0257	
1813.4		14.7	0.0475		
1797.5		17.9	0.00203		
1754.5	10+18	11.1	0.00398	0.00598	
1713.1	6+8	6.2	0.00057		
1702.5		20.4	0.00039		
1671.0	2+4; 8+19	12.7	0.00391	0.00858	
1644.5	14+18	7.9	0.00017		
1636.7		40.4	0.00140		
1617.9	6+18	9.6	0.00330	0.00567	
1605.8	2+18	17.0	0.00244		
1586.0	16	21.6	0.00538	0.00731	ν_{16}
1527.9	4+11	18.2	0.0330	0.0184	
1479.2	13	5.7	0.221	0.0499	ν_{13}
1472.6	13 of ^{13}C **	7.0	0.0132		
1393.2	7+20	12.1	0.0140	0.0126	
1310.0	9	26.2	0.00342	0.00907	ν_9
1249.5	11+20	14.5	0.00363	0.00676	
1227.8		29.7	0.00192		
1203.3		25.9	0.00280		
1177.3	17	24.4	0.0233	0.0176	ν_{17}
1147.6	10	27.4	0.0121	0.0182	ν_{10}
1093.2	14	184.1	0.00687	0.0445	ν_{14}
1036.6		8.1	0.0701		
1033.4		10.0	0.0483		
1025.5	14 of ^{13}C	15.4	0.00506		

Table 5.2. Continued.

Peak Position / cm^{-1}	Assignment of wavenumber [a]	Γ_j / cm^{-1}	C_j / km mole^{-1}	$\lvert \bar{R}_j \rvert$ [b]	Assignment of intensity
1010.3	6; 18+20	9.8	0.00500	0.0125	ν_6
993.9	2; 7	20.7	0.00642	0.0143	ν_2
970.9	19	41.8	0.0163	0.0162	ν_{19}
850.4	11	23.0	0.0155	0.0169	ν_{11}
677.8	4	7.5	0.686	0.244	ν_4
675.3		5.2	0.396		
672.3		6.1	0.193		
446.4	11-20	12.2	0.00015		
418.8		16.1	0.00025		
402.7	20	17.2	0.00087	0.0058	ν_{20}
398.6		62.7	0.00221		
346.9		26.1	0.00004		
302.2		14.7	0.00032		
270.0		28.6	0.00009		
232.1		186.2	0.00329		
170.2		17.3	0.00011		
105.4		62.3	0.00089		
77.8		76.6	0.00337		
48.4		7.6	0.00010		
44.0		72.7	0.00207		

[a] The assignments are from Brodersen and Langseth[79] except those marked with * which are from Maslen *et al.*[50] and those marked with ** which are proposed in this work. Not assigned indicates that the peak was observed by Brodersen and Langseth[79] but not assigned. A blank entry indicates that the peak was not observed by Brodersen and Langseth[79].

[b] The unit is Debye.

Table 5.3. Classical damped harmonic oscillator peaks used to fit the imaginary molar polarizability spectrum of benzene-d_6.

Peak Position / cm^{-1}	Assignment of wavenumber [a]	Γ_j / cm^{-1}	C_j / km mole^{-1}	$\lvert \bar{R}_j \rvert$ [b]	Assignment of intensity
4965.3		11.1	0.00001		
4958.6		9.6	0.00001		
4914.5		7.3	0.00001		
4886.4		8.4	0.00002		
4866.3		14.4	0.00003		
4847.0		17.6	0.00013		
4826.2		15.5	0.00003		
4797.2		14.1	0.00001		
4772.4		12.4	0.00002		
4743.2		13.8	0.00008		
4629.1	not assigned	14.9	0.00015		
4602.5	not assigned	11.8	0.00035		
4557.8	12+15	5.3	0.00004		
4482.6	1+12;1+2+13	23.8	0.0140	0.00993	
4451.7	5+15	17.1	0.00269	0.00436	
4434.7		25.3	0.00233		
4404.6	not assigned	13.7	0.00055		
4390.7	not assigned	15.0	0.00077		
4372.6		13.3	0.00024		
4337.3		17.9	0.00018		
4172.1		27.3	0.00021		
4135.3		16.9	0.00029		
4035.3		78.2	0.00052		
3937.4		9.2	0.00021		
3919.6		48.3	0.00079		
3902.3		4.2	0.00002		
3888.1		7.7	0.00035		
3873.9		25.6	0.00040		

Table 5.3. Continued.

Peak Position / cm^{-1}	Assignment of wavenumber [a]	Γ_j / cm^{-1}	C_j / km mole^{-1}	$\lvert\vec{R}_j\rvert$ [b]	Assignment of intensity
3857.0		19.5	0.00022		
3828.8	12+16; 2+13+16	11.9	0.00244	0.00317	
3815.8		7.7	0.00040		
3802.3	5+16	11.3	0.00436	0.00425	
3773.1		16.5	0.00026		
3740.5		9.6	0.00041		
3718.1		27.8	0.00067		
3685.0		18.3	0.00016		
3654.1		5.9	0.00003		
3621.3	1+13	13.8	0.00179		
3577.6	13+15	9.8	0.00028		
3570.0		127.9	0.00172		
3546.4	9+15	10.3	0.00010		
3463.6		5.0	0.00002		
3453.3		19.3	0.00017		
3428.6		6.2	0.00007		
3421.2		23.5	0.00033		
3386.5		14.9	0.00013		
3361.2		20.9	0.00037		
3323.7	3+12; 2+3+13	9.0	0.00062		
3316.1		17.0	0.00020		
3272.8	not assigned	20.2	0.00234	0.00475	
3234.9	6+15	11.2	0.01397	0.00825	
3227.3		12.4	0.00344		
3208.4		8.2	0.00035		
3166.2		5.8	0.00003		
3148.2	12+17	9.4	0.00043		
3134.7	2+13+17	17.8	0.00072		
3111.4	1+14; 5+7	5.7	0.00027		
3107.0		73.3	0.00360		
3105.1		14.9	0.00039		

Table 5.3. Continued.

Peak Position / cm^{-1}	Assignment of wavenumber [a]	Γ_j / cm^{-1}	C_j / km mole^{-1}	$\lvert\vec{R}_j\rvert$ [b]	Assignment of intensity
3075.9	14+15	11.3	0.00163	0.00289	
3048.7	C_6D_5H	16.5	0.00182		
3000.1	not assigned	13.5	0.00055		
2965.7	not assigned	5.5	0.00017		
2955.1	not assigned	8.3	0.00007		
2943.1		44.9	0.00142		
2940.7	11+12; 2+11+13	9.8	0.00007		
2919.4	not assigned	13.6	0.00031		
2876.6	13+16	8.4	0.00013		
2858.0	12+18; 2+13+18	8.3	0.00317	0.00591	
2854.5		69.4	0.00261		
2845.2		6.2	0.00055		
2830.2	10+16	9.4	0.00147	0.00286	
2792.7	1+4	10.2	0.00016		
2771.3	not assigned	19.8	0.00092		
2649.9	not assigned	33.0	0.00035		
2614.2	15+20	12.7	0.00108		
2606.2		27.3	0.00043		
2572.5	not assigned	16.7	0.00022		
2558.1		22.5	0.00016		
2545.5		12.9	0.00006		
2537.9		7.2	0.00002		
2522.5	6+16	3.5	0.00022		
2520.3		4.7	0.00025		
2517.2		7.9	0.00018		
2498.4		34.1	0.00033		
2470.4		38.7	0.00066		
2447.9	not assigned	27.3	0.00041		
2388.4	3+13	7.4	0.01054	0.00834	
2375.9	9+16	7.6	0.00571	0.00615	
2362.4	14+16	9.6	0.00349	0.00482	

Table 5.3. Continued.

Peak Position / cm^{-1}	Assignment of wavenumber [a]	Γ_j / cm^{-1}	C_j / km mole^{-1}	$\lvert\vec{R}_j\rvert$ [b]	Assignment of intensity
2345.2	16+19	10.2	0.00119	0.00400	
2333.7		19.5	0.00395	0.00730	
2280.2	12	8.1	0.139	0.0430	ν_{12}
2269.0	2+13	10.8	0.0963		
2257.8		29.0	0.0277		
2214.8		52.6	0.00494		
2195.7	13+17	6.0	0.00025	0.00134	
2149.1	9+17	15.2	0.00110		
2033.0	not assigned	15.0	0.00010		
1995.1	11+13	4.6	0.00013		
1992.6		5.4	0.00017		
1988.4		10.2	0.00019		
1953.3	not assigned	7.2	0.00001		
1902.4	16+20	8.9	0.00102		
1888.8		138.7	0.00140		
1868.0	3+14	7.8	0.00112	0.00307	
1861.3	9+18	8.4	0.00167	0.00376	
1847.8		38.9	0.00114		
1798.6	6+7	4.9	0.00044		
1794.6		10.1	0.00028		
1769.0	2+14	9.5	0.00004		
1755.8		24.5	0.00013		
1692.2	10+17	12.1	0.00177	0.00406	
1680.7	14+17	8.3	0.00192	0.00424	
1671.5	5-8	15.0	0.00083		
1657.1	17+19	17.8	0.00122		
1619.5	7+19	6.7	0.0108	0.0159	
1616.9		7.2	0.0105		
1612.2		11.8	0.00470		
1570.1	6+8	5.1	0.00066	0.00364	
1555.6	16	42.9	0.00642	0.0081	ν_{16}
1549.9	6+18	7.6	0.00272	0.00526	

Table 5.3. Continued.

Peak Position / cm^{-1}	Assignment of wavenumber [a]	Γ_j / cm^{-1}	c_j / km mole^{-1}	$\lvert\vec{R}_j\rvert$ [b]	Assignment of intensity
1521.7		23.4	0.00043		
1499.7		15.5	0.00060		
1476.3	11+14	3.0	0.00007		
1453.7	11+19	9.9	0.0233	0.0159	
1448.8	2+4	12.1	0.00765		
1403.1	10+18	10.7	0.00108		
1393.4	14+18	6.3	0.00199	0.00474	
1389.2	8+19	8.4	0.00349	0.00629	
1332.4		34.0	0.00170	0.0284	ν_{13}
1330.6	13	5.7	0.0429		
1328.4		6.3	0.0195		
1322.3	13 of ^{13}C *	7.1	0.00382		
1287.4	9	22.7	0.00136	0.0058	ν_9
1272.2		23.2	0.00061		
1225.5	17+20	8.7	0.00023		
1202.3	16-20; 3+14-11	4.0	0.00014		
1181.9	7+20	7.2	0.00062		
1163.1	4+11	12.3	0.0137	0.0136	
1156.2		10.7	0.00334		
1056.0	3	10.6	0.00017	0.0023	ν_3
1037.7		9.7	0.00004		
1012.2	11+20	13.4	0.00242	0.00614	
984.8		4.4	0.00014		
970.7	6	28.5	0.00380	0.0111	ν_6
951.7	8+20	9.0	0.00114		
944.3	2	10.6	0.00222	0.00861	ν_2
930.3	18+20	7.1	0.00113	0.00619	
923.8	C_6D_5H	10.5	0.00142		
864.9	17	42.2	0.0183	0.0182	ν_{17}
812.5	14	7.0	0.115	0.0507	ν_{14}
805.2		34.5	0.0170		
709.8	C_6D_5H	7.2	0.00070		

Table 5.3. Continued.

Peak Position / cm^{-1}	Assignment of wavenumber [a]	Γ_j / cm^{-1}	C_j / km $mole^{-1}$	$\lvert\vec{R}_j\rvert$ [b]	Assignment of intensity
663.9	11; 13-11	21.2	0.00879	0.0144	ν_{11}
577.6	18	56.9	0.00865	0.0154	ν_{18}
496.4 [c]	4		0.725 [c]	0.214 [c]	ν_4

[a] The assignments are from Brodersen and Langseth[79] except those marked with * which are proposed in this work. Not assigned indicates that the peak was observed by Brodersen and Langseth[79] but not assigned. A blank entry indicates that the peak was not observed by Brodersen and Langseth[79].

[b] The unit is Debye.

[c] Determined from binary mixtures of C_6H_6 and C_6D_6. See Chapter 7.

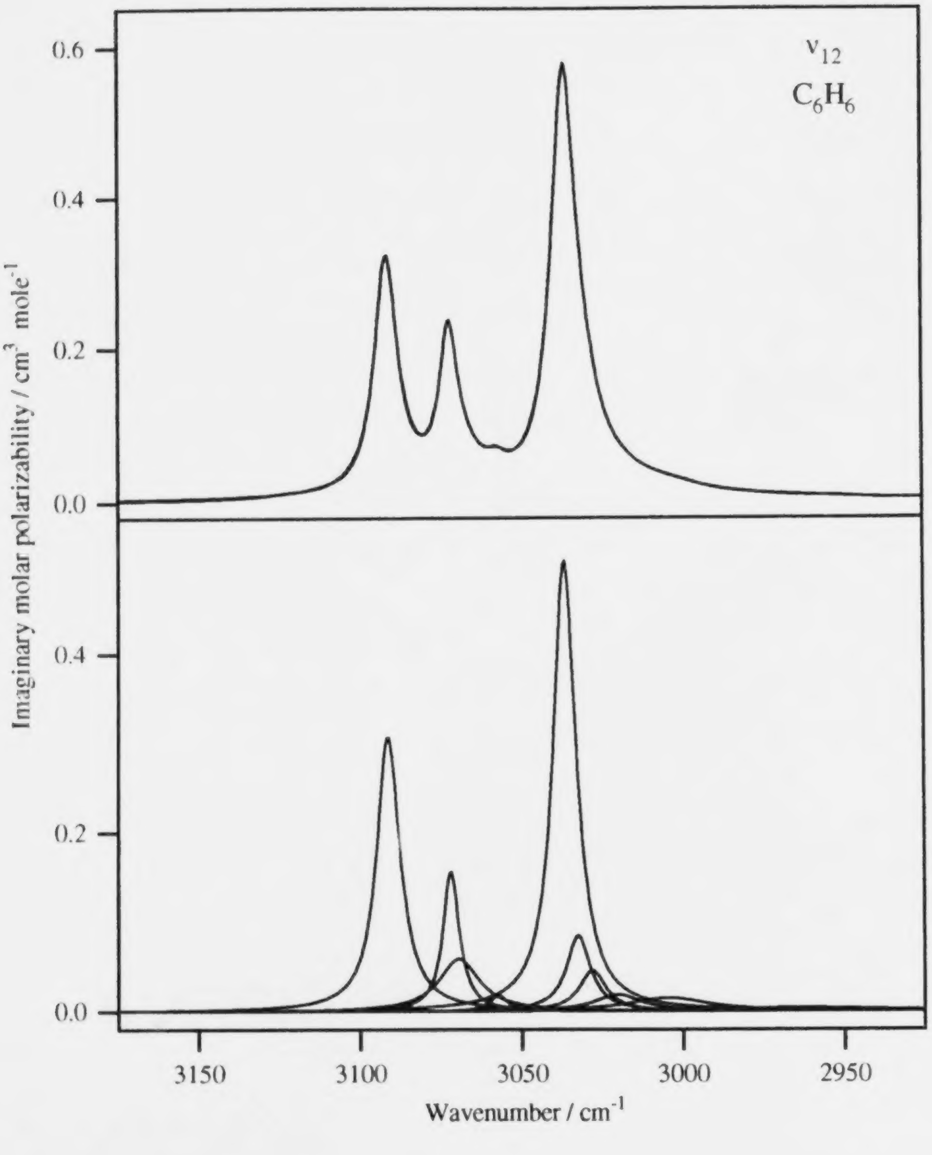

Figure 5.10. Shown in the top box are the experimental and fitted imaginary molar polarizability spectra of ν_{12} of benzene-h_6. The two spectra practically coincide. The fitted spectrum is the sum of all the bands given in Table 5.2. Shown in the bottom box are the 12 component CDHO bands of the fitted spectrum in this region.

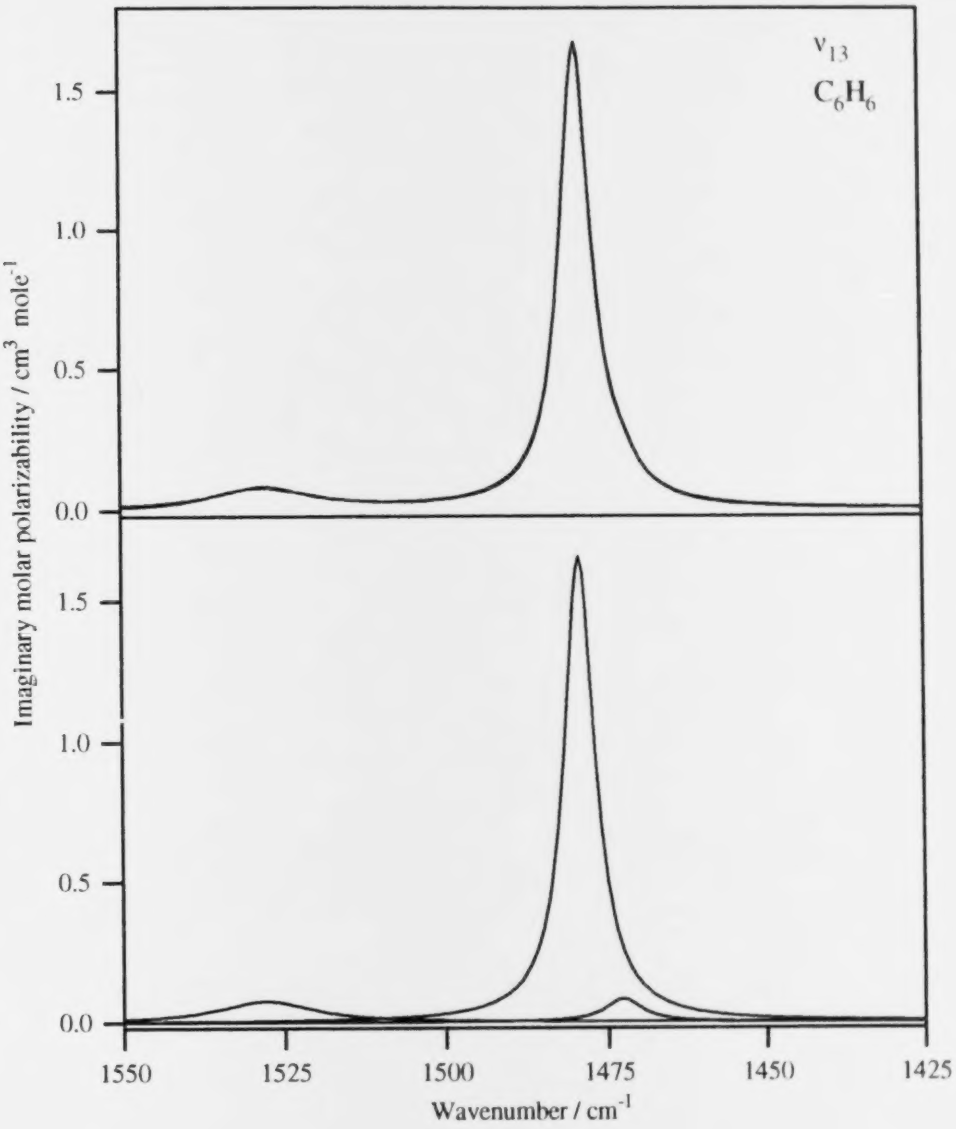

Figure 5.11. Shown in the top box are the experimental and fitted imaginary molar polarizability spectra of ν_{13} of benzene-h_6. The two spectra practically coincide. The fitted spectrum is the sum of all the bands given in Table 5.2. Shown in the bottom box are the 3 component CDHO bands of the fitted spectrum in this region.

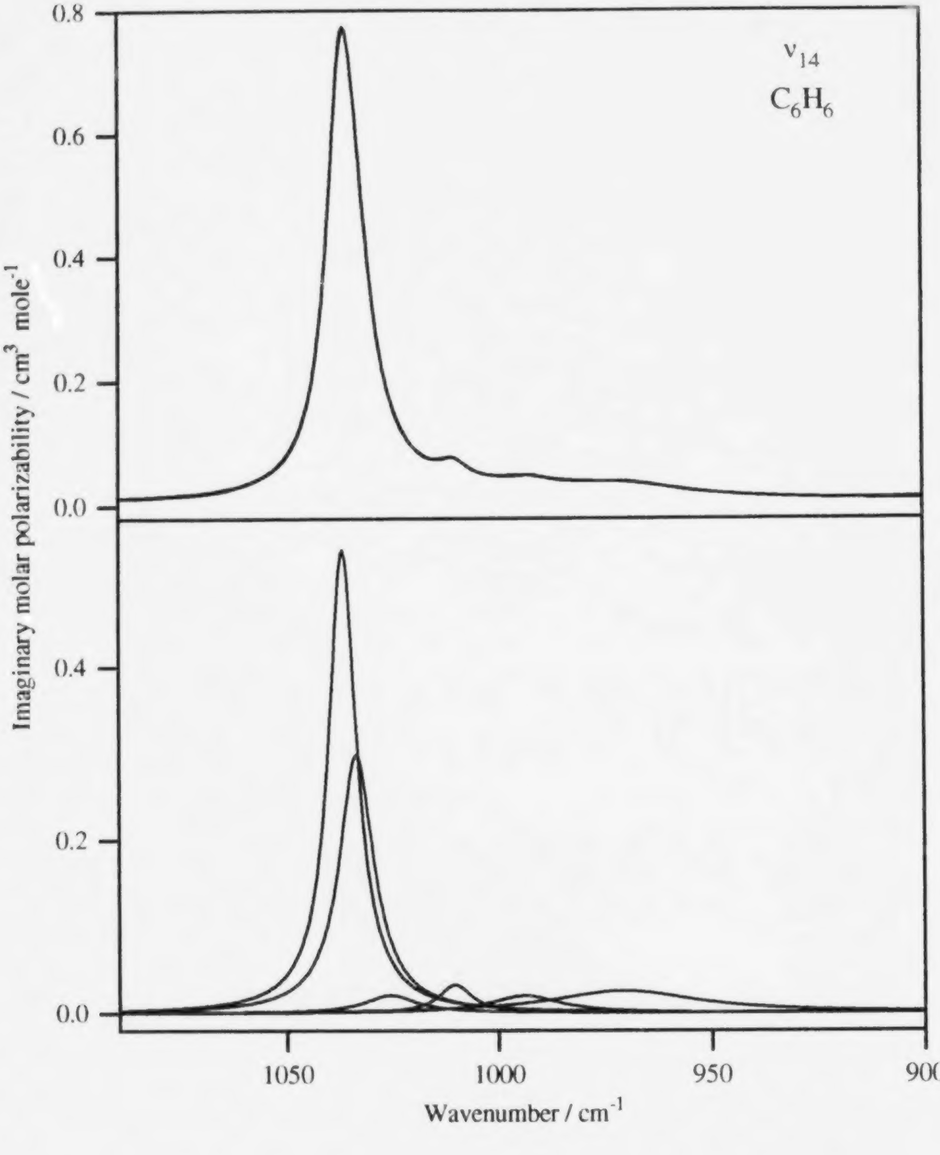

Figure 5.12. Shown in the top box are the experimental and fitted imaginary molar polarizability spectra of ν_{14} of benzene-h$_6$. The two spectra practically coincide. The fitted spectrum is the sum of all the bands given in Table 5.2. Shown in the bottom box are the 7 component CDHO bands of the fitted spectrum in this region.

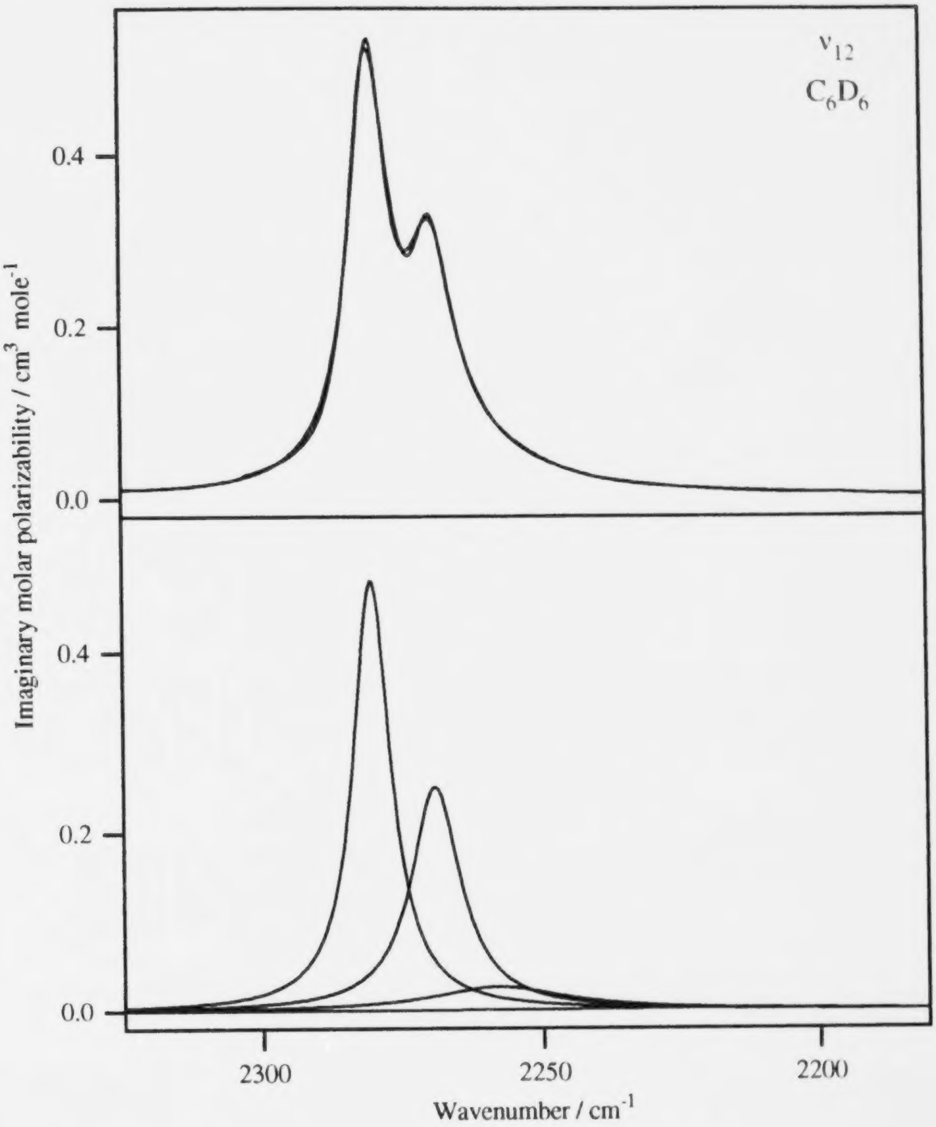

Figure 5.13. Shown in the top box are the experimental and fitted imaginary molar polarizability spectra of ν_{12} of benzene-d_6. The fitted spectrum is the sum of all the bands given in Table 5.3. Shown in the bottom box are the 4 component CDHO bands of the fitted spectrum in this region.

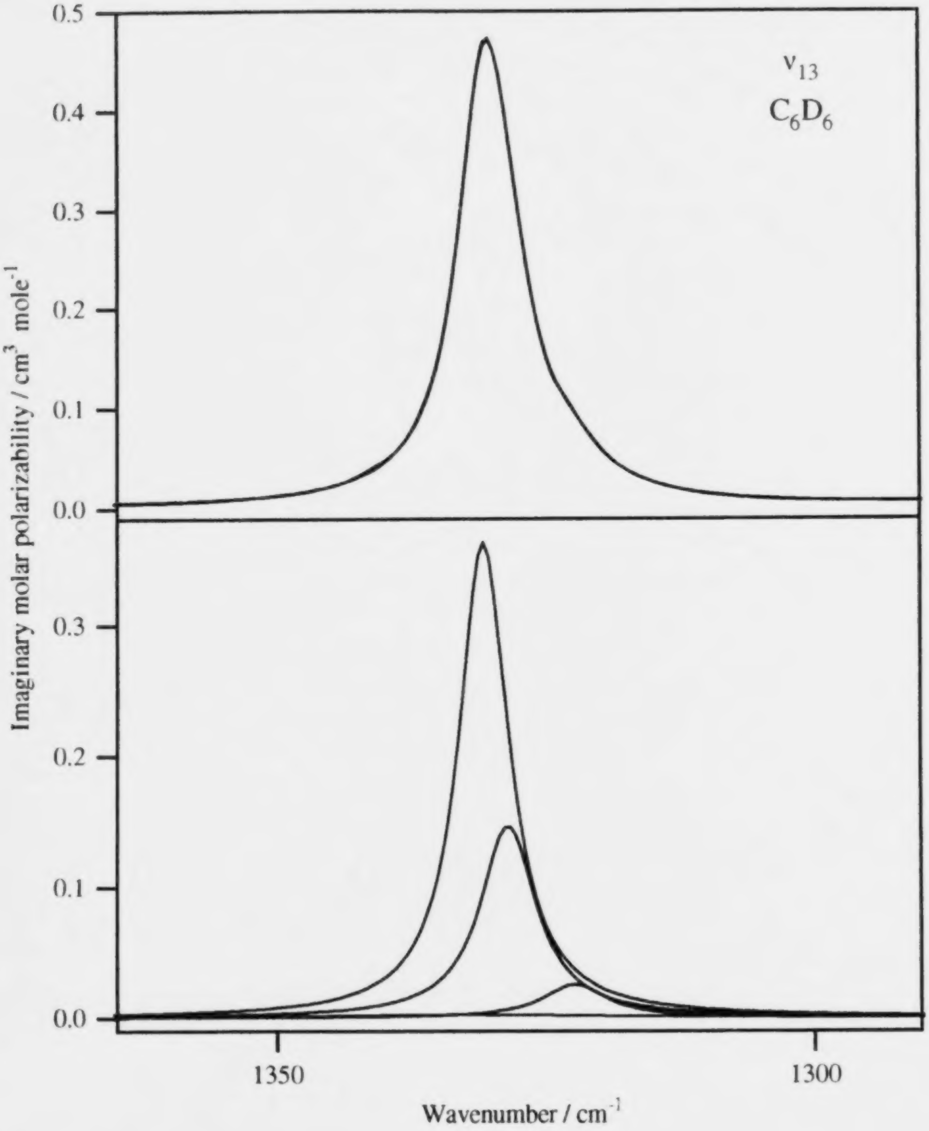

Figure 5.14. Shown in the top box are the experimental and fitted imaginary molar polarizability spectra of ν_{13} of benzene-d$_6$. The two spectra practically coincide. The fitted spectrum is the sum of all the bands given in Table 5.3. Shown in the bottom box are the 5 component CDHO bands of the fitted spectrum in this region.

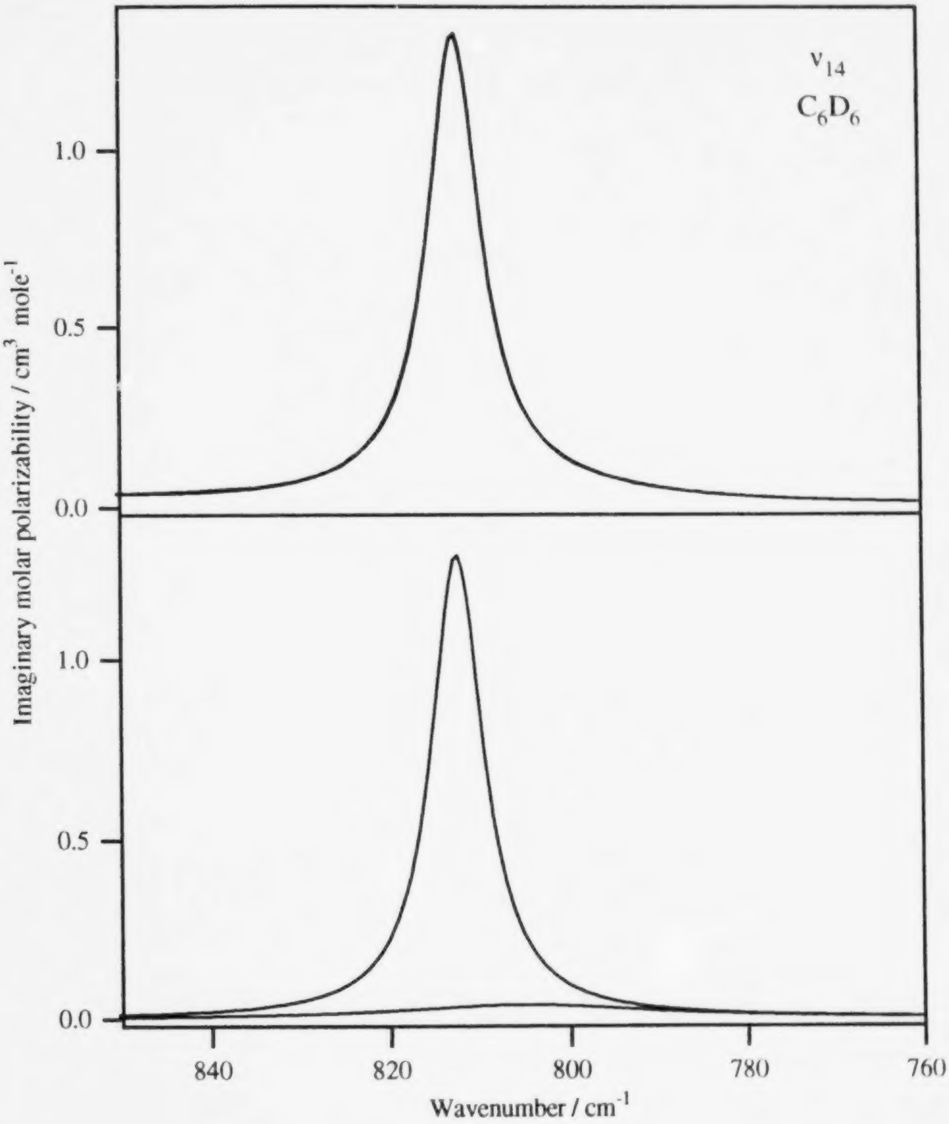

Figure 5.15. Shown in the top box are the experimental and fitted imaginary molar polarizability spectra of ν_{14} of benzene-d_6. The two spectra practically coincide. The fitted spectrum is the sum of all the bands given in Table 5.3. Shown in the bottom box are the 2 component CDHO bands of the fitted spectrum in this region.

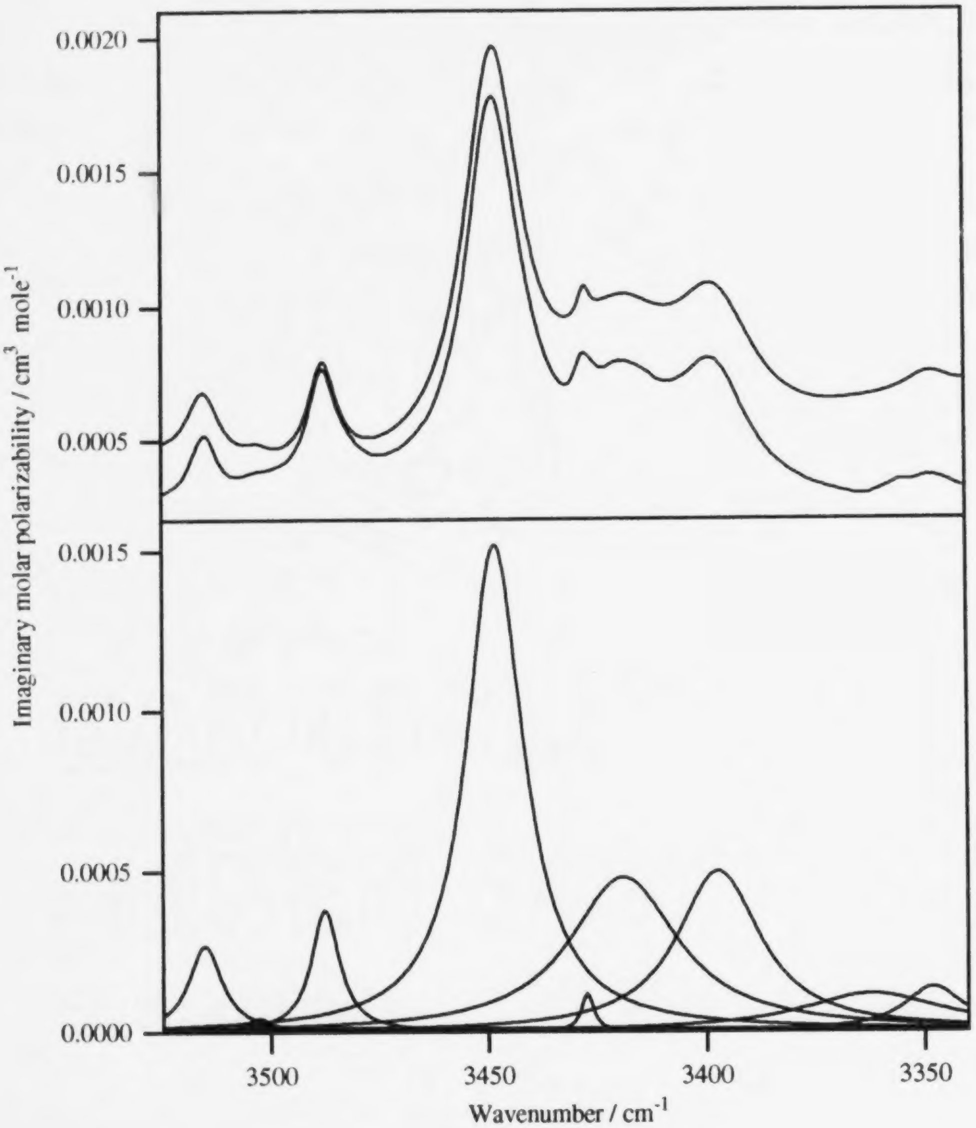

Figure 5.16. Shown in the top box are the experimental and fitted imaginary molar polarizability spectra of benzene-h_6 between 3535 and 3340 cm^{-1}. The fitted spectrum is the sum of all the bands given in Table 5.3. Shown in the bottom box are the 9 component CDHO bands of the fitted spectrum in this region.

bands are too high because their far wings are too high. This was explored, with the conclusion that the error due to the high wings of the fitted band is less than 1%.

As stated earlier, the areas C_j under the $\tilde{\nu}\alpha''_{\mathrm{m}}$ spectrum of the fitted bands were calculated from the CDHO parameters of the band through equation (1.3.43). Numerical integration under the α''_{m} spectrum was also done, to check that the total area under the fitted α''_{m} spectrum is very close to that under the experimental spectrum. Over the entire fitted range from 6225 to 30 cm^{-1} the area under the fitted spectrum was 1.2% greater than the area under the experimental α''_{m} spectrum for benzene-h_6 and over the range 5000 cm^{-1} to 450 cm^{-1} the area under the fitted spectrum was 2.5% greater than the area under the experimental α''_{m} spectrum for benzene-d_6. Over ranges of about 500 cm^{-1} broad in the regions of weaker absorption the areas agreed to within ±5 to ±15% but most of the difference came from the wings of bands in other regions of the spectrum, so the integrated intensities of the bands in these regions are generally much better than this.

It is estimated that the C_j values determined for the four infrared active fundamentals are accurate to within ±5%, since the uncertainty of the experimental optical constants is on the order of ±2 to ±3%. The C_j values of the infrared active combinations and infrared inactive fundamentals are conservatively estimated to be accurate to within ±15%.

The curve fit and assignment of the bands required to fit the infrared active fundamental regions of benzene-h_6 and benzene-d_6 are discussed in the following subsections.

5.2.1 The ν_{12} Band

The experimental and fitted imaginary molar polarizability spectra are shown in the top boxes of Figures 5.10 and 5.13 for the ν_{12} regions of benzene-h_6 and benzene-d_6, respectively. The component CDHO bands of the fitted spectra are shown in the bottom boxes.

For benzene-h_6, 12 bands were required to fit the region between 3175 and 2925 cm^{-1}. The bands at 3091, 3072, 3057, 3036 and 3020 are obviously present in the spectrum. The weaker bands are also clearly required because the peaks at 3071 and 3036 are obviously asymmetric and can not be fitted by a single band. The peaks at 3005, 2964 and 2927 cm^{-1} are very weak peaks that are can be seen in the experimental spectrum when it is plotted on an expanded scale.

The three major peaks in this region, at 3091, 3072 and 3036 cm^{-1} have been assigned[79] to $\nu_2+\nu_{13}+\nu_{18}$, $\nu_{13}+\nu_{16}$, and ν_{12}. The component peaks at 3069 and 3032 cm^{-1} are also assigned to the $\nu_2+\nu_{13}+\nu_{18}$ and ν_{12} transitions, respectively. The band asymmetry, and the 3 to 4 cm^{-1} splitting of the component peaks may be due to the way in which benzene is packed in the liquid phase. It is believed[51, 177, 178], that liquid benzene has a local structure similar to that of solid benzene. Harada and Shimanouchi[179] have found that the bands of solid benzene broaden at 250 °K and the multiplet structures observed at 85 and 155 °K[180] become less obvious. They estimated that the splitting due to local structure is about 2 to 3 cm^{-1} in solid benzene at -3°C.

The peaks at 3057 and 3028 can be assigned to $\nu_{13}+\nu_{16}$ and ν_{12} of $^{13}CC_5H_6$, respectively, on the basis that the 1.1% natural abundance of ^{13}C results in benzene-

h_6 containing about 6% $^{13}C^{12}C_5H_6$. The total intensity of the group of bands at 3072, 3069 and 3057 cm^{-1} is 0.0949 km $mole^{-1}$, and the intensity of the 3057 cm^{-1} band is 0.00595 km $mole^{-1}$, or 6.3% of the total intensity of the group. The total intensity of the 3036, 3032 and 3028 cm^{-1} group is 0.262 km $mole^{-1}$ and the intensity of the 3028 cm^{-1} band is 0.0216 km $mole^{-1}$, or about 8% of the total intensity of the group.

Painter and Koenig[101] measured the spectrum of neat $^{13}C^{12}C_5H_6$ and observed four peaks, at 3082, 3076, 3056 and 3028 cm^{-1}, grouped to form 3 features with intensity patterns comparable to those of C_6H_6 in Figure 5.10. Thus, if the 3056 and 3028 cm^{-1} peaks of $^{13}C^{12}C_5H_6$ are included in the spectrum, peaks at 3082 and 3076 cm^{-1} should also be included with comparable intensities. This was done with no degradation of the fit, but also with no significant improvement. Thus, the assignment of 3057 and 3028 cm^{-1} to $^{13}C^{12}C_5H_6$ was justified, but the two additional peaks at 3082 and 3056 were not included in the final fit.

The intensity of ν_{12} is taken as the sum of the intensity of all 12 peaks used to fit this region. Maslen *et al.*[50] have calculated that the $\nu_{13}+\nu_{16}$ transition has ~7% of the intensity of ν_{12} and that the $\nu_2+\nu_{13}+\nu_{18}$ has zero intensity in the gas phase. It is obvious from Figure 5.10 that the intensities of these peaks do not follow the pattern predicted by Maslen *et al.* and that their intensities are greatly affected by Fermi resonance. All the intensity in this region is, therefore, assigned to ν_{12}, although some of the intensity may belong to the combination bands.

The ν_{12} region of benzene-d_6 (Figure 5.13) is considerably simpler and only 4 peaks were needed to fit the spectrum. The fit is not as good as for benzene-h_6, but the addition of extra peaks did not improve it. The peaks at 2280 and 2268 cm^{-1} have been assigned[79] to ν_{12} and $\nu_2+\nu_{13}$. The peak at 2258 cm^{-1} is broad and contains about 10% of the total intensity in this region. This seems too high to be attributed to $^{13}C^{12}C_5D_6$. Also no splitting of the component bands was observed in the sense that it was not necessary to use two component bands split by a few cm^{-1} to fit the main peaks. All of the intensity in this region was assigned to ν_{12} on the assumption that the intensity at 2268 cm^{-1} is gained by Fermi resonance with ν_{12} and is not intrinsic to $\nu_2 + \nu_{13}$.

5.2.2 The ν_{13} Band

The experimental and fitted imaginary molar polarizability spectra are shown, almost coincident, in the top boxes of Figures 5.11 and 5.14 for the ν_{13} region of benzene-h_6 and benzene-d_6, respectively. The component CDHO bands of the fitted spectra are shown in the bottom boxes.

For benzene-h_6, 3 peaks were required to fit the region 1550 to 1425 cm^{-1}. The weak peak at 1527 cm^{-1} has been assigned[79] to $\nu_4+\nu_{11}$. The peak at 1479 cm^{-1} has been assigned[79] to ν_{13}. The intensity of the 1472 cm^{-1} band is about 6% of that of the 1479 cm^{-1} peak. Painter and Koenig[101] observed that ν_{13} of $^{13}C^{12}C_5H_6$ is at 1472 cm^{-1}, so the 1472 cm^{-1} peak is assigned to ν_{13} of $^{13}C^{12}C_5H_6$. No splitting of the component bands was observed. The intensity of the peak at 1527 cm^{-1} is assigned to the intrinsic intensity of $\nu_4+\nu_{11}$ and the intensity of the other two peaks is assigned to ν_{13}.

For benzene-d_6 5 peaks were required to fit the ν_{13} region between 1370 and 1275 cm^{-1}. The peak at 1330 cm^{-1} has been assigned[79] to ν_{13}. The intensity of the peak at 1322 cm^{-1} is about 6% of that of the other peaks. On this basis this peak can be assigned to ν_{13} of $^{13}C^{12}C_5D_6$. The peak at 1328 cm^{-1} is assigned to the splitting of the ν_{13} transition by the local structure of liquid benzene-d_6. The peak at 1287 cm^{-1} has been assigned[79] to the infrared inactive fundamental ν_9. The intensity of this peak is assigned to ν_9 and the sum of the intensities of the other 4 peaks in this region are assigned to ν_{13}.

5.2.3 The ν_{14} Band

The experimental and fitted imaginary molar polarizability spectra are shown, almost coincident, in the top boxes of Figures 5.12 and 5.15 for the ν_{14} region of benzene-h_6 and benzene-d_6, respectively. The component CDHO bands of the fitted spectra are shown in the bottom boxes.

Seven peaks are required to fit the region between 1095 and 900 cm^{-1} for benzene-h_6. The peaks at 1036 and 1033 cm^{-1} are assigned to ν_{14} of benzene-h_6 under the influence of the liquid structure. The peak at 1025 cm^{-1} contains about 4% of the total intensity in this region and therefore is assigned to ν_{14} of $^{13}C^{12}C_5H_6$. Painter and Koenig observed[101] that this band was at 1033 cm^{-1} in the infrared, but at 1027 cm^{-1} in the Raman. It is therefore not improbable that it appears as a shoulder at 1025 cm^{-1} under the stronger absorption by $^{12}C_6H_6$. The other 3 peaks have been assigned[79] to infrared active combinations and infrared inactive fundamentals. The intensity of these peaks are assigned to the corresponding transitions and the intensity of ν_{14} is assigned the sum of the intensity of the peaks at 1093, 1036, 1033 and 1025 cm^{-1}.

Only two peaks were required to fit the region between 850 and 750 cm^{-1} for benzene-d_6. The peak at 812 cm^{-1} is assigned[79] to ν_{14}. The intensity of the broad weak peak at 805 cm^{-1} is about 15% of the intensity of the peak at 812 cm^{-1}. This seems too high to be assigned to $^{13}C^{12}C_5D_6$.

5.2.4 The ν_4 Band

The experimental imaginary molar polarizability spectrum in the ν_4 region of benzene-h_6 and of benzene-d_6 were not measured in this work. The ν_4 region of benzene-h_6 was taken from Jones and co-workers[18]. The ν_4 region of benzene-d_6 was estimated by shifting and scaling the ν_4 peak of benzene-h_6. Jones's measurements were made on a 1968-model dispersive spectrometer[18] and were far noisier than the spectra recorded in this work. For these reasons the curve fitting results are less significant in these regions. The ν_4 peak of benzene-h_6 required 3 peaks to fit it. The individual peaks were not considered important but their total intensity was accepted as a good estimate of the true value. This is confirmed in Chapter 7, where it is found that the intensity of ν_4 band of benzene-h_6 is linear in molar fraction and that the C_j value for pure benzene-h_6 agrees well with that expected from the other mole fractions. The value of C_j for ν_4 of benzene-d_6 was taken from that determined from the binary mixtures in Chapter 7.

5.2.5 Other Peaks

Of the remaining peaks required to fit the imaginary molar polarizability spectra of benzene-h_6 and benzene-d_6, the majority have been assigned or observed by Brodersen and Langseth[79], especially those below the CH or CD stretching region. The value of C_j is given for all peaks used to fit the imaginary molar polarizability spectra in Tables 5.2 and 5.3. For the peaks with a height >0.00015 cm^3 $mole^{-1}$ in the $\tilde{\nu}\alpha''_m$ spectra the transition moment is listed.

For the fundamentals it is straightforward to calculate the dipole moments derivatives with respect to the normal coordinates from the transition moments under the double harmonic approximation. These dipole moment derivatives are mass-weighted and they must be converted to dipole moment derivatives with respect to symmetry coordinates or internal coordinates so that the dipole moment derivatives of benzene-h_6 and benzene-d_6 relay the same information. In order to do this the descriptions of the normal coordinates in terms of the symmetry or internal coordinates are required. In the next section the normal coordinates are calculated from the wavenumbers of the fundamental transitions of benzene-h_6 and benzene-d_6. In section 5.3, the dipole moment derivatives with respect to the normal coordinates of the fundamentals calculated from the transition moments given in Table 5.2 and 5.3 are presented. These dipole moment derivatives and the definition of the normal coordinates are then used to obtain the dipole moment derivatives with respect to the symmetry coordinates.

5.3 Normal Coordinate Calculations

5.3.1 Principles

The calculation of empirical force constants using the Wilson ***GF*** matrix method has been fully discussed in the literature[62]. A brief outline is given here only for convenience.

The ***G*** matrix elements depend only on the atomic masses and the geometry of the molecule. The ***F*** matrix elements are the force constants and need to be determined. The procedure to determine ***F***, is to use an estimate of the force constants and calculate the eigenvalues and eigenvectors of ***GF***. That is determine ***L*** and Λ in

$$\boldsymbol{GFL} = \boldsymbol{L\Lambda} \tag{5.3.1}$$

where Λ is a diagonal matrix of the eigenvalues. The eigenvalues, Λ, are the squares of the wavenumbers (apart from a numerical constant) of the fundamentals. These calculated wavenumbers are then compared with the observed wavenumbers and the $\boldsymbol{F}$ matrix is adjusted until the best fit to the observed wavenumbers is obtained.

$\boldsymbol{L}$ is the eigenvector matrix and is the transformation matrix between the internal coordinates and the normal coordinates defined by

$$\boldsymbol{R} = \boldsymbol{LQ} \tag{5.3.2}$$

where $\boldsymbol{R}$ is a column vector of the internal coordinates and $\boldsymbol{Q}$ is a column vector of the normal coordinates. The elements of $\boldsymbol{L}$ are the derivatives of the internal coordinates with respect to the normal coordinates, i.e.

$$L_{ij} = \left(\frac{\partial R_i}{\partial Q_j} \right) \tag{5.3.3}$$

It is common to transform the internal coordinates to symmetry coordinates through an orthogonal transformation matrix $\boldsymbol{U}$, before calculating the eigenvalues and eigenvectors.

$$\boldsymbol{S} = \boldsymbol{UR} \tag{5.3.4}$$

where $\boldsymbol{S}$ is a column vector of symmetry coordinates. The symmetry coordinates are linear combinations of the internal coordinates such that they have the symmetry of one of the irreducible representations of the point group of the molecule. The symmetry coordinates in the same irreducible representation are grouped together in the $\boldsymbol{S}$ vector. The irreducible representations are usually called the symmetry species in vibrational spectroscopy.

Equations (5.3.1) and (5.3.2) become

$$\boldsymbol{G}_\mathbf{s}\boldsymbol{F}_\mathbf{s}\boldsymbol{L}_\mathbf{s} = \boldsymbol{L}_\mathbf{s}\boldsymbol{\Lambda} \tag{5.3.5}$$

and
$$\boldsymbol{S} = \boldsymbol{L}_\mathbf{s}\boldsymbol{Q} \tag{5.3.6}$$

where

$$\boldsymbol{G}_\mathbf{s} = \boldsymbol{UGU}^\mathrm{T} \tag{5.3.7}$$

$$\boldsymbol{F}_\mathbf{s} = \boldsymbol{UFU}^\mathrm{T} \tag{5.3.8}$$

$$\boldsymbol{L}_\mathbf{s} = \boldsymbol{UL} \tag{5.3.9}$$

The elements of $\boldsymbol{L}_\mathbf{s}$ are the derivatives of the symmetry coordinates with respect to the normal coordinates,

$$\left(L_\mathrm{s}\right)_{ij} = \left(\frac{\partial S_i}{\partial Q_j}\right) \tag{5.3.10}$$

and the elements of $\boldsymbol{L}_\mathbf{s}^{-1}$ are the derivatives of the normal coordinates with respect to the symmetry coordinates,

$$\left(L_\mathrm{s}^{-1}\right)_{ij} = \left(\frac{\partial Q_i}{\partial S_j}\right) \tag{5.3.10}$$

When the internal coordinates are transformed to symmetry coordinates, the eigenvalues and eigenvectors of the $\boldsymbol{G}_\mathbf{s}\boldsymbol{F}_\mathbf{s}$ matrix are calculated instead of the eigenvalues and eigenvectors of the $\boldsymbol{GF}$ matrix. This has the advantage that the $\boldsymbol{G}_\mathbf{s}\boldsymbol{F}_\mathbf{s}$ matrix is a block diagonal matrix. That is the elements are arranged so that all the elements for a particular symmetry species are blocked together and thus the order of the matrix equation to be solved is reduced to the number of vibrations in the particular symmetry species .

5.3.2 Geometry, Internal Coordinates and Symmetry Coordinates of Benzene

The internal coordinates used for the normal coordinate calculations of benzene-h_6 and benzene-d_6 are given in Table 5.4. The geometry and the in-plane internal coordinates are shown in Figure 5.17 and the out-of-plane internal coordinates are shown in Figure 5.18. The internal coordinates are those used by Pulay *et al.*[124], except the coordinates R_{13} to R_{18} use 2 in the denominator instead of $\sqrt{2}$, and R_{29} is defined as the negative of that used by Pulay. Pulay's internal coordinates were based on those used by Whiffen[105] but have the redundancies removed. The geometry of benzene used in this work is that of Plíva *et al.*[99] who gave r_{CC} = 1.3920 Å and r_{CH} = 1.0862 Å. The carbon 12 scale of atomic masses was used, i.e. m_C = 12.000000 amu, m_H = 1.007825 amu and m_D = 2.014000 amu.

The symmetry coordinates used in this work are given in Table 5.5. They were chosen to be the same as those used by Whiffen[105] to be consistent with most of the normal coordinate calculations of benzene in the literature[40, 41, 50, 100, 105-111, 113-131].

5.3.3 Reproducing Literature Calculations

The first step of any normal coordinate calculation is to repeat the best literature calculation of the same molecule. This is not always trivial to do since there are many different ways of defining internal coordinates and many different computer programs are used to do the normal coordinate calculation.

The benzene force field was first studied by Wilson in 1934[102]. He developed a potential surface using only six diagonal force constants. Many different empirical[40, 41, 100, 103-111, 113-121] force field calculations have been carried out on

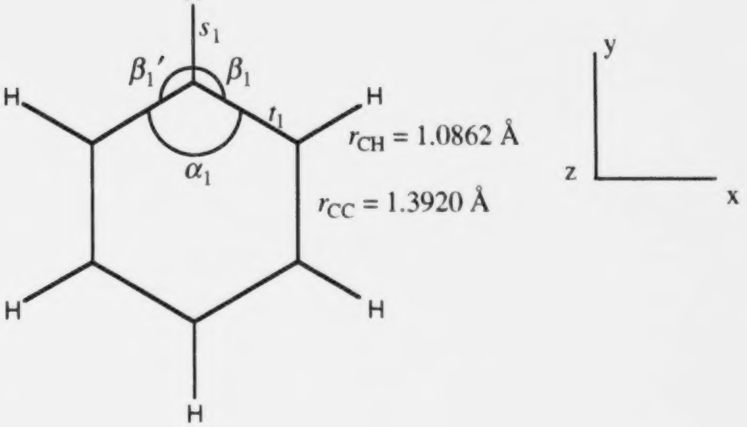

Figure 5.17. Geometry and in-plane internal coordinates of benzene. s_i is defined as the increase in the CH bond length, t_i is defined as the increase in the CC bond length, β_i is the increase in the HCC angle and α_i is the increase in the CCC bond angle.

Table 5.4. Internal coordinates.[a]

$$R_1 \rightarrow R_6 : s_1 \rightarrow s_6$$

$$R_7 \rightarrow R_{12} : t_1 \rightarrow t_6$$

$$R_{13} \rightarrow R_{18} : \frac{1}{2}(\beta_1 - \beta_1') \rightarrow \frac{1}{2}(\beta_6 - \beta_6')$$

$$R_{19} = \frac{1}{\sqrt{6}}(\alpha_1 - \alpha_2 + \alpha_3 - \alpha_4 + \alpha_5 - \alpha_6)$$

$$R_{20} = \frac{1}{\sqrt{12}}(2\alpha_1 - \alpha_2 - \alpha_3 + 2\alpha_4 - \alpha_5 - \alpha_6)$$

$$R_{21} = \frac{1}{2}(\alpha_2 - \alpha_3 + \alpha_5 - \alpha_6)$$

$$R_{22} \rightarrow R_{27} : \gamma_1 \rightarrow \gamma_6$$

$$R_{28} = \frac{1}{\sqrt{6}}(\delta_1 - \delta_2 + \delta_3 - \delta_4 + \delta_5 - \delta_6)$$

$$R_{29} = \frac{1}{2}(\delta_1 - \delta_3 + \delta_4 - \delta_6)$$

$$R_{30} = \frac{1}{\sqrt{12}}(-\delta_1 + 2\delta_2 - \delta_3 - \delta_4 + 2\delta_5 - \delta_6)$$

[a] R_{13} through R_{30} are all multiplied by 1Å^{-1} to provide uniform units for the force constants and displacement derivatives.

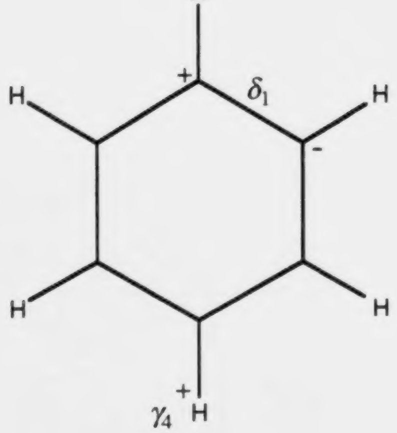

Figure 5.18. Out-of-plane internal coordinates of benzene. γ_i is defined as the change in the HCCC out-of-plane angle by motion of the hydrogen atom towards $+z$ and δ_i is defined as the CCCC torsion, i.e. the dihedral angle between the planes of the planes of $C_{i-1}C_iC_{i+1}$ and $C_iC_{i+1}C_{i+2}$. The + indicates that the atom moves in the positive z direction and the - indicates that the atom moves in the negative z direction.

Table 5.5. Symmetry coordinates. [a]

Symmetry	Coordinate
A_{1g}	$S_1 = \frac{1}{\sqrt{6}}(R_1 + R_2 + R_3 + R_4 + R_5 + R_6)$
A_{1g}	$S_2 = \frac{1}{\sqrt{6}}(R_7 + R_8 + R_9 + R_{10} + R_{11} + R_{12})$
A_{2g}	$S_3 = \frac{1}{\sqrt{6}}(R_{13} + R_{14} + R_{15} + R_{16} + R_{17} + R_{18})$
A_{2u}	$S_4 = \frac{1}{\sqrt{6}}(R_{22} + R_{23} + R_{24} + R_{25} + R_{26} + R_{27})$
B_{1u}	$S_5 = \frac{1}{\sqrt{6}}(-R_1 + R_2 - R_3 + R_4 - R_5 + R_6)$
B_{1u}	$S_6 = R_{19}$
B_{2g}	$S_7 = \frac{1}{\sqrt{6}}(R_{22} - R_{23} + R_{24} - R_{25} + R_{26} - R_{27})$
B_{2g}	$S_8 = R_{28}$
B_{2u}	$S_9 = \frac{1}{\sqrt{6}}(-R_7 + R_8 - R_9 + R_{10} - R_{11} + R_{12})$
B_{2u}	$S_{10} = \frac{1}{\sqrt{6}}(-R_{13} + R_{14} - R_{15} + R_{16} - R_{17} + R_{18})$
E_{1g}	$S_{11a} = \frac{1}{2}(-R_{23} - R_{24} + R_{26} + R_{27})$
E_{1g}	$S_{11b} = \frac{1}{\sqrt{12}}(2R_{22} + R_{23} - R_{24} - 2R_{25} - R_{26} + R_{27})$
E_{1u}	$S_{12a} = \frac{1}{\sqrt{12}}(-2R_1 - R_2 + R_3 + 2R_4 + R_5 - R_6)$
E_{1u}	$S_{13a} = \frac{1}{2}(-R_7 + R_9 + R_{10} - R_{12})$
E_{1u}	$S_{14a} = \frac{1}{2}(R_{14} + R_{15} - R_{17} - R_{18})$
E_{1u}	$S_{12b} = \frac{1}{2}(R_2 + R_3 - R_5 - R_6)$
E_{1u}	$S_{13b} = \frac{1}{\sqrt{12}}(R_7 + 2R_8 + R_9 - R_{10} - 2R_{11} - R_{12})$
E_{1u}	$S_{14b} = \frac{1}{\sqrt{12}}(2R_{13} + R_{14} - R_{15} - 2R_{16} - R_{17} + R_{18})$
E_{2g}	$S_{15a} = \frac{1}{\sqrt{12}}(-2R_1 + R_2 + R_3 - 2R_4 + R_5 + R_6)$
E_{2g}	$S_{16a} = \frac{1}{\sqrt{12}}(-R_7 + 2R_8 - R_9 - R_{10} + 2R_{11} - R_{12})$
E_{2g}	$S_{17a} = R_{20}$
E_{2g}	$S_{18a} = \frac{1}{2}(-R_{14} + R_{15} - R_{17} + R_{18})$

Table 5.5. Continued. [a]

Symmetry	Coordinate
E_{2g}	$S_{15b} = \frac{1}{2}(-R_2 + R_3 - R_5 + R_6)$
E_{2g}	$S_{16b} = \frac{1}{2}(-R_7 + R_9 - R_{10} + R_{12})$
E_{2g}	$S_{17b} = R_{21}$
E_{2g}	$S_{18b} = \frac{1}{\sqrt{12}}(2R_{13} - R_{14} - R_{15} + 2R_{16} - R_{17} - R_{18})$
E_{2u}	$S_{19a} = \frac{1}{2}(-R_{23} + R_{24} - R_{26} + R_{27})$
E_{2u}	$S_{20a} = R_{30}$
E_{2u}	$S_{19b} = \frac{1}{\sqrt{12}}(-2R_{22} + R_{23} + R_{24} - 2R_{25} + R_{26} + R_{27})$
E_{2u}	$S_{20b} = R_{29}$

[a] The internal coordinates are defined in Table 5.4 and Figures 5.17 and 5.18.

benzene since this first study by Wilson. The most recent normal coordinate calculation for benzene was done by Goodman *et al.*[100] for the gas. Goodman *et al.*[100] did not directly give the internal or symmetry coordinates used for their work, but it is indirectly indicated that they were similar to Pulay's. Goodman *et al.*[100] used the bond lengths determined by Stoicheff[181], r_{CC} = 1.397 Å, r_{CH} = 1.084 Å. With this geometry it was found that Goodman *et al.*'s calculated wavenumbers were reproduced within 1 cm^{-1} under the assumption that Goodman's internal and symmetry coordinates were identical to those used in this work.

5.3.4 Assignment and Wavenumbers of the Fundamentals of Liquid Benzene-h_6 and Benzene-d_6

The assignment and best current values of the wavenumbers of the fundamentals of gaseous benzene-h_6 and benzene-d_6 were given by Goodman *et al.*[100] Brodersen and Langseth[79] gave the assignments and wavenumbers of the fundamentals of liquid benzene-h_6 and benzene-d_6. Painter and Koenig[101] gave improved wavenumbers of the fundamentals of liquid benzene-h_6 based on the assignment of Brodersen and Langseth[79]. The assignments given in these three papers were adopted in this work and the wavenumbers of the fundamentals observed in the infrared spectra of liquid benzene-h_6 and benzene-d_6 are given as the $\tilde{\nu}_j$ parameter of the dominant component band used to fit the α''_m spectra (section 5.2). The wavenumbers of the fundamentals not observed in the α''_m spectra of liquid benzene-h_6 and benzene-d_6 where taken from Painter and Koenig[101], and Brodersen and Langseth[79], respectively, who estimated the wavenumbers of these inactive fundamentals from the wavenumbers of active combination bands.

Goodman et al.[100] estimated the anharmonic correction to the wavenumbers of the fundamentals of gaseous benzene-h_6 and benzene-d_6. These anharmonic corrections were applied in this work to the wavenumbers of the fundamentals of the liquids. The observed anharmonic wavenumbers and the resulting harmonic wavenumbers of the fundamental vibrations of liquid benzene-h_6 and benzene-d_6 are given in Table 5.6.

5.3.5 Present Normal Coordinate Calculation for Liquid Benzene-h_6 and Benzene-d_6

The harmonic wavenumbers of the liquid (Table 5.6) were used with Goodman's force constants of the gas[100] (Table 5.8) as the initial force constants, in program FPERT. The program refined the force constants to a set which calculated the wavenumbers of the liquid with an average error of 0.9 cm^{-1} or 0.1%. The calculated wavenumbers and the harmonic observed wavenumbers (Table 5.6) are compared in Table 5.7. The refined force constants are given in Table 5.8 and the eigenvectors and inverse eigenvectors calculated from them are presented in Tables 5.9 and 5.10 for liquid benzene-h_6 and benzene-d_6, respectively. The force constants generally agree with those given by Goodman *et al.*[100] and Pulay *et al.*[124] for the gas, indicating that there is very little difference in the force fields of the gas and the liquid.

The eigenvectors and inverse eigenvectors are used in the next section to determine the dipole moment derivatives with respect to symmetry coordinates and with respect to internal coordinates from the dipole moment derivatives with respect to normal coordinates determined from the experimental imaginary molar polarizability spectra of benzene-h_6 and benzene-d_6 by curve fitting in section 5.1.

Table 5.6. Anharmonic and harmonic wavenumbers of benzene-h_6 and benzene-d_6.

		Wavenumber / cm^{-1}			
Vibration	Symmetry	C_6H_6 obs [a]	C_6H_6 harmonic [b]	C_6D_6 obs [c]	C_6D_6 harmonic [b]
ν_1	A_{1g}	3059 *	3176 (117)	2293 **	2352 (59)
ν_2	A_{1g}	992.9	994.7 (1.8)	944.3	945.7 (1.4)
ν_3	A_{2g}	1346 *	1363 (17)	1056.0	1056.0
ν_4	A_{2u}	676.1	676.1	496.4	496.4
ν_5	B_{1u}	3062 *	3179 (117)	2275 **	2334 (59)
ν_6	B_{1u}	1010.3	1010.3	970.7	970.7
ν_7	B_{2g}	993.9	993.9	830 **	830
ν_8	B_{2g}	703 *	703	599 **	599
ν_9	B_{2u}	1310.0	1310.0	1287.4	1287.4
ν_{10}	B_{2u}	1147.6	1147.6	823 **	827 (4)
ν_{11}	E_{1g}	850.4	850.4	663.9	663.9
ν_{12}	E_{1u}	3036.5	3153.5 (117)	2280.2	2336.8 (56.6)
ν_{13}	E_{1u}	1479.2	1489.2 (10.0)	1330.6	1336.6 (6.0)
ν_{14}	E_{1u}	1036.6	1036.6	812.5	812.5
ν_{15}	E_{2g}	3046 *	3163 (117)	2267 **	2326 (59)
ν_{16}	E_{2g}	1586.0	1592.0 (6.0)	1555.6	1561.6 (6.0)
ν_{17}	E_{2g}	1177.3	1177.3	864.9	864.9
ν_{18}	E_{2g}	606 *	606	577.6	577.9 (0.3)
ν_{19}	E_{2u}	970.9	970.9	789 **	789
ν_{20}	E_{2u}	402.7	402.7	351 **	351

[a] Values marked by * were not observed in the spectrum, the values given are from Painter and Koenig[101]. The other values are the $\tilde{\nu}_j$ values of the component bands of the fit in section 5.2.

[b] Anharmonic corrections after Goodman *et al.*[100] are in parentheses.

[c] Values marked by ** were not observed in the spectrum, the values given are from Brodersen and Langseth[79]. The other values are the $\tilde{\nu}_j$ values of the component bands of the fit in section 5.2.

Table 5.7. Observed and calculated harmonic wavenumbers of benzene-h_6 and benzene-d_6.

		Wavenumber / cm^{-1}			
Vibration	Symmetry	C_6H_6 obs [a]	C_6H_6 calc [b]	C_6D_6 obs [a]	C_6D_6 calc [b]
ν_1	A_{1g}	3176	3175.4	2352	2352.8
ν_2	A_{1g}	994.7	992.7	945.7	947.8
ν_3	A_{2g}	1363	1360.8	1056.0	1058.8
ν_4	A_{2u}	676.1	676.1	496.4	496.4
ν_5	B_{1u}	3179	3178.6	2334	2334.5
ν_6	B_{1u}	1010.3	1009.1	970.7	971.9
ν_7	B_{2g}	993.9	994.7	830	829.0
ν_8	B_{2g}	703	704.1	599	597.7
ν_9	B_{2u}	1310.0	1310.3	1287.4	1287.1
ν_{10}	B_{2u}	1147.6	1147.9	827	826.7
ν_{11}	E_{1g}	850.4	851.5	663.9	662.5
ν_{12}	E_{1u}	3153.5	3153.8	2336.8	2336.4
ν_{13}	E_{1u}	1489.2	1489.9	1336.6	1335.9
ν_{14}	E_{1u}	1036.6	1037.5	812.5	811.3
ν_{15}	E_{2g}	3163	3163.4	2326	2325.2
ν_{16}	E_{2g}	1592.0	1592.7	1561.6	1560.9
ν_{17}	E_{2g}	1177.3	1178.3	864.9	863.6
ν_{18}	E_{2g}	606	607.6	577.9	575.9
ν_{19}	E_{2u}	970.9	971.0	789	788.9
ν_{20}	E_{2u}	402.7	402.9	351	350.8

[a] From Table 5.6.

[b] Calculated using the force constants given in Table 5.8.

Table 5.8. Internal coordinate force constants of benzene. [a]

Force Constant	Potential Term	This Work	Ref. 100 [b]	Ref. 124 [c]
f_1	$t_i t_i$	6.616	6.616	6.578
f_2	$s_i s_i$	5.468	5.547	5.176
f_3	$R_{19}R_{19}$	1.262	1.284	1.269
f_4	$R_{20}R_{20}$	1.225	1.257	1.247
f_5	$R_{13}R_{13}$	1.082	1.047	0.514 [d]
f_6	$t_i t_{i+1}$	0.728	0.728	0.710
f_7	$t_i t_{i+2}$	-0.428	-0.419	-0.407
f_8	$t_i t_{i+3}$	0.365	0.383	0.425
f_9	$s_i s_{i+1}$	-0.015	0.007	0.016
f_{10}	$s_i s_{i+2}$	0.048	0.008	0.005
f_{11}	$s_i s_{i+3}$	-0.025	-0.022	0.001
f_{12}	$R_{13}R_{14}$	-0.004	0.016	0.007 [d]
f_{13}	$R_{13}R_{15}$	-0.042	-0.023	-0.012 [d]
f_{14}	$R_{13}R_{16}$	0.034	-0.002	-0.001 [d]
f_{15}	$t_i s_i$	0.145	0.200	0.079
f_{16}	$t_i s_{i+2}$	0.000	0.008	-0.002
f_{17}	$t_i s_{i+3}$	-0.040	-0.130	-0.022
f_{18}	$t_1 R_{20}$	0.129	0.124	0.113
f_{19}	$s_1 R_{19}$	-0.140	-0.135	-0.105
f_{20}	$s_1 R_{20}$	0.030	-0.110	-0.099
f_{21}	$t_1 R_{13}$	0.216	0.216	0.158 [e]
f_{22}	$t_1 R_{15}$	-0.020	-0.022	-0.019 [e]
f_{23}	$t_1 R_{16}$	0.036	0.033	0.028 [e]
f_{24}	$s_1 R_{14}$	0.172	-0.068	0.005 [e]
f_{25}	$s_1 R_{15}$	-0.273	-0.027	-0.007 [e]
f_{26}	$R_{14}R_{20}$	-0.067	-0.106	-0.067 [e]
f_{27}	$\gamma_i \gamma_i$	0.454	0.447	0.4389
f_{28}	$R_{28}R_{28}$	0.393	0.394	0.3763
f_{29}	$R_{29}R_{29}$	0.323	0.312	0.3156
f_{30}	$\gamma_i \gamma_{i+1}$	-0.071	-0.069	-0.0690

Table 5.8. Continued.

Force Constant	Potential Term	This Work	Ref. 100 [b]	Ref. 124 [c]
f_{31}	$\gamma_i\gamma_{i+2}$	0.001	0.002	-0.0003
f_{32}	$\gamma_i\gamma_{i+3}$	-0.019	-0.021	-0.0176
f_{33}	$\gamma_1 R_{28}$	0.155	0.154	-0.1456
f_{34}	$\gamma_1 R_{29}$	0.154	-0.147 [f]	-0.147 [f]

[a] The unit of the force constants is mdyne Å^{-1}.

[b] These force constants where calculated from 55 harmonic gas phase wavenumbers of C_6H_6, C_6D_6, $^{13}C_6H_6$ and $^{13}C_6D_6$.

[c] These force constants are scaled and adjusted harmonic *ab initio* force constants, designated "Set II" by Pulay *et al.*[124].

[d] These values had to be multiplied by 2 when used with the internal coordinates in Table 5.1 to reproduce the wavenumbers given by Pulay *et al.*[124]

[e] These values had to be multiplied by $\sqrt{2}$ when used with the internal coordinates in Table 5.1 to reproduce the wavenumbers given by Pulay *et al.*[124]

[f] This force constant is the negative of that used in the present work following the definitions of R_{29} in the two studies.

Table 5.9. Eigenvectors of benzene-h_6 and benzene-d_6.

Symmetry Coordinate	C_6H_6	C_6D_6
S_1	$1.0369Q_1 + 0.0210Q_2$	$0.7598Q_1 + 0.0500Q_2$
S_2	$- 0.0859Q_1 + 0.2756Q_2$	$- 0.1267Q_1 + 0.2594Q_2$
S_3	$1.4594Q_3$	$1.1355Q_3$
S_4	$0.9548Q_4$	$0.7011Q_4$
S_5	$1.0370Q_5 - 0.0136Q_6$	$0.7613Q_5 + 0.0159Q_6$
S_6	$- 0.1909Q_5 + 0.6926Q_6$	$- 0.2862Q_5 + 0.6589Q_6$
S_7	$1.3217Q_7 - 0.5420Q_8$	$1.2730Q_7 + 0.0062Q_8$
S_8	$- 0.6693Q_7 + 1.2714Q_8$	$-1.2397Q_7 + 0.7262Q_8$
S_9	$0.4522Q_9 + 0.2134Q_{10}$	$0.4968Q_9 + 0.0563Q_{10}$
S_{10}	$- 0.8933Q_9 + 1.0125Q_{10}$	$- 0.4768Q_9 + 0.8692Q_{10}$
S_{11}	$1.0319Q_{11}$	$0.8029Q_{11}$
S_{12}	$1.0356Q_{12} + 0.0554Q_{13} - 0.0096\ Q_{14}$	$0.7562Q_{12} + 0.0892Q_{13} - 0.0066Q_{14}$
S_{13}	$- 0.0810Q_{12} + 0.2525Q_{13} + 0.2339Q_{14}$	$- 0.1299Q_{12} + 0.3015Q_{13} + 0.1312Q_{14}$
S_{14}	$0.1370Q_{12} - 1.3108Q_{13} + 0.5903Q_{14}$	$0.1935Q_{12} - 0.8796Q_{13} + 0.6587Q_{14}$
S_{15}	$-1.0261Q_{15} + 0.0863Q_{16} + 0.1194Q_{17}$ $- 0.0316Q_{18}$	$0.7553Q_{15} - 0.0261Q_{16} + 0.0809Q_{17}$ $- 0.0466Q_{18}$
S_{16}	$0.0214Q_{15} - 0.4278Q_{16} + 0.1535Q_{17}$ $- 0.0357Q_{18}$	$- 0.0464Q_{15} + 0.4465Q_{16} + 0.0781Q_{17}$ $- 0.0272Q_{18}$
S_{17}	$0.1386Q_{15} - 0.3720Q_{16} + 0.0510Q_{17}$ $+ 0.4029Q_{18}$	$- 0.2088Q_{15} + 0.3624Q_{16} - 0.0730Q_{17}$ $+ 0.3772Q_{18}$
S_{18}	$- 0.1394Q_{15} - 0.8966Q_{16} - 1.0417Q_{17}$ $- 0.1537Q_{18}$	$0.0370Q_{15} + 0.6370Q_{16} + 0.7982Q_{17}$ $- 0.2179Q_{18}$
S_{19}	$1.2496Q_{19} + 0.2606Q_{20}$	$1.0904Q_{19} + 0.1421Q_{20}$
S_{20}	$0.4432Q_{19} + 0.7012Q_{20}$	$0.6010Q_{19} + 0.5718Q_{20}$

Table 5.10. Inverse eigenvectors of benzene-h_6 and benzene-d_6.

Normal Coordinate	C_6H_6	C_6D_6
Q_1	$0.9584S_1 - 0.0730S_2$	$1.2751S_1 - 0.2456S_2$
Q_2	$0.2989S_1 + 3.6059S_2$	$0.6230S_1 + 3.7355S_2$
Q_3	$0.6852S_3$	$0.8806S_3$
Q_4	$1.0473S_4$	$1.4264S_4$
Q_5	$0.9678S_5 + 0.0191S_6$	$1.3017S_5 - 0.0314S_6$
Q_6	$0.2667S_5 + 1.4492S_6$	$0.5653S_5 + 1.5040S_6$
Q_7	$0.9649S_7 + 0.4114S_8$	$0.7791S_7 - 0.0066S_8$
Q_8	$0.5080S_7 + 1.0031S_8$	$1.3301S_7 + 1.3657S_8$
Q_9	$1.5614S_9 - 0.3290S_{10}$	$1.8949S_9 - 0.1228S_{10}$
Q_{10}	$1.3776S_9 + 0.6973S_{10}$	$1.0395S_9 + 1.0838S_{10}$
Q_{11}	$0.9691S_{11}$	$1.2454S_{11}$
Q_{12}	$0.9581S_{12} - 0.0423S_{13} + 0.0324S_{14}$	$1.2714S_{12} - 0.2146S_{13} + 0.0554S_{14}$
Q_{13}	$0.1679S_{12} + 1.2884S_{13} - 0.5077S_{14}$	$0.4491S_{12} + 2.0219S_{13} - 0.3982S_{14}$
Q_{14}	$0.1506S_{12} + 2.8704S_{13} + 0.5592S_{14}$	$0.2263S_{12} + 2.7629S_{13} + 0.9701S_{14}$
Q_{15}	$-0.9553S_{15} + 0.0027S_{16} + 0.0341S_{17} - 0.1074S_{18}$	$1.2910S_{15} - 0.0467S_{16} - 0.0852S_{17} + 0.1341S_{18}$
Q_{16}	$-0.0312S_{15} - 1.6094S_{16} - 0.2365S_{17} - 0.2522S_{18}$	$0.1625S_{15} + 1.8258S_{16} + 0.2130S_{17} + 0.1757S_{18}$
Q_{17}	$0.1126S_{15} + 1.6346S_{16} - 0.1357S_{17} - 0.7129S_{18}$	$0.0351S_{15} + 1.8434S_{16} - 0.4645S_{17} - 1.0263S_{18}$
Q_{18}	$0.2856S_{15} - 1.6935S_{16} + 2.2688S_{17} - 0.1057S_{18}$	$0.5654S_{15} - 1.4231S_{16} + 2.3093S_{17} - 0.2931S_{18}$
Q_{19}	$0.9218S_{19} - 0.3425S_{20}$	$1.0625S_{19} - 0.2640S_{20}$
Q_{20}	$-0.5826S_{19} + 1.6426S_{20}$	$-1.1168S_{19} + 2.0263S_{20}$

5.4 Dipole Moment Derivatives of Benzene-h_6 and Benzene-d_6 With Respect to Symmetry and Internal Coordinates

For a fundamental vibration it is straightforward and useful to use the approximations of mechanical and electrical harmonicity to convert the magnitude of the transition moment, $|\bar{R}_j|$, to the magnitude of the dipole moment derivative with respect to the normal coordinate, $|\partial\bar{\mu}/\partial Q_j| = \mu_j$. The appropriate equation is

$$\mu_j = \sqrt{\frac{8\pi^2 c\tilde{v}_j}{h}}\,|\bar{R}_j| \qquad (5.4.1)$$

When $\tilde{v}_j$ is in cm^{-1} and $|\bar{R}_j|$ is in Debye, equation (5.4.1) takes the following form to give μ_j in Debye $Å^{-1}$ $amu^{-1/2}$

$$\mu_j = \sqrt{0.05932\,\tilde{v}_j}\,|\bar{R}_j| \qquad (5.4.2)$$

The experimental measurements have given the magnitudes of the transition moments of the four infrared active fundamentals, Q_4 (A_{2u}), Q_{12} (E_{1u}), Q_{13} (E_{1u}) and Q_{14} (E_{1u}) as well as the magnitudes of the transitions moments of the fundamentals that are infrared inactive in the gas but active in the liquid. These transition moments are given in Tables 5.2 and 5.3 and were used to calculate the dipole moment derivatives with respect to the normal coordinates. These values are given in Table 5.11, with the values of the integrated intensity, C_j, for all of the fundamentals of benzene-h_6 and benzene-d_6.

The dipole moment derivative with respect to the normal coordinate is weighted by the effective mass of the oscillator, and this weighting must be removed before the values obtained can be compared between isotopic molecules. The mass-weighting is removed through the inverse eigenvectors or the eigenvectors from the normal coordinate calculations presented in the previous section, through the equations

$$\frac{\partial\bar{\mu}}{\partial S_i} = \sum_{j=1}^{3n-6} \frac{\partial\bar{\mu}}{\partial Q_j}\frac{\partial Q_j}{\partial S_i} = \sum_{j=1}^{3n-6} \frac{\partial\bar{\mu}}{\partial Q_j}\left(L_s^{-1}\right)_{ji} \qquad i = 1,2,\ldots,3n-6 \quad (5.4.3)$$

or

$$\frac{\partial\bar{\mu}}{\partial Q_j} = \sum_{i=1}^{3n-6} \frac{\partial\bar{\mu}}{\partial S_i}\frac{\partial S_i}{\partial Q_j} = \sum_{i=1}^{3n-6} \frac{\partial\bar{\mu}}{\partial S_i}\left(L_s\right)_{ij} \qquad j = 1,2,\ldots,3n-6 \quad (5.4.4)$$

In equations (5.4.3) and (5.4.4), the elements of $\boldsymbol{L}_s$ and $\boldsymbol{L}_s^{-1}$ are block diagonal and the sums need only be considered over the coordinates in a particular symmetry species. These sums are vector sums, and only the magnitude of $\partial\bar{\mu}/\partial Q_j$ is known. For vibrations that are infrared active under the D_{6h} point group of the isolated molecule, $\partial\bar{\mu}/\partial Q_j$ and $\partial\bar{\mu}/\partial S_i$ must point along the *x*, *y* and *z* axes of the molecule (Figure 5.17), so the only unknown is the sense of the vector with respect to positive *x*, *y* or *z*. This is not quite true for the liquid, but it is as valid as the use of the D_{6h} point group is for a molecule in liquid benzene. The treatment of vibrations that are active in the liquid but inactive under D_{6h} is rather less certain, and is discussed later in section 5.4.2.

The conversion of the dipole moment derivatives with respect to the normal coordinates to dipole moment derivatives with respect to symmetry coordinates and to dipole moment derivatives with respect to internal coordinates is discussed for the fundamentals of different symmetry in the following subsections.

5.4.1 Dipole Moment Derivatives With Respect to Symmetry Coordinates for the Infrared Active Fundamentals

5.4.1a A_{2u} Vibrations

The conversion of the dipole moment derivatives with respect to normal coordinates to dipole moment derivatives with respect to symmetry coordinates is straightforward for the A_{2u} symmetry species since only one vibration, ν_4, has this symmetry. In this case, equation (5.4.3) takes the form

$$\frac{\partial \bar{\mu}}{\partial S_4} = \frac{\partial \bar{\mu}}{\partial Q_4} \frac{\partial Q_4}{\partial S_4} \tag{5.4.5}$$

where both vectors are perpendicular to the molecular plane.

From the inverse eigenvectors given in Table 5.10 and the $|\partial \bar{\mu}/\partial Q_4|$ values in Table 5.11, equation (5.4.5) gives equations (5.4.6) and (5.4.7) for benzene-h_6 and benzene-d_6, respectively.

$$\left|\frac{\partial \bar{\mu}}{\partial S_4}\right| = 1.0473\left|\frac{\partial \bar{\mu}}{\partial Q_4}\right| = 1.0473 \times 1.54 \text{ Debye Å}^{-1} \tag{5.4.6}$$

$$\left|\frac{\partial \bar{\mu}}{\partial S_4}\right| = 1.4264\left|\frac{\partial \bar{\mu}}{\partial Q_4}\right| = 1.4264 \times 1.16 \text{ Debye Å}^{-1} \tag{5.4.7}$$

Thus $|\partial \bar{\mu}/\partial S_4| = 1.61 \pm 0.04$ Debye Å^{-1} for benzene-h_6 and $|\partial \bar{\mu}/\partial S_4| = 1.66 \pm 0.04$ Debye Å^{-1} for benzene-d_6. These values agree. The best value of $|\partial \bar{\mu}/\partial S_4|$ is taken to be the average of these two values and is tabulated in Table 5.12 with the other values of the dipole moment derivatives with respect to the symmetry coordinates.

Table 5.11. Dipole moment derivative with respect to the normal coordinates.

Normal Coordinate	Symmetry	C_6H_6		C_6D_6	
		C_j / km mole^{-1}	$\mu_j = \left\lvert\frac{\partial \bar{\mu}}{\partial Q_j}\right\rvert$ [a]	C_j / km mole^{-1}	$\mu_j = \left\lvert\frac{\partial \bar{\mu}}{\partial Q_j}\right\rvert$ [a]
Q_1	A_{1g}	0	0	0	0
Q_2	A_{1g}	0.00642 [b]	0.110 ± 0.008	0.00222	0.064 ± 0.005
Q_3	A_{2g}	0	0	0.00017	0.0178 ± 0.0013
Q_4	A_{2u}	1.27	1.54 ± 0.04	0.725	1.16 ± 0.03
Q_5	B_{1u}	0	0	0	0
Q_6	B_{1u}	0.00500 [c]	0.097 ± 0.007	0.00380	0.084 ± 0.006
Q_7	B_{2g}	0 [b]	0	0	0
Q_8	B_{2g}	0	0	0	0
Q_9	B_{2u}	0.00342	0.080 ± 0.006	0.00136	0.050 ± 0.004
Q_{10}	B_{2u}	0.0121	0.150 ± 0.011	0	0
Q_{11}	E_{1g}	0.0155	0.120 ± 0.009	0.00879 [d]	0.091 ± 0.007
Q_{12}	E_{1u}	0.539	0.710 ± 0.018	0.268	0.500 ± 0.012
Q_{13}	E_{1u}	0.234	0.468 ± 0.012	0.0679	0.252 ± 0.006
Q_{14}	E_{1u}	0.130	0.349 ± 0.009	0.132	0.352 ± 0.009
Q_{15}	E_{2g}	0	0	0	0
Q_{16}	E_{2g}	0.00538	0.071 ± 0.005	0.00642	0.077 ± 0.06
Q_{17}	E_{2g}	0.0233	0.148 ± 0.011	0.0183	0.131 ± 0.010
Q_{18}	E_{2g}	0	0	0.00865	0.090 ± 0.007
Q_{19}	E_{2u}	0.0163	0.123 ± 0.009	0	0
Q_{20}	E_{2u}	0.0087	0.029 ± 0.002	0 [e]	0

[a] The unit of μ_j is Debye Å^{-1} amu$^{-1/2}$.

[b] ν_2 and ν_7 are assigned to the same peak, the intensity is assumed to be all due to ν_2.

[c] ν_6 and $\nu_{18} + \nu_{20}$ are assigned to the same peak, this is the total intensity.

[d] ν_{11} and $\nu_{13} - \nu_{11}$ are assigned to the same peak, this is the total intensity.

[e] This peak is at 351 cm^{-1}, below the region measured in this work. The intensity is assumed to be 0.

Table 5.12. Dipole moment derivative with respect to symmetry coordinates.

Coordinate	Symmetry	Motion	$\frac{\partial \bar{\mu}}{\partial S_i}$ [a]
S_1	A_{1g}	CH stretch	0.025 ± 0.002
S_2	A_{1g}	CC stretch	0.34 ± 0.03
S_3	A_{2g}	HCC in plane bend	0.0078 ± 0.0006
S_4	A_{2u}	HCCC out-of-plane bend	1.63 ± 0.04
S_5	B_{1u}	CH stretch	0.031 ± 0.002
S_6	B_{1u}	CCC in-plane bend	0.14 ± 0.01
S_7	B_{2g}	HCCC out-of-plane bend	0
S_8	B_{2g}	CCCC torsion	0
S_9	B_{2u}	CC stretch	0.24 ± 0.02
S_{10}	B_{2u}	HCC in-plane bend	0.083 ± 0.006
S_{11}	E_{1g}	HCCC out-of-plane bend	0.12 ± 0.01
S_{12}	E_{1u}	CH stretch	0.64 ± 0.06
S_{13}	E_{1u}	CC stretch	0.39 ± 0.04
S_{14}	E_{1u}	HCC in-plane bend	0.46 ± 0.01
S_{15}	E_{2g}	CH stretch	0.024 ± 0.002
S_{16}	E_{2g}	CC stretch	-0.22 ± 0.02
S_{17}	E_{2g}	CCC in-plane bend	0.19 ± 0.01
S_{18}	E_{2g}	HCC in-plane bend	0.12 ± 0.01
S_{19}	E_{2u}	HCCC out-of-plane bend	0.13 ± 0.01
S_{20}	E_{2u}	CCCC torsion	-0.11 ± 0.01

[a] The unit is Debye Å^{-1}. Only relative signs are given. Within each symmetry species the values can all be multiplied by -1 and fit the experimental intensities equally well.

5.4.1b E_{1u} Vibrations

For the other three infrared active fundamentals, the conversion of the dipole moment derivatives with respect to the normal coordinate to the dipole moment derivatives with respect to the symmetry coordinate is a little more complicated. These three fundamentals all have E_{1u} symmetry. Consequently, equation (5.4.3), the expressions for the dipole moment derivatives with respect to the symmetry coordinates in terms of the dipole moment derivatives with respect to the normal coordinates, are linear equations in the three dipole moment derivatives with respect to the normal coordinates. With the inverse eigenvectors given in Table 5.10 equation (5.4.3) gives the following equations for benzene-h_6

$$\frac{\partial\bar{\mu}}{\partial S_{12}} = 0.9581\frac{\partial\bar{\mu}}{\partial Q_{12}} + 0.1679\frac{\partial\bar{\mu}}{\partial Q_{13}} + 0.1506\frac{\partial\bar{\mu}}{\partial Q_{14}} \tag{5.4.8}$$

$$\frac{\partial\bar{\mu}}{\partial S_{13}} = -0.0423\frac{\partial\bar{\mu}}{\partial Q_{12}} + 1.2884\frac{\partial\bar{\mu}}{\partial Q_{13}} + 2.8704\frac{\partial\bar{\mu}}{\partial Q_{14}} \tag{5.4.9}$$

$$\frac{\partial\bar{\mu}}{\partial S_{14}} = 0.0324\frac{\partial\bar{\mu}}{\partial Q_{12}} - 0.5077\frac{\partial\bar{\mu}}{\partial Q_{13}} + 0.5592\frac{\partial\bar{\mu}}{\partial Q_{14}} \tag{5.4.10}$$

and for benzene-d_6

$$\frac{\partial\bar{\mu}}{\partial S_{12}} = 1.2714\frac{\partial\bar{\mu}}{\partial Q_{12}} + 0.4491\frac{\partial\bar{\mu}}{\partial Q_{13}} + 0.2263\frac{\partial\bar{\mu}}{\partial Q_{14}} \tag{5.4.11}$$

$$\frac{\partial\bar{\mu}}{\partial S_{13}} = -0.2146\frac{\partial\bar{\mu}}{\partial Q_{12}} + 2.0219\frac{\partial\bar{\mu}}{\partial Q_{13}} + 2.7629\frac{\partial\bar{\mu}}{\partial Q_{14}} \tag{5.4.12}$$

$$\frac{\partial\bar{\mu}}{\partial S_{14}} = 0.0554\frac{\partial\bar{\mu}}{\partial Q_{12}} - 0.3982\frac{\partial\bar{\mu}}{\partial Q_{13}} + 0.9701\frac{\partial\bar{\mu}}{\partial Q_{14}} \tag{5.4.13}$$

The magnitudes of the dipole moment derivatives with respect to Q_{12}, Q_{13} and Q_{14} are given in Table 5.11. The values are $\mu_{12} = 0.710 \pm 0.018$, $\mu_{13} = 0.468 \pm 0.012$, $\mu_{14} = 0.349 \pm 0.009$ Debye Å^{-1} amu$^{-1/2}$ for benzene-h$_6$ and $\mu_{12} = 0.500 \pm 0.012$, $\mu_{13} = 0.252 \pm 0.006$, $\mu_{14} = 0.352 \pm 0.009$ Debye Å^{-1} amu$^{-1/2}$ for benzene-d$_6$.

The intensities depend on μ_j^2 and only the magnitudes of the dipole moment derivatives with respect to the normal coordinates are known. The signs can not be determined. But for E$_{1u}$ symmetry, all of the $\partial\bar{\mu}/\partial Q_j$ and $\partial\bar{\mu}/\partial S_i$ vectors lie along the x axis for the E_{1u}^a coordinates and along the y axis for all of the E_{1u}^b coordinates. The dipole moment derivatives must be the same for the a and the b coordinates, so it is only necessary to consider the a coordinates. Thus the $\partial\bar{\mu}/\partial S_i$ are either parallel or antiparallel to each other and to the $\partial\bar{\mu}/\partial Q_j$. Therefore, it is necessary to consider the possible sign combinations for the dipole moment derivatives with respect to normal coordinates Q_{12}, Q_{13} and Q_{14} in equation (5.4.8) to (5.4.13). There are eight possible sign combinations. The combinations '+++', '++-', '+-+' and '+--' provide independent values of the magnitude of the dipole moment derivatives with respect to the symmetry coordinates. The other four combinations are dependent on the first four, only providing a change in the sign of the dipole moment derivatives determined by these four combinations.

Table 5.13 lists the values of $\partial\bar{\mu}/\partial S_i$ obtained for these four sign combinations when the dipole moment derivatives with respect to the normal coordinates are substituted into equations (5.4.8) to (5.4.13). The '+-+' combination gives the best agreement between the calculated $\partial\bar{\mu}/\partial S_i$ values for benzene-h$_6$ and benzene-d$_6$. Goodman *et al.*[41] and Pulay *et al.*[124] have found the same sign combination appropriate to gaseous benzene, given the fact that their Q_{13} is defined in the opposite direction to that used here.

Table 5.13. Dipole moment derivatives with respect to symmetry coordinates of E_{1u} symmetry.

Results from inverse eigenvectors through equations (5.4.8) to (5.4.13)

Sign of $\frac{\partial\mu}{\partial Q}$	Molecule	$\partial\bar{\mu}/\partial S_{12}$	$\partial\bar{\mu}/\partial S_{13}$	$\partial\bar{\mu}/\partial S_{14}$
+++	C_6H_6	0.810 ± 0.020	1.552 ± 0.038	-0.022 ± 0.007
	C_6D_6	0.824 ± 0.021	1.353 ± 0.034	0.273 ± 0.009
++-	C_6H_6	0.707 ± 0.018	-0.411 ± 0.027	-0.405 ± 0.007
	C_6D_6	0.664 ± 0.017	-0.593 ± 0.028	-0.410 ± 0.009
+-+	C_6H_6	0.654 ± 0.017	0.351 ± 0.027	0.451 ± 0.007
	C_6D_6	0.607 ± 0.016	0.378 ± 0.028	0.465 ± 0.009
+--	C_6H_6	0.551 ± 0.017	-1.612 ± 0.027	0.068 ± 0.007
	C_6D_6	0.448 ± 0.016	-1.567 ± 0.028	-0.218 ± 0.009

Results of nonlinear least squares fit of equations (5.4.14) to (5.4.19)

	C_6H_6		C_6D_6	
	$\lvert\partial\bar{\mu}/\partial Q_j\rvert^2$ obs	$\lvert\partial\bar{\mu}/\partial Q_j\rvert^2$ calc	$\lvert\partial\bar{\mu}/\partial Q_j\rvert^2$ obs	$\lvert\partial\bar{\mu}/\partial Q_j\rvert^2$ calc
Q_{12}	0.50	0.49	0.25	0.28
Q_{13}	0.22	0.22	0.063	0.053
Q_{14}	0.12	0.13	0.12	0.12

$\partial\bar{\mu}/\partial S_{12}$	0.645 ± 0.012
$\partial\bar{\mu}/\partial S_{13}$	0.386 ± 0.063
$\partial\bar{\mu}/\partial S_{14}$	0.459 ± 0.015

Equation (5.4.4) can be used instead of equation (5.4.3) to relate the dipole moment derivative with respect to the symmetry coordinates to the dipole moment derivative with respect to the normal coordinates. Equation (5.4.4) and the eigenvectors given in Table 5.9 give the following equations for benzene-h_6

$$\left|\frac{\partial\bar{\mu}}{\partial Q_{12}}\right|^2 = \left|1.0356\frac{\partial\bar{\mu}}{\partial S_{12}} - 0.0810\frac{\partial\bar{\mu}}{\partial S_{13}} + 0.1370\frac{\partial\bar{\mu}}{\partial S_{14}}\right|^2 \qquad (5.4.14)$$

$$\left|\frac{\partial\bar{\mu}}{\partial Q_{13}}\right|^2 = \left|0.0554\frac{\partial\bar{\mu}}{\partial S_{12}} + 0.2525\frac{\partial\bar{\mu}}{\partial S_{13}} - 1.3108\frac{\partial\bar{\mu}}{\partial S_{14}}\right|^2 \qquad (5.4.15)$$

$$\left|\frac{\partial\bar{\mu}}{\partial Q_{14}}\right|^2 = \left|-0.0096\frac{\partial\bar{\mu}}{\partial S_{12}} + 0.2339\frac{\partial\bar{\mu}}{\partial S_{13}} + 0.5903\frac{\partial\bar{\mu}}{\partial S_{14}}\right|^2 \qquad (5.4.16)$$

and for benzene-d_6

$$\left|\frac{\partial\bar{\mu}}{\partial Q_{12}}\right|^2 = \left|0.7562\frac{\partial\bar{\mu}}{\partial S_{12}} - 0.1299\frac{\partial\bar{\mu}}{\partial S_{13}} + 0.1935\frac{\partial\bar{\mu}}{\partial S_{14}}\right|^2 \qquad (5.4.17)$$

$$\left|\frac{\partial\bar{\mu}}{\partial Q_{13}}\right|^2 = \left|0.0892\frac{\partial\bar{\mu}}{\partial S_{12}} + 0.3015\frac{\partial\bar{\mu}}{\partial S_{13}} - 0.8796\frac{\partial\bar{\mu}}{\partial S_{14}}\right|^2 \qquad (5.4.18)$$

$$\left|\frac{\partial\bar{\mu}}{\partial Q_{14}}\right|^2 = \left|-0.0066\frac{\partial\bar{\mu}}{\partial S_{12}} + 0.1312\frac{\partial\bar{\mu}}{\partial S_{13}} + 0.6587\frac{\partial\bar{\mu}}{\partial S_{14}}\right|^2 \qquad (5.4.19)$$

The $\left|\partial\bar{\mu}/\partial Q_j\right|^2$ on the left hand side of equations (5.4.14) to (5.4.19) are the quantities that are obtained from the measurement of the intensities. Therefore, these equations provide 6 equations with three unknown; $\partial\bar{\mu}/\partial S_{12}$, $\partial\bar{\mu}/\partial S_{13}$ and $\partial\bar{\mu}/\partial S_{14}$. The last row of Table 5.13 gives the $\partial\bar{\mu}/\partial S_j$ values obtained from a nonlinear least squares fit of the three $\partial\bar{\mu}/\partial S_j$ values to the six $\left|\partial\bar{\mu}/\partial Q_j\right|^2$ values. The values obtained from the least squares fit agree with the values determined above from equations (5.4.8) to (5.4.13) with the '+-+' sign combination.

The best values of the dipole moment derivatives with respect to the symmetry coordinates are taken as $\partial\bar{\mu}/\partial S_{12} = 0.64 \pm 0.06$, $\partial\bar{\mu}/\partial S_{13} = 0.39 \pm 0.04$ and $\partial\bar{\mu}/\partial S_{14} = 0.46 \pm 0.01$ Debye Å^{-1}. These values are the values obtained from the least squares fit. Each error limit is the larger of the deviations from the best value of the two values obtained for benzene-h$_6$ and benzene-d$_6$ from equations (5.4.8) to (5.4.13) plus the error due to estimated accuracy of the dipole moment derivatives with respect to the normal coordinates (about 2.5%).

5.4.2 Dipole Moment Derivatives With Respect to Symmetry Coordinates for the Vibrations that are not Infrared Active Under D_{6h}

For these vibrations, the displacements of the different parts of the molecule in the gas phase are such that the dipole moment induced by the displacements in one part are exactly cancelled by the dipole moments induced by the displacements in the remainder of the molecule. Thus, all $\partial\bar{\mu}/\partial Q_j$ and $\partial\bar{\mu}/\partial S_i$ magnitudes are zero in the gas phase. In the liquid phase some of these vibrations are observed, usually with low intensity. Two mechanisms are envisaged for the activation of these vibrations, and both result from the fact that the there is no symmetry at all at the site in the liquid occupied by the molecule. The liquid molecules are asymmetrically arranged about the molecule of interest, so there is no symmetry to the intermolecular forces that act on the molecule in the liquid.

The first activating mechanism is the slight distortion of the molecular geometry from the D_{6h} symmetry of the gas by the asymmetric arrangement of the surrounding molecules. Thus, the dipole moment induced by atomic displacements in one part of the molecule is not quite cancelled by those induced in other parts . The second activating mechanism arises without the need for distortion of the molecular geometry, because the dipole moment change induced in one part of the molecule by the atomic displacements itself induces a responding dipole moment in the surrounding molecules. Because the arrangement of the surrounding molecules is not symmetric, the dipole moment change induced in a different part of the molecule by the atomic displacements induces a different responding dipole moment in the surrounding molecules. These responding dipole moments do not cancel each other, even if the dipole moment changes in the molecule do cancel.

It is clear that these two mechanisms are not independent. But both argue that the activity is caused by the asymmetric arrangement of molecules about the molecule of interest, and that the direction of the dipole moment change is determined by the asymmetry of the surrounding molecules.

The distortion of benzene from D_{6h} symmetry in the liquid is clearly small[182], so it is useful and meaningful to consider the direction and values of $\partial\bar{\mu}/\partial S_i$ vectors that are zero for the gaseous molecule. The above activation mechanisms argue that the $\partial\bar{\mu}/\partial S_i$ vectors are all parallel for symmetry coordinates of a given symmetry, because their direction is determined by the asymmetry of the surrounding molecules.

Thus, equation (5.3.4) is used in the following sub-sections, with the assumption that the $\partial\bar{\mu}/\partial S_i$ and $\partial\bar{\mu}/\partial Q_j$ vectors are all parallel, to determine values of $\partial\bar{\mu}/\partial S_i$ for these liquid-activated vibrations. The resulting $\partial\bar{\mu}/\partial S_i$ values are summarized in Table 5.12.

5.4.2a A_{1g} Vibrations

Equation (5.4.4) gives the following equations with the eigenvectors given in Table 5.9 and the $\left|\partial\bar{\mu}/\partial Q_j\right|$ values in Table 5.11 for benzene-h_6

$$\left|\frac{\partial\bar{\mu}}{\partial Q_1}\right|^2 = 0 = \left|1.0369\frac{\partial\bar{\mu}}{\partial S_1} - 0.0859\frac{\partial\bar{\mu}}{\partial S_2}\right|^2 \tag{5.4.20}$$

$$\left|\frac{\partial\bar{\mu}}{\partial Q_2}\right|^2 = 0.0121 = \left|0.0210\frac{\partial\bar{\mu}}{\partial S_1} + 0.2756\frac{\partial\bar{\mu}}{\partial S_2}\right|^2 \tag{5.4.21}$$

and for benzene-d_6

$$\left|\frac{\partial\bar{\mu}}{\partial Q_1}\right|^2 = 0 = \left|0.7598\frac{\partial\bar{\mu}}{\partial S_1} - 0.1267\frac{\partial\bar{\mu}}{\partial S_2}\right|^2 \tag{5.4.22}$$

$$\left|\frac{\partial\bar{\mu}}{\partial Q_2}\right|^2 = 0.00410 = \left|-0.0500\frac{\partial\bar{\mu}}{\partial S_1} + 0.2594\frac{\partial\bar{\mu}}{\partial S_2}\right|^2 \tag{5.4.23}$$

The values $\left|\partial\bar{\mu}/\partial S_1\right| = 0.025 \pm 0.002$ Debye Å^{-1} and $\left|\partial\bar{\mu}/\partial S_2\right| = 0.336 \pm 0.025$ Debye Å^{-1} were obtained by nonlinear least squares fit to equations (5.4.20) to (5.4.23).

5.4.2b A_{2g} Vibrations

From equation (5.3.4), Table 5.9 and Table 5.11, the equations are for benzene-h_6

$$\left|\frac{\partial\bar{\mu}}{\partial Q_3}\right|^2 = 0 = \left|1.4594\frac{\partial\bar{\mu}}{\partial S_3}\right|^2 \tag{5.4.24}$$

and for benzene-d_6

$$\left|\frac{\partial\bar{\mu}}{\partial Q_3}\right|^2 = 0.00032 = \left|1.1355\frac{\partial\bar{\mu}}{\partial S_3}\right|^2 \tag{5.4.25}$$

Clearly $|\partial\bar{\mu}/\partial S_3| = 0.0$ Debye Å^{-1} for benzene-h$_6$ and 0.0157 ± 0.0011 Debye Å^{-1} for benzene-d$_6$, for an average value 0.008 Debye Å^{-1}.

5.4.2c B_{1u} Vibrations

The eigenvectors given in Table 5.9, the $|\partial\bar{\mu}/\partial Q_j|$ values in Table 5.11, and equation (5.4.4) give the following equations for benzene-h$_6$

$$\left|\frac{\partial\bar{\mu}}{\partial Q_5}\right|^2 = 0 = \left|1.0370\frac{\partial\bar{\mu}}{\partial S_5} - 0.1909\frac{\partial\bar{\mu}}{\partial S_6}\right|^2 \tag{5.4.26}$$

$$\left|\frac{\partial\bar{\mu}}{\partial Q_6}\right|^2 = 0.0094 = \left|-0.0136\frac{\partial\bar{\mu}}{\partial S_5} + 0.6926\frac{\partial\bar{\mu}}{\partial S_6}\right|^2 \tag{5.4.27}$$

and for benzene-d$_6$

$$\left|\frac{\partial\bar{\mu}}{\partial Q_5}\right|^2 = 0 = \left|0.7613\frac{\partial\bar{\mu}}{\partial S_5} - 0.2862\frac{\partial\bar{\mu}}{\partial S_6}\right|^2 \tag{5.4.28}$$

$$\left|\frac{\partial\bar{\mu}}{\partial Q_6}\right|^2 = 0.0071 = \left|0.0159\frac{\partial\bar{\mu}}{\partial S_5} + 0.6589\frac{\partial\bar{\mu}}{\partial S_6}\right|^2 \tag{5.4.29}$$

Nonlinear least squares solution gave $|\partial\bar{\mu}/\partial S_5| = 0.031 \pm 0.002$ Debye Å^{-1} and $|\partial\bar{\mu}/\partial S_6| = 0.135 \pm 0.010$ Debye Å^{-1}.

5.4.2d B_{2g} Vibrations

Normal coordinates Q_7 and Q_8 have B$_{2g}$ symmetry, but neither vibration was observed in the α''_{m} spectrum of benzene-h$_6$ or benzene-d$_6$ (Table 5.11). Thus $|\partial\bar{\mu}/\partial S_7| = |\partial\bar{\mu}/\partial S_8| = 0.0$.

5.4.2e B_{2u} Vibrations

The eigenvectors given in Table 5.9, the $\left|\partial\bar{\mu}/\partial Q_j\right|$ values in Table 5.11, and equation (5.4.4) give the following equations for benzene-h_6

$$\left|\frac{\partial\bar{\mu}}{\partial Q_9}\right|^2 = 0.0064 = \left|0.4522\frac{\partial\bar{\mu}}{\partial S_9} - 0.8933\frac{\partial\bar{\mu}}{\partial S_{10}}\right|^2 \tag{5.4.30}$$

$$\left|\frac{\partial\bar{\mu}}{\partial Q_{10}}\right|^2 = 0.0225 = \left|0.2134\frac{\partial\bar{\mu}}{\partial S_9} + 1.0125\frac{\partial\bar{\mu}}{\partial S_{10}}\right|^2 \tag{5.4.31}$$

and for benzene-d_6

$$\left|\frac{\partial\bar{\mu}}{\partial Q_9}\right|^2 = 0.0025 = \left|0.4968\frac{\partial\bar{\mu}}{\partial S_9} - 0.4768\frac{\partial\bar{\mu}}{\partial S_{10}}\right|^2 \tag{5.4.32}$$

$$\left|\frac{\partial\bar{\mu}}{\partial Q_{10}}\right|^2 = 0 = \left|0.0563\frac{\partial\bar{\mu}}{\partial S_9} + 0.8692\frac{\partial\bar{\mu}}{\partial S_{10}}\right|^2 \tag{5.4.33}$$

Nonlinear least squares solution gave $\left|\partial\bar{\mu}/\partial S_9\right| = 0.243 \pm 0.018$ Debye Å^{-1} and $\left|\partial\bar{\mu}/\partial S_{10}\right| = 0.083 \pm 0.006$ Debye Å^{-1}.

5.4.2f E_{1g} Vibrations

The eigenvectors given in Table 5.9, the $\left|\partial\bar{\mu}/\partial Q_j\right|$ values in Table 5.11, and equation (5.4.4) give the following equations for benzene-h_6

$$\left|\frac{\partial\bar{\mu}}{\partial Q_{11}}\right|^2 = 0.0144 = \left|1.0319\frac{\partial\bar{\mu}}{\partial S_{11}}\right|^2 \tag{5.4.34}$$

and for benzene-d_6

$$\left|\frac{\partial\bar{\mu}}{\partial Q_{11}}\right|^2 = 0.0083 = \left|0.8029\frac{\partial\bar{\mu}}{\partial S_{11}}\right|^2 \tag{5.4.35}$$

Thus $|\partial\bar{\mu}/\partial S_{11}| = 0.116 \pm 0.009$ for benzene-h$_6$ and 0.113 ± 0.009 for benzene-d$_6$ for an average value of 0.115 ± 0.009 Debye Å^{-1}.

5.4.2g E_{2g} Vibrations

The eigenvectors given in Table 5.9, the $|\partial\bar{\mu}/\partial Q_j|$ values in Table 5.11, and equation (5.4.4) give the following equations for benzene-h$_6$

$$\left|\frac{\partial\bar{\mu}}{\partial Q_{15}}\right|^2 = \left|-1.0261\frac{\partial\bar{\mu}}{\partial S_{15}} + 0.0214\frac{\partial\bar{\mu}}{\partial S_{16}} + 0.1386\frac{\partial\bar{\mu}}{\partial S_{17}} - 0.1394\frac{\partial\bar{\mu}}{\partial S_{18}}\right|^2 \tag{5.4.36}$$

$$\left|\frac{\partial\bar{\mu}}{\partial Q_{16}}\right|^2 = \left|0.0863\frac{\partial\bar{\mu}}{\partial S_{15}} - 0.4278\frac{\partial\bar{\mu}}{\partial S_{16}} - 0.3720\frac{\partial\bar{\mu}}{\partial S_{17}} - 0.8966\frac{\partial\bar{\mu}}{\partial S_{18}}\right|^2 \tag{5.4.37}$$

$$\left|\frac{\partial\bar{\mu}}{\partial Q_{17}}\right|^2 = \left|0.1194\frac{\partial\bar{\mu}}{\partial S_{15}} + 0.1535\frac{\partial\bar{\mu}}{\partial S_{16}} + 0.0510\frac{\partial\bar{\mu}}{\partial S_{17}} - 1.0417\frac{\partial\bar{\mu}}{\partial S_{18}}\right|^2 \tag{5.4.38}$$

$$\left|\frac{\partial\bar{\mu}}{\partial Q_{18}}\right|^2 = \left|-0.0316\frac{\partial\bar{\mu}}{\partial S_{15}} - 0.0357\frac{\partial\bar{\mu}}{\partial S_{16}} + 0.4029\frac{\partial\bar{\mu}}{\partial S_{17}} - 0.1537\frac{\partial\bar{\mu}}{\partial S_{18}}\right|^2 \tag{5.4.39}$$

and for benzene-d$_6$

$$\left|\frac{\partial\bar{\mu}}{\partial Q_{15}}\right|^2 = \left|0.7553\frac{\partial\bar{\mu}}{\partial S_{15}} - 0.0464\frac{\partial\bar{\mu}}{\partial S_{16}} - 0.2088\frac{\partial\bar{\mu}}{\partial S_{17}} + 0.0370\frac{\partial\bar{\mu}}{\partial S_{18}}\right|^2 \tag{5.4.40}$$

$$\left|\frac{\partial\bar{\mu}}{\partial Q_{16}}\right|^2 = \left|-0.0261\frac{\partial\bar{\mu}}{\partial S_{15}} + 0.4465\frac{\partial\bar{\mu}}{\partial S_{16}} + 0.3624\frac{\partial\bar{\mu}}{\partial S_{17}} + 0.6370\frac{\partial\bar{\mu}}{\partial S_{18}}\right|^2 \tag{5.4.41}$$

$$\left|\frac{\partial\bar{\mu}}{\partial Q_{17}}\right|^2 = \left|0.0809\frac{\partial\bar{\mu}}{\partial S_{15}} + 0.0781\frac{\partial\bar{\mu}}{\partial S_{16}} - 0.0730\frac{\partial\bar{\mu}}{\partial S_{17}} + 0.7982\frac{\partial\bar{\mu}}{\partial S_{18}}\right|^2 \tag{5.4.42}$$

$$\left|\frac{\partial\bar{\mu}}{\partial Q_{18}}\right|^2 = \left|-0.0466\frac{\partial\bar{\mu}}{\partial S_{15}} - 0.0272\frac{\partial\bar{\mu}}{\partial S_{16}} + 0.3772\frac{\partial\bar{\mu}}{\partial S_{17}} - 0.2179\frac{\partial\bar{\mu}}{\partial S_{18}}\right|^2 \tag{5.4.43}$$

The magnitudes of the dipole moment derivative with respect to normal coordinates 15, 16, 17 and 18 are given in Table 5.11. The values of $\partial\bar{\mu}/\partial S_{15}$, $\partial\bar{\mu}/\partial S_{16}$, $\partial\bar{\mu}/\partial S_{17}$ and $\partial\bar{\mu}/\partial S_{18}$ were obtained by nonlinear least squares fit to the observed dipole moment derivative with respect to the normal coordinates through equations (5.4.36) to (5.4.43) and are given in Table 5.12.

5.4.2h E_{2u} Vibrations

The eigenvectors given in Table 5.9, the $\left|\partial\bar{\mu}/\partial Q_j\right|$ values in Table 5.11, and equation (5.4.4) give the following equations for benzene-h_6

$$\left|\frac{\partial\bar{\mu}}{\partial Q_{19}}\right|^2 = 0.0151 = \left|1.2496\frac{\partial\bar{\mu}}{\partial S_{19}} + 0.4432\frac{\partial\bar{\mu}}{\partial S_{20}}\right|^2 \qquad (5.4.44)$$

$$\left|\frac{\partial\bar{\mu}}{\partial Q_{20}}\right|^2 = 0.0008 = \left|0.2606\frac{\partial\bar{\mu}}{\partial S_{19}} + 0.7012\frac{\partial\bar{\mu}}{\partial S_{20}}\right|^2 \qquad (5.4.45)$$

and for benzene-d_6

$$\left|\frac{\partial\bar{\mu}}{\partial Q_{19}}\right|^2 = 0 = \left|1.0904\frac{\partial\bar{\mu}}{\partial S_{19}} + 0.6010\frac{\partial\bar{\mu}}{\partial S_{20}}\right|^2 \qquad (5.4.46)$$

$$\left|\frac{\partial\bar{\mu}}{\partial Q_{20}}\right|^2 = 0 = \left|0.1421\frac{\partial\bar{\mu}}{\partial S_{19}} + 0.5718\frac{\partial\bar{\mu}}{\partial S_{20}}\right|^2 \qquad (5.4.47)$$

Nonlinear least squares solution gave $\left|\partial\bar{\mu}/\partial S_{19}\right| = 0.13 \pm .01$ Debye Å^{-1} and $\left|\partial\bar{\mu}/\partial S_{20}\right| = 0.112 \pm 0.008$ Debye Å^{-1}.

5.4.2i The Validity of the Parallel Dipole Approximation For Vibrations Inactive Under D_{6h}

The above calculations assumed that all of the induced $\partial\bar{\mu}/\partial S_i$ vectors in a symmetry species are parallel. To check on the possible error incurred by this assumption, values of $\partial\bar{\mu}/\partial S_i$ were also calculated under the other extreme assumption, that the angle between the different $\partial\bar{\mu}/\partial S_i$ vectors of the same symmetry vary randomly from molecule to molecule. In this case, the squares of sums in equations (5.4.20) to (5.4.47) become sums of squared terms. The resulting equations can be solved for some symmetries if it is accepted that the zero intensity of some vibrations may, in fact, be small but not zero. The magnitudes of $\partial\bar{\mu}/\partial S_i$ obtained from this assumption were very similar to those obtained above. Thus, the values of $\partial\bar{\mu}/\partial S_i$ summarized in Table 5.12 are not believed to be greatly in error because of the assumption used to obtain them from the $\partial\bar{\mu}/\partial S_i$ values.

5.4.2j Summary and Discussion of Vibrations Inactive Under D_{6h}

Table 5.12 includes the values of $\partial\bar{\mu}/\partial S_i$ calculated in this subsection, 5.4.2, for the symmetry coordinates S_1 to S_3, S_5 to S_{11} and S_{15} to S_{20} which do not yield infrared activity under D_{6h}. For the coordinates that deal primarily with motion of the hydrogen atoms, CH stretching and HCC deformation, the $\partial\bar{\mu}/\partial S_i$ values are all small, 0.025 ± 0.005 Debye Å^{-1} for the stretch and 0.08 ± 0.08 Debye Å^{-1} for the deformation, with no distinction between in-plane and out-of-plane deformation. The $\partial\bar{\mu}/\partial S_i$ values for the out-of-plane CCCC torsion coordinates are of the same magnitude, 0 to 0.11 Debye Å^{-1}. For the coordinates that deal with the in-plane motion of the carbon atoms, the $\partial\bar{\mu}/\partial S_i$ values are larger, 0.27 ± 0.07 Debye Å^{-1} for the stretching coordinates and 0.17 ± 0.03 Debye Å^{-1} for the CCC deformation coordinates. It is natural to relate this greater intensity associated with in-plane displacements of the carbon atoms to a greater sensitivity of the π electron cloud above and below the ring to the anisotropy of the intermolecular forces. The π electrons are known to be more polarizable than the σ electrons of the CH bonds, so this provides a satisfactory qualitative understanding of the pattern of infrared activation by the liquid of vibrations that are inactive in the gas.

5.4.3 Dipole Moment Derivatives With Respect to the Internal Coordinates

From the definition of the symmetry coordinates in terms of the internal coordinates (Table 5.5) and the dipole moment derivatives with respect to the symmetry coordinates (Table 5.12), the dipole moment derivatives with respect to the internal coordinates can be calculated. The appropriate equation is

$$\frac{\partial \bar{\mu}}{\partial R_j} = \sum_{i=1}^{3n-6} \frac{\partial \bar{\mu}}{\partial S_i} \frac{\partial S_i}{\partial R_j} = \sum_{i=1}^{3n-6} \frac{\partial \bar{\mu}}{\partial S_i} U_{ij} \qquad j = 1, 2, \ldots, 3n-6 \qquad (5.4.48)$$

Only the modes that are infrared active under D_{6h} are included in the sum. The $\partial\bar{\mu}/\partial S_i$ vectors that are non-zero only because of the asymmetry in the surrounding molecules reflect that asymmetry rather than properties intrinsic to the pseudo-D_{6h} molecule. It is important to note that the sum is over $\partial\bar{\mu}/\partial S_i$ vectors of all infrared active species, A_{1u} and E_{1u}, so not all of the vectors are parallel. The vector sum must therefore be taken.

In the next subsections, the dipole moment derivatives with respect to the symmetry coordinates are converted to dipole moment derivatives with respect to the CH stretch coordinates, the CC stretch coordinates, the HCC deformation coordinates and the HCCC out-of-plane angle coordinates.

5.4.3a Dipole Moment Derivatives With Respect to CH Stretch Coordinates

$S_{12}(E_{1u})$ is the only symmetry coordinate which involves the CH stretching displacement in infrared active vibrations. From the definition of the symmetry coordinates in Table 5.5 and equation (5.4.48), the dipole moment derivatives with respect to the CH stretch coordinates, R_1 to R_6, can be obtained. Equation (5.4.48), simplifies to equation (5.4.49) in this case.

$$\frac{\partial \bar{\mu}}{\partial R_j} = \frac{\partial \bar{\mu}}{\partial S_{12a}} \frac{\partial S_{12a}}{\partial R_j} + \frac{\partial \bar{\mu}}{\partial S_{12b}} \frac{\partial S_{12b}}{\partial R_j} \qquad j = 1, 2, \ldots, 6 \qquad (5.4.49)$$

$\partial \bar{\mu}/\partial S_{12a}$ and $\partial \bar{\mu}/\partial S_{12b}$ are orthogonal and have the same magnitude. The dipole moment derivatives with respect to internal coordinates R_1 to R_6 all have the same magnitude but point in different directions. The magnitudes of the dipole moment derivatives with respect to R_1 to R_6, called $\partial \mu/\partial s$, are, thus, given by

$$\frac{\partial \mu}{\partial s} = \frac{1}{\sqrt{3}} \left| \frac{\partial \bar{\mu}}{\partial S_{12}} \right| \qquad (5.4.50)$$

With the value of $|\partial \bar{\mu}/\partial S_{12}|$ given in Table 5.12, this gives $\partial \mu/\partial s = 0.37 \pm 0.03$ Debye Å^{-1}.

5.4.3b Dipole Moment Derivatives With Respect to CC Stretch Coordinates

The only infrared-active CC stretching symmetry coordinate is S_{13} which is also in E_{1u}. Thus, equation (5.3.48) for the CC stretching coordinates R_7 to R_{12} is

$$\frac{\partial \bar{\mu}}{\partial R_j} = \frac{\partial \bar{\mu}}{\partial S_{13a}} \frac{\partial S_{13a}}{\partial R_j} + \frac{\partial \bar{\mu}}{\partial S_{13b}} \frac{\partial S_{13b}}{\partial R_j} \qquad j = 7, 8, \ldots, 12 \qquad (5.4.51)$$

By analogous arguments to those for the CH stretching coordinates, the magnitudes of the dipole moment derivatives with respect to R_7 to R_{12}, called $\partial \mu/\partial t$, are given by

$$\frac{\partial \mu}{\partial t} = \frac{1}{\sqrt{3}} \left| \frac{\partial \bar{\mu}}{\partial S_{13}} \right| \qquad (5.4.52)$$

From the value of $|\partial \bar{\mu}/\partial S_{13}|$ given in Table 5.12, it is determined that $\partial \mu/\partial t = 0.23 \pm 0.02$ Debye Å^{-1}.

5.4.3c Dipole Moment Derivatives With Respect to HCC Deformation Coordinates

The treatment of the HCC deformation coordinates R_{13} to R_{18} is identical to that of the CH and CC stretching modes. The only symmetry coordinate involved is S_{14} (Table 5.5) so equation (5.4.48), simplifies to

$$\frac{\partial\mu}{\partial R_j} = \frac{\partial\mu}{\partial S_{14\mathrm{a}}}\frac{\partial S_{14\mathrm{a}}}{\partial R_j} + \frac{\partial\mu}{\partial S_{14\mathrm{b}}}\frac{\partial S_{14\mathrm{b}}}{\partial R_j} \qquad j = 13,14,\ldots,18 \qquad (5.4.53)$$

$\partial\bar{\mu}/\partial S_{14\mathrm{a}}$ and $\partial\bar{\mu}/\partial S_{14\mathrm{b}}$ are orthogonal and have the same magnitude. The dipole moment derivatives with respect to internal coordinates R_{13} to R_{18} all have the same magnitude, $\partial\mu/\partial\beta$, but point in different directions. The value of $\partial\mu/\partial\beta$, is given by

$$\frac{\partial\mu}{\partial\beta} = \frac{1}{\sqrt{3}}\left|\frac{\partial\bar{\mu}}{\partial S_{14}}\right| \qquad (5.4.54)$$

Table 5.12 gives $|\partial\bar{\mu}/\partial S_{14}|$ =0.46 ± 0.01 Debye Å^{-1}, so $\partial\mu/\partial\beta = 0.263 \pm 0.006$ Debye Å^{-1}.

5.4.3d Dipole Moment Derivatives With Respect to HCCC Out-Of-Plane Angle Coordinates

The only infrared active symmetry coordinate formed by the HCCC out-of-plane angle coordinates, R_{22} to R_{27}, is $S_4(\mathrm{A}_{2u})$ (Table 5.5) so equation (5.4.48) simplifies to equation (5.4.55).

$$\frac{\partial\bar{\mu}}{\partial R_j} = \frac{\partial\bar{\mu}}{\partial S_4}\frac{\partial S_4}{\partial R_j} \qquad j = 22,23,\ldots,27 \qquad (5.4.55)$$

The dipole moment derivatives with respect to internal coordinates R_{22} to R_{27} are all perpendicular to the plane of the ring and all have the same magnitude, $\partial\mu/\partial\gamma$. The value of $\partial\mu/\partial\gamma$ is given by

$$\frac{\partial\mu}{\partial\gamma} = \frac{1}{\sqrt{6}}\left|\frac{\partial\bar{\mu}}{\partial S_4}\right| \tag{5.4.56}$$

where $|\partial\bar{\mu}/\partial S_4| = 1.63 \pm 0.04$ (Table 5.12). Thus $\partial\mu/\partial\gamma = 0.665 \pm 0.016$ Debye Å^{-1}.

5.4.3e Summary of Dipole Moment Derivatives of Vibrations Active Under D_{6h}

The dipole moment derivatives with respect to symmetry coordinates are summarized in Table 5.12. They are $\partial\bar{\mu}/\partial S_i = 1.63\pm0.04$, 0.64 ± 0.06, 0.39 ± 0.04 and 0.46 ± 0.01 Debye Å^{-1} for $i = 4, 12, 13, 14$, respectively. The dipole moment derivatives with respect to the internal coordinates calculated in this subsection, 5.4.3, are

$$\partial\mu/\partial R_{\mathrm{CH}} = \partial\mu/\partial s = 0.37 \pm 0.03 \text{ Debye Å}^{-1}$$

$$\partial\mu/\partial R_{\mathrm{CC}} = \partial\mu/\partial t = 0.23 \pm 0.02 \text{ Debye Å}^{-1}$$

$$\partial\mu/\partial(1\text{Å} \times \phi_{\mathrm{HCC}}) = \partial\mu/\partial\beta = 0.263 \pm 0.006 \text{ Debye Å}^{-1}$$

$$\partial\mu/\partial(1\text{Å} \times \gamma_{\mathrm{HCCC}}) = \partial\mu/\partial\gamma = 0.665 \pm 0.016 \text{ Debye Å}^{-1}$$

These values are discussed in conjunction with those obtained for gaseous benzene in section 6.2

Chapter 6

Comparison of Liquid and Gas Phase Intensities of Benzene-h_6 and Benzene-d_6

In Chapter 5, the integrated intensities of benzene-h_6 and benzene-d_6 in the liquid phase were discussed. It was found that many of the fundamentals that were inactive in the gas phase are active in the liquid phase due to the asymmetric intermolecular interactions in the liquid. In this chapter, the integrated intensities of the active fundamentals of benzene-h_6 and benzene-d_6 in the liquid phase are compared to the gas phase integrated intensities to explore the effect of the intermolecular interactions on these fundamentals.

The integrated intensities of benzene-h_6 in the liquid[5-8, 12, 18-20, 32, 33, 36-38, 43] and the gas[2, 31, 35, 39-42] phases have been measured by many workers. The intensities of benzene-d_6 in the liquid have only been measured once[36] while those in the gas have been measured 5 times[34, 39-42].

The most recent summary of the results and comparison of the intensities in the two phases was made by Zelano and King in 1970[36]. Since 1970 the integrated intensities of benzene-h_6 gas and benzene-d_6 gas have each been measured four times[39-42] and the integrated intensities of liquid benzene-h_6 have been measured four times[12, 37, 38, 43], apart from those measured in this work, but those of liquid benzene-d_6 were not measured until the present work.

The necessary theory required to compare the integrated intensities of the gas and liquid is developed in section 6.1. In section 6.2, the experimental intensities of the gas and liquid phases are compared for the infrared active fundamentals of benzene-h_6 and benzene-d_6. In section 6.3, the experimental gas phase and liquid phase intensities of benzene-h_6 are compared with the *ab initio* intensities in the literature.

6.1 Principles

The quantities that are usually compared are the integrated intensities A_j of vibration j in the gas and liquid phases. The intensity A_j is defined[133] by equation (1.3.34).

The theoretical quantities of interest are the transition moment, $\vec{R}_j$, and the magnitude of the dipole moment derivative with respect to normal coordinate Q_j, $\mu_j = \left|\frac{\partial \mu}{\partial Q_j}\right|$. Under the usual assumption that the oscillators are mechanically and electrically harmonic the transition moment is for the fundamental transition, i.e. that between the ground state and the first excited state of vibration j. Under these assumptions and the additional usual assumption that the Lorentz local field is valid for the liquid, the integrated intensities A_j are related to these theoretical quantities by equations (1.3.47) and (1.3.48), where for the gas $\underline{n} = 1$[62]. From these equations, the ratio of $A_{j,\text{liq}}$ to $A_{j,\text{gas}}$ is

$$\frac{A_{j,\text{liq}}}{A_{j,\text{gas}}} = \frac{1}{\underline{n}}\left(\frac{\underline{n}^2+2}{3}\right)^2 \frac{\tilde{\nu}_{j,\text{liq}}\left|\vec{R}_{j,\text{liq}}\right|^2}{\tilde{\nu}_{j,\text{gas}}\left|\vec{R}_{j,\text{gas}}\right|^2} = \frac{1}{\underline{n}}\left(\frac{\underline{n}^2+2}{3}\right)^2 \frac{\mu^2_{j,\text{liq}}}{\mu^2_{j,\text{gas}}} \qquad (6.1.1)$$

The comparison of gas and liquid intensities is usually made relative to the unperturbed case, in which the molecular properties are the same in the gas and liquid phases. Thus, in the unperturbed case $\tilde{\nu}_j \left|\vec{R}_j\right|^2$ is the same for gas and liquid phases, $\mu^2_{j,\text{liq}} = \mu^2_{j,\text{gas}}$, and equation (6.1.1) becomes

$$\frac{A_{j,\text{liq}}}{A_{j,\text{gas}}} = \frac{1}{\underline{n}}\left(\frac{\underline{n}^2+2}{3}\right)^2 = \frac{1}{\sqrt{\underline{\varepsilon}}}\left(\frac{\underline{\varepsilon}+2}{3}\right)^2 \qquad (6.1.2)$$

This is the Polo-Wilson equation[61, 63], the equation that is usually used to compare intensities in the two phases. It is convenient to call the numerical value of the right hand side of equation (6.1.2) the *Polo-Wilson value*.

Equation (6.1.2) gives the Polo-Wilson equation in terms of both the real refractive index, $\underline{n}$, and the real dielectric constant, $\underline{\varepsilon}$. Refractive indices are near 1.5 for many liquids, which gives 1.35 for the Polo-Wilson value. However, both the refractive index and the dielectric constant are different for different compounds and are wavenumber-dependent. Thus, the Polo-Wilson value is different for bands of different compounds and even for different bands of the same compound.

Consideration of the spectrum of the imaginary molar polarizability of the liquid,[27, 29, 30] $\alpha''_{\text{m}}(\tilde{\nu})$, yields a more convenient ratio. This ratio equals unity for all bands of all compounds in the unperturbed case, $\mu^2_{j,\text{liq}} = \mu^2_{j,\text{gas}}$. It is obtained in the following way.

The Polo-Wilson equation assumes the Lorentz local field. Under the same assumption, it was shown in section 1.3 that the complex molar polarizability, $\hat{\alpha}_{\text{m}}(\tilde{\nu})$, can be calculated from the complex dielectric constant, $\hat{\varepsilon}(\tilde{\nu})$, or from the complex refractive index, $\hat{n}(\tilde{\nu})$ through the generalized form of the Lorentz-Lorenz formula[54].

The area C_j was defined in section 1.3 as the area under the band due to vibration j in the spectrum of $\tilde{\nu}\alpha''_{\text{m}}$. C_j is related to the transition moment and dipole moment derivative through equations (1.3.37) and (1.3.38), respectively.

Equations (1.3.38) and (1.3.48) give

$$8\pi^2 \frac{C_{j,\mathrm{liq}}}{A_{j,\mathrm{gas}}} = \frac{\mu_{j,\mathrm{liq}}^2}{\mu_{j,\mathrm{gas}}^2} \qquad (6.1.3)$$

which means that

$$8\pi^2 \frac{C_{j,\mathrm{liq}}}{A_{j,\mathrm{gas}}} = 1 \qquad (6.1.4)$$

for all bands of all liquids in the unperturbed case.

6.2 Comparison of Experimental Gas Phase and Liquid Phase Intensities

In this section the intensities of the four infrared active fundamentals of benzene in the gas and liquid phases are compared through ratio $A_{j,\mathrm{liq}} / A_{j,\mathrm{gas}}$ for convenient comparison with previous studies, and are compared in more detail through the ratio $8\pi^2 \frac{C_{j,\mathrm{liq}}}{A_{j,\mathrm{gas}}}$. For three reasons it is recommended that the latter ratio be used. First, it is clear from equation (6.1.3) that a value of 1.35 or 0.65 means that $\mu_{j,\mathrm{liq}}^2$ is 35% greater than or 35% less than $\mu_{j,\mathrm{gas}}^2$, respectively. Second, it has been shown[30] that the appropriate value of $\underline{n}$ or $\underline{\varepsilon}$ can not be found with accuracy if the spectrum contains strong bands, so the Polo-Wilson value can not be used when accurate comparison is desired. Third, the ratio $8\pi^2 \frac{C_{j,\mathrm{liq}}}{A_{j,\mathrm{gas}}}$ is independent of compound and, consequently, more convenient. The ratio $8\pi^2 \frac{C_{j,\mathrm{liq}}}{A_{j,\mathrm{gas}}}$ is required for convenient and accurate comparison.

6.2.1 Results

The values of $A_{j,\mathrm{liq}}$ of the four infrared active fundamentals of liquid benzene-h$_6$ and benzene-d$_6$ measured in this work over the specified integration ranges are given in Table 6.1. They were measured from the molar absorption coefficient spectra reported in Chapter 3. It should be noted that the areas given in Chapter 3 are not A_j values. They are areas under the molar absorption coefficient spectrum, not multiplied by 2.303, and areas under the imaginary refractive index spectrum. The integration limits in this chapter were selected for compatibility with the literature and to coincide with the apparent ends of the bands. They differ slightly from those used in Chapters 3 and 4 for the secondary infrared intensity standards.

The values of $A_{j,\mathrm{liq}}$ measured in this work for benzene-h_6 and benzene-d_6 are compared in Table 6.1 with the literature values. The values in Table 6.1 differ significantly, especially those recorded before 1976. Some of the poor agreement may be because the integration range is not always known and tests have shown that different probable integration limits can change the integrated intensity by up to ~5%; this contribution is not included in the uncertainties reported in Table 6.1. A more detailed analysis of the previous measurements is not presented. It is simply noted that the average of the literature values of benzene-h_6 is never outside the error limits of the present values by more than 2%. The benzene-h_6 spectra which yielded the present values were recorded on modern Fourier transform spectrometers by different workers in several different laboratories, and have been corrected for baseline variations using the method described in Chapter 2. These values of benzene-h_6 agree well with those measured by Jones and co-workers[12] and by Zolotarev[38]. They are taken as the best available for benzene-h_6. The benzene-d_6 values measured in this work are taken as the best available for benzene-d_6 since the only other measurement was made in 1970. The 1970 measurements[36] were made by measuring the dispersion of the real refractive index. This method is an approximate and low resolution method that is based on the interference fringe pattern generated when the liquid is placed between two high refractive index plates.

Table 6.1. Absorption intensities A_j of liquid benzene-h$_6$ and benzene-d$_6$.

Reference	Year	Integration range / cm^{-1}	$A_{j,\mathrm{liq}}$ / km mole^{-1} [a]
		Benzene-h$_6$	
ν_{12} (3071.7 cm^{-1})			
32	1959	3250 - 2850	49.94 (29)
33	1960	not given	49.9 (3)
7	1960	not given	84 (29) *
6	1967	3110 - 3000	48
36	1970	not given	31.5 (64) *
12	1976	3125 - 2950	55.6
43	1993	not given	59.2
Average[b]			54.0 (52.5 without *)
Present work	1993	3175 - 2925	54.3 (6)
ν_{13} (1479.2 cm^{-1})			
32	1959	1590 - 1350	22.36 (28)
33	1960	not given	22.4 (3)
7	1960	not given	28 (11)
36	1970	not given	32.2 (25)
12	1976	1540 - 1450	25.9
Average[b]			26.2
Present work	1993	1550 - 1425	26.2 (2)
Present work	1993	1508 - 1425	23.3 (2)
ν_{14} (1035.9 cm^{-1})			
32	1959	1130 - 920	10.92 (90)
33	1960	not given	11.5 [c]
7	1960	not given	18 (7)
5	1966	not given	15.4 (11)[d]
6	1967	1080 - 1000	15
36	1970	not given	19.3 (13)
37	1973	1080 - 990	19.4 [e]
12	1976	1080 - 920	15.48
38	1976	1076 - 990	15.7 [e]
Average[b]			15.6
Present work	1993	1095 - 910	15.6 (1)

Table 6.1. Continued.

Reference	Year	Integration range / cm^{-1}	$A_{j,\mathrm{liq}}$ / km mole^{-1} [a]
ν_4 (676.1 cm^{-1})			
32	1959	770 - 600	89.71 (128)
33	1960	not given	99.0 [f]
7	1960	not given	141 (12)
8	1961	not given	165 (21)
5	1966	not given	142 (6)
6	1967	640 - 730	146
36	1970	not given	144.2 (11)
12	1976	700 - 650	147
Average[b]			134
Present work	1993	730 - 615	127 (5)
		Benzene-d$_6$	
ν_{12} (2284 cm^{-1}			
36	1970	not given	38.8 (6)
Present work	1994	2325 - 2180	26.3 (8)
ν_{13} (1334 cm^{-1})			
36	1970	not given	9.5 (11)
Present work	1994	1370 - 1275	6.96 (21)
ν_{14} (812 cm^{-1})			
36	1970	not given	18.8 (9)
Present work	1994	850 - 760	13.3 (4)
ν_4 (496 cm^{-1})			
36	1970	not given	86.4 (11)
Present work	1994	538 - 458	66.9 (20) [g]

[a] The number in parentheses is the stated uncertainty in the terminal digit. The stars indicate values that are omitted from the average labelled "without *".

[b] The average of all $A_{j,\mathrm{liq}}$ values except the present values.

[c] Ref. 33 gives values from 10.9 to 11.9 for different wing corrections. This value is the average.

[d] The authors[5] state 12.9 (9) "was obtained by eliminating the hot band".

[e] This value was calculated by computing the area under the tabulated spectra in the Ref.

[f] Ref. 33 gives values from 89.7 to 105.8 for different wing corrections. This value is the average.

[g] Determined from mixtures of benzene-h$_6$ and benzene-d$_6$, see Chapter 7.

The values of $A_{j,\mathrm{gas}}$ of the four infrared active fundamentals of benzene-h_6 and benzene-d_6 were taken from the literature and are summarized in Table 6.2. For each band they agree within ±15%. The intensity of ν_{13} of benzene-h_6 has been given in the literature both with and without including the intensity of $\nu_4+\nu_{11}$, the 1528 cm^{-1} band. Both values are considered in the present study. The integration ranges were given only by Goodman *et al.*[41] and Akiyama[39]. Goodman *et al.*[41] used 1569 - 1421 and 1088 - 973 cm^{-1} for ν_{13} and ν_{14} of benzene-h_6, respectively and 1280 - 1365 and 888 - 740 cm^{-1} for ν_{13} and ν_{14} of benzene-d_6. Akiyama[39] used the range 3140 - 3010 cm^{-1} for ν_{12} of benzene-h_6.

The most recent values were measured by Goodman *et al.*[41] They are ~10 to 15% lower than the previous values for ν_{14} of benzene-h_6 and for ν_{13} and ν_{14} of benzene-d_6. For these three bands the values reported by Goodman *et al.*[41] are considered separately from the average of the other values. For the other bands, the best value of $A_{j,\mathrm{gas}}$ is taken as the average of all values reported in the literature.

Absorbance spectra of the four infrared active fundamentals are shown for both liquid and gas phases in Figure 6.1 for benzene-h_6 and Figure 6.2 for benzene-d_6. The range shown is the integration range used in this work for the liquid intensities A_j given in Table 6.1. The spectra show that, with one exception, integration over the range shown includes the same bands for the gas and liquid phases. The exception is ν_{14} of benzene-h_6, which is accompanied by weak bands to low wavenumber in the spectrum of the liquid that are much weaker, if present, for the gas. This case is discussed later.

Table 6.2. Absorption intensities A_j of gaseous benzene-h$_6$ and benzene-d$_6$.[a]

Ref.	Year	$A_{j,\text{gas}}$ / km mole^{-1} [b,c]				
		Benzene-h$_6$				
		ν_{12} (3064.4 cm^{-1})	ν_{13} [d] (1484.0 cm^{-1})	ν_{13} [e] (1484.0 cm^{-1})	ν_{14} (1038.3 cm^{-1})	ν_4 (674.0 cm^{-1})
31	1956	75.9	14.9	13.0	8.8	88.2
2	1963	68.7 (12)	16.1 (2)		8.5 (1)	84.6 (20)
35	1965					99.6 (28)
39	1980					96
40	1982	73.3		13.0	8.82	
41	1989		14.2 (5)	13.2 (12)	7.48 (15)	
42	1989					104 (5)
Average[f]		73 (9)	15.1 (24)	13.1 (3)	8.7 (4) 7.5 (2)	94 (10)
		Benzene-d$_6$				
		ν_{12} (2284 cm^{-1})		ν_{13} (1330 cm^{-1})	ν_{14} (812 cm^{-1})	ν_4 (496 cm^{-1})
34	1962	35.3 (30)		2.90 (15)	8.0 (4)	49.8 (25)
39	1980					52.23
40	1982	33.7 (17)		2.85 (14)	8.38 (42)	
41	1989			2.51 (12)	7.09 (14)	
42	1989					66 (5)
Average[f]		34.5 (8)		2.88 (3) 2.51 (12)	8.19 (19) 7.09 (14)	56 (10)

[a] The value of $\tilde{\nu}_j$ is taken from Goodman *et al.*[100].

[b] The number given in parentheses is the stated uncertainty in the terminal digit.

[c] The only known integration ranges are: for benzene-h$_6$ 1569 - 1421 cm^{-1} and 1088 - 973 cm^{-1} for ν_{13} and ν_{14} in Ref. 41 and 3140 - 3010 cm^{-1} for ν_{12} in Ref. 40; for benzene-d$_6$ 1280 - 1365 and 888 - 740 cm^{-1} for ν_{13} and ν_{14} in Ref. 41.

[d] This is the total intensity including $\nu_4 + \nu_{11}$ at 1528 cm^{-1}.

[e] This is the intensity excluding $\nu_4 + \nu_{11}$ at 1528 cm^{-1}.

[f] The number given in parentheses is the estimated uncertainty in the terminal digit. For three of the fundamentals two values are considered due to disagreement among the literature values, see text.

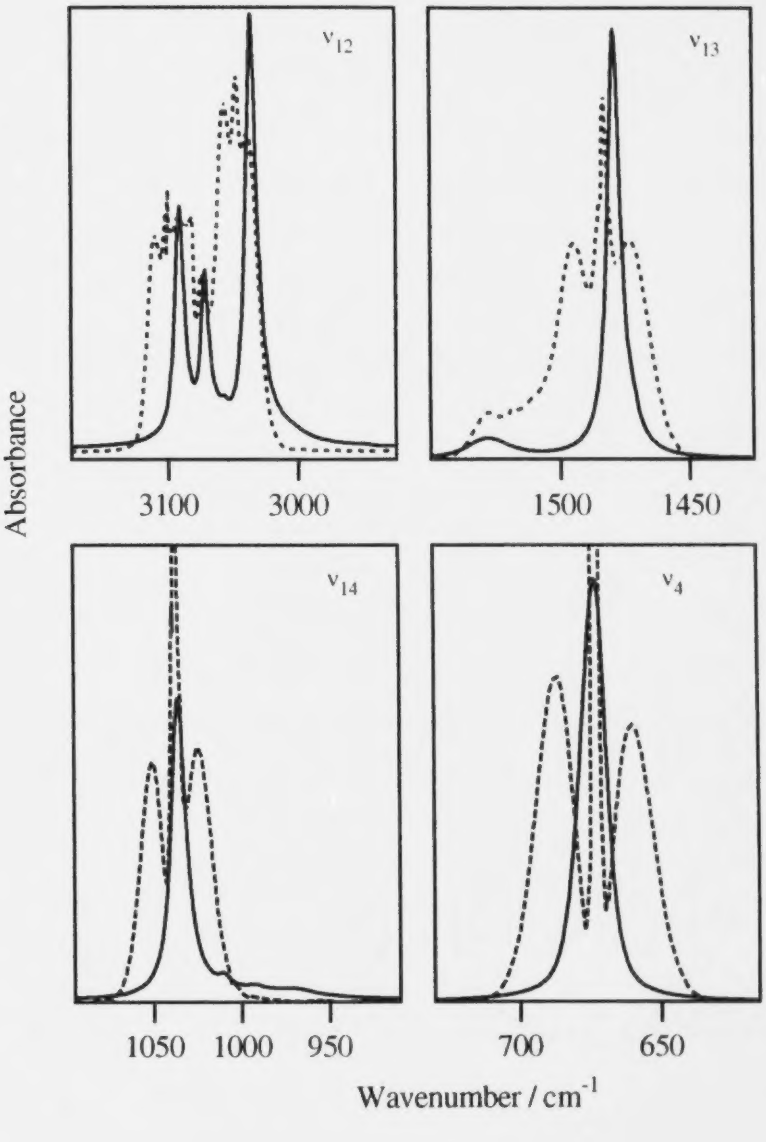

Figure 6.1. Absorbance spectra of benzene-h_6 liquid (solid) and gas (dotted). Top left: the ν_{12} (E_{1u}) CH stretching vibration; Top right: the ν_{13} (E_{1u}) HCC in-plane deformation and ring vibration; Bottom left: the ν_{14} (E_{1u}) HCC in-plane deformation and ring vibration; Bottom right: the ν_4 (A_{2u}) out-of-plane hydrogen motion. The intensities shown for gaseous and liquid benzene-h_6 are not comparable.

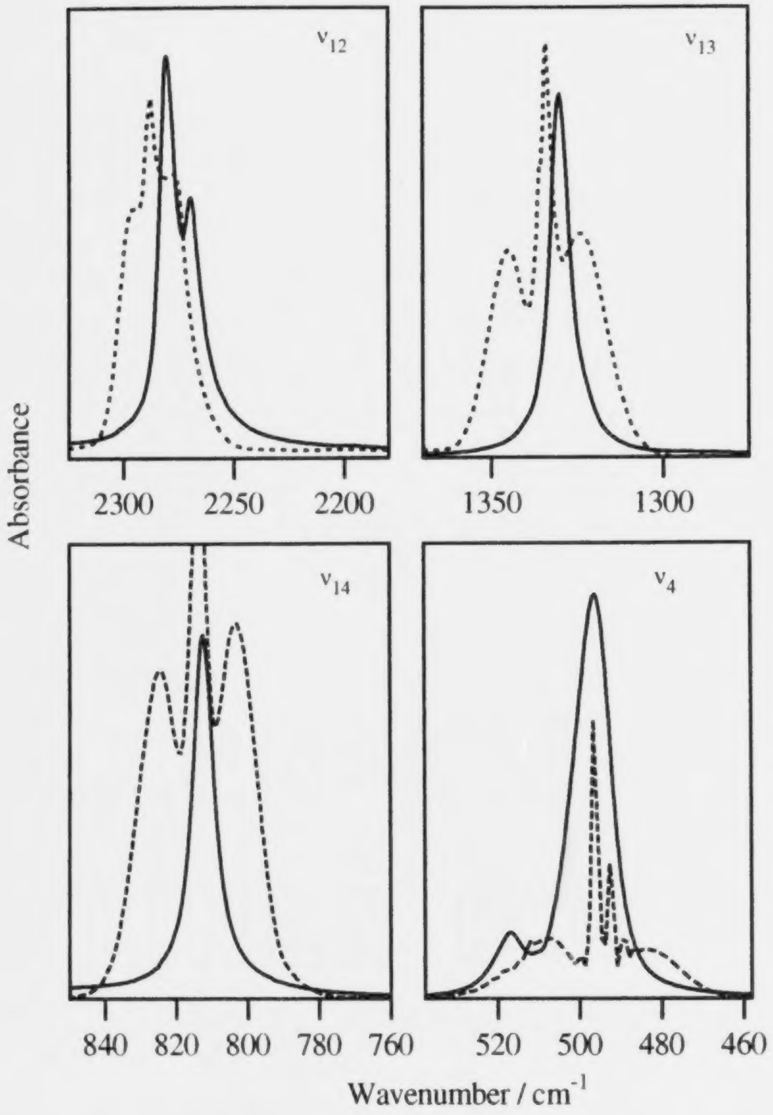

Figure 6.2. Absorbance spectra of benzene-d_6 liquid (solid) and gas (dotted). Top left: the ν_{12} (E_{1u}) CD stretching vibration; Top right: the ν_{13} (E_{1u}) DCC in-plane deformation and ring vibration; Bottom left: the ν_{14} (E_{1u}) DCC in-plane deformation and ring vibration; Bottom right: the ν_4 (A_{2u}) out-of-plane hydrogen motion. The intensities shown for gaseous and liquid benzene-d_6 are not comparable.

Table 6.3 presents the values of C_j for the bands of liquid benzene-h$_6$ and benzene-d$_6$ and compares them with the values of A_j for the bands of the gas. The values of C_j were determined in Chapter 5 from the parameters of the CDHO bands that fitted the α_m'' spectra. It must be noted that the fitted and experimental curves were visually indistinguishable except for ν_{12} of benzene-d$_6$, as is shown in the top box of Figure 6.3 for ν_{14} of benzene-h$_6$. The values of C_j were also found by integrating the $\tilde{\nu}\alpha_m''$ spectra between the integration limits given in Table 6.1. These values are listed in footnote c of Table 6.3 and differ from the values calculated from the fitted bands by less than 6% for all but ν_4 of benzene-d$_6$. The reason for this exception is described in section 7.2. The C_j values determined by fitting the α_m'' spectra are preferred because they include the effects of the wings. The values of C_j given in Table 6.3 include any areas that were assigned to $^{13}C^{12}C_5H_6$ in Chapter 5, as is required for comparison because the A_j values for the gas includes these contribution.

Traditionally the ratio of the integrated intensity A_j for the liquid phase to the integrated intensity A_j for the gas phase was compared. As pointed out in section 6.1, this ratio is not as convenient as the ratio $8\pi^2 \dfrac{C_{j,\text{liq}}}{A_{j,\text{gas}}}$ but to compare the results of this study with those in the literature it is necessary to tabulate $\frac{A_{j,\text{liq}}}{A_{j,\text{gas}}}$. The best values of A_j for the liquid from Table 6.1 and the best values of A_j for the gas from Table 6.2 are collected in Table 6.4 along with their ratio. These ratios are compared with the Polo-Wilson value for each band and with the ratios reported previously.

Table 6.3. Absorption intensities C_j of liquid benzene compared with intensities A_j of gaseous benzene.

Band			$8\pi^2 \frac{C_{j,\mathrm{liq}}}{A_{j,\mathrm{gas}}}$	
$(\tilde{\nu}_j / \mathrm{cm}^{-1})$ [a]	$C_{j,\mathrm{liq}}$ [b,c]	$A_{j,\mathrm{gas}}$ [d]	This Work [e]	Unperturbed case [f]
Benzene-h_6				
ν_{12} (~3070)	0.539 (27)	73 (9)	0.58 (8)	1
ν_{13} (~1480)	0.267 (13) [g]	15.1 (24) [g]	1.40 (23) [g]	1
	0.234 (12) [h]	13.1 (3) [h]	1.41 (8) [h]	1
ν_{14} (~1036)	0.158 (7)	8.7 (4)	1.43 (9)	1
		7.5 (2)	1.66 (9)	1
	0.130 (6) [i]	8.7 (4)	1.18 (8)	1
		7.5 (2)	1.37 (7)	1
ν_4 (~675)	1.27 (6)	94 (10)	1.07 (12)	1
Benzene-d_6				
ν_{12} (~2280)	0.268 (14)	34.5 (8)	0.61 (4)	1
ν_{13} (~1330)	0.068 (3)	2.88 (3)	1.86 (10)	1
		2.51 (12)	2.14 (16)	1
ν_{14} (~812)	0.132 (7)	8.19 (19)	1.27 (7)	1
		7.09 (14)	1.47 (8)	1
ν_4 (~496)	0.73 (4)	56 (10)	1.02 (19)	1

[a] The value of $\tilde{\nu}_j$ given is approximate since it differs slightly for the gas and liquid phases.

[b] The number given in parentheses is the uncertainty in the terminal digit.

[c] The full area under the CDHO bands which fitted the $\tilde{\nu}\alpha''_m$ spectrum in the integration range. The C_j values obtained by integrating under $\tilde{\nu}\alpha''_m$ between the integration limits given in Table 6.1 are for benzene-h_6: 0.532, 0.253, 0.225, 0.151, 0.119, 1.21 km mole^{-1}; and for benzene-d_6: 0.257, 0.0654, 0.131, 0.636 km mole^{-1}.

[d] From Table 6.2.

[e] The number in parentheses is the uncertainty in the terminal digit due to the uncertainties in $C_{j,\mathrm{liq}}$ and $A_{j,\mathrm{gas}}$.

[f] The ratio $8\pi^2\, C_{j,\mathrm{liq}} / A_{j,\mathrm{gas}}$ equals unity for all bands of all compounds in the unperturbed case that $\tilde{\nu}_j \left|\bar{R}_j\right|^2$ and μ_j^2 are the same for gas and liquid phases.

[g] Includes $\nu_4 + \nu_{11}$ at 1528 cm^{-1}.

[h] Excludes $\nu_4 + \nu_{11}$ at 1528 cm^{-1}.

[i] Corrected for the three low wavenumber bands not seen in the gas spectrum. See text and Figure 6.3.

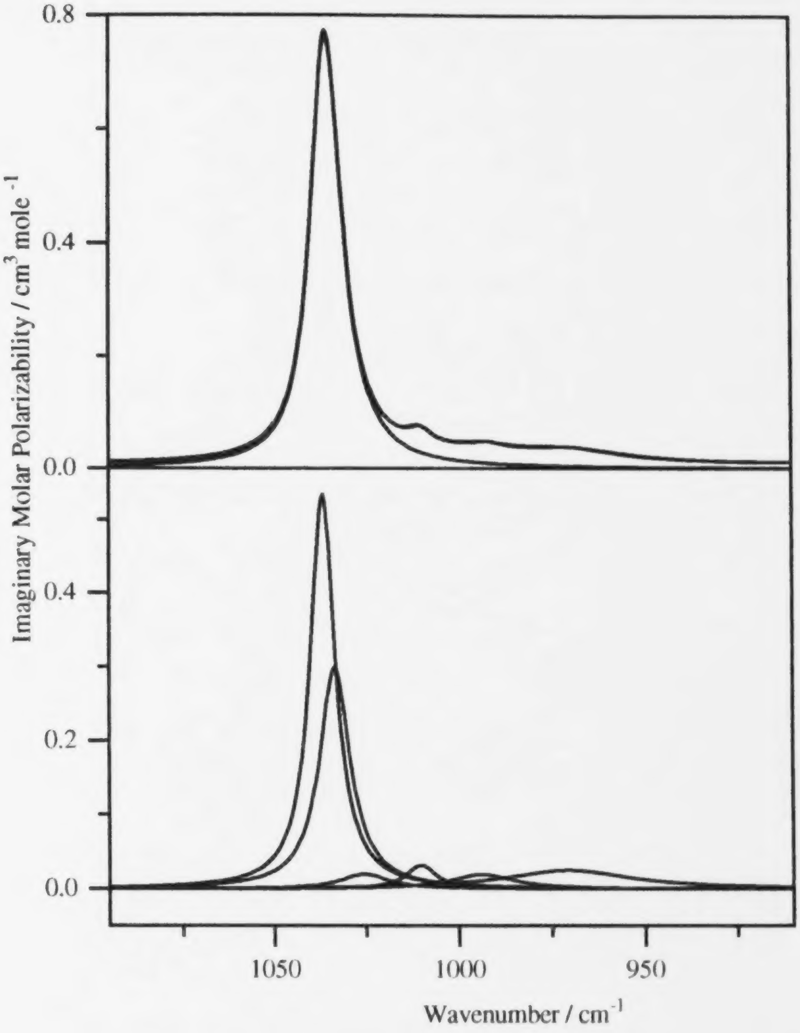

Figure 6.3. Top box, upper curve: The imaginary molar polarizability spectrum of ν_{14} (E_{1u}) of liquid benzene-h_6 coincident with the sum of the seven Classical Damped Harmonic Oscillator bands fitted to it. Top box lower curve: The sum of the three higher-wavenumber CDHO bands. Bottom box: The seven CDHO bands required to fit the imaginary molar polarizability spectrum.

Table 6.4. Comparison of intensities A_j of liquid and gaseous benzene-h$_6$ and benzene-d$_6$.

			$\frac{A_{j,\text{liq}}}{A_{j,\text{gas}}}$				
					Previous Studies		
Band ($\tilde{\nu}_j$ / cm^{-1})[a]	$A_{j,\text{liq}}$[b]	$A_{j,\text{gas}}$[c]	This Work[d]	Polo-Wilson value[e]	Ref. 36	Ref. 183	Ref. 7
Benzene-h$_6$							
ν_{12} (~3070)	54.3 (6)	73 (9)	0.74 (9)	1.32	0.46	0.74	0.74
ν_{13} (~1480)	26.2 (2)	15.1 (24)	1.74 (28)	1.31	2.0	1.47	
	23.3 (2)	13.1 (3)	1.78 (4)	1.31			1.46
ν_{14} (~1036)	15.6 (1)	8.7 (4)	1.79 (8)	1.31	2.3	1.31	1.33
		7.5 (2)	2.08 (6)	1.31			
ν_4 (~675)	127 (5)	94 (10)	1.35 (15)	1.39	1.7	1.09	1.60
Benzene-d$_6$							
ν_{12} (~2280)	26.3 (8)	34.5 (8)	0.76 (3)	1.31	1.10		
ν_{13} (~1330)	6.96 (21)	2.88 (3)	2.42 (8)	1.31	3.28		
		2.51 (12)	2.77 (16)	1.31			
ν_{14} (~812)	13.3 (4)	8.19 (19)	1.62 (6)	1.31	2.35		
		7.09 (14)	1.88 (7)	1.31			
ν_4 (~496)	66.9 (20)	56 (10)	1.19 (22)	1.36	1.73		

[a] Herzberg's notation is used to number the vibrations. The value of $\tilde{\nu}_j$ is given approximately since it differs slightly for the gas and liquid phases.

[b] From Table 6.1.

[c] From Table 6.2.

[d] The number in parentheses is the uncertainty in the terminal digit found by propagating the uncertainties in $A_{j,\text{liq}}$ and $A_{j,\text{gas}}$.

[e] Predicted by equation (6.1.6) using $\underline{n}$ equal to 1.479, 1.474, 1.467, and 1.550 respectively for benzene-h$_6$ and 1.472, 1.475, 1.471, and 1.526 respectively for benzene-d$_6$.

6.2.2 Discussion

The reported values of $\frac{A_{j,\mathrm{liq}}}{A_{j,\mathrm{gas}}}$ for each band of benzene-h$_6$ differ significantly (Table 6.4). The values obtained in this work do not agree overall with any previous set. For the CH stretching band, ν_{12}, of benzene-h$_6$ the present value does agree with the values reported in 1964 and 1960. For ν_{12} of benzene-h$_6$ and benzene-d$_6$, all reports agree that the intensity is weaker in the liquid than in the gas, and much weaker than that expected from the Polo-Wilson equation. For the other bands the reports agree that the liquid intensity is greater than that of the gas. However, they only agree in the sense that the intensities reported for the ν_{13} and ν_{14} bands of liquid benzene-h$_6$ and benzene-d$_6$ are greater than those predicted by the Polo-Wilson equation.

The current values of the ratio $8\pi^2 \frac{C_{j,\mathrm{liq}}}{A_{j,\mathrm{gas}}}$ are given in Table 6.3. The ratio is the same for the CH and CD stretching vibration, ν_{12}, 0.58 ± 0.08 for benzene-h$_6$ and 0.61 ± 0.04 for benzene-d$_6$, indicating that μ_j^2 and $\tilde{\nu}_j\left|\vec{R}_j\right|^2$ are ~65% greater for the gases than for the liquids.

The ratio is 1.40 for the HCC in-plane and ring deformation, ν_{13}, of benzene-h$_6$, indicating that μ_j^2 and $\tilde{\nu}_j\left|\vec{R}_j\right|^2$ are 40% greater in the liquid than in the gas. The inclusion or exclusion of $\nu_4+\nu_{11}$ at 1528 cm^{-1} does not affect this ratio significantly. For benzene-d$_6$, the ratios for ν_{13} are much greater, 1.86 or 2.14 depending on which value of $A_{j,\mathrm{gas}}$ is used. This indicates that μ_j^2 and $\tilde{\nu}_j\left|\vec{R}_j\right|^2$ are about twice as large in the liquid as in the gas. The fact that the ratio for ν_{13} is significantly different for benzene-h$_6$ and benzene-d$_6$ is an indication that the eigenvectors of these vibrations are significantly different for the two isotopomers (Table 5.9). This is discussed again later in this section.

For the very intense butterfly vibration, the A_{2u} out-of-plane hydrogen vibration ν_4, the ratio is the same for benzene-h_6 and benzene-d_6, 1.07 ± 0.12 and 1.02 ± 0.19, respectively, showing that μ_j^2 and $\tilde{\nu}_j\left|\vec{R}_j\right|^2$ have the same values in gas and liquid phases within experimental error.

For ν_{14} of benzene-d_6, the ratio is 1.27 or 1.47 depending on which value of $A_{j,\text{gas}}$ is used, indicating that μ_j^2 and $\tilde{\nu}_j\left|\vec{R}_j\right|^2$ are ~30 to 50% larger in the liquid. The situation is more confused for ν_{14} of benzene-h_6. There are several weak bands to low wavenumber of the main ν_{14} peak in the spectrum of liquid benzene-h_6. They are much less noticeable in the spectrum of the gas, and raise concern about whether the comparison of the areas of gas and liquid over the same integration range compares the intensities of the same transitions. To determine the effect of these weak bands, the imaginary molar polarizability spectrum was fitted with the seven classical damped harmonic oscillator bands shown in the lower box of Figure 6.3. The upper curve in the top box shows both the experimental spectrum and the (indistinguishable) sum of the fitted bands. The lower curve in the top box of Figure 6.3 shows the result of omitting the three lowest-wavenumber CDHO bands from the sum. The area under this lower curve multiplied by wavenumber gives the value of C_j when these additional bands are neglected. This area (Table 6.3) is 0.130 km mole^{-1} instead of the total area of 0.158 km mole^{-1}.

The conclusions concerning ν_{14} of benzene-h_6 are as follows. If the older and larger value, 8.7 ± 0.4 km mole^{-1}, is the correct integrated intensity for the gas, and if the weak bands to low wavenumber of the main peak in the spectrum of the liquid do exhibit new intensity rather than intensity taken from the fundamental. $8\pi^2 \frac{C_{j,\text{liq}}}{A_{j,\text{gas}}} =$ 1.18 and μ_j^2 and $\tilde{\nu}_j\left|\vec{R}_j\right|^2$ of the liquid are about 18% greater than those of the gas. If the new, lower value 7.5 km mole^{-1} is correct for the gas, and the weak bands in the liquid spectrum steal their intensity from the fundamental, $8\pi^2 \frac{C_{j,\text{liq}}}{A_{j,\text{gas}}} = 1.66$ and μ_j^2 and $\tilde{\nu}_j\left|\vec{R}_j\right|^2$ of the liquid are ~65% greater than those of the gas. The other two possibilities yield intermediate results.

Maslen *et al.*[50] have calculated that $\nu_{18}+\nu_{20}$, at 1010 cm^{-1} has 1.8% of the intensity of ν_{14}. This may indicate that most of the intensity of the weak combinations and inactive fundamentals is stolen from the fundamental. If this is accepted, and the intensity of the weak peaks to low wavenumber of ν_{14} of benzene-h_6 is included in the intensity of ν_{14}, the ratio $8\pi^2 \frac{C_{j,\text{liq}}}{A_{j,\text{gas}}}$ is very similar for benzene-h_6 and benzene-d_6. The ratios are either 1.43 ± 0.09 for benzene-h_6 and 1.27 ± 0.07 for benzene-d_6 or 1.66 ± 0.09 for benzene-h_6 and 1.47 ± 0.08 for benzene-d_6 depending on which values of A_j are used for the gas. It is not clear, however, that the ratio should be the same for benzene-h_6 and benzene-d_6, because the eigenvectors of this vibration are different in the two compounds, as is the case for ν_{13}. The HCC deformation and CC stretching displacements contribute to ν_{13} and ν_{14} in both molecules, but to different extents.

The fact that the out-of-plane ν_4 vibrations are not affected by condensation while the in-plane vibrations ν_{12}, ν_{13} and ν_{14} are drastically different in the liquid and gas phases can be explained qualitatively by the liquid structure. The local structure in the liquid is very similar to the structure in the solid[51, 177, 178]. The molecules in solid benzene are arranged[184] in a T-like arrangement, such that the plane of a molecule is perpendicular to the planes of its nearest neighbours. Thus the out-of-plane motion is relatively unhindered while the in-plane motion is hindered.

The ratios of the integrated intensities, C_j, of the active fundamentals of liquid benzene-h$_6$ to those of liquid benzene-d$_6$ are given in Table 6.5 along with corresponding ratios of A_j for the gases. For ν_{12} and ν_4, the ratios of the liquid phase intensities and the ratios of the gas phase intensities are close to 2, indicating that these vibrations mostly involve motion of the hydrogen atoms. For ν_{14} the ratio of the liquid phase intensities and the ratio of the gas phase intensities are very close to 1. It is tempting to conclude from this that the eigenvectors must be the same in both molecules. The eigenvectors presented in Table 5.8 are not the same for both molecules, but indicate that ν_{14} is mainly one unit of the CC stretching coordinate S_{13} mixed with one quarter unit of the HCC deformation coordinate S_{14} in C_6H_6 and is one unit of S_{13} mixed with three quarters units of S_{14} plus one quarter unit of the CD stretching coordinate S_{12} in C_6D_6. Further, these eigenvectors yield a set of three dipole moment derivatives with respect to symmetry coordinates that fit the observed intensity very well (Table 5.13). Thus, it is not safe to draw the conclusion that equal intensity for the two molecules implies identical eigenvectors in the two molecules. For ν_{13}, the ratios of the intensity for benzene-h$_6$ and benzene-d$_6$ are 3.9 for the liquid and 5.2 for the gas. The eigenvectors show that both are mixtures of S_{13} and S_{14}, with S_{12} also involved for benzene-d$_6$.

Table 6.5. Ratios of integrated intensities of benzene-h_6 to integrated intensities benzene-d_6 for liquid and gas phases.

Vibration	C_6H_6	C_6D_6	Ratio	Motion
	$C_{j,\mathrm{liq}}$			
ν_{12}	0.539	0.268	2.0	CH (D) Stretch
ν_{13}	0.267 [a] 0.234 [b]	0.068	3.9 3.4	HCC (DCC) and CCC deformations
ν_{14}	0.158 0.130 [c]	0.132	1.1 1.0	HCC (DCC) and CCC deformations
ν_4	1.27	0.73	1.7	HCCC (DCCC) out-of-plane bend
	$A_{j,\mathrm{gas}}$			
ν_{12}	73	34.5	2.1	CH (D) Stretch
ν_{13}	15.1 [d] 13.1 [d]	2.88 [d] 2.51 [d]	5.2 5.2	HCC (DCC) and CCC deformations
ν_{14}	8.7 7.5	8.19 [d] 7.09 [d]	1.1 1.1	HCC (DCC) and CCC deformations
ν_4	94	56	1.7	HCCC (DCCC) out-of-plane bend

[a] This is the total intensity including $\nu_4 + \nu_{11}$ at 1528 cm^{-1}.

[b] This is the intensity excluding $\nu_4 + \nu_{11}$ at 1528 cm^{-1}.

[c] Corrected for the three low wavenumber bands not seen in the gas spectrum. See text and Figure 6.3.

[d] Two values of the intensity are listed because of disagreement among the literature values. See text and Table 6.2.

6.2.3 Comparison of Transition Moments and Dipole Moment Derivatives of Liquid Benzene-h_6 and Benzene-d_6 With Those of Gaseous Benzene-h_6 and Benzene-d_6

The transition moments and dipole moment derivatives with respect to the normal coordinates for the liquid and gas phases are given in Table 6.6. The values for the liquid were taken from Tables 5.2, 5.3, and 5.11 and those for the gas were calculated from A_j through equations (1.3.47) and (1.3.48). It should be recalled that the signs of the dipole moment derivatives with respect to Q_{12}, Q_{13} and Q_{14} are + - +, or - + -, for both the liquid and the gas.

In this subsection the dipole moment derivatives with respect to the symmetry and internal coordinates are calculated for gaseous benzene and compared with the values given for liquid benzene in Chapter 5 and with values calculated from quantum mechanical theory by Pulay *et al.*[124] and by Goodman, Ozkabak and Wiberg[41]. Then, to determine the origin of the intensity differences noted in the previous section between the liquid and gas phases and between benzene-h_6 and benzene-d_6, the contributions to the dipole moment derivatives with respect to the normal coordinates from the different symmetry coordinates are presented and discussed.

It may be helpful to note that 1 Debye equals 0.208 electron Å, so that the values of the dipole moment derivatives with respect to internal or symmetry coordinates can be thought of in terms of electrons instead of Debye $Å^{-1}$. Caution should be used, however, when thinking of these quantities as effective charges on the atoms. This is sometimes a useful concept for bending vibrations, as is noted later, but it should not be used for stretching vibrations because considerable charge redistribution occurs when a bond is stretched.

In Table 6.2, Goodman's values of the integrated intensities of the gas are presented, as well as the averages of all of the literature values except those of Goodman. These two sets of values were converted to the dipole moment derivatives with respect to the normal coordinates, $\partial\bar{\mu}/\partial Q_j$, tabulated in Table 6.6. Both sets of $\partial\bar{\mu}/\partial Q_j$ values were then converted to dipole moment derivatives with respect to symmetry coordinates, $\partial\bar{\mu}/\partial S_i$ and with respect to internal coordinates, $\partial\bar{\mu}/\partial R_i$. These conversions require the eigenvectors of the gas. It was noted in Section 5.3.3 that Goodman's normal coordinates for the gas were reproduced in this work, and the eigenvectors from that calculation were used.

The following equations were solved by non-linear least squares for the E_{1u} vibrations.

For C_6H_6

$$\left|\frac{\partial\bar{\mu}}{\partial Q_{12}}\right|^2 = \left|1.0362\frac{\partial\bar{\mu}}{\partial S_{12}} - 0.0740\frac{\partial\bar{\mu}}{\partial S_{13}} + 0.1196\frac{\partial\bar{\mu}}{\partial S_{14}}\right|^2 \qquad (6.2.1)$$

$$\left|\frac{\partial\bar{\mu}}{\partial Q_{13}}\right|^2 = \left|0.0371\frac{\partial\bar{\mu}}{\partial S_{12}} + 0.2521\frac{\partial\bar{\mu}}{\partial S_{13}} - 1.3189\frac{\partial\bar{\mu}}{\partial S_{14}}\right|^2 \qquad (6.2.2)$$

$$\left|\frac{\partial\bar{\mu}}{\partial Q_{14}}\right|^2 = \left|-0.0203\frac{\partial\bar{\mu}}{\partial S_{12}} + 0.2366\frac{\partial\bar{\mu}}{\partial S_{13}} + 0.5813\frac{\partial\bar{\mu}}{\partial S_{14}}\right|^2 \qquad (6.2.3)$$

For C_6D_6

$$\left|\frac{\partial\bar{\mu}}{\partial Q_{12}}\right|^2 = \left|0.7586\frac{\partial\bar{\mu}}{\partial S_{12}} - 0.1191\frac{\partial\bar{\mu}}{\partial S_{13}} + 0.1698\frac{\partial\bar{\mu}}{\partial S_{14}}\right|^2 \qquad (6.2.4)$$

Table 6.6. Transition moments and dipole moment derivatives of liquid and gaseous benzene-h_6 and benzene-d_6.

Band	Sym-	Liquid			Gas		
($\tilde{\nu}_j$ / cm^{-1})[a]	metry	$C_{j,\mathrm{liq}}$ [b]	$\lvert\vec{R}_j\rvert$ [c,d]	μ_j [c,d]	$A_{j,\mathrm{gas}}$ [b]	$\lvert\vec{R}_j\rvert$ [c,d]	μ_j [c,d]
Benzene-h_6							
ν_{12} (~3070)	E_{1u}	0.539 (27)	0.0529 (13)	0.710 (18)	73 (9)	0.069 (4)	0.93 (6)
ν_{13} (~1480)	E_{1u}	0.267 (13) [e] 0.234 (12) [f]	0.0533 (13) 0.0499 (13)	0.499 (13) 0.468 (12)	15.1 (24) [e] 13.1 (3) [f]	0.045 (4) 0.0420 (5)	0.42 (3) 0.394 (5)
ν_{14} (~1036)	E_{1u}	0.158 (7) 0.130 (6) [g]	0.0490 (11) 0.0445 (10)	0.384 (9) 0.349 (8)	8.7 (4) [h] 7.5 (2) [h]	0.0409 (9) 0.0380 (5)	0.321 (7) 0.298 (4)
ν_4 (~675)	A_{2u}	1.27 (6)	0.244 (5)	1.54 (4)	94 (10)	0.236 (13)	1.49 (8)
Benzene-d_6							
ν_{12} (~2280)	E_{1u}	0.268 (14)	0.0430 (11)	0.500 (13)	34.5 (8)	0.0549 (6)	0.639 (7)
ν_{13} (~1330)	E_{1u}	0.068 (3)	0.0284 (6)	0.252 (6)	2.88(3) [h] 2.51 (12) [h]	0.0208 (1) 0.0194 (5)	0.185 (1) 0.172 (4)
ν_{14} (~812)	E_{1u}	0.132 (7)	0.0507 (13)	0.352 (9)	8.19 (19) [h] 7.09 (14) [h]	0.0449 (5) 0.0417 (4)	0.311 (4) 0.290 (3)
ν_4 (~496)	A_{2u}	0.73 (4)	0.214 (6)	1.16 (3)	56 (10)	0.212 (19)	1.15 (10)

[a] The value of $\tilde{\nu}_j$ is given approximately since it differs slightly for the gas and liquid phases.

[b] $C_{j,\mathrm{liq}}$ is from Table 6.3 and $A_{j,\mathrm{gas}}$ is from Table 6.2.

[c] The number given in parentheses is the uncertainty in the terminal digit.

[d] The unit of $\lvert\vec{R}_j\rvert$ is Debye and the unit of μ_j is Debye Å^{-1} amu$^{-1/2}$.

[e] Includes $\nu_4 + \nu_{11}$ at 1528 cm^{-1}.

[f] Excludes $\nu_4 + \nu_{11}$ at 1528 cm^{-1}.

[g] Corrected for the three low wavenumber bands not seen in the gas spectrum. See text and Figure 6.3.

[h] Two values are listed for $A_{j,\mathrm{gas}}$ because of the disagreement among the literature values, see text.

$$\left|\frac{\partial\bar{\mu}}{\partial Q_{13}}\right|^2 = \left|0.0649\frac{\partial\bar{\mu}}{\partial S_{12}} + 0.3052\frac{\partial\bar{\mu}}{\partial S_{13}} - 0.8874\frac{\partial\bar{\mu}}{\partial S_{14}}\right|^2 \tag{6.2.5}$$

$$\left|\frac{\partial\bar{\mu}}{\partial Q_{14}}\right|^2 = \left|-0.0121\frac{\partial\bar{\mu}}{\partial S_{12}} + 0.1329\frac{\partial\bar{\mu}}{\partial S_{13}} + 0.6571\frac{\partial\bar{\mu}}{\partial S_{14}}\right|^2 \tag{6.2.6}$$

The values of $\partial\bar{\mu}/\partial S_i$ obtained are listed in Table 6.7 with their standard deviations. To show the quality of the fit, the experimental and calculated μ_j^2 values are included in the table, with the standard deviation of the fit. The latter were 0.033 for the fit to Goodman's data and 0.031 to the average values of all of the data except Goodman's, both of which indicate fairly good fits.

The two sets of $\partial\bar{\mu}/\partial S_i$ values are within ~10% of each other, and the averages of the two sets are included in Table 6.8 and are used in the following discussion.

For the A_{2u} vibration, ν_4, the equations are

$$\left|\frac{\partial\bar{\mu}}{\partial S_4}\right| = 1.0453\left|\frac{\partial\bar{\mu}}{\partial Q_4}\right| \tag{6.2.7}$$

$$\left|\frac{\partial\bar{\mu}}{\partial S_4}\right| = 1.4235\left|\frac{\partial\bar{\mu}}{\partial Q_4}\right| \tag{6.2.8}$$

With the values of μ_j^2 given in Table 6.6, these equations give $\partial\bar{\mu}/\partial S_4 = 1.56 \pm 0.08$ Debye Å^{-1} for benzene-h_6 and 1.64 ± 0.08 Debye Å^{-1} for benzene-d_6. The average of these values, 1.60 ± 0.10 Debye Å^{-1} is used as the value of $\partial\bar{\mu}/\partial S_4$ for the gas.

Table 6.7. $\partial\bar{\mu}/\partial S_i$ of gaseous benzene-h_6 and benzene-d_6 from nonlinear least squares fit of experimental $\partial\bar{\mu}/\partial Q_j$ for E_{1u} vibrations.

	All but Goodman	Goodman
$\partial\bar{\mu}/\partial S_{12}$	0.872 ± 0.017	0.869 ± 0.018
$\partial\bar{\mu}/\partial S_{13}$	0.477 ± 0.115	0.423 ± 0.127
$\partial\bar{\mu}/\partial S_{14}$	0.407 ± 0.028	0.393 ± 0.031

j	μ_j^2 obs	μ_j^2 calc	μ_j^2 obs	μ_j^2 calc
C_6H_6 12	0.865	0.840	0.865	0.839
$C_6H_6$13	0.155	0.147	0.155	0.144
C_6H_6 14	0.103	0.110	0.088	0.097
C_6D_6 12	0.408	0.454	0.408	0.456
$C_6D_6$13	0.034	0.025	0.030	0.027
C_6D_6 14	0.097	0.103	0.084	0.093
Standard Deviation		0.031		0.033

Table 6.8 shows the dipole moment derivatives with respect to the symmetry and internal coordinates for benzene-h_6 and benzene-d_6 from the experimental intensities of the gas and liquid phases, and also the values calculated for isolated benzene molecules in the two most recent calculations. Neither of the two sets of calculated values were obtained by the best current methods and they show significant dependence on basis set. Nevertheless, it is clear that they agree with the experimental values for the gas within ~20% except for $\partial\mu/\partial t$ calculated by Pulay *et al.*[124]. It should be noted that in the literature[41, 124], the $\partial\bar{\mu}/\partial S_i$ values are given with positive signs while the $\partial\bar{\mu}/\partial R_i$ values are given with negative signs. From the definition of the symmetry coordinates, the $\partial\bar{\mu}/\partial S_i$ values and the $\partial\bar{\mu}/\partial R_i$ should have the same sign. The pattern of the experimental values for the gas and liquid is like that of the intensities (section 6.2.2). For the CH stretching coordinate (S_{12}) the liquid phase value is about 26% smaller than that of the gas, which follows from the 40% lower intensity of the liquid and the lack of coupling with other coordinates. For the out-of-plane hydrogen coordinate, S_4, the dipole moment derivative is essentially the same in both phases. For S_{13} and S_{14} which mix heavily in the normal vibrations and whose dipole moment derivatives are similar, the values are similar for gas and liquid phases, but in the reverse order.

The intensity differences between liquid and gas phases that were discussed in subsection 6.2.2 can now be explored more fully, with the help of the eigenvectors and the $\partial\bar{\mu}/\partial S_i$ values (Table 6.8) of the two phases. Table 6.9 shows the experimental and fitted values of $\partial\bar{\mu}/\partial Q_j$ and the contributions to the fitted value from the three E_{1u} symmetry coordinates. The increase in the CH stretching intensity in the gas is essentially all due to the increase in the dipole moment derivative with respect to CH bond stretching.

Table 6.8. Dipole moment derivatives with respect to symmetry coordinates and internal coordinates for liquid and gaseous benzene-h_6 and benzene-d_6.

		Gas		
	Liquid	This work	Goodman[41 a]	Pulay[124 b]
$\partial\bar{\mu}/\partial S_4$	1.63 (4)	1.60 (10)		
$\partial\bar{\mu}/\partial S_{12}$	0.64 (6)	0.87 (2)	0.9 ± 0.1	
$\partial\bar{\mu}/\partial S_{13}$	0.39 (4)	0.45 (12)	0.4 ± 0.2	
$\partial\bar{\mu}/\partial S_{14}$	0.46 (1)	0.40 (2)	0.51 ± 0.4	
$\partial\mu/\partial s$	0.37 (3)	0.50 (1)	-0.55 ± 0.08	-0.65
$\partial\mu/\partial t$	0.23 (1)	0.26 (7)	-0.23 ± 0.12	0.74
$\partial\mu/\partial\beta$	0.26 (1)	0.23 (1)	-0.30 ± 0.02	-0.22
$\partial\mu/\partial\gamma$	0.66 (2)	0.65 (4)		0.61

[a] Average of the values reported by Goodman *et al.*[41]. These values were calculated by *ab initio* calculations with Møller-Plesset perturbation.

[b] Values reported by Pulay *et al.*[124], calculated by *ab initio* calculations with 4-21P basis set except $\partial\mu/\partial t$ which was calculated with 4-21P + bond functions.

Table 6.9. Contribution of $\partial\bar{\mu}/\partial S_i$ to $\partial\bar{\mu}/\partial Q_j$ for liquid and gaseous benzene-h_6 and benzene-d_6 for E_{1u} vibrations.

				Percentage Contribution of		
j	Phase	$\partial\bar{\mu}/\partial Q_j$ obs	$\partial\bar{\mu}/\partial Q_j$ calc	S_{12}	S_{13}	S_{14}
C_6H_6 12	Liquid	0.71	0.69	95.5	-4.6	9.1
	Gas	0.93	0.92	98.4	-3.6	5.2
C_6H_6 13	Liquid	-0.47	-0.47	-7.6	-21.0	128.6
	Gas	-0.40	-0.38	-8.5	-29.7	138.2
C_6H_6 14	Liquid	0.35	0.36	-1.7	25.6	76.1
	Gas	0.31	0.32	-5.5	33.1	72.4
C_6D_6 12	Liquid	0.50	0.52	92.7	-9.7	17.0
	Gas	0.64	0.67	97.9	-7.9	10.0
C_6D_6 13	Liquid	-0.25	-0.23	-24.8	-51.1	176.0
	Gas	-0.18	-0.16	-35.0	-85.2	220.3
C_6D_6 14	Liquid	0.35	0.35	-1.2	14.6	86.6
	Gas	0.30	0.31	-3.4	19.2	84.2

The relative intensities of corresponding vibrations of benzene-h_6 and benzene-d_6 were noted in the previous section and can now be explored fully with the intensity contributions listed in Table 6.9. For ν_{13}, there is a big difference between the intensities for benzene-h_6 and benzene-d_6. From Table 6.9, it is obvious that this difference is due to the differences in the eigenvectors of the two molecules. For ν_{14}, the intensities for benzene-h_6 and benzene-d_6 are very similar and, as was noted in the previous section, it is tempting to associate this with the molecules having the same eigenvectors. From Table 6.9, it is obvious that the contributions of the different symmetry coordinates is different for the two molecules and the fact that the intensities are very similar is only coincidental.

Before ending this discussion of the relative intensities of liquid and gaseous benzene, it is necessary to consider the recent work of Akiyama[42]. Akiyama has presented values of the effective charge on the hydrogen atom during the out-of-plane hydrogen motion. This quantity is closely related to $\partial\mu/\partial\gamma$ and, for reference, the value 0.66 Debye $Å^{-1}$ for this quantity in Table 6.8 yields an effective charge on the hydrogen atom for this motion of 0.127 electrons.

Akiyama *et al.*[42] have recently presented a charge distribution of benzene determined from the infrared band intensities through a new relation of Akiyama's[185-187] between, effectively, the molar polarizability spectra and the dielectric constant spectra. His expression for the imaginary molar polarizability is equation (1.3.41) multiplied on the right hand side by $(\varepsilon_D+2)/3$, where ε_D is the real dielectric constant of the liquid at the sodium-D line. Akiyama *et al.*[42] calculated the effective charge on the hydrogen atom from their experimental data for gaseous benzene (0.129 electrons) and for benzene in cyclohexane or carbon disulfide solution. They found

Crawford's equation, and thus equation (1.3.41), gave the effective charge in solution within 8% of that in the gas, while Akiyama's new equation gave values higher than those from Crawford's equation by 14% for benzene in cyclohexane and 25% for benzene in carbon disulfide. They then argued that the reaction field in the liquid should make the effective charges on benzene in solution larger than those in the gas, and that their calculation of this effect supported the validity of the Akiyama equation.

These higher values of the effective charge of benzene are believed to be wrong, because Akiyama's equation is believed to be wrong for the following reasons. In his derivation, Akiyama used the Lorentz local field but divided the polarization into two parts, a complex part resonant with the infrared radiation, and a real part that is always in phase with the infrared radiation field and arises from the electronic polarization. Akiyama argued that Crawford's derivation of equation (1.3.41) (in which Crawford used the local susceptibility $\hat{C}$ instead of, $\hat{\alpha}_{\mathrm{m}}$, where $V_m\hat{C} = \hat{\alpha}_{\mathrm{m}}$) omitted this second contribution to the polarizability. This argument is wrong. The polarization in Crawford's derivation[58], and in the derivation of equation (1.3.41), is the total polarization at the wavenumber of the radiation. The real part is the sum of the contribution from the electronic polarization and the in-phase part of the infrared polarization, and the imaginary part reflects the absorption at the wavenumber of the radiation.

The derivation of equation (1.3.41)[58] uses generally applicable equations of electromagnetism with the one assumption that the Lorentz local field is valid for liquids. It is believed that it relates the molecular properties to the optical properties as correctly as the assumption of the Lorentz local field allows. It must be kept in mind that the Lorentz local field accounts for interactions over a sufficient range that the liquid is effectively isotropic, and the effect of short range interactions between molecules should remain visible in the molar polarizability spectra. This is perhaps, the most desirable situation from the chemists point of view.

6.3 Comparison of *Ab Initio* Intensities with Experimental Intensities

Maslen *et al.*[50] have reported the gas phase intensity, $A_{j,\mathrm{gas}}$, of all fundamental, combination and overtone transitions of benzene-h_6 below 6150 cm^{-1} calculated by an *ab initio* calculation that included mechanical and electrical anharmonic effects. Table 6.10 lists the magnitudes of the transition moments calculated from the intensities given by Maslen *et al.*[50] along with the magnitudes of the experimental gas and liquid phase transition moments. Also given in Table 6.10 are the ratios of the experimental gas and liquid phase transition moments to *ab initio* transition moments. These ratios should be unity if the *ab initio* transition moments are exact and if the transition moments of the liquid phase are the same as those for the gas phase.

The *ab initio* transition moments are 5 to 30% larger than the experimental gas phase transition moments for the four infrared active fundamentals, and about 1.7 times larger for $\nu_4+\nu_{11}$.

The *ab initio* transition moments of ν_{13}, ν_{14} and ν_4 are about 2 to 25% larger than the experimental liquid phase transition moments; that for ν_{12} is about 80% larger, because ν_{12} is much weaker in the liquid (Table 6.6). For the combination transitions, 45 of the 48 *ab initio* transition moments are within a factor of 2 of the experimental liquid phase transition moments. This quality of calculated intensities is very encouraging and very helpful to the assignment of spectra.

Table 6.10. Calculated and experimental intensities of benzene-h_6. [a,b]

Transition[c]	$\tilde{\nu}_{j,\mathrm{ab}}$ / cm^{-1}	$\lvert R_{j,\mathrm{ab}} \rvert$	$\lvert R_{j,\mathrm{gas}} \rvert$	$\frac{\lvert R_{j,\mathrm{gas}} \rvert}{\lvert R_{j,\mathrm{ab}} \rvert}$	$\tilde{\nu}_{j,\mathrm{liq}}$ / cm^{-1}	$\lvert R_{j,\mathrm{liq}} \rvert$	$\frac{\lvert R_{j,\mathrm{liq}} \rvert}{\lvert R_{j,\mathrm{ab}} \rvert}$
1+12	6087	0.00304			6089	0.0153	0.50
12+15	6074	0.00694			6072	0.00198	0.29
12+13+13	6023	0.00973			6023	0.00184	0.19
12+16	4659	0.00575			4642	0.00357	0.62
5+16	4631	0.0645			4583	0.00416	0.65
1+13	4549	0.00209			4543	0.00313	1.16
13+15	4543	0.00061			4538		
3+12	4403	0.00131			4378	0.00135	1.03
9+15	4368	0.00107			4372	0.00139	1.21
12+17	4231	0.00025			4195	0.00178	7.2
10+15	4207	0.00131			4173	0.00113	0.86
5+17	4208	0.00152			4219	0.00139	0.91
1+14	4107	0.00406			4097	0.00320	0.79
14+15	4095	0.00349			4081	0.00420	1.20
6+15	4068	0.0129			4057	0.0115	0.89
2+12	4048	0.00370			4024	0.00303	0.46
15+19	4022	0.00386			4024		
5+7	4018	0.00411					
11+12	3899	0.00452			3898	0.00341	0.75
1+4	3742	0.00452			3738	0.00404	0.89
5+8	3739	0.00099					
12+18	3663	0.00702			3642	0.00433	0.62
5+18	3640	0.00464			3611	0.00588	1.27
15+20	3457	0.00546			3448	0.00343	0.63
2+13+18	3080		0.069	0.76	3091	0.0~~495~~ 521	0.5~~5~~ 8
13+16	3084	0.0229			3071		
12	3055	0.0879			3036		
9+16	2901	0.00710			2887	0.00514	0.72
3+13	2831	0.00312			2819	0.00427	1.35
10+16	2746	0.00320					

Table 6.10. Continued.

Transition	$\tilde{\nu}_{j,\mathrm{ab}}$ / cm^{-1}	$\lvert R_{j,\mathrm{ab}}\rvert$	$\lvert R_{j,\mathrm{gas}}\rvert$	$\frac{\lvert R_{j,\mathrm{gas}}\rvert}{\lvert R_{j,\mathrm{ab}}\rvert}$	$\tilde{\nu}_{j,\mathrm{liq}}$ / cm^{-1}	$\lvert R_{j,\mathrm{liq}}\rvert$	$\frac{\lvert R_{j,\mathrm{liq}}\rvert}{\lvert R_{j,\mathrm{ab}}\rvert}$
13+17	2660	0.00345			2653	0.00416	1.21
14+16	2633	0.00021					
6+16	2609	0.00924			2595	0.00385	0.42
16+19	2567	0.00431			2554	0.00267	0.62
9+17	2488	0.00497			2485	0.00190	0.38
2+13	2474	0.00062			2469	0.00129	2.09
3+14	2388	0.00542			2382	0.00382	0.70
10+17	2327	0.00464			2325	} 0.0104	1.44
11+13	2331	0.00308			2325		
14+17	2215	0.00624			2210	0.00552	0.79
6+17	2188	0.00263					
17+19	2145	0.00053					
13+18	2090	0.00066					
2+14	2029	0.00070					
6+7	2000	0.00957			2005	} 0.00289	0.65
2+18+20	2000	0.00390			2005		
16+20	1998	0.00390			1988	0.00390	1.00
7+19	1955	0.0202			1960	0.0200	0.99
9+18	1916	0.00041					
11+14	1885	0.00448			1883	0.00292	0.65
11+19	1810	0.0293			1815	0.0257	0.88
10+18	1756	0.00598			1755	0.00598	1.00
6+8	1717	0.00099			1713	0.00324	3.29
8+19	1674	0.00275			1671	} 0.00859	1.41
2+4	1666	0.00472			1671		
14+18	1646	0.00177			1645	0.00128	0.72
6+18	1618	0.00657			1618	0.00567	0.86
17+20	1576	0.00292					
18+19	1575	0.00123					
4+11	1519	0.0276	0.0162	0.59	1528	0.0184	0.45
13	1484	0.0517	0.420	0.81	1479	0.0~~485~~97	0.9~~4~~7

Table 6.10. Continued.

Transition	$\tilde{\nu}_{j,\mathrm{ab}}$ / cm^{-1}	$\lvert R_{j,\mathrm{ab}}\rvert$	$\lvert R_{j,\mathrm{gas}}\rvert$	$\frac{\lvert R_{j,\mathrm{gas}}\rvert}{\lvert R_{j,\mathrm{ab}}\rvert}$	$\tilde{\nu}_{j,\mathrm{liq}}$ / cm^{-1}	$\lvert R_{j,\mathrm{liq}}\rvert$	$\frac{\lvert R_{j,\mathrm{liq}}\rvert}{\lvert R_{j,\mathrm{ab}}\rvert}$
7+20	1387	0.0105			1393	0.0126	1.20
11+20	1243	0.00538			1250	0.00676	1.26
8+20	1108	<0.00012					
14	1038	0.0431	0.0409 [d]	0.95	1036	0.0445	1.03
			0.0380 [d]	0.88			
18+20	1006	0.00821			1010	0.0125	1.52
4	674	0.306	0.236	0.77	676	0.244	0.80

[a] $\tilde{\nu}_{j,\mathrm{ab}}$ is the *ab initio* anharmonic wavenumber of the transition calculated by Maslen *et al.*[50] and $\tilde{\nu}_{j,\mathrm{liq}}$ is the wavenumber of the transition observed in the $\tilde{\nu}\alpha''_{\mathrm{m}}$ spectrum of liquid benzene-h$_6$.

[b] The transition moments are in Debye. $\lvert R_{j,\mathrm{ab}}\rvert$ is the magnitude of the *ab initio* transition moment calculated from the intensity given by Maslen *et al.*[50], $\lvert R_{j,\mathrm{liq}}\rvert$ and $\lvert R_{j,\mathrm{gas}}\rvert$ are the magnitude of the experimental liquid and gas phase transition moments from Chapter 5 and section 6.2, respectively.

[c] The entries in this column are the numbers of the transitions. For example, 1+12 means $\nu_1+\nu_{12}$.

[d] Two values are listed due to the disagreement between the literature values. See section 6.2.

Chapter 7

Binary Mixtures of Liquid Benzene-h_6 and Liquid Benzene-d_6

In this chapter the measurement and analysis of the optical constant spectra of binary mixtures of benzene-h_6 and benzene-d_6 are described. The optical constants have been determined from transmission spectra for 8 mole fractions of benzene-h_6 in benzene-d_6, in addition to the optical constants of pure benzene-h_6 and benzene-d_6 that were discussed in Chapter 3. Section 7.1 describes the experimental measurements from which the optical constants were calculated. In section 7.2 the change in integrated intensity with composition is examined for the four infrared active fundamentals of both benzene-h_6 and benzene-d_6 and in section 7.4 the peak shifts and changes in band width with composition are compared with those reported in the literature.

7.1 Method and Experimental

The experimental and instrumental details are the same as for benzene, described in section 3.1. Solutions were prepared by mixing known masses of benzene-h_6 and benzene-d_6. All concentrations are referred to in terms of the mole fraction of benzene-h_6.

Experimental absorbance spectra of mixtures of benzene-h_6 and benzene-d_6 were measured in cells with KBr windows and fixed path lengths between 11 and 1500 μm, in cells with CaF_2 windows and fixed path lengths of 110 and 1180 μm, and in variable path NaCl and CaF_2 cells with path lengths up to 3.8 mm.

Tables 7.1 and 7.2 list the linear absorption coefficients, and their 95% confidence limits at the anchor points for the different mixtures of benzene-h_6 and benzene-d_6 measured in this work. The path lengths used to measure these linear absorption coefficients were between 0.5 mm and 3.8 mm, always at least twice the path length used to measure the neighbouring peaks. The determination of the linear absorption coefficients at the anchor points requires an approximate real refractive index value at each anchor point. These approximate real refractive indices were determined by converting an experimental absorbance spectrum of the mixture in an 11 μm cell into real and imaginary refractive index spectra with program RNJ46A, not using the baseline correction (section 2.5).

The experimental absorbance spectra were converted to imaginary refractive index spectra using RNJ46A with the linear absorption coefficients given in Table 7.1 and 7.2. Each imaginary refractive index spectrum was only used in those regions where the corresponding experimental absorbance was between 0.2 and 2.0. For each mixture, the imaginary refractive index spectra were averaged over common suitable regions, and a final imaginary refractive index spectrum was obtained by merging these averaged spectra.

The benzene-h_6 ν_4 band (~760 - 550 cm^{-1}) is too strong to measure accurately in 11 μm cells for mole fractions of benzene-h_6 greater than or equal to 0.40. But it is necessary to include this band in the $k(\tilde{\nu})$ spectrum that is Kramers-Kronig transformed to give $n(\tilde{\nu})$. The determination of this band for 100% benzene-h_6 was described in section 3.1.3b. This region was approximated for mole fractions of benzene-h_6 greater than or equal to 0.40 by a mole-fraction-weighted linear combination of the pure benzene-h_6 and benzene-d_6 imaginary refractive index spectra.

Table 7.1. Linear absorption coefficients at anchor points for binary mixtures up to 52% benzene-h_6 in benzene-d_6 at 25°C.

Mole fraction of benzene-h_6							
0.1001		0.2538		0.4000		0.5195	
$\tilde{\nu}$ / cm^{-1}	$K(\tilde{\nu})$ / cm^{-1}	$\tilde{\nu}$ / cm^{-1}	$K(\tilde{\nu})$ / cm^{-1}	$\tilde{\nu}$ / cm^{-1}	$K(\tilde{\nu})$ / cm^{-1}	$\tilde{\nu}$ / cm^{-1}	$K(\tilde{\nu})$ / cm^{-1}
6231.8	0 [a]	6317.1	0.052 (5)	6319.5	0.074 (18)	6231.8	0 [a]
6068.8	0 [a]	6062.6	0.17 (5)	6064.5	0.304 (16)	6063.1	0.29 (8)
5829.7	0.06 (5)	5822.5	0.159 (18)	5819.6	0.200 (9)	5816.2	0.233 (11)
5631.6	0 [a]	5630.6	0.084 (4)	5629.2	0.186 (12)	5631.6	0.15 (7)
5473.9	0 [a]	5471.0	0.057 (28)	5462.8	0.114 (7)	5468.1	0.111 (28)
5169.7	0 [a]	5167.3	0.068 (12)	5171.1	0.095 (5)	5285.4	0.20 (4)
5020.7	0 [a]	4942.6	0.074 (18)	4948.4	0.138 (6)	5169.2	0.135 (17)
4806.2	0.042 (15)	4804.7	0.109 (17)	4804.7	0.177 (5)	4950.3	0.153 (22)
4567.5	0.753 (13)	4529.0	1.167 (11)	4525.6	1.158 (5)	4804.3	0.200 (18)
4351.5	0.450 (12)	4350.6	0.522 (8)	4349.6	0.5737 (19)	4523.2	1.213 (9)
4196.3	0.523 (11)	4149.5	0.754 (6)	4147.6	1.051 (7)	4315.4	0.544 (6)
3995.3	0.379 (9)	3971.6	0.729 (7)	3971.6	1.041 (5)	4147.1	1.342 (6)
3755.6	0.643 (5)	3853.0	1.181 (10)	3851.6	1.220 (4)	3971.1	1.310 (5)
3661.6	0.642 (6)	3756.1	0.833 (5)	3757.1	0.994 (5)	3852.1	1.246 (5)
3558.5	0.586 (5)	3659.7	0.971 (7)	3497.7	0.4423 (22)	3756.6	1.147 (5)
3472.2	0.263 (4)	3497.2	0.373 (9)	3375.3	0.5701 (21)	3525.7	0.511 (4)
3343.9	0.582 (4)	3375.7	0.565 (8)	3193.5	2.629 (22)	3342.0	0.616 (4)
3180.0	1.481 (5)	3181.4	2.203 (26)	2916.3	3.208 (11)	3195.9	2.938 (8)
2972.2	2.614 (8)	2915.3	2.550 (12)	2707.5	0.5228 (23)	2916.8	3.978 (22)
2802.0	1.071 (4)	2799.6	1.265 (9)	2533.5	0.6943 (26)	2721.0	0.610 (5)
2695.0	0.334 (4)	2699.8	0.444 (6)	2499.7	0.8056 (23)	2534.4	0.782 (4)
2638.6	0.717 (4)	2534.0	0.607 (6)	2352.2	6.71 (3)	2440.4	1.252 (6)
2582.7	0.690 (4)	2499.7	0.721 (7)	2160.8	1.943 (7)	2352.2	5.801 (29)
2533.5	0.511 (4)	2160.8	2.237 (8)	2065.3	0.5654 (23)	2160.3	1.731 (6)
2498.3	0.624 (4)	2063.9	0.464 (6)	1892.7	2.047 (6)	1997.4	4.257 (8)
2352.2	9.146 (22)	1891.8	1.813 (8)	1729.8	1.147 (5)	1893.7	2.231 (5)
2161.3	2.534 (9)	1731.7	0.936 (6)	1648.3	3.615 (20)	1729.3	1.319 (7)

Table 7.1. Continued.

Mole fraction of benzene-h_6							
0.1001		0.2538		0.4000		0.5195	
$\tilde{\nu}$ / cm^{-1}	$K(\tilde{\nu})$ / cm^{-1}	$\tilde{\nu}$ / cm^{-1}	$K(\tilde{\nu})$ / cm^{-1}	$\tilde{\nu}$ / cm^{-1}	$K(\tilde{\nu})$ / cm^{-1}	$\tilde{\nu}$ / cm^{-1}	$K(\tilde{\nu})$ / cm^{-1}
1981.5	1.607 (8)	1648.3	3.610 (22)	1563.0	6.43 (4)	1647.8	3.654 (6)
1923.1	1.035 (9)	1563.5	6.47 (4)	1418.8	4.079 (18)	1563.0	6.441 (12)
1890.8	1.501 (8)	1418.8	3.843 (18)	1364.8	3.736 (15)	1418.8	4.313 (7)
1842.1	2.533 (9)	1366.3	3.685 (16)	1267.0	3.001 (14)	1364.3	3.791 (6)
1735.1	0.685 (7)	1263.6	2.668 (16)	1095.3	2.97 (9)	1267.9	3.230 (5)
1647.3	3.524 (11)	1095.8	2.159 (7)	908.8	5.37 (7)	1095.3	3.554 (18)
1578.9	4.431 (13)	909.3	5.240 (9)	757.9	8.54 (6)	908.8	5.482 (10)
1508.0	3.973 (10)	757.4	7.525 (19)	587.7	7.72 (10)	835.5	17.32 (7)
1418.3	3.561 (13)	595.4	7.888 (21)	446.9	9.17 (7)	783.4	11.94 (10)
1368.2	3.580 (11)	447.4	11.17 (28)			760.3	9.25 (3)
1236.6	1.688 (17)					567.9	6.79 (16)
1098.7	1.392 (15)					451.7	8.36 (11)
996.5	5.133 (6)						
909.3	5.155 (12)						
755.0	6.183 (25)						
623.4	6.376 (17)						
447.4	13.92 (22)						

[a] Set to zero because the absorbance is too weak to determine accurately in a 3.8 mm cell.

Table 7.2. Linear absorption coefficients at anchor points for binary mixtures greater than 60% benzene-h_6 in benzene-d_6 at 25°C.

Mole fraction of benzene-h_6							
0.6196		0.7008		0.7934		0.9426	
$\tilde{\nu}$ / cm^{-1}	$K(\tilde{\nu})$ / cm^{-1}	$\tilde{\nu}$ / cm^{-1}	$K(\tilde{\nu})$ / cm^{-1}	$\tilde{\nu}$ / cm^{-1}	$K(\tilde{\nu})$ / cm^{-1}	$\tilde{\nu}$ / cm^{-1}	$K(\tilde{\nu})$ / cm^{-1}
6328.7	0.191 (3)	6231.8	0 [a]	6231.8	0.029 (14)	6231.8	0.158 (18)
6062.1	0.55 (4)	6061.6	0.43 (5)	6063.1	0.431 (22)	6061.6	0.668 (25)
5817.7	0.324 (20)	5817.2	0.283 (16)	5816.2	0.307 (10)	5815.2	0.377 (20)
5631.1	0.34 (3)	5631.6	0.24 (4)	5631.6	0.210 (7)	5727.0	0.415 (17)
5459.9	0.198 (23)	5461.4	0.136 (29)	5468.1	0.134 (11)	5630.6	0.347 (21)
5170.7	0.168 (17)	5288.8	0.20 (4)	5285.4	0.184 (12)	5463.8	0.181 (15)
4948.9	0.224 (21)	5169.7	0.15 (3)	5169.2	0.184 (6)	5281.1	0.223 (14)
4804.7	0.265 (20)	4948.9	0.179 (24)	4950.3	0.198 (7)	5169.2	0.202 (10)
4521.7	1.134 (11)	4804.3	0.231 (25)	4804.3	0.262 (4)	5113.3	0.222 (11)
4316.3	0.593 (10)	4520.3	1.067 (17)	4517.4	1.068 (9)	5026.5	0.244 (11)
4146.2	1.518 (11)	4317.8	0.607 (10)	4319.2	0.683 (4)	4949.8	0.244 (11)
3971.6	1.518 (10)	4146.2	1.674 (17)	4145.2	1.913 (5)	4803.8	0.305 (9)
3850.6	1.238 (9)	3971.1	1.674 (11)	3971.1	1.899 (7)	4510.2	0.871 (5)
3757.1	1.236 (8)	3848.7	1.227 (8)	3844.8	1.221 (5)	4321.7	0.732 (5)
3658.7	1.600 (9)	3757.1	1.316 (11)	3757.6	1.431 (5)	4143.8	2.202 (7)
3526.2	0.520 (6)	3525.7	0.503 (5)	3525.7	0.536 (3)	3971.1	2.215 (8)
3373.8	0.593 (6)	3342.0	0.577 (4)	3340.1	0.597 (3)	3840.0	1.100 (5)
3198.3	3.131 (25)	3201.2	3.199 (17)	3204.1	3.284 (8)	3757.6	1.569 (7)
2917.2	4.244 (10)	2919.7	4.657 (16)	2916.8	5.089 (19)	3526.6	0.515 (3)
2871.4	3.567 (11)	2721.5	0.663 (5)	2722.0	0.729 (4)	3365.1	0.521 (3)
2836.7	3.522 (10)	2533.5	0.859 (4)	2534.4	0.931 (4)	3216.6	2.902 (5)
2721.5	0.639 (3)	2440.4	1.173 (8)	2440.4	1.173 (6)	2917.7	6.042 (28)
2534.0	0.825 (3)	2352.2	4.359 (10)	2352.2	3.675 (12)	2864.7	3.743 (23)
2500.7	0.934 (3)	2160.3	1.358 (8)	2159.8	1.213 (7)	2789.5	1.595 (10)
2440.4	1.209 (8)	1996.9	5.377 (15)	1997.8	6.109 (17)	2722.5	0.773 (10)
2352.2	4.982 (17)	1894.7	2.438 (7)	1895.6	2.539 (5)	2533.0	0.986 (10)
2160.3	1.524 (8)	1727.4	1.532 (9)	1725.9	1.650 (7)	2439.9	1.109 (10)

Table 7.2. Continued.

Mole fraction of benzene-h_6							
0.6196		0.7008		0.7934		0.9426	
$\tilde{\nu}$ / cm^{-1}	$K(\tilde{\nu})$ / cm^{-1}	$\tilde{\nu}$ / cm^{-1}	$K(\tilde{\nu})$ / cm^{-1}	$\tilde{\nu}$ / cm^{-1}	$K(\tilde{\nu})$ / cm^{-1}	$\tilde{\nu}$ / cm^{-1}	$K(\tilde{\nu})$ / cm^{-1}
2066.8	0.7213 (28)	1650.2	3.654 (9)	1650.2	3.655 (7)	2353.2	2.475 (15)
1894.2	2.355 (8)	1562.5	6.370 (15)	1563.0	6.307 (17)	2303.5	3.356 (15)
1727.9	1.454 (4)	1420.8	4.640 (13)	1420.7	4.775 (9)	2229.3	2.192 (16)
1649.3	3.675 (20)	1361.5	3.804 (22)	1360.5	3.731 (6)	2123.7	0.633 (9)
1563.0	6.400 (28)	1271.3	3.459 (13)	1276.6	3.524 (6)	1898.0	2.612 (15)
1420.3	4.493 (16)	1095.8	4.430 (5)	1094.8	4.935 (19)	1725.0	1.847 (18)
1362.9	3.786 (15)	907.8	5.516 (11)	906.9	5.571 (15)	1651.7	3.627 (16)
1269.8	3.374 (14)	833.1	15.70 (8)	831.2	14.11 (9)	1560.6	6.46 (6)
1095.3	4.13 (9)	785.9	10.579 (23)	786.8	9.57 (3)	1421.2	5.07 (3)
909.3	5.50 (6)	761.3	10.26 (5)	761.7	10.64 (4)	1355.7	3.567 (18)
760.3	9.86 (8)	566.5	5.045 (10)	569.9	4.37 (16)	1279.0	3.522 (12)
567.9	6.07 (3)	447.4	6.03 (3)	453.7	4.68 (5)	1098.7	6.42 (8)
447.9	6.41 (7)					913.1	5.73 (4)
						825.4	10.43 (3)
						792.6	7.096 (22)
						554.0	2.224 (8)
						455.1	1.994 (12)

[a] Set to zero because the absorbance is too weak to determine accurately in a 3.8 mm cell.

Similarly, the benzene-d_6 ν_4 region (~510 - 450 cm^{-1}) is too strong to measure accurately in 11 μm cells for 0.10 mole fraction of benzene-h_6. To obtain an accurate $n(\tilde{\nu})$ spectrum, this region of the $k(\tilde{\nu})$ spectrum was also approximated by a mole-fraction-weighted linear combination of the pure benzene-h_6 and benzene-d_6 imaginary refractive index spectra.

These approximated ν_4 regions of certain mixtures were only included to improve the real refractive index spectra in the surrounding regions and were not included in the analysis of the mixtures in section 7.2 and 7.4.

The real refractive index spectra were calculated by Kramers-Kronig transformation of the imaginary refractive index spectra using the values of n_{8000} given in Table 7.3. There is only a 0.16% difference between the real refractive indices of benzene-h_6 and benzene-d_6 at 8000 cm^{-1} (section 3.2.2) so it was assumed that n_{8000} is linear in mole fraction of benzene-h_6.

The real and imaginary refractive index spectra are tabulated in compact table format[44] in Appendix VI. They are shown between 3200 to 400 cm^{-1} in Figures 7.1 to 7.4 for pure benzene-d_6, 0.4 benzene-h_6, 0.6 benzene-h_6 and pure benzene-h_6. From the real and imaginary refractive index spectra the molar absorption coefficient (E_m) spectra, the real and imaginary dielectric constant spectra and the imaginary molar polarizability (α_m'') spectra were calculated using the equations summarized in section 1.3. The required molar volumes are given in Table 7.3. These molar volumes were calculated from the molar volumes of benzene-h_6 and benzene-d_6 (section 3.2.2) under the assumption that there is no volume change when the two liquids are mixed, so the molar volume is linear in mole fraction.

Table 7.3. Real refractive indices at 8000 cm^{-1} and molar volumes for binary mixtures of benzene-h$_6$ and benzene-d$_6$ at 25°C.

Mole fraction of benzene-h$_6$	n_{8000}	V_m / cm^3 mole^{-1}
0.0000	1.4780	88.59
0.1001	1.4782	88.67
0.2538	1.4786	88.80
0.4000	1.4790	88.92
0.5195	1.4792	89.01
0.6196	1.4795	89.10
0.7008	1.4797	89.16
0.7934	1.4799	89.24
0.9426	1.4803	89.36
1.0000	1.4804	89.41

7.2 Change in Intensity upon Isotopic Dilution

Figures 7.5 to 7.12 show the $\tilde{\nu}\alpha''_{\mathrm{m}}$ spectra of mixtures of benzene-h_6 and benzene-d_6 in the regions of the 4 infrared active fundamentals of each isotopomer. Figure 7.13 shows the integrated intensities of the 4 infrared active fundamentals of both benzene-h_6 and benzene-d_6 plotted against the mole fraction of benzene-h_6. The intensities shown are the integrated intensities C_j, (equation 1.3.36) over the integration ranges given in the figure caption, which are the ranges shown in Figures 7.5 to 7.12. The C_j values are tabulated in Table 7.4. Note that in this comparison the areas between specific integration limits are compared. Thus, the C_j values quoted for pure benzene-h_6 and pure benzene-d_6 are smaller than the C_j values determined from the parameters of the fitted bands (Tables 5.2 and 5.3).

The parameters obtained by linear least squares fits of the C_j values are given in Table 7.5. From the plots and parameters, it is clear that the intensity of each band is linear in the mole fraction of the absorbing molecule. This is the result expected from the CDHO theory of molar polarizability spectra of liquids if the interaction between different molecules is the same as that between like molecules. These interactions are essentially the same for benzene-h_6 and benzene-d_6, which form essentially ideal solutions, so this result confirms this aspect of the CDHO theory. This is a possibly unspectacular result, but is a necessary basis for the application of this technique to the study of the intermolecular interactions in liquids.

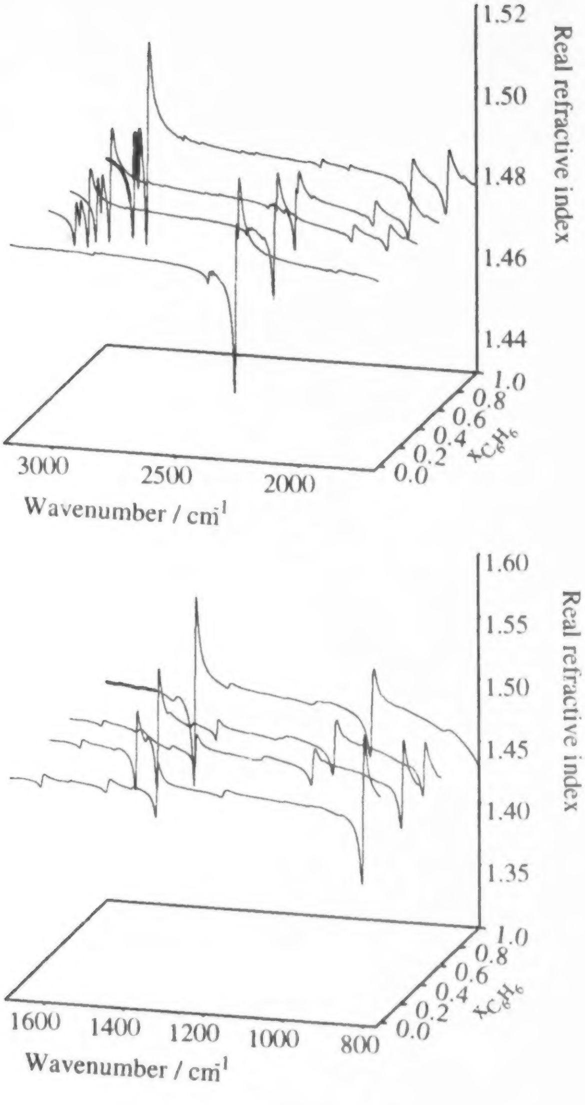

Figure 7.1. Real refractive index spectra for binary mixtures of benzene-h$_6$ and benzene-d$_6$ between 3200 and 800 cm^{-1}. The mole fractions of benzene-h$_6$ are 0.0000, 0.4000, 0.6196 and 1.0000.

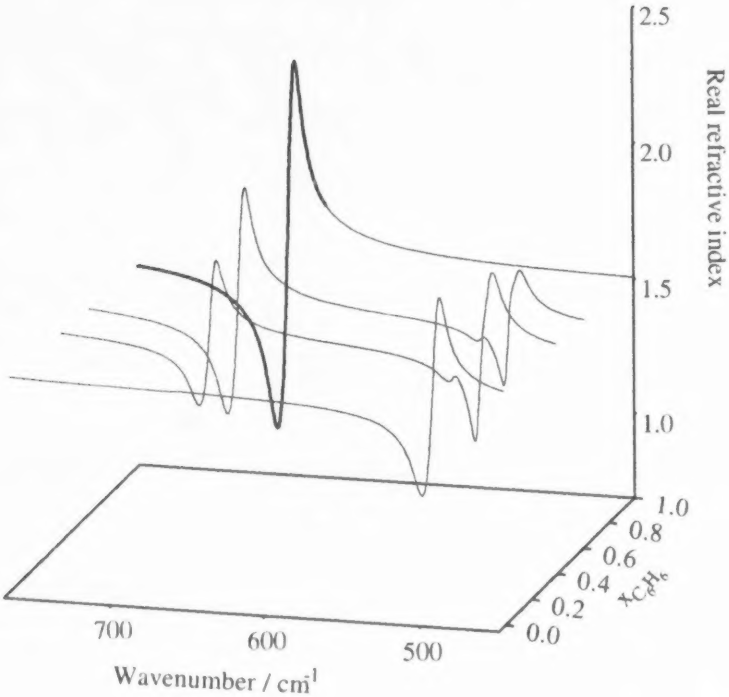

Figure 7.2. Real refractive index spectra for binary mixtures of benzene-h_6 and benzene-d_6 between 800 and 400 cm^{-1}. The mole fractions of benzene-h_6 are 0.0000, 0.4000, 0.6196 and 1.0000.

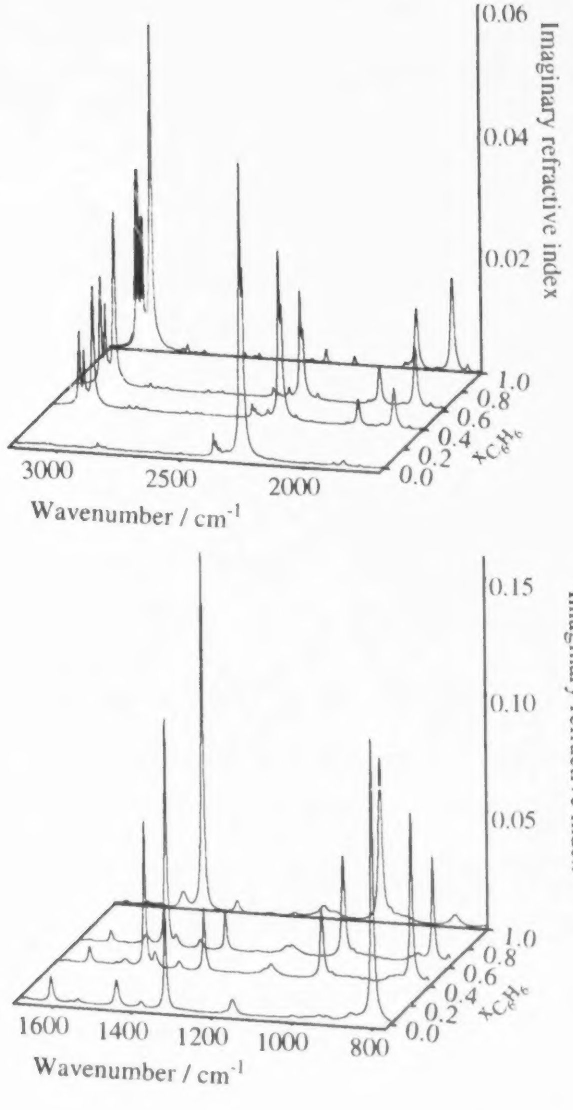

Figure 7.3. Imaginary refractive index spectra for binary mixtures of benzene-h$_6$ and benzene-d$_6$ between 3200 and 800 cm^{-1}. The mole fractions of benzene-h$_6$ are 0.0000, 0.4000, 0.6196 and 1.0000.

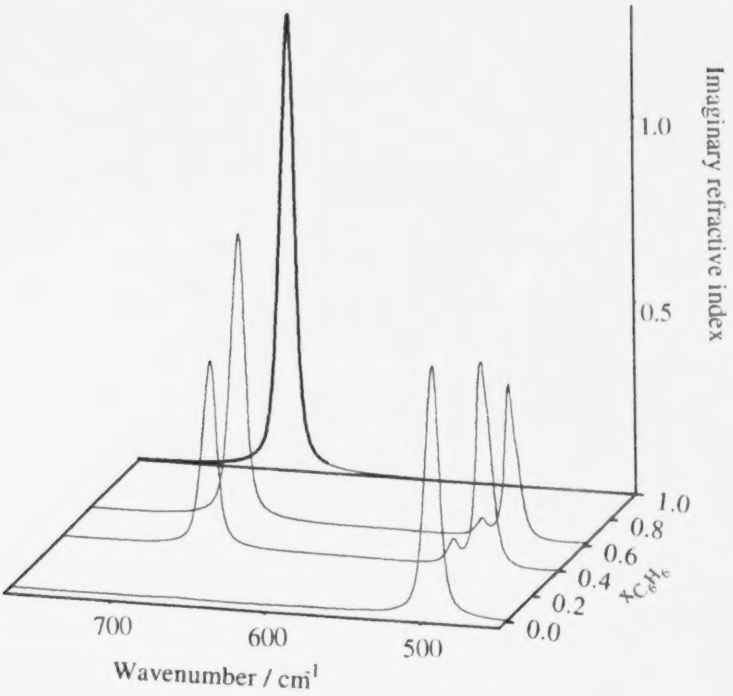

Figure 7.4. Imaginary refractive index spectra for binary mixtures of benzene-h$_6$ and benzene-d$_6$ between 800 and 400 cm^{-1}. The mole fractions of benzene-h$_6$ are 0.0000, 0.4000, 0.6196 and 1.0000. The bands of benzene-h$_6$ at $x_{C_6H_6}$ = 0.40 and 0.6196 and that of benzene-d$_6$ at $x_{C_6H_6}$ = 0.0 are approximate, as described in the text.

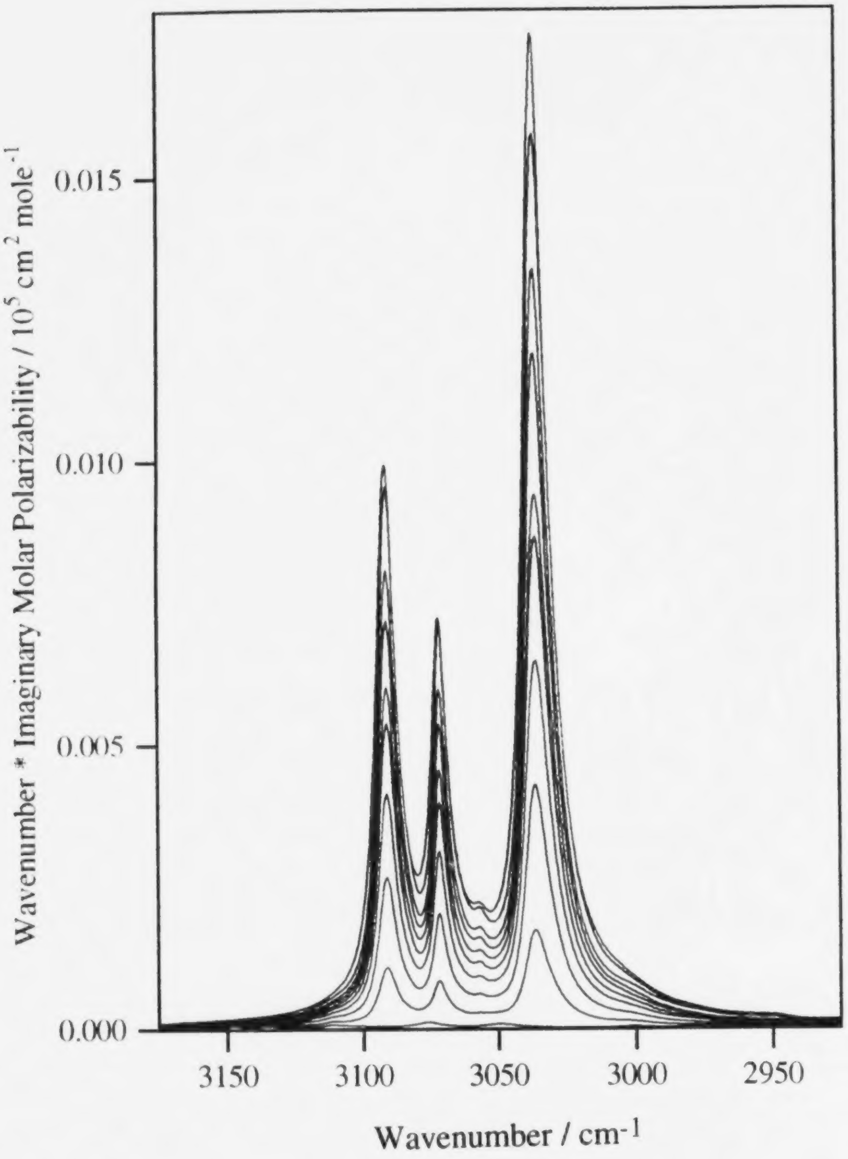

Figure 7.5. Wavenumber times the imaginary molar polarizability spectra for binary mixtures of benzene-h_6 and benzene-d_6 in the ν_{12} region of benzene-h_6. The mole fractions of benzene-h_6 are, from top to bottom; 1.0000, 0.9426, 0.7934, 0.7008, 0.6196, 0.5195, 0.4000, 0.2538, 0.1001 and 0.0000.

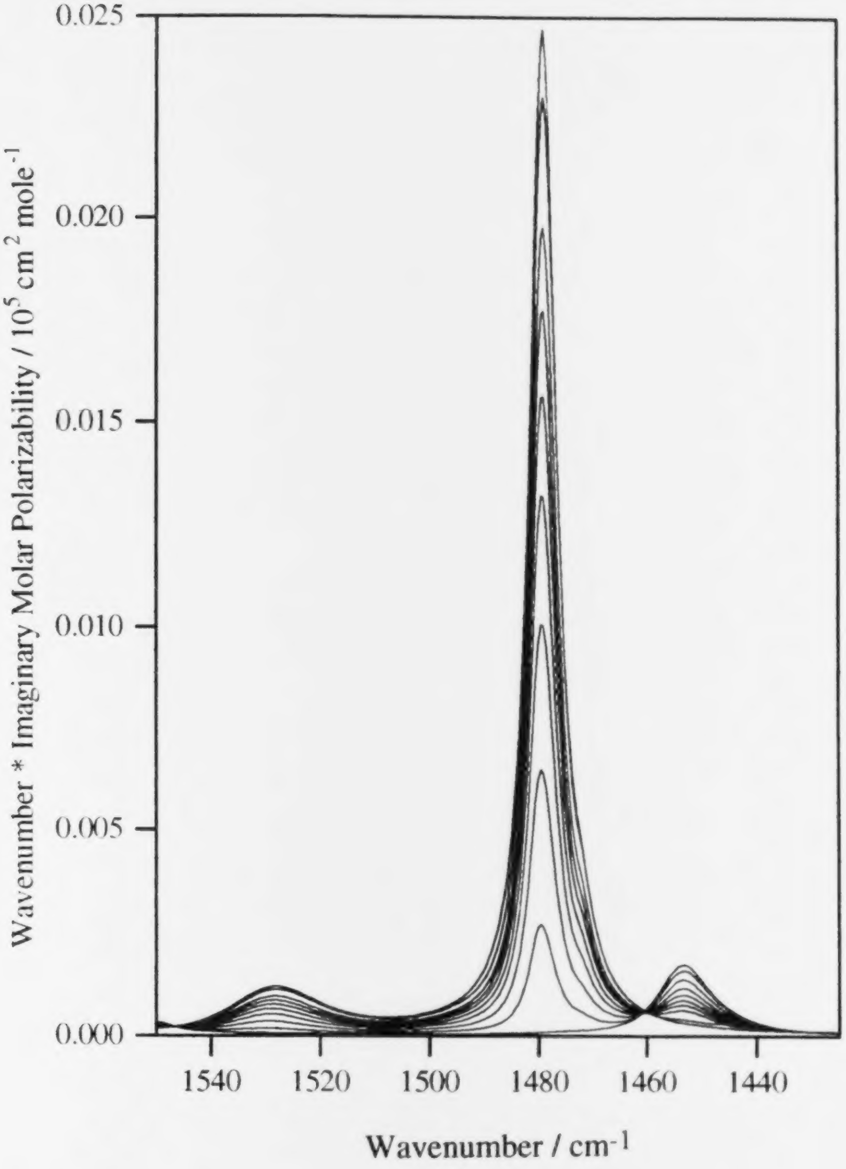

Figure 7.6. Wavenumber times the imaginary molar polarizability spectra for binary mixtures of benzene-h_6 and benzene-d_6 in the ν_{13} region of benzene-h_6. The mole fractions of benzene-h_6 are, from top to bottom of the main peak; 1.0000, 0.9426, 0.7934, 0.7008, 0.6196, 0.5195, 0.4000, 0.2538, 0.1001 and 0.0000.

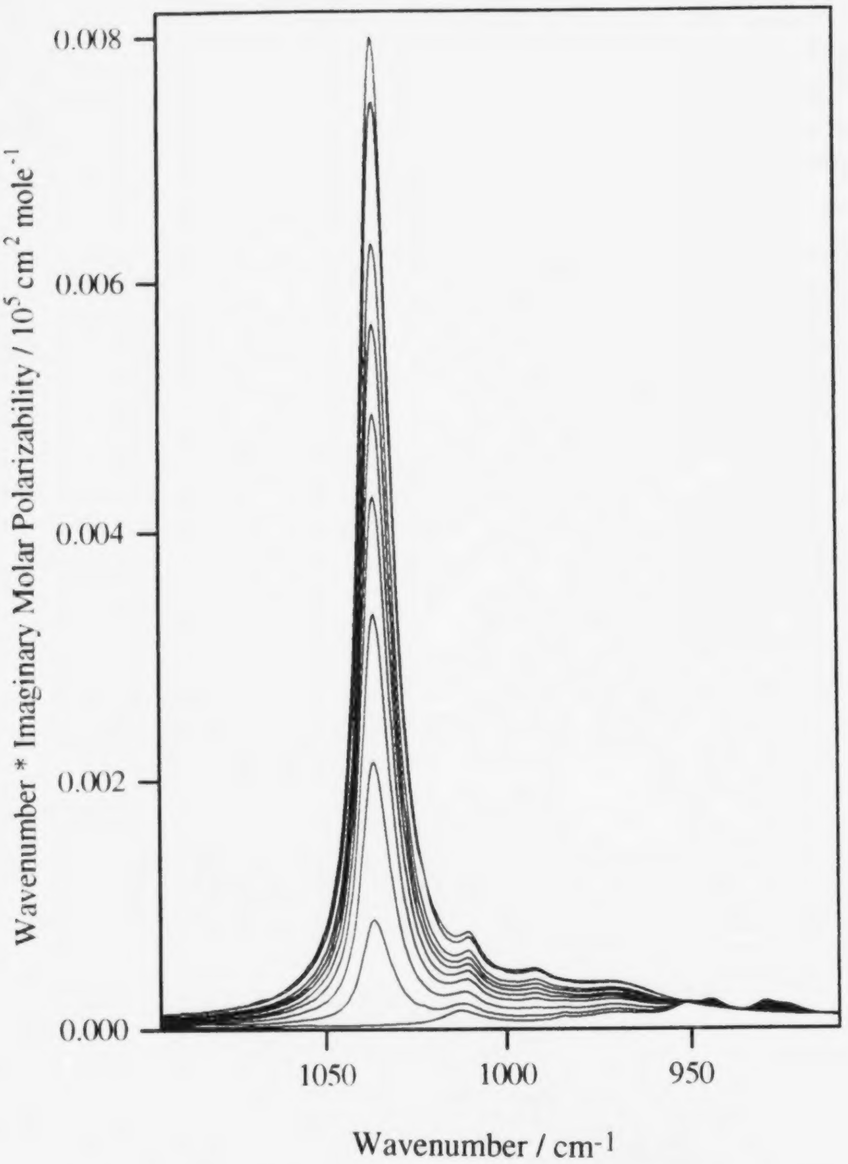

Figure 7.7. Wavenumber times the imaginary molar polarizability spectra for binary mixtures of benzene-h_6 and benzene-d_6 in the ν_{14} region of benzene-h_6. The mole fractions of benzene-h_6 are, from top to bottom of the main peak; 1.0000, 0.9426, 0.7934, 0.7008, 0.6196, 0.5195, 0.4000, 0.2538, 0.1001 and 0.0000.

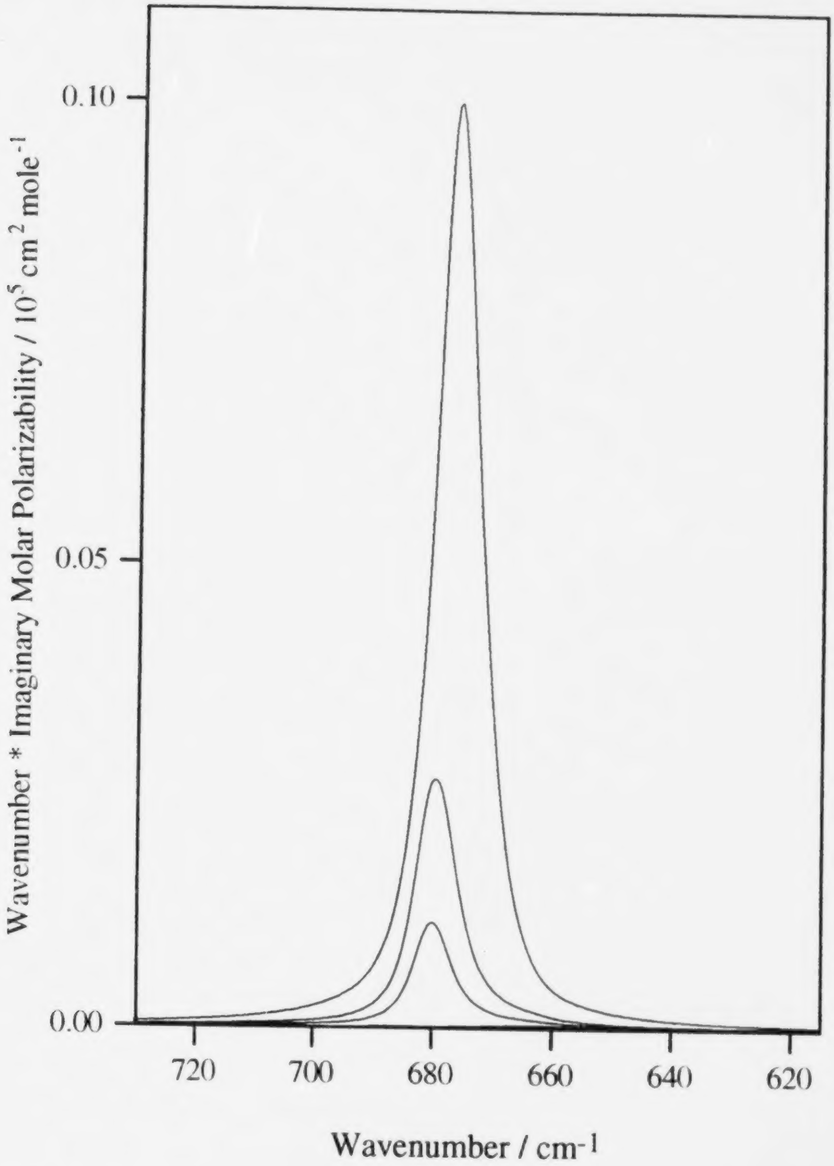

Figure 7.8. Wavenumber times the imaginary molar polarizability spectra for binary mixtures of benzene-h_6 and benzene-d_6 in the ν_4 region of benzene-h_6. The mole fractions of benzene-h_6 are, from top to bottom; 1.0000, 0.2538, 0.1001 and 0.0000.

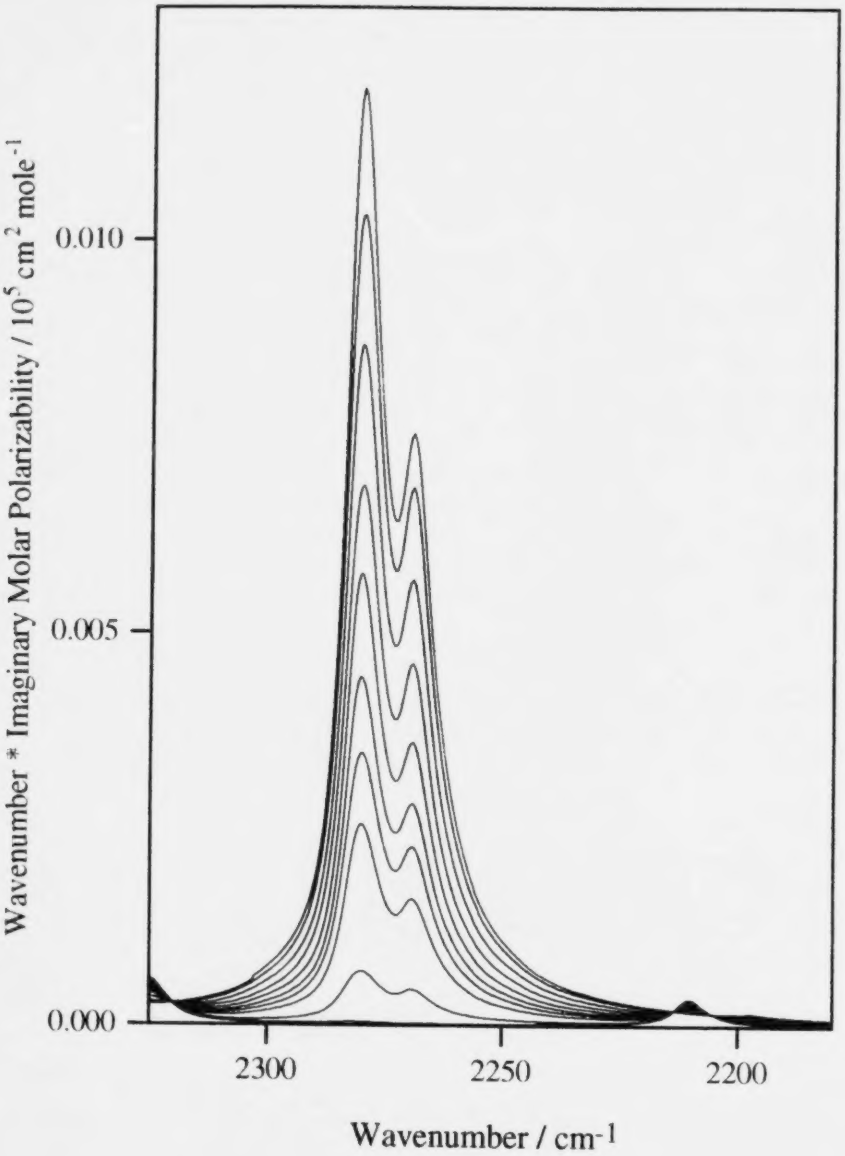

Figure 7.9. Wavenumber times the imaginary molar polarizability spectra for binary mixtures of benzene-h_6 and benzene-d_6 in the ν_{12} region of benzene-d_6. The mole fractions of benzene-h_6 are, from top to bottom of the main peak; 0.0000, 0.1001, 0.2538, 0.4000, 0.5195, 0.6196, 0.7008, 0.7934, 0.9426 and 1.0000.

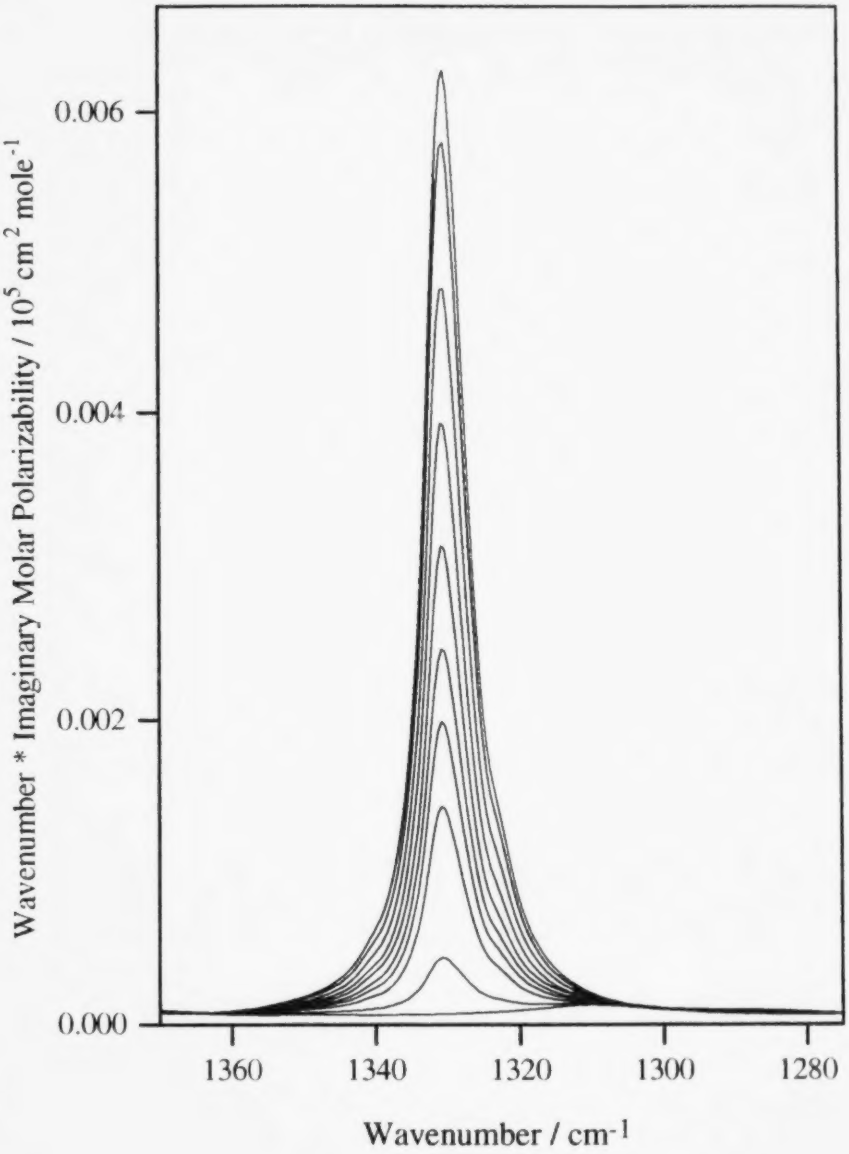

Figure 7.10. Wavenumber times the imaginary molar polarizability spectra for binary mixtures of benzene-h_6 and benzene-d_6 in the ν_{13} region of benzene-d_6. The mole fractions of benzene-h_6 are, from top to bottom; 0.0000, 0.1001, 0.2538, 0.4000, 0.5195, 0.6196, 0.7008, 0.7934, 0.9426 and 1.0000.

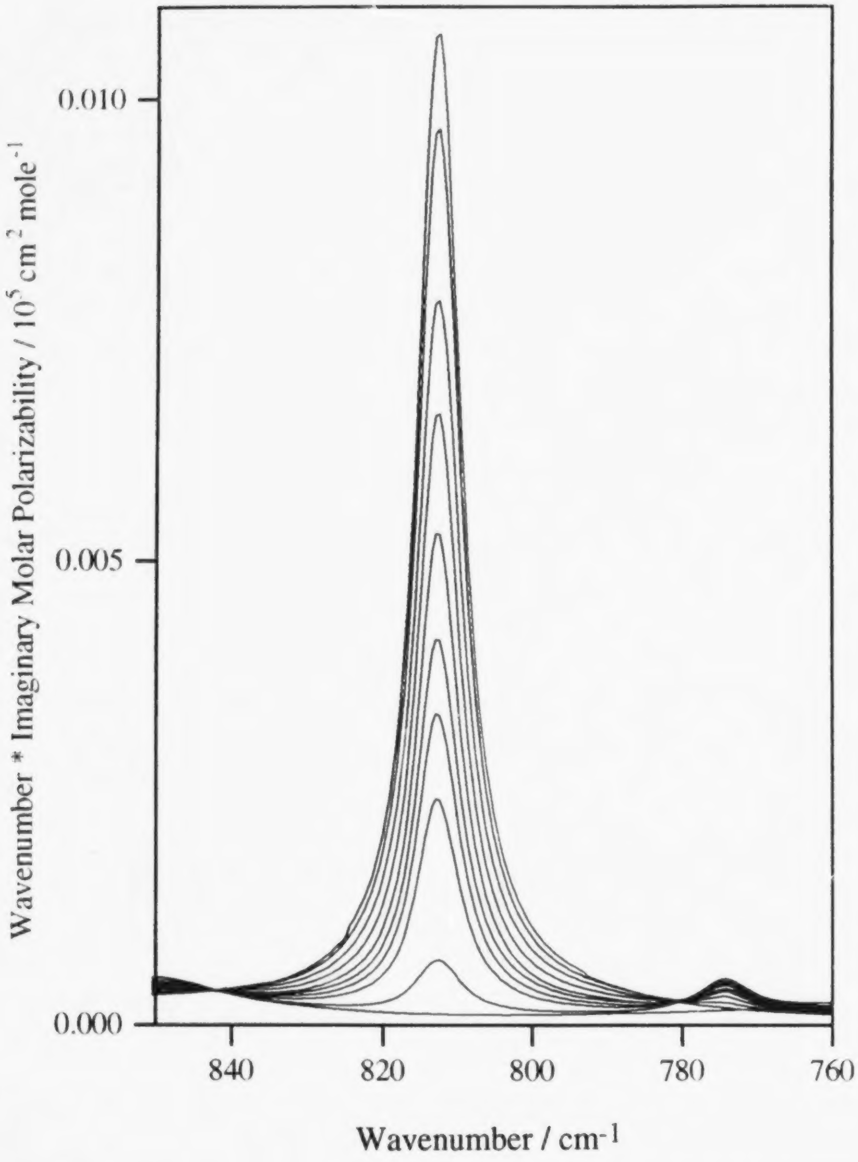

Figure 7.11. Wavenumber times the imaginary molar polarizability spectra for binary mixtures of benzene-h_6 and benzene-d_6 in the ν_{14} region of benzene-d_6. The mole fractions of benzene-h_6 are, from top to bottom of the main peak; 0.0000, 0.1001, 0.2538, 0.4000, 0.5195, 0.6196, 0.7008, 0.7934, 0.9426 and 1.0000.

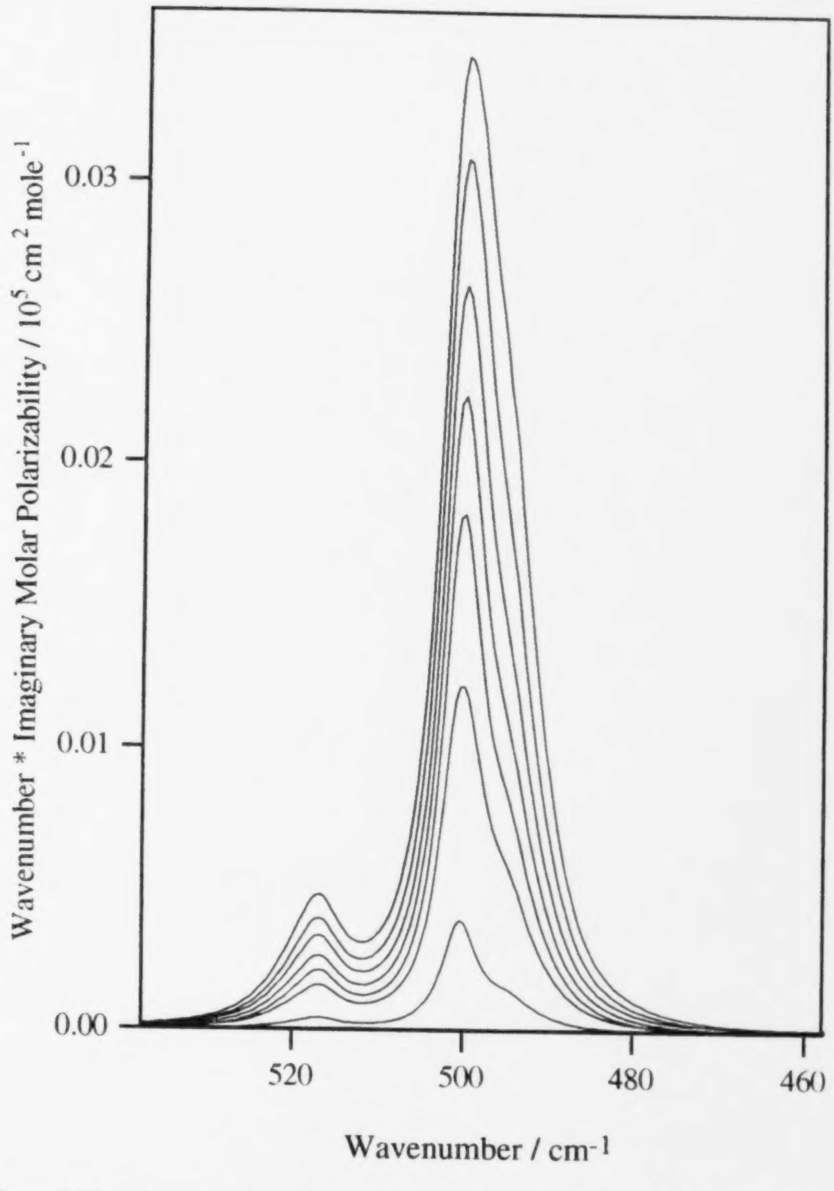

Figure 7.12. Wavenumber times the imaginary molar polarizability spectra for binary mixtures of benzene-h_6 and benzene-d_6 in the ν_4 region of benzene-d_6. The mole fractions of benzene-h_6 are, from top to bottom; 0.2538, 0.4000, 0.5195, 0.6196, 0.7008, 0.7934, 0.9426 and 1.0000.

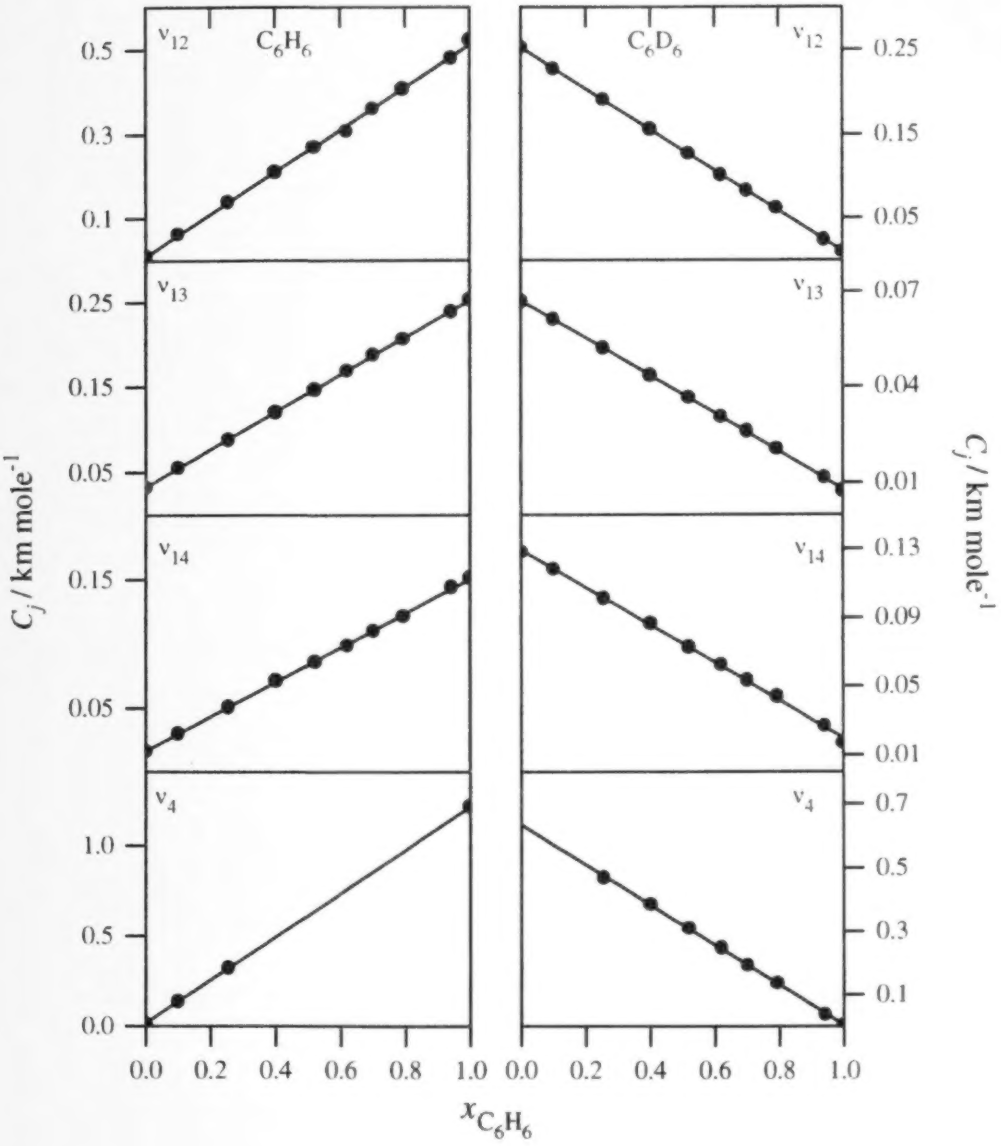

Figure 7.13. Integrated intensity versus mole fraction of benzene-h_6 for the infrared active fundamentals of benzene-h_6 and benzene-d_6. The areas shown are the areas under the bands in the $\tilde{\nu}\alpha''_m$ spectra. The integration ranges are 3175 - 2925, 1550 - 1425, 1095 - 910 and 730 - 615 cm^{-1} for benzene-h_6 and 2325 - 2180, 1370 - 1275, 850 - 760 and 538 - 458 cm^{-1} for benzene-d_6.

Table 7.4. Integrated intensities of mixtures of benzene-h_6 and benzene-d_6.

	C_j / km mole^{-1}							
$x_{C_6H_6}$	3175 - 2925 cm^{-1}	1550 - 1425 cm^{-1}	1095 - 910 cm^{-1}	730 - 615 cm^{-1}	2325 - 2180 cm^{-1}	1370 - 1275 cm^{-1}	850 - 760 cm^{-1}	538 - 458 cm^{-1}
0.0000	0.011	0.033	0.017	0.015	0.253	0.0669	0.129	
0.1001	0.062	0.055	0.030	0.137	0.227	0.0612	0.118	
0.2538	0.138	0.088	0.051	0.234	0.191	0.0518	0.101	0.469
0.4000	0.211	0.120	0.071		0.156	0.0434	0.087	0.386
0.5195	0.270	0.146	0.086		0.127	0.0365	0.072	0.311
0.6196	0.308	0.169	0.098		0.102	0.0304	0.062	0.249
0.7008	0.362	0.187	0.110		0.083	0.0257	0.053	0.193
0.7934	0.407	0.206	0.121		0.062	0.0205	0.044	0.137
0.9246	0.476	0.239	0.144		0.024	0.0115	0.027	0.037
1.0000	0.522	0.253	0.151	1.214	0.010	0.0074	0.017	0.003

Table 7.5. Least squares equations for C_j versus mole fraction. [a]

	Integration Range / cm^{-1}	*a*	*b*
Benzene-h$_6$ ν_{12}	3175 - 2925	0.502 (±0.006)	0.009 (±0.004)
Benzene-h$_6$ ν_{13}	1550 - 1425	0.2192 (±0.0007)	0.0329 (±0.0004)
Benzene-h$_6$ ν_{14}	1095 - 910	0.1338 (±0.0010)	0.0166 (±0.0006)
Benzene-h$_6$ ν_4	730 - 615	1.197 (±0.003)	0.017 (±0.002)
Benzene-d$_6$ ν_{12}	2325 - 2180	-0.2419 (±0.0008)	0.2524 (±0.0005)
Benzene-d$_6$ ν_{13}	1370 - 1275	-0.0591 (±0.0003)	0.0670 (±0.0002)
Benzene-d$_6$ ν_{14}	850 - 760	-0.1095 (±0.0012)	0.1295 (±0.0008)
Benzene-d$_6$ ν_4	538 - 458	-0.631 (±0.006)	0.636 (±0.004)

[a] $C_j = ax_{C_6H_6} + b$. The values in parentheses are the standard deviations in the parameters obtained from the least squares fits.

7.3 The Integrated Intensity of ν_4 of Benzene-d_6

It was stated earlier in this chapter as well as in section 3.2.1, that the intensity of ν_4 of benzene-d_6 could not be measured accurately in the pure liquid because it is too strong to measure in 11 μm cells. The band was approximated by scaling the ν_4 band of benzene-h_6 and shifting it to the correct position. The integrated intensity of ν_4 of benzene-d_6 used in Table 5.11, $C_j = 0.725$ km mole^{-1}, was not the area under this approximated band. It was determined in the following way. Extrapolation of the line in the bottom right box of Figure 7.13 to $x_{C_6H_6} = 0.0$ yields an integrated intensity C_j of 0.636 km mole^{-1} between 538 and 458 cm^{-1} for pure liquid benzene-d_6 (Table 7.5).

This value of C_j is not the full area under the band. The ν_4 band of benzene-d_6 has a FWHH of about 12 cm^{-1}. The 538 to 458 cm^{-1} integration range used for this band is ~±3.3 FWHH, and for CDHO bands integration over ±3.3 FWHH gives only about 90% of the total area[30]. Thus, the total area of the band is 0.636/0.9 = 0.71 km mole^{-1}.

To obtain an estimate of the reliability of this result, because the ν_4 band of benzene-d_6 is not a single CDHO band (Figure 7.12), the area was calculated from the parameters of the CDHO bands fitted to the ν_4 band of benzene-d_6 in mixtures with $x_{C_6H_6}$ between 0.25 and 0.95. The α''_m spectra of the mixtures were fitted between 538 and 458 cm^{-1} with 4 CDHO bands. The fits were as good as those for the other fundamentals (section 5.2). The total integrated intensity of the 4 CDHO bands used to fit the spectrum of each mixture was 14% larger than the area between 538 and 458

cm^{-1}. Therefore, the total intensity of ν_4 of benzene-d_6 is 0.725 km mole^{-1}, within 1.5% of the value above. C_j = 0.725 km mole^{-1} is given in Tables 5.3 and 5.11.

The area under the approximated ν_4 band of benzene-d_6 is 0.475 km mole^{-1} between 538 and 458 cm^{-1}. The method used to approximate the band was clearly not perfect. The only use made of this approximated band was to improve the real refractive index spectrum calculated from the imaginary refractive index spectrum by KK transform, this error is not serious and it is definitely better than not including this band at all.

7.4 Changes in Peak Wavenumber and Band Width Upon Isotopic Dilution

In 1986 Ikawa, Ito, Fukuda and Kimura measured[51] absorbance spectra of various mole fractions of benzene-h_6 in benzene-d_6. They studied the ν_{13}, ν_{14} and ν_4 vibrations of both benzene-h_6 and benzene-d_6. They found[51] that the peak wavenumbers of ν_{13} and ν_{14} of both molecules shifted by 1 cm^{-1} or less as the concentration changed between pure benzene-h_6 and pure benzene-d_6. For the ν_4 vibrations, they found that the peak wavenumber shifted by about 7 cm^{-1} for benzene-h_6 and about 4 cm^{-1} for benzene-d_6 over this concentration range.

Ikawa *et al.* also found[51] that the full width at half height (FWHH) changed by 1 cm^{-1} or less for the ν_{13} and ν_{14} vibrations, while for ν_4 it changed by 3.5 and 2.5 cm^{-1} for benzene-h_6 and benzene-d_6, respectively.

Ikawa *et al.* measured the peak shifts and band widths in experimental absorbance spectra. The comparison of experimental absorbance spectra does not take account of changes in the local field with concentration. These arise because the real dielectric constant in the vicinity of the band is different for each mixture, so the local field is different for each mixture. Under the approximation of the Lorentz local field, the α_m'' spectrum is completely corrected for local field effects. In this section the changes with concentration of the peak position and band width in the α_m'' spectra and in the E_m spectra are compared to those found by Ikawa *et al.*[51] for experimental absorbance spectra. The E_m spectrum is simply the absorbance spectrum divided by path length and concentration, and the changes in the E_m spectrum are directly comparable to those found by Ikawa *et al.*[51] The comparison of the molar absorption coefficient spectra with the imaginary molar polarizability spectra will reveal the local field effects.

Figures 7.5 to 7.12 show the $\tilde{\nu}\alpha_m''$ spectra of mixtures of benzene-h_6 and benzene-d_6 in the regions of the 4 infrared active fundamentals of each isotopomer. The peak positions and FWHH's of these bands are tabulated in Tables 7.6 and 7.7. As shown in Figure 7.9, the peaks due to ν_{12} and $\nu_2+\nu_{13}$ of benzene-d_6 are heavily overlapped. The contribution from each peak was separated by curve fitting the imaginary molar polarizability spectrum in this region. As for pure benzene-d_6 (Figure 5.13 and Table 5.3) two strong and two weak CDHO bands were used in the fit and a linear baseline was included to account for the wings of bands outside this region. The fit was of the quality of that shown in Figure 5.13. The peak wavenumbers and FWHH values of the two strong fitted bands are attributed in Table 7.7 to ν_{12} and $\nu_2+\nu_{13}$. The ν_4 region of benzene-d_6 also has peaks that overlap. This region was fitted with 4 CDHO bands and a linear baseline. The fit was not perfect but was similar to the quality of fit obtained in Chapter 5. The peak positions and FWHH's of the three peaks that make up the major peak in this region are tabulated in Table 7.7 with those of the experimental $\tilde{\nu}\alpha_m''$ peaks.

Table 7.6. Peak wavenumbers and FWHH's of the benzene-h_6 vibrations in the $\tilde{\nu}\alpha''_m$ spectra of mixtures of benzene-h_6 and benzene-d_6.

	Peak wavenumber / cm^{-1}					
$x_{C_6H_6}$	$\nu_2+\nu_{13}+\nu_{18}$	ν_{13} $+\nu_{16}$	ν_{12}	ν_{13}	ν_{14}	ν_4
0.000						
0.100	3091.0	3071.8	3036.3	1479.6	1036.3	680.0
0.254	3091.0	3071.7	3036.2	1479.5	1036.3	679.6
0.400	3090.9	3071.7	3035.9	1479.4	1036.2	
0.520	3090.9	3071.6	3035.9	1479.4	1036.1	
0.620	3090.9	3071.6	3035.8	1479.4	1036.1	
0.701	3090.9	3071.6	3036.1	1479.3	1036.0	
0.793	3090.9	3071.5	3036.0	1479.2	1035.9	
0.925	3090.9	3071.5	3036.0	1479.2	1035.8	
1.000	3091.1	3071.7	3036.2	1479.2	1035.9	676.1

	FWHH / cm-1					
$x_{C_6H_6}$	$\nu_2+\nu_{13}$ $+\nu_{18}$	ν_{13} $+\nu_{16}$	ν_{12}	ν_{13}	ν_{14}	ν_4
0.000						
0.100	9.3	9.3	11.3	6.0	10.1	7.8
0.254	9.0	8.3	11.2	5.9	10.0	8.4
0.400	8.9	8.3	11.5	5.9	10.0	
0.520	8.9	8.2	11.1	5.8	10.0	
0.620	9.2	8.4	11.8	5.9	10.2	
0.701	8.9	8.2	11.0	5.9	10.2	
0.793	8.9	8.1	11.0	5.9	10.3	
0.925	8.9	8.1	11.1	6.0	10.3	
1.000	9.4	9.3	10.5	6.0	10.4	9.0

Table 7.7. Peak wavenumbers and FWHH's of the benzene-d_6 vibrations in the $\tilde{\nu}\alpha''_m$ spectra of mixtures of benzene-h_6 and benzene-d_6.

	Peak wavenumber / cm^{-1}							
$x_{C_6H_6}$	ν_{12}	ν_2 $+\nu_{13}$	ν_{13}	ν_{14}	ν_4			
0.000	2280.3	2269.0	1330.3	812.6				
0.100	2280.3	2269.0	1330.3	812.5	Fitted Bands			Experimental
0.254	2280.3	2269.0	1330.4	812.6	500.8	498.1	494.2	499.8
0.400	2280.2	2268.9	1330.4	812.6	500.8	498.5	494.4	499.8
0.520	2280.2	2269.0	1330.5	812.6	500.9	498.9	494.7	499.9
0.620	2280.3	2269.0	1330.5	812.6	500.8	499.0	494.6	500.0
0.701	2280.2	2268.9	1330.5	812.7	500.8	499.1	494.7	500.1
0.793	2280.2	2268.9	1330.5	812.7	501.0	499.2	494.8	500.2
0.925	2280.2	2268.9	1330.6	812.6	500.9	499.5	494.9	500.3
1.000								

	FWHH / cm-1							
$x_{C_6H_6}$	ν_{12}	ν_2 $+\nu_{13}$	ν_{13}	ν_{14}	ν_4			
0.000	7.7	13.3	6.9	7.3				
0.100	8.0	13.1	6.8	7.3	Fitted Bands			Experimental
0.254	7.9	13.3	6.8	7.6	5.2	5.6	7.8	10.4
0.400	8.2	13.0	6.8	7.3	5.0	5.3	7.7	9.5
0.520	7.8	13.4	6.8	7.3	4.6	5.2	8.4	8.7
0.620	7.8	13.6	7.0	7.4	4.6	5.0	7.9	8.0
0.701	8.1	13.4	6.9	7.4	4.5	4.8	7.9	7.3
0.793	7.9	13.4	7.1	7.5	4.5	4.8	7.9	7.9
0.925	8.4	12.8	8.4	9.0	4.2	4.2	7.9	5.7
1.000								

For the other bands the peak wavenumbers are those in the $\tilde{\nu}\alpha''_{\mathrm{m}}$ spectra. The FWHH values were determined at half the peak height above zero ordinate, not above the baseline.

Figure 7.14 shows the peak wavenumber plotted against mole fraction for the four infrared active fundamentals of benzene-h_6 and benzene-d_6. The solid circles are the peak wavenumbers in the $\tilde{\nu}\alpha''_{\mathrm{m}}$ spectra and the open circles are the peak wavenumbers in the E_{m} spectra. The solid and open circles coincide for all vibrations except ν_4. For the ν_{12} (3036 cm^{-1}) region of benzene-h_6, the peak positions of the two infrared active combinations, $\nu_2+\nu_{13}+\nu_{18}$ (3090 cm^{-1}) and $\nu_{13}+\nu_{16}$ (3070 cm^{-1}), are included and for the ν_{12} (2280 cm^{-1}) region of benzene-d_6 the peak position of $\nu_2+\nu_{13}$ (2270 cm^{-1}) is included. In order to compare the present results with those of Ikawa *et al.*[51], the peak positions plotted for ν_4 of benzene-d_6 are the maxima in the $\tilde{\nu}\alpha''_{\mathrm{m}}$ spectra not the positions of the fitted bands given in Table 7.7.

Ikawa *et al.*[51] found that the peak wavenumbers in the experimental absorbance spectrum varied linearly with mole fraction for the six fundamentals they studied, ν_{13}, ν_{14} and ν_4 of both benzene-h_6 and benzene-d_6. Figure 7.14 includes as dotted lines the straight lines they determined. The present work indicates that the peak wavenumbers of ν_{12}, $\nu_2+\nu_{13}$ and ν_{14} of benzene-d_6 and $\nu_2+\nu_{13}+\nu_{18}$ and $\nu_{13}+\nu_{16}$ of benzene-h_6 are independent of concentration, as is probably that of ν_{12} (Table 7.6) while the wavenumbers of the remaining bands change linearly with the mole fraction. The wavenumbers in the E_{m} spectra measured in the present work agree with those of Ikawa *et al.*[51], except for ν_4 of benzene-d_6.

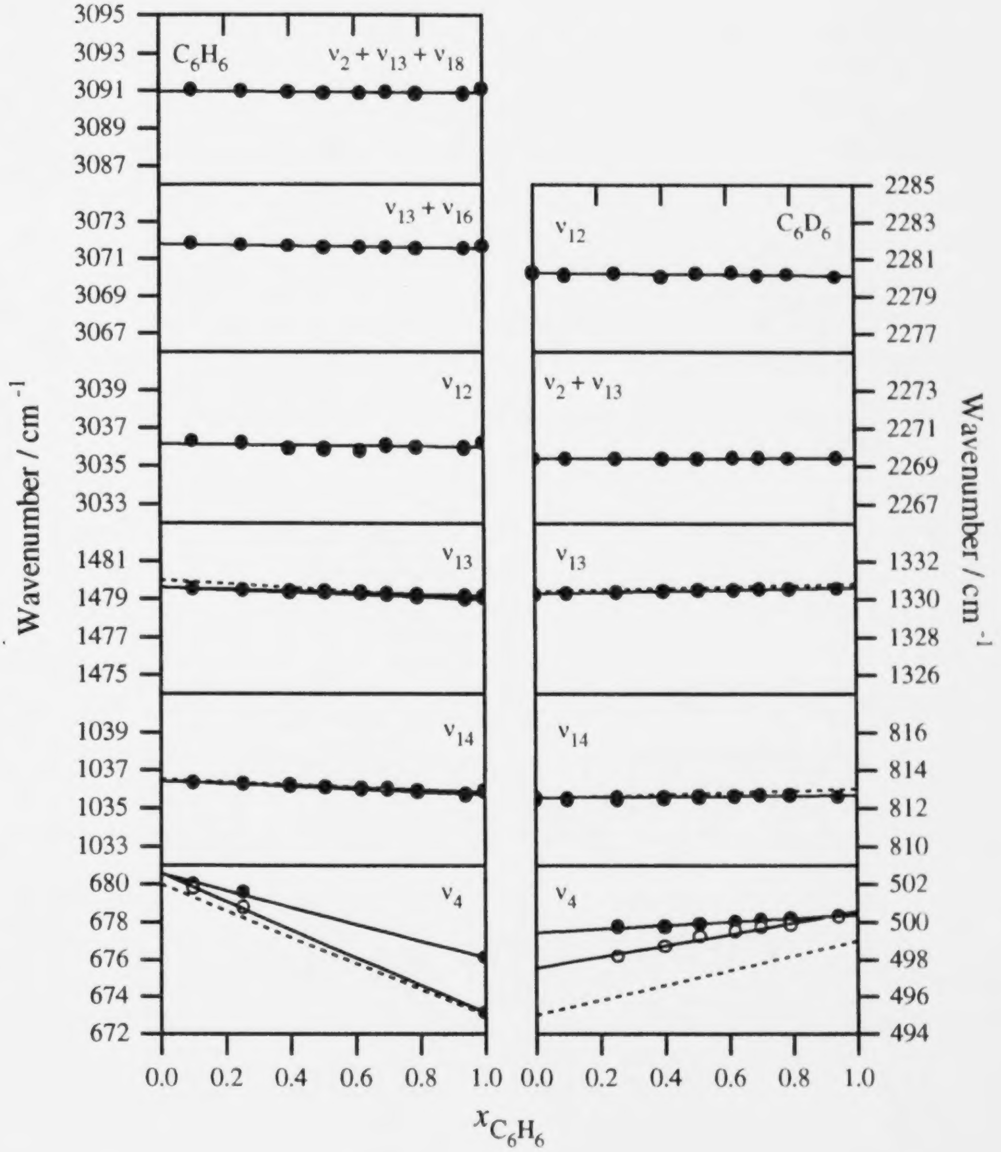

Figure 7.14. Peak wavenumber versus mole fraction of benzene-h_6 for the infrared active fundamentals and related bands of benzene-h_6 and benzene-d_6. The solid circles are for peaks in the $\tilde{\nu}\alpha''_m$ spectra and the open circles are for peaks in the E_m spectra. The two coincide except for ν_4. The dotted lines indicate the wavenumbers given by Ikawa *et al.*[51]

The differences between peak wavenumbers in the $\tilde{\nu}\alpha''_m$ spectra and the corresponding peak wavenumbers in the E_m spectra are due to the local field effects. From the data shown in Figure 7.14, it is clear that the local field has little effect on the peak wavenumbers apart from those of ν_4 of benzene-h$_6$ and benzene-d$_6$. For ν_4 of benzene-h$_6$, the peaks in the E_m spectra shift by ~7.0 cm^{-1} over the composition range from pure benzene-h$_6$ to pure benzene-d$_6$ while the peaks in the $\tilde{\nu}\alpha''_m$ spectrum only shift by ~4.0 cm^{-1}. For ν_4 of benzene-d$_6$, the peaks in the E_m spectra shift by ~3.0 cm^{-1} while the peaks in the $\tilde{\nu}\alpha''_m$ spectrum only shift by ~1.0 cm^{-1}.

The FWHH values for the four infrared active fundamentals and related bands of both benzene-h$_6$ and benzene-d$_6$ are tabulated for the different mole fractions in Tables 7.6 and 7.7 and are shown in Figure 7.15. As in Figure 7.14, the solid circles are the values from the $\tilde{\nu}\alpha''_m$ spectra and the open circles are from the molar absorption coefficient spectra, and they coincide except for ν_4. For the ν_{12} (3036 cm^{-1}) region of benzene-h$_6$, the FWHH's of the two infrared active combinations, $\nu_2+\nu_{13}+\nu_{18}$ (3090 cm^{-1}) and $\nu_{13}+\nu_{16}$ (3070 cm^{-1}), are shown and for the ν_{12} (2280 cm^{-1}) region of benzene-d$_6$ the FWHH's of $\nu_2+\nu_{13}$ (2270 cm^{-1}) are shown. In order to compare the present results with those of Ikawa *et al.*[51], the FWHH values plotted for ν_4 of benzene-d$_6$ are the FWHH values in the $\tilde{\nu}\alpha''_m$ spectra not the FWHH of the component bands (Table 7.7) used to fit the α''_m spectra.

The FWHH values determined[51] by Ikawa *et al.* are included in Figure 7.15 as dotted curves, for ν_{13}, ν_{14} and ν_4 of both benzene-h$_6$ and benzene-d$_6$. Ikawa *et al.* found that the FWHH varied linearly with mole fraction for all but ν_4 of benzene-h$_6$. This was verified in this work, however no conclusion about whether or not the change in FWHH of ν_4 of benzene-h$_6$ is linear could be made since only three values

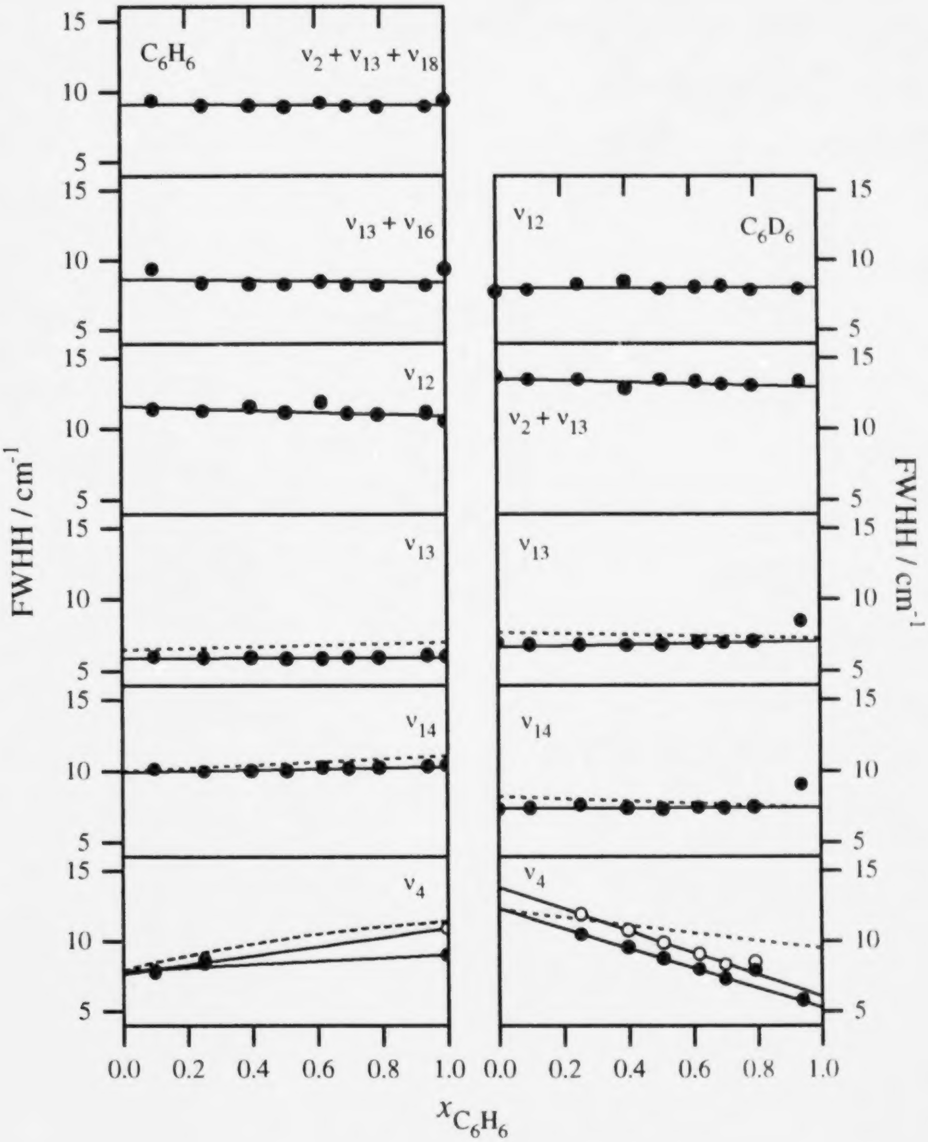

Figure 7.15. Full width at half height versus mole fraction of benzene-h$_6$ for the infrared active fundamentals and related bands of benzene-h$_6$ and benzene-d$_6$. The solid circles are for peaks in the $\tilde{\nu}\alpha''_m$ spectra and the open circles are for peaks in the E_m spectra. The two sets coincide except for ν_4. The dotted curves indicate the FWHH's given by Ikawa *et al.*[51]

could be measured in this work. This band absorbs so strongly that it should be studied by reflection spectroscopy. For ν_4 of benzene-d_6 the change in half width with concentration found in the present work was about 7 cm^{-1}; greater than the 3 cm^{-1} found by Ikawa *et al.*

As was the case for the peak wavenumbers shown in Figure 7.14, there is little difference between the FWHH values in the $\tilde{\nu}\alpha''_m$ and the E_m spectra, except for the ν_4 vibrations. For ν_4 of benzene-h_6, the FWHH in the E_m spectra change by ~3.2 cm^{-1} while they only change by ~1.4 cm^{-1} in the $\tilde{\nu}\alpha''_m$. For ν_4 of benzene-d_6, the FWHH values in the E_m and $\tilde{\nu}\alpha''_m$ spectra shift by approximately the same amount (~7.0 cm^{-1}) but the FWHH in the $\tilde{\nu}\alpha''_m$ spectra are smaller than those in the E_m spectra.

Although, the trend of the changes in FWHH, determined by Ikawa *et al.*[51] agree with the trend found in the present work, their values are generally larger than those determined in the present work. As stated above, Ikawa *et al.*[51] used experimental absorbance spectra so their spectra were not corrected for reflection losses. This increases the apparent FWHH, particularly at low concentrations, if the FWHH is measured above zero ordinate rather than above the baseline, as seems likely from the trends observed in Figure 7.15. The FWHH measured in the present work were also measured above zero ordinate but this had very little effect because the baselines of these bands are very close to zero since they were corrected for reflection losses. Some of the disagreement may be because the spectra measured by Ikawa *et al.*[51] were recorded with 2 cm^{-1} nominal resolution at 22°C while those measured in this work were recorded with 1 cm^{-1} nominal resolution at 25°C. There is evidence to support this possibility in the plots in Figure 7.15 because the largest difference between the FWHH values determined in the present work and that determined by Ikawa *et al.*[51] is for the sharpest peaks. Also trapezoidal apodization was used in this work and the apodization used by Ikawa *et al.*[51] is not known. For these reasons, the significance of the differences between the FWHH values found by Ikawa *et al.*[51] and in this work is not clear.

Ikawa *et al.*[51] attributed the change in wavenumber and FWHH of ν_4 of benzene-h_6 to vibrational resonance coupling. The fact that the peak wavenumbers in the $\tilde{\nu}\alpha''_\mathrm{m}$ spectra change with concentration by much less than those in the E_m spectra shows that the change in local field with concentration amounts for much of the effect. The residual change in peak wavenumber of ν_4 over the whole concentration range is ~4 cm^{-1} for benzene-h_6 and ~1.2 cm^{-1} for benzene-d_6.

7.5 Summary of Changes in the Molecular CDHO Properties $\tilde{\nu}_j$, Γ_j and μ_j Upon Isotopic Dilution

It was shown in section 1.3 that the classical damped harmonic oscillator (CDHO) model predicts that the imaginary molar polarizability bands have band shapes defined by the molecular parameters $\tilde{\nu}_j$, Γ_j and μ_j. Under the CDHO model the only effect of the surrounding molecules on a particular molecule is to modify the applied electric field, $\boldsymbol{E}$, to an effective local electric field, $\boldsymbol{E}_\mathrm{eff}$. Under the approximation of a Lorentz local field, the imaginary molar polarizability spectra are corrected for all local field effects and the molecular properties, $\tilde{\nu}_j$, Γ_j and μ_j should be independent of mole fraction in an ideal solution.

$\tilde{\nu}_j$ and Γ_j are the peak wavenumber and full width at half height, respectively, of band j in the $\tilde{\nu}\alpha''_\mathrm{m}$ spectrum, while μ_j^2 is linearly proportional to the area under band j in the $\tilde{\nu}\alpha''_{\mathrm{m}}$ spectrum through equation (1.3.38). The straight line graphs in Figure 7.13 show that the integrated intensities are linear functions of composition for all fundamentals, which means that μ_j^2 is independent of composition for all fundamental vibrations. For all fundamentals, except ν_4, the nearly flat straight lines in Figure 7.14 and 7.15 show that the peak wavenumbers, $\tilde{\nu}_j$, and the band widths, Γ_j, are almost independent of composition. For ν_4, the most intense band in the spectra, the evidence is clear that $\tilde{\nu}_j$ and Γ_j change slightly with composition for benzene-d$_6$, and they also clearly do so for benzene-h$_6$ but the evidence obtained in this work for ν_4 of benzene-h$_6$ is minimal.

Figures 7.16 and 7.17 show the measured imaginary molar polarizability spectrum of 0.2538 mole fraction benzene-h$_6$ in benzene-d$_6$ and that calculated by adding 0.2538 times the imaginary molar polarizability spectrum of benzene-h$_6$ to 0.7462 times the imaginary molar polarizability spectrum of benzene-d$_6$. For an ideal solution these spectra should be identical. The spectra agree well, with differences of up to ~2% at some peaks, for all but the ν_4 vibrations for which the disagreement is that expected from the above discussion.

There are two bands in the measured spectrum (~775 and ~515 cm^{-1}) that are not present in the calculated spectrum. They are assigned[79] to ν_{17} - ν_{20} (~775 cm^{-1}) of benzene-h$_6$ and ν_{17} - ν_{20} (~515 cm^{-1}) of benzene-d$_6$. They are not present in the calculated spectrum because of the way in which the ν_4 regions of benzene-h$_6$ and benzene-d$_6$ were obtained. For ν_4 of benzene-h$_6$, the region between 800 and 500 cm^{-1} was obtained by digitizing the graph published by Jones and co-workers[18] (section 3.1.3b). With the 670 cm^{-1} band on scale, ν_{17} - ν_{20} (~775 cm^{-1}) of benzene-h$_6$ could not be seen. For ν_4 of benzene-d$_6$, the region between 550 and 450 cm^{-1}

was obtained by scaling and shifting the ν_4 region of benzene-h_6, as described in Chapter 3 and this band was neglected.

Figures 7.18 and 7.19 show the measured molar absorption coefficient spectrum of 0.2538 mole fraction benzene-h_6 in benzene-d_6 and that calculated by adding 0.2538 times the molar absorption coefficient spectrum of benzene-h_6 to 0.7462 times the molar absorption coefficient spectrum of benzene-d_6. These are expected to be very similar for transitions that are sufficiently weak to cause very little anomalous dispersion in the real refractive index[30]. It is clear from Figures 7.18 and 7.19 that, as was the case for the imaginary molar polarizability spectra, the measured and calculated spectra agree very well for all but the ν_4 vibrations.

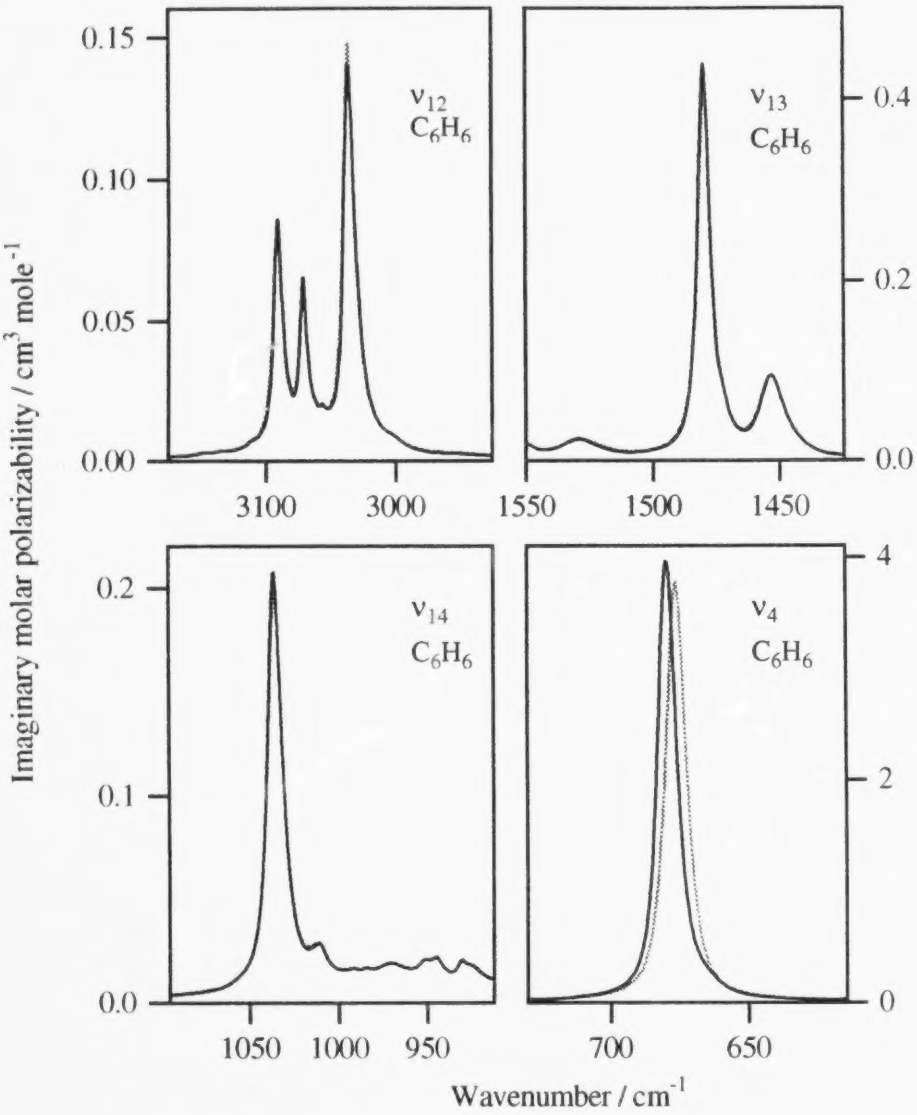

Figure 7.16. Imaginary molar polarizability spectra of 0.25 mole fraction of benzene-h_6 in the regions of the infrared active fundamentals of benzene-h_6. The solid curves are the measured imaginary molar polarizability spectra and the dotted curves are the imaginary molar polarizability spectra calculated as a mole fraction weighted linear combination of the imaginary molar polarizability spectra of pure benzene-h_6 and pure benzene-d_6.

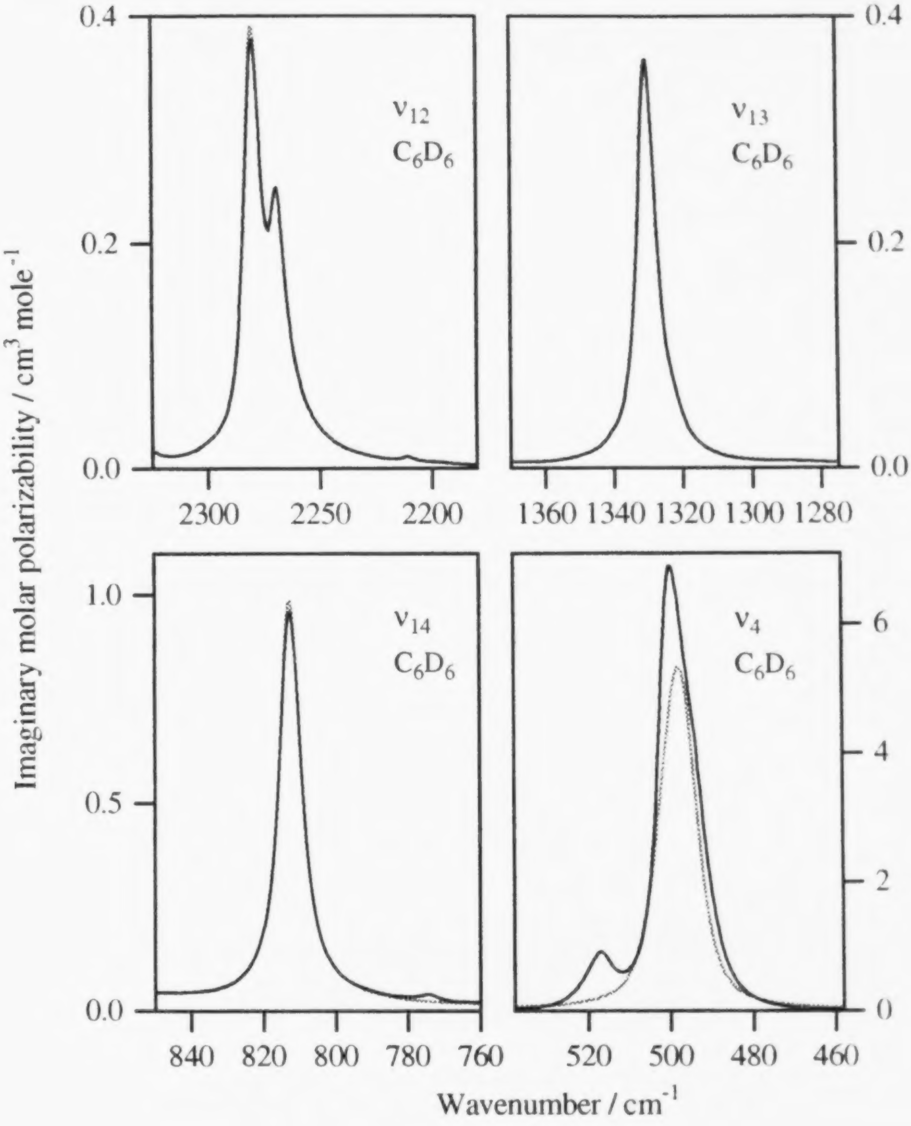

Figure 7.17. Imaginary molar polarizability spectra of 0.25 mole fraction of benzene-h_6 in the regions of the infrared active fundamentals of benzene-d_6. The solid curves are the measured imaginary molar polarizability spectra and the dotted curves are the imaginary molar polarizability spectra calculated as a mole fraction weighted linear combination of the imaginary molar polarizability spectra of pure benzene-h_6 and pure benzene-d_6.

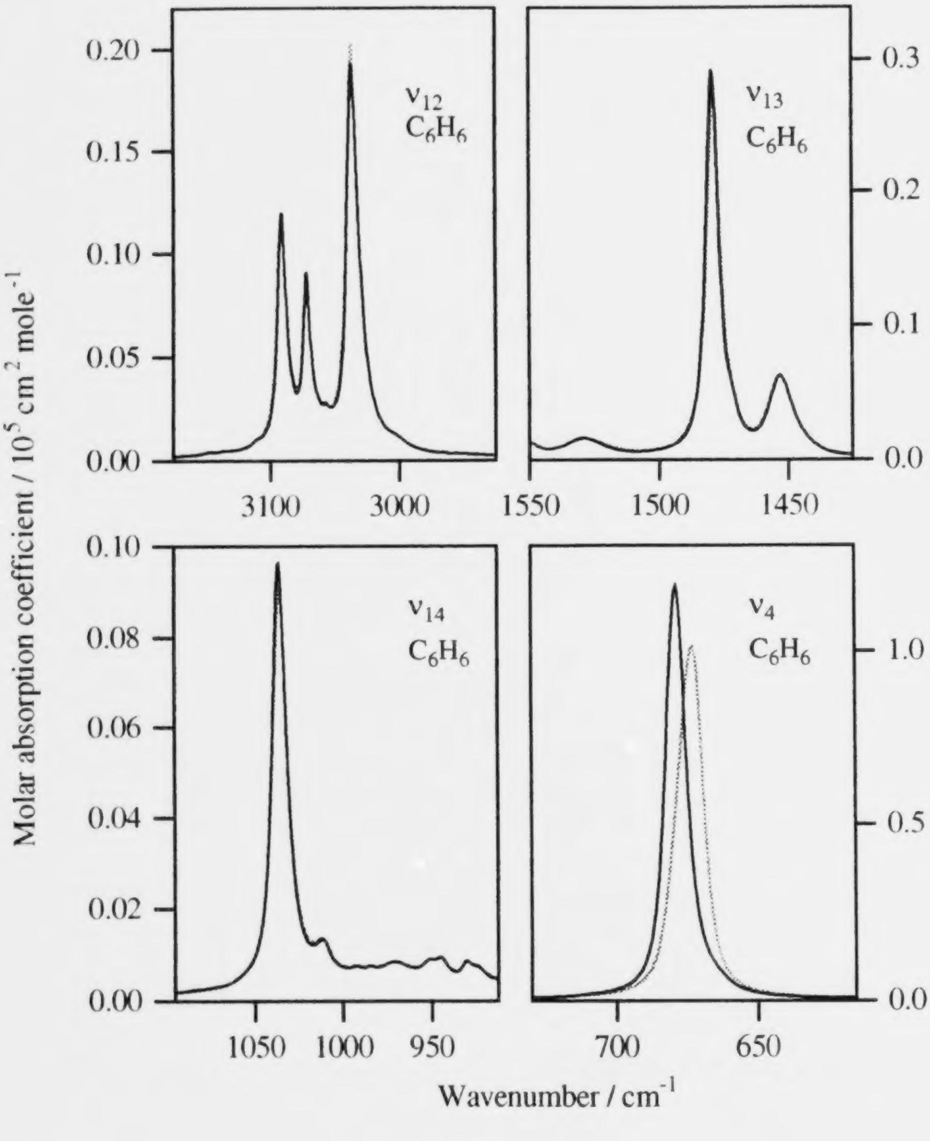

Figure 7.18. Molar absorption coefficient spectra of 0.25 mole fraction of benzene-h_6 in the regions of the infrared active fundamentals of benzene-h_6. The solid curves are the measured molar absorption coefficient spectra and the dotted curves are the molar absorption coefficient spectra calculated as a mole fraction weighted linear combination of the molar absorption coefficient spectra of pure benzene-h_6 and pure benzene-d_6.

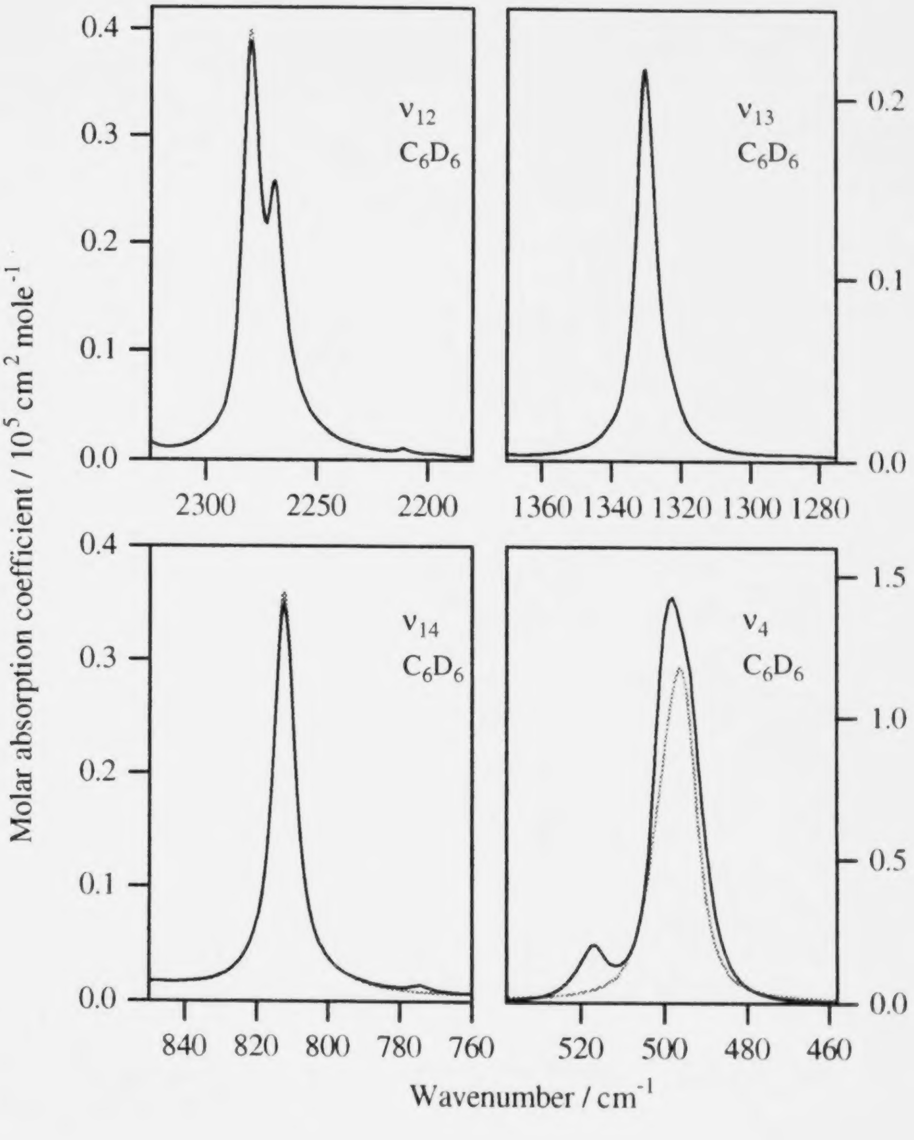

Figure 7.19. Molar absorption coefficient spectra of 0.25 mole fraction of benzene-h_6 in the regions of the infrared active fundamentals of benzene-d_6. The solid curves are the measured molar absorption coefficient spectra and the dotted curves are the molar absorption coefficient spectra calculated as a mole fraction weighted linear combination of the molar absorption coefficient spectra of pure benzene-h_6 and pure benzene-d_6.

Chapter 8

Summary

In this work transmission spectra of benzene-h_6, benzene-d_6 and mixtures of benzene-h_6 and benzene-d_6 were measured. It was shown in Chapter 2 that transmission spectra typically suffer from baseline variations. A method was developed to correct for these variations and was incorporated into the procedure and programs used to calculate optical constants from transmission spectra.

From the transmission spectra of benzene-h_6, benzene-d_6 and mixtures of benzene-h_6 and benzene-d_6 the imaginary refractive indices of these liquids and solutions were calculated by program RNJ46A. A study of the systematic errors in imaginary refractive index spectra of benzene-h_6 calculated from transmission spectra was made by comparing spectra measured by different spectroscopists in different laboratories with different instruments, samples and operating conditions. From this study it was estimated that the imaginary refractive index spectra obtained from transmission spectra in this laboratory are accurate to about ±2.5%.

From the imaginary refractive index spectra the real refractive index spectra were calculated by Kramers-Kronig transformation. The real refractive index spectra are estimated to be accurate to within ±0.2%. The molar absorption coefficient spectra, complex dielectric constant spectra and complex molar polarizability spectra were calculated from the complex refractive index spectra. The molar absorption coefficient spectra and the imaginary components of the dielectric constant and molar polarizability spectra have approximately the same accuracy as the imaginary refractive index spectra. The real components of the dielectric constant and molar polarizability spectra have approximately the same accuracy as the real refractive index spectra.

The complex refractive index spectra and molar absorption coefficient spectra of benzene-h_6, along with the corresponding spectra for toluene, chlorobenzene and dichloromethane have been used to develop secondary infrared intensity standards. The most accurate standards are areas measured under bands in the spectra but above a baseline through the curve at the integration limits; these are believed accurate to ~±1.5%. These standards have been accepted by the International Union of Pure and Applied Chemistry. They can be used to calibrate other intensity measurements, both transmission measurements and measurements with other techniques such as attenuated total reflection.

The imaginary molar polarizability spectra of benzene-h_6 and benzene-d_6 were fitted with CDHO bands. The purpose of this was to assign the overall integrated intensity to specific vibrations. For the fundamentals of each molecule, the integrated intensities were converted to dipole moment derivatives with respect to normal coordinates. The magnitudes of the dipoles moment derivatives with respect to the normal coordinates, μ_j, for the infrared active fundamentals are, for benzene-h_6; $\mu_{12} = 0.710 \pm 0.010$, $\mu_{13} = 0.468 \pm 0.012$, $\mu_{14} = 0.349 \pm 0.009$, $\mu_4 = 1.54 \pm 0.04$ Debye Å^{-1} $\text{amu}^{-1/2}$ and for benzene-d_6; $\mu_{12} = 0.500 \pm 0.012$, $\mu_{13} = 0.252 \pm 0.006$, $\mu_{14} = 0.352 \pm 0.009$, $\mu_4 = 1.16 \pm 0.03$ Debye Å^{-1} $\text{amu}^{-1/2}$.

Using the wavenumbers of all 40 fundamentals of benzene-h_6 and benzene-d_6, a normal coordinate calculation was performed for the liquid using as the starting point of the refinement a complete harmonic force field for the gas taken from the literature. From the normal coordinates calculated in this work, the dipole moment derivatives with respect to normal coordinates were converted to dipole moment derivatives with respect to symmetry coordinates for all fundamentals. The magnitudes of the dipole moment derivatives with respect to the symmetry coordinates for the infrared active fundamentals are $|\partial\bar{\mu}/\partial S_4| = 1.63 \pm 0.04$ Debye Å^{-1}, $|\partial\bar{\mu}/\partial S_{12}| = 0.66 \pm 0.06$ Debye Å^{-1}, $|\partial\bar{\mu}/\partial S_{13}| = 0.39 \pm 0.04$ Debye Å^{-1} and $|\partial\bar{\mu}/\partial S_{14}| = 0.46 \pm 0.01$ Debye Å^{-1}.

The magnitudes of the dipole moment derivatives with respect to the internal coordinates are

$$\partial\mu/\partial R_{\mathrm{CH}} = \partial\mu/\partial s = 0.37 \pm 0.03 \text{ Debye Å}^{-1},$$

$$\partial\mu/\partial R_{\mathrm{CC}} = \partial\mu/\partial t = 0.23 \pm 0.02 \text{ Debye Å}^{-1},$$

$$\partial\mu/\partial\left(1\text{Å} \times \phi_{\mathrm{HCC}}\right) = \partial\mu/\partial\beta = 0.263 \pm 0.006 \text{ Debye Å}^{-1} \text{ and}$$

$$\partial\mu/\partial\left(1\text{Å} \times \gamma_{\mathrm{HCCC}}\right) = \partial\mu/\partial\gamma = 0.665 \pm 0.016 \text{ Debye Å}^{-1}$$

The integrated intensities of liquid benzene-h$_6$ and benzene-d$_6$ were compared with those of the gaseous molecules taken from the literature. It was found that for both molecules the transition moment for ν_4 remains the same in the gas and liquid phases. For ν_{12}, the transition moments for the liquid phase are about 20% smaller than those for the gas phase. For ν_{13}, the transition moments for the liquid phase are between 20 and 40% larger than those for the gas phase. For ν_{14}, the transition moments for the liquid phase are between 5 and 30% larger than those for the gas phase. There is disagreement among the literature integrated intensities for ν_{13} of benzene-h$_6$ and ν_{14} and ν_{13} of benzene-d$_6$. To increase our knowledge of the comparison of the liquid phase intensities and the gas phase intensities, reliable remeasurement of the gas phase intensities is needed.

The integrated intensities of the fundamentals and combination transitions observed in the liquid were compared to literature values for the gas calculated by *ab initio* methods. It was found that the calculated transition moments are generally within a factor of 2 of the experimentally determined transition moments. Calculated intensities of this quality are very useful in assigning spectra because the observed intensities cover a much greater range of values.

From the imaginary molar polarizability spectra of mixtures of benzene-h_6 and benzene-d_6, the changes in molecular properties upon isotopic dilution were studied. The dipole moment derivatives with respect to normal coordinates for all the infrared active fundamentals of benzene-h_6 and benzene-d_6 remain the same in the mixtures. Only for the ν_4 vibrations do the peak wavenumbers and full widths at half height change significantly. For the other infrared active fundamentals (ν_{12}, ν_{13} and ν_{14}), the solutions behave ideally and the measured imaginary molar polarizability spectra agree with those calculated as a sum of the imaginary molar polarizability spectra of the pure liquids weighted by mole fraction. For ν_{12}, ν_{13} and ν_{14}, the sum of the molar absorption coefficient spectra of the pure liquids weighted by mole fraction also agree with the measured spectra.

The ν_4 regions of benzene-h_6 and benzene-d_6 are too strong to measure accurately by transmission spectroscopy for the pure liquids as well as for some of the higher concentrations in the mixtures. Reflection spectroscopy should enable accurate spectra and intensities to be measured in these regions for the compositions that are too strong to measure in transmission.

References

1. B. Crawford Jr. in *Vibrational Intensities in Infrared and Raman Spectroscopy*, W.B. Person and G. Zerbi, Ed. (Elsevier, Amsterdam, 1982), p. 3.

2. J. Overend in *Infra-Red Spectroscopy and Molecular Structure: An Outline of the Principles*, M. Davies, Ed. (Elsevier, Amsterdam, 1963), p. 345.

3. T.L. Brown, Chem. Rev., **58**, 581 (1958).

4. B. Crawford Jr., T.G. Goplen, and D. Swanson in *Advances in Infrared and Raman Spectrocopy*, R. J. H. Clark and R. E. Hester, Ed. (Heyden, London, 1978), Vol. 4.

5. A.C. Gilby, J. Burr Jr., W. Krueger, and B. Crawford Jr., J. Phys. Chem., **70**, 1525 (1966).

6. G.M. Irons and H.W. Thompson, Proc. Roy. Soc., **298A**, 160 (1967).

7. P.N. Schatz, J. Chem. Phys., **32**, 894 (1960).

8. P.N. Schatz, S. Maeda, J.L. Hollenberg, and D.A. Dows, J. Chem. Phys., **34**, 175 (1961).

9. C.W. Robertson, B. Curnutte, and D. Williams, Mol. Phys., **26**, 183 (1973).

10. C.W. Robertson and D. Williams, J. Opt. Soc. Am., **61**, 1316 (1971).

11. W.B. Person and G. Zerbi, ed. *Vibrational Intensities in Infrared and Raman Spectroscopy*. (Amsterdam, Elsevier, 1982).

12. J.P. Hawranek and R.N. Jones, Spectrochim. Acta, **32A**, 111 (1976).

13. J.P. Hawranek and R.N. Jones, Spectrochim. Acta, **32A**, 99 (1976).

14. J.P. Hawranek, P. Neelakantan, R.P. Young, and R.N. Jones, Spectrochim. Acta, **32A**, 85 (1976).

15. J.P. Hawranek, P. Neelakantan, R.P. Young, and R.N. Jones, Spectrochim. Acta, **32A**, 75 (1976).

16. R.N. Jones and R.P. Young, *Computer Programs for Infrared Spectrophotometry XVI to XXII*. 2nd ed. (Ottawa, National Research Council of Canada Bulletin 13, 1976).

17. D.G. Cameron, J.P. Hawranek, P. Neelakantan, R.P. Young, and R.N. Jones, *Computer Programs for Infrared Spectrophotometry XLII to XLVII*. (Ottawa, National Research Council of Canada Bulletin 16, 1977).

18. T.G. Goplen, D.G. Cameron, and R.N. Jones, Appl. Spectrosc., **34**, 657 (1980).

19. J.E. Bertie, R.N. Jones, and V. Behnam, Appl. Spectrosc., **40**, 427 (1986).

20. J.E. Bertie, R.N. Jones, and V. Behnam, Appl. Spectrosc., **39**, 401 (1985).

21. J.W.C. Johns, Mikochim. Acta, **III**, 171 (1987).

22. M. Gussoni, C. Castiglioni, M.N. Ramos, M. Rui, and G. Zerbi, J. Mol. Struct., **224**, 445 (1990).

23. M. Gussoni, C. Castiglioni, and G. Zerbi, J. Phys. Chem., **88**, 600 (1984).

24. C. Castiglioni, M. Gussoni, and G. Zerbi, J. Mol. Struct., **198**, 475 (1989).

25. J. Fahrenfort in *Infra-Red Spectroscopy and Molecular Structure: An Outline of the Principles*, M. Davies, Ed. (Elsevier, Amsterdam, 1963), p. 377.

26. J.W. Warner and M. Wolfsberg, J. Chem. Phys., **78**, 1722 (1983).

27. M.J. Dignam, Appl. Spectrosc. Rev., **21**, 99 (1988).

28. J.E. Bertie, H. Harke, M.K. Ahmed, and H.H. Eysel, Croat. Chem. Acta, **61**, 391 (1988).

29. J.E. Bertie, S.L. Zhang, H.H. Eysel, S. Baluja, and M.K. Ahmed, Appl. Spectrosc., **47**, 1100 (1993).

30. J.E. Bertie, S.L. Zhang, and C.D. Keefe, J. Mol. Struct., **324**, 157 (1994).

31. H. Spedding and D.H. Whiffen, Proc. Roy. Soc., **238A**, 245 (1956).

32. I.C. Hisatsune and E.S. Jayadevappa, J. Chem. Phys., **30**, 848 (1959).

33. I.C. Hisatsune and E.S. Jayadevappa, J. Chem. Phys., **32**, 565 (1960).

34. D.A. Dows and A.L. Pratt, Spectrochim. Acta, **18**, 433 (1962).

35. E.V. Broun and A.V. Iogansen, Opt. Spectrosc., **18**, 348 (1965).

36. A.J. Zelano and W.T. King, J. Chem. Phys., **53**, 4444 (1970).

37. A.E. Tshmel and V.I. Vettegren, Spectrochim. Acta, **29A**, 1681 (1973).

38. V.M. Zolotarev, Sov. J. Opt. Technol, **43**, 494 (1976).

39. M. Akiyama, J. Mol. Spectrosc., **84**, 49 (1980).

40. M. Akiyama, J. Mol. Spectrosc., **93**, 154 (1982).

41. L. Goodman, A.G. Ozkabak, and K.B. Wiberg, J. Chem. Phys., **91**, 2069 (1989).

42. M. Akiyama, Y. Shimizu, H. Itaya, and M. Kakihana, J. Phys. Chem., **93**, 2280 (1989).

43. D.H. Son, C.H. Choi, and K. Kim, Vib. Spectrosc., **4**, 349 (1993).

44. J.E. Bertie, R.N. Jones, and Y. Apelblat, Appl. Spectrosc., **47**, 1989 (1993).

45. T.G. Goplen, D.G. Cameron, and R.N. Jones, Appl. Spectrosc., **34**, 652 (1980).

46. R.N. Jones, D. Escolar, J.P. Hawranek, P. Neelakatan, and R.P. Young, J. Mol. Struct., **19**, 21 (1973).

47. J.E. Bertie, R.N. Jones, Y. Apelblat, and C.D. Keefe, Appl. Spectrosc., **48**, 127 (1994).

48. J.E. Bertie, R.N. Jones, and Y. Apelblat, Appl. Spectrosc., **48**, 144 (1994).

49. J.E. Bertie, Z. Lan, R.N. Jones, and Y. Apelblat, In preparation, (1994).

50. P.E. Maslen, N.C. Handy, R.D. Amos, and D. Jayatilaka, J. Chem. Phys., **97**, 4233 (1992).

51. S. Ikawa, M. Ito, T. Fukuda, and M. Kimura, J. Mol. Liq., **32**, 219 (1986).

52. J.R. Meyer-Arendt, *Introduction to Classical and Modern Optics*. 3rd ed. (Englewood Cliffs, Prentice Hall, 1989).

53. E. Hecht, *Optics*. 2nd ed. (Reading, Addison - Wesley Publishing Company, 1987).

54. M. Born and E. Wolf, *Principles of Optics: Electromagnetic Theory of Propagation, Interference and Diffraction of Light*. 6th ed. (Oxford, Pergamon Press, 1980).

55. E.R. Cohen and B.N. Taylor, Phys. Today, **August**, BG8 (1989).

56. W.E. Harris and B. Kratochvil, *An Introduction to Chemical Analysis*. (Philadelphia, Saunders College Publishing, 1981).

57. H. Fröhlich, *Theory of Dielectrics, Dielectric Constant, and Dielectric Loss*. 2nd ed. (London, Oxford University Press, 1958).

58. A.A. Clifford and B. Crawford Jr., J. Phys. Chem., **70**, 1536 (1966).

59. M.A. Czarnecki, J.P. Hawranek, and W. Wrzeszcz, J. Mol. Struct., **275**, 111 (1992).

60. T. Motojima, S.-I. Ikawa, and M.J. Kimura, J. Quant. Spectrosc. Radiat. Trans., **25**, 29 (1981).

61. P.N. Schatz, Spectrochim. Acta, **21**, 617 (1965).

62. E.B. Wilson Jr., J.C. Decius, and P.C. Cross, *Molecular Vibrations: The Theory of Infrared and Raman Vibrational Spectra*. (New York, McGraw-Hill Book Company, Inc., 1955).

63. S.R. Polo and M.K. Wilson, J. Chem. Phys., **23**, 2376 (1955).

64. W.R. Angus, C.R. Bailey, J.B. Hale, C.K. Ingold, A.H. Leckie, C.G. Raisin, J.W. Thompson, and C.L. Wilson, J. Chem. Soc., 966 (1936).

65. W.R. Angus, C.R. Bailey, J.B. Hale, C.K. Ingold, A.H. Leckie, C.G. Raisin, J.W. Thompson, and C.L. Wilson, J. Chem. Soc., 971 (1936).

66. W.R. Angus, C.R. Bailey, C.K. Ingold, and C.L. Wilson, J. Chem. Soc., 912 (1936).

67. C.K. Ingold, C.G. Raisin, and C.L. Wilson, J. Chem. Soc., 915 (1936).

68. W.R. Angus, C.K. Ingold, and A.H. Leckie, J. Chem. Soc., 925 (1936).

69. C.R. Bailey, J.B. Hale, C.K. Ingold, and J.W. Thompson, J. Chem. Soc., 931 (1936).

70. C.R. Bailey, C.K. Ingold, H.G. Poole, and C.L. Wilson, J. Chem. Soc., 222 (1946).

71. C.R. Bailey, S.C. Carson, and C.K. Ingold, J. Chem. Soc., 252 (1946).

72. C.R. Bailey, J.B. Hale, N. Herzfeld, C.K. Ingold, A.H. Leckie, and H.G. Poole, J. Chem. Soc., 255 (1946).

73. C.R. Bailey, R.R. Gordon, J.B. Hale, N. Herzfeld, C.K. Ingold, and H.G. Poole, J. Chem. Soc., 299 (1946).

74. N. Herzfeld, C.K. Ingold, and H.G. Poole, J. Chem. Soc., 316 (1946).

75. C.R. Bailey, S.C. Carson, R.R. Gordon, and C.K. Ingold, J. Chem. Soc., 288 (1946).

76. N. Herzfeld, J.W. Hobden, C.K. Ingold, and H.G. Poole, J. Chem. Soc., 255 (1946).

77. R.D. Mair and D.F. Hornig, J. Chem. Phys., **17**, 1236 (1949).

78. S. Brodersen and A. Langseth, Kgl. Danske Videnskab Selskab, Mat. Fys. Skr., **1**, 36 (1959).

79. S. Brodersen and A. Langseth, Mat. Fys. Skr. Dan. Vid. Selsk., **1**, 1 (1956).

80. A. Cabana, J. Bachand, and J. Giguère, Can. J. Phys., **52**, 1949 (1974).

81. A.B. Hollinger and H.L. Welsh, Can. J. Phys., **56**, 974 (1978).

82. A.B. Hollinger and H.L. Welsh, Can. J. Phys., **56**, 1513 (1978).

83. A.B. Hollinger, H.L. Welsh, and K.S. Jammu, Can. J. Phys., **57**, 767 (1979).

84. H.B. Jensen and S. Brodersen, J. Raman Spectrosc., **8**, 103 (1979).

85. J. Plíva and A.S. Pine, J. Mol. Spectrosc., **93**, 209 (1982).

86. J. Plíva and J.W.C. Johns, Can. J. Phys., **61**, 269 (1983).

87. J. Plíva and J.W.C. Johns, J. Mol. Spectrosc., **107**, 318 (1984).

88. P. Esherick, A. Owyoung, and J. Plíva, J. Chem. Phys., **83**, 3311 (1985).

89. S.N. Thakur, L. Goodman, and A.G. Ozkabak, J. Chem. Phys., **84**, 6642 (1986).

90. J. Plíva and A.S. Pine, J. Mol. Spectrosc., **126**, 82 (1987).

91. J. Plíva, P. Esherick, and A. Owyoung, J. Mol. Spectrosc., **125**, 393 (1987).

92. L. Goodman and Y. Nibu, Chem. Phys. Lett., **143**, 551 (1988).

93. L. Goodman, J.M. Berman, and A.G. Ozkabak, J. Chem. Phys., **90**, 2544 (1989).

94. J. Plíva, J.W.C. Johns, and L. Goodman, J. Mol. Spectrosc., **134**, 227 (1989).

95. J. Plíva, A. Velentin, J. Chazelas, and L. Henry, J. Mol. Spectrosc., **134**, 220 (1989).

96. J. Plíva, A. Valentin, J. Chazelas, and L. Henry, J. Mol. Spectrosc., **134**, 220 (1989).

97. J. Plíva, J.W.C. Johns, and L. Goodman, J. Mol. Spectrosc., **140**, 214 (1990).

98. H. Hollenstein, S. Piccirillo, M. Quack, and M. Snels, Mol. Phys., **71**, 759 (1990).

99. J. Plíva, J.W.C. Johns, and L. Goodman, J. Mol. Spectrosc., **148**, 427 (1991).

100. L. Goodman, A.G. Ozkabak, and S.N. Thakur, J. Phys. Chem., **95**, 9044 (1991).

101. P.C. Painter and J.L. Koenig, Spectrochim. Acta, **33A**, 1003 (1977).

102. E.B. Wilson Jr., Phys. Rev., **45**, 706 (1934).

103. F.A. Miller and B.L. Crawford Jr., J. Chem. Phys., **14**, 282 (1946).

104. B.L. Crawford Jr. and F.A. Miller, J. Chem. Phys., **17**, 249 (1949).

105. D.H. Whiffen, Philos. Trans. R. Soc. London, **248A**, 131 (1955).

106. S. Califano and B. Crawford Jr., Spectrochim. Acta, **16**, 889 (1960).

107. J.R. Scherer and J. Overend, Spectrochim. Acta, **17**, 719 (1961).

108. J.R. Scherer, J.C. Evans, W.W. Muelder, and J. Overend, Spectrochim. Acta, **18**, 57 (1962).

109. N. Neto, M. Scrocco, and S. Califano, Spectrochim. Acta, **22**, 1981 (1966).

110. J.C. Duinker and I.M. Mills, Spectrochim. Acta, **24A**, 417 (1968).

111. Y. Kakiuti, H. Saito, and T. Yokoyama, J. Mol. Spectrosc., **32**, 247 (1969).

112. R.A. Kydd, Spectrochim. Acta, **27A**, 2067 (1971).

113. J. Favrot, P. Caillet, and M. Forel, J. Chim. Phys., **10**, 1337 (1974).

114. L.M. Sverdlov, M.A. Kovner, and E.P. Krainov in *Vibrational Spectra of Polyatomic Molecules*, (John Wiley and Sons, New York, 1974), p. 324.

115. P.C. Painter and J.L. Koenig, Spectrochim. Acta, **33A**, 1019 (1977).

116. P.C. Painter and R.W. Snyder, Spectrochim. Acta, **36A**, 337 (1980).

117. A.G. Ozkabak, L. Goodman, S.N. Thakur, and K. Krogh-Jespersen, J. Chem. Phys., **83**, 6047 (1985).

118. A.G. Ozkabak, L. Goodman, S.N. Thakur, and K. Krogh-Jespersen, J. Chem. Phys., **85**, 2346 (1986).

119. J.M. Berman and L. Goodman, J. Chem. Phys., **87**, 1479 (1987).

120. A.G. Ozkabak and L. Goodman, J. Chem. Phys., **87**, 2564 (1987).

121. A.G. Ozkabak, L. Goodman, and K.B. Wiberg, J. Chem. Phys., **92**, 4115 (1990).

122. R.E. Bruns and W.B. Person, J. Chem. Phys., **57**, 324 (1972).

123. K. Ohno, J. Mol. Spectrosc., **72**, 238 (1978).

124. P. Pulay, G. Fogarasi, and J.E. Boggs, J. Chem. Phys., **74**, 3999 (1981).

125. P. Pulay, J. Chem. Phys., **85**, 1703 (1986).

126. H. Guo and M. Karplus, J. Chem. Phys., **89**, 4235 (1988).

127. E. Albertazzi and F. Zerbetto, Chem. Phys., **164**, 91 (1992).

128. M.V. Korolevich, J. Mol. Struct. (Theochem), **276**, 1 (1992).

129. A. Berces and T. Ziegler, Chem. Phys. Lett., **203**, 592 (1993).

130. A. Berces and T. Ziegler, J. Chem. Phys., **98**, 4793 (1993).

131. G. Baranovic and B. Schrader, J. Mol. Struct. (Theochem), **306**, 165 (1994).

132. N. Sheppard, H.A. Willis, and J.C. Rigg, Spectrochim. Acta, **43A**, 1 (1987).

133. I. Mills, T. Cvitas, K. Homann, N. Kallay, and K. Kuchitsu, *Quantities, Units and Symbols in Physical Chemistry*. 2nd ed. (Oxford, Blackwell Scientific Publications, 1993).

134. K. Ohta and H. Ishida, Appl. Opt., **29**, 1952 (1990).

135. J.E. Bertie, R.N. Jones, and C.D. Keefe, Appl. Spectrosc., **47**, 891 (1993).

136. J.B. Conway, *Functions of One Complex Variable*. 2nd ed. (New York, Spriner-Verlag New York Inc., 1978).

137. R.V. Churchill and J.W. Brown, *Complex Variables and Applications*. 4th ed. (New York, McGraw-Hill Book Company, 1984).

138. J.S. Toll, Phys. Rev., **104**, 1760 (1956).

139. G.H. Goedecke, J. Opt. Soc. Am., **65**, 146 (1975).

140. C.W. Peterson and B.W. Knight, J. Opt. Soc. Amer., **63**, 1238 (1973).

141. J.E. Bertie and S.L. Zhang, Can. J. Chem., **70**, 520 (1992).

142. J.E. Bertie and Z. Lan, To be Published., (1994).

143. R.K. Ahrenkiel, J. Opt. Soc. Am., **61**, 1651 (1971).

144. R.Z. Bachrach and F.C. Brown, Phys. Rev., **1B**, 818 (1970).

145. R.K. Ahrenkiel, J. Opt. Soc. Am., **61**, 1009 (1972).

146. C.W. Robertson, H.D. Downing, B. Curnutte, and D. Williams, J. Opt. Soc. Am., **65**, 432 (1975).

147. R.E. Stephens, E.K. Plyler, W.S. Rodney, and R.J. Spindler, J. Opt. Soc. Am., **43**, 110 (1953).

148. K.R. June, Appl. Opt., **11**, 1655 (1972).

149. E.W. Washburn, ed. *International Critical Tables of Numerical Data, Physics, Chemistry and Technology*. 1st ed. Vol. 7. (New York, McGraw-Hill Book Company, 1930).

150. W.W. Coblentz, J. Opt. Soc. Am., **4**, 432 (1920).

151. K. Ohta and H. Ishida, Appl. Opt., **29**, 2466 (1990).

152. K. Ohta and H. Ishida, Appl. Spectrosc., **42**, 952 (1988).

153. J.E. Bertie in *Vibrational Spectra and Structure*, J.R. Durig, Ed. (Elsevier, Amsterdam, 1985), Vol. 14, p. 221.

154. P.R. Griffiths and J.A. de Haseth, *Fourier Transform Infrared Spectrometry*. (New York, J. Wiley & Sons, 1986).

155. J.E. Bertie and H.H. Eysel, Appl. Spectrosc., **39**, 392 (1985).

156. Commission on Molecular Structure and Spectroscopy of IUPAC, *Tables of Wavenumbers for the Calibration of Infra-red Spectrometers*. (London, Butterworths, 1961).

157. A.R.H. Cole, *Tables of Wavenumbers for the Calibration of Infrared Spectrometers*. 2nd ed. (Oxford, Pergamon Press, 1977).

158. S.K. Garg, J.E. Bertie, H. Kilp, and C.P. Smyth, J. Chem. Phys., **49**, 2551 (1968).

159. J. Timmermans in *Physico-Chemical Constants of Pure Organic Compounds*, (Elsevier, Amsterdam, 1965), Vol. 2, p. 98.

160. M.N. Asfar and G.W. Chantry, IEE Conf. Pub., **152**, 64 (1977).

161. M.N. Asfar, Proc IEEE, **67**, 1460 (1979).

162. J.E. Bertie, S.L. Zhang, and R. Manji, Appl. Spectrosc., **46**, 1660 (1992).

163. *Catalog Handbook of Fine Chemicals*. (Milwaukee, Aldrich Chemical Company, Inc., 1992).

164. J.A. Reddick and E.E. Toops Jr. in *Techniques of Organic Chemistry*, A. Weissberger, Ed. (Interscience, New York, 1955), Vol. VII, p. 72.

165. A.R.H. Cole, R.N. Jones, and R.C. Lord, Pure and Appl. Chem., **33**, 605 (1973).

166. A.R.H. Cole, R.N. Jones, and R.C. Lord, Pure and Appl. Chem., **33**, 647 (1973).

167. J.E. Bertie, C.D. Keefe, and R.N. Jones, *Tables of Intensities for the Calibration of Infrared Spectroscopic Measurements in the Liquid Phase*. (Oxford, Blackwell Scientific Publications Ltd., 1994).

168. M. Windolz, S. Budavari, R.F. Blumetti, and E.S. Otterbein, ed. *The Merck Index. An Encyclopedia of Chemicals and Drugs*. 10th ed. (Rahway, Merck and Co., Inc., 1983).

169. R.E. Lenga, ed. *The Sigma-Aldrich Library of Chemical Safety Data*. 1st ed. (Milwaukee, Aldrich Chemical Company, Inc., 1985).

170. M.A. Armour, *Hazardous Laboratory Chemicals. Disposal Guide*. (Boca Raton, CRC Press, Inc., 1991).

171. J.E. Bertie, C.D. Keefe, R.N. Jones, H.H. Mantsch, and D.J. Moffatt, Appl. Spectrosc., **45**, 1233 (1991).

172. J.E. Bertie, M.K. Ahmed, and S. Baluja. "Absolute Infrared Intensities of Water-Alcohol Mixtures," 7th International Conference on Fourier Transform Spectroscopy, D. Cameron, Ed., Proc. SPIE **1145**, 518 (1989).

173. J.E. Bertie, M.K. Ahmed, and H.H. Eysel, J. Phys. Chem., **93**, 2210 (1989).

174. J.E. Bertie and S.L. Zhang, Appl. Spectrosc., **48**, 176 (1994).

175. G. Herzberg, *Molecular Spectra and Molecular Structure. II. Infrared and Raman Spectra of Polyatomic Molecules*. (Princeton, D. Van Nostrand Company, Inc., 1945).

176. F.A. Miller, J. Raman Spectrosc., **19**, 219 (1988).

177. R. LeSar and R. Kopelman, J. Chem. Phys., **66**, 5035 (1977).

178. A.H. Narten, J. Chem. Phys., **67**, 2102 (1977).

179. I. Harada and T. Shimanouchi, J. Chem. Phys., **44**, 2016 (1966).

180. J.L. Hollenberg and D.A. Dows, J. Chem. Phys., **37**, 1300 (1962).

181. B.P. Stoicheff, Can. J. Phys., **32**, 339 (1954).

182. E.G. Cox, Rev. Mod. Phys., **30**, 159 (1958).

183. D. Steele, Quart. Rev., **18**, 21 (1964).

184. E.G. Cox, D.W.J. Cruickshank, and J.A.S. Smith, Proc. Roy. Soc. (London), **A247**, 1 (1958).

185. M. Akiyama, J. Chem. Phys., **84**, 631 (1986).

186. M. Akiyama, J. Chem. Phys., **85**, 7 (1986).

187. M. Akiyama, J. Phys. Chem., **92**, 27 (1988).

Appendix I

Proof of the Hilbert and KK Transforms

Let $f(z) = u(z) + iv(z), \qquad z = x + iy$

such that $f(z)$ is analytic and $f(z) \to 0$ as $|z| \to \infty$ in either the lower or upper half of the complex plane. (It will be assumed here that this is true on the lower half of the complex plane. The proof is exactly the same for the upper half plane.) Note that if $f(z) \to a$ as $|z| \to \infty$, where a is a constant (which may be complex), then the following is valid for the function $f(z)-a$.

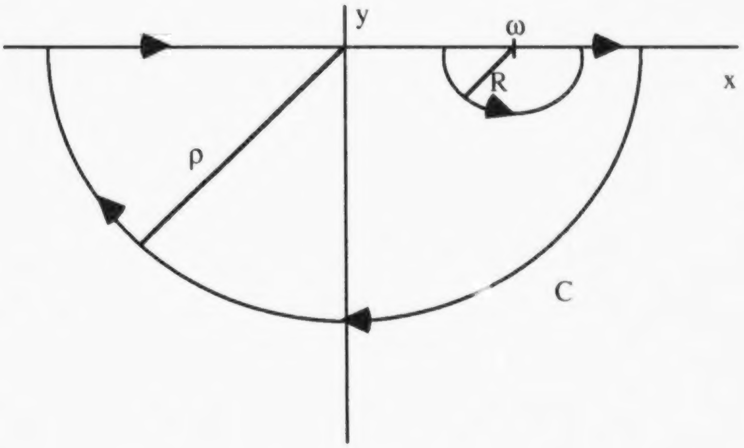

Figure AI.1. Closed curve used to prove the Hilbert and Kramers-Kronig transforms. The curve C is defined as the larger semi circle with radius ρ centered on the origin minus the smaller semi circle with radius R centered on ω.

Consider the integral

$$\oint_C \frac{f(z)}{z-\omega} dz$$

where C is the curve defined in Figure AI.1.

By the Cauchy-Goursat integral theorem[136, 137]

$$\oint_C \frac{f(z)}{z-\omega}\mathrm{d}z = 0 \tag{AI.1}$$

Now consider the limit as $\rho \to \infty$, the integral over this part of the curve is 0, since $f(z) \to 0$. Therefore, the integral over the real axis and the semi circle centered about ω is also 0.

$$\int_{-\infty}^{\omega-R}\frac{f(z)}{z-\omega}\mathrm{d}z + \int_{\omega+R}^{\infty}\frac{f(z)}{z-\omega}\mathrm{d}z + \int_{\pi}^{2\pi}\frac{f(\omega+Re^{\mathrm{i}\theta})R\mathrm{i}e^{\mathrm{i}\theta}}{Re^{\mathrm{i}\theta}}\mathrm{d}\theta = 0$$

$$\int_{-\infty}^{\omega-R}\frac{f(z)}{z-\omega}\mathrm{d}z + \int_{\omega+R}^{\infty}\frac{f(z)}{z-\omega}\mathrm{d}z + \mathrm{i}\int_{\pi}^{2\pi} f(\omega+Re^{\mathrm{i}\theta})\mathrm{d}\theta = 0$$

Now consider the limit of this equation as $R \to 0$

$$\begin{aligned}\lim_{R\to 0} \int_{-\infty}^{\omega-R}\frac{f(z)}{z-\omega}\mathrm{d}z + \int_{\omega+R}^{\infty}\frac{f(z)}{z-\omega}\mathrm{d}z + \mathrm{i}\int_{\pi}^{2\pi} f(\omega+Re^{\mathrm{i}\theta})d\theta \\ = \mathrm{P}\int_{-\infty}^{\infty}\frac{f(z)}{z-\omega}dz + \mathrm{i}\pi f(\omega) = 0\end{aligned} \tag{AI.2}$$

where the P stands for the Cauchy Principal value[137] of the integral.

Separating the real and imaginary parts, one obtains

$$u(\omega) = \frac{1}{\pi}\mathrm{P}\int_{-\infty}^{\infty}\frac{v(z)}{z-\omega}\mathrm{d}z \tag{AI.3}$$

$$v(\omega) = \frac{-1}{\pi}\mathrm{P}\int_{-\infty}^{\infty}\frac{u(z)}{z-\omega}\mathrm{d}z \tag{AI.4}$$

These have been called the Hilbert transforms in the physics and chemistry literature.

If $f(z)=f^*(-z)$, then

$$u(\omega)=\frac{2}{\pi}\mathrm{P}\int_0^\infty \frac{zv(z)}{z^2-\omega^2}\mathrm{d}z \tag{AI.5}$$

$$v(\omega)=\frac{-2}{\pi}\omega\mathrm{P}\int_0^\infty \frac{u(z)}{z^2-\omega^2}\mathrm{d}z \tag{AI.6}$$

These are the Kramers-Kronig (KK) transforms in the physics and chemistry literature. It should be noted that the Hilbert transform does not require the real part of the function to be even and the imaginary part to be odd. This is a requirement of the KK transform. This has been confused in the physics and chemistry literature and sometimes the KK transform has been assumed general and that the even and odd conditions are necessary for the Hilbert transforms to hold. It is more of a technical point because causality ensures that the real parts of the optical and dielectric constants are even and the imaginary parts are odd[140].

Appendix II

Numerical Constants in Equations (1.3.37), (1.3.38), (1.3.44), (1.3.45), (1.3.47) and (1.3.48)

If A_j, B_j and C_j are in km mole^{-1}, the numerical constants in equations (1.3.37), (1.3.38), (1.3.44), (1.3.45), (1.3.47) and (1.3.48) taken on the following values to give $\left|\bar{R}_j\right|$ in Debye and μ_j in Debye Å^{-1} amu$^{-1/2}$.

$$\left|\bar{R}_j\right|^2 = \frac{31.50C_j}{g_j\tilde{\nu}_j} \qquad \mu_j^2 = \frac{1.8686C_j}{g_j}$$

$$\left|\bar{R}_j\right|^2 = \frac{2.5066B_j}{g_j\tilde{\nu}_j} \qquad \mu_j^2 = \frac{0.1487B_j}{g_j}$$

$$\left|\bar{R}_j\right|^2 = \frac{3.5905A_j}{g_j\tilde{\nu}_j}\frac{\underline{n}}{(\underline{n}^2+2)^2} \qquad \mu_j^2 = \frac{0.21294A_j}{g_j}\frac{\underline{n}}{(\underline{n}^2+2)^2}$$

The values of the fundamental constants were taken from E. R. Cohen and B. N. Taylor, Phys. Today, August, BG8 (1989). They have the values

$c = 2.99792458 \times 10^{10}$ cm s^{-1} $\quad$ $h = 6.6260755 \times 10^{-34}$ J s

$N_A = 6.0221367 \times 10^{23}$ mol^{-1}

Substitution of the above constants into equations (1.3.37), (1.3.38), (1.3.44), (1.3.45), (1.3.47) and (1.3.48) give $\left|\bar{R}_j\right|$ in esu cm and μ_j^2 in esu^2 g^{-1}. The conversion factors 1 Debye = 10^{-18} esu. cm and 1 amu = $1.6605402 \times 10^{-24}$ g are then necessary to convert to units of Debye and Debye Å^{-1} amu$^{-1/2}$.

Appendix III

Numerical KK Transform

The KK transforms given in equations (2.3.6) and (2.3.10) have to be calculated for a $k(\tilde{\nu})$ spectrum that is digitized at discrete wavenumbers with constant spacing between the wavenumbers, i.e. $k(\tilde{\nu})$ is known at a collection of $\tilde{\nu}$'s, $\{\tilde{\nu}_i\}$, i=1,n with

$$\Delta = \tilde{\nu}_i - \tilde{\nu}_{i-1} \qquad \text{(AIII.1)}$$

The only complication in calculating the numerical integral is that there is a singularity at $\tilde{\nu} = \tilde{\nu}_i$. To overcome this several methods have been presented in the literature[14, 152].

The algorithm that was used in this work to calculate the numerical transform is the one presented by Ohta and Ishida[152] which they have termed the MacLaurin Formula. The algorithm amounts to calculating the integral using a trapezoid numerical integral but ignoring every second point. The points are chosen so that $\tilde{\nu}_i$ is not included in the set of points used to calculate the integral. Thus the set of points used to calculate the integral is different when the integral is calculated for an even than for an odd point.

The value of the integral is

$$\frac{2}{\pi}\mathrm{P}\int_{\tilde{\nu}_{\text{low}}}^{\tilde{\nu}_{\text{high}}} \frac{\tilde{\nu}k(\tilde{\nu})}{\tilde{\nu}^2 - \tilde{\nu}_i^2}\,\mathrm{d}\tilde{\nu} = \frac{2}{\pi} \times 2\Delta \times \sum_j \frac{\tilde{\nu}_j k_j}{\tilde{\nu}_j^2 - \tilde{\nu}_i^2} \qquad \text{(AIII.2)}$$

where

$$j = \begin{cases} 2, 4, 6, \ldots i-1, i+1, \ldots & i \text{ odd} \\ 1, 3, 5, \ldots i-1, i+1, \ldots & i \text{ even} \end{cases} \tag{AIII.3}$$

Appendix IV

Optical Constants of Benzene-h_6

Table IV.1. Imaginary refractive indices between 6225 and 30 cm^{-1} of liquid benzene-h_6 at 25°C.[a,b]

cm^{-1}	*XE*	*YE*	0	1	2	3	4	5	6	7	8	9	10	11	12	13	14	15	16
6225.09	0	-7	192	168	150	128	123	106	97	91	85	79	71	68	75	68	68	64	63
6208.70	0	-7	65	66	70	66	68	72	71	73	75	77	77	78	82	83	91	95	96
6192.31	0	-7	99	104	109	120	130	149	155	152	129	111	97	86	83	82	82	82	84
6175.91	0	-7	87	96	89	93	94	99	96	102	102	116							
6159.52	3	-7	215	437	581	425	379	438	533	590	579	648	502	396	321	241	224	252	370
6028.39	3	-7	563	687	780	1154	1636	2441	3293	2681	2430	2090	2011	1680	1425				
5931.96	2	-7	1691	1786	1570	1513	1915	2325	2119	1665	1361	1182	982	778	710	780	795	741	720
5866.39	2	-7	756	749	658	567	494	406	307	233	185	151	121	96	76	66	72	89	110
5800.83	2	-7	123	119	120	122	137	151	180	190	209	211	180	149	142	142	147	159	153
5735.26	2	-7	132	125	117	129	164	233	268	278	326	415	525	631	615	440	297	225	182
5669.69	2	-7	164	163	164	168	177	156	125	106	96	92	97	100	113	135	161	199	217
5604.12	2	-7	221	222	214	217	244	292	366	395	342	255	178	144	139	149	182	226	247
5538.56	2	-7	277	296	297	295	310	352	345	268	210	187	181	162	146	126	102	84	81
5472.99	2	-7	72	65	56	55	57	61											
5451.77	1	-7	67	69	76	73	76	82	85	96	106	113	121	136	139	143	142	140	137
5418.99	1	-7	136	135	128	115	103	100	101	111	122	120	117	112	106	101	98	95	95
5386.21	1	-7	97	100	108	117	126	135	137	138	134	131	128	125	125	125	128	130	132
5353.42	1	-7	138	148	163	172	176	171	161	151	140	131	124	122	128	134	137	129	128
5320.64	1	-7	127	133	138	147	156	167	189	209	220	189	137	106	96	93	101	112	125
5287.85	1	-7	136	140	118	90	74	64	66	72	82	91	102	113	129	145	163	190	207
5255.07	1	-7	227	248	271	294	302	268	211	170	140	121	108	99	95	85	83	81	78
5222.29	1	-7	73	70	65	63	65	65	64	62	57	53	50	48	48	48	50	47	50
5189.50	1	-7	54	56	53	58	57	57	55	55	49	48	47	44	43	48	53	63	74
5156.72	1	-7	80	83	85	86	84	83	81	78	72	73	73	72	77	80	84	84	82
5123.93	1	-7	79	74	67	60	57												
5112.36	2	-7	52	56	78	100	118	133	150	160	160	120	82	78	85	93	97	103	117
5046.80	2	-7	123	101	83	82	88	93	110	139	168	171	130	110	124	148	137	96	81
4981.23	2	-7	92	100	104	103	114	125	125	123	118	115	118	123	133	141	148	151	151
4915.66	2	-7	152	154	161	173	176	169	162	156	156	163	179	200	218	223	221	224	228
4850.09	2	-7	232	231	228	218	206	189	169	157	152	156	160	152	147	149	153	158	169
4784.52	2	-7	187	190	180	171	165	167	171	177	180	184	192	203	219	242	266	293	326
4718.96	2	-7	366	414	464	542	691	855	1160	1717	1832	1633	1714	2363	4021	5263			
4666.89	1	-7	4615	3653	2883	2361	2026	1840	1783	1876	2158	2645	3277	3839	4096	4114	3957	3474	2824
4634.10	1	-7	2304	2005	1937	2153	2703	3473	3882	3578	3007	2523	2159	1925	1826	1843	1930	2010	1999
4601.32	1	-7	1896	1768	1684	1688	1809	2087	2576	3309	4154	4693	4591	4110	3580	3070	2566	2131	1790
4568.54	1	-7	1529	1331	1170	1047	965	910	880	878	911	996	1150	1366	1573	1643	1530	1328	1121
4535.75	1	-7	947	810	698	606	534	476	431	395	366	344	325	312	302	295	289	282	278
4502.97	1	-7	270	267	263	256	253	254	254	261	270	286	303	316	320	310	302	297	298
4470.18	1	-7	297	301	314	328	345	355	354	353	353	355	359	364	368	374	382	392	410
4437.40	1	-7	437	480	530	570	575	557	534	515	502	500	523	580	651	652	611	594	591
4404.62	1	-7	577	554	529	507	491	474	464	459	466	494	561	687	881	1110	1225		
4373.76	2	-7	1013	755	581	461	393	356	330	319	314	308	310	311	311	307	312	326	347
4308.19	2	-7	378	417	462	511	545	550	535	533	560	624	743	978	1318				
4259.98	1	-7	1369	1299	1190	1100	1024	972	963	985	1017	1032	1026	1003	980	964	955	942	943
4227.20	1	-7	969	1025	1108	1221	1313	1328	1297	1269	1258	1262	1267	1260	1264	1300	1391	1543	1697
4194.41	1	-7	1735	1636	1487	1354	1255	1191	1162	1171	1218	1295	1390	1451	1396	1291	1213	1162	1126
4161.63	1	-7	1093	1068	1064	1067	1065	1057	1044	1034	1024	1028	1008	993	997	1019	1032	1058	1087
4128.84	1	-7	1106	1141	1192	1239	1287	1333	1386	1448	1540	1646	1789	1964	2165	2411	2726	3083	3451
4096.06	1	-6	376	403	429	462	509	575	658	740	786	790	774	777	820	911	1052	1252	1544
4063.28	1	-6	1957	2474	2996	3315	3266	2862	2316	1812	1418	1119	888	711	579	483	415	368	339
4030.49	1	-7	3290	3419	3651	3648	3256	2719	2256	1891	1605	1389	1235	1097	965	841	717	609	532
3997.71	1	-7	474	415	374	361	378	409	423	411	402	343	251						
3977.94	-1	-7	232	214	191	167	151	135	118	101	89	78	70	62	56	51	48	56	67
3969.75	-1	-7	83	103	131	166	211	267	333	412	504	606	713	820	922	1014	1092	1157	1214
3961.55	-1	-7	1264	1313	1365	1421	1482	1546	1611	1672	1721	1755	1769	1761	1732	1685	1622	1547	1465
3953.35	-1	-7	1380	1295	1211	1132	1057	989	928	869	823	783	745	715	688	668	654	644	640
3945.16	-1	-7	642	649	662	683	710	744	787	840	906	985	1081	1196	1332	1489	1668	1862	2062
3936.96	-1	-7	2254	2414	2524	2567	2547	2474	2368	2243	2113	1983	1859	1740	1628	1521			
3926.84	2	-7	904	622	514	468	441	445	445	440	444	445	440	435	410	361	322	307	296
3861.27	2	-7	296	301	299	296	294	297	309	344	389	419	421	426	453	471	488		
3805.34	1	-7	487	500	527	549	576	616	678	775	871	908	861	781	730	713	715	740	789
3772.56	1	-7	851	920	951	935	894	845	815	796	791	815	859	914	973	1043	1126	1195	1248
3739.78	1	-7	1282	1294	1289	1266	1248	1234	1234	1246	1268	1301	1338	1378	1420	1483	1578	1732	1956
3706.99	1	-7	2247	2613	3120	3965	5417	7227	7675	6324	5038	4391	4144	3890	3422	2871	2409	2083	1849
3674.21	1	-7	1670	1546	1480	1455	1454	1402	1293	1199	1154	1177	1278	1482	1864	2606	3986	6263	8633
3641.42	1	-7	8604	6437	4463	3249	2584	2181	1893	1673	1538	1491	1552	1737	2060	2545	3114	3557	3623
3608.64	1	-7	3301	2780	2260	1832	1526	1310	1154	1025	920	829	751	680	605	545	497	467	428
3575.86	1	-7	386	345	318	306	306	312	316	314	300	290	283	281	286	286	294	298	299
3543.07	1	-7	304	304	293	280	264	258	254										

Table IV.1. Continued.

cm^{-1}	*XE*	*YE*	0	1	2	3	4	5	6	7	8	9	10	11	12	13	14	15	16
3531.02	-1	-7	253	253	253	252	250	249	250	251	271	271	271	273	275	277	281	285	289
3521.38	1	-7	307	343	409	471	463	394	351	337	338	348	353	359	369	383	413	470	569
3488.59	1	-7	685	692	595	523	473	439	419	411	412	423	438	464	496	534	593	675	783
3455.81	1	-7	929	1131	1367	1571	1645	1553	1371	1175	1010	876	774	702	656	656	724	760	725
3423.02	1	-7	711	723	734	729	717	701	677	663	662	673	691	719	739	740	715	666	601
3390.24	1	-7	538	488	443	407	380	356	338	323	311	302	292	285	278	272	271	277	288
3357.46	1	-7	301	316	318	320	329	332	328	318	305	297	296	307	319	326	332	344	364
3324.67	1	-7	374	368															
3322.26	-1	-7	367	364	362	361	359	553	548	553	531	513	531	511	486	517	521	486	482
3314.07	-1	-7	497	510	513	519	522	531	520	517	549	523	525	531	505	530	511	504	512
3305.87	-1	-7	494	488	461	443	436	439	438	431	423	413	396	382	396	381	387	397	394
3297.67	-1	-7	396	398	423	427	441	456	458	481	480	482	489	484	502	535	549	558	570
3289.48	-1	-7	573	581	595	607	600	599	603	596	589	595	605	598	599	596	594	581	578
3281.28	-1	-7	614	631	629	641	669	681	698	724	755	801	820	812	816	828	812	814	836
3273.09	-1	-7	828	834	858	853	837	825	809	820	828	819	809	803	831	823	805	809	797
3264.89	-1	-7	805	829	837	840	835	851	884	908	918	918	944	948	956	1006	1029	1046	1092
3256.69	-1	-7	1083	1075	1116	1092	1096	1110	1088	1093	1087	1096	1083	1076	1099	1115	1123	1105	1119
3248.50	-1	-7	1124	1122	1145	1133	1139	1147	1148	1146	1140	1146	1129	1143	1144	1129	1135	1119	1109
3240.30	-1	-7	1126	1117	1124	1147	1138	1133	1141	1137	1143	1142	1142	1164	1168	1166	1180	1197	1184
3232.11	-1	-7	1185	1190	1183	1191	1183	1176	1164	1177	1192	1187	1198	1210	1225	1244	1251	1241	1243
3223.91	-1	-7	1260	1274	1286	1281	1301	1345	1346	1374	1401	1413	1461	1480	1508	1531	1524	1524	1507
3215.71	-1	-7	1510	1512	1493	1472	1488	1521	1512	1520									
3211.38	0	-7	1540	1534	1592	1639	1673	1719	1763	1793	1833	1870	1928	1953	1982	2029	2067	2096	2143
3194.98	0	-7	2208	2288	2320	2387	2464	2566	2630	2709	2796	2853	2884	2919	2934	2942	2950	2941	2971
3178.59	0	-7	2989	2978	3022	3081	3096	3159	3202	3298	3345	3453	3528	3617	3680	3730	3780	3795	3865
3162.20	0	-7	3897	3972	4035	4102	4204	4271	4390	4477	4594	4632	4712	4783	4865	4947	5040	5177	5279
3145.81	0	-7	5430	5561	5681	5794	5898	6031	6167	6348	6494	6662	6819	7007	7226	7395	7594	7804	8004
3129.42	0	-6	825	851	879	910	945	979	1017	1058	1100	1146	1200	1254	1320	1391	1472	1556	1644
3113.02	0	-6	1739	1842	1954	2073	2203	2349	2518	2716	2950	3243	3606	4066	4654	5410	6369	7606	9222
3096.63	0	-5	1133	1405	1749	2155	2568	2873	2948	2767	2434	2068	1736	1466	1257	1100	984	898	840
3080.24	0	-5	808	806	836	902	1015	1191	1445	1764	2066	2182	2036	1766	1503	1284	1109	976	877
3063.85	0	-6	8026	7481	7084	6811	6651	6599	6625	6646	6565	6397	6250	6174	6198	6323	6572	6958	7511
3047.46	0	-5	827	929	1064	1243	1480	1791	2196	2704	3318	4003	4681	5200	5338				
3033.96	1	-5	4533	3465	2634	2020	1557	1221	985	818	697	605	535	479	434	399	370	344	318
3001.17	1	-6	2939	2707	2483	2273	2088	1925	1788	1658	1536	1440	1360	1288	1216	1145	1076	1008	954
2968.39	1	-7	9048	8687	8435	8225	7980	7810	7696	7585	7510	7399	7259	6896	6364	5891	5482	5114	4897
2935.60	1	-7	4798	4804	4803	4819	4780	4671	4466	4276	4009	3826	3849						
2915.36	0	-7	4038	4198	4438	4766	5205	5759	6424	7138	7755	8095	8029	7606	7013	6362	5808	5355	5017
2898.96	0	-6	479	467	466	478	502	542	606	703	842	1033	1268	1491	1598	1511	1283	1046	858
2881.61	1	-7	6169	4661	3695	3141	2811	2608	2502	2409	2291	2243	2262	2384	2637	3013	3405	3587	3465
2848.82	1	-7	3175	2854	2584	2405	2303	2225	2127	2031	1969	1977	2118	2474	3192	4387	5749	6829	6936
2816.04	1	-7	5828	4578	3701	3034	2466	2021	1690	1429	1218	1061	961	888	848	827	833	847	856
2783.25	1	-7	856	836	804	750	700	650	609	577	554	528	515	511	496	482	469	457	457
2750.47	1	-7	446	421	397	375	363	356	353	361	371	385	392	376	350	332	325	323	326
2717.69	1	-7	330	334	336	345	348	355	367	381	391	409	428	446	463	483	495	519	538
2684.90	1	-7	570	597	632	659	677	695	724	770	836	923	1061	1269	1595	2116	3008	4632	
2655.01	0	-7	5770	6896	7487	7153	6138	4995	4033	3307	2776	2378	2068	1818	1616	1461	1343	1246	1166
2638.62	0	-7	1099	1037	982	935	906	882	872	868	870	878	897	929	970	1021	1088	1176	1287
2622.23	0	-7	1434	1626	1883	2195	2548	2954	3407	3868	4180	4196	3931	3531	3128	2781	2520	2332	2219
2605.84	0	-7	2170	2182	2255	2401	2637	2990	3498	4215	5195	6423	7604	8083	7536	6391	5215		
2590.41	1	-7	3494	2443	1840	1537	1384	1306	1274	1261	1304	1351	1266	1134	1050	1021	1053	1128	1228
2557.62	1	-7	1386	1580	1639	1448	1189	989	854	773	716	663	631	605	594	596	615	638	678
2524.84	1	-7	726	779	838	850	828	818	806	788	759	733	710	701	694	701	724	768	834
2492.06	1	-7	927	1049	1196	1363	1479	1388	1198	1057	985	976	1045	1169	1241	1151	1040	941	869
2459.27	1	-7	843	858	911	981	992	936	853	791	746	724	723	745	794	882	1031	1195	1236
2426.49	1	-7	1211	1206	1234	1305	1418	1603	1858	2154	2406	2549	2570	2507	2423	2358	2315	2279	2265
2393.70	1	-7	2315	2490	2817	3380	4211	5134	5549	5165	4460	3782	3184	2689	2319	2065	1900	1855	1897
2360.92	1	-6	180	162	156	155	157	160	164	170	180	196	216	247	296	373	494	694	1019
2328.14	1	-6	1526	2105	2233	1739	1174	782	542	399	309	250	207	176	154	138	126	117	111
2295.35	1	-7	1068	1053	1076	1139	1265	1439	1598	1637	1518	1331	1169	1049	976	922	865	801	754
2262.57	1	-7	715	683	668	665	669	691	718	735	737	738	744	763	784	809	841	890	955
2229.78	1	-6	104	114	126	143	170	215	295	439	710	1138							
2211.95	-1	-6	1246	1329	1389	1401	1385	1330	1260	1175	1089	1002	918	839	764	694			
2203.75	1	-7	4660	3200	2324	1792	1472	1275	1153	1086	1044	1010	971	929	888	854	821	795	770
2170.97	1	-7	750	741	727	718	703	693	684	672	657	645	639	629	632	629	616	592	569
2138.18	1	-7	551	533	524	516	509	509	509	521	535	543	545	534	559	583	597	594	594
2105.40	1	-7	584	611	660	725	765	776	791	819	846	872	886	899	902	910	898	862	828
2072.61	1	-7	797	783	784	813	806	833	857	904	981	1113	1241	1402	1582	1751	1849	1861	1840
2039.83	1	-7	1857	1904	1981	2038	2063	2104	2173	2228	2318	2408	2540	2743	3076	3624	4511	5847	7575
2007.05	1	-6	921	1022	979	850	742	683	677	728	847	1022	1104	1063	1052	1100	1208	1383	1635
1974.26	1	-6	1997	2536	3325	4439	5907	7599	9135	9963	9757	8670	7199	5747	4506	3530	2797	2268	1899
1941.48	1	-6	1639	1443	1266	1099	947	817	706	615	542	482	437	409	387	376	359	328	297
1908.69	1	-7	2744	2602	2489	2426	2389	2377	2408	2488	2712	3070	3529	4110	4582	4869	5067	5291	5619
1875.91	1	-7	5828	5717	5349	4932	4620	4484	4417	4455	4596	4807	5079	5423	5816	6329	6900	7646	8476
1843.13	1	-5	96	111	129	151	181	221	275	348	449	581	754	963	1194	1405	1537	1531	1388
1810.34	1	-5	1173	950	753	593	470	378	312	266	232	203	176	150	127	107	91	78	69
1777.56	1	-6	617	564	517	479	472	464	477	512	587	723	943	1217	1361	1211	920	686	541
1744.77	1	-7	4383	3639	3140	2784	2525	2343	2203	2088	2011	1969	1949	1968	2061	2298	2785	3689	
1715.37	-1	-7	3993	4305	4617	4863	5042	5060	4972	4752	4487	4201	3927	3691	3478	3315	3175	3071	2981
1705.72	1	-7	2800	2719	2647	2619	2610	2634	2667	2743	2855	3024	3269	3638	4155	4905	5996	7568	9647
1672.94	1	-6	1172	1267	1182	995	807	659	553	483	440	417	407	405	412	425	450	481	469
1640.15	1	-6	457	459	469	489	521	566	629	718	850	1054	1360	1696	1758	1522	1303	1190	1157
1607.37	1	-6	1169	1161	1124	1080	1047	1041	1066	1117	1183	1264	1336	1362	1326	1249	1162	1083	1018

Table IV.1. Continued.

cm^{-1}	*XE*	*YE*	0	1	2	3	4	5	6	7	8	9	10	11	12	13	14	15	16
1574.59	1	-7	9549	8853	8290	7866	7567	7482	7295	7434									
1560.12	0	-6	784	784	808	800	801	829	872	886	919	957	1008	1071	1131	1215	1318	1443	1583
1543.73	0	-6	1750	1962	2200	2467	2796	3152	3503	3928	4393	4881	5389	5871	6303	6682	6984	7181	7268
1527.34	0	-6	7243	7103	6886	6582	6244	5886	5517	5141	4768	4434	4146	3875	3631	3424	3250	3108	2993
1510.95	0	-6	2892	2831	2788	2775	2802	2819	2855	2900	2993	3109	3254	3431	3653	3897	4194	4574	4974
1494.56	0	-4	55	61	68	77	89	104	123	148	181	227	292	387	528	737	1025	1344	1533
1478.16	0	-4	1413	1134	855	631	477	383	324	270	217	173	140	116	98	84	72	62	54
1461.77	0	-6	4796	4253	3800	3435	3109	2857	2589	2369	2188	2036	1914	1807	1706	1603	1511	1419	1339
1445.38	0	-6	1262	1193	1132	1082	1033	990	952	915	890	874	825	791	771	747	729	721	717
1428.99	0	-7	7036	6967	6894	6834	6797	6820	6778	6773	6755	6591	6603	6715	6864	7010	7183	7367	7573
1412.60	0	-6	783	813	847	890	941	1005	1082	1177	1295	1447	1627	1851	2123	2454	2859	3330	3838
1396.20	0	-6	4340	4780	5083	5179	5054	4747	4323	3857	3392	2956	2577	2258	1981				
1380.78	2	-6	1218	865	681	575	505	450	422	419	431	434	422	419	437	462	503	564	653
1315.21	2	-6	772	870	862	777	672	584	525	486	464	458	468	495	547	637	781	1024	1405
1249.64	2	-6	1709	1524	1227	1091	1066	1081	1115	1165	1233	1325	1459	1673	1922	2088	2378	2820	3510
1184.07	2	-6	4438	5275	5654	5105	4252	3657	3329	3243	3321	3447	3333	2898	2399	2008	1722	1515	1361
1118.50	2	-6	1236	1157	1124	1115	1057	992	1001	1029	1079	1150	1267	1422	1587	1825	2206	2811	3700
1052.93	2	-6	5101	7714															
1047.15	1	-5	996	1346	1917	2885	4447	6306	7065	6183	4709	3379	2414	1772	1357	1087	908	791	718
1014.37	1	-6	6838	6912	7132	6560	5627	4988	4605	4407	4326	4311	4372	4475	4444	4174	3896		
983.51	2	-6	3624	3512	3537	3564	3447	3128	2740	2358	2061	1839	1664	1511	1392	1287	1217	1157	1111
917.94	2	-6	1102	1107	1127	1129	1134	1148	1186	1241	1318	1424	1566	1766	2021	2357	2853	3572	4499
852.38	2	-6	5319	5455	4731	3798	3072	2547	2148	1838	1610	1439	1328	1242	1210	1207	1246	1315	1402
786.81	2	-6	1476	1543	1659	1788	1932	2095	2279	2489	2729	3005	3325	3700	4141	4665	5296	6063	7009
721.24	2	-5	819	970	1167	1429	1790	2303	3069	4292									
692.31	1	-3	52	66	88	125	190	297	455	661	893	1108	1209	1065	727	423	248	156	105
659.53	1	-5	7616	5884	4754	3949	3339	2861	2478	2166	1909	1695	1514	1361	1230	1116	1018	932	856
626.74	1	-6	7893	7300	6771	6297	5871	5487	5139	4823	4535	4272	4032	3811	3608	3420	3247	3086	2937
593.96	1	-6	2799	2670	2550	2438	2333	2235	2142	2056	1974	1897	1825	1757	1692	1631	1573	1518	1466
561.17	1	-6	1417	1370	1325	1283	1242	1204	1167	1132	1098	1066	1035	1006	978	951	925	900	876
528.39	1	-7	8531	8310	8098	7894	7697	7508	7326	7150	6981	6817	6659	6470	6326	6233	6226	6257	6308
495.61	1	-7	6348	6371	6398	6438	6488	6538	6588	6641	6692	6735	6785	6852	6921	6978	7032	7093	7163
462.82	1	-7	7264	7413	7599	7823	8091	8392	8712	9243	9443	9191	8952	8833	8841	8950	9121	9315	9522
430.04	1	-6	975	1002	1036	1080	1137	1202	1269	1327	1372	1411	1456	1523	1625	1744	1821	1795	1687
397.25	1	-6	1563	1452	1359	1276	1201	1136	1077	1025	980	938	899	866	838	814	795	778	764
364.47	1	-7	7510	7386	7246	7081	6906	6744	6605	6495	6411	6347	6301	6265	6231	6197	6164	6134	6114
331.69	1	-6	611	612	615	620	626	630	635	642	655	675	705	750	811	880	955	1018	1022
298.90	1	-7	9606	8807	8150	7685	7383	7217	7158	7173	7210	7232	7232	7227	7246	7305	7394	7502	7603
266.12	1	-7	7666	7684	7676	7663	7649	7641	7654	7688	7732	7784	7840	7903	7970	8033	8105	8189	8276
233.33	1	-7	8361	8440	8508	8559	8599	8665	8760	8866	8982	9092	9163	9285	9383	9450	9507	9581	9687
200.55	1	-6	982	998	1013	1023	1033	1043	1053	1068	1087	1108	1137	1173	1217	1268	1318	1357	1381
167.77	1	-6	1385	1374	1359	1353	1360	1379	1401	1423	1447	1472	1499	1531	1571	1616	1667	1721	1777
134.98	1	-6	1838	1903	1977	2061	2159	2270	2392	2518	2559	2687	2815	2938	3055	3172	3294	3422	3555
102.20	1	-6	3690	3831	3981	4141	4304	4459	4600	4729	4858	5003	5170	5344	5500	5610	5656	5675	5762
69.41	1	-6	5948	6151	6299	6382	6433	6488	6577	6711	6879	7040	7942	8023	7775	7416	7066	6804	6673
36.63	1	-6	6646	6646	6597	6454	6214												

a. The column headed cm^{-1} contains the wavenumber of the first $k(\tilde{\nu})$ value in the row. The columns headed *XE* and *YE* contain the X-exponent and the Y-exponent, respectively, for the row. The columns headed 0,1,2,····16, contain the ordinate values, and the headings give the indices of the ordinate values in the row. In a row which starts with $\tilde{\nu}(0)$, the wavenumber corresponding to the ordinate indexed *J* is $\tilde{\nu}(J) = \tilde{\nu}(0) - \frac{15798.002}{16384} \cdot J \cdot 2^{XE}$. The $k(\tilde{\nu})$ values in that row are the ordinate value shown times 10^{YE}. Thus the entry indexed 16 in the first row of the table shows that $k = 63 \times 10^{-7} = 6.3 \times 10^{-6}$ at $\tilde{\nu} = 6225.09 - \frac{15798.002}{16384} \cdot 16 \cdot 2^0 = 6209.66\ cm^{-1}$.

b. The $k(\tilde{\nu})$ values in the table can be interpolated to the original wavenumber spacing, 0.482117 cm^{-1}, and yield the original $k(\tilde{\nu})$ values accurate to 1% below 4500 cm^{-1}, 2% between 4500 and 5000 cm^{-1} and 5% above 5000 cm^{-1}, via the 4-point spline interpolation program TRECOVER[44].

Table IV.2. Real refractive indices between 6225 and 30 cm^{-1} of liquid benzene-h$_6$ at 25°C.[a,b]

cm^{-1}	*XE*	0	1	2	3	4	5	6	7	8	9	10	11	12	13	14	15	16
6225.09	0	14799	14799	14799	14799	14799	14799	14799	14799	14799	14799	14799	14799	14799	14799	14799	14799	14799
6208.70	0	14799	14799	14799	14799	14799	14799	14799	14799	14799	14799	14799	14799	14799	14799	14799	14799	14799
6192.31	0	14799	14799	14799	14799	14799	14799	14799	14799	14799	14799	14799	14799	14799	14799	14799	14799	14799
6175.91	0	14798	14798	14798	14798	14798	14798	14798	14798	14798	14798							
6159.52	3	14798	14798	14798	14799	14798	14798	14798	14798	14798	14799	14799	14799	14798	14798	14798	14798	14798
6028.39	3	14798	14798	14797	14797	14797	14797	14798	14799	14799	14799	14799	14799	14799				
5931.96	2	14799	14799	14799	14799	14799	14799	14800	14800	14800	14800	14800	14800	14800	14800	14800	14800	14800
5866.39	2	14800	14800	14800	14800	14800	14800	14800	14800	14800	14800	14799	14799	14799	14799	14799	14799	14799
5800.83	2	14799	14799	14799	14799	14799	14799	14799	14799	14799	14799	14799	14799	14799	14799	14799	14799	14799
5735.26	2	14799	14799	14799	14799	14799	14798	14798	14798	14798	14798	14798	14799	14799	14799	14799	14799	14799
5669.69	2	14799	14799	14799	14799	14799	14799	14799	14799	14798	14798	14798	14798	14798	14798	14798	14798	14798
5604.12	2	14798	14798	14798	14798	14798	14798	14798	14798	14798	14798	14798	14798	14798	14798	14798	14798	14798
5538.56	2	14798	14798	14798	14798	14798	14798	14798	14798	14798	14798	14798	14798	14798	14798	14798	14798	14798
5472.99	2	14798	14798	14798	14798	14798	14798											
5451.77	1	14798	14798	14798	14798	14798	14798	14798	14798	14798	14798	14798	14798	14798	14798	14798	14798	14798
5418.99	1	14798	14798	14798	14798	14798	14798	14798	14798	14798	14798	14798	14798	14798	14798	14798	14798	14798
5386.21	1	14798	14798	14798	14798	14798	14798	14798	14798	14798	14798	14798	14798	14798	14798	14798	14798	14798
5353.42	1	14798	14798	14798	14798	14798	14798	14798	14798	14798	14798	14798	14798	14798	14797	14797	14797	14797
5320.64	1	14797	14797	14797	14797	14797	14797	14797	14797	14797	14798	14798	14797	14797	14797	14797	14797	14797
5287.85	1	14797	14797	14797	14797	14797	14797	14797	14797	14797	14797	14797	14797	14797	14797	14797	14797	14797
5255.07	1	14797	14797	14797	14797	14797	14797	14797	14797	14797	14797	14797	14797	14797	14797	14797	14797	14797
5222.29	1	14797	14797	14797	14797	14797	14797	14797	14797	14797	14797	14797	14797	14797	14797	14797	14797	14797
5189.50	1	14797	14797	14797	14797	14797	14797	14797	14797	14797	14797	14797	14797	14797	14797	14797	14797	14797
5156.72	1	14797	14797	14797	14797	14797	14797	14797	14797	14797	14797	14797	14797	14797	14797	14797	14797	14797
5123.93	1	14797	14797	14797	14797	14797												
5112.36	2	14797	14797	14797	14797	14797	14797	14797	14797	14797	14797	14797	14797	14796	14796	14796	14796	14796
5046.80	2	14796	14796	14796	14796	14796	14796	14796	14796	14796	14796	14796	14796	14796	14796	14796	14796	14796
4981.23	2	14796	14796	14796	14796	14796	14796	14796	14796	14796	14796	14796	14796	14796	14796	14796	14796	14796
4915.66	2	14796	14796	14796	14796	14796	14796	14796	14796	14796	14795	14795	14795	14795	14795	14795	14795	14795
4850.09	2	14795	14795	14795	14795	14795	14795	14795	14795	14795	14795	14795	14795	14795	14795	14795	14795	14795
4784.52	2	14795	14795	14795	14795	14795	14795	14794	14794	14794	14794	14794	14794	14794	14794	14794	14794	14794
4718.96	2	14794	14793	14793	14793	14793	14793	14792	14792	14793	14793	14792	14792	14792	14794			
4666.89	1	14795	14796	14795	14795	14795	14795	14794	14794	14793	14793	14793	14794	14794	14795	14795	14796	14796
4634.10	1	14796	14795	14795	14794	14794	14794	14795	14796	14796	14796	14796	14796	14795	14795	14795	14795	14795
4601.32	1	14795	14795	14795	14795	14794	14794	14794	14794	14794	14795	14796	14797	14797	14797	14797	14797	14797
4568.54	1	14797	14797	14797	14796	14796	14796	14796	14796	14796	14795	14795	14795	14796	14796	14796	14796	14796
4535.75	1	14796	14796	14796	14796	14796	14796	14796	14796	14796	14795	14795	14795	14795	14795	14795	14795	14795
4502.97	1	14795	14795	14795	14795	14795	14795	14795	14795	14795	14795	14795	14795	14795	14794	14794	14794	14794
4470.18	1	14794	14794	14794	14794	14794	14794	14794	14794	14794	14794	14794	14794	14794	14794	14794	14794	14794
4437.40	1	14794	14794	14794	14794	14794	14794	14794	14794	14794	14794	14794	14794	14794	14794	14794	14794	14794
4404.62	1	14794	14794	14794	14794	14794	14794	14793	14793	14793	14793	14793	14793	14793	14793	14793		
4373.76	2	14794	14794	14794	14794	14793	14793	14793	14793	14793	14793	14793	14793	14793	14793	14793	14793	14792
4308.19	2	14792	14792	14792	14792	14792	14792	14792	14792	14792	14792	14791	14791	14791				
4259.98	1	14792	14792	14792	14792	14792	14792	14792	14792	14792	14792	14792	14792	14792	14791	14791	14791	14791
4227.20	1	14791	14791	14791	14791	14791	14791	14791	14791	14791	14791	14791	14791	14791	14791	14791	14791	14791
4194.41	1	14791	14791	14791	14791	14791	14791	14791	14791	14791	14791	14791	14791	14791	14791	14791	14791	14791
4161.63	1	14790	14790	14790	14790	14790	14790	14790	14790	14790	14790	14790	14789	14789	14789	14789	14789	14789
4128.84	1	14789	14788	14788	14788	14788	14788	14788	14787	14787	14787	14787	14786	14786	14786	14785	14785	14785
4096.06	1	14785	14785	14784	14784	14784	14783	14783	14783	14784	14784	14784	14783	14782	14781	14780	14779	14778
4063.28	1	14778	14779	14783	14790	14798	14805	14808	14809	14809	14808	14807	14806	14805	14804	14803	14802	14801
4030.49	1	14800	14800	14799	14800	14800	14800	14799	14799	14799	14798	14798	14798	14797	14797	14797	14797	14796
3997.71	1	14796	14796	14796	14795	14795	14795	14795	14795	14795	14795	14794						
3977.94	-1	14794	14794	14794	14794	14794	14794	14794	14794	14794	14794	14794	14794	14794	14794	14794	14793	14793
3969.75	-1	14793	14793	14793	14793	14793	14793	14793	14793	14793	14793	14793	14793	14793	14793	14793	14793	14793
3961.55	-1	14793	14793	14793	14793	14793	14793	14793	14793	14793	14793	14793	14793	14793	14793	14794	14794	14794
3953.35	-1	14794	14794	14794	14794	14794	14794	14794	14793	14793	14793	14793	14793	14793	14793	14793	14793	14793
3945.16	-1	14793	14793	14793	14793	14793	14792	14792	14792	14792	14792	14792	14792	14792	14792	14792	14792	14792
3936.96	-1	14792	14792	14793	14793	14793	14793	14793	14794	14794	14794	14794	14794	14794	14794			
3926.84	2	14794	14793	14793	14793	14793	14792	14792	14792	14792	14792	14792	14792	14792	14792	14791	14791	14791
3861.27	2	14791	14791	14791	14791	14791	14790	14790	14790	14790	14790	14790	14790	14790	14790	14789		
3805.34	1	14789	14789	14789	14789	14789	14789	14789	14789	14789	14789	14789	14789	14789	14789	14789	14789	14789
3772.56	1	14789	14789	14789	14789	14789	14789	14788	14788	14788	14788	14788	14788	14788	14788	14788	14788	14788
3739.78	1	14788	14788	14788	14788	14788	14787	14787	14787	14787	14787	14787	14787	14787	14786	14786	14786	14786
3706.99	1	14785	14785	14785	14784	14784	14785	14788	14790	14790	14790	14790	14790	14790	14790	14790	14790	14789
3674.21	1	14789	14789	14788	14788	14788	14788	14788	14787	14787	14787	14786	14786	14785	14784	14784	14784	14786
3641.42	1	14789	14791	14791	14791	14790	14790	14790	14789	14789	14788	14788	14788	14787	14787	14787	14788	14789
3608.64	1	14789	14789	14790	14789	14789	14789	14789	14789	14789	14788	14788	14788	14788	14788	14788	14788	14788
3575.86	1	14787	14787	14787	14787	14787	14787	14787	14787	14787	14786	14786	14786	14786	14786	14786	14786	14786
3543.07	1	14786	14786	14786	14785	14785	14785	14785										
3531.02	-1	14785	14785	14785	14785	14785	14785	14785	14785	14785	14785	14785	14785	14785	14785	14785	14785	14785
3521.38	1	14785	14785	14785	14784	14784	14784	14784	14784	14784	14784	14784	14784	14784	14784	14784	14783	14783
3488.59	1	14783	14783	14783	14783	14783	14783	14783	14783	14783	14783	14783	14782	14782	14782	14782	14782	14782
3455.81	1	14782	14782	14782	14782	14782	14782	14782	14782	14782	14782	14782	14782	14782	14781	14781	14781	14781
3423.02	1	14781	14781	14781	14781	14781	14781	14781	14780	14780	14780	14780	14780	14780	14780	14780	14780	14780
3390.24	1	14780	14779	14779	14779	14779	14779	14779	14779	14779	14778	14778	14778	14778	14778	14778	14778	14777
3357.46	1	14777	14777	14777	14777	14777	14777	14776	14776	14776	14776	14776	14776	14775	14775	14775	14775	14775
3324.67	1	14775	14774															
3322.26	-1	14774	14774	14774	14774	14774	14774	14774	14774	14774	14774	14774	14774	14774	14774	14774	14774	14774
3314.07	-1	14774	14774	14774	14774	14774	14773	14773	14773	14773	14773	14773	14773	14773	14773	14773	14773	14773
3305.87	-1	14773	14773	14773	14773	14773	14773	14773	14773	14773	14773	14772	14772	14772	14772	14772	14772	14772
3297.67	-1	14772	14772	14772	14772	14772	14772	14772	14772	14772	14772	14771	14771	14771	14771	14771	14771	14771

Table IV.2. Continued.

cm^{-1}	*XE*	0	1	2	3	4	5	6	7	8	9	10	11	12	13	14	15	16
3289.48	-1	14771	14771	14771	14771	14771	14771	14771	14771	14771	14771	14771	14771	14770	14770	14770	14770	14770
3281.28	-1	14770	14770	14770	14770	14770	14770	14770	14770	14770	14770	14770	14770	14769	14769	14769	14769	14769
3273.09	-1	14769	14769	14769	14769	14769	14769	14769	14769	14769	14769	14769	14769	14769	14768	14768	14768	14768
3264.89	-1	14768	14768	14768	14768	14768	14768	14768	14768	14768	14768	14767	14767	14767	14767	14767	14767	14767
3256.69	-1	14767	14767	14767	14767	14767	14767	14767	14767	14767	14766	14766	14766	14766	14766	14766	14766	14766
3248.50	-1	14766	14766	14766	14766	14766	14766	14766	14765	14765	14765	14765	14765	14765	14765	14765	14765	14765
3240.30	-1	14765	14765	14764	14764	14764	14764	14764	14764	14764	14764	14764	14764	14764	14764	14763	14763	14763
3232.11	-1	14763	14763	14763	14763	14763	14763	14763	14762	14762	14762	14762	14762	14762	14762	14762	14762	14762
3223.91	-1	14761	14761	14761	14761	14761	14761	14761	14761	14761	14760	14760	14760	14760	14760	14760	14760	14760
3215.71	-1	14760	14760	14760	14759	14759	14759	14759	14759									
3211.38	0	14759	14758	14758	14758	14758	14757	14757	14757	14757	14756	14756	14756	14756	14755	14755	14755	14754
3194.98	0	14754	14754	14754	14753	14753	14753	14752	14752	14752	14752	14751	14751	14751	14750	14750	14750	14749
3178.59	0	14749	14749	14748	14748	14748	14747	14747	14746	14746	14745	14745	14745	14744	14744	14743	14743	14742
3162.20	0	14742	14741	14741	14740	14740	14739	14739	14738	14737	14737	14736	14736	14735	14734	14734	14733	14732
3145.81	0	14731	14731	14730	14729	14728	14727	14727	14726	14725	14724	14723	14722	14721	14720	14719	14717	14716
3129.42	0	14715	14714	14712	14711	14709	14708	14706	14704	14703	14701	14699	14697	14695	14692	14690	14688	14685
3113.02	0	14682	14679	14676	14673	14669	14665	14661	14656	14651	14645	14638	14630	14622	14613	14603	14593	14583
3096.63	0	14574	14567	14566	14577	14605	14653	14712	14765	14801	14819	14824	14821	14813	14804	14793	14782	14770
3080.24	0	14757	14744	14731	14717	14704	14693	14688	14695	14722	14765	14805	14827	14835	14835	14830	14823	14815
3063.85	0	14807	14799	14791	14783	14776	14769	14763	14758	14753	14748	14741	14732	14723	14712	14701	14689	14675
3047.46	0	14661	14645	14628	14610	14592	14574	14560	14552	14557	14582	14633	14716	14820				
3033.96	1	14977	15037	15049	15044	15031	15013	14995	14979	14965	14953	14942	14933	14925	14918	14913	14907	14903
3001.17	1	14899	14895	14892	14888	14885	14881	14878	14876	14873	14870	14868	14865	14863	14861	14859	14858	14856
2968.39	1	14854	14852	14850	14849	14848	14846	14845	14844	14843	14842	14841	14840	14840	14839	14838	14836	14835
2935.60	1	14834	14833	14832	14832	14831	14830	14829	14829	14828	14827	14826						
2915.36	0	14825	14825	14824	14823	14823	14822	14822	14822	14823	14823	14824	14824	14825	14824	14824	14824	14823
2898.96	0	14822	14822	14821	14820	14820	14819	14818	14817	14816	14816	14817	14818	14822	14825	14827	14828	14827
2881.61	1	14826	14825	14824	14823	14822	14821	14820	14820	14819	14818	14818	14817	14816	14816	14816	14816	14816
2848.82	1	14816	14816	14815	14815	14815	14814	14814	14813	14813	14812	14811	14811	14810	14810	14810	14811	14813
2816.04	1	14814	14814	14814	14814	14813	14813	14813	14812	14812	14811	14811	14811	14810	14810	14810	14809	14809
2783.25	1	14809	14809	14808	14808	14808	14808	14808	14807	14807	14807	14807	14806	14806	14806	14806	14806	14805
2750.47	1	14805	14805	14805	14805	14805	14804	14804	14804	14804	14804	14803	14803	14803	14803	14803	14803	14802
2717.69	1	14802	14802	14802	14802	14802	14801	14801	14801	14801	14801	14801	14800	14800	14800	14800	14800	14800
2684.90	1	14799	14799	14799	14799	14799	14798	14798	14798	14798	14797	14797	14797	14796	14796	14795	14795	
2655.01	0	14795	14796	14798	14799	14801	14801	14801	14801	14801	14800	14800	14800	14800	14799	14799	14799	14799
2638.62	0	14799	14798	14798	14798	14798	14798	14798	14797	14797	14797	14797	14797	14797	14796	14796	14796	14796
2622.23	0	14795	14795	14795	14795	14795	14795	14795	14795	14796	14796	14797	14797	14797	14797	14797	14797	14796
2605.84	0	14796	14796	14795	14795	14795	14794	14794	14794	14794	14794	14795	14797	14799	14800	14800		
2590.41	1	14800	14799	14799	14798	14798	14797	14797	14797	14797	14796	14796	14796	14796	14796	14796	14795	14795
2557.62	1	14795	14795	14795	14795	14795	14795	14795	14795	14795	14795	14794	14794	14794	14794	14794	14794	14793
2524.84	1	14793	14793	14793	14793	14793	14793	14793	14793	14793	14792	14792	14792	14792	14792	14792	14792	14791
2492.06	1	14791	14791	14791	14791	14791	14791	14791	14791	14791	14791	14791	14791	14791	14791	14791	14790	14790
2459.27	1	14790	14790	14790	14790	14790	14790	14789	14789	14789	14789	14789	14788	14788	14788	14788	14788	14788
2426.49	1	14788	14788	14787	14787	14787	14787	14786	14786	14786	14787	14787	14787	14787	14787	14787	14786	14786
2393.70	1	14786	14785	14785	14785	14785	14785	14786	14787	14788	14788	14788	14788	14787	14787	14787	14786	14786
2360.92	1	14786	14786	14785	14785	14785	14784	14784	14783	14783	14782	14782	14781	14780	14779	14778	14776	14775
2328.14	1	14776	14780	14789	14795	14797	14796	14795	14793	14792	14791	14791	14790	14789	14789	14788	14788	14787
2295.35	1	14787	14787	14786	14786	14786	14786	14785	14785	14786	14785	14785	14785	14785	14785	14784	14784	14784
2262.57	1	14784	14784	14783	14783	14783	14783	14782	14782	14782	14782	14782	14781	14781	14781	14781	14780	14780
2229.78	1	14780	14779	14779	14778	14778	14777	14776	14775	14774	14775							
2211.95	-1	14776	14777	14779	14780	14782	14783	14784	14785	14786	14786	14787	14787	14787	14787			
2203.75	1	14786	14786	14785	14784	14783	14783	14782	14782	14782	14781	14781	14781	14780	14780	14780	14780	14780
2170.97	1	14779	14779	14779	14779	14779	14778	14778	14778	14778	14778	14777	14777	14777	14777	14777	14777	14776
2138.18	1	14776	14776	14776	14776	14775	14775	14775	14775	14775	14774	14774	14774	14774	14774	14773	14773	14773
2105.40	1	14773	14772	14772	14772	14772	14772	14771	14771	14771	14771	14771	14770	14770	14770	14770	14769	14769
2072.61	1	14769	14769	14768	14768	14768	14767	14767	14766	14766	14766	14765	14765	14765	14764	14764	14764	14764
2039.83	1	14763	14763	14762	14762	14761	14761	14760	14760	14759	14758	14758	14757	14756	14755	14754	14753	14752
2007.05	1	14753	14754	14755	14755	14755	14753	14751	14749	14748	14747	14747	14746	14744	14742	14739	14735	14731
1974.26	1	14727	14723	14718	14715	14715	14721	14736	14757	14781	14799	14810	14815	14815	14813	14809	14806	14802
1941.48	1	14799	14796	14794	14793	14791	14789	14787	14785	14784	14782	14781	14779	14778	14777	14776	14775	14774
1908.69	1	14773	14772	14771	14769	14768	14767	14766	14765	14764	14763	14762	14761	14761	14760	14760	14759	14758
1875.91	1	14758	14758	14757	14756	14755	14754	14753	14751	14750	14748	14746	14745	14743	14741	14739	14736	14734
1843.13	1	14731	14728	14724	14720	14716	14710	14705	14699	14693	14688	14686	14689	14699	14720	14750	14785	14814
1810.34	1	14833	14842	14844	14842	14837	14832	14827	14822	14818	14815	14812	14809	14806	14803	14801	14798	14795
1777.56	1	14793	14791	14789	14787	14785	14783	14781	14780	14778	14776	14775	14776	14778	14781	14782	14781	14780
1744.77	1	14779	14777	14776	14775	14774	14773	14772	14771	14770	14769	14768	14767	14766	14765	14764	14763	
1715.37	-1	14763	14763	14763	14763	14763	14764	14764	14764	14764	14764	14764	14764	14764	14764	14763	14763	14763
1705.72	1	14762	14761	14761	14760	14759	14758	14757	14757	14756	14755	14754	14753	14752	14751	14749	14749	14749
1672.94	1	14750	14752	14754	14755	14755	14755	14753	14752	14751	14750	14749	14748	14747	14746	14745	14744	14744
1640.15	1	14743	14741	14740	14739	14738	14737	14735	14734	14732	14731	14730	14732	14736	14738	14737	14736	14735
1607.37	1	14734	14734	14733	14732	14731	14730	14728	14727	14726	14725	14725	14725	14725	14725	14724	14723	14722
1574.59	1	14720	14719	14717	14715	14712	14710	14707	14704									
1560.12	0	14703	14702	14701	14699	14698	14696	14694	14693	14691	14689	14687	14685	14682	14680	14678	14675	14673
1543.73	0	14670	14667	14665	14662	14660	14658	14656	14654	14653	14653	14654	14656	14658	14661	14665	14669	14674
1527.34	0	14678	14682	14686	14688	14690	14691	14691	14690	14689	14686	14683	14680	14677	14673	14668	14664	14659
1510.95	0	14654	14648	14643	14637	14631	14624	14618	14610	14603	14594	14586	14576	14566	14555	14543	14530	14516
1494.56	0	14500	14482	14462	14439	14414	14384	14351	14312	14266	14213	14153	14086	14020	13981	14024	14239	14671
1478.16	0	15133	15393	15490	15483	15428	15368	15326	15299	15269	15234	15199	15167	15139	15114	15092	15072	15054
1461.77	0	15038	15023	15010	14997	14986	14976	14967	14958	14950	14943	14936	14929	14924	14918	14913	14908	14903
1445.38	0	14899	14895	14891	14887	14883	14880	14876	14873	14870	14867	14864	14861	14859	14856	14854	14851	14849
1428.99	0	14847	14844	14842	14840	14838	14836	14834	14832	14831	14829	14827	14825	14823	14821	14820	14818	14816
1412.60	0	14814	14813	14811	14809	14807	14805	14803	14801	14799	14797	14794	14792	14790	14789	14788	14787	14789
1396.20	0	14791	14795	14801	14808	14814	14820	14824	14826	14828	14828	14827	14826	14825				

Table IV.2. Continued.

cm^{-1}	*XE*	0	1	2	3	4	5	6	7	8	9	10	11	12	13	14	15	16
1380.78	2	14818	14812	14807	14803	14799	14796	14792	14790	14787	14785	14782	14780	14778	14775	14773	14771	14769
1315.21	2	14768	14767	14767	14767	14766	14764	14762	14760	14757	14755	14753	14750	14748	14745	14742	14740	14739
1249.64	2	14741	14744	14743	14740	14738	14735	14733	14730	14728	14725	14722	14719	14717	14714	14711	14708	14705
1184.07	2	14706	14712	14724	14734	14737	14736	14732	14729	14728	14728	14731	14732	14731	14727	14724	14719	14715
1118.50	2	14710	14706	14701	14697	14692	14686	14681	14674	14668	14660	14652	14642	14632	14619	14603	14584	14560
1052.93	2	14528	14482															
1047.15	1	14450	14413	14369	14329	14327	14443	14687	14900	15005	15027	15010	14978	14946	14917	14891	14870	14851
1014.37	1	14836	14824	14819	14820	14815	14806	14797	14789	14783	14777	14772	14769	14768	14767	14763		
983.51	2	14756	14749	14744	14740	14739	14736	14733	14728	14723	14717	14712	14706	14700	14695	14689	14684	14678
917.94	2	14672	14666	14661	14655	14650	14644	14637	14631	14624	14618	14611	14603	14596	14588	14580	14574	14571
852.37	2	14573	14581	14585	14581	14574	14565	14554	14544	14532	14520	14507	14494	14480	14466	14451	14435	14419
786.81	2	14402	14384	14364	14343	14321	14297	14271	14243	14212	14178	14141	14100	14054	14003	13945	13879	13803
721.24	2	13715	13611	13487	13337	13152	12915	12604	12172									
692.31	1	11883	11519	11055	10472	09792	09123	08698	08843	09894	12193	15911	19953	22077	21908	20918	19977	19221
659.53	1	18633	18181	17830	17551	17322	17130	16966	16825	16702	16593	16497	16411	16334	16264	16200	16142	16089
626.74	1	16040	15995	15953	15914	15878	15845	15813	15784	15756	15730	15705	15682	15660	15639	15620	15601	15583
593.96	1	15566	15550	15535	15520	15506	15492	15480	15467	15455	15444	15433	15422	15412	15402	15393	15384	15375
561.18	1	15366	15358	15350	15342	15335	15328	15321	15314	15307	15301	15295	15289	15283	15277	15272	15266	15261
528.39	1	15256	15251	15246	15241	15236	15232	15227	15223	15219	15215	15211	15207	15203	15199	15195	15191	15188
495.61	1	15184	15181	15178	15174	15171	15168	15165	15162	15159	15156	15154	15151	15148	15146	15143	15140	15138
462.82	1	15135	15133	15131	15128	15126	15124	15122	15120	15118	15117	15115	15113	15110	15108	15106	15104	15103
430.04	1	15101	15099	15097	15095	15093	15092	15091	15089	15088	15087	15086	15085	15084	15083	15084	15085	15085
397.26	1	15084	15084	15083	15081	15080	15079	15078	15076	15075	15074	15072	15071	15070	15069	15067	15066	15065
364.47	1	15064	15063	15061	15060	15059	15058	15057	15056	15055	15054	15053	15052	15051	15050	15049	15048	15047
331.69	1	15046	15045	15044	15043	15042	15041	15040	15039	15038	15037	15036	15035	15034	15033	15033	15033	15034
298.90	1	15034	15034	15033	15032	15031	15030	15029	15028	15028	15027	15026	15026	15025	15024	15024	15023	15022
266.12	1	15022	15021	15021	15020	15020	15019	15019	15018	15017	15017	15016	15016	15015	15015	15014	15014	15013
233.34	1	15012	15012	15012	15011	15011	15010	15010	15009	15009	15008	15008	15007	15007	15006	15006	15005	15005
200.55	1	15004	15004	15003	15003	15003	15002	15002	15001	15001	15000	14999	14999	14998	14998	14998	14998	14998
167.77	1	14998	14998	14997	14997	14996	14996	14995	14994	14994	14993	14993	14992	14992	14991	14990	14990	14989
134.98	1	14989	14988	14987	14987	14986	14986	14985	14985	14985	14984	14984	14984	14984	14984	14984	14984	14985
102.20	1	14985	14985	14985	14986	14986	14987	14988	14989	14990	14991	14992	14993	14995	14997	14999	15000	15001
69.42	1	15001	15003	15006	15008	15010	15012	15013	15015	15017	15017	15021	15031	15039	15044	15047	15049	15050
36.63	1	15053	15056	15060	15065	15070	14801											

a. The column headed cm^{-1} contains the wavenumber of the first $n(\tilde{\nu})$ value in the row. The column headed *XE* contains the X-exponent for the row. The columns headed 0,1,2,⋯16, contain the $n(\tilde{\nu})$ values with the decimal point implicitly after the first digit in each value, and the headings give the indices of the $n(\tilde{\nu})$ values in the row. In a row which starts with $\tilde{\nu}(0)$, the wavenumber corresponding to the ordinate indexed J is $\tilde{\nu}(J) = \tilde{\nu}(0) - \frac{15798.002}{16384} \cdot J \cdot 2^{XE}$. Thus the entry indexed 16 in the first row of the table shows that $n = 1.4799$ at $\tilde{\nu} = 6225.09 - \frac{15798.002}{16384} \cdot 16 \cdot 2^0 = 6209.66\ cm^{-1}$, and the entry indexed 4 in the row which starts with 692.31 cm^{-1} shows that $n = 0.9794$ at $\tilde{\nu} = 684.60\ cm^{-1}$.

b. The $n(\tilde{\nu})$ values in the table can be interpolated to the original wavenumber spacing, 0.482117 cm^{-1}, and yield the original $n(\tilde{\nu})$ values accurate to 0.1%, via the 4-point spline interpolation program TRECOVER[44].

Appendix V

Optical Constants of Benzene-d_6

Table V.1. Imaginary refractive indices between 5000 and 550 cm^{-1} of liquid benzene-d_6 at 25 °C.[a,b]

cm^{-1}	*XE*	*YE*	0	1	2	3	4	5	6	7	8	9	10	11	12	13	14	15	16
5000.03	2	-7	0	0	1	3	5	7	8	8	10	14	16	14	10	7	4	2	2
4934.47	2	-7	3	1	2	4	12	18	14	11	7	5	5	15	31	29	24	23	30
4868.90	2	-7	42	49	50	52	69	98	97	78	58	45	39	41	33	23	17	14	13
4803.33	2	-7	15	17	16	14	11	11	14	19	22	21	18	16	18	25	44	74	72
4737.76	2	-7	49	32	21	15	13	13	16	18	18	19	19	18	16	17	21	29	31
4672.19	2	-7	33	39	41	44	49	59	73	86	111	141	169	201	201	180	167	176	238
4606.63	2	-7	370	463	391	280	206	166	147	144	140	145	171	225	294	320	310	295	292
4541.06	2	-7	318	355	391	434	491	573	699	873	1121	1492	2069	2946	4182	5664	7006	7771	7605
4475.49	2	-7	6352	4751	3588	3062	3077	3366	3535	3270	2804	2450	2264	2030	1739	1488	1189	949	903
4409.92	2	-7	1008	1122	1084	1021	1028	1107	891	680	577	549	514	408	313	241	198	176	188
4344.35	2	-7	236	263	234	198	177	160	135	116	100	93	84	69	60	56	59	65	62
4278.79	2	-7	53	45	38	36	36	32	27	22	19	16	15	14	14	15	17	19	20
4213.22	2	-7	23	30	41	64	72	77	94	95	102	119	137	144	131	125	128	116	105
4147.65	2	-7	113	156	243	288	236	189	144	103	77	64	60	59	60	60	60	55	49
4082.08	2	-7	47	53	76	113	121	106	94	83	75	70	71	85	102	125	139	130	111
4016.51	2	-7	92	74	63	58	55	55	60	68	81	86	88	90	101	109	112	121	137
3952.88	1	-7	147	158	172	197	235	303	416	490	539	515	449	397	371	361	352	340	329
3920.09	1	-7	327	341	363	362	347	336	333	340	356	378	385	373	368	396	486	717	984
3887.31	1	-7	908	787	674	578	507	474	474	495	512	507	487	474	480	498	516	528	531
3854.52	1	-7	528	528	545	579	623	691	761	866	1032	1302	1726	2348	3078	3539	3435	2986	2508
3821.74	1	-7	2161	2026	2122	2312	2363	2395	2626	3222	4335	5790	6427	5625	4365	3289	2476	1871	1434
3788.96	1	-7	1135	942	825	738	655	596	587	582	582	565	532	487	427	369	324	291	269
3756.17	1	-7	258	259	276	312	379	490	653	833	895	812	702	607	530	475	446	443	464
3721.46	2	-7	530	515	472	424	364	310	287	280	284	314	302	265	232	211	202	204	229
3655.89	2	-7	275	297	289	296	337	427	634	1107	1882	2273	1753	1154	787	579	482	434	406
3590.32	2	-7	388	410	546	730	661	466	349	296	278	294	358	403	363	309	254	216	193
3526.68	1	-7	183	177	174	176	181	186	190	190	184	172	158	144	133	126	120	117	116
3493.90	1	-7	116	113	107	102	98	96	96	100	108	114	108	105	107	117	141	184	204
3461.12	1	-7	199	201	224	252	250	231	219	221	229	225	216	210	208	215	243	307	411
3428.33	1	-7	466	432	395	375	363	365	350	312	275	245	221	207	203	207	207	207	213
3395.55	1	-7	223	243	273	308	327	327	320	310	299	292	291	298	316	344	380	418	453
3362.76	1	-7	477	485	477	454	424	394	367	347	334	326	326	334	354	387	435	487	560
3329.98	1	-7	697	949	1322	1594	1523	1268	1037	876	768	698	648	620	609	605	602	605	619
3297.20	1	-7	645	687	749	833	950	1106	1300	1522	1744	1949	2140	2370	2701	2935	2849	2601	2354
3264.41	1	-6	218	211	211	221	242	271	305	349	401	472	586	779	1093	1555	2087	2452	2434
3231.63	1	-6	2108	1717	1399	1145	909	702	537	417	336	294	276	269	249	214	181	154	133
3198.84	1	-7	1174	1046	935	842	766	707	666	638	618	602	594	596	606	626	661	707	745
3166.06	1	-7	761	766	775	796	841	919	1049	1241	1490	1705	1738	1616	1497	1465	1535	1677	1748
3133.28	1	-7	1671	1576	1521	1491	1480	1485	1491	1479	1485	1599	1957	2398	2329	2121	1972	1866	1779
3100.49	1	-7	1713	1630	1540	1483	1466	1479	1514	1592	1738	2000	2423	2995	3534	3664	3245	2662	2190
3067.71	1	-7	1874	1675	1554	1500	1522	1629	1820	2100	2423	2663	2681	2471	2149	1827	1552	1334	1164
3034.93	1	-7	1021	902	807	732	675	630	598	575	559	549	546	552	575	624	710	841	1002
3002.14	1	-7	1137	1167	1094	973	849	744	662	601	558	530	514	506	508	518	536	571	636
2969.36	1	-7	761	1037	1207	1023	897	872	904	959	994	983	964	965	992	1039	1085	1083	1050
2936.57	1	-7	1010	971	940	922	917	929	966	1031	1094	1094	1022	928	848	791	749	715	690
2903.79	1	-7	677	675	677	688	711	734	745	731	762	808	881	997	1159	1329	1445	1507	1581
2871.01	1	-7	1721	1966	2360	2985	4017	5819	8241	8960	7095	5073	3830	3230	3284	3788	3414	2754	2335
2838.22	1	-7	2227	2397	2861	3713	4269	3643	2840	2179	1725	1421	1190	997	850	746	679	635	616
2803.51	2	-7	603	674	800	849	797	754	813	1059	1311	1162	878	680	563	483	419	358	311
2737.94	2	-7	283	269	263	262	246	237	233	222	210	201	190	183	182	184	187	192	202
2672.37	2	-7	213	227	255	305	357	402	414	393	398	429	475	537	670	1006	1694	2288	1905
2606.81	2	-7	1301	899	683	548	453	395	375	411	497	529	483	436	405	377	368	352	351
2544.13	0	-7	349	346	342	339	335	332	329	326	325	324	324	325	328	333	346	370	410
2527.74	0	-7	475	581	763	1083	1622	2276	2601	2508	2238	1914	1596	1326	1113	942	804	697	616
2511.35	0	-7	555	509	475	451	436	428	427	428	428	424	419	417	416	416	415	415	416
2492.06	2	-7	435	428	424	441	469	502	539	587	664	758	887	1133	1155	1046	1055	1101	1199
2429.39	0	-7	1231	1266	1304	1347	1391	1438	1486	1536	1584	1633	1682	1730	1781	1832	1886	1943	2007
2412.99	0	-7	2078	2155	2244	2344	2456	2585	2731	2899	3090	3307	3557	3847	4185	4589	4909	5406	6076
2396.60	0	-6	702	837	1023	1287	1665	2196	2874	3530	3847	3705	3310	2869	2482	2178	1933	1736	1625
2380.21	0	-6	1625	1740	1967	2261	2481	2433	2171	1871	1603	1392	1238	1137	1083	1074	1109	1191	1308
2362.85	1	-6	1445	1301	1088	926	827	779	776	808	875	959	1012	994	969	1002	1109	1162	1090
2330.07	1	-6	1047	1041	1028	1028	1047	1081	1127	1189	1267	1361	1473	1609	1778	1990	2256	2727	3123
2297.29	1	-5	358	417	495	606	787	1118	1740	2855	4290	4841	4164	3286	2740	2680	3026	3012	2457
2262.57	2	-5	1459	941	652	485	377	292	233	193	166	140	120	105	92	81	72	65	63
2197.01	2	-7	6629	5540	4716	4070	3590	3312	3123	2804	2513	2343	2430	3097	3745	3037	2500	2138	1811
2131.44	2	-7	1648	1496	1288	1121	980	912	840	754	671	592	512	449	403	366	334	306	282
2065.87	2	-7	263	251	254	262	263	243	229	244	290	310	266	223	203	199	207	228	281
2002.23	1	-7	347	488	781	1315	1863	1839	1483	1163	927	729	574	468	401	364	344	333	325
1967.52	2	-7	305	299	317	357	383	370	363	373	398	443	507	593	687	787	954	1461	2800
1903.88	1	-7	3917	4121	3330	2541	1968	1590	1363	1263	1232	1212	1223	1286	1410	1605	1916	2429	3259

Table V.1. Continued.

cm^{-1}	*XE*	*YE*	0	1	2	3	4	5	6	7	8	9	10	11	12	13	14	15	16
1871.10	1	-7	4602	6440	7432	7383	7956	8588	7312	5360	3905	3041	2576	2281	2048	1924	1777	1612	1473
1838.31	1	-7	1359	1258	1165	1083	1010	950	901	860	828	800	775	759	750	747	761	773	785
1806.49	0	-7	817	878	980	1147	1421	1874	2579	3403	3841	3684	3208	2681	2227	1880	1637	1464	1311
1790.10	0	-7	1155	1016	900	806	732	673	625	585	552	525	503	486	474	467	464	467	476
1773.71	0	-7	491	512	533	550	553	546	535	523	514	508	502	497	491	485	479	474	470
1754.42	2	-7	449	440	458	489	520	556	608	703	811	875	977	1132	1412	1990	2910	4691	6950
1690.78	1	-6	710	666	659	744	926	1102	1023	801	655	582	535	498	471	451	442	446	463
1658.00	1	-6	480	478	455	429	406	393	391	402	428	470	529	605	704	817	984	1263	1757
1625.22	1	-5	268	438	717	1007	1048	840	598	422	308	228	170	130	102	82	69	61	55
1592.43	1	-7	5183	4934	4807	4690	4638	4547	4485	4530	4763	5365	6920	9599	9832	8468	7818	7656	7803
1559.65	1	-6	831	924	1077	1324	1705	1982	1694	1247	940	753	653	571	498	450	418	392	373
1526.86	1	-7	3567	3395	3227	3065	2898	2745	2618	2514	2444	2409	2413	2486	2628	2771	2812	2774	2748
1494.08	1	-6	276	283	296	313	334	362	404	466	554	663	756	825	920	1079	1333	1724	2335
1461.30	1	-5	334	491	715	963	1107	1046	854	650	486	367	281	215	166	129	102	82	68
1428.51	1	-6	589	527	483	457	445	439	444	463	498	545	613	710	809	911	996	1089	1287
1395.73	1	-6	1756	2468	2640	2614	2296	1644	1174	881	706	603	541	508	488	475	469	475	491
1362.94	1	-5	52	56	62	70	80	93	109	129	154	189	243	332	444	618	972	1741	3292
1331.12	0	-5	4095	4393	4089	3454	2763	2136	1639	1305	1104	953	795	652	538	449	379	325	281
1313.77	1	-6	2191	1732	1402	1172	1006	884	806	750	722	702	691	673	660	649	633	612	581
1280.98	1	-7	5434	5086	4885	4878	4454	3947	3570	3293	3080	2910	2772	2642	2524	2403	2277	2145	2022
1246.27	2	-7	1825	1690	1607	1613	1810	2191	2280	1984	1762	1785	2164	3413	3515	3062	3686	5399	8446
1180.70	2	-6	1140	1268	1783	3250	5513	6156	4747	3094	1857	1104	693	462	341	278	231	205	192
1115.14	2	-7	1802	1745	1721	1637	1554	1525	1507	1523	1567	1621	1678	1754	1856	2010	2281	2658	2639
1049.57	2	-6	249	247	258	281	311	350	406	520	777	1208	1288	980	746	633	603	628	726
985.93	1	-6	852	935	903	923	978	1054	1135	1207	1243	1240	1215	1187	1173	1182	1229	1336	1524
953.15	1	-6	1776	1968	2010	2065	2229	2186	1884	1637	1493	1456	1591	1922	2160	2034	1931	1874	1735
920.36	1	-6	1528	1340	1199	1105	1052	1030	1028	1042	1068	1105	1149	1203	1265	1335	1415	1503	1604
885.65	2	-5	185	219	267	332	395	408	377	351	342	350	372	400	443	496	604	814	1261
822.01	1	-4	163	224	338	562	953	1224	967	598	373	252	183	140	112	93	80	68	58
787.30	2	-6	4510	3551	2865	2377	2026	1767	1565	1412	1300	1339	1172	1052	1009	953	907	878	858
723.66	1	-6	854	855	864	886	936	1051	1368	1712	1419	1204	1105	1068	1060	1069	1093	1124	1166
688.95	2	-6	1287	1469	1748	2070	2578	3403	4284	4368	3598	2790	2223	1858	1627	1480	1401	1357	1351
623.38	2	-6	1387	1484	1762	1878	1845	1992	2161	2297	2457	2688	3031	3466	3620	3540	3541	3672	3914
557.81	2	-6	4231	4668	5257														

---

[a] See footnote a to Table IV.1.

[b] The $k(\tilde{\nu})$ values in the table can be interpolated to the original wavenumber spacing, 0.482117 cm^{-1}, and yield the original $k(\tilde{\nu})$ values accurate 1% via the 4-point spline interpolation program TRECOVER[44].

Table V.2. Real refractive indices between 5000 and 550 cm^{-1} of liquid benzene-d$_6$ at 25 °C.[a,b]

cm^{-1}	*XE*	0	1	2	3	4	5	6	7	8	9	10	11	12	13	14	15	16
5000.03	2	14776	14776	14776	14776	14776	14776	14776	14776	14776	14776	14776	14776	14776	14776	14776	14776	14776
4934.47	2	14776	14776	14776	14776	14776	14776	14776	14776	14776	14776	14776	14776	14776	14776	14776	14776	14776
4868.90	2	14776	14776	14776	14776	14776	14776	14776	14776	14776	14776	14776	14776	14776	14776	14776	14776	14776
4803.33	2	14776	14776	14776	14776	14776	14776	14776	14775	14775	14775	14775	14775	14775	14775	14775	14775	14775
4737.76	2	14775	14775	14775	14775	14775	14775	14775	14775	14775	14775	14775	14775	14775	14775	14775	14775	14775
4672.19	2	14775	14775	14775	14775	14775	14775	14775	14775	14775	14775	14775	14775	14775	14775	14775	14775	14775
4606.63	2	14775	14775	14775	14775	14775	14775	14775	14774	14774	14774	14774	14774	14774	14774	14774	14774	14774
4541.06	2	14774	14774	14773	14773	14773	14773	14773	14772	14772	14772	14771	14771	14771	14771	14772	14774	14776
4475.49	2	14778	14778	14778	14777	14777	14777	14777	14778	14778	14778	14778	14778	14778	14778	14778	14777	14777
4409.92	2	14777	14777	14777	14777	14777	14777	14777	14777	14777	14777	14777	14777	14777	14777	14776	14776	14776
4344.35	2	14776	14776	14776	14776	14776	14776	14776	14776	14776	14776	14776	14776	14776	14776	14776	14776	14776
4278.79	2	14776	14776	14776	14775	14775	14775	14775	14775	14775	14775	14775	14775	14775	14775	14775	14775	14775
4213.22	2	14775	14775	14775	14775	14775	14775	14775	14775	14775	14775	14775	14775	14775	14775	14775	14775	14775
4147.65	2	14775	14775	14775	14775	14775	14775	14775	14775	14775	14775	14775	14775	14775	14775	14775	14775	14775
4082.08	2	14774	14774	14774	14774	14774	14774	14774	14774	14774	14774	14774	14774	14774	14774	14774	14774	14774
4016.51	2	14774	14774	14774	14774	14774	14774	14774	14774	14774	14774	14774	14774	14774	14774	14774	14774	14774
3952.88	1	14774	14773	14773	14773	14773	14773	14773	14773	14773	14774	14774	14774	14774	14774	14774	14773	14773
3920.09	1	14773	14773	14773	14773	14773	14773	14773	14773	14773	14773	14773	14773	14773	14773	14773	14773	14773
3887.31	1	14773	14773	14773	14773	14773	14773	14773	14773	14773	14773	14773	14773	14773	14773	14773	14773	14773
3854.52	1	14773	14773	14772	14772	14772	14772	14772	14772	14772	14771	14771	14771	14771	14772	14773	14773	14773
3821.74	1	14773	14773	14773	14773	14773	14772	14772	14772	14772	14772	14774	14776	14777	14777	14777	14777	14776
3788.96	1	14776	14776	14776	14775	14775	14775	14775	14775	14775	14775	14775	14775	14775	14775	14774	14774	14774
3756.17	1	14774	14774	14774	14774	14774	14774	14774	14774	14774	14774	14774	14774	14774	14774	14774	14774	14774
3721.46	2	14774	14774	14774	14774	14774	14774	14774	14774	14773	14773	14773	14773	14773	14773	14773	14773	14773
3655.89	2	14773	14773	14773	14773	14773	14772	14772	14772	14772	14773	14774	14774	14774	14774	14773	14773	14773
3590.32	2	14773	14773	14773	14773	14773	14773	14773	14773	14773	14773	14773	14773	14773	14773	14773	14773	14773
3526.68	1	14773	14773	14772	14772	14772	14772	14772	14772	14772	14772	14772	14772	14772	14772	14772	14772	14772
3493.90	1	14772	14772	14772	14772	14772	14772	14772	14772	14772	14772	14772	14772	14772	14772	14772	14772	14772
3461.12	1	14772	14772	14772	14772	14772	14772	14772	14772	14771	14771	14771	14771	14771	14771	14771	14771	14771
3428.33	1	14771	14771	14771	14771	14771	14771	14771	14771	14771	14771	14771	14771	14771	14771	14771	14771	14771
3395.55	1	14771	14771	14771	14771	14771	14771	14771	14771	14771	14771	14771	14770	14770	14770	14770	14770	14770
3362.76	1	14770	14770	14770	14770	14770	14770	14770	14770	14770	14770	14770	14770	14770	14769	14769	14769	14769
3329.98	1	14769	14769	14769	14769	14770	14770	14770	14770	14770	14769	14769	14769	14769	14769	14769	14769	14769
3297.20	1	14768	14768	14768	14768	14768	14767	14767	14767	14767	14767	14767	14767	14767	14767	14767	14767	14767
3264.41	1	14767	14767	14766	14766	14765	14765	14764	14763	14763	14762	14760	14759	14758	14758	14760	14766	14773
3231.63	1	14778	14781	14782	14782	14782	14782	14781	14780	14779	14778	14777	14777	14777	14777	14776	14776	14776
3198.84	1	14775	14775	14775	14774	14774	14774	14774	14773	14773	14773	14773	14773	14773	14772	14772	14772	14772
3166.06	1	14772	14772	14772	14771	14771	14771	14771	14771	14771	14771	14771	14771	14771	14771	14771	14771	14771
3133.28	1	14771	14771	14771	14771	14771	14771	14771	14771	14771	14770	14770	14771	14771	14771	14771	14771	14771
3100.49	1	14771	14771	14771	14771	14771	14770	14770	14770	14770	14770	14770	14770	14770	14771	14772	14772	14772
3067.71	1	14772	14771	14771	14771	14771	14771	14770	14770	14771	14771	14771	14772	14772	14772	14772	14772	14772
3034.93	1	14772	14771	14771	14771	14771	14771	14771	14771	14771	14770	14770	14770	14770	14770	14770	14770	14770
3002.14	1	14770	14770	14770	14770	14770	14770	14770	14770	14770	14770	14770	14770	14769	14769	14769	14769	14769
2969.36	1	14769	14769	14769	14769	14769	14769	14769	14769	14769	14769	14769	14769	14769	14769	14769	14769	14769
2936.57	1	14769	14769	14769	14769	14769	14768	14768	14768	14768	14768	14768	14768	14768	14768	14768	14768	14768
2903.79	1	14768	14768	14768	14768	14767	14767	14767	14767	14767	14767	14767	14766	14766	14766	14766	14766	14766
2871.01	1	14765	14765	14765	14764	14764	14763	14765	14768	14770	14771	14770	14770	14769	14769	14770	14770	14769
2838.22	1	14769	14768	14768	14768	14769	14770	14771	14770	14770	14770	14770	14770	14769	14769	14769	14769	14769
2803.51	2	14768	14768	14768	14768	14768	14767	14767	14767	14767	14767	14767	14767	14767	14767	14767	14767	14766
2737.94	2	14766	14766	14766	14766	14766	14766	14765	14765	14765	14765	14765	14765	14765	14764	14764	14764	14764
2672.37	2	14764	14764	14763	14763	14763	14763	14763	14763	14762	14762	14762	14762	14761	14761	14761	14761	14762
2606.81	2	14762	14762	14762	14761	14761	14761	14761	14760	14760	14760	14760	14759	14759	14759	14759	14758	14758
2544.13	0	14758	14758	14758	14758	14758	14758	14757	14757	14757	14757	14757	14757	14757	14757	14757	14756	14756
2527.74	0	14756	14756	14755	14755	14755	14755	14756	14756	14757	14757	14757	14757	14757	14757	14757	14757	14756
2511.35	0	14756	14756	14756	14756	14756	14756	14755	14755	14755	14755	14755	14755	14755	14755	14754	14754	14754
2492.06	2	14754	14753	14753	14752	14752	14751	14751	14750	14750	14749	14748	14748	14747	14746	14746	14745	14744
2429.39	0	14743	14743	14743	14743	14742	14742	14742	14741	14741	14741	14740	14740	14740	14739	14739	14739	14738
2412.99	0	14738	14737	14737	14736	14736	14735	14735	14734	14733	14733	14732	14731	14730	14729	14728	14727	14726
2396.60	0	14724	14722	14720	14718	14717	14716	14717	14722	14730	14738	14743	14745	14746	14746	14745	14743	14742
2380.21	0	14739	14737	14736	14737	14740	14744	14747	14748	14747	14746	14745	14744	14742	14740	14739	14738	14737
2362.85	1	14739	14740	14740	14738	14736	14734	14732	14730	14728	14727	14726	14725	14724	14722	14720	14719	14718
2330.07	1	14716	14714	14712	14709	14706	14703	14699	14695	14691	14687	14682	14676	14670	14663	14655	14647	14638
2297.29	1	14627	14614	14597	14576	14547	14510	14471	14452	14524	14695	14826	14866	14857	14834	14851	14924	14972
2262.57	2	14974	14949	14924	14905	14890	14878	14867	14858	14851	14845	14839	14834	14830	14827	14823	14820	14817
2197.01	2	14815	14814	14812	14810	14808	14806	14805	14803	14802	14800	14799	14798	14797	14797	14796	14796	14795
2131.44	2	14794	14793	14792	14792	14791	14790	14790	14789	14788	14788	14787	14787	14786	14786	14785	14785	14784
2065.87	2	14784	14783	14783	14782	14782	14782	14781	14781	14781	14780	14780	14780	14779	14779	14778	14778	14777
2002.23	1	14777	14777	14777	14776	14777	14777	14778	14777	14777	14777	14777	14777	14777	14776	14776	14776	14776
1967.52	2	14775	14775	14775	14774	14774	14774	14774	14773	14773	14772	14772	14772	14771	14771	14770	14770	14769
1903.88	1	14770	14771	14772	14772	14772	14771	14771	14770	14770	14770	14769	14769	14769	14768	14767	14767	14766
1871.10	1	14766	14766	14768	14769	14769	14771	14773	14774	14774	14773	14773	14772	14772	14771	14771	14771	14771
1838.31	1	14770	14770	14770	14770	14770	14769	14769	14769	14769	14768	14768	14768	14768	14768	14767	14767	14767
1806.49	0	14766	14766	14766	14766	14765	14765	14765	14765	14766	14767	14768	14768	14768	14768	14768	14768	14767
1790.10	0	14767	14767	14767	14767	14767	14767	14766	14766	14766	14766	14766	14766	14766	14765	14765	14765	14765
1773.71	0	14765	14765	14765	14765	14765	14765	14764	14764	14764	14764	14764	14764	14764	14764	14764	14764	14763
1754.42	2	14763	14763	14762	14762	14761	14761	14760	14759	14759	14758	14758	14757	14756	14755	14753	14752	14753
1690.78	1	14754	14754	14754	14753	14753	14755	14758	14758	14758	14757	14757	14756	14755	14755	14754	14753	14753
1658.00	1	14752	14752	14751	14751	14750	14748	14747	14746	14744	14742	14740	14738	14735	14732	14728	14723	14716
1625.22	1	14708	14701	14702	14727	14769	14797	14807	14806	14802	14798	14794	14790	14786	14783	14780	14777	14775

Table V.2. Continued.

cm^{-1}	*XE*	0	1	2	3	4	5	6	7	8	9	10	11	12	13	14	15	16
1592.43	1	14773	14771	14770	14769	14767	14766	14765	14764	14762	14761	14759	14760	14762	14762	14761	14760	14759
1559.65	1	14758	14757	14756	14756	14757	14762	14767	14769	14768	14767	14765	14764	14764	14763	14762	14761	14760
1526.86	1	14759	14759	14758	14757	14757	14756	14755	14755	14754	14753	14752	14751	14750	14750	14749	14748	14747
1494.08	1	14746	14745	14744	14743	14741	14740	14738	14736	14734	14732	14731	14728	14725	14722	14717	14712	14705
1461.30	1	14699	14694	14695	14710	14741	14774	14795	14803	14803	14801	14797	14793	14789	14784	14781	14777	14774
1428.51	1	14771	14768	14766	14764	14761	14760	14758	14756	14754	14752	14750	14749	14747	14746	14745	14743	14740
1395.73	1	14738	14740	14747	14751	14757	14759	14757	14754	14751	14748	14745	14743	14740	14738	14735	14732	14729
1362.94	1	14726	14723	14719	14715	14710	14705	14700	14693	14685	14675	14663	14648	14631	14606	14571	14531	14550
1331.12	0	14628	14744	14853	14925	14960	14970	14962	14946	14932	14924	14917	14908	14899	14890	14881	14873	14866
1313.77	1	14854	14845	14836	14829	14823	14818	14813	14809	14806	14803	14800	14798	14796	14794	14793	14791	14790
1280.98	1	14789	14788	14786	14785	14784	14783	14782	14781	14780	14779	14778	14777	14776	14775	14774	14774	14773
1246.27	2	14771	14769	14768	14766	14765	14763	14762	14761	14759	14758	14755	14754	14753	14751	14748	14744	14742
1180.70	2	14740	14737	14730	14725	14734	14762	14782	14787	14785	14780	14775	14771	14767	14765	14762	14760	14758
1115.14	2	14757	14755	14754	14753	14752	14750	14749	14748	14747	14746	14744	14743	14742	14741	14740	14739	14738
1049.57	2	14737	14735	14734	14733	14731	14729	14728	14725	14723	14724	14728	14729	14728	14725	14723	14720	14718
985.93	1	14717	14717	14717	14716	14715	14714	14713	14713	14713	14713	14713	14712	14711	14709	14708	14706	14705
953.15	1	14704	14705	14706	14706	14707	14710	14711	14710	14708	14705	14702	14701	14703	14705	14705	14705	14706
920.36	1	14705	14704	14702	14699	14697	14694	14692	14690	14688	14685	14683	14681	14678	14676	14674	14671	14669
885.65	2	14664	14658	14653	14649	14649	14652	14650	14643	14634	14623	14611	14596	14576	14552	14515	14466	14390
822.01	1	14340	14271	14186	14110	14201	14709	15204	15315	15259	15185	15121	15070	15030	14997	14972	14953	14932
787.30	2	14902	14879	14860	14843	14829	14817	14807	14798	14789	14781	14776	14769	14763	14757	14751	14745	14740
723.66	1	14737	14734	14731	14728	14725	14721	14718	14720	14721	14719	14716	14713	14710	14707	14704	14701	14698
688.95	2	14692	14686	14680	14675	14669	14665	14669	14677	14681	14679	14672	14665	14657	14649	14641	14632	14624
623.38	2	14615	14605	14595	14589	14578	14567	14556	14544	14532	14518	14503	14490	14477	14460	14439	14415	14389
557.81	2	14359	14326	14288														

[a,b] See footnotes a and b to Table IV.2.

Appendix VI

Optical Constants of Benzene-h$_6$ and Benzene-d$_6$ Mixtures

Table VI.1. Imaginary refractive indices between 6500 and 450 cm^{-1} of 10.01% liquid benzene-h$_6$ in liquid benzene-d$_6$ at 25 °C.[a,b]

cm^{-1}	*XE*	*YE*	0	1	2	3	4	5	6	7	8	9	10	11	12	13	14	15	16
6499.90	3	-7	41	38	36	32	32	29	28	26	24	24	23	21	21	21	22	20	19
6368.76	3	-7	17	17	16	16	18	15	17	14	13	12	10	8	5	4	3	4	2
6237.63	3	-7	0	0	0	0	0	6	11	13	18	19	23	35	37	47	35	32	28
6106.49	3	-7	22	18	27	12	2	0	1	5	10	23	43	66	81	130	177	291	420
5975.36	3	-7	308	241	190	169	138	106	151	133	221	163	103	73	89	83	81	73	56
5844.22	3	-7	36	22	18	23	28	24	19	16	20	24	26	12	5	8	4	0	1
5713.09	3	-7	12	15	25	28	20	9	5	6	7	2	1	1	2	12	15	9	4
5581.95	3	-7	6	7	3	4	7	19	29	26	20	18	9	4	1	0	0	2	2
5450.81	3	-7	3	8	17	26	22	16	19	18	14	10	33	34	36	48	48	39	35
5319.68	3	-7	36	29	22	27	29	36	38	30	27	20	22	15	11	8	8	5	4
5188.54	3	-7	3	2	1	1	6	12	16	13	14	24	19	19	38	44	26	16	10
5057.41	3	-7	8	5	1	1	0	0	3	7	8	10	13	14	18	17	10	8	7
4926.27	3	-7	8	15	15	10	12	33	26	37	53	57	102	80	47	42	25	18	17
4798.99	2	-7	19	19	18	18	22	25	28	31	28	26	26	27	36	58	85	79	61
4733.42	2	-7	48	42	41	42	47	54	61	71	88	106	146	201	191	180	209	316	542
4667.86	2	-7	555	357	254	222	259	390	510	522	438	365	389	520	552	420	368	423	569
4602.29	2	-7	625	513	419	433	578	635	518	403	326	303	318	358	366	366	390	431	433
4536.72	2	-7	421	425	453	496	574	688	851	1086	1442	1998	2835	4027	5419	6715	7444	7187	5860
4471.15	2	-7	4310	3257	2827	2877	3170	3282	2992	2555	2249	2099	1880	1616	1380	1097	905	905	1037
4405.58	2	-7	1101	1035	976	1004	1031	815	680	647	609	533	411	314	246	207	189	206	250
4340.02	2	-7	264	232	201	183	166	146	131	119	116	107	97	92	91	94	98	95	91
4274.45	2	-7	90	95	115	151	147	122	107	104	107	101	93	91	93	106	128	128	127
4208.88	2	-7	136	144	180	221	230	212	192	196	226	263	250	222	211	209	201	193	200
4143.31	2	-7	243	325	354	310	279	247	223	218	226	249	292	359	432	481	547	683	837
4077.74	2	-7	842	877	1086	1479	2289	3272	3253	2136	1336	879	631	514	487	534	516	401	321
4014.10	1	-7	291	268	250	235	219	205	193	184	178	175	174	177	184	195	205	210	212
3981.32	1	-7	212	205	197	193	189	190	195	210	245	297	326	352	391	400	374	344	325
3948.54	1	-7	321	332	366	447	575	689	824	793	673	587	534	499	469	443	426	422	433
3915.75	1	-7	444	433	417	407	407	416	431	446	445	430	432	472	580	830	984	870	765
3882.97	1	-7	668	591	535	512	516	536	546	533	512	501	510	526	542	553	554	553	557
3850.18	1	-7	574	604	642	690	758	865	1035	1302	1715	2294	2913	3215	3032	2607	2196	1929	1863
3817.40	1	-7	1993	2141	2166	2230	2495	3090	4102	5224	5602	4869	3741	2812	2129	1637	1295	1066	913
3784.62	1	-7	811	729	656	605	588	592	599	591	568	522	461	408	368	339	321	314	320
3751.83	1	-7	342	384	458	575	740	896	914	824	728	646	580	536	517	523	552	591	617
3719.05	1	-7	616	602	588	576	566	560	558	559	573	620	731	930	1051	921	776	715	714
3686.27	1	-7	707	654	576	505	450	408	375	350	336	330	331	330	323	322	331	350	374
3653.48	1	-7	397	424	474	580	789	1093	1200	1024	855	784	797	879	1041	1295	1636	1953	2131
3620.70	1	-7	2123	1939	1700	1502	1346	1199	1046	889	762	668	602	555	520	492	469	454	445
3587.91	1	-7	451	474	534	597	657	742	717	625	530	454	399	361	335	318	306	302	305
3555.13	1	-7	318	344	378	403	407	390	366	341	316	289	265	246	231	218	207	198	194
3522.35	1	-7	193	198	208	219	224	216	204	191	178	168	160	153	148	145	146	150	155
3489.56	1	-7	163	165	154	143	139	139	145	145	140	139	144	158	185	226	240	243	258
3456.78	1	-7	294	333	350	358	366	369	359	334	308	288	276	277	301	364	462	495	457
3423.99	1	-7	428	412	406	405	381	344	310	282	263	254	255	262	262	263	265	271	284
3391.21	1	-7	308	333	340	334	323	311	299	292	291	299	316	343	376	410	440	457	462
3358.43	1	-7	452	430	402	375	353	337	326	320	320	329	349	384	430	481	558	704	964
3325.64	1	-7	1304	1471	1341	1109	919	790	703	646	606	586	579	575	580	590	607	640	683
3292.86	1	-7	742	826	938	1091	1276	1483	1681	1867	2043	2275	2558	2695	2572	2366	2182	2064	2031
3260.07	1	-6	206	218	239	266	297	337	393	472	594	787	1074	1450	1826	2099	2154	1880	1511
3227.29	1	-6	1223	992	782	606	472	376	313	276	261	251	229	199	173	153	137	125	115
3194.51	1	-7	1062	992	943	908	888	874	864	855	857	883	911	968	1008	1049	1105	1124	1132
3161.72	1	-7	1159	1177	1235	1307	1463	1674	1921	2122	2155	2049	1981	2005	2102	2243	2281	2230	2200
3128.94	1	-7	2206	2231	2282	2370	2489	2602	2785	3077	3640	4129	4188	4250	4460	4829	5438	6582	8749
3096.15	1	-6	1286	2027	3000	3202	2502	1821	1416	1194	1063	1063	1204	1550	2296	2485	1828	1362	1105
3063.37	1	-6	963	872	840	865	859	841	862	904	968	1095	1394	2006	3106	4551	5289	4783	3830
3030.59	1	-6	3005	2353	1829	1434	1149	948	800	686	601	539	497	467	451	439	433	418	395
2997.80	1	-7	3635	3275	2959	2672	2452	2280	2126	2014	1934	1856	1798	1732	1649	1608	1620	1699	1926
2965.02	1	-7	1914	1703	1582	1551	1572	1612	1627	1614	1599	1580	1560	1555	1544	1491	1424	1359	1303
2932.23	1	-7	1260	1231	1215	1216	1239	1285	1318	1290	1220	1163	1156	1214	1325	1418	1366	1233	1128
2899.45	1	-7	1066	1046	1078	1186	1418	1852	2313	2108	1722	1600	1613	1652	1664	1672	1724	1857	2101
2866.67	1	-7	2491	3104	4126	5843	7802	8033	6232	4564	3574	3143	3350	3685	3166	2598	2288	2251	2455
2833.88	1	-7	2933	3743	3920	3288	2655	2238	2043	1950	1759	1463	1219	1057	936	842	779	731	702
2801.10	1	-7	705	738	785	829	855	853	830	802	780	772	786	836	932	1072	1207	1259	1202
2768.31	1	-7	1078	943	824	729	656	601	557	519	486	457	427	395	368	345	327	313	305
2735.53	1	-7	300	296	293	291	291	285	277	270	266	265	264	262	257	251	245	241	239
2702.75	1	-7	236	233	230	228	227	228	230	232	236	241	246	251	256	261	267	273	280
2669.96	1	-7	290	304	323	350	386	445	541	710	1062	1292	961	735	632	571	524	502	497
2637.18	1	-7	501	510	526	549	584	640	733	883	1118	1466	1913	2348	2532	2312	1937	1595	1325
2604.39	1	-7	1126	1007	981	1076	1326	1342	1019	789	650	563	512	491	494	520	558	603	630
2571.61	1	-7	614	578	545	521	508	503	500	503	520	524	492	457	434	423	413	402	390

Table VI.1. Continued

cm^{-1}	*XE*	*YE*	0	1	2	3	4	5	6	7	8	9	10	11	12	13	14	15	16
2539.79	0	-7	384	379	375	372	370	369	369	370	373	380	397	426	474	551	679	900	1285
2523.40	0	-7	1864	2362	2427	2230	1954	1662	1399	1188	1021	886	776	691	626	576	538	509	490
2507.01	0	-7	478	472	471	471	467	462	459	457	457	458	456	456	457	461	468	476	483
2489.65	1	-7	490	496	510	519	504	489	484	488	499	519	547	562	565	577	597	626	662
2456.87	1	-7	706	762	836	936	1047	1076	998	932	901	996	1038	1057	1091	1134	1205	1278	1349
2424.08	1	-6	143	151	159	171	186	204	223	243	265	288	319	360	411	485	606	845	1324
2391.30	1	-6	2274	3383	3202	2447	1906	1594	1579	1928	2259	1893	1404	1112	1007	1058	1249	1310	1147
2358.51	1	-6	961	830	751	716	720	756	818	900	929	909	895	942	1053	1074	1032	1054	1113
2325.73	1	-6	1177	1158	1095	1072	1088	1127	1187	1274	1387	1526	1713	1935	2202	2518	2877	3317	3895
2292.95	1	-5	470	586	780	1131	1776	2845	3937	4146	3518	2799	2410	2479	2803	2622	2074	1583	1236
2260.16	1	-6	9896	8095	6727	5692	4899	4276	3771	3326	2925	2588	2313	2083	1894	1734	1599	1471	1367
2227.38	1	-6	1263	1168	1083	1010	950	894	855	847	870	840	754	692	642	610	605	616	604
2194.60	1	-7	5553	4954	4552	4159	3886	3597	3376	3220	3019	2947	2929	2844	2719	2553	2465	2285	2236
2161.81	1	-7	2137	2166	2278	2537	2957	3359	3378	3051	2697	2436	2251	2090	1922	1762	1641	1561	1505
2129.03	1	-7	1446	1359	1264	1178	1105	1035	969	917	884	860	830	790	752	715	680	647	614
2096.24	1	-7	579	545	516	492	474	456	438	421	406	390	374	358	343	330	319	310	302
2063.46	1	-7	298	297	301	311	323	338	356	371	382	387	379	372	377	396	423	451	468
2030.68	1	-7	465	449	430	414	404	403	413	435	477	551	680	881	1115	1320	1283	1178	1199
1997.89	1	-7	1436	1949	2392	2343	2221	2095	1809	1593	1495	1499	1594	1789	2103	2594	3363	4508	6083
1965.11	1	-6	794	966	1069	1059	940	771	608	474	372	297	245	210	187	171	156	141	128
1932.32	1	-7	1177	1097	1037	1000	987	987	994	1020	1062	1114	1175	1312	1665	2199	3041	3981	3748
1899.54	1	-7	2964	2334	1896	1617	1476	1461	1506	1538	1572	1652	1803	2043	2401	2919	3712	5017	6601
1866.76	1	-7	7130	7094	7760	7937	6541	4918	3804	3183	2879	2686	2580	2564	2530	2523	2565	2669	2844
1833.97	1	-6	311	352	415	507	644	834	1081	1354	1589	1692	1626	1434	1196	967	776	638	555
1801.19	1	-7	5567	6387	5735	4507	3616	3025	2488	2026	1688	1437	1247	1103	1009	949	919	927	931
1768.40	1	-7	911	895	920	962	1073	1300	1667	1944	1755	1369	1100	973	879	806	766	744	728
1735.62	1	-7	723	727	740	766	808	863	911	948	993	1071	1208	1431	1528	1472	1535	1706	1979
1702.84	1	-6	234	276	334	420	531	632	670	638	618	674	823	1011	1019	835	702	653	627
1670.05	1	-7	5828	5311	4896	4632	4538	4609	4753	4761	4572	4314	4094	3956	3933	4065	4312	4668	5163
1637.27	1	-6	576	653	738	875	1093	1479	2192	3509	5784	8633	9833	8372	6074	4268	3109	2330	1754
1604.48	1	-6	1338	1047	855	728	646	599	575	564	561	568	585	583	550	521	521	556	657
1571.70	1	-6	877	976	860	781	758	766	804	880	1006	1208	1526	1855	1729	1340	1058	900	847
1538.92	1	-6	845	871	936	1019	1080	1090	1046	960	859	764	682	618	569	532	506	489	483
1507.10	0	-6	499	499	519	534	555	579	602	624	646	670	695	734	766	807	862	926	1013
1490.70	0	-5	113	126	145	171	208	262	341	460	644	925	1308	1641	1673	1423	1112	841	636
1474.31	0	-6	5044	4312	3893	3450	2981	2620	2383	2248	2197	2217	2317	2481	2743	3111	3611	4260	5074
1457.92	0	-5	606	717	829	930	1000	1023	997	930	841	745	651	565	492	429	372	324	284
1441.53	0	-6	2486	2182	1918	1690	1497	1338	1185	1060	956	867	790	727	675	628	593	560	535
1424.17	1	-6	498	476	463	460	471	499	542	593	677	788	904	1021	1131	1309	1653	2289	2933
1391.39	1	-6	2883	2734	2235	1617	1199	920	755	656	588	550	516	492	480	480	485	496	529
1359.57	0	-6	555	584	614	654	693	752	821	886	972	1059	1156	1241	1352	1483	1640	1830	2064
1343.18	0	-5	237	277	323	369	422	497	606	765	997	1345	1867	2607	3456	4011	3943	3422	2780
1326.78	0	-5	2181	1673	1307	1076	931	793	654	538	446	375	318	274	239	212	188	167	150
1309.43	1	-6	1238	1058	922	824	750	709	688	678	659	660	664	670	665	649	629	600	562
1276.64	1	-7	5360	5252	4826	4513	4318	4257	4267	4152	4134	4108	4029	4149	4101	4045	3773	3427	3063
1243.86	1	-7	2765	2653	2532	2468	2482	2499	2533	2629	2808	3032	3075	3046	2925	2770	2714	2712	2812
1211.08	1	-6	297	319	351	418	504	533	497	481	493	532	595	692	828	1019	1233	1440	1588
1178.29	1	-6	1673	1763	1916	2215	2740	3557	4595	5562	6019	5814	5189	4421	3654	2960	2378	1918	1559
1145.51	1	-6	1277	1058	886	751	644	558	497	456	421	393	377	368	362	344	328	314	300
1112.72	1	-7	2929	2796	2653	2654	2580	2501	2457	2336	2293	2331	2422	2498	2723	3041	3501	3958	3936
1079.94	1	-7	3691	3490	3468	3467	3528	3667	3989	4138	4367	4707	5127	5651	6235	6772	7465	8448	9911
1047.16	1	-6	1209	1564	2188	3313	5229	7376	7704	6382	4800	3511	2618	2056	1757	1629	1461	1466	1588
1014.37	1	-6	1751	1843	1796	1583	1361	1193	1095	1015	965	943	952	977	997	1005	1053	1161	1190
981.59	1	-6	1160	1184	1239	1312	1389	1448	1468	1450	1410	1370	1341	1335	1369	1465	1639	1857	1988
948.80	1	-6	1996	2059	2178	2051	1770	1573	1458	1454	1620	1941	2070	1932	1870	1814	1665	1469	1299
916.02	1	-6	1175	1095	1052	1038	1051	1055	1093	1105	1141	1190	1248	1295	1379	1457	1575	1687	1812
883.24	1	-6	1967	2142	2382	2647	2930	3258	3582	3854	3984	3944	3835	3711	3566	3517	3505	3561	3645
850.45	1	-5	373	382	391	399	413	426	447	469	495	534	594	678	796	964	1210	1587	2243
817.67	1	-4	346	584	952	1083	780	474	299	205	151	117	95	80	69	61	54	48	43
784.88	1	-6	3877	3550	3254	3045	2909	2942	2785	2416	2144	1974	1843	1756	1666	1589	1524	1456	1516
752.10	1	-6	1613	1572	1569	1697	1985	2040	1833	1668	1580	1563	1605	1632	1614	1625	1683	1708	1797
719.32	1	-5	187	199	213	239	289	326	322	338	376	425	475	543	637	774	988	1328	1935
686.53	1	-4	311	551	996	1461	1465	1037	638	406	281	213	175	151	130	109	90	74	62
653.75	1	-6	5192	4485	3938	3479	3093	2860	2637	2459	2352	2248	2120	2080	2008	1988	1954	1867	1834
620.97	1	-6	1754	1719	1748	1920	1934	1885	1766	1667	1583	1557	1462	1449	1328	1319	1242	1203	1211
588.18	1	-6	1184	1183	1225	1311	1445	1464	1430	1363	1370	1334	1327	1355	1328	1333	1284	1260	1317
555.40	1	-5	141	157	176	204	231	259	293	336	384	452	536	646	781	997	1325	1836	2665
522.61	1	-4	396	578	799	927	795	657	640	703	1039	1621	2459	3512	4652	5624	5865	4844	3131
489.83	1	-4	1803	1075	688	472	348	273	222	186	158	136	118	103	91	81	73	66	59
457.05	1	-6	5411	4949	4544	4189													

---

[a] See footnote a to Table IV.1.

[b] See footnote b to Table V.1 .

Table VI.2. Real refractive indices between 6500 and 450 cm^{-1} of 10.01% liquid benzene-h$_6$ in liquid benzene-d$_6$ at 25 °C.^{a,b}

cm^{-1}	*XE*	0	1	2	3	4	5	6	7	8	9	10	11	12	13	14	15	16
6499.90	3	14779	14779	14779	14779	14779	14779	14779	14779	14779	14779	14779	14779	14779	14779	14779	14779	14779
6368.76	3	14779	14779	14779	14779	14779	14779	14779	14779	14779	14779	14779	14779	14779	14779	14779	14779	14779
6237.63	3	14779	14779	14779	14779	14779	14779	14779	14779	14779	14779	14779	14779	14779	14779	14779	14779	14779
6106.49	3	14779	14779	14779	14779	14779	14779	14779	14779	14779	14779	14779	14779	14779	14779	14779	14779	14779
5975.36	3	14779	14779	14779	14779	14779	14779	14779	14779	14779	14779	14779	14779	14779	14779	14779	14779	14779
5844.22	3	14779	14779	14779	14779	14779	14779	14779	14779	14779	14779	14779	14779	14779	14779	14779	14779	14779
5713.09	3	14779	14779	14779	14779	14779	14779	14779	14779	14779	14779	14779	14779	14779	14779	14779	14779	14779
5581.95	3	14779	14779	14779	14778	14778	14778	14778	14778	14778	14778	14778	14778	14778	14778	14778	14778	14778
5450.81	3	14778	14778	14778	14778	14778	14778	14778	14778	14778	14778	14778	14778	14778	14778	14778	14778	14778
5319.68	3	14778	14778	14778	14778	14778	14778	14778	14778	14778	14778	14778	14778	14778	14778	14778	14778	14778
5188.54	3	14778	14778	14778	14778	14778	14778	14778	14778	14778	14778	14778	14778	14778	14778	14778	14778	14778
5057.41	3	14778	14778	14778	14778	14778	14778	14778	14778	14778	14778	14777	14777	14777	14777	14777	14777	14777
4926.27	3	14777	14777	14777	14777	14777	14777	14777	14777	14777	14777	14777	14777	14777	14777	14777	14777	14777
4798.99	2	14777	14777	14777	14777	14777	14777	14777	14777	14777	14777	14777	14777	14777	14777	14777	14777	14777
4733.42	2	14777	14777	14777	14777	14777	14777	14776	14776	14776	14776	14776	14776	14776	14776	14776	14776	14776
4667.86	2	14776	14776	14776	14776	14776	14776	14776	14776	14776	14776	14776	14776	14776	14776	14776	14776	14776
4602.29	2	14776	14776	14776	14776	14776	14776	14776	14776	14776	14776	14776	14776	14776	14776	14775	14775	14775
4536.72	2	14775	14775	14775	14775	14774	14774	14774	14774	14773	14773	14772	14772	14773	14774	14776	14778	14779
4471.15	2	14779	14779	14778	14778	14778	14778	14779	14779	14779	14779	14779	14779	14779	14779	14778	14778	14778
4405.58	2	14778	14778	14778	14778	14778	14778	14778	14778	14778	14778	14778	14778	14778	14778	14777	14777	14777
4340.02	2	14777	14777	14777	14777	14777	14777	14777	14777	14777	14777	14777	14777	14777	14777	14777	14777	14777
4274.45	2	14777	14777	14777	14777	14777	14776	14776	14776	14776	14776	14776	14776	14776	14776	14776	14776	14776
4208.88	2	14776	14776	14776	14776	14776	14776	14776	14776	14776	14776	14776	14776	14776	14776	14776	14776	14776
4143.31	2	14776	14776	14776	14776	14776	14776	14775	14775	14775	14775	14775	14775	14775	14775	14775	14775	14775
4077.74	2	14775	14775	14774	14774	14774	14775	14776	14777	14777	14777	14777	14776	14776	14776	14776	14776	14776
4014.10	1	14776	14776	14776	14776	14776	14776	14776	14776	14776	14776	14776	14775	14775	14775	14775	14775	14775
3981.32	1	14775	14775	14775	14775	14775	14775	14775	14775	14775	14775	14775	14775	14775	14775	14775	14775	14775
3948.54	1	14775	14775	14775	14775	14775	14775	14775	14775	14775	14775	14775	14775	14775	14775	14775	14775	14775
3915.75	1	14775	14775	14775	14775	14775	14775	14775	14775	14775	14775	14774	14774	14774	14774	14774	14775	14775
3882.97	1	14775	14775	14775	14774	14774	14774	14774	14774	14774	14774	14774	14774	14774	14774	14774	14774	14774
3850.18	1	14774	14774	14774	14773	14773	14773	14773	14773	14772	14772	14773	14774	14774	14775	14775	14774	14774
3817.40	1	14774	14774	14774	14774	14773	14773	14773	14774	14776	14777	14778	14778	14778	14777	14777	14777	14777
3784.62	1	14776	14776	14776	14776	14776	14776	14776	14776	14776	14775	14775	14775	14775	14775	14775	14775	14775
3751.83	1	14775	14775	14775	14774	14774	14775	14775	14775	14775	14775	14775	14775	14775	14775	14775	14775	14775
3719.05	1	14775	14775	14775	14774	14774	14774	14774	14774	14774	14774	14774	14774	14774	14775	14775	14774	14774
3686.27	1	14774	14775	14774	14774	14774	14774	14774	14774	14774	14774	14774	14774	14774	14774	14774	14774	14774
3653.48	1	14774	14774	14773	14773	14773	14773	14774	14774	14774	14774	14773	14773	14773	14773	14773	14773	14774
3620.70	1	14774	14774	14775	14775	14775	14775	14775	14775	14775	14774	14774	14774	14774	14774	14774	14774	14774
3587.91	1	14774	14774	14774	14774	14774	14774	14774	14774	14774	14774	14774	14774	14774	14774	14774	14774	14774
3555.13	1	14774	14773	14773	14773	14773	14773	14773	14773	14773	14773	14773	14773	14773	14773	14773	14773	14773
3522.35	1	14773	14773	14773	14773	14773	14773	14773	14773	14773	14773	14773	14773	14773	14773	14773	14773	14773
3489.56	1	14773	14773	14773	14773	14772	14772	14772	14772	14772	14772	14772	14772	14772	14772	14772	14772	14772
3456.78	1	14772	14772	14772	14772	14772	14772	14772	14772	14772	14772	14772	14772	14772	14772	14772	14772	14772
3423.99	1	14772	14772	14772	14772	14772	14772	14772	14772	14771	14771	14771	14771	14771	14771	14771	14771	14771
3391.21	1	14771	14771	14771	14771	14771	14771	14771	14771	14771	14771	14771	14770	14770	14770	14770	14770	14770
3358.43	1	14770	14770	14770	14770	14770	14770	14770	14770	14770	14770	14770	14769	14769	14769	14769	14769	14769
3325.64	1	14769	14769	14770	14770	14770	14769	14769	14769	14769	14769	14769	14769	14769	14768	14768	14768	14768
3292.86	1	14768	14767	14767	14767	14767	14767	14767	14767	14767	14766	14767	14767	14767	14767	14767	14766	14766
3260.07	1	14766	14765	14765	14764	14764	14763	14762	14761	14760	14759	14758	14759	14762	14766	14771	14776	14778
3227.29	1	14779	14779	14779	14779	14778	14777	14776	14775	14775	14774	14774	14774	14773	14773	14773	14772	14772
3194.51	1	14772	14771	14771	14771	14771	14770	14770	14770	14770	14769	14769	14769	14769	14769	14768	14768	14768
3161.72	1	14768	14768	14767	14767	14767	14767	14767	14767	14767	14767	14766	14766	14766	14766	14766	14765	14765
3128.94	1	14765	14764	14764	14764	14763	14763	14762	14762	14761	14761	14760	14760	14759	14758	14756	14754	14752
3096.15	1	14749	14748	14753	14766	14774	14775	14773	14771	14769	14766	14764	14762	14763	14773	14778	14777	14775
3063.37	1	14774	14772	14771	14769	14768	14767	14765	14764	14761	14758	14754	14750	14748	14754	14771	14787	14794
3030.59	1	14797	14798	14797	14795	14793	14792	14790	14789	14787	14786	14785	14784	14784	14783	14783	14782	14782
2997.80	1	14782	14782	14781	14781	14780	14780	14780	14779	14779	14779	14778	14778	14778	14777	14777	14777	14777
2965.02	1	14777	14777	14776	14776	14776	14776	14776	14776	14775	14775	14775	14775	14775	14775	14775	14775	14775
2932.23	1	14774	14774	14774	14774	14774	14774	14774	14774	14774	14773	14773	14773	14773	14773	14773	14773	14773
2899.45	1	14772	14772	14772	14772	14771	14771	14772	14772	14772	14772	14771	14771	14771	14771	14771	14770	14770
2866.67	1	14769	14769	14768	14768	14770	14773	14774	14775	14774	14773	14773	14773	14774	14773	14773	14773	14772
2833.88	1	14772	14772	14773	14774	14774	14774	14773	14773	14773	14773	14773	14773	14773	14772	14772	14772	14772
2801.10	1	14772	14772	14771	14771	14771	14771	14771	14771	14771	14771	14771	14771	14770	14770	14770	14771	14771
2768.31	1	14771	14771	14771	14771	14770	14770	14770	14770	14770	14770	14770	14770	14770	14770	14770	14769	14769
2735.53	1	14769	14769	14769	14769	14769	14769	14769	14769	14769	14769	14768	14768	14768	14768	14768	14768	14768
2702.75	1	14768	14768	14768	14768	14768	14767	14767	14767	14767	14767	14767	14767	14767	14767	14767	14767	14766
2669.96	1	14766	14766	14766	14766	14766	14766	14766	14765	14765	14766	14766	14766	14766	14766	14765	14765	14765
2637.18	1	14765	14765	14765	14765	14764	14764	14764	14764	14764	14763	14764	14764	14764	14765	14765	14765	14765
2604.39	1	14765	14765	14764	14764	14764	14764	14764	14764	14764	14764	14764	14763	14763	14763	14763	14763	14763
2571.61	1	14763	14763	14763	14762	14762	14762	14762	14762	14762	14762	14762	14761	14761	14761	14761	14761	14761
2539.79	0	14761	14760	14760	14760	14760	14760	14760	14760	14760	14760	14759	14759	14759	14759	14759	14758	14758
2523.40	0	14758	14759	14759	14760	14760	14760	14760	14760	14760	14760	14759	14759	14759	14759	14759	14759	14759
2507.01	0	14759	14758	14758	14758	14758	14758	14758	14758	14758	14758	14757	14757	14757	14757	14757	14757	14757
2489.65	1	14757	14756	14756	14756	14756	14756	14755	14755	14755	14755	14754	14754	14754	14753	14753	14753	14753
2456.87	1	14752	14752	14752	14751	14751	14751	14751	14750	14750	14749	14749	14749	14748	14748	14747	14747	14746
2424.08	1	14746	14745	14744	14744	14743	14742	14742	14741	14740	14739	14738	14736	14735	14733	14730	14727	14724
2391.30	1	14722	14731	14744	14749	14748	14746	14743	14741	14746	14750	14750	14748	14745	14743	14742	14743	14744
2358.51	1	14743	14742	14740	14738	14736	14734	14733	14732	14731	14730	14728	14726	14725	14724	14723	14721	14719

Table VI.2. Continued.

cm^{-1}	*XE*	0	1	2	3	4	5	6	7	8	9	10	11	12	13	14	15	16
2325.73	1	14718	14716	14714	14711	14708	14704	14700	14696	14691	14686	14680	14674	14667	14660	14651	14640	14628
2292.95	1	14612	14591	14565	14532	14501	14502	14589	14730	14827	14852	14839	14823	14855	14923	14957	14959	14950
2260.16	1	14939	14927	14916	14906	14897	14889	14882	14876	14871	14865	14861	14856	14852	14848	14845	14842	14839
2227.38	1	14836	14834	14831	14829	14827	14825	14823	14821	14820	14819	14818	14817	14815	14814	14813	14812	14811
2194.60	1	14810	14809	14809	14808	14807	14806	14805	14804	14803	14802	14802	14801	14800	14800	14799	14798	14798
2161.81	1	14797	14796	14795	14795	14794	14794	14794	14794	14794	14794	14793	14793	14793	14792	14792	14791	14791
2129.03	1	14791	14790	14790	14790	14789	14789	14788	14788	14788	14787	14787	14787	14787	14786	14786	14786	14785
2096.24	1	14785	14785	14785	14784	14784	14784	14783	14783	14783	14783	14782	14782	14782	14782	14782	14781	14781
2063.46	1	14781	14781	14780	14780	14780	14780	14779	14779	14779	14779	14779	14778	14778	14778	14778	14778	14777
2030.68	1	14777	14777	14777	14777	14776	14776	14776	14775	14775	14775	14775	14774	14774	14774	14774	14774	14773
1997.89	1	14773	14773	14773	14773	14773	14773	14773	14773	14772	14772	14771	14771	14770	14769	14769	14768	14768
1965.11	1	14768	14770	14772	14774	14776	14777	14777	14777	14777	14776	14776	14775	14775	14774	14774	14774	14773
1932.32	1	14773	14773	14772	14772	14772	14771	14771	14771	14770	14770	14770	14769	14769	14768	14768	14769	14770
1899.54	1	14770	14770	14770	14769	14769	14768	14768	14768	14767	14767	14766	14766	14765	14765	14764	14764	14764
1866.76	1	14766	14766	14767	14768	14770	14770	14769	14769	14768	14767	14767	14766	14766	14765	14765	14764	14763
1833.97	1	14763	14762	14761	14760	14759	14759	14759	14760	14762	14766	14769	14772	14773	14773	14773	14772	14771
1801.19	1	14770	14770	14771	14771	14771	14771	14770	14770	14769	14768	14768	14767	14767	14767	14766	14766	14765
1768.40	1	14765	14765	14764	14764	14763	14763	14763	14763	14763	14763	14763	14763	14762	14762	14762	14761	14761
1735.62	1	14761	14760	14760	14759	14759	14759	14758	14758	14758	14757	14757	14756	14756	14756	14755	14755	14754
1702.84	1	14753	14753	14752	14752	14751	14752	14753	14753	14752	14752	14751	14752	14755	14756	14756	14755	14755
1670.05	1	14755	14754	14754	14753	14752	14751	14751	14750	14750	14749	14748	14747	14746	14744	14743	14741	14739
1637.27	1	14738	14735	14732	14729	14724	14718	14711	14704	14701	14717	14753	14785	14798	14798	14795	14791	14787
1604.48	1	14784	14780	14777	14774	14771	14769	14767	14765	14764	14763	14762	14761	14760	14759	14757	14756	14754
1571.70	1	14753	14755	14755	14755	14754	14752	14751	14750	14749	14748	14748	14751	14756	14758	14757	14755	14753
1538.92	1	14752	14751	14750	14749	14749	14750	14750	14750	14750	14749	14748	14747	14745	14744	14742	14740	14738
1507.10	0	14737	14736	14735	14734	14733	14731	14730	14729	14728	14726	14725	14723	14721	14719	14717	14714	14711
1490.70	0	14708	14704	14699	14694	14688	14680	14672	14663	14654	14650	14661	14698	14752	14791	14808	14812	14807
1474.31	0	14799	14791	14786	14782	14778	14773	14768	14762	14757	14752	14747	14743	14738	14733	14728	14725	14722
1457.92	0	14721	14723	14729	14738	14751	14766	14781	14793	14802	14808	14811	14812	14812	14811	14809	14807	14805
1441.53	0	14803	14801	14799	14796	14794	14792	14790	14788	14786	14784	14782	14781	14779	14777	14776	14775	14773
1424.17	1	14771	14768	14766	14764	14762	14760	14758	14756	14753	14752	14750	14749	14747	14745	14742	14741	14747
1391.39	1	14754	14759	14763	14763	14761	14758	14755	14752	14750	14747	14745	14742	14740	14737	14734	14731	14727
1359.57	0	14726	14724	14722	14720	14717	14715	14713	14710	14707	14705	14702	14698	14695	14691	14686	14681	14676
1343.18	0	14669	14663	14656	14648	14639	14627	14612	14595	14577	14557	14543	14548	14595	14694	14806	14888	14931
1326.78	0	14949	14947	14935	14921	14910	14905	14897	14889	14881	14873	14865	14858	14852	14847	14842	14837	14833
1309.43	1	14826	14819	14814	14809	14805	14802	14799	14796	14793	14791	14789	14788	14786	14785	14784	14783	14782
1276.64	1	14780	14779	14778	14777	14776	14775	14774	14773	14772	14771	14771	14770	14769	14769	14768	14767	14767
1243.86	1	14766	14765	14764	14763	14762	14761	14760	14760	14759	14758	14758	14757	14756	14755	14754	14754	14753
1211.08	1	14751	14750	14749	14748	14748	14747	14747	14746	14744	14743	14741	14739	14737	14736	14735	14735	14735
1178.29	1	14734	14733	14730	14727	14724	14723	14726	14734	14747	14760	14769	14775	14778	14778	14777	14776	14774
1145.51	1	14772	14769	14767	14765	14764	14762	14760	14759	14757	14756	14755	14753	14752	14752	14751	14750	14749
1112.72	1	14748	14747	14746	14745	14744	14744	14743	14742	14741	14740	14739	14738	14737	14736	14735	14734	14734
1079.94	1	14733	14732	14731	14730	14729	14728	14727	14725	14724	14723	14721	14719	14718	14716	14713	14711	14707
1047.16	1	14703	14699	14693	14687	14686	14702	14731	14750	14757	14757	14754	14749	14745	14742	14738	14735	14733
1014.37	1	14732	14733	14734	14735	14734	14733	14731	14729	14727	14726	14724	14723	14721	14720	14718	14717	14717
981.59	1	14716	14715	14714	14713	14712	14712	14712	14712	14711	14710	14709	14707	14706	14704	14702	14702	14703
948.80	1	14703	14703	14704	14706	14706	14705	14702	14699	14696	14696	14698	14699	14698	14698	14698	14697	14696
916.02	1	14693	14691	14688	14686	14683	14681	14679	14677	14674	14672	14669	14667	14664	14661	14659	14656	14653
883.24	1	14650	14648	14645	14642	14640	14638	14638	14638	14639	14639	14639	14637	14633	14629	14625	14620	14616
850.45	1	14611	14605	14599	14593	14585	14577	14567	14556	14543	14527	14509	14487	14461	14429	14389	14338	14271
817.67	1	14192	14142	14307	14821	15182	15221	15157	15089	15033	14988	14952	14924	14900	14881	14865	14851	14838
784.88	1	14826	14816	14806	14796	14787	14781	14776	14771	14763	14756	14750	14743	14737	14731	14725	14719	14713
752.10	1	14707	14703	14697	14690	14686	14684	14680	14675	14669	14662	14656	14650	14643	14636	14629	14620	14612
719.32	1	14603	14593	14582	14570	14558	14550	14537	14521	14502	14482	14459	14431	14396	14353	14299	14228	14133
686.53	1	14009	13877	13878	14301	14989	15395	15427	15337	15238	15158	15098	15056	15025	15001	14976	14952	14930
653.75	1	14909	14890	14873	14857	14844	14830	14818	14806	14796	14787	14777	14768	14760	14752	14744	14737	14729
620.97	1	14722	14714	14707	14700	14694	14690	14683	14676	14669	14662	14655	14648	14640	14632	14624	14616	14607
588.18	1	14598	14589	14580	14570	14561	14552	14543	14532	14520	14508	14495	14482	14468	14453	14436	14419	14400
555.40	1	14380	14358	14335	14311	14286	14257	14226	14192	14154	14111	14062	14009	13946	13871	13785	13686	13576
522.61	1	13470	13403	13428	13610	13722	13586	13330	12980	12528	12171	11988	12134	12769	14058	15993	17821	18532
489.83	1	18274	17771	17328	16976	16703	16493	16328	16195	16085	15993	15913	15844	15784	15730	15683	15640	15601
457.05	1	15566	15533	15504	15476													

[a] See footnotes a and b to Table IV.2.

Table VI.3. Imaginary refractive indices between 6500 and 450 cm^{-1} of 25.38% liquid benzene-h$_6$ in liquid benzene-d$_6$ at 25 °C.[a,b]

cm^{-1}	*XE*	*YE*	0	1	2	3	4	5	6	7	8	9	10	11	12	13	14	15	16
6499.90	3	-7	19	18	17	16	20	20	18	18	17	16	18	18	19	18	19	18	20
6368.76	3	-7	18	19	20	18	16	16	15	15	14	18	21	22	19	20	17	18	18
6237.63	3	-7	18	20	20	19	19	14	16	16	23	28	46	92	115	100	91	93	106
6106.49	3	-7	105	101	124	92	65	55	52	63	85	117	157	186	222	350	513	658	931
5975.36	3	-7	776	644	524	482	407	329	436	369	597	467	302	202	212	221	217	196	151
5844.22	3	-7	104	69	55	51	54	60	59	59	70	84	87	68	61	54	48	45	50
5713.09	3	-7	80	84	106	112	90	62	52	52	50	35	28	28	33	56	62	49	39
5581.95	3	-7	43	44	41	41	50	70	85	73	71	73	51	37	28	24	20	18	23
5450.81	3	-7	24	25	37	51	49	37	42	42	45	56	45	57	65	80	79	69	67
5319.68	3	-7	62	64	57	53	64	55	52	56	69	75	49	38	36	31	29	27	25
5188.54	3	-7	27	26	25	25	36	42	45	47	45	43	40	43	61	68	54	45	36
5057.41	3	-7	36	35	30	23	22	24	27	30	34	28	35	34	40	38	29	27	31
4926.27	3	-7	32	38	40	38	38	54	51	67	82	88	125	107	75	66	49	45	42
4798.99	2	-7	45	45	46	50	56	59	60	62	61	60	60	62	70	87	111	109	97
4733.42	2	-7	92	92	95	102	115	130	146	174	218	266	366	506	482	456	528	780	1299
4667.86	2	-7	1390	858	589	517	603	888	1150	1171	918	686	700	1010	1140	833	657	667	814
4602.29	2	-7	867	744	676	792	1162	1411	1157	840	598	491	457	467	467	475	548	652	615
4536.72	2	-7	532	485	472	496	542	631	754	950	1239	1706	2404	3428	4693	5938	6719	6602	5386
4471.15	2	-7	3943	2955	2527	2539	2807	2915	2669	2274	2014	1900	1739	1509	1296	1045	877	852	921
4405.58	2	-7	993	945	887	901	939	780	706	749	699	592	457	354	284	243	221	229	263
4340.02	2	-7	275	252	229	215	200	180	168	161	163	163	162	165	169	172	174	172	170
4274.45	2	-7	176	195	245	338	343	284	247	243	256	245	230	224	226	256	312	315	305
4208.88	2	-7	313	318	365	455	473	409	359	354	400	465	434	384	362	354	345	334	337
4143.31	2	-7	371	443	478	453	441	430	434	453	496	567	675	838	1006	1116	1298	1665	2075
4077.75	2	-7	2094	2142	2592	3550	5633	8308	8399	5568	3478	2245	1555	1192	1071	1163	1143	871	688
4014.11	1	-7	624	573	534	500	467	436	410	389	373	362	356	358	368	384	399	404	407
3981.32	1	-7	405	387	367	352	341	336	342	371	450	571	635	692	781	806	736	647	581
3948.54	1	-7	546	536	557	630	767	947	1218	1241	1053	906	797	720	659	613	582	567	568
3915.75	1	-7	569	553	535	524	523	528	537	548	547	534	534	563	646	846	976	887	801
3882.97	1	-7	720	652	600	575	573	583	589	576	557	546	550	561	571	575	571	564	563
3850.19	1	-7	573	595	624	661	717	804	941	1159	1494	1964	2471	2736	2604	2256	1913	1686	1629
3817.40	1	-7	1741	1870	1894	1949	2162	2637	3440	4364	4735	4186	3250	2460	1895	1502	1239	1062	927
3784.62	1	-7	825	746	677	632	616	625	643	652	645	605	544	491	454	427	411	406	412
3751.83	1	-7	433	473	542	651	804	948	970	898	820	751	695	657	641	648	677	718	747
3719.05	1	-7	752	747	744	748	759	782	822	874	953	1100	1389	1891	2219	1921	1553	1380	1349
3686.27	1	-7	1323	1201	1027	875	765	685	621	574	548	537	541	537	514	492	486	498	522
3653.48	1	-7	560	624	752	1012	1514	2254	2548	2092	1590	1294	1168	1150	1221	1390	1655	1911	2042
3620.70	1	-7	2022	1906	1799	1751	1730	1658	1499	1285	1087	928	813	732	671	621	582	552	530
3587.91	1	-7	519	523	561	606	649	711	684	606	526	465	421	391	369	356	344	337	337
3555.13	1	-7	346	366	393	413	417	403	383	363	341	317	295	278	264	251	239	230	227
3522.35	1	-7	227	235	252	273	284	266	247	232	223	216	210	204	198	195	200	211	229
3489.56	1	-7	258	274	250	229	218	212	213	213	208	208	215	229	255	293	313	327	355
3456.78	1	-7	406	469	524	574	607	606	574	522	471	430	398	382	389	436	524	568	531
3423.99	1	-7	503	491	487	484	460	425	392	366	349	342	348	358	362	362	358	353	354
3391.21	1	-7	364	375	373	361	347	331	319	310	307	312	325	345	372	401	426	442	446
3358.43	1	-7	440	424	401	379	362	351	344	337	334	339	355	383	422	464	528	653	876
3325.64	1	-7	1165	1299	1183	992	841	738	666	617	583	566	561	560	559	565	580	605	641
3292.86	1	-7	691	760	857	985	1144	1323	1502	1662	1812	1996	2233	2354	2269	2101	1953	1871	1868
3260.07	1	-6	193	206	224	246	270	301	341	399	493	652	911	1276	1663	1879	1808	1550	1274
3227.29	1	-6	1058	874	701	553	437	351	294	260	245	236	220	196	178	166	154	146	139
3194.51	1	-7	1348	1318	1297	1299	1295	1278	1269	1244	1259	1293	1314	1364	1430	1471	1568	1634	1659
3161.72	1	-7	1652	1713	1842	1945	2070	2200	2424	2616	2623	2614	2596	2732	2860	3027	3097	3118	3159
3128.94	1	-6	321	332	344	362	395	415	456	507	584	659	702	745	817	923	1094	1389	1935
3096.16	1	-6	2969	4800	7226	7803	6076	4343	3283	2680	2272	2174	2455	3316	5238	5870	4276	3130	2498
3063.37	1	-5	215	193	184	188	184	174	174	182	199	236	315	471	745	1106	1306	1196	959
3030.59	1	-6	7494	5846	4528	3524	2808	2300	1919	1637	1423	1259	1141	1054	991	941	893	842	787
2997.80	1	-7	7186	6540	5925	5331	4881	4506	4191	3912	3697	3480	3327	3135	2937	2834	2678	2665	2763
2965.02	1	-7	2653	2466	2383	2366	2384	2416	2382	2367	2286	2226	2107	2051	2021	2003	1991	1928	1876
2932.24	1	-7	1816	1772	1738	1713	1704	1711	1713	1673	1617	1607	1694	1909	2244	2539	2456	2138	1869
2899.45	1	-7	1705	1641	1695	1919	2446	3468	4590	4110	3010	2476	2220	2072	1967	1894	1887	1972	2156
2866.67	1	-7	2451	2926	3730	5074	6604	6998	5751	4416	3556	3135	3263	3534	3079	2585	2308	2255	2403
2833.88	1	-7	2783	3443	3585	3112	2698	2559	2680	2868	2755	2293	1866	1583	1365	1182	1047	946	871
2801.10	1	-7	832	830	846	870	886	879	860	839	821	813	819	852	924	1036	1146	1184	1128
2768.32	1	-7	1019	904	804	724	663	616	577	543	516	491	462	431	404	382	366	355	348
2735.53	1	-7	346	347	347	343	339	331	323	318	316	315	315	314	311	306	302	300	301
2702.75	1	-7	302	301	301	301	303	307	312	317	324	334	343	353	361	368	376	384	394
2669.96	1	-7	409	430	461	502	562	671	874	1266	2068	2574	1802	1254	1006	862	747	681	645
2637.18	1	-7	623	612	615	628	656	707	796	944	1188	1576	2089	2630	2876	2571	2122	1758	1494
2604.40	1	-7	1319	1261	1365	1710	2410	2572	1854	1332	1027	843	736	684	666	684	713	762	797
2571.61	1	-7	765	706	661	636	631	640	656	686	740	759	696	620	568	536	514	494	475
2539.79	0	-7	465	457	450	446	442	440	439	438	438	442	454	480	525	594	707	898	1224
2523.40	0	-7	1719	2153	2207	2033	1798	1552	1335	1163	1030	923	835	762	703	657	620	592	572
2507.01	0	-7	559	551	547	543	539	534	530	528	529	530	533	535	541	550	563	579	596
2489.65	1	-7	628	666	714	742	703	658	636	634	646	678	730	754	737	731	734	752	783
2456.87	1	-7	828	889	965	1050	1135	1149	1077	1019	992	992	1009	1037	1084	1158	1239	1295	1353
2424.08	1	-6	142	150	159	171	186	204	226	245	264	284	309	341	386	450	556	752	1132
2391.30	1	-6	1861	2659	2617	2101	1681	1415	1390	1678	1982	1655	1223	964	868	910	1074	1128	986
2358.52	1	-6	828	716	652	623	626	657	715	783	816	797	791	838	941	982	978	1058	1220

Table VI.3. Continued.

cm^{-1}	*XE*	*YE*	0	1	2	3	4	5	6	7	8	9	10	11	12	13	14	15	16
2325.73	1	-6	1396	1366	1199	1086	1037	1030	1053	1106	1188	1304	1451	1644	1867	2132	2428	2792	3261
2292.95	1	-5	392	487	646	939	1478	2379	3307	3456	2914	2327	2006	2062	2320	2174	1724	1319	1032
2260.16	1	-6	8267	6772	5629	4762	4101	3584	3158	2790	2457	2179	1942	1756	1597	1459	1348	1247	1154
2227.38	1	-6	1064	987	921	865	818	791	788	844	975	955	805	696	617	567	538	536	523
2194.60	1	-7	4742	4294	3960	3631	3370	3174	2978	2809	2686	2652	2592	2499	2373	2243	2122	2021	1943
2161.81	1	-7	1900	1908	1995	2206	2554	2893	2914	2645	2351	2136	1980	1844	1701	1566	1464	1396	1350
2129.03	1	-7	1303	1232	1153	1084	1027	972	921	880	853	833	807	774	744	718	692	669	644
2096.24	1	-7	618	595	579	570	565	558	545	531	519	505	487	468	451	436	425	417	413
2063.46	1	-7	412	416	426	444	468	498	538	582	628	656	651	640	646	671	704	735	753
2030.68	1	-7	755	748	740	734	736	753	790	854	961	1142	1450	1921	2454	2919	2828	2471	2260
1997.89	1	-6	232	271	320	335	361	379	345	321	317	330	360	410	485	605	795	1090	1507
1965.11	1	-6	2014	2485	2733	2657	2340	1928	1529	1193	927	731	588	489	424	377	336	298	265
1932.33	1	-7	2377	2150	1971	1807	1695	1617	1560	1544	1541	1540	1523	1569	1814	2245	2960	3757	3526
1899.54	1	-7	2846	2332	2003	1811	1755	1825	1963	2060	2103	2161	2301	2559	2920	3366	3958	5008	6352
1866.76	1	-7	6784	6721	7224	7332	6195	4893	4026	3558	3380	3305	3350	3500	3677	3920	4271	4733	5325
1833.97	1	-6	613	728	894	1130	1474	1953	2572	3268	3878	4173	4040	3580	2989	2410	1917	1532	1253
1801.19	1	-6	1094	1050	924	771	649	553	462	384	322	278	242	214	193	179	172	169	165
1768.41	1	-7	1595	1575	1613	1742	2030	2589	3486	4199	3795	2858	2164	1808	1543	1342	1213	1127	1064
1735.62	1	-7	1023	998	990	1000	1028	1074	1120	1157	1222	1354	1612	2066	2203	1908	1835	1938	2154
1702.84	1	-7	2423	2750	3211	3913	4823	5689	6056	5825	5665	6154	7446	9131	9409	8110	7353	7419	7548
1670.05	1	-7	7083	6255	5515	5016	4755	4708	4772	4742	4548	4315	4128	4026	4046	4241	4472	4693	5081
1637.27	1	-6	558	625	699	819	1007	1335	1930	3041	4982	7454	8534	7287	5325	3795	2815	2160	1676
1604.49	1	-6	1325	1080	910	798	733	700	691	695	714	724	714	685	649	621	614	632	701
1571.70	1	-6	870	958	856	784	759	761	800	862	969	1154	1426	1713	1632	1340	1151	1079	1115
1538.92	1	-6	1235	1396	1640	1907	2110	2182	2110	1932	1699	1481	1283	1131	1011	921	865	833	830
1507.10	0	-6	846	851	878	901	932	969	1013	1052	1103	1161	1231	1312	1406	1522	1663	1830	2038
1490.71	0	-5	230	263	307	371	461	589	778	1060	1497	2165	3069	3890	4040	3483	2714	2025	1499
1474.31	0	-5	1156	963	850	733	606	504	431	379	343	319	306	302	308	326	356	400	461
1457.92	0	-6	5375	6278	7217	8073	8662	8836	8590	8011	7249	6421	5626	4899	4267	3729	3270	2884	2548
1441.53	0	-6	2252	1988	1755	1557	1380	1237	1101	991	896	815	746	692	648	607	578	555	529
1424.17	1	-6	499	484	479	496	514	547	584	622	715	829	967	1119	1299	1583	2067	2797	3410
1391.39	1	-6	3258	2957	2398	1786	1367	1075	877	747	655	596	553	526	504	494	493	500	529
1359.57	0	-6	551	575	605	628	669	713	756	805	872	937	1016	1102	1195	1304	1432	1583	1777
1343.18	0	-5	203	235	275	313	357	419	511	645	842	1137	1580	2203	2911	3349	3258	2806	2278
1326.79	0	-5	1789	1377	1081	896	778	664	551	455	380	321	275	239	212	188	169	152	138
1309.43	1	-6	1146	987	867	789	739	681	640	621	607	589	587	584	580	555	533	507	486
1276.65	1	-7	4735	4634	4186	3918	3808	3741	3791	3872	3939	4094	4385	4843	5415	5911	6024	5686	5158
1243.86	1	-7	4680	4334	4099	3969	3915	3916	3982	4123	4298	4457	4559	4587	4548	4501	4505	4573	4710
1211.08	1	-6	493	526	576	654	746	776	761	767	803	866	957	1083	1257	1487	1745	1983	2193
1178.29	1	-6	2353	2471	2571	2733	3061	3631	4385	5107	5449	5335	4836	4201	3560	2995	2529	2166	1876
1145.51	1	-6	1628	1409	1221	1064	936	831	748	680	624	577	538	506	480	459	441	425	413
1112.73	1	-7	4041	4015	4038	4026	3918	3792	3699	3635	3611	3584	3537	3607	3872	4109	4283	4453	4673
1079.94	1	-6	476	494	525	557	587	609	633	669	734	805	912	1021	1151	1302	1497	1743	2112
1047.16	1	-5	267	354	508	784	1251	1786	1888	1571	1173	841	609	457	361	301	264	248	248
1014.37	1	-6	2578	2688	2691	2397	2049	1807	1655	1573	1522	1501	1516	1559	1577	1527	1520	1589	1598
981.59	1	-6	1550	1562	1611	1680	1749	1808	1816	1787	1726	1659	1602	1567	1567	1614	1736	1897	1990
948.81	1	-6	1973	2001	2078	1955	1712	1543	1435	1425	1558	1847	1949	1817	1763	1718	1604	1437	1312
916.02	1	-6	1194	1124	1086	1069	1070	1088	1100	1148	1191	1230	1287	1329	1398	1481	1563	1669	1780
883.24	1	-6	1926	2067	2273	2504	2773	3072	3374	3609	3743	3754	3696	3660	3631	3660	3717	3826	3943
850.46	1	-5	404	408	410	408	409	416	430	443	461	491	535	602	696	833	1034	1349	1893
817.67	1	-5	2909	4874	7779	8695	6352	3884	2471	1714	1275	1001	820	697	608	537	481	433	390
784.89	1	-6	3588	3341	3212	3193	3333	3645	3526	2921	2463	2219	2050	1979	1908	1869	1830	1811	1839
752.10	1	-6	1954	1937	1895	1906	1921	1996	1954	2064	2110	2212	2349	2420	2587	2695	2835	2992	3149
719.32	1	-5	337	357	391	430	493	550	581	634	713	820	954	1123	1344	1651	2114	2858	4166
686.54	1	-4	661	1144	2032	3106	3600	3075	2038	1259	813	569	428	340	275	219	173	138	113
653.75	1	-6	9362	7999	6815	6115	5341	4827	4455	4097	3823	3566	3400	3179	2988	2867	2752	2590	2549
620.97	1	-6	2446	2478	2591	2677	2892	3053	2946	2827	2734	2667	2643	2516	2494	2419	2311	2194	2077
588.18	1	-6	1911	1778	1740	1602	1647	1639	1399	1300	1221	1164	1186	1140	1075	962	806	722	610
555.40	1	-5	53	60	68	86	101	121	146	180	217	266	324	408	508	684	953	1388	2099
522.62	1	-4	321	484	679	798	672	541	521	611	845	1358	2467	4348	5668	5830	5431	4847	3527
489.83	1	-4	2277	1381	841	532	353	246	176	128	95	70	50	40	33	27	20	20	19
457.05	1	-6	2138	2633	2994	3478													

[a] See footnote a to Table IV.1.

[b] See footnote b to Table V.1 .

Table VI.4. Real refractive indices between 6500 and 450 cm^{-1} of 25.38% liquid benzene-h$_6$ in liquid benzene-d$_6$ at 25 °C.^{a,b}

cm^{-1}	XE	0	1	2	3	4	5	6	7	8	9	10	11	12	13	14	15	16
6499.90	3	14783	14783	14783	14783	14783	14783	14783	14783	14783	14783	14783	14783	14783	14783	14783	14783	14783
6368.76	3	14783	14783	14783	14783	14783	14783	14783	14783	14783	14783	14783	14783	14783	14783	14783	14783	14783
6237.63	3	14783	14783	14783	14783	14783	14782	14782	14782	14782	14782	14782	14782	14782	14782	14782	14782	14782
6106.49	3	14782	14782	14782	14782	14782	14782	14782	14782	14782	14782	14782	14782	14782	14782	14782	14782	14782
5975.36	3	14782	14782	14783	14783	14783	14782	14782	14782	14782	14783	14783	14783	14782	14783	14782	14783	14783
5844.22	3	14782	14782	14782	14782	14782	14782	14782	14782	14782	14782	14782	14782	14782	14782	14782	14782	14782
5713.09	3	14782	14782	14782	14782	14782	14782	14782	14782	14782	14782	14782	14782	14782	14782	14782	14782	14782
5581.95	3	14782	14782	14782	14782	14782	14782	14782	14782	14782	14782	14782	14782	14782	14782	14782	14782	14782
5450.81	3	14782	14782	14782	14782	14782	14782	14782	14782	14782	14782	14782	14782	14781	14781	14781	14781	14781
5319.68	3	14781	14781	14781	14781	14781	14781	14781	14781	14781	14781	14781	14781	14781	14781	14781	14781	14781
5188.54	3	14781	14781	14781	14781	14781	14781	14781	14781	14781	14781	14781	14781	14781	14781	14781	14781	14781
5057.41	3	14781	14781	14781	14781	14781	14781	14781	14781	14781	14781	14781	14781	14781	14781	14781	14780	14780
4926.27	3	14780	14780	14780	14780	14780	14780	14780	14780	14780	14780	14780	14780	14780	14780	14780	14780	14780
4798.99	2	14780	14780	14780	14780	14780	14780	14780	14780	14780	14780	14780	14780	14780	14780	14780	14780	14780
4733.42	2	14780	14779	14779	14779	14779	14779	14779	14779	14779	14779	14779	14779	14779	14779	14779	14779	14779
4667.86	2	14779	14780	14779	14779	14779	14779	14779	14779	14780	14779	14779	14779	14779	14780	14779	14779	14779
4602.29	2	14779	14779	14779	14779	14779	14779	14780	14780	14780	14779	14779	14779	14779	14779	14779	14779	14779
4536.72	2	14779	14778	14778	14778	14778	14778	14777	14777	14777	14776	14776	14776	14776	14777	14778	14780	14782
4471.15	2	14782	14782	14781	14781	14781	14781	14781	14781	14781	14781	14781	14781	14781	14781	14781	14781	14781
4405.58	2	14781	14781	14781	14781	14781	14781	14780	14780	14781	14781	14780	14780	14780	14780	14780	14780	14780
4340.02	2	14780	14780	14780	14780	14780	14780	14780	14780	14780	14779	14779	14779	14779	14779	14779	14779	14779
4274.45	2	14779	14779	14779	14779	14779	14779	14779	14779	14779	14779	14779	14779	14779	14779	14779	14779	14779
4208.88	2	14778	14778	14778	14778	14778	14778	14778	14778	14778	14778	14778	14778	14778	14778	14778	14778	14778
4143.31	2	14778	14778	14778	14778	14778	14777	14777	14777	14777	14777	14777	14777	14776	14776	14776	14776	14776
4077.75	2	14776	14776	14775	14775	14774	14776	14780	14782	14782	14782	14781	14781	14780	14780	14780	14780	14780
4014.11	1	14780	14779	14779	14779	14779	14779	14779	14779	14779	14779	14779	14779	14779	14779	14779	14779	14778
3981.32	1	14778	14778	14778	14778	14778	14778	14778	14778	14778	14778	14778	14778	14778	14778	14778	14778	14778
3948.54	1	14778	14778	14778	14778	14778	14777	14778	14778	14778	14778	14778	14778	14778	14778	14778	14778	14778
3915.75	1	14778	14778	14778	14778	14778	14778	14778	14777	14777	14777	14777	14777	14777	14777	14777	14777	14777
3882.97	1	14777	14777	14777	14777	14777	14777	14777	14777	14777	14777	14777	14777	14777	14777	14777	14777	14777
3850.19	1	14777	14776	14776	14776	14776	14776	14776	14776	14775	14775	14776	14776	14777	14777	14777	14777	14777
3817.40	1	14776	14776	14776	14776	14776	14776	14776	14776	14778	14779	14779	14779	14779	14779	14779	14779	14779
3784.62	1	14778	14778	14778	14778	14778	14778	14778	14778	14778	14778	14778	14777	14777	14777	14777	14777	14777
3751.83	1	14777	14777	14777	14777	14777	14777	14777	14777	14777	14777	14777	14777	14777	14777	14777	14776	14776
3719.05	1	14776	14776	14776	14776	14776	14776	14776	14776	14776	14776	14776	14776	14776	14777	14777	14777	14777
3686.27	1	14777	14777	14777	14777	14777	14777	14777	14777	14776	14776	14776	14776	14776	14776	14776	14776	14776
3653.48	1	14776	14775	14775	14775	14775	14775	14776	14776	14776	14776	14776	14776	14776	14776	14776	14776	14776
3620.70	1	14776	14776	14776	14776	14777	14777	14777	14777	14777	14777	14777	14777	14777	14776	14776	14776	14776
3587.91	1	14776	14776	14776	14776	14776	14776	14776	14776	14776	14776	14776	14776	14776	14776	14776	14776	14776
3555.13	1	14775	14775	14775	14775	14775	14775	14775	14775	14775	14775	14775	14775	14775	14775	14775	14775	14775
3522.35	1	14775	14775	14775	14775	14775	14775	14775	14775	14775	14775	14775	14774	14774	14774	14774	14774	14774
3489.56	1	14774	14774	14774	14774	14774	14774	14774	14774	14774	14774	14774	14774	14774	14774	14774	14773	14773
3456.78	1	14773	14773	14773	14773	14773	14773	14773	14773	14773	14773	14773	14773	14773	14773	14773	14773	14773
3423.99	1	14773	14773	14773	14773	14773	14773	14773	14773	14773	14773	14773	14773	14772	14772	14772	14772	14772
3391.21	1	14772	14772	14772	14772	14772	14772	14772	14772	14772	14772	14772	14772	14771	14771	14771	14771	14771
3358.43	1	14771	14771	14771	14771	14771	14771	14771	14771	14771	14770	14770	14770	14770	14770	14770	14770	14770
3325.64	1	14770	14770	14770	14770	14770	14770	14770	14770	14769	14769	14769	14769	14769	14769	14769	14768	14768
3292.86	1	14768	14768	14768	14767	14767	14767	14767	14767	14767	14767	14767	14767	14767	14767	14767	14766	14766
3260.07	1	14766	14765	14765	14764	14764	14763	14762	14762	14761	14759	14758	14759	14761	14766	14771	14774	14775
3227.29	1	14776	14776	14776	14775	14775	14774	14773	14772	14772	14771	14771	14771	14770	14770	14770	14769	14769
3194.51	1	14769	14768	14768	14768	14767	14767	14767	14766	14766	14766	14765	14765	14765	14764	14764	14764	14764
3161.72	1	14763	14763	14763	14762	14762	14761	14761	14761	14761	14760	14760	14759	14759	14758	14758	14757	14757
3128.94	1	14756	14755	14755	14754	14753	14752	14750	14749	14748	14747	14746	14744	14741	14738	14735	14730	14724
3096.16	1	14717	14715	14728	14760	14780	14783	14780	14775	14770	14763	14755	14748	14750	14776	14787	14786	14782
3063.37	1	14779	14775	14771	14768	14766	14763	14758	14753	14747	14739	14728	14718	14713	14728	14769	14809	14830
3030.59	1	14837	14838	14837	14833	14828	14824	14821	14817	14814	14812	14809	14807	14805	14804	14803	14802	14801
2997.80	1	14800	14799	14799	14798	14797	14796	14795	14794	14794	14793	14792	14792	14791	14791	14790	14789	14789
2965.02	1	14789	14788	14788	14787	14787	14787	14786	14786	14786	14786	14785	14785	14785	14785	14784	14784	14784
2932.24	1	14784	14783	14783	14783	14783	14782	14782	14782	14782	14781	14781	14781	14781	14781	14781	14781	14781
2899.45	1	14780	14780	14779	14779	14778	14778	14779	14781	14781	14780	14780	14780	14779	14779	14779	14778	14778
2866.67	1	14777	14777	14776	14776	14777	14779	14781	14781	14781	14780	14779	14780	14780	14780	14779	14779	14778
2833.88	1	14778	14778	14779	14779	14779	14779	14779	14779	14779	14779	14779	14779	14779	14779	14779	14778	14778
2801.10	1	14778	14778	14777	14777	14777	14777	14777	14777	14777	14777	14776	14776	14776	14776	14776	14776	14776
2768.32	1	14776	14776	14776	14776	14776	14776	14776	14776	14775	14775	14775	14775	14775	14775	14775	14775	14775
2735.53	1	14774	14774	14774	14774	14774	14774	14774	14774	14774	14774	14773	14773	14773	14773	14773	14773	14773
2702.75	1	14773	14773	14773	14773	14772	14772	14772	14772	14772	14772	14772	14772	14772	14771	14771	14771	14771
2669.96	1	14771	14771	14771	14771	14770	14770	14770	14770	14770	14771	14771	14771	14771	14771	14771	14770	14770
2637.18	1	14770	14770	14770	14769	14769	14769	14769	14769	14768	14768	14768	14768	14769	14770	14770	14770	14769
2604.40	1	14769	14769	14769	14768	14768	14769	14770	14770	14769	14769	14769	14769	14768	14768	14768	14768	14768
2571.61	1	14768	14768	14767	14767	14767	14767	14767	14767	14767	14767	14767	14766	14766	14766	14766	14766	14766
2539.79	0	14766	14765	14765	14765	14765	14765	14765	14765	14765	14765	14764	14764	14764	14764	14764	14764	14763
2523.40	0	14763	14764	14764	14765	14765	14765	14765	14765	14765	14764	14764	14764	14764	14764	14764	14764	14764
2507.01	0	14763	14763	14763	14763	14763	14763	14763	14763	14763	14763	14762	14762	14762	14762	14762	14762	14762
2489.65	1	14762	14761	14761	14761	14761	14761	14761	14760	14760	14760	14760	14759	14759	14759	14759	14758	14758
2456.87	1	14758	14758	14757	14757	14757	14757	14756	14756	14756	14755	14755	14755	14754	14754	14753	14753	14752
2424.08	1	14752	14751	14751	14750	14750	14749	14748	14748	14747	14746	14745	14744	14743	14741	14739	14737	14734
2391.30	1	14733	14739	14749	14753	14753	14752	14749	14748	14752	14756	14756	14754	14751	14749	14748	14750	14750
2358.52	1	14749	14748	14747	14745	14743	14742	14740	14739	14739	14738	14736	14734	14733	14732	14731	14729	14727

Table VI.4. Continued.

cm^{-1}	XE	0	1	2	3	4	5	6	7	8	9	10	11	12	13	14	15	16
2325.73	1	14727	14728	14727	14724	14721	14718	14715	14711	14707	14702	14698	14692	14687	14680	14673	14664	14654
2292.95	1	14640	14623	14601	14573	14547	14547	14621	14741	14820	14840	14829	14816	14843	14898	14926	14928	14921
2260.16	1	14911	14902	14893	14884	14877	14870	14864	14859	14855	14850	14846	14842	14839	14836	14833	14830	14828
2227.38	1	14826	14823	14821	14819	14817	14816	14814	14812	14811	14812	14812	14811	14809	14808	14807	14806	14805
2194.60	1	14805	14804	14803	14802	14801	14800	14800	14799	14798	14797	14797	14796	14796	14795	14794	14794	14793
2161.81	1	14793	14792	14791	14791	14790	14790	14790	14790	14790	14790	14789	14789	14789	14788	14788	14787	14787
2129.03	1	14787	14786	14786	14786	14785	14785	14785	14784	14784	14784	14784	14783	14783	14783	14782	14782	14782
2096.24	1	14782	14781	14781	14781	14781	14780	14780	14780	14780	14779	14779	14779	14779	14778	14778	14778	14777
2063.46	1	14777	14777	14777	14776	14776	14776	14776	14775	14775	14775	14775	14775	14774	14774	14774	14774	14773
2030.68	1	14773	14773	14773	14772	14772	14772	14771	14771	14770	14770	14769	14769	14769	14769	14769	14769	14769
1997.89	1	14768	14768	14768	14767	14767	14767	14767	14766	14766	14765	14764	14763	14761	14760	14758	14757	14756
1965.11	1	14757	14761	14768	14774	14779	14782	14783	14783	14782	14781	14780	14779	14778	14777	14776	14775	14775
1932.33	1	14774	14774	14773	14772	14772	14771	14771	14770	14770	14770	14769	14768	14768	14767	14767	14767	14768
1899.54	1	14768	14768	14767	14767	14766	14766	14765	14765	14765	14764	14763	14763	14762	14762	14761	14761	14761
1866.76	1	14762	14762	14763	14764	14765	14764	14764	14763	14762	14761	14760	14759	14758	14757	14756	14755	14754
1833.97	1	14752	14751	14749	14747	14745	14743	14744	14747	14753	14762	14771	14778	14782	14784	14784	14783	14781
1801.19	1	14779	14778	14778	14778	14777	14776	14775	14774	14773	14772	14771	14770	14770	14769	14768	14768	14767
1768.41	1	14766	14766	14765	14764	14764	14763	14763	14764	14765	14765	14764	14764	14763	14763	14762	14762	14761
1735.62	1	14761	14760	14760	14759	14759	14758	14758	14757	14757	14756	14756	14756	14756	14755	14755	14754	14753
1702.84	1	14753	14752	14751	14751	14751	14751	14751	14751	14751	14750	14749	14750	14752	14753	14752	14752	14752
1670.05	1	14752	14752	14752	14751	14750	14749	14749	14748	14748	14747	14746	14745	14743	14742	14741	14739	14738
1637.27	1	14736	14734	14731	14728	14724	14719	14712	14706	14703	14716	14747	14775	14785	14786	14783	14779	14776
1604.49	1	14773	14770	14767	14764	14762	14760	14758	14756	14755	14754	14753	14753	14752	14750	14749	14748	14746
1571.70	1	14745	14746	14746	14745	14744	14742	14741	14739	14738	14736	14736	14738	14741	14742	14740	14738	14735
1538.92	1	14733	14732	14731	14731	14732	14735	14737	14738	14738	14737	14736	14733	14731	14728	14725	14722	14718
1507.10	0	14716	14714	14712	14710	14708	14705	14703	14700	14698	14694	14691	14687	14683	14679	14674	14668	14662
1490.71	0	14654	14646	14636	14624	14610	14593	14574	14553	14533	14523	14548	14635	14764	14866	14915	14928	14918
1474.31	0	14900	14883	14871	14865	14857	14847	14837	14828	14819	14811	14803	14796	14789	14782	14776	14770	14765
1457.92	0	14762	14762	14764	14771	14781	14792	14804	14813	14819	14823	14825	14825	14824	14822	14820	14818	14816
1441.53	0	14813	14811	14808	14806	14804	14802	14799	14797	14795	14793	14791	14789	14787	14786	14784	14783	14781
1424.17	1	14778	14776	14773	14771	14768	14766	14764	14761	14759	14757	14755	14753	14750	14748	14746	14747	14754
1391.39	1	14762	14767	14771	14770	14768	14765	14763	14760	14757	14755	14752	14749	14747	14744	14742	14739	14736
1359.57	0	14734	14732	14730	14729	14727	14725	14723	14720	14718	14715	14713	14710	14707	14703	14700	14695	14691
1343.18	0	14685	14680	14674	14667	14659	14649	14636	14622	14607	14590	14579	14584	14625	14710	14802	14868	14902
1326.79	0	14915	14913	14902	14890	14882	14877	14872	14865	14858	14851	14845	14839	14834	14829	14825	14822	14818
1309.43	1	14812	14807	14802	14798	14795	14792	14789	14787	14784	14783	14781	14779	14778	14777	14775	14774	14773
1276.65	1	14772	14771	14770	14768	14767	14766	14765	14764	14763	14761	14760	14759	14759	14758	14758	14758	14758
1243.86	1	14757	14756	14755	14754	14753	14752	14751	14751	14750	14749	14748	14748	14747	14746	14745	14744	14743
1211.08	1	14742	14741	14739	14738	14738	14737	14736	14735	14734	14732	14730	14729	14727	14726	14725	14725	14725
1178.29	1	14726	14726	14725	14724	14722	14721	14723	14729	14739	14749	14757	14761	14764	14764	14763	14762	14760
1145.51	1	14759	14757	14756	14754	14752	14750	14749	14747	14746	14744	14743	14741	14740	14739	14738	14736	14735
1112.73	1	14734	14733	14732	14731	14730	14728	14727	14726	14725	14723	14722	14721	14719	14718	14717	14715	14714
1079.94	1	14712	14711	14709	14707	14705	14704	14701	14699	14696	14693	14690	14687	14683	14679	14674	14668	14661
1047.16	1	14652	14641	14628	14614	14614	14653	14725	14775	14796	14798	14791	14782	14772	14764	14757	14750	14745
1014.37	1	14742	14740	14741	14742	14740	14737	14734	14731	14729	14726	14724	14722	14721	14720	14718	14716	14716
981.59	1	14714	14712	14711	14710	14709	14708	14708	14708	14707	14706	14704	14703	14701	14699	14697	14696	14697
948.81	1	14697	14696	14696	14697	14697	14695	14692	14689	14686	14685	14687	14687	14686	14685	14685	14683	14681
916.02	1	14679	14676	14674	14671	14669	14666	14663	14661	14658	14656	14653	14651	14648	14645	14642	14640	14637
883.24	1	14634	14631	14627	14625	14622	14620	14619	14619	14619	14618	14617	14614	14611	14608	14604	14600	14597
850.46	1	14593	14589	14585	14579	14572	14564	14556	14546	14535	14521	14505	14486	14463	14436	14403	14359	14304
817.67	1	14240	14203	14347	14747	15035	15067	15015	14959	14912	14875	14845	14820	14800	14782	14767	14754	14741
784.89	1	14730	14718	14708	14698	14689	14683	14682	14678	14669	14660	14651	14643	14635	14627	14619	14611	14603
752.10	1	14595	14588	14580	14572	14563	14554	14544	14534	14524	14514	14502	14491	14479	14466	14452	14438	14421
719.32	1	14404	14385	14363	14340	14315	14291	14261	14226	14185	14139	14085	14022	13946	13850	13729	13569	13359
686.54	1	13087	12784	12687	13308	14648	15995	16526	16448	16218	15996	15824	15694	15596	15516	15442	15375	15316
653.75	1	15264	15218	15178	15143	15111	15083	15057	15034	15012	14992	14974	14958	14942	14926	14911	14897	14884
620.97	1	14870	14858	14845	14834	14825	14816	14808	14799	14790	14781	14772	14763	14754	14744	14735	14726	14716
588.18	1	14706	14696	14685	14673	14662	14653	14641	14628	14614	14601	14587	14572	14557	14541	14523	14505	14484
555.40	1	14464	14438	14416	14389	14362	14332	14300	14265	14226	14183	14135	14081	14018	13944	13858	13759	13650
522.62	1	13541	13465	13465	13608	13689	13529	13246	12879	12410	11813	11222	11462	13090	14885	16201	17474	18316
489.83	1	18405	18088	17665	17281	16969	16721	16525	16362	16228	16115	16020	15934	15862	15798	15742	15690	15644
457.05	1	15602	15569	15535	15508													

[a,b] See footnotes a and b to Table IV.2.

Table VI.5. Imaginary refractive indices between 6500 and 450 cm^{-1} of 40.00% liquid benzene-h_6 in liquid benzene-d_6 at 25 °C.[a,b]

cm^{-1}	*XE*	*YE*	0	1	2	3	4	5	6	7	8	9	10	11	12	13	14	15	16
6499.90	3	-7	16	16	14	17	19	18	18	18	18	17	18	21	22	22	23	23	23
6368.76	3	-7	24	25	25	24	24	23	21	22	23	25	29	30	30	30	29	27	29
6237.63	3	-7	29	30	32	33	35	33	32	42	45	48	76	143	188	182	149	150	168
6106.49	3	-7	172	166	203	152	108	95	93	110	135	189	256	308	361	540	796	1067	1338
5975.36	3	-7	1105	955	797	737	630	520	690	601	931	740	472	339	350	339	334	298	231
5844.22	3	-7	155	98	73	63	66	77	80	81	99	118	127	95	91	95	81	72	86
5713.09	3	-7	134	144	182	191	155	112	99	99	96	73	62	61	69	106	116	95	79
5581.95	3	-7	82	86	81	81	96	123	140	120	122	126	92	72	58	50	42	39	39
5450.81	3	-7	43	46	59	76	71	61	68	63	60	78	86	81	84	100	107	90	90
5319.68	3	-7	83	81	80	73	80	77	70	74	93	104	93	61	52	44	42	37	37
5188.54	3	-7	39	38	35	35	51	57	59	62	64	57	52	60	77	83	74	69	61
5057.41	3	-7	59	60	57	50	45	47	55	59	62	54	57	57	62	59	52	52	56
4926.27	3	-7	56	61	66	68	65	76	77	99	113	118	150	134	103	90	74	71	67
4798.99	2	-7	68	70	72	78	87	91	89	91	90	91	90	92	99	113	134	134	130
4733.42	2	-7	130	136	144	157	176	199	225	269	338	412	572	794	755	710	817	1212	2031
4667.86	2	-7	2169	1327	903	777	900	1346	1761	1764	1348	967	979	1478	1682	1202	922	903	1060
4602.29	2	-7	1086	939	902	1130	1726	2051	1657	1203	844	659	575	552	540	562	685	839	759
4536.72	2	-7	612	522	478	471	499	559	661	810	1053	1434	2016	2862	3900	4929	5593	5441	4339
4471.15	2	-7	3148	2388	2089	2123	2337	2407	2186	1874	1673	1599	1496	1316	1137	928	813	819	877
4405.58	2	-7	927	872	814	824	851	735	738	857	779	629	485	374	304	265	242	247	275
4340.02	2	-7	282	259	242	228	213	197	185	187	193	196	216	228	236	242	243	242	245
4274.45	2	-7	258	292	372	515	529	445	389	382	400	383	361	352	354	401	488	492	476
4208.88	2	-7	485	488	550	688	707	595	514	503	564	652	601	530	499	487	482	468	462
4143.31	2	-7	480	536	572	557	565	581	603	654	718	820	995	1250	1537	1765	2045	2620	3270
4077.74	2	-6	329	336	412	572	916	1342	1339	859	533	343	236	180	161	176	173	131	104
4014.11	1	-7	937	859	794	754	700	667	615	595	569	550	541	543	550	572	588	593	600
3981.32	1	-7	593	559	533	516	494	481	486	528	649	837	942	1030	1167	1203	1089	943	833
3948.54	1	-7	765	730	733	804	964	1221	1630	1688	1417	1205	1046	930	839	772	727	701	694
3915.75	1	-7	685	665	647	637	636	640	646	650	644	630	627	648	716	878	973	897	826
3882.97	1	-7	760	702	654	627	619	621	621	607	588	576	576	583	590	594	590	583	579
3850.19	1	-7	585	601	621	649	690	756	865	1041	1315	1704	2119	2324	2204	1919	1641	1456	1409
3817.40	1	-7	1499	1602	1618	1661	1834	2227	2906	3662	3863	3355	2642	2051	1628	1341	1156	1028	913
3784.62	1	-7	814	738	676	639	630	646	674	699	704	669	610	559	523	499	486	484	493
3751.83	1	-7	517	557	623	724	861	990	1014	957	893	835	786	753	742	752	782	822	851
3719.05	1	-7	860	863	872	889	918	970	1051	1155	1296	1529	1970	2724	3219	2784	2215	1932	1868
3686.27	1	-7	1821	1633	1370	1145	987	877	790	727	692	682	691	689	653	616	601	611	643
3653.48	1	-7	701	809	1015	1414	2175	3274	3747	3074	2249	1735	1479	1377	1373	1460	1638	1818	1911
3620.70	1	-7	1907	1856	1853	1929	2026	2019	1856	1590	1325	1105	944	831	745	678	625	588	558
3587.91	1	-7	539	532	555	581	609	650	620	554	488	439	406	384	368	357	347	339	337
3555.13	1	-7	345	360	380	397	400	389	373	356	338	317	299	285	273	260	249	242	241
3522.35	1	-7	244	256	279	310	325	299	273	258	251	247	243	238	234	232	239	256	286
3489.56	1	-7	334	364	328	294	274	263	259	257	254	255	263	279	305	341	366	391	431
3456.78	1	-7	495	580	671	760	817	813	759	681	607	545	495	462	455	486	565	618	583
3423.99	1	-7	555	548	546	542	519	485	455	429	415	412	420	434	441	443	435	421	410
3391.21	1	-7	406	404	393	376	357	340	326	315	310	311	321	335	355	378	399	412	417
3358.43	1	-7	414	402	384	367	355	348	343	335	330	333	345	369	403	440	491	592	776
3325.64	1	-7	1012	1116	1020	865	743	661	604	564	537	524	537	535	535	539	555	571	603
3292.86	1	-7	646	705	784	894	1034	1191	1342	1481	1602	1748	1937	2027	1961	1831	1718	1653	1646
3260.07	1	-6	169	179	195	215	236	264	301	352	432	558	753	1018	1294	1469	1454	1271	1048
3227.29	1	-7	8669	7183	5808	4645	3745	3101	2670	2419	2316	2261	2124	1935	1783	1678	1602	1553	1523
3194.51	1	-7	1504	1491	1580	1532	1540	1608	1563	1517	1572	1592	1661	1732	1726	1815	1934	2047	2096
3161.72	1	-7	2152	2164	2292	2351	2472	2640	2826	3021	3134	3140	3168	3352	3536	3708	3833	3885	3971
3128.94	1	-6	407	430	450	480	528	572	630	695	789	886	959	1055	1176	1358	1639	2124	2987
3096.15	1	-5	455	734	1110	1214	951	674	504	405	341	325	365	495	795	907	664	485	383
3063.37	1	-5	327	293	278	283	276	260	258	271	301	363	488	724	1134	1657	1974	1873	1523
3030.59	1	-5	1183	915	704	547	435	357	299	256	223	198	179	165	154	145	135	127	118
2997.80	1	-6	1082	994	899	820	753	697	650	606	570	537	508	478	453	422	401	386	385
2965.02	1	-7	3710	3513	3359	3298	3270	3279	3313	3280	3264	3066	2867	2746	2692	2573	2509	2404	2395
2932.23	1	-7	2374	2363	2362	2299	2258	2244	2227	2149	2029	2048	2217	2574	3120	3602	3494	2998	2574
2899.45	1	-7	2313	2207	2279	2613	3417	4974	6658	6004	4236	3306	2797	2468	2252	2109	2049	2085	2209
2866.67	1	-7	2414	2789	3462	4633	5996	6211	5235	4236	3544	3157	3196	3362	2970	2555	2314	2252	2352
2833.88	1	-7	2649	3182	3291	2952	2732	2847	3246	3665	3645	3055	2460	2065	1758	1492	1290	1138	1024
2801.10	1	-7	946	909	899	904	908	898	881	867	855	848	848	867	916	997	1079	1103	1050
2768.32	1	-7	956	858	775	708	658	619	585	558	536	516	489	459	433	413	399	389	384
2735.53	1	-7	385	390	393	387	379	370	363	359	358	360	361	361	359	356	354	354	356
2702.75	1	-7	359	362	365	368	372	379	386	393	405	418	433	447	457	465	475	486	502
2669.96	1	-7	523	553	596	656	747	908	1211	1807	2979	3683	2577	1738	1346	1117	944	840	779
2637.18	1	-7	734	709	702	709	735	784	871	1019	1269	1683	2244	2874	3195	2827	2300	1906	1646
2604.40	1	-7	1502	1506	1727	2300	3398	3705	2636	1837	1371	1093	937	860	825	834	854	906	947
2571.61	1	-7	901	822	765	739	740	760	794	849	936	971	882	768	686	635	601	573	546
2539.79	0	-7	535	524	515	509	505	502	502	502	503	506	517	539	579	638	733	891	1156
2523.40	0	-7	1551	1898	1947	1820	1637	1440	1264	1126	1018	932	861	801	751	711	679	653	635
2507.01	0	-7	621	612	607	603	598	594	590	590	591	594	596	602	610	622	639	659	683
2489.65	1	-7	736	798	873	914	849	774	732	721	732	773	844	870	831	804	789	790	813
2456.87	1	-7	855	917	989	1054	1107	1104	1034	979	953	931	975	976	1029	1094	1205	1273	1318
2424.08	1	-7	1368	1426	1494	1595	1765	1972	2231	2443	2629	2771	2927	3173	3498	3960	4722	6313	9514
2391.30	1	-6	1587	2328	2238	1783	1460	1259	1218	1416	1654	1408	1049	829	744	771	895	941	822
2358.52	1	-6	693	601	551	527	526	550	598	659	691	682	678	721	815	870	908	1045	1305

Table VI.5. Continued

cm^{-1}	*XE*	*YE*	0	1	2	3	4	5	6	7	8	9	10	11	12	13	14	15	16
2325.73	1	-6	1586	1542	1280	1082	981	939	936	965	1016	1092	1198	1338	1509	1721	1968	2268	2665
2292.95	1	-5	322	403	537	773	1202	1904	2608	2761	2365	1886	1616	1660	1881	1762	1391	1060	828
2260.16	1	-6	6633	5446	4543	3853	3321	2903	2562	2262	1990	1763	1574	1418	1290	1185	1096	1019	946
2227.38	1	-6	882	822	769	727	692	684	714	824	1039	1054	856	695	578	509	475	467	453
2194.60	1	-7	4085	3673	3385	3164	2958	2762	2593	2457	2353	2285	2236	2156	2050	1945	1846	1760	1694
2161.81	1	-7	1655	1654	1723	1896	2183	2461	2474	2246	2007	1835	1708	1593	1476	1366	1279	1223	1186
2129.03	1	-7	1147	1089	1028	974	930	891	854	823	804	790	767	741	720	701	686	674	657
2096.24	1	-7	638	627	622	625	634	637	628	620	613	599	579	558	537	520	511	504	502
2063.46	1	-7	505	514	529	556	592	637	697	768	844	894	894	882	887	919	958	992	1013
2030.68	1	-7	1021	1024	1027	1033	1048	1082	1144	1246	1412	1695	2179	2919	3744	4459	4323	3710	3281
1997.89	1	-6	317	343	390	424	486	532	491	465	470	497	549	630	747	934	1225	1669	2296
1965.11	1	-6	3063	3794	4207	4133	3666	3034	2409	1880	1463	1150	923	766	660	586	520	456	399
1932.32	1	-7	3526	3130	2793	2538	2330	2174	2060	1993	1998	1993	1943	1914	2064	2364	2912	3560	3360
1899.54	1	-7	2812	2398	2129	1996	2003	2159	2398	2587	2683	2776	2950	3238	3598	3928	4302	5014	5995
1866.76	1	-7	6312	6268	6724	6858	5968	4970	4333	4047	3997	4052	4212	4486	4813	5248	5781	6550	7542
1833.97	1	-6	889	1074	1337	1707	2237	2960	3889	4945	5901	6428	6308	5646	4733	3817	3025	2397	1924
1801.19	1	-6	1609	1438	1248	1061	908	777	654	545	456	386	334	293	261	238	221	210	196
1768.40	1	-7	1907	1888	1936	2112	2550	3428	4858	5955	5372	3995	2930	2410	2000	1710	1513	1456	1347
1735.62	1	-7	1297	1277	1234	1215	1227	1261	1298	1337	1419	1598	1966	2634	2820	2306	2105	2145	2305
1702.84	1	-7	2492	2733	3090	3651	4390	5116	5450	5270	5147	5575	6682	8186	8639	7805	7567	8134	8617
1670.05	1	-7	8184	7124	6088	5353	4921	4742	4714	4637	4441	4234	4088	4023	4085	4315	4528	4680	4998
1637.27	1	-6	542	599	657	757	914	1184	1673	2588	4197	6299	7268	6232	4580	3302	2493	1966	1575
1604.48	1	-6	1286	1075	931	838	786	768	772	791	823	847	841	808	762	722	702	702	741
1571.70	1	-6	862	931	840	776	755	758	797	853	937	1094	1321	1569	1538	1346	1241	1251	1377
1538.92	1	-6	1614	1911	2305	2723	3054	3200	3132	2888	2550	2217	1916	1677	1494	1360	1265	1207	1190
1507.10	0	-6	1207	1212	1246	1276	1320	1371	1433	1504	1591	1685	1785	1924	2062	2252	2470	2742	3061
1490.71	0	-5	348	399	468	563	700	894	1179	1605	2261	3262	4632	5928	6305	5565	4361	3243	2381
1474.31	0	-5	1817	1495	1307	1115	910	742	618	529	464	415	382	358	346	345	358	385	427
1457.92	0	-6	4827	5531	6244	6926	7390	7528	7318	6814	6184	5495	4834	4226	3705	3253	2878	2556	2264
1441.53	0	-6	2021	1791	1585	1414	1273	1157	1035	940	868	792	748	702	664	622	591	574	547
1424.17	1	-6	522	502	515	528	543	572	613	667	746	855	991	1178	1429	1806	2385	3141	3717
1391.39	1	-6	3553	3144	2469	1780	1316	1019	835	718	642	592	553	525	507	500	501	504	516
1359.57	0	-6	526	541	562	579	607	646	694	742	810	869	933	998	1075	1158	1259	1384	1547
1343.18	0	-5	174	200	232	262	296	347	423	533	695	939	1305	1819	2397	2736	2630	2251	1822
1326.79	0	-5	1433	1107	872	726	633	543	452	376	316	269	232	204	182	164	149	137	126
1309.43	1	-6	1099	972	870	790	714	666	632	606	586	576	585	582	581	564	542	519	500
1276.65	1	-7	4947	4948	4701	4494	4382	4340	4356	4452	4633	4955	5477	6220	7158	8022	8322	7920	7175
1243.86	1	-7	6463	5927	5589	5401	5306	5299	5370	5494	5660	5829	5947	6012	6054	6085	6160	6327	6561
1211.08	1	-6	687	731	795	885	984	1021	1022	1050	1109	1196	1314	1471	1682	1959	2266	2545	2814
1178.29	1	-6	3025	3151	3193	3228	3385	3759	4351	4940	5224	5049	4578	4036	3514	3070	2711	2434	2203
1145.51	1	-6	1982	1761	1559	1382	1232	1108	1005	921	850	790	737	696	662	631	606	585	566
1112.73	1	-7	5555	5517	5528	5523	5386	5205	5080	5018	4978	4969	4994	5007	5222	5519	5835	5965	6026
1079.94	1	-6	632	671	705	746	786	820	871	945	1030	1134	1282	1446	1634	1863	2165	2565	3145
1047.16	1	-5	400	538	777	1200	1914	2744	2948	2477	1852	1320	945	699	542	441	377	344	334
1014.37	1	-6	3394	3540	3622	3257	2792	2477	2286	2181	2136	2125	2164	2232	2243	2150	2087	2102	2099
981.59	1	-6	2056	2057	2096	2157	2223	2269	2273	2228	2148	2054	1962	1887	1844	1849	1918	2030	2084
948.81	1	-6	2045	2042	2084	1965	1749	1590	1487	1459	1552	1768	1845	1723	1668	1627	1525	1389	1270
916.02	1	-6	1182	1126	1094	1082	1083	1093	1109	1133	1161	1197	1239	1290	1349	1415	1493	1579	1680
883.24	1	-6	1800	1945	2117	2320	2559	2825	3095	3325	3463	3509	3496	3505	3549	3648	3795	3984	4169
850.45	1	-5	428	432	428	420	411	407	408	413	423	441	473	522	596	705	863	1115	1556
817.67	1	-5	2387	4025	6533	7252	5138	3132	2005	1397	1045	823	677	577	506	454	411	377	351
784.89	1	-6	3310	3196	3167	3290	3628	4214	4095	3316	2746	2424	2259	2173	2111	2084	2065	2054	1914
752.10	1	-6	2015	2017	2021	2053	2107	2176	2260	2344	2432	2538	2660	2796	2949	3123	3317	3539	3792
719.32	1	-5	408	442	482	533	605	672	719	786	875	985	1122	1292	1507	1785	2161	2709	3585
686.53	1	-4	509	769	1196	1831	2656	3585	4447	4852	4278	2928	1718	1019	651	446	328	256	209
653.75	1	-5	1742	1480	1275	1110	976	866	774	697	632	577	530	489	454	423	397	374	354
620.97	1	-6	3381	3250	3167	3146	3094	2928	2803	2726	2680	2651	2628	2607	2584	2564	2554	2555	2571
588.18	1	-6	2607	2286	2226	2139	1997	1967	1841	1677	1680	1614	1501	1533	1456	1251	1074	923	801
555.40	1	-5	76	69	75	91	104	115	137	168	182	217	273	327	404	561	773	1124	1712
522.61	1	-4	265	400	566	673	561	446	430	506	705	1152	2149	3935	5266	5101	4349	3679	2573
489.83	1	-4	1632	994	609	385	258	177	126	90	66	48	37	29	24	21	15	14	14

---

[a] See footnote a to Table IV.1.

[b] See footnote b to Table V.1 .

Table VI.6. Real refractive indices between 6500 and 450 cm^{-1} of 40.00% liquid benzene-h_6 in liquid benzene-d_6 at 25 °C.[a,b]

cm^{-1}	*XE*	0	1	2	3	4	5	6	7	8	9	10	11	12	13	14	15	16
6499.90	3	14786	14786	14786	14786	14786	14786	14786	14786	14786	14786	14786	14786	14786	14786	14786	14786	14786
6368.76	3	14786	14786	14786	14786	14786	14786	14786	14786	14786	14786	14786	14786	14786	14786	14786	14786	14786
6237.63	3	14786	14786	14786	14786	14786	14786	14786	14786	14786	14786	14786	14786	14786	14786	14786	14786	14786
6106.49	3	14786	14786	14786	14786	14786	14786	14786	14786	14786	14786	14786	14785	14785	14785	14785	14785	14786
5975.36	3	14786	14786	14786	14786	14786	14786	14786	14786	14786	14787	14786	14786	14786	14786	14786	14786	14786
5844.22	3	14786	14786	14786	14786	14786	14786	14786	14786	14786	14786	14786	14786	14786	14786	14786	14786	14786
5713.09	3	14786	14786	14786	14786	14786	14786	14786	14786	14786	14786	14786	14786	14786	14786	14786	14786	14786
5581.95	3	14786	14786	14785	14785	14785	14785	14785	14785	14785	14785	14785	14785	14785	14785	14785	14785	14785
5450.81	3	14785	14785	14785	14785	14785	14785	14785	14785	14785	14785	14785	14785	14785	14785	14785	14785	14785
5319.68	3	14785	14785	14785	14785	14785	14785	14785	14785	14785	14785	14785	14785	14785	14785	14785	14785	14785
5188.54	3	14785	14785	14785	14785	14785	14785	14785	14785	14785	14784	14784	14784	14784	14784	14784	14784	14784
5057.41	3	14784	14784	14784	14784	14784	14784	14784	14784	14784	14784	14784	14784	14784	14784	14784	14784	14784
4926.27	3	14784	14784	14784	14784	14784	14784	14784	14784	14784	14784	14784	14784	14784	14783	14783	14783	14783
4798.99	2	14783	14783	14783	14783	14783	14783	14783	14783	14783	14783	14783	14783	14783	14783	14783	14783	14783
4733.42	2	14783	14783	14783	14783	14783	14782	14782	14782	14782	14782	14782	14782	14782	14782	14782	14782	14782
4667.86	2	14783	14783	14783	14783	14782	14782	14782	14783	14783	14783	14783	14782	14783	14783	14783	14783	14783
4602.29	2	14783	14783	14783	14782	14782	14783	14783	14784	14783	14783	14783	14783	14783	14783	14782	14782	14783
4536.72	2	14782	14782	14782	14782	14782	14782	14781	14781	14781	14780	14780	14780	14780	14781	14782	14784	14785
4471.15	2	14785	14785	14784	14784	14784	14784	14784	14784	14784	14784	14784	14784	14784	14784	14784	14784	14784
4405.58	2	14784	14784	14784	14783	14783	14783	14783	14783	14784	14784	14783	14783	14783	14783	14783	14783	14783
4340.02	2	14783	14783	14783	14783	14783	14783	14783	14782	14782	14782	14782	14782	14782	14782	14782	14782	14782
4274.45	2	14782	14782	14782	14782	14782	14782	14782	14782	14782	14782	14782	14782	14782	14781	14781	14781	14781
4208.88	2	14781	14781	14781	14781	14781	14781	14781	14781	14781	14781	14781	14781	14781	14781	14781	14781	14781
4143.31	2	14780	14780	14780	14780	14780	14780	14780	14780	14779	14779	14779	14779	14778	14778	14778	14778	14778
4077.74	2	14778	14777	14776	14775	14775	14778	14785	14788	14788	14787	14786	14785	14785	14784	14784	14784	14784
4014.11	1	14784	14784	14783	14783	14783	14783	14783	14783	14783	14783	14783	14782	14782	14782	14782	14782	14782
3981.32	1	14782	14782	14782	14782	14782	14782	14782	14781	14781	14781	14781	14781	14781	14781	14782	14782	14782
3948.54	1	14781	14781	14781	14781	14781	14781	14781	14781	14782	14782	14782	14782	14782	14781	14781	14781	14781
3915.75	1	14781	14781	14781	14781	14781	14781	14781	14781	14781	14781	14781	14781	14781	14781	14781	14781	14781
3882.97	1	14781	14781	14781	14781	14781	14781	14781	14780	14780	14780	14780	14780	14780	14780	14780	14780	14780
3850.19	1	14780	14780	14780	14780	14779	14779	14779	14779	14779	14779	14779	14780	14780	14780	14780	14780	14780
3817.40	1	14780	14780	14780	14779	14779	14779	14779	14780	14781	14781	14782	14782	14782	14782	14781	14781	14781
3784.62	1	14781	14781	14781	14781	14780	14780	14780	14780	14780	14780	14780	14780	14780	14780	14780	14780	14780
3751.83	1	14780	14779	14779	14779	14779	14779	14779	14779	14779	14779	14779	14779	14779	14779	14779	14779	14779
3719.05	1	14779	14779	14779	14779	14779	14779	14778	14778	14778	14778	14778	14778	14779	14780	14780	14780	14780
3686.27	1	14780	14780	14780	14780	14780	14780	14780	14779	14779	14779	14779	14779	14779	14779	14779	14778	14778
3653.48	1	14778	14778	14777	14777	14777	14777	14779	14780	14780	14780	14779	14779	14779	14779	14779	14779	14779
3620.70	1	14779	14779	14779	14779	14779	14779	14780	14780	14780	14780	14780	14779	14779	14779	14779	14779	14779
3587.91	1	14779	14779	14779	14779	14779	14779	14779	14779	14779	14779	14778	14778	14778	14778	14778	14778	14778
3555.13	1	14778	14778	14778	14778	14778	14778	14778	14778	14778	14778	14778	14778	14778	14778	14777	14777	14777
3522.35	1	14777	14777	14777	14777	14777	14777	14777	14777	14777	14777	14777	14777	14777	14777	14777	14777	14776
3489.56	1	14776	14776	14776	14776	14776	14776	14776	14776	14776	14776	14776	14776	14776	14776	14776	14776	14776
3456.78	1	14775	14775	14775	14775	14775	14776	14776	14776	14776	14776	14775	14775	14775	14775	14775	14775	14775
3423.99	1	14775	14775	14775	14775	14775	14775	14775	14775	14775	14775	14775	14774	14774	14774	14774	14774	14774
3391.21	1	14774	14774	14774	14774	14774	14774	14774	14774	14774	14774	14773	14773	14773	14773	14773	14773	14773
3358.43	1	14773	14773	14773	14773	14773	14773	14772	14772	14772	14772	14772	14772	14772	14772	14771	14771	14771
3325.64	1	14771	14771	14771	14771	14771	14771	14771	14771	14771	14771	14770	14770	14770	14770	14770	14770	14769
3292.86	1	14769	14769	14769	14769	14768	14768	14768	14768	14768	14768	14768	14768	14768	14768	14767	14767	14767
3260.07	1	14766	14766	14766	14765	14765	14764	14764	14763	14762	14761	14761	14761	14763	14766	14769	14772	14773
3227.29	1	14774	14774	14774	14773	14772	14772	14771	14770	14770	14769	14769	14769	14768	14768	14767	14767	14767
3194.51	1	14766	14766	14765	14765	14765	14765	14764	14764	14763	14763	14763	14762	14762	14761	14761	14761	14760
3161.72	1	14760	14759	14759	14758	14758	14757	14756	14756	14756	14755	14754	14754	14753	14752	14752	14751	14750
3128.94	1	14749	14748	14746	14745	14743	14742	14740	14738	14736	14734	14732	14729	14725	14721	14715	14708	14699
3096.15	1	14689	14685	14705	14754	14787	14792	14787	14779	14771	14760	14748	14737	14739	14779	14797	14796	14790
3063.37	1	14784	14779	14773	14768	14765	14760	14753	14745	14735	14722	14707	14691	14684	14706	14763	14825	14862
3030.59	1	14875	14878	14875	14869	14862	14855	14849	14844	14840	14836	14832	14829	14827	14824	14823	14821	14820
2997.80	1	14818	14817	14816	14814	14813	14812	14811	14809	14808	14807	14807	14806	14805	14804	14803	14802	14802
2965.02	1	14801	14801	14800	14799	14799	14798	14798	14797	14797	14797	14796	14796	14795	14795	14795	14794	14794
2932.23	1	14793	14793	14793	14792	14792	14792	14791	14791	14791	14790	14790	14789	14789	14789	14790	14790	14789
2899.45	1	14789	14788	14788	14787	14786	14786	14787	14790	14790	14790	14789	14789	14788	14788	14787	14787	14786
2866.67	1	14786	14785	14784	14784	14785	14787	14788	14788	14788	14787	14787	14787	14787	14787	14786	14786	14786
2833.88	1	14785	14785	14786	14786	14785	14785	14785	14785	14786	14786	14786	14786	14786	14786	14786	14785	14785
2801.10	1	14785	14785	14784	14784	14784	14784	14784	14783	14783	14783	14783	14783	14783	14783	14783	14783	14783
2768.32	1	14783	14782	14782	14782	14782	14782	14782	14782	14782	14781	14781	14781	14781	14781	14781	14781	14781
2735.53	1	14780	14780	14780	14780	14780	14780	14780	14780	14780	14779	14779	14779	14779	14779	14779	14779	14779
2702.75	1	14779	14778	14778	14778	14778	14778	14778	14778	14778	14778	14777	14777	14777	14777	14777	14777	14777
2669.96	1	14777	14776	14776	14776	14776	14775	14775	14775	14775	14776	14777	14777	14777	14777	14777	14776	14776
2637.18	1	14776	14776	14775	14775	14775	14775	14774	14774	14774	14774	14774	14774	14775	14775	14775	14775	14775
2604.40	1	14775	14774	14774	14773	14774	14775	14776	14776	14776	14775	14775	14775	14774	14774	14774	14774	14774
2571.61	1	14774	14774	14773	14773	14773	14773	14773	14773	14772	14773	14772	14772	14772	14772	14772	14772	14772
2539.79	0	14771	14771	14771	14771	14771	14771	14771	14771	14771	14771	14770	14770	14770	14770	14770	14770	14770
2523.40	0	14769	14770	14770	14770	14771	14771	14771	14770	14770	14770	14770	14770	14770	14770	14770	14770	14770
2507.01	0	14769	14769	14769	14769	14769	14769	14769	14769	14769	14769	14768	14768	14768	14768	14768	14768	14768
2489.65	1	14768	14768	14767	14767	14767	14767	14767	14767	14766	14766	14766	14766	14766	14765	14765	14765	14765
2456.87	1	14764	14764	14764	14764	14763	14763	14763	14763	14763	14762	14762	14761	14761	14761	14760	14760	14760
2424.08	1	14759	14759	14758	14758	14757	14757	14756	14756	14755	14754	14754	14753	14752	14750	14749	14746	14744
2391.30	1	14743	14748	14757	14760	14760	14759	14757	14756	14759	14762	14762	14761	14759	14757	14756	14757	14758
2358.52	1	14757	14756	14754	14753	14752	14750	14749	14748	14748	14747	14745	14744	14742	14741	14740	14738	14737

Table VI.6. Continued.

cm^{-1}	*XE*	0	1	2	3	4	5	6	7	8	9	10	11	12	13	14	15	16
2325.73	1	14738	14741	14741	14739	14736	14733	14730	14727	14724	14720	14716	14712	14707	14702	14695	14688	14679
2292.95	1	14669	14655	14637	14616	14596	14598	14655	14746	14811	14830	14821	14810	14831	14877	14899	14901	14895
2260.16	1	14887	14879	14871	14865	14859	14853	14849	14845	14841	14837	14834	14831	14828	14825	14823	14821	14819
2227.38	1	14817	14815	14813	14812	14810	14808	14806	14805	14804	14807	14807	14806	14805	14804	14803	14802	14801
2194.60	1	14801	14800	14799	14798	14798	14797	14796	14796	14795	14794	14794	14793	14793	14792	14792	14791	14791
2161.81	1	14790	14790	14789	14789	14788	14788	14788	14788	14788	14787	14787	14787	14786	14786	14786	14785	14785
2129.03	1	14785	14785	14784	14784	14784	14783	14783	14783	14782	14782	14782	14782	14781	14781	14781	14780	14780
2096.24	1	14780	14780	14779	14779	14779	14779	14778	14778	14778	14778	14777	14777	14777	14777	14776	14776	14776
2063.46	1	14776	14775	14775	14775	14774	14774	14774	14774	14773	14773	14773	14773	14772	14772	14772	14772	14771
2030.68	1	14771	14771	14770	14770	14770	14769	14769	14768	14768	14767	14766	14766	14766	14766	14767	14767	14766
1997.89	1	14766	14765	14764	14764	14763	14763	14763	14762	14761	14760	14759	14757	14755	14753	14751	14749	14748
1965.11	1	14750	14756	14765	14775	14783	14788	14790	14790	14789	14787	14785	14784	14782	14781	14780	14779	14778
1932.32	1	14777	14777	14776	14775	14774	14774	14773	14772	14772	14771	14770	14770	14769	14768	14768	14768	14769
1899.54	1	14768	14768	14767	14767	14766	14765	14765	14764	14764	14763	14763	14762	14762	14761	14761	14760	14760
1866.76	1	14761	14761	14761	14761	14762	14761	14760	14759	14758	14757	14756	14755	14753	14752	14751	14749	14747
1833.97	1	14745	14742	14739	14737	14734	14732	14732	14737	14746	14759	14774	14785	14793	14796	14796	14795	14793
1801.19	1	14790	14788	14787	14786	14784	14783	14782	14781	14779	14778	14777	14776	14775	14774	14773	14772	14771
1768.40	1	14770	14769	14768	14767	14766	14765	14765	14766	14768	14768	14768	14767	14766	14766	14765	14764	14764
1735.62	1	14763	14763	14762	14762	14761	14760	14760	14759	14759	14758	14757	14757	14757	14757	14757	14756	14755
1702.84	1	14755	14754	14753	14753	14752	14752	14752	14752	14752	14751	14750	14750	14752	14752	14752	14751	14752
1670.05	1	14753	14753	14753	14752	14751	14750	14749	14749	14748	14747	14746	14745	14744	14743	14742	14740	14739
1637.27	1	14737	14735	14733	14730	14727	14722	14717	14711	14708	14719	14744	14767	14776	14776	14774	14771	14768
1604.48	1	14765	14763	14760	14758	14756	14754	14752	14751	14749	14749	14748	14747	14746	14745	14744	14743	14741
1571.70	1	14740	14740	14740	14739	14737	14735	14734	14732	14730	14728	14727	14728	14730	14729	14727	14724	14721
1538.92	1	14719	14716	14716	14716	14719	14722	14726	14729	14729	14729	14727	14724	14720	14717	14712	14708	14702
1507.10	0	14700	14697	14694	14691	14687	14684	14680	14676	14672	14668	14662	14657	14651	14644	14637	14628	14618
1490.71	0	14608	14595	14580	14562	14541	14516	14487	14455	14424	14408	14441	14566	14761	14929	15017	15043	15031
1474.31	0	15003	14976	14958	14949	14938	14923	14908	14895	14882	14871	14860	14850	14841	14832	14824	14817	14810
1457.92	0	14806	14803	14803	14807	14813	14821	14829	14835	14840	14842	14842	14841	14839	14837	14835	14832	14830
1441.53	0	14827	14824	14822	14819	14817	14814	14812	14810	14808	14805	14803	14801	14800	14798	14796	14794	14793
1424.17	1	14790	14787	14784	14781	14779	14776	14774	14771	14769	14766	14764	14761	14758	14756	14754	14756	14764
1391.39	1	14773	14779	14782	14782	14779	14776	14772	14770	14767	14764	14762	14759	14757	14755	14752	14750	14747
1359.57	0	14745	14744	14742	14741	14739	14737	14735	14733	14731	14729	14727	14724	14722	14719	14716	14712	14708
1343.18	0	14704	14699	14694	14689	14682	14674	14663	14652	14639	14625	14616	14621	14656	14727	14802	14852	14878
1326.79	0	14888	14886	14877	14867	14861	14857	14852	14846	14840	14835	14830	14825	14821	14817	14814	14811	14808
1309.43	1	14803	14799	14795	14792	14789	14787	14784	14782	14780	14778	14776	14775	14774	14773	14771	14770	14769
1276.65	1	14768	14767	14766	14765	14763	14762	14761	14760	14759	14757	14756	14755	14755	14755	14755	14755	14755
1243.86	1	14754	14754	14753	14751	14750	14749	14748	14747	14747	14746	14745	14744	14743	14742	14741	14740	14739
1211.08	1	14738	14736	14735	14734	14733	14733	14732	14731	14729	14727	14726	14724	14722	14721	14721	14721	14722
1178.29	1	14723	14725	14726	14726	14725	14723	14725	14730	14738	14746	14752	14756	14757	14757	14756	14755	14754
1145.51	1	14753	14752	14751	14750	14748	14746	14745	14743	14741	14740	14738	14737	14735	14734	14732	14731	14729
1112.73	1	14728	14726	14725	14724	14723	14721	14720	14718	14717	14715	14713	14712	14710	14708	14706	14704	14702
1079.94	1	14700	14698	14696	14693	14691	14688	14685	14682	14678	14674	14669	14665	14659	14653	14646	14637	14626
1047.16	1	14612	14595	14575	14555	14554	14611	14722	14804	14840	14845	14835	14821	14806	14794	14782	14772	14764
1014.37	1	14759	14755	14755	14756	14754	14750	14746	14742	14739	14735	14733	14731	14730	14729	14726	14724	14723
981.59	1	14721	14719	14718	14716	14715	14715	14714	14714	14713	14712	14711	14709	14707	14705	14703	14702	14702
948.81	1	14701	14700	14700	14701	14699	14697	14695	14692	14689	14687	14688	14688	14686	14685	14684	14683	14680
916.02	1	14678	14675	14673	14670	14667	14665	14662	14660	14657	14654	14652	14649	14646	14643	14640	14637	14634
883.24	1	14631	14628	14625	14622	14619	14616	14615	14614	14613	14612	14610	14608	14604	14601	14598	14594	14592
850.45	1	14590	14587	14584	14580	14575	14568	14560	14551	14541	14529	14515	14498	14478	14455	14426	14390	14342
817.67	1	14286	14251	14370	14720	14946	14963	14917	14869	14830	14798	14772	14750	14731	14715	14701	14688	14676
784.89	1	14665	14654	14643	14633	14624	14620	14622	14618	14609	14599	14589	14580	14571	14562	14553	14545	14534
752.10	1	14524	14515	14505	14494	14483	14472	14461	14449	14436	14423	14409	14394	14378	14362	14344	14325	14305
719.32	1	14283	14259	14233	14205	14175	14145	14109	14068	14022	13969	13910	13841	13760	13664	13546	13398	13211
686.53	1	12975	12701	12431	12259	12315	12733	13651	15136	16751	17600	17533	17138	16764	16464	16230	16049	15907
653.75	1	15793	15699	15620	15552	15493	15441	15394	15353	15315	15281	15250	15222	15195	15171	15148	15127	15106
620.97	1	15087	15069	15052	15036	15022	15007	14993	14979	14966	14953	14940	14928	14917	14905	14894	14883	14872
588.18	1	14863	14852	14841	14830	14818	14807	14796	14783	14769	14757	14743	14729	14715	14700	14684	14667	14648
555.40	1	14629	14608	14586	14563	14539	14513	14484	14455	14421	14384	14342	14296	14241	14177	14107	14021	13927
522.61	1	13834	13765	13761	13885	13954	13812	13566	13247	12832	12291	11731	11928	13625	15502	16557	17391	17879
489.83	1	17801	17501	17158	16856	16611	16416	16259	16130	16024	15931	15853	15786	15727	15679	15633	15589	15553

[a,b] See footnotes a and b to Table IV.2.

Table VI.7. Imaginary refractive indices between 6500 and 450 cm^{-1} of 51.95% liquid benzene-h$_6$ in liquid benzene-d$_6$ at 25 °C.[a,b]

cm^{-1}	*XE*	*YE*	0	1	2	3	4	5	6	7	8	9	10	11	12	13	14	15	16
6499.90	3	0	0	0	0	0	0	0	0	0	0	0	0	0	0	0	0	0	0
6368.76	3	-7	3	6	6	6	7	6	5	7	8	7	14	14	13	10	8	10	11
6237.63	3	-7	9	9	13	14	18	19	27	33	52	58	92	167	211	216	179	174	187
6106.49	3	-7	190	180	229	163	109	90	88	109	140	206	292	382	461	727	1048	1496	2231
5975.36	3	-7	1744	1304	1033	917	759	591	815	699	1180	945	592	381	442	457	443	407	307
5844.22	3	-7	213	133	99	78	75	94	101	99	121	144	152	104	91	96	87	70	82
5713.09	3	-7	146	156	203	215	171	115	97	99	95	67	51	51	60	105	123	95	72
5581.95	3	-7	76	82	76	74	92	129	148	123	123	131	89	67	51	46	40	37	41
5450.81	3	-7	42	49	66	87	85	68	85	78	71	84	99	102	103	115	118	104	99
5319.68	3	-7	91	85	70	67	70	67	74	86	109	116	103	78	68	60	57	54	53
5188.54	3	-7	57	55	49	51	71	76	72	73	72	65	58	69	84	82	70	71	64
5057.41	3	-7	64	67	62	53	50	51	60	69	72	62	67	64	69	63	56	57	63
4926.27	3	-7	63	66	71	76	73	80	83	108	124	130	156	143	114	99	82	80	76
4798.99	2	-7	79	82	86	94	107	111	109	109	109	110	113	115	121	135	154	159	159
4733.42	2	-7	164	174	186	202	225	255	288	345	435	531	726	1016	990	935	1045	1548	2661
4667.86	2	-7	2875	1770	1181	988	1128	1719	2332	2360	1803	1254	1211	1844	2209	1596	1201	1132	1295
4602.29	2	-7	1324	1157	1118	1419	2252	2799	2240	1608	1115	846	711	662	645	679	842	1057	949
4536.72	2	-7	740	600	523	494	499	538	614	731	913	1207	1659	2318	3136	3950	4473	4381	3553
4471.15	2	-7	2593	1963	1712	1744	1924	2013	1847	1593	1428	1385	1328	1189	1039	867	777	804	836
4405.58	2	-7	875	824	770	770	793	713	765	952	872	692	531	414	339	301	277	280	300
4340.02	2	-7	306	290	275	265	253	237	232	234	243	257	269	284	297	298	297	298	305
4274.45	2	-7	326	375	477	663	688	575	507	504	534	517	489	475	477	535	645	654	626
4208.88	2	-7	633	629	695	878	919	774	665	640	709	823	766	676	630	611	609	597	593
4143.31	2	-7	609	664	703	708	728	752	792	855	948	1086	1305	1637	2003	2288	2649	3398	4313
4077.74	2	-6	437	439	521	719	1165	1734	1707	1144	714	452	304	227	205	228	226	172	135
4014.11	1	-7	1224	1126	1053	988	923	862	810	768	733	707	694	692	707	734	758	765	770
3981.32	1	-7	766	729	686	653	625	606	609	658	808	1049	1195	1317	1500	1560	1417	1219	1064
3948.54	1	-7	961	898	882	946	1117	1429	1952	2090	1771	1503	1291	1128	1005	918	858	823	807
3915.75	1	-7	792	771	753	744	743	745	746	747	741	727	720	734	785	912	989	929	872
3882.97	1	-7	814	760	711	680	665	661	657	643	624	609	606	609	613	613	608	600	593
3850.19	1	-7	594	602	613	631	659	707	789	927	1151	1472	1823	2003	1914	1684	1449	1287	1232
3817.40	1	-7	1294	1374	1383	1415	1552	1877	2457	3136	3321	2876	2291	1816	1477	1252	1116	1022	918
3784.62	1	-7	820	743	687	656	653	674	711	751	771	745	687	636	599	575	562	560	571
3751.83	1	-7	596	636	701	797	925	1048	1082	1040	988	936	890	858	847	856	884	925	956
3719.05	1	-7	970	980	996	1023	1065	1138	1252	1396	1588	1896	2472	3481	4221	3681	2891	2477	2360
3686.27	1	-7	2283	2041	1702	1409	1203	1061	953	875	835	825	840	842	797	745	719	722	755
3653.48	1	-7	825	960	1222	1731	2705	4161	4991	4138	2943	2190	1796	1600	1514	1525	1628	1754	1834
3620.70	1	-7	1858	1869	1951	2130	2329	2389	2228	1915	1585	1314	1100	955	848	763	699	654	619
3587.91	1	-7	594	580	592	600	612	637	607	548	489	446	418	399	385	375	365	357	354
3555.13	1	-7	358	370	386	401	405	398	386	371	355	337	320	307	296	283	272	266	267
3522.35	1	-7	272	286	316	356	378	346	314	297	290	287	284	280	275	274	282	304	343
3489.56	1	-7	407	451	408	362	335	315	305	300	296	298	306	321	346	382	412	446	496
3456.78	1	-7	571	672	789	911	994	996	926	822	723	640	573	526	506	523	593	658	629
3423.99	1	-7	604	601	602	598	577	547	517	493	478	477	487	504	516	520	511	492	471
3391.21	1	-7	456	444	425	403	382	363	347	335	327	326	331	341	356	374	390	402	408
3358.43	1	-7	408	401	387	372	363	359	355	346	339	339	347	367	397	431	472	552	699
3325.64	1	-7	892	984	914	789	687	615	566	532	509	498	496	498	500	507	520	540	567
3292.86	1	-7	603	652	718	807	919	1048	1179	1298	1405	1528	1682	1768	1727	1626	1530	1473	1465
3260.07	1	-6	150	158	172	188	207	232	260	301	362	462	617	834	1070	1227	1215	1063	879
3227.29	1	-7	7308	6086	4977	4038	3302	2778	2430	2232	2163	2135	2045	1925	1820	1749	1707	1687	1683
3194.51	1	-7	1693	1720	1770	1835	1890	1915	1927	1934	1955	1987	2045	2112	2199	2305	2396	2479	2544
3161.72	1	-7	2607	2677	2762	2880	3029	3216	3436	3636	3743	3804	3876	4016	4210	4454	4660	4819	4998
3128.94	1	-6	523	549	581	618	660	708	765	839	939	1055	1168	1280	1444	1674	2034	2632	3724
3096.15	1	-5	572	931	1425	1588	1254	888	657	521	430	402	447	611	992	1166	866	631	496
3063.37	1	-5	420	372	351	357	348	327	323	340	377	457	616	918	1448	2159	2626	2505	2017
3030.59	1	-5	1553	1194	913	705	557	453	377	321	280	248	224	207	193	181	169	159	147
2997.80	1	-6	1345	1237	1103	993	925	847	784	730	676	645	613	573	538	501	474	446	443
2965.02	1	-7	4330	4266	4091	3942	3979	3905	3894	3779	3777	3562	3355	3193	3150	3096	3050	3044	3006
2932.24	1	-7	2970	2933	2885	2830	2761	2693	2628	2552	2499	2551	2774	3239	3959	4618	4517	3869	3294
2899.45	1	-7	2928	2751	2807	3216	4245	6302	8727	7902	5446	4139	3392	2885	2559	2354	2246	2239	2311
2866.67	1	-7	2438	2721	3281	4295	5555	5802	5051	4282	3695	3296	3230	3300	2951	2590	2369	2283	2329
2833.88	1	-7	2546	2977	3090	2868	2800	3109	3718	4333	4428	3763	3021	2515	2123	1778	1510	1316	1165
2801.10	1	-7	1054	987	954	944	941	930	919	911	912	911	907	913	941	997	1058	1072	1025
2768.32	1	-7	942	857	784	726	683	650	620	595	577	560	535	506	481	461	447	439	435
2735.53	1	-7	437	445	451	442	431	422	415	411	412	414	415	416	415	412	411	412	415
2702.75	1	-7	420	426	433	438	445	453	461	472	485	502	520	537	550	560	569	582	600
2669.96	1	-7	626	665	721	801	924	1131	1504	2234	3635	4641	3365	2229	1671	1346	1114	977	893
2637.18	1	-7	830	792	778	782	807	858	947	1095	1346	1773	2364	3075	3517	3128	2514	2068	1797
2604.40	1	-7	1672	1716	2011	2732	4108	4706	3398	2325	1691	1313	1109	1010	960	964	978	1029	1079
2571.61	1	-7	1033	940	874	845	847	873	919	994	1108	1164	1060	915	808	736	689	653	620
2539.79	0	-7	606	593	582	575	569	566	565	566	568	572	583	603	635	685	763	889	1100
2523.40	0	-7	1416	1702	1761	1679	1544	1388	1246	1131	1041	968	904	851	806	769	739	714	696
2507.01	0	-7	682	672	666	661	656	652	650	650	652	656	662	670	681	696	716	741	770
2489.65	1	-7	839	921	1020	1074	992	892	832	809	817	864	950	982	927	884	852	841	856
2456.87	1	-7	894	956	1028	1078	1109	1094	1025	971	944	941	958	994	1058	1164	1270	1312	1342
2424.08	1	-7	1389	1452	1533	1644	1803	2009	2238	2440	2596	2725	2870	3071	3378	3842	4561	5754	7948
2391.30	1	-6	1293	1886	1845	1517	1279	1114	1062	1199	1387	1194	898	710	632	646	745	785	690
2358.52	1	-6	588	512	473	454	454	473	517	567	602	602	602	642	730	793	862	1048	1374

Table VI.7. Continued.

cm^{-1}	*XE*	*YE*	0	1	2	3	4	5	6	7	8	9	10	11	12	13	14	15	16
2325.73	1	-6	1726	1685	1358	1093	940	862	829	832	861	909	992	1109	1259	1427	1619	1857	2159
2292.95	1	-5	257	317	417	604	956	1554	2194	2288	1908	1513	1296	1317	1468	1378	1101	845	661
2260.16	1	-6	5285	4319	3584	3039	2618	2296	2027	1795	1578	1399	1257	1139	1041	960	891	830	776
2227.38	1	-6	724	680	643	611	592	599	655	811	1095	1138	909	718	577	485	432	409	392
2194.60	1	-7	3535	3184	2924	2703	2514	2350	2213	2110	2019	1973	1941	1891	1807	1742	1658	1589	1527
2161.81	1	-7	1475	1462	1494	1634	1878	2112	2146	1971	1766	1626	1530	1442	1369	1289	1213	1136	1092
2129.03	1	-7	1063	1008	951	895	861	830	815	811	812	804	777	753	724	700	682	668	660
2096.24	1	-7	630	627	629	639	647	647	651	651	641	647	623	600	579	570	559	551	546
2063.46	1	-7	545	560	599	648	717	799	867	979	1097	1159	1165	1140	1139	1170	1225	1263	1295
2030.68	1	-7	1305	1316	1316	1345	1360	1425	1502	1645	1864	2220	2854	3815	4866	5780	5642	4817	4183
1997.89	1	-6	391	405	448	493	583	651	609	581	593	630	701	810	963	1199	1564	2112	2889
1965.11	1	-6	3846	4781	5351	5320	4767	3969	3162	2467	1920	1507	1209	1000	860	763	676	595	522
1932.32	1	-7	4583	4058	3601	3257	2963	2743	2580	2480	2452	2430	2326	2228	2281	2484	2901	3400	3220
1899.54	1	-7	2753	2433	2234	2159	2214	2437	2766	3006	3130	3194	3356	3628	3971	4232	4475	4958	5721
1866.76	1	-7	5964	5903	6248	6348	5717	4967	4505	4332	4370	4520	4812	5225	5731	6343	7129	8120	9427
1833.97	1	-6	1116	1357	1694	2165	2827	3722	4867	6170	7391	8132	8091	7322	6173	4981	3941	3104	2469
1801.19	1	-6	2021	1746	1505	1327	1170	1017	867	731	618	528	458	405	364	334	310	293	280
1768.41	1	-7	2721	2712	2815	3092	3661	4725	6411	7847	7303	5501	4043	3247	2682	2254	1973	1781	1638
1735.62	1	-7	1537	1466	1421	1399	1401	1425	1459	1499	1593	1806	2256	3088	3340	2663	2352	2331	2437
1702.84	1	-7	2555	2725	2997	3436	4026	4627	4942	4832	4750	5125	6072	7414	8009	7591	7763	8700	9497
1670.05	1	-7	9164	7947	6662	5702	5102	4801	4692	4574	4383	4202	4088	4051	4100	4343	4489	4530	4763
1637.27	1	-6	513	563	630	716	847	1069	1461	2195	3496	5232	6108	5308	3951	2889	2217	1795	1489
1604.49	1	-6	1254	1080	953	874	837	830	842	875	919	950	943	907	854	807	775	763	777
1571.70	1	-6	858	906	835	780	757	756	783	829	904	1036	1229	1446	1460	1353	1323	1401	1594
1538.92	1	-6	1906	2312	2815	3340	3765	3979	3930	3648	3245	2822	2440	2132	1890	1711	1591	1510	1476
1507.10	0	-6	1481	1489	1517	1554	1603	1665	1742	1831	1938	2065	2217	2398	2607	2840	3123	3456	3868
1490.71	0	-5	439	502	587	702	870	1112	1465	2000	2823	4093	5884	7703	8271	7265	5710	4262	3132
1474.31	0	-5	2386	1954	1701	1445	1170	944	776	653	563	494	441	400	377	367	367	380	405
1457.92	0	-6	4434	4931	5484	6012	6370	6469	6279	5865	5325	4742	4177	3664	3214	2835	2513	2243	2011
1441.53	0	-6	1805	1619	1455	1315	1195	1094	998	920	852	794	743	702	667	636	612	592	578
1424.17	1	-6	560	549	550	558	578	608	648	699	780	894	1037	1239	1530	1982	2662	3507	4070
1391.39	1	-6	3806	3293	2592	1909	1434	1113	912	779	688	623	575	539	519	507	509	515	533
1359.57	0	-6	547	562	579	596	623	652	683	719	759	805	855	909	972	1044	1127	1233	1363
1343.18	0	-5	153	176	203	229	259	300	360	445	571	758	1048	1462	1921	2181	2087	1782	1446
1326.79	0	-5	1140	885	702	586	511	438	368	308	262	228	202	181	166	154	144	135	128
1309.43	1	-6	1152	1044	949	869	801	743	699	666	638	616	600	585	571	555	536	517	503
1276.65	1	-6	498	500	484	470	466	469	478	496	525	570	637	734	855	969	1020	980	889
1243.86	1	-7	7983	7292	6846	6589	6478	6459	6523	6655	6825	6992	7128	7240	7321	7418	7576	7801	8100
1211.08	1	-6	849	902	975	1076	1180	1221	1239	1285	1361	1467	1606	1787	2027	2342	2681	2987	3294
1178.29	1	-6	3541	3678	3680	3617	3626	3823	4240	4704	4936	4758	4347	3892	3472	3125	2853	2644	2459
1145.51	1	-6	2258	2040	1825	1632	1466	1326	1208	1110	1026	955	894	841	797	760	728	700	679
1112.73	1	-7	6639	6582	6612	6611	6446	6244	6085	5996	5941	5944	5991	6075	6203	6358	6561	6805	7049
1079.94	1	-6	730	762	797	834	882	941	1014	1103	1212	1345	1511	1719	1976	2297	2727	3242	3986
1047.16	1	-5	508	683	984	1518	2418	3477	3777	3203	2404	1713	1224	900	691	555	469	420	398
1014.37	1	-6	3965	4118	4254	3844	3284	2905	2675	2554	2502	2491	2535	2617	2625	2498	2397	2381	2367
981.59	1	-6	2311	2305	2334	2387	2446	2489	2487	2436	2344	2236	2121	2022	1950	1920	1948	2016	2041
948.81	1	-6	1989	1965	1979	1872	1690	1553	1459	1429	1494	1665	1729	1631	1594	1566	1481	1363	1260
916.02	1	-6	1186	1137	1114	1107	1105	1109	1120	1137	1161	1192	1228	1272	1324	1383	1451	1529	1620
883.24	1	-6	1728	1856	2006	2187	2398	2633	2877	3092	3242	3318	3364	3424	3538	3707	3914	4137	4342
850.45	1	-5	445	446	436	418	402	389	383	381	381	390	412	448	506	591	713	908	1257
817.67	1	-5	1918	3245	5283	5786	4058	2487	1605	1128	841	659	547	467	417	378	347	319	298
784.89	1	-6	2838	2796	2915	3173	3705	4456	4430	3583	2923	2563	2374	2279	2234	2230	2246	2287	2360
752.10	1	-6	2475	2520	2575	2666	2785	2904	3030	3157	3305	3472	3661	3863	4071	4301	4567	4863	5199
719.32	1	-5	557	602	652	699	754	823	893	986	1103	1248	1425	1646	1924	2284	2771	3481	4617
686.53	1	-4	657	994	1549	2372	3444	4650	5769	6294	5547	3792	2219	1311	832	567	415	322	262
653.75	1	-5	2181	1850	1591	1382	1084	889	773	698	638	586	541	502	468	438	412	390	371
620.97	1	-6	3566	3469	3430	3502	3651	3753	3609	3341	3101	2902	2743	2619	2481	2319	2154	2208	2213
588.18	1	-6	2099	2088	2056	2066	2095	2072	2184	2239	2230	2308	2300	2357	2301	2156	1891	1685	1445
555.40	1	-5	141	139	142	150	167	179	194	216	234	258	277	318	393	487	686	965	1450
522.62	1	-4	225	341	483	581	480	375	357	421	586	962	1824	3480	4633	4148	3363	2731	1875
489.83	1	-3	119	73	45	29	19	13	9	7	5	1656	1739	1788	1780	1750	1716	1686	1661
457.05	1	-3	1642	1626	1613	1602	1593												

---

[a] See footnote a to Table IV.1.

[b] See footnote b to Table V.1.

Table VI.8. Real refractive indices between 6500 and 450 cm^{-1} of 51.95% liquid benzene-h_6 in liquid benzene-d_6 at 25 °C.[a,b]

cm^{-1}	*XE*	0	1	2	3	4	5	6	7	8	9	10	11	12	13	14	15	16
6499.90	3	14788	14788	14788	14788	14788	14788	14788	14788	14788	14788	14788	14788	14788	14788	14788	14788	14788
6368.76	3	14788	14788	14788	14788	14788	14788	14788	14788	14788	14788	14788	14788	14788	14788	14788	14788	14788
6237.63	3	14788	14788	14788	14788	14788	14788	14788	14788	14788	14788	14788	14788	14788	14788	14788	14788	14788
6106.49	3	14788	14788	14788	14788	14788	14787	14787	14787	14787	14787	14787	14787	14787	14787	14787	14787	14787
5975.36	3	14788	14788	14788	14788	14788	14788	14788	14788	14788	14788	14788	14788	14788	14788	14788	14788	14788
5844.22	3	14788	14788	14788	14788	14788	14788	14788	14788	14788	14788	14788	14788	14788	14788	14788	14788	14787
5713.09	3	14787	14787	14787	14788	14788	14788	14787	14787	14787	14787	14787	14787	14787	14787	14787	14787	14787
5581.95	3	14787	14787	14787	14787	14787	14787	14787	14787	14787	14787	14787	14787	14787	14787	14787	14787	14787
5450.81	3	14787	14787	14787	14787	14787	14787	14787	14787	14787	14787	14787	14787	14787	14787	14787	14787	14787
5319.68	3	14787	14787	14787	14787	14787	14787	14787	14787	14786	14786	14786	14786	14786	14786	14786	14786	14786
5188.54	3	14786	14786	14786	14786	14786	14786	14786	14786	14786	14786	14786	14786	14786	14786	14786	14786	14786
5057.41	3	14786	14786	14786	14786	14786	14786	14786	14786	14786	14786	14786	14786	14786	14786	14786	14785	14785
4926.27	3	14785	14785	14785	14785	14785	14785	14785	14785	14785	14785	14785	14785	14785	14785	14785	14785	14785
4798.99	2	14785	14785	14785	14785	14785	14785	14785	14785	14785	14784	14784	14784	14784	14784	14784	14784	14784
4733.42	2	14784	14784	14784	14784	14784	14784	14784	14784	14783	14783	14783	14783	14783	14783	14783	14783	14783
4667.86	2	14784	14785	14785	14784	14784	14783	14784	14784	14785	14785	14784	14784	14785	14785	14785	14784	14784
4602.29	2	14784	14784	14784	14784	14784	14785	14785	14786	14785	14785	14785	14785	14785	14784	14784	14784	14784
4536.72	2	14784	14784	14784	14784	14784	14784	14783	14783	14783	14782	14782	14782	14782	14783	14784	14785	14786
4471.15	2	14786	14786	14785	14785	14785	14785	14785	14785	14785	14785	14785	14785	14785	14785	14785	14785	14785
4405.58	2	14785	14785	14785	14785	14785	14785	14784	14785	14785	14785	14785	14785	14785	14784	14784	14784	14784
4340.02	2	14784	14784	14784	14784	14784	14784	14784	14784	14784	14784	14783	14783	14783	14783	14783	14783	14783
4274.45	2	14783	14783	14783	14783	14783	14783	14783	14783	14783	14783	14783	14783	14783	14783	14782	14783	14782
4208.88	2	14782	14782	14782	14782	14782	14782	14782	14782	14782	14782	14782	14782	14782	14782	14782	14782	14782
4143.31	2	14781	14781	14781	14781	14781	14781	14780	14780	14780	14780	14779	14779	14779	14779	14778	14778	14778
4077.74	2	14778	14778	14777	14775	14775	14779	14788	14792	14791	14790	14789	14788	14787	14786	14786	14786	14786
4014.11	1	14786	14786	14785	14785	14785	14785	14785	14785	14785	14784	14784	14784	14784	14784	14784	14784	14784
3981.32	1	14784	14784	14784	14784	14783	14783	14783	14783	14783	14783	14783	14783	14783	14783	14783	14783	14783
3948.54	1	14783	14783	14783	14783	14782	14782	14782	14783	14783	14783	14783	14783	14783	14783	14783	14783	14783
3915.75	1	14783	14783	14783	14783	14783	14783	14783	14783	14782	14782	14782	14782	14782	14782	14782	14782	14782
3882.97	1	14782	14782	14782	14782	14782	14782	14782	14782	14782	14782	14782	14782	14782	14782	14782	14782	14781
3850.19	1	14781	14781	14781	14781	14781	14781	14781	14781	14780	14780	14781	14781	14781	14781	14781	14781	14781
3817.40	1	14781	14781	14781	14781	14781	14780	14780	14781	14782	14782	14783	14783	14783	14782	14782	14782	14782
3784.62	1	14782	14782	14782	14782	14781	14781	14781	14781	14781	14781	14781	14781	14781	14781	14781	14781	14781
3751.83	1	14781	14780	14780	14780	14780	14780	14780	14780	14780	14780	14780	14780	14780	14780	14780	14780	14780
3719.05	1	14780	14780	14780	14780	14779	14779	14779	14779	14779	14779	14778	14779	14780	14781	14781	14781	14781
3686.27	1	14781	14781	14781	14781	14781	14781	14781	14781	14780	14780	14780	14780	14780	14780	14780	14779	14779
3653.48	1	14779	14779	14778	14778	14777	14778	14780	14781	14781	14781	14781	14781	14780	14780	14780	14780	14780
3620.70	1	14780	14780	14780	14780	14780	14780	14781	14781	14781	14781	14781	14781	14781	14780	14780	14780	14780
3587.91	1	14780	14780	14780	14780	14780	14780	14780	14780	14780	14780	14779	14779	14779	14779	14779	14779	14779
3555.13	1	14779	14779	14779	14779	14779	14779	14779	14779	14779	14779	14778	14778	14778	14778	14778	14778	14778
3522.35	1	14778	14778	14778	14778	14778	14778	14778	14778	14778	14778	14778	14778	14777	14777	14777	14777	14777
3489.56	1	14777	14777	14777	14777	14777	14777	14777	14777	14777	14777	14777	14776	14776	14776	14776	14776	14776
3456.78	1	14776	14776	14776	14776	14776	14776	14776	14776	14776	14776	14776	14776	14776	14776	14776	14776	14776
3423.99	1	14776	14776	14775	14775	14775	14775	14775	14775	14775	14775	14775	14775	14775	14775	14775	14775	14775
3391.21	1	14775	14774	14774	14774	14774	14774	14774	14774	14774	14774	14774	14774	14774	14773	14773	14773	14773
3358.43	1	14773	14773	14773	14773	14773	14773	14773	14772	14772	14772	14772	14772	14772	14772	14771	14771	14771
3325.64	1	14771	14771	14771	14771	14771	14771	14771	14771	14771	14770	14770	14770	14770	14770	14770	14769	14769
3292.86	1	14769	14769	14769	14768	14768	14768	14768	14768	14768	14767	14767	14767	14767	14767	14767	14767	14766
3260.07	1	14766	14766	14765	14765	14764	14764	14763	14763	14762	14761	14761	14761	14762	14764	14767	14770	14771
3227.29	1	14771	14771	14771	14770	14769	14769	14768	14768	14767	14767	14766	14766	14765	14765	14764	14764	14764
3194.51	1	14763	14763	14762	14762	14762	14761	14761	14760	14760	14759	14759	14759	14758	14758	14757	14757	14756
3161.72	1	14756	14755	14754	14754	14753	14752	14752	14751	14750	14750	14749	14748	14747	14746	14745	14744	14743
3128.94	1	14742	14740	14739	14737	14735	14733	14731	14729	14726	14723	14720	14717	14712	14706	14698	14689	14677
3096.15	1	14664	14658	14682	14746	14791	14799	14793	14783	14772	14758	14742	14726	14728	14777	14803	14803	14796
3063.37	1	14788	14780	14773	14766	14763	14756	14747	14736	14723	14706	14686	14665	14654	14679	14755	14842	14892
3030.59	1	14909	14912	14908	14899	14890	14881	14873	14866	14860	14855	14850	14846	14843	14840	14838	14836	14834
2997.80	1	14832	14830	14829	14827	14825	14824	14822	14821	14819	14818	14817	14816	14815	14814	14813	14812	14811
2965.02	1	14810	14809	14808	14807	14807	14806	14806	14805	14805	14804	14804	14803	14802	14802	14801	14801	14800
2932.24	1	14800	14800	14799	14799	14798	14798	14798	14797	14797	14796	14795	14795	14794	14795	14796	14796	14795
2899.45	1	14795	14794	14793	14792	14791	14791	14793	14796	14797	14796	14795	14795	14794	14794	14793	14792	14792
2866.67	1	14791	14791	14790	14790	14790	14792	14793	14793	14793	14792	14792	14792	14792	14792	14791	14791	14790
2833.88	1	14790	14790	14790	14790	14790	14789	14789	14789	14790	14791	14791	14791	14791	14791	14790	14790	14790
2801.10	1	14789	14789	14789	14789	14788	14788	14788	14788	14788	14787	14787	14787	14787	14787	14787	14787	14787
2768.32	1	14787	14787	14786	14786	14786	14786	14786	14786	14786	14785	14785	14785	14785	14785	14785	14785	14784
2735.53	1	14784	14784	14784	14784	14784	14784	14784	14783	14783	14783	14783	14783	14783	14783	14783	14783	14782
2702.75	1	14782	14782	14782	14782	14782	14782	14782	14781	14781	14781	14781	14781	14781	14781	14781	14780	14780
2669.96	1	14780	14780	14780	14779	14779	14779	14778	14778	14778	14780	14781	14781	14781	14781	14780	14780	14780
2637.18	1	14780	14779	14779	14779	14779	14778	14778	14778	14777	14777	14777	14777	14778	14779	14779	14779	14779
2604.40	1	14778	14778	14777	14777	14777	14779	14780	14780	14780	14779	14779	14778	14778	14778	14778	14778	14777
2571.61	1	14777	14777	14777	14777	14777	14777	14776	14776	14776	14776	14776	14776	14776	14776	14776	14776	14775
2539.79	0	14775	14775	14775	14775	14775	14775	14775	14775	14775	14774	14774	14774	14774	14774	14774	14774	14774
2523.40	0	14773	14774	14774	14774	14774	14774	14774	14774	14774	14774	14774	14774	14774	14774	14774	14774	14773
2507.01	0	14773	14773	14773	14773	14773	14773	14773	14773	14773	14772	14772	14772	14772	14772	14772	14772	14772
2489.65	1	14772	14771	14771	14771	14771	14771	14771	14771	14771	14770	14770	14770	14770	14770	14769	14769	14769
2456.87	1	14769	14769	14768	14768	14768	14768	14768	14767	14767	14767	14766	14766	14766	14765	14765	14765	14764
2424.08	1	14764	14764	14763	14763	14762	14762	14762	14761	14761	14760	14760	14759	14758	14757	14756	14754	14752
2391.30	1	14751	14755	14762	14764	14764	14764	14763	14762	14764	14767	14767	14765	14764	14762	14761	14762	14762
2358.52	1	14762	14761	14760	14759	14757	14756	14755	14754	14754	14753	14752	14750	14749	14748	14746	14744	14744

Table VI.8. Continued.

cm^{-1}	*XE*	0	1	2	3	4	5	6	7	8	9	10	11	12	13	14	15	16
2325.73	1	14746	14750	14751	14750	14747	14745	14742	14739	14736	14733	14730	14726	14722	14718	14713	14707	14700
2292.95	1	14692	14681	14666	14647	14629	14628	14677	14759	14811	14824	14817	14808	14824	14857	14875	14876	14872
2260.16	1	14866	14859	14853	14848	14843	14838	14835	14831	14828	14825	14822	14820	14818	14815	14814	14812	14810
2227.38	1	14809	14807	14806	14804	14802	14801	14799	14797	14798	14801	14802	14802	14801	14800	14799	14798	14797
2194.60	1	14796	14796	14795	14794	14794	14793	14792	14792	14791	14791	14790	14790	14789	14789	14788	14788	14788
2161.81	1	14787	14787	14786	14786	14785	14785	14785	14785	14785	14785	14784	14784	14784	14783	14783	14783	14783
2129.03	1	14782	14782	14782	14781	14781	14781	14781	14780	14780	14780	14779	14779	14779	14779	14778	14778	14778
2096.24	1	14778	14777	14777	14777	14777	14776	14776	14776	14776	14775	14775	14775	14775	14774	14774	14774	14774
2063.46	1	14773	14773	14773	14772	14772	14772	14771	14771	14771	14771	14771	14770	14770	14770	14769	14769	14769
2030.68	1	14768	14768	14768	14767	14767	14766	14766	14765	14765	14764	14763	14763	14762	14763	14764	14764	14764
1997.89	1	14763	14762	14761	14760	14759	14760	14759	14758	14757	14755	14754	14752	14749	14747	14744	14741	14740
1965.11	1	14742	14749	14761	14774	14785	14791	14794	14794	14793	14791	14789	14787	14785	14784	14782	14781	14780
1932.32	1	14779	14778	14777	14776	14775	14774	14774	14773	14772	14771	14771	14770	14769	14769	14768	14768	14768
1899.54	1	14768	14767	14766	14766	14765	14764	14764	14763	14763	14762	14762	14761	14761	14760	14760	14759	14759
1866.76	1	14759	14759	14758	14759	14759	14758	14757	14756	14754	14753	14752	14750	14749	14747	14745	14743	14741
1833.97	1	14738	14735	14731	14728	14725	14723	14723	14728	14739	14755	14774	14789	14799	14804	14805	14803	14801
1801.19	1	14797	14795	14793	14791	14789	14788	14786	14785	14783	14782	14780	14779	14778	14776	14775	14774	14773
1768.41	1	14772	14771	14770	14769	14768	14767	14767	14768	14770	14771	14770	14769	14768	14768	14767	14766	14765
1735.62	1	14765	14764	14763	14763	14762	14761	14761	14760	14760	14759	14758	14758	14758	14758	14757	14757	14756
1702.84	1	14755	14755	14754	14753	14753	14753	14753	14752	14752	14751	14750	14750	14751	14751	14750	14750	14751
1670.05	1	14753	14753	14753	14752	14751	14750	14749	14749	14748	14747	14746	14745	14744	14743	14742	14740	14739
1637.27	1	14737	14736	14734	14731	14728	14725	14720	14715	14713	14720	14741	14760	14768	14768	14765	14763	14761
1604.49	1	14758	14756	14754	14752	14750	14748	14746	14745	14744	14743	14743	14742	14742	14740	14739	14738	14736
1571.70	1	14735	14735	14734	14733	14731	14729	14727	14725	14723	14721	14719	14719	14720	14718	14716	14712	14709
1538.92	1	14706	14704	14703	14704	14707	14712	14716	14720	14721	14721	14719	14715	14711	14706	14701	14695	14689
1507.10	0	14686	14682	14678	14674	14670	14666	14661	14656	14650	14644	14638	14631	14624	14615	14606	14595	14583
1490.71	0	14569	14553	14534	14511	14484	14452	14415	14373	14331	14305	14338	14496	14760	14984	15099	15134	15121
1474.31	0	15087	15052	15030	15019	15004	14986	14967	14949	14934	14919	14906	14894	14883	14873	14863	14855	14847
1457.92	0	14841	14837	14835	14836	14839	14844	14850	14854	14856	14857	14856	14854	14852	14849	14846	14843	14840
1441.53	0	14837	14835	14832	14829	14827	14824	14822	14819	14817	14815	14813	14811	14809	14807	14805	14803	14802
1424.17	1	14798	14795	14792	14789	14787	14784	14781	14779	14776	14773	14770	14767	14764	14761	14760	14763	14772
1391.39	1	14782	14787	14791	14790	14787	14784	14781	14778	14775	14773	14770	14768	14765	14763	14761	14758	14756
1359.57	0	14754	14753	14752	14750	14749	14747	14746	14744	14742	14740	14738	14736	14734	14732	14729	14726	14723
1343.18	0	14719	14715	14711	14707	14702	14695	14687	14678	14668	14657	14649	14653	14682	14738	14797	14836	14856
1326.79	0	14863	14861	14854	14847	14842	14838	14834	14829	14824	14820	14816	14812	14809	14806	14803	14801	14799
1309.43	1	14795	14792	14789	14787	14784	14782	14780	14778	14776	14775	14773	14772	14771	14769	14768	14767	14766
1276.65	1	14765	14764	14762	14761	14760	14759	14758	14756	14755	14754	14753	14752	14751	14751	14752	14753	14753
1243.86	1	14752	14751	14750	14749	14748	14747	14746	14745	14744	14743	14742	14741	14740	14739	14738	14737	14736
1211.08	1	14734	14733	14732	14731	14730	14729	14728	14727	14725	14724	14722	14720	14719	14718	14718	14718	14720
1178.29	1	14722	14724	14727	14728	14727	14726	14726	14730	14737	14744	14748	14750	14751	14751	14750	14750	14749
1145.51	1	14749	14748	14747	14746	14745	14743	14741	14739	14738	14736	14735	14733	14731	14730	14728	14726	14725
1112.73	1	14723	14721	14720	14719	14717	14715	14714	14712	14710	14708	14706	14704	14702	14700	14698	14696	14694
1079.94	1	14691	14688	14686	14683	14679	14676	14672	14668	14663	14658	14653	14647	14640	14632	14622	14611	14598
1047.16	1	14581	14559	14534	14509	14506	14578	14718	14825	14874	14881	14870	14852	14834	14818	14804	14792	14781
1014.37	1	14773	14768	14768	14769	14765	14761	14756	14751	14747	14743	14740	14738	14737	14736	14733	14731	14729
981.59	1	14727	14725	14723	14721	14720	14719	14719	14718	14718	14717	14715	14714	14711	14709	14707	14706	14705
948.81	1	14704	14703	14702	14702	14700	14698	14695	14693	14690	14688	14688	14687	14685	14684	14683	14681	14679
916.02	1	14676	14674	14671	14668	14666	14663	14660	14658	14655	14652	14650	14647	14644	14641	14638	14635	14632
883.24	1	14629	14625	14622	14619	14616	14614	14611	14610	14609	14607	14605	14602	14599	14596	14593	14591	14589
850.45	1	14588	14587	14585	14582	14577	14571	14564	14556	14547	14536	14524	14509	14493	14473	14449	14419	14379
817.67	1	14332	14302	14398	14684	14855	14864	14826	14788	14755	14728	14705	14686	14669	14655	14642	14630	14618
784.89	1	14606	14595	14583	14573	14563	14560	14563	14560	14551	14540	14530	14519	14508	14498	14487	14476	14465
752.10	1	14454	14443	14431	14419	14406	14393	14379	14365	14349	14333	14317	14299	14280	14260	14238	14215	14190
719.32	1	14163	14134	14103	14070	14032	13990	13943	13890	13831	13763	13687	13598	13494	13370	13218	13028	12785
686.53	1	12480	12125	11776	11553	11627	12172	13364	15294	17392	18495	18408	17896	17409	17018	16714	16480	16297
653.75	1	16151	16031	15932	15853	15775	15704	15636	15580	15531	15487	15447	15411	15378	15348	15319	15293	15268
620.97	1	15245	15223	15202	15182	15165	15150	15137	15123	15109	15094	15080	15067	15053	15040	15026	15012	15001
588.18	1	14988	14975	14964	14952	14940	14927	14916	14903	14892	14880	14867	14856	14845	14832	14817	14803	14786
555.40	1	14768	14750	14731	14712	14692	14668	14644	14620	14592	14561	14526	14487	14440	14386	14325	14253	14173
522.62	1	14093	14034	14031	14140	14213	14091	13882	13612	13259	12794	12285	12450	14180	15875	16590	17122	17376
489.83	1	17259	17005	16735	16501	16310	16159	16033	15931	15845	16557	17391	17879	17801	17501	17158	16856	16611
457.05	1	16416	16259	16130	16024	15931												

[a,b] See footnotes a and b to Table IV.2.

Table VI.9. Imaginary refractive indices between 6500 and 450 cm^{-1} of 61.96% liquid benzene-h_6 in liquid benzene-d_6 at 25 °C.^{a,b}

cm^{-1}	*XE*	*YE*	0	1	2	3	4	5	6	7	8	9	10	11	12	13	14	15	16
6499.90	3	-7	43	45	44	45	47	49	50	50	50	50	53	52	54	54	55	55	55
6368.76	3	-7	56	57	59	59	56	54	56	56	57	59	65	68	67	68	64	66	65
6237.63	3	-7	66	69	70	72	76	73	75	95	95	103	142	245	310	313	261	260	283
6106.49	3	-7	289	279	335	258	192	172	165	172	202	292	389	464	538	772	1113	1499	1944
5975.36	3	-7	1631	1471	1284	1203	1026	855	1133	974	1449	1145	763	573	546	524	506	457	360
5844.22	3	-7	242	161	124	103	104	124	127	130	153	179	190	146	144	152	130	118	139
5713.09	3	-7	212	231	293	310	256	189	169	167	164	129	111	109	121	174	192	161	135
5581.95	3	-7	138	144	139	138	158	197	219	189	193	202	150	121	100	89	76	69	66
5450.81	3	-7	71	76	94	118	112	101	109	98	91	115	131	118	119	137	151	126	123
5319.68	3	-7	116	113	111	101	104	104	97	106	136	158	152	104	87	73	71	64	63
5188.54	3	-7	67	66	60	62	83	89	87	90	95	83	78	90	107	108	104	104	96
5057.41	3	-7	95	99	96	84	79	83	93	101	104	92	94	90	95	91	83	85	90
4926.27	3	-7	91	94	100	107	103	106	112	139	155	161	181	171	142	124	107	107	102
4798.99	2	-7	106	109	110	120	133	134	129	128	127	130	130	130	134	146	160	164	169
4733.42	2	-7	177	189	204	222	252	286	324	390	494	607	843	1184	1139	1072	1242	1849	3091
4667.86	2	-7	3325	2063	1400	1195	1358	1995	2582	2576	1978	1386	1372	2079	2421	1744	1304	1221	1376
4602.29	2	-7	1393	1223	1218	1567	2411	2889	2387	1753	1218	921	764	694	673	712	897	1125	998
4536.72	2	-7	758	601	511	469	460	479	531	620	760	985	1327	1813	2386	2913	3223	3150	2625
4471.15	2	-7	1993	1552	1382	1413	1555	1618	1488	1295	1175	1154	1127	1023	901	765	712	758	769
4405.58	2	-7	794	741	692	690	705	663	758	977	886	693	534	422	351	312	288	286	299
4340.02	2	-7	302	288	278	271	263	254	251	256	271	286	306	328	345	352	352	354	363
4274.45	2	-7	392	450	568	778	815	696	616	604	634	612	578	564	567	634	762	775	747
4208.88	2	-7	757	757	836	1038	1073	894	767	742	817	940	868	765	716	697	697	682	671
4143.31	2	-7	701	762	784	835	830	888	928	993	1120	1291	1564	1978	2425	2699	3076	3908	4960
4077.75	2	-6	511	516	613	827	1326	1949	1905	1301	835	540	363	272	238	262	262	202	162
4014.11	1	-7	1471	1350	1243	1193	1082	1008	943	892	852	821	802	799	814	843	868	874	878
3981.32	1	-7	872	832	783	745	717	701	709	770	944	1214	1373	1499	1700	1780	1625	1396	1216
3948.54	1	-7	1099	1034	1020	1084	1257	1584	2120	2274	1953	1659	1420	1239	1105	1011	947	908	888
3915.75	1	-7	868	841	821	810	806	805	803	800	792	780	774	784	821	919	972	922	875
3882.97	1	-7	828	782	739	708	689	680	672	656	638	623	616	616	618	616	609	600	591
3850.19	1	-7	589	594	601	613	634	671	736	845	1020	1269	1538	1673	1604	1422	1240	1114	1078
3817.40	1	-7	1133	1199	1207	1232	1341	1590	2024	2512	2640	2321	1880	1523	1279	1131	1053	996	909
3784.62	1	-7	814	740	689	661	660	682	722	769	795	772	718	669	635	614	604	605	617
3751.83	1	-7	643	684	747	837	950	1060	1094	1065	1023	982	945	920	912	923	951	988	1012
3719.05	1	-7	1034	1050	1074	1111	1170	1264	1406	1587	1819	2177	2830	3918	4665	4135	3291	2834	2710
3686.27	1	-7	2637	2360	1968	1628	1393	1230	1104	1010	959	944	958	956	900	837	804	806	843
3653.48	1	-7	926	1088	1396	1984	3064	4548	5349	4617	3323	2459	1997	1754	1622	1577	1621	1695	1749
3620.70	1	-7	1783	1838	1982	2231	2496	2600	2445	2111	1749	1435	1203	1041	916	817	741	686	640
3587.91	1	-7	603	573	566	567	572	583	552	502	454	420	400	386	376	368	358	349	345
3555.13	1	-7	347	355	368	380	384	379	370	358	344	329	316	305	296	285	275	270	273
3522.35	1	-7	279	296	330	375	400	363	325	308	303	303	302	298	294	294	304	330	377
3489.56	1	-7	453	504	453	399	367	344	332	325	322	325	334	350	375	408	441	482	540
3456.78	1	-7	623	737	875	1020	1119	1122	1038	919	805	710	632	576	547	556	619	687	657
3423.99	1	-7	629	628	634	630	610	582	555	532	519	518	530	549	563	567	556	532	503
3391.21	1	-7	479	457	433	407	384	363	347	334	325	322	324	330	341	354	367	376	383
3358.43	1	-7	386	384	374	363	357	356	354	345	337	335	342	358	385	414	448	513	634
3325.64	1	-7	789	857	797	698	619	565	528	502	484	476	475	476	480	497	509	526	549
3292.86	1	-7	578	622	680	756	856	964	1076	1176	1261	1359	1474	1539	1507	1442	1381	1355	1373
3260.07	1	-7	1421	1504	1620	1754	1892	2060	2289	2603	3094	3881	5111	6824	8662	9822	9686	8550	7186
3227.29	1	-7	6064	5134	4272	3539	2971	2553	2283	2124	2069	2053	1988	1905	1836	1804	1791	1793	1783
3194.51	1	-7	1788	1845	1842	1872	1944	1962	1942	1866	1933	1981	2020	2132	2117	2246	2361	2505	2596
3161.72	1	-7	2635	2718	2803	2862	3016	3143	3324	3519	3701	3822	3919	4199	4357	4559	4755	4844	5064
3128.94	1	-6	527	552	585	632	696	767	847	950	1068	1193	1321	1466	1660	1941	2366	3078	4346
3096.16	1	-5	664	1067	1603	1777	1420	1017	759	608	508	476	527	714	1143	1336	998	731	577
3063.37	1	-5	491	438	414	420	408	383	378	396	441	534	718	1060	1644	2380	2842	2751	2267
3030.59	1	-5	1775	1380	1067	829	660	540	453	388	337	299	269	247	229	214	199	185	171
2997.80	1	-6	1579	1449	1314	1194	1106	1013	940	880	821	781	728	679	629	584	545	516	496
2965.02	1	-7	4732	4493	4453	4338	4223	4221	4214	4207	4169	3926	3666	3420	3347	3233	3125	3072	3005
2932.24	1	-7	2990	2941	2921	2884	2789	2702	2605	2666	2673	2754	3043	3608	4461	5228	5108	4357	3693
2899.45	1	-7	3276	3091	3174	3664	4873	7222	9829	8924	6153	4615	3721	3105	2707	2454	2312	2271	2307
2866.67	1	-7	2371	2574	3013	3822	4831	5053	4541	4005	3555	3214	3122	3137	2835	2537	2355	2278	2298
2833.88	1	-7	2455	2786	2876	2752	2821	3297	4076	4819	4981	4260	3420	2845	2401	2008	1695	1466	1287
2801.10	1	-7	1150	1061	1007	980	966	950	938	934	932	928	922	923	935	970	1010	1012	966
2768.32	1	-7	894	823	763	715	679	650	625	603	587	572	548	519	494	476	463	456	454
2735.53	1	-7	457	466	474	464	450	440	433	430	431	434	436	438	437	436	436	437	442
2702.75	1	-7	450	458	465	472	481	490	501	512	528	547	568	588	604	616	626	641	662
2669.96	1	-7	694	739	805	900	1046	1294	1742	2609	4201	5192	3792	2529	1894	1522	1255	1092	989
2637.18	1	-7	909	858	834	832	853	901	988	1136	1393	1838	2456	3206	3667	3249	2609	2160	1902
2604.40	1	-7	1801	1890	2268	3143	4763	5385	3878	2649	1921	1486	1250	1133	1070	1066	1072	1119	1171
2571.61	1	-7	1118	1011	936	905	911	944	1002	1092	1226	1295	1178	1007	880	796	740	698	659
2539.79	0	-7	642	628	616	608	601	598	596	597	599	602	612	631	660	705	772	877	1049
2523.40	0	-7	1304	1531	1580	1521	1415	1290	1178	1088	1018	962	913	871	834	801	774	751	733
2507.01	0	-7	720	710	703	697	692	687	685	685	687	692	698	707	720	737	760	789	822
2489.65	1	-7	904	1002	1118	1177	1080	962	891	863	871	925	1021	1052	983	926	881	860	869
2456.87	1	-7	904	966	1036	1073	1082	1053	986	936	911	911	927	964	1035	1150	1262	1296	1312
2424.08	1	-7	1346	1402	1480	1598	1770	2000	2252	2464	2607	2700	2790	2919	3125	3452	3997	4990	6919
2391.30	1	-6	1067	1495	1486	1274	1116	992	945	1048	1195	1018	765	605	539	551	633	664	584
2358.52	1	-6	495	436	403	389	391	409	441	483	508	508	516	561	650	735	835	1047	1414

Table VI.9. Continued.

cm⁻¹	*XE*	*YE*	0	1	2	3	4	5	6	7	8	9	10	11	12	13	14	15	16
2325.73	1	-6	1814	1794	1421	1094	895	785	726	711	724	762	825	913	1023	1156	1309	1488	1730
2292.95	1	-5	205	253	332	482	760	1224	1703	1762	1472	1176	1014	1035	1152	1079	863	664	522
2260.16	1	-6	4189	3430	2852	2420	2089	1830	1620	1433	1267	1128	1014	921	844	775	725	675	635
2227.38	1	-6	595	558	532	514	512	538	618	805	1118	1179	935	717	553	451	393	366	345
2194.60	1	-7	3075	2756	2540	2382	2236	2099	1979	1878	1801	1750	1714	1655	1583	1512	1442	1382	1333
2161.81	1	-7	1301	1295	1333	1438	1618	1797	1808	1663	1512	1398	1309	1229	1149	1073	1015	974	948
2129.03	1	-7	923	885	846	815	793	774	758	744	736	728	714	699	688	683	684	685	681
2096.24	1	-7	676	678	690	712	741	758	761	761	760	748	726	698	673	655	645	640	636
2063.46	1	-7	632	628	668	722	785	879	993	1111	1211	1271	1240	1224	1211	1258	1307	1346	1375
2030.68	1	-7	1393	1428	1461	1504	1533	1610	1700	1868	2142	2578	3337	4470	5702	6744	6595	5664	4905
1997.89	1	-6	455	460	504	563	672	760	716	686	700	749	830	956	1137	1413	1840	2479	3377
1965.11	1	-6	4485	5572	6256	6254	5636	4714	3769	2953	2303	1813	1456	1204	1035	914	809	709	620
1932.33	1	-7	5412	4763	4236	3778	3423	3146	2949	2827	2791	2744	2603	2452	2431	2556	2846	3221	3064
1899.54	1	-7	2699	2442	2308	2281	2385	2657	3027	3331	3487	3579	3736	3993	4345	4558	4664	4957	5486
1866.76	1	-6	564	558	586	596	550	496	467	462	474	499	537	588	652	727	822	943	1101
1833.97	1	-6	1311	1597	1999	2556	3333	4372	5693	7205	8648	9574	9604	8754	7421	6013	4771	3768	3000
1801.19	1	-6	2444	2078	1784	1544	1344	1163	990	834	705	604	525	462	415	379	350	332	323
1768.41	1	-7	3136	3131	3257	3589	4270	5524	7467	9098	8504	6438	4735	3791	3122	2609	2269	2036	1863
1735.62	1	-7	1736	1645	1585	1550	1542	1556	1582	1625	1730	1973	2496	3460	3745	2933	2538	2474	2548
1702.84	1	-6	262	273	294	329	376	425	452	446	442	477	561	681	748	738	790	916	1019
1670.05	1	-7	9917	8599	7145	6028	5302	4896	4705	4543	4343	4179	4094	4093	4227	4515	4710	4728	4923
1637.27	1	-6	521	563	603	671	782	968	1299	1919	3010	4489	5243	4555	3417	2554	2017	1685	1440
1604.49	1	-6	1247	1096	985	912	880	882	906	946	1001	1041	1045	1004	943	882	844	822	815
1571.70	1	-6	860	889	824	772	753	752	787	831	890	1007	1167	1355	1395	1348	1373	1506	1761
1538.92	1	-6	2151	2632	3230	3853	4367	4642	4610	4313	3853	3364	2908	2541	2250	2035	1883	1785	1746
1507.10	0	-6	1756	1761	1799	1839	1896	1968	2057	2163	2289	2442	2621	2841	3055	3337	3666	4053	4546
1490.71	0	-5	516	591	693	834	1035	1321	1740	2368	3331	4807	6889	9022	9779	8694	6884	5146	3777
1474.31	0	-5	2870	2347	2040	1734	1404	1132	928	778	665	577	510	455	415	389	378	379	391
1457.92	0	-6	4145	4493	4883	5273	5532	5581	5404	5044	4585	4099	3631	3206	2840	2529	2261	2036	1841
1441.53	0	-6	1666	1509	1368	1250	1146	1065	978	911	852	803	759	718	688	657	633	617	601
1424.17	1	-6	586	578	579	588	606	634	676	728	810	928	1083	1300	1629	2139	2888	3781	4316
1391.39	1	-6	4000	3391	2653	1977	1504	1172	960	819	718	646	590	550	525	508	505	508	520
1359.57	0	-6	528	539	552	565	589	615	642	673	707	744	785	829	877	933	998	1077	1175
1343.18	0	-5	130	147	168	188	211	244	293	364	468	624	856	1178	1525	1713	1639	1407	1146
1326.79	0	-6	9084	7094	5662	4761	4187	3631	3085	2626	2264	1982	1766	1600	1473	1372	1290	1218	1155
1309.43	1	-6	1053	960	878	810	754	705	664	633	607	588	577	567	557	544	531	517	504
1276.65	1	-6	502	504	495	487	488	496	510	534	572	628	710	825	969	1106	1172	1132	1028
1243.86	1	-7	9213	8390	7859	7546	7402	7367	7417	7528	7683	7838	7984	8121	8250	8401	8612	8896	9258
1211.08	1	-6	972	1032	1114	1224	1333	1377	1407	1470	1561	1684	1842	2044	2308	2654	3020	3349	3689
1178.29	1	-6	3968	4110	4072	3939	3840	3910	4180	4523	4665	4484	4123	3749	3422	3159	2963	2813	2671
1145.51	1	-6	2491	2276	2052	1847	1666	1513	1382	1273	1179	1098	1030	971	922	879	842	810	785
1112.73	1	-7	7688	7614	7646	7638	7441	7212	7046	6944	6902	6911	7016	7162	7509	7783	8286	8568	8742
1079.94	1	-6	905	939	993	1032	1085	1144	1234	1344	1465	1638	1834	2081	2374	2735	3196	3822	4705
1047.16	1	-5	601	809	1162	1778	2799	3989	4364	3753	2839	2029	1452	1070	823	666	560	493	458
1014.37	1	-6	4496	4615	4777	4327	3716	3307	3065	2920	2858	2850	2884	2971	2968	2817	2680	2620	2575
981.59	1	-6	2511	2491	2512	2561	2620	2660	2651	2604	2496	2382	2249	2123	2007	1938	1927	1955	1951
948.81	1	-6	1889	1851	1844	1751	1591	1461	1378	1340	1392	1532	1582	1499	1467	1430	1359	1271	1197
916.02	1	-6	1131	1105	1075	1091	1112	1141	1149	1165	1192	1203	1232	1264	1305	1362	1435	1505	1591
883.24	1	-6	1684	1797	1920	2073	2267	2492	2729	2932	3093	3205	3297	3400	3556	3770	3998	4281	4532
850.46	1	-5	468	470	457	436	413	394	383	373	368	371	385	407	448	512	605	760	1036
817.67	1	-5	1562	2608	4191	4523	3175	1968	1293	926	704	567	475	412	370	340	319	299	284
784.89	1	-6	2817	2853	3042	3375	3984	4859	4811	3862	3131	2721	2506	2423	2386	2366	2298	2287	2273
752.10	1	-6	2378	2435	2498	2584	2690	2811	2948	3094	3250	3427	3625	3844	4089	4363	4668	5013	5403
719.32	1	-5	585	635	694	765	855	949	1039	1153	1295	1468	1680	1943	2274	2702	3282	4128	5481
686.54	1	-4	780	1183	1844	2826	4104	5542	6876	7502	6610	4516	2639	1555	984	668	487	378	306
653.75	1	-5	2549	2161	1855	1611	1412	1248	1111	996	899	816	745	683	629	582	541	504	473
620.97	1	-6	4448	4209	4016	3876	3727	3516	3341	3204	3094	3001	2918	2841	2768	2701	2644	2597	2564
588.18	1	-6	2545	2544	2557	2586	2608	2598	2550	2489	2433	2392	2361	2109	2032	1811	1609	1432	1292
555.40	1	-5	115	102	107	104	103	110	117	136	148	159	183	211	263	340	476	726	1116
522.62	1	-4	175	270	385	464	378	293	281	335	477	800	1549	3051	4016	3306	2570	2052	1381
489.83	1	-5	8712	5297	3271	2058	1340	892	597	404	252	192	114	73	61	35	5	23	63
457.05	1	-6	590	1132	1441	2127													

---

[a] See footnote a to Table IV.1.

[b] See footnote b to Table V.1.

Table VI.10. Real refractive indices between 6500 and 450 cm^{-1} of 61.96% liquid benzene-h_6 in liquid benzene-d_6 at 25 °C.^{a,b}

cm^{-1}	*XE*	0	1	2	3	4	5	6	7	8	9	10	11	12	13	14	15	16
6499.90	3	14791	14791	14791	14791	14791	14791	14791	14791	14791	14791	14791	14791	14791	14791	14791	14791	14791
6368.76	3	14791	14791	14791	14791	14791	14791	14791	14791	14791	14791	14791	14791	14791	14791	14791	14791	14791
6237.63	3	14791	14791	14791	14791	14791	14791	14790	14790	14790	14790	14790	14790	14790	14790	14790	14790	14790
6106.49	3	14790	14790	14790	14790	14790	14790	14790	14790	14790	14790	14790	14790	14790	14789	14789	14790	14790
5975.36	3	14791	14791	14791	14791	14791	14791	14791	14791	14791	14791	14791	14791	14791	14791	14791	14791	14791
5844.22	3	14791	14791	14791	14791	14791	14791	14791	14791	14790	14790	14790	14790	14790	14790	14790	14790	14790
5713.09	3	14790	14790	14790	14790	14790	14790	14790	14790	14790	14790	14790	14790	14790	14790	14790	14790	14790
5581.95	3	14790	14790	14790	14790	14790	14790	14790	14790	14790	14790	14790	14790	14790	14790	14790	14790	14790
5450.81	3	14790	14790	14790	14790	14790	14790	14790	14790	14790	14790	14790	14790	14789	14789	14789	14789	14789
5319.68	3	14789	14789	14789	14789	14789	14789	14789	14789	14789	14789	14789	14789	14789	14789	14789	14789	14789
5188.54	3	14789	14789	14789	14789	14789	14789	14789	14789	14789	14789	14789	14789	14789	14789	14789	14789	14789
5057.41	3	14789	14789	14789	14789	14789	14788	14788	14788	14788	14788	14788	14788	14788	14788	14788	14788	14788
4926.27	3	14788	14788	14788	14788	14788	14788	14788	14788	14788	14788	14788	14788	14788	14788	14788	14788	14787
4798.99	2	14787	14787	14787	14787	14787	14787	14787	14787	14787	14787	14787	14787	14787	14787	14787	14787	14787
4733.42	2	14787	14787	14787	14786	14786	14786	14786	14786	14786	14786	14786	14786	14786	14786	14785	14785	14785
4667.86	2	14787	14788	14787	14787	14786	14786	14787	14787	14788	14787	14787	14787	14788	14788	14788	14787	14787
4602.29	2	14787	14787	14787	14786	14786	14787	14788	14788	14788	14788	14788	14788	14787	14787	14787	14787	14787
4536.72	2	14787	14787	14787	14787	14787	14787	14786	14786	14786	14786	14785	14785	14786	14786	14787	14787	14788
4471.15	2	14788	14788	14788	14787	14787	14787	14788	14788	14788	14787	14787	14788	14787	14787	14787	14787	14787
4405.58	2	14787	14787	14787	14787	14787	14787	14787	14787	14787	14787	14787	14787	14787	14787	14787	14787	14786
4340.02	2	14786	14786	14786	14786	14786	14786	14786	14786	14786	14786	14786	14786	14786	14786	14786	14786	14785
4274.45	2	14785	14785	14785	14785	14785	14785	14785	14785	14785	14785	14785	14785	14785	14785	14785	14785	14785
4208.88	2	14785	14785	14785	14785	14785	14785	14785	14784	14784	14784	14784	14784	14784	14784	14784	14784	14784
4143.31	2	14784	14783	14783	14783	14783	14783	14783	14782	14782	14782	14781	14781	14781	14780	14780	14780	14780
4077.75	2	14780	14779	14778	14777	14776	14781	14791	14795	14795	14794	14792	14791	14790	14789	14789	14789	14789
4014.11	1	14789	14789	14788	14788	14788	14788	14788	14788	14787	14787	14787	14787	14787	14787	14787	14787	14787
3981.32	1	14786	14786	14786	14786	14786	14786	14786	14786	14785	14785	14785	14785	14785	14786	14786	14786	14786
3948.54	1	14786	14786	14785	14785	14785	14785	14785	14786	14786	14786	14786	14786	14786	14786	14786	14786	14786
3915.75	1	14786	14785	14785	14785	14785	14785	14785	14785	14785	14785	14785	14785	14785	14785	14785	14785	14785
3882.97	1	14785	14785	14785	14785	14785	14785	14785	14785	14785	14784	14784	14784	14784	14784	14784	14784	14784
3850.19	1	14784	14784	14784	14784	14784	14784	14783	14783	14783	14783	14783	14784	14784	14784	14784	14784	14784
3817.40	1	14784	14783	14783	14783	14783	14783	14783	14783	14784	14784	14785	14785	14785	14784	14784	14784	14784
3784.62	1	14784	14784	14784	14784	14784	14784	14783	14783	14783	14783	14783	14783	14783	14783	14783	14783	14783
3751.83	1	14783	14783	14783	14782	14782	14782	14783	14783	14783	14783	14783	14782	14782	14782	14782	14782	14782
3719.05	1	14782	14782	14782	14782	14782	14781	14781	14781	14781	14781	14780	14781	14782	14783	14783	14783	14783
3686.27	1	14783	14784	14784	14784	14783	14783	14783	14783	14783	14783	14782	14782	14782	14782	14782	14782	14781
3653.48	1	14781	14781	14780	14780	14779	14780	14782	14783	14784	14784	14783	14783	14783	14783	14782	14782	14782
3620.70	1	14782	14782	14782	14782	14782	14783	14783	14783	14783	14783	14783	14783	14783	14783	14783	14783	14782
3587.91	1	14782	14782	14782	14782	14782	14782	14782	14782	14782	14782	14782	14782	14781	14781	14781	14781	14781
3555.13	1	14781	14781	14781	14781	14781	14781	14781	14781	14781	14781	14781	14781	14780	14780	14780	14780	14780
3522.35	1	14780	14780	14780	14780	14780	14780	14780	14780	14780	14780	14780	14780	14779	14779	14779	14779	14779
3489.56	1	14779	14779	14779	14779	14779	14779	14779	14779	14779	14779	14779	14778	14778	14778	14778	14778	14778
3456.78	1	14778	14778	14778	14778	14778	14778	14778	14778	14778	14778	14778	14778	14778	14778	14778	14778	14778
3423.99	1	14778	14777	14777	14777	14777	14777	14777	14777	14777	14777	14777	14777	14777	14777	14777	14777	14777
3391.21	1	14776	14776	14776	14776	14776	14776	14776	14776	14776	14776	14775	14775	14775	14775	14775	14775	14775
3358.43	1	14775	14775	14775	14775	14774	14774	14774	14774	14774	14774	14774	14774	14773	14773	14773	14773	14773
3325.64	1	14773	14773	14773	14773	14773	14773	14772	14772	14772	14772	14772	14772	14771	14771	14771	14771	14771
3292.86	1	14771	14770	14770	14770	14770	14769	14769	14769	14769	14769	14769	14769	14769	14768	14768	14768	14768
3260.07	1	14767	14767	14767	14766	14766	14766	14765	14765	14764	14763	14763	14763	14764	14766	14768	14769	14770
3227.29	1	14770	14770	14770	14769	14769	14768	14768	14767	14767	14766	14766	14765	14765	14765	14764	14764	14763
3194.51	1	14763	14762	14762	14762	14761	14761	14760	14760	14759	14759	14758	14758	14757	14757	14756	14756	14755
3161.72	1	14754	14754	14753	14752	14752	14751	14750	14749	14749	14748	14747	14746	14745	14744	14742	14741	14740
3128.94	1	14738	14737	14735	14733	14731	14728	14726	14723	14720	14717	14714	14709	14704	14697	14689	14678	14665
3096.16	1	14651	14645	14672	14742	14792	14802	14795	14785	14772	14756	14739	14722	14724	14779	14809	14808	14800
3063.37	1	14792	14784	14775	14768	14764	14756	14746	14734	14719	14701	14679	14657	14647	14677	14756	14844	14901
3030.59	1	14923	14928	14924	14916	14907	14897	14889	14881	14874	14869	14863	14859	14855	14852	14849	14847	14845
2997.80	1	14843	14841	14839	14837	14835	14833	14831	14830	14828	14827	14826	14824	14823	14822	14821	14820	14818
2965.02	1	14818	14816	14816	14815	14814	14813	14812	14812	14811	14811	14810	14810	14809	14808	14808	14807	14807
2932.24	1	14806	14805	14805	14805	14804	14804	14803	14802	14802	14801	14800	14800	14800	14800	14801	14801	14801
2899.45	1	14800	14799	14798	14797	14796	14796	14798	14802	14802	14802	14801	14800	14800	14799	14798	14798	14797
2866.67	1	14797	14796	14796	14795	14795	14796	14797	14797	14797	14797	14796	14796	14796	14796	14796	14795	14795
2833.88	1	14794	14794	14794	14794	14793	14793	14793	14794	14795	14795	14796	14795	14795	14795	14795	14794	14794
2801.10	1	14794	14793	14793	14793	14793	14792	14792	14792	14792	14792	14792	14791	14791	14791	14791	14791	14791
2768.32	1	14791	14791	14790	14790	14790	14790	14790	14790	14790	14789	14789	14789	14789	14789	14789	14789	14788
2735.53	1	14788	14788	14788	14788	14788	14788	14788	14787	14787	14787	14787	14787	14787	14787	14787	14786	14786
2702.75	1	14786	14786	14786	14786	14786	14785	14785	14785	14785	14785	14785	14785	14785	14784	14784	14784	14784
2669.96	1	14784	14784	14783	14783	14783	14782	14782	14781	14782	14784	14785	14785	14785	14785	14784	14784	14784
2637.18	1	14784	14783	14783	14783	14783	14782	14782	14782	14781	14781	14781	14781	14782	14783	14783	14783	14782
2604.40	1	14782	14781	14781	14780	14781	14783	14784	14784	14784	14783	14783	14783	14782	14782	14782	14782	14782
2571.61	1	14781	14781	14781	14781	14781	14781	14780	14780	14780	14780	14780	14780	14780	14780	14780	14780	14780
2539.79	0	14779	14779	14779	14779	14779	14779	14779	14779	14779	14779	14779	14778	14778	14778	14778	14778	14778
2523.40	0	14778	14778	14778	14778	14778	14778	14778	14778	14778	14778	14778	14778	14778	14778	14778	14778	14778
2507.01	0	14777	14777	14777	14777	14777	14777	14777	14777	14777	14777	14777	14776	14776	14776	14776	14776	14776
2489.65	1	14776	14776	14776	14776	14776	14775	14775	14775	14775	14775	14775	14774	14774	14774	14774	14774	14774
2456.87	1	14773	14773	14773	14773	14773	14773	14772	14772	14772	14772	14771	14771	14771	14770	14770	14770	14770
2424.08	1	14769	14769	14768	14768	14768	14767	14767	14767	14766	14766	14766	14765	14764	14763	14762	14761	14759
2391.30	1	14759	14762	14766	14768	14769	14769	14768	14767	14769	14771	14771	14770	14769	14768	14767	14767	14768
2358.52	1	14767	14766	14765	14764	14763	14762	14761	14761	14760	14759	14758	14757	14755	14754	14753	14751	14751

Table VI.10. Continued.

cm^{-1}	*XE*	0	1	2	3	4	5	6	7	8	9	10	11	12	13	14	15	16
2325.73	1	14753	14759	14761	14760	14758	14756	14753	14751	14748	14746	14743	14740	14737	14733	14729	14725	14719
2292.95	1	14713	14704	14692	14678	14664	14664	14703	14766	14804	14814	14809	14802	14815	14841	14854	14856	14852
2260.16	1	14847	14842	14838	14833	14830	14826	14823	14821	14818	14816	14814	14812	14810	14808	14806	14805	14804
2227.38	1	14802	14801	14800	14798	14797	14795	14794	14792	14793	14797	14799	14799	14798	14797	14796	14795	14794
2194.60	1	14794	14793	14792	14792	14791	14790	14790	14789	14789	14788	14788	14788	14787	14787	14787	14786	14786
2161.81	1	14785	14785	14784	14784	14784	14784	14784	14783	14783	14783	14783	14782	14782	14782	14782	14781	14781
2129.03	1	14781	14781	14780	14780	14780	14779	14779	14779	14779	14778	14778	14778	14778	14777	14777	14777	14777
2096.24	1	14776	14776	14776	14776	14775	14775	14775	14775	14774	14774	14774	14774	14774	14773	14773	14773	14772
2063.46	1	14772	14772	14771	14771	14771	14770	14770	14770	14770	14769	14769	14769	14769	14768	14768	14768	14767
2030.68	1	14767	14767	14766	14766	14765	14765	14764	14763	14763	14762	14761	14760	14760	14761	14762	14762	14762
1997.89	1	14761	14760	14759	14758	14757	14757	14757	14756	14754	14752	14750	14748	14745	14742	14739	14736	14735
1965.11	1	14737	14745	14759	14774	14787	14794	14798	14798	14797	14795	14793	14790	14788	14786	14785	14784	14782
1932.33	1	14781	14780	14779	14778	14777	14776	14775	14774	14773	14772	14772	14771	14770	14769	14769	14768	14768
1899.54	1	14768	14767	14766	14766	14765	14764	14763	14763	14762	14762	14761	14761	14760	14760	14759	14759	14758
1866.76	1	14758	14758	14757	14757	14757	14756	14754	14753	14752	14750	14749	14747	14745	14743	14741	14739	14736
1833.97	1	14733	14729	14725	14721	14718	14715	14716	14721	14733	14752	14774	14793	14805	14811	14813	14811	14808
1801.19	1	14805	14802	14799	14797	14795	14793	14791	14789	14787	14786	14784	14782	14781	14779	14778	14777	14776
1768.41	1	14774	14773	14772	14771	14769	14768	14768	14770	14772	14773	14772	14771	14771	14770	14769	14768	14767
1735.62	1	14766	14766	14765	14764	14764	14763	14762	14761	14761	14760	14759	14759	14759	14759	14759	14758	14757
1702.84	1	14756	14756	14755	14754	14754	14753	14753	14753	14752	14751	14750	14750	14751	14751	14750	14750	14751
1670.05	1	14753	14753	14753	14753	14752	14751	14750	14749	14748	14747	14746	14745	14744	14743	14742	14741	14740
1637.27	1	14738	14737	14735	14733	14730	14727	14723	14718	14716	14722	14739	14755	14761	14761	14759	14757	14755
1604.49	1	14753	14751	14749	14747	14745	14744	14742	14741	14740	14739	14739	14739	14738	14737	14736	14734	14733
1571.70	1	14731	14731	14730	14728	14726	14724	14722	14720	14718	14715	14713	14712	14712	14710	14707	14703	14699
1538.92	1	14696	14693	14692	14694	14697	14703	14708	14713	14715	14714	14712	14708	14704	14698	14692	14685	14678
1507.10	0	14674	14670	14666	14661	14656	14651	14645	14639	14633	14626	14619	14610	14602	14592	14581	14568	14554
1490.71	0	14537	14518	14496	14469	14437	14400	14356	14307	14259	14228	14266	14445	14749	15018	15162	15210	15196
1474.31	0	15157	15115	15089	15076	15059	15038	15016	14996	14977	14961	14946	14933	14920	14908	14897	14887	14879
1457.92	0	14871	14866	14862	14861	14862	14865	14868	14870	14870	14870	14868	14866	14863	14860	14856	14853	14850
1441.53	0	14847	14844	14841	14839	14836	14833	14831	14828	14826	14824	14822	14819	14817	14815	14813	14812	14810
1424.17	1	14806	14803	14800	14797	14794	14791	14788	14785	14782	14779	14776	14773	14770	14767	14766	14769	14780
1391.39	1	14790	14796	14798	14797	14795	14791	14788	14785	14783	14780	14778	14775	14773	14771	14768	14766	14764
1359.57	0	14762	14761	14760	14759	14757	14756	14755	14753	14752	14750	14748	14747	14745	14743	14741	14738	14736
1343.18	0	14733	14729	14726	14723	14718	14713	14706	14699	14690	14682	14677	14681	14704	14748	14792	14823	14838
1326.79	0	14844	14842	14837	14831	14826	14824	14820	14817	14813	14810	14806	14803	14801	14798	14796	14794	14792
1309.43	1	14789	14787	14784	14782	14780	14778	14777	14775	14773	14772	14770	14769	14768	14767	14765	14764	14763
1276.65	1	14762	14761	14760	14759	14757	14756	14755	14754	14752	14751	14750	14749	14748	14749	14750	14750	14751
1243.86	1	14750	14749	14748	14747	14746	14745	14744	14743	14742	14741	14740	14739	14738	14737	14735	14734	14733
1211.08	1	14732	14730	14729	14728	14727	14727	14725	14724	14722	14721	14719	14717	14716	14715	14715	14716	14717
1178.29	1	14720	14724	14727	14729	14729	14728	14728	14731	14736	14741	14745	14746	14746	14746	14745	14745	14745
1145.51	1	14745	14745	14744	14743	14741	14740	14738	14736	14735	14733	14731	14729	14728	14726	14724	14722	14721
1112.73	1	14719	14717	14715	14714	14712	14710	14708	14706	14704	14702	14700	14698	14695	14693	14691	14688	14686
1079.94	1	14683	14680	14677	14674	14670	14666	14662	14657	14652	14646	14640	14633	14625	14616	14605	14592	14576
1047.16	1	14556	14532	14503	14475	14474	14554	14711	14837	14897	14908	14895	14875	14854	14836	14820	14807	14795
1014.37	1	14785	14778	14777	14778	14774	14768	14763	14758	14753	14749	14746	14744	14743	14741	14739	14736	14734
981.59	1	14732	14729	14727	14725	14724	14723	14722	14722	14721	14720	14719	14717	14715	14712	14710	14708	14707
948.81	1	14706	14704	14703	14702	14700	14698	14695	14692	14689	14687	14687	14685	14683	14682	14680	14678	14676
916.02	1	14673	14670	14668	14665	14662	14660	14657	14654	14652	14649	14646	14643	14640	14637	14634	14631	14628
883.24	1	14625	14622	14619	14615	14612	14609	14607	14605	14603	14601	14599	14596	14593	14590	14587	14585	14584
850.46	1	14584	14584	14583	14581	14577	14571	14565	14558	14550	14541	14530	14518	14504	14487	14467	14442	14409
817.67	1	14372	14348	14426	14646	14774	14779	14748	14717	14690	14668	14649	14632	14617	14604	14592	14581	14569
784.89	1	14558	14546	14535	14525	14516	14513	14518	14515	14506	14494	14482	14471	14460	14449	14437	14425	14412
752.10	1	14399	14386	14373	14358	14344	14328	14312	14295	14277	14259	14239	14218	14195	14171	14146	14118	14088
719.32	1	14056	14021	13983	13942	13896	13849	13794	13732	13662	13583	13492	13387	13264	13117	12936	12710	12421
686.54	1	12058	11635	11219	10955	11043	11693	13116	15418	17921	19237	19133	18520	17939	17471	17108	16828	16610
653.75	1	16435	16292	16171	16068	15979	15900	15831	15770	15714	15664	15619	15578	15540	15504	15472	15442	15414
620.97	1	15387	15362	15339	15317	15297	15278	15259	15241	15224	15208	15192	15177	15162	15148	15135	15121	15108
588.18	1	15095	15083	15071	15059	15048	15037	15026	15015	15004	14993	14983	14972	14960	14947	14933	14919	14903
555.40	1	14888	14871	14854	14837	14819	14798	14778	14755	14732	14705	14675	14641	14604	14557	14506	14446	14379
522.62	1	14313	14263	14259	14345	14401	14295	14117	13888	13587	13187	12742	12905	14630	16059	16474	16827	16952
489.83	1	16827	16618	16403	16222	16071	15951	15853	15772	15703	15645	15596	15552	15513	15482	15451	15421	15396
457.05	1	15377	15355	15336	15325													

[a,b] See footnotes a and b to Table IV.2.

Table VI.11. Imaginary refractive indices between 6500 and 450 cm^{-1} of 70.08% liquid benzene-h_6 in liquid benzene-d_6 at 25 °C.[a,b]

cm^{-1}	XE	YE	0	1	2	3	4	5	6	7	8	9	10	11	12	13	14	15	16
6499.90	3	0	0	0	0	0	0	0	0	0	0	0	0	0	0	0	0	0	0
6368.76	3	-7	-1	2	5	5	3	1	1	3	5	6	13	14	13	14	15	14	11
6237.63	3	-7	11	15	19	22	28	30	32	56	67	73	111	217	296	306	241	235	258
6106.49	3	-7	265	257	322	235	157	133	133	164	206	291	414	521	630	984	1433	2120	3133
5975.36	3	-7	2160	1668	1368	1241	1049	840	1152	990	1598	1278	785	562	636	634	614	555	421
5844.22	3	-7	293	183	129	97	92	120	126	127	154	182	192	132	122	137	117	96	117
5713.09	3	-7	198	214	283	303	244	167	144	144	141	100	81	79	92	151	175	137	107
5581.95	3	-7	111	117	112	111	133	177	203	168	170	184	125	94	74	65	54	48	46
5450.81	3	-7	49	59	76	105	96	84	100	85	73	92	123	110	105	118	133	109	102
5319.68	3	-7	94	85	76	71	69	74	78	89	120	137	137	97	77	63	63	56	56
5188.54	3	-7	61	60	53	55	80	84	79	79	82	70	63	77	90	87	83	87	81
5057.41	3	-7	79	84	80	68	62	65	78	88	91	79	80	75	80	75	66	71	76
4926.27	3	-7	76	78	85	94	90	89	96	128	144	149	167	159	131	111	95	95	89
4798.99	2	-7	91	95	101	112	128	132	128	128	129	130	133	136	141	152	169	176	184
4733.42	2	-7	196	214	233	256	288	326	372	449	569	697	964	1362	1318	1227	1398	2046	3380
4667.86	2	-7	3961	2344	1541	1323	1535	2293	3067	3138	2315	1575	1558	2413	2878	2049	1505	1400	1574
4602.29	2	-7	1586	1402	1417	1853	2891	3551	2882	2041	1395	1040	849	763	736	787	1007	1280	1128
4536.72	2	-7	831	634	519	458	434	441	477	544	654	836	1120	1534	2046	2538	2834	2751	2240
4471.15	2	-7	1673	1304	1164	1184	1296	1354	1260	1111	1017	1014	1015	933	824	708	676	736	737
4405.58	2	-7	754	698	648	640	654	634	768	1036	944	720	543	423	353	315	292	288	298
4340.02	2	-7	300	290	281	274	266	258	258	265	282	300	322	348	366	373	375	378	389
4274.45	2	-7	421	486	618	856	910	778	688	676	710	689	650	633	634	707	851	867	832
4208.88	2	-7	840	837	923	1155	1208	1004	854	820	900	1041	966	847	788	764	766	754	741
4143.31	2	-7	734	782	811	839	868	939	1029	1098	1200	1399	1721	2187	2693	3030	3537	4542	5779
4077.74	2	-6	591	594	705	969	1567	2314	2274	1540	976	624	423	314	274	304	302	229	179
4014.11	1	-7	1624	1495	1395	1308	1221	1137	1066	1007	961	925	904	900	916	948	978	985	989
3981.32	1	-7	983	938	881	835	799	774	778	843	1037	1345	1544	1703	1935	2025	1847	1584	1373
3948.54	1	-7	1231	1140	1104	1160	1345	1726	2372	2594	2209	1867	1595	1385	1222	1112	1036	987	961
3915.75	1	-7	935	906	886	876	874	872	869	864	854	840	832	832	858	932	971	931	892
3882.97	1	-7	851	807	765	731	708	694	683	668	649	633	625	622	621	618	609	598	588
3850.19	1	-7	584	584	586	592	605	631	680	764	902	1103	1322	1439	1388	1244	1092	984	947
3817.40	1	-7	985	1035	1040	1059	1144	1341	1691	2101	2229	1974	1620	1338	1152	1050	1009	976	902
3784.62	1	-7	809	736	688	664	665	691	737	791	827	810	758	709	674	652	643	645	660
3751.83	1	-7	689	732	795	881	988	1090	1131	1114	1082	1046	1010	985	974	983	1010	1047	1079
3719.05	1	-7	1098	1119	1149	1193	1260	1368	1532	1742	2012	2428	3191	4504	5503	4828	3784	3219	3052
3686.27	1	-7	2950	2630	2183	1798	1527	1344	1202	1098	1041	1026	1043	1043	981	906	866	864	902
3653.48	1	-7	993	1174	1525	2195	3446	5263	6399	5471	3817	2770	2206	1900	1713	1613	1603	1639	1680
3620.70	1	-7	1730	1827	2032	2356	2697	2848	2693	2325	1915	1558	1291	1105	963	850	765	702	650
3587.91	1	-7	602	560	536	547	544	545	513	466	424	395	377	366	356	349	340	331	327
3555.13	1	-7	329	334	344	354	358	355	348	338	327	314	301	292	284	275	265	261	265
3522.35	1	-7	272	292	329	381	411	370	328	309	304	303	303	301	297	298	309	338	391
3489.56	1	-7	477	540	487	425	388	359	342	333	329	332	341	358	382	415	451	497	562
3456.78	1	-7	651	775	932	1100	1220	1230	1136	999	866	755	665	598	560	558	613	688	662
3423.99	1	-7	636	638	646	643	626	600	574	551	538	537	549	569	587	595	585	558	523
3391.21	1	-7	490	460	431	401	375	354	336	322	312	307	307	310	316	325	335	344	351
3358.43	1	-7	356	357	351	342	338	339	338	329	319	315	319	332	355	381	408	460	558
3325.64	1	-7	684	742	696	618	554	509	477	455	440	434	434	437	441	449	461	477	498
3292.86	1	-7	525	559	605	667	744	835	930	1018	1097	1183	1283	1343	1329	1278	1231	1208	1223
3260.07	1	-7	1264	1337	1435	1548	1670	1821	2012	2278	2674	3288	4231	5529	6927	7873	7889	7025	5924
3227.29	1	-7	5026	4284	3618	3054	2623	2312	2110	2004	1975	1975	1938	1883	1843	1828	1947	2115	2142
3194.51	1	-7	2065	2102	2113	2168	2255	2158	2246	2277	2295	2393	2603	2575	2785	2456	2710	2863	2998
3161.72	1	-7	3007	3021	3154	3405	3548	3696	3744	3914	4054	4280	4403	4581	4843	5059	5128	5169	5442
3128.94	1	-6	581	618	653	696	785	880	970	1090	1223	1371	1496	1650	1841	2159	2640	3448	4941
3096.15	1	-5	769	1258	1918	2120	1668	1188	887	706	580	539	602	819	1331	1576	1165	848	670
3063.37	1	-5	570	507	478	484	471	438	430	447	495	599	816	1232	1969	2982	3613	3357	2692
3030.59	1	-5	2090	1622	1248	963	761	618	515	436	378	333	299	276	258	241	225	209	194
2997.80	1	-6	1792	1646	1479	1347	1244	1145	1064	984	896	851	800	744	680	634	593	561	541
2965.02	1	-7	5334	5263	5203	4796	4684	4518	4494	4338	4261	4117	3730	3607	3448	3497	3403	3227	3613
2932.23	1	-7	3509	3633	3429	3452	3331	3165	3242	2941	2860	2970	3306	3953	4933	5827	5727	4884	4118
2899.45	1	-6	363	340	347	401	538	810	1131	1019	693	515	410	337	289	260	243	234	235
2866.67	1	-7	2377	2520	2858	3501	4327	4595	4305	3940	3564	3223	3078	3036	2760	2505	2347	2268	2261
2833.88	1	-7	2368	2627	2717	2679	2850	3433	4320	5165	5473	4770	3808	3133	2620	2174	1821	1563	1364
2801.10	1	-7	1208	1102	1035	1000	980	962	951	950	952	950	942	932	931	948	970	964	922
2768.32	1	-7	861	799	748	706	675	650	627	607	592	579	557	530	505	487	474	467	465
2735.53	1	-7	469	481	490	479	465	454	447	446	447	451	453	455	455	455	455	457	464
2702.75	1	-7	473	483	492	501	510	520	532	544	562	584	607	631	651	665	677	693	716
2669.96	1	-7	751	801	873	979	1142	1420	1926	2897	4657	5823	4301	2851	2112	1678	1366	1176	1055
2637.18	1	-7	962	901	871	865	884	934	1021	1167	1426	1882	2526	3325	3851	3422	2740	2265	1997
2604.40	1	-7	1901	2013	2445	3422	5219	6026	4382	2977	2144	1641	1365	1226	1150	1138	1137	1181	1238
2571.61	1	-7	1187	1073	992	960	966	1003	1066	1168	1317	1403	1282	1091	945	848	782	735	693
2539.79	0	-7	674	658	645	635	627	624	621	622	624	627	636	652	678	717	774	860	999
2523.40	0	-7	1202	1388	1437	1403	1326	1226	1135	1063	1006	961	919	883	850	820	794	773	756
2507.01	0	-7	742	731	723	716	712	707	705	706	708	714	721	733	748	767	792	823	861
2489.65	1	-7	953	1065	1195	1263	1158	1024	940	904	910	966	1072	1106	1027	961	904	872	876
2456.87	1	-7	909	971	1039	1069	1062	1023	958	910	885	885	903	942	1019	1143	1266	1296	1303
2424.08	1	-7	1330	1380	1457	1574	1753	1991	2256	2478	2618	2689	2746	2831	2978	3217	3631	4405	5936
2391.30	1	-6	894	1245	1254	1103	997	905	852	914	1019	874	664	528	468	472	536	562	497
2358.52	1	-6	425	378	352	340	342	357	384	418	443	447	460	504	590	684	807	1046	1451

Table VI.11. Continued.

cm^{-1}	*XE*	*YE*	0	1	2	3	4	5	6	7	8	9	10	11	12	13	14	15	16
2325.73	1	-6	1894	1895	1480	1103	867	736	668	638	635	652	692	751	833	934	1052	1202	1398
2292.95	1	-5	167	207	274	394	614	972	1328	1390	1185	948	813	828	923	865	689	529	415
2260.16	1	-6	3330	2737	2286	1942	1681	1479	1312	1162	1028	914	822	747	685	637	598	563	530
2227.38	1	-6	500	477	455	443	450	488	582	781	1078	1199	988	735	544	426	360	326	302
2194.60	1	-7	2685	2406	2220	2087	1967	1852	1747	1658	1587	1540	1507	1457	1397	1338	1282	1231	1189
2161.81	1	-7	1161	1152	1178	1258	1396	1537	1550	1437	1318	1224	1148	1079	1012	949	899	864	841
2129.03	1	-7	821	791	760	737	721	710	701	695	691	686	676	665	659	660	665	672	673
2096.24	1	-7	672	679	698	727	762	786	794	796	796	785	761	733	706	689	679	675	678
2063.46	1	-7	689	707	736	779	837	913	1015	1139	1275	1374	1392	1381	1392	1433	1481	1520	1546
2030.68	1	-7	1563	1587	1616	1646	1689	1762	1881	2067	2365	2850	3647	4848	6160	7345	7364	6372	5482
1997.89	1	-6	500	499	538	605	734	837	795	763	779	837	933	1078	1285	1600	2080	2797	3802
1965.11	1	-6	5050	6293	7108	7150	6471	5420	4330	3383	2635	2069	1657	1370	1175	1035	918	803	698
1932.32	1	-7	6070	5301	4668	4150	3749	3425	3202	3070	3005	2951	2769	2589	2492	2549	2768	3072	2943
1899.54	1	-7	2658	2463	2366	2377	2517	2813	3221	3584	3785	3911	4102	4414	4762	4934	4925	5044	5371
1866.76	1	-6	544	537	559	569	536	502	487	484	503	534	580	640	713	802	910	1048	1229
1833.97	1	-5	147	180	225	289	376	493	641	811	975	1087	1098	1008	856	693	549	432	342
1801.19	1	-6	2767	2325	1984	1720	1502	1301	1104	931	786	670	581	511	458	416	383	357	336
1768.40	1	-7	3231	3466	3616	3991	4740	6095	8174	9993	9540	7277	5312	4208	3440	2857	2471	2205	2008
1735.62	1	-7	1863	1760	1688	1643	1626	1632	1655	1699	1813	2076	2647	3708	4050	3149	2678	2572	2608
1702.84	1	-6	263	270	286	313	350	390	414	412	413	445	518	625	699	717	794	940	1064
1670.05	1	-6	1051	914	754	626	541	491	465	446	426	412	406	409	420	455	473	469	484
1637.27	1	-6	510	544	585	649	742	897	1177	1700	2624	3885	4560	3987	3017	2291	1844	1577	1385
1604.48	1	-6	1222	1092	996	938	916	926	956	1006	1069	1114	1113	1070	1009	947	902	871	850
1571.70	1	-6	870	880	821	774	750	748	766	807	866	970	1116	1286	1346	1349	1425	1606	1910
1538.92	1	-6	2355	2924	3603	4303	4889	5217	5207	4892	4386	3829	3313	2884	2545	2299	2122	2006	1952
1507.10	0	-6	1953	1935	1985	2050	2141	2230	2333	2469	2606	2761	2926	3148	3410	3708	4086	4549	5109
1490.71	0	-4	58	67	78	95	117	149	196	265	372	535	766	1011	1108	996	792	592	434
1474.31	0	-5	3281	2667	2307	1951	1574	1263	1031	860	730	630	550	488	437	402	378	367	377
1457.92	0	-6	3897	4122	4392	4667	4846	4862	4691	4383	3998	3590	3196	2841	2531	2265	2046	1857	1690
1441.53	0	-6	1540	1405	1285	1182	1094	1023	950	893	843	797	761	727	699	673	652	636	622
1424.17	1	-6	606	599	598	604	621	650	695	751	830	951	1115	1351	1712	2266	3080	4019	4548
1391.39	1	-6	4215	3551	2775	2075	1585	1234	1009	862	751	673	616	578	549	529	516	511	514
1359.57	0	-6	521	530	543	554	570	593	616	641	664	697	730	764	802	847	898	962	1037
1343.18	0	-5	114	127	144	159	176	202	241	298	382	508	696	957	1238	1383	1311	1118	911
1326.79	0	-6	7242	5697	4588	3894	3442	3007	2572	2215	1927	1705	1542	1416	1323	1253	1194	1147	1103
1309.43	1	-6	1028	950	878	825	775	726	682	643	614	594	584	580	571	561	548	532	516
1276.65	1	-6	511	504	501	499	513	541	558	581	627	698	800	938	1107	1270	1358	1323	1208
1243.86	1	-6	1081	980	913	873	852	845	847	855	867	877	886	895	904	916	936	964	1000
1211.08	1	-6	1048	1112	1199	1314	1424	1470	1510	1585	1689	1827	2002	2229	2526	2906	3303	3644	3989
1178.29	1	-6	4272	4409	4348	4158	3973	3931	4075	4317	4418	4239	3920	3617	3360	3160	3021	2917	2800
1145.51	1	-6	2636	2421	2194	1979	1788	1627	1489	1372	1270	1182	1107	1043	989	946	907	873	849
1112.73	1	-7	8327	8277	8325	8331	8118	7850	7645	7505	7428	7428	7483	7520	7731	7909	8230	8526	8946
1079.94	1	-6	938	984	1050	1102	1157	1232	1322	1451	1588	1773	1993	2256	2595	3016	3548	4272	5274
1047.16	1	-5	677	914	1314	2013	3172	4534	5003	4324	3263	2323	1653	1213	928	744	623	547	504
1014.37	1	-6	4903	5042	5236	4758	4065	3608	3337	3193	3144	3145	3200	3304	3303	3120	2945	2882	2838
981.59	1	-6	2775	2753	2771	2815	2865	2903	2894	2830	2719	2579	2432	2293	2177	2095	2054	2048	2020
948.81	1	-6	1945	1891	1863	1766	1626	1516	1434	1394	1417	1511	1540	1463	1432	1409	1355	1283	1216
916.02	1	-6	1162	1126	1112	1111	1113	1114	1118	1127	1142	1163	1191	1226	1268	1316	1371	1436	1512
883.24	1	-6	1600	1705	1829	1975	2146	2340	2544	2741	2906	3041	3171	3328	3536	3807	4122	4436	4705
850.45	1	-6	4853	4848	4675	4404	4122	3882	3709	3572	3477	3454	3500	3645	3915	4395	5133	6335	8512
817.67	1	-5	1271	2108	3389	3633	2535	1570	1031	740	569	461	390	345	312	288	268	255	247
784.89	1	-6	2480	2589	2880	3329	4072	5036	5002	4006	3233	2814	2599	2507	2475	2162	2225	2299	2389
752.10	1	-6	2512	2590	2675	2781	2905	3046	3203	3371	3552	3755	3981	4232	4510	4821	5168	5558	5998
719.32	1	-5	650	707	773	851	947	1051	1158	1289	1450	1646	1886	2183	2558	3042	3697	4653	6183
686.53	1	-4	881	1336	2084	3194	4639	6265	7774	8481	7473	5103	2979	1753	1107	750	545	423	342
653.75	1	-5	2848	2412	2070	1796	1573	1389	1236	1107	998	904	824	754	693	640	594	553	516
620.97	1	-6	4843	4564	4330	4145	3961	3734	3539	3381	3247	3130	3025	2928	2836	2751	2677	2613	2561
588.18	1	-6	2522	2499	2488	2491	2490	2465	2410	2347	2289	2242	2205	2183	1680	1423	1231	935	809
555.40	1	-6	668	589	518	574	481	545	630	611	717	735	861	1001	1432	1994	3217	4941	8188
522.61	1	-4	134	212	310	378	304	230	219	260	377	641	1271	2574	3307	2528	1918	1512	1008
489.83	1	-5	6325	3838	2328	1423	881	563	315	194	105	41							

[a] See footnote a to Table IV.1.

[b] See footnote b to Table V.1.

Table VI.12. Real refractive indices between 6500 and 450 cm^{-1} of 70.08% liquid benzene-h$_6$ in liquid benzene-d$_6$ at 25 °C.^{a,b}

cm^{-1}	*XE*	0	1	2	3	4	5	6	7	8	9	10	11	12	13	14	15	16
6499.90	3	14793	14793	14793	14793	14793	14793	14793	14793	14793	14793	14793	14793	14793	14793	14793	14793	14793
6368.76	3	14793	14793	14793	14793	14793	14793	14793	14793	14793	14793	14793	14793	14792	14792	14792	14792	14792
6237.63	3	14792	14792	14792	14792	14792	14792	14792	14792	14792	14792	14792	14792	14792	14792	14792	14792	14792
6106.49	3	14792	14792	14792	14792	14792	14792	14792	14792	14792	14791	14791	14791	14791	14791	14791	14791	14792
5975.36	3	14793	14793	14793	14793	14793	14793	14793	14792	14793	14793	14793	14793	14793	14793	14793	14793	14793
5844.22	3	14793	14793	14793	14793	14793	14792	14792	14792	14792	14792	14792	14792	14792	14792	14792	14792	14792
5713.09	3	14792	14792	14792	14792	14792	14792	14792	14792	14792	14792	14792	14792	14792	14792	14792	14792	14792
5581.95	3	14792	14792	14792	14792	14792	14792	14792	14792	14792	14792	14792	14792	14792	14792	14792	14792	14792
5450.81	3	14791	14791	14791	14791	14791	14791	14791	14791	14791	14791	14791	14791	14791	14791	14791	14791	14791
5319.68	3	14791	14791	14791	14791	14791	14791	14791	14791	14791	14791	14791	14791	14791	14791	14791	14791	14791
5188.54	3	14791	14791	14791	14791	14791	14791	14791	14791	14791	14791	14790	14790	14790	14790	14790	14790	14790
5057.41	3	14790	14790	14790	14790	14790	14790	14790	14790	14790	14790	14790	14790	14790	14790	14790	14790	14790
4926.27	3	14790	14790	14790	14790	14790	14789	14789	14789	14789	14789	14789	14789	14789	14789	14789	14789	14789
4798.99	2	14789	14789	14789	14789	14789	14789	14789	14789	14789	14789	14789	14789	14788	14788	14788	14788	14788
4733.42	2	14788	14788	14788	14788	14788	14788	14788	14787	14787	14787	14787	14787	14787	14787	14787	14786	14787
4667.86	2	14789	14789	14789	14788	14788	14787	14788	14789	14790	14789	14788	14788	14789	14790	14789	14789	14789
4602.29	2	14789	14789	14788	14788	14788	14789	14790	14790	14790	14790	14790	14789	14789	14789	14789	14789	14789
4536.72	2	14789	14789	14789	14789	14789	14788	14788	14788	14788	14788	14787	14787	14787	14788	14788	14789	14789
4471.15	2	14790	14789	14789	14789	14789	14789	14789	14789	14789	14789	14789	14789	14789	14789	14789	14789	14788
4405.58	2	14788	14788	14788	14788	14788	14788	14788	14788	14788	14789	14788	14788	14788	14788	14788	14788	14788
4340.02	2	14788	14788	14788	14788	14788	14787	14787	14787	14787	14787	14787	14787	14787	14787	14787	14787	14787
4274.45	2	14787	14787	14786	14786	14787	14787	14787	14787	14787	14786	14786	14786	14786	14786	14786	14786	14786
4208.88	2	14786	14786	14786	14786	14786	14786	14786	14786	14786	14786	14786	14786	14785	14785	14785	14785	14785
4143.31	2	14785	14785	14784	14784	14784	14784	14783	14783	14783	14782	14782	14781	14781	14781	14780	14780	14780
4077.74	2	14781	14780	14778	14776	14776	14782	14793	14798	14798	14797	14795	14794	14792	14792	14792	14792	14791
4014.11	1	14791	14791	14790	14790	14790	14790	14790	14789	14789	14789	14789	14789	14789	14789	14788	14788	14788
3981.32	1	14788	14788	14788	14788	14788	14788	14787	14787	14787	14787	14787	14787	14787	14787	14788	14788	14788
3948.54	1	14788	14787	14787	14787	14787	14786	14787	14787	14788	14788	14788	14788	14788	14788	14787	14787	14787
3915.75	1	14787	14787	14787	14787	14787	14787	14787	14787	14787	14787	14787	14787	14786	14786	14787	14787	14787
3882.97	1	14786	14786	14786	14786	14786	14786	14786	14786	14786	14786	14786	14786	14786	14786	14786	14786	14786
3850.19	1	14786	14785	14785	14785	14785	14785	14785	14785	14785	14785	14785	14785	14785	14785	14785	14785	14785
3817.40	1	14785	14785	14785	14785	14785	14784	14784	14785	14785	14786	14786	14786	14786	14785	14785	14785	14785
3784.62	1	14785	14785	14785	14785	14785	14785	14785	14785	14785	14785	14785	14784	14784	14784	14784	14784	14784
3751.83	1	14784	14784	14784	14784	14784	14784	14784	14784	14784	14784	14784	14784	14783	14783	14783	14783	14783
3719.05	1	14783	14783	14783	14783	14782	14782	14782	14782	14782	14781	14781	14781	14783	14785	14785	14785	14785
3686.27	1	14785	14785	14785	14785	14785	14785	14784	14784	14784	14784	14784	14784	14783	14783	14783	14783	14782
3653.48	1	14782	14782	14781	14781	14780	14781	14783	14785	14786	14785	14785	14785	14784	14784	14784	14784	14784
3620.70	1	14783	14783	14783	14783	14783	14784	14784	14785	14785	14785	14785	14784	14784	14784	14784	14784	14784
3587.91	1	14784	14783	14783	14783	14783	14783	14783	14783	14783	14783	14783	14783	14783	14782	14782	14782	14782
3555.13	1	14782	14782	14782	14782	14782	14782	14782	14782	14782	14782	14782	14782	14781	14781	14781	14781	14781
3522.35	1	14781	14781	14781	14781	14781	14781	14781	14781	14781	14781	14780	14780	14780	14780	14780	14780	14780
3489.56	1	14780	14780	14780	14780	14780	14780	14780	14780	14780	14779	14779	14779	14779	14779	14779	14779	14779
3456.78	1	14779	14779	14778	14779	14779	14779	14779	14779	14779	14779	14779	14779	14779	14778	14778	14778	14778
3423.99	1	14778	14778	14778	14778	14778	14778	14778	14778	14778	14778	14777	14777	14777	14777	14777	14777	14777
3391.21	1	14777	14777	14777	14777	14777	14777	14776	14776	14776	14776	14776	14776	14776	14776	14776	14775	14775
3358.43	1	14775	14775	14775	14775	14775	14775	14775	14774	14774	14774	14774	14774	14774	14774	14773	14773	14773
3325.64	1	14773	14773	14773	14773	14773	14773	14772	14772	14772	14772	14772	14772	14771	14771	14771	14771	14771
3292.86	1	14770	14770	14770	14770	14770	14769	14769	14769	14769	14769	14769	14768	14768	14768	14768	14768	14767
3260.07	1	14767	14767	14766	14766	14766	14765	14765	14764	14764	14763	14763	14763	14763	14765	14766	14768	14768
3227.29	1	14768	14768	14768	14767	14767	14766	14765	14765	14764	14764	14764	14763	14763	14762	14762	14761	14761
3194.51	1	14761	14760	14760	14759	14759	14758	14758	14757	14757	14756	14756	14755	14754	14754	14753	14752	14752
3161.72	1	14751	14750	14749	14749	14748	14747	14746	14745	14744	14743	14742	14741	14740	14739	14737	14736	14734
3128.94	1	14732	14730	14728	14726	14723	14720	14718	14715	14711	14708	14704	14698	14692	14684	14674	14661	14644
3096.15	1	14627	14619	14653	14739	14798	14808	14800	14788	14773	14754	14732	14712	14712	14780	14815	14814	14804
3063.37	1	14794	14784	14774	14766	14761	14752	14739	14725	14707	14684	14655	14626	14609	14644	14757	14873	14936
3030.59	1	14957	14961	14957	14946	14934	14922	14912	14902	14894	14887	14880	14875	14870	14866	14863	14860	14858
2997.80	1	14855	14853	14851	14849	14846	14844	14842	14840	14839	14837	14835	14834	14832	14831	14829	14828	14827
2965.02	1	14826	14824	14824	14823	14822	14821	14820	14819	14818	14818	14817	14816	14815	14815	14814	14813	14813
2932.23	1	14812	14812	14811	14811	14810	14810	14809	14808	14808	14807	14806	14805	14805	14805	14806	14807	14806
2899.45	1	14805	14804	14803	14802	14801	14800	14803	14807	14808	14808	14807	14806	14805	14805	14804	14803	14803
2866.67	1	14802	14801	14801	14800	14800	14801	14801	14802	14802	14801	14801	14801	14801	14800	14800	14800	14799
2833.88	1	14799	14798	14798	14798	14797	14797	14797	14798	14799	14800	14800	14800	14800	14799	14799	14799	14798
2801.10	1	14798	14798	14797	14797	14797	14797	14796	14796	14796	14796	14796	14795	14795	14795	14795	14795	14795
2768.32	1	14795	14794	14794	14794	14794	14794	14794	14793	14793	14793	14793	14793	14793	14793	14792	14792	14792
2735.53	1	14792	14792	14792	14792	14791	14791	14791	14791	14791	14791	14791	14790	14790	14790	14790	14790	14790
2702.75	1	14790	14789	14789	14789	14789	14789	14789	14789	14788	14788	14788	14788	14788	14788	14788	14787	14787
2669.96	1	14787	14787	14787	14786	14786	14785	14785	14785	14785	14787	14789	14789	14789	14788	14788	14788	14787
2637.18	1	14787	14787	14786	14786	14786	14786	14785	14785	14785	14784	14784	14784	14785	14786	14786	14786	14786
2604.40	1	14785	14784	14784	14783	14784	14786	14788	14788	14787	14787	14786	14786	14786	14785	14785	14785	14785
2571.61	1	14785	14785	14785	14784	14784	14784	14784	14784	14784	14784	14784	14784	14784	14783	14783	14783	14783
2539.79	0	14783	14783	14783	14783	14783	14782	14782	14782	14782	14782	14782	14782	14782	14782	14782	14781	14781
2523.40	0	14781	14781	14781	14782	14782	14782	14782	14782	14782	14781	14781	14781	14781	14781	14781	14781	14781
2507.01	0	14781	14781	14781	14781	14781	14780	14780	14780	14780	14780	14780	14780	14780	14780	14780	14780	14779
2489.65	1	14779	14779	14779	14779	14779	14779	14779	14779	14778	14778	14778	14778	14778	14778	14778	14777	14777
2456.87	1	14777	14777	14777	14777	14776	14776	14776	14776	14776	14775	14775	14775	14774	14774	14774	14774	14774
2424.08	1	14773	14773	14773	14772	14772	14772	14771	14771	14771	14771	14770	14770	14769	14768	14768	14766	14765
2391.30	1	14764	14767	14770	14772	14773	14773	14772	14772	14773	14775	14775	14774	14773	14772	14771	14772	14772
2358.52	1	14771	14770	14770	14769	14768	14767	14766	14765	14765	14764	14763	14762	14760	14759	14758	14756	14756

Table VI.12. Continued.

cm^{-1}	*XE*	0	1	2	3	4	5	6	7	8	9	10	11	12	13	14	15	16
2325.73	1	14759	14765	14768	14768	14766	14764	14762	14760	14757	14755	14753	14750	14748	14745	14742	14738	14733
2292.95	1	14728	14721	14712	14701	14690	14691	14721	14767	14799	14808	14804	14799	14809	14830	14841	14842	14839
2260.16	1	14835	14831	14827	14823	14820	14817	14815	14813	14811	14809	14807	14806	14804	14803	14801	14800	14799
2227.38	1	14798	14797	14796	14794	14793	14792	14790	14789	14790	14793	14796	14796	14796	14795	14794	14793	14792
2194.60	1	14792	14791	14790	14790	14789	14789	14788	14788	14787	14787	14787	14786	14786	14786	14785	14785	14785
2161.81	1	14784	14784	14783	14783	14783	14783	14783	14782	14782	14782	14782	14781	14781	14781	14781	14780	14780
2129.03	1	14780	14780	14779	14779	14779	14779	14778	14778	14778	14778	14777	14777	14777	14777	14776	14776	14776
2096.24	1	14776	14775	14775	14775	14775	14774	14774	14774	14774	14774	14773	14773	14773	14773	14772	14772	14772
2063.46	1	14771	14771	14771	14770	14770	14770	14769	14769	14769	14769	14768	14768	14768	14767	14767	14767	14766
2030.68	1	14766	14766	14765	14765	14764	14763	14763	14762	14761	14760	14759	14759	14759	14759	14761	14761	14761
1997.89	1	14759	14758	14757	14756	14755	14755	14755	14754	14752	14750	14747	14745	14742	14738	14735	14732	14730
1965.11	1	14733	14742	14757	14774	14789	14798	14802	14803	14801	14799	14796	14793	14791	14789	14787	14786	14785
1932.32	1	14783	14782	14781	14779	14778	14777	14776	14775	14774	14773	14773	14772	14771	14770	14769	14769	14769
1899.54	1	14768	14767	14766	14766	14765	14764	14763	14763	14762	14762	14761	14760	14760	14760	14759	14758	14758
1866.76	1	14757	14757	14756	14756	14755	14754	14753	14751	14750	14748	14746	14745	14743	14740	14738	14735	14732
1833.97	1	14729	14725	14720	14716	14711	14709	14709	14715	14728	14750	14774	14797	14811	14819	14820	14819	14816
1801.19	1	14812	14808	14805	14802	14800	14798	14796	14794	14791	14789	14787	14786	14784	14782	14781	14779	14778
1768.40	1	14777	14775	14774	14773	14771	14770	14770	14771	14774	14775	14775	14774	14773	14772	14771	14770	14769
1735.62	1	14768	14767	14766	14766	14765	14764	14763	14763	14762	14761	14760	14760	14761	14761	14760	14759	14758
1702.84	1	14758	14757	14756	14755	14755	14754	14754	14754	14753	14752	14751	14751	14751	14750	14750	14750	14751
1670.05	1	14753	14754	14754	14753	14752	14751	14750	14750	14749	14748	14747	14746	14744	14743	14743	14742	14740
1637.27	1	14739	14737	14736	14734	14731	14728	14725	14721	14719	14723	14738	14752	14757	14756	14754	14752	14751
1604.48	1	14749	14748	14746	14744	14742	14740	14739	14738	14737	14737	14736	14736	14735	14734	14733	14732	14730
1571.70	1	14729	14728	14727	14725	14723	14721	14718	14716	14714	14711	14709	14707	14706	14703	14700	14696	14691
1538.92	1	14688	14685	14684	14686	14690	14696	14702	14707	14710	14710	14707	14703	14698	14692	14685	14678	14670
1507.10	0	14665	14660	14655	14650	14644	14639	14633	14626	14619	14612	14603	14594	14584	14573	14560	14546	14530
1490.71	0	14511	14490	14464	14434	14399	14358	14309	14255	14200	14164	14201	14394	14734	15045	15217	15276	15264
1474.31	0	15219	15172	15142	15126	15107	15082	15057	15034	15014	14995	14979	14964	14950	14937	14925	14914	14905
1457.92	0	14896	14890	14885	14882	14881	14882	14883	14883	14882	14881	14878	14875	14872	14869	14865	14862	14859
1441.53	0	14855	14852	14849	14847	14844	14841	14838	14836	14833	14831	14829	14827	14825	14823	14821	14819	14817
1424.17	1	14813	14810	14807	14803	14800	14797	14794	14791	14788	14785	14781	14778	14774	14771	14770	14775	14785
1391.39	1	14796	14802	14805	14804	14801	14798	14795	14792	14789	14786	14784	14782	14779	14777	14775	14773	14771
1359.57	0	14769	14768	14767	14766	14765	14764	14762	14761	14760	14758	14757	14755	14754	14752	14750	14748	14746
1343.18	0	14743	14741	14738	14735	14732	14727	14722	14715	14709	14702	14697	14701	14720	14756	14791	14814	14826
1326.79	0	14830	14828	14824	14819	14815	14813	14811	14808	14805	14802	14799	14796	14794	14792	14791	14789	14788
1309.43	1	14785	14783	14781	14779	14778	14776	14775	14773	14772	14770	14769	14768	14766	14765	14764	14763	14762
1276.65	1	14761	14760	14758	14757	14756	14755	14753	14752	14751	14749	14748	14747	14747	14747	14748	14750	14750
1243.86	1	14750	14749	14748	14747	14746	14744	14743	14742	14741	14740	14739	14738	14737	14736	14735	14733	14732
1211.08	1	14731	14729	14728	14727	14726	14725	14724	14722	14721	14719	14717	14716	14714	14713	14714	14715	14717
1178.29	1	14720	14724	14728	14731	14731	14730	14730	14732	14736	14740	14742	14743	14743	14743	14742	14742	14742
1145.51	1	14743	14743	14742	14741	14739	14738	14736	14734	14733	14731	14729	14727	14725	14723	14722	14720	14718
1112.73	1	14716	14714	14712	14711	14709	14707	14705	14703	14701	14698	14696	14694	14691	14688	14686	14683	14680
1079.94	1	14677	14673	14670	14666	14662	14658	14653	14647	14642	14635	14628	14620	14611	14601	14588	14574	14556
1047.16	1	14533	14506	14473	14441	14439	14528	14706	14854	14924	14937	14923	14900	14876	14855	14837	14821	14808
1014.37	1	14797	14789	14787	14788	14783	14777	14771	14765	14760	14755	14752	14749	14748	14747	14744	14741	14739
981.59	1	14736	14734	14731	14729	14728	14727	14726	14726	14725	14724	14723	14721	14719	14716	14714	14712	14711
948.81	1	14709	14707	14706	14705	14703	14700	14697	14695	14692	14689	14688	14687	14685	14683	14681	14679	14677
916.02	1	14674	14671	14668	14666	14663	14660	14658	14655	14652	14649	14646	14643	14640	14637	14634	14631	14628
883.24	1	14625	14621	14618	14615	14611	14608	14605	14603	14601	14598	14596	14593	14589	14587	14584	14583	14583
850.45	1	14584	14584	14584	14582	14579	14574	14569	14562	14555	14547	14537	14526	14514	14499	14482	14460	14433
817.67	1	14402	14381	14443	14620	14720	14721	14694	14667	14644	14625	14608	14593	14579	14567	14555	14544	14532
784.89	1	14521	14509	14498	14487	14478	14476	14482	14480	14470	14458	14445	14433	14422	14409	14395	14382	14368
752.10	1	14355	14341	14326	14310	14294	14277	14260	14241	14221	14200	14178	14155	14130	14103	14075	14044	14011
719.32	1	13975	13936	13894	13847	13796	13742	13680	13611	13532	13443	13341	13223	13084	12918	12714	12458	12132
686.53	1	11722	11244	10774	10475	10576	11312	12921	15526	18357	19846	19728	19035	18377	17848	17436	17120	16873
653.75	1	16676	16514	16379	16263	16162	16075	15997	15928	15866	15810	15760	15714	15672	15633	15597	15563	15532
620.97	1	15503	15476	15451	15427	15405	15384	15364	15344	15326	15308	15292	15276	15260	15246	15231	15217	15204
588.18	1	15191	15178	15166	15154	15143	15132	15121	15110	15099	15089	15079	15070	15061	15047	15034	15021	15007
555.40	1	14992	14977	14961	14947	14930	14912	14895	14875	14855	14832	14807	14778	14746	14707	14665	14615	14559
522.61	1	14503	14461	14457	14532	14583	14496	14349	14161	13913	13581	13202	13365	14951	16058	16278	16503	16569
489.83	1	16454	16291	16124	15985	15869	15773	15697	15631	15577	15532							

[a,b] See footnotes a and b to Table IV.2.

Table VI.13. Imaginary refractive indices between 6500 and 450 cm^{-1} of 79.34% liquid benzene-h_6 in liquid benzene-d_6 at 25 °C.[a,b]

cm^{-1}	XE	YE	0	1	2	3	4	5	6	7	8	9	10	11	12	13	14	15	16
6499.90	3	0	0	0	0	0	0	0	0	0	0	0	0	0	0	0	0	0	0
6368.76	3	-7	-2	-1	0	0	-1	-1	-1	0	2	3	11	13	8	8	6	5	8
6237.63	3	-7	8	9	10	13	18	22	30	46	63	77	126	249	324	331	270	260	284
6106.49	3	-7	289	277	353	251	163	135	149	210	287	382	517	618	742	1152	1654	2394	3503
5975.36	3	-7	2719	2041	1609	1403	1128	887	1215	1061	1854	1466	923	576	713	741	725	662	491
5844.22	3	-7	348	222	153	104	98	126	139	141	168	202	215	148	131	142	125	100	122
5713.09	3	-7	214	232	308	326	257	173	145	144	141	95	71	69	85	151	178	138	104
5581.95	3	-7	109	117	110	109	135	186	212	175	178	194	127	95	71	61	51	44	46
5450.81	3	-7	51	58	80	108	104	84	102	91	79	97	122	115	112	126	133	110	103
5319.68	3	-7	94	88	71	65	64	63	72	91	133	150	142	101	86	73	71	66	66
5188.54	3	-7	74	73	66	68	97	101	94	94	95	79	73	89	103	96	90	95	91
5057.41	3	-7	90	97	91	78	72	75	87	98	103	88	91	85	89	83	74	79	87
4926.27	3	-7	86	87	95	105	100	97	107	140	157	164	178	170	145	122	105	106	100
4798.99	2	-7	104	109	116	129	147	152	148	147	149	154	159	162	165	176	190	204	217
4733.42	2	-7	230	251	276	305	338	381	431	518	655	801	1109	1566	1519	1408	1585	2336	3961
4667.86	2	-7	4526	2717	1781	1498	1707	2546	3462	3588	2715	1822	1735	2656	3276	2375	1737	1582	1749
4602.29	2	-7	1766	1561	1561	2036	3242	4150	3374	2383	1625	1201	960	851	813	870	1122	1444	1276
4536.72	2	-7	934	703	561	482	441	433	449	488	558	675	861	1140	1494	1849	2071	2031	1682
4471.15	2	-7	1287	1023	931	951	1030	1072	1010	910	851	869	903	854	764	672	660	735	713
4405.58	2	-7	724	672	625	610	620	626	784	1099	1026	776	585	461	388	348	324	316	321
4340.02	2	-7	321	313	308	303	296	291	292	302	323	346	375	404	425	432	432	435	451
4274.45	2	-7	489	567	715	979	1046	898	793	779	823	804	761	742	744	826	987	1007	965
4208.88	2	-7	972	968	1057	1310	1376	1147	980	940	1025	1181	1104	969	902	873	876	863	848
4143.31	2	-7	850	882	921	959	1012	1070	1146	1253	1399	1610	1943	2462	3047	3472	4014	5141	6538
4077.75	2	-6	663	661	787	1086	1760	2622	2601	1752	1098	699	471	352	311	344	348	268	212
4014.11	1	-7	1888	1723	1601	1489	1391	1297	1216	1150	1096	1056	1030	1024	1039	1074	1106	1114	1119
3981.32	1	-7	1112	1061	997	945	904	878	885	957	1170	1503	1719	1895	2165	2298	2106	1800	1549
3948.54	1	-7	1380	1276	1237	1292	1475	1869	2534	2821	2462	2090	1769	1523	1342	1218	1135	1081	1050
3915.75	1	-7	1020	990	969	959	954	951	944	935	925	912	904	903	916	964	985	953	922
3882.97	1	-7	886	847	807	771	743	724	708	691	673	656	645	639	636	630	621	610	598
3850.19	1	-7	590	585	583	582	587	601	631	689	789	934	1094	1175	1137	1035	926	846	816
3817.40	1	-7	841	876	876	886	944	1087	1344	1644	1719	1533	1298	1120	1009	965	967	966	906
3784.62	1	-7	816	745	700	680	684	713	764	826	871	859	810	762	727	707	698	701	717
3751.83	1	-7	749	793	858	942	1042	1135	1175	1169	1146	1115	1083	1061	1052	1061	1088	1121	1153
3719.05	1	-7	1174	1199	1233	1284	1362	1484	1671	1913	2218	2685	3537	5000	6140	5463	4256	3592	3387
3686.27	1	-7	3272	2915	2412	1976	1673	1468	1312	1198	1139	1124	1147	1151	1084	1002	952	948	988
3653.48	1	-7	1090	1294	1686	2431	3817	5826	7286	6399	4360	3108	2440	2067	1822	1667	1597	1590	1615
3620.70	1	-7	1683	1823	2090	2484	2901	3109	2964	2563	2102	1696	1389	1176	1013	883	788	721	665
3587.91	1	-7	613	567	537	526	522	516	483	443	409	386	373	365	356	349	341	333	329
3555.13	1	-7	330	334	343	352	356	355	351	344	334	323	313	306	299	290	281	278	284
3522.35	1	-7	293	314	356	414	449	404	358	338	333	334	335	334	331	332	345	377	437
3489.56	1	-7	535	609	549	479	436	403	382	372	368	371	381	398	422	453	491	544	616
3456.78	1	-7	713	848	1023	1214	1351	1364	1260	1105	956	832	731	655	608	598	646	725	700
3423.99	1	-7	672	676	688	686	671	647	623	600	588	587	601	623	643	654	644	613	572
3391.21	1	-7	531	494	458	425	397	374	355	341	329	323	321	320	322	327	333	339	347
3358.43	1	-7	354	359	356	350	349	353	354	345	334	328	329	339	359	382	402	440	515
3325.64	1	-7	611	651	615	557	510	478	455	439	428	424	425	429	434	442	455	469	488
3292.86	1	-7	509	537	573	621	682	753	828	899	963	1031	1107	1155	1151	1124	1101	1098	1118
3260.07	1	-7	1161	1226	1307	1398	1493	1606	1748	1941	2224	2655	3311	4217	5199	5908	5957	5352	4571
3227.29	1	-7	3929	3414	2957	2578	2292	2086	1957	1898	1894	1911	1902	1883	1889	1904	2096	2273	2245
3194.51	1	-7	2254	2316	2322	2402	2459	2571	2432	2561	2574	2565	2658	2812	2955	2752	2894	3044	3096
3161.72	1	-7	3165	3208	3216	3562	3590	3769	3907	4058	4221	4521	4664	4742	5058	5266	5404	5608	5834
3128.94	1	-6	619	652	695	747	837	940	1047	1172	1328	1491	1649	1822	2080	2420	2945	3836	5460
3096.16	1	-5	846	1385	2130	2385	1891	1346	1000	792	649	596	658	894	1466	1768	1318	958	753
3063.37	1	-5	636	561	529	536	524	488	479	499	554	672	908	1361	2171	3301	4051	3807	3063
3030.59	1	-5	2372	1832	1402	1081	851	692	572	487	423	372	337	309	288	271	259	244	227
2997.80	1	-6	2104	1936	1778	1646	1529	1424	1324	1240	1168	1103	1045	988	932	879	832	791	758
2965.02	1	-7	7256	6931	6670	6480	6352	6277	6253	6260	6248	6045	5666	5266	4917	4619	4380	4193	4053
2932.24	1	-7	3944	3862	3781	3682	3560	3431	3311	3217	3197	3322	3695	4426	5540	6587	6504	5549	4668
2899.45	1	-6	410	382	389	448	599	905	1276	1164	787	577	451	364	309	275	255	246	244
2866.67	1	-7	2410	2482	2716	3191	3837	4134	4055	3887	3619	3302	3105	2997	2750	2539	2406	2321	2281
2833.88	1	-7	2330	2504	2587	2632	2914	3633	4660	5625	6058	5350	4270	3502	2921	2419	2018	1724	1498
2801.10	1	-7	1320	1193	1110	1062	1034	1014	1005	1008	1014	1014	1004	986	969	964	966	949	908
2768.32	1	-7	856	806	764	731	706	684	664	646	634	623	602	575	551	532	519	513	512
2735.53	1	-7	517	530	540	528	512	499	492	491	493	496	500	502	503	503	505	509	517
2702.75	1	-7	526	538	549	560	570	583	597	611	629	652	679	705	728	744	757	774	801
2669.96	1	-7	840	897	980	1100	1285	1599	2168	3248	5160	6468	4852	3218	2368	1870	1515	1297	1159
2637.18	1	-7	1051	980	943	935	953	1001	1090	1236	1496	1964	2632	3481	4068	3625	2892	2393	2123
2604.40	1	-7	2038	2180	2675	3770	5765	6750	4946	3350	2400	1827	1511	1353	1265	1246	1238	1282	1347
2571.61	1	-7	1295	1171	1080	1042	1047	1087	1158	1271	1438	1542	1416	1204	1037	924	848	795	749
2539.79	0	-7	728	711	697	686	679	674	673	673	676	681	690	705	727	759	804	870	973
2523.40	0	-7	1122	1261	1307	1294	1244	1172	1107	1055	1014	980	949	921	894	869	846	826	810
2507.01	0	-7	796	785	776	770	764	761	759	760	764	771	780	792	810	831	859	893	935
2489.65	1	-7	1036	1161	1307	1383	1267	1116	1020	976	980	1042	1159	1198	1107	1028	960	918	917
2456.87	1	-7	947	1008	1076	1096	1070	1019	955	910	885	882	899	942	1025	1161	1292	1317	1313
2424.08	1	-7	1334	1379	1453	1570	1751	1998	2271	2500	2630	2682	2702	2739	2823	2983	3265	3796	4866
2391.30	1	-7	6939	9305	9642	9036	8643	8070	7529	7757	8398	7172	5495	4404	3896	3878	4325	4537	4037
2358.52	1	-6	348	313	294	287	289	301	323	352	374	383	399	442	523	624	773	1050	1506

Table VI.13. Continued.

cm^{-1}	*XE*	*YE*	0	1	2	3	4	5	6	7	8	9	10	11	12	13	14	15	16
2325.73	1	-6	2003	2018	1549	1117	841	681	590	542	519	515	532	571	627	699	780	886	1023
2292.95	1	-5	121	149	194	279	437	702	980	1023	858	681	582	589	654	614	492	379	297
2260.16	1	-6	2380	1950	1626	1386	1203	1062	946	841	743	664	601	550	507	472	446	424	405
2227.38	1	-6	387	373	361	358	377	430	546	788	1168	1290	1024	750	543	410	332	289	261
2194.60	1	-7	2290	2047	1890	1780	1686	1595	1515	1444	1386	1345	1315	1274	1228	1183	1140	1100	1064
2161.81	1	-7	1039	1029	1043	1095	1189	1286	1296	1217	1133	1063	1003	949	897	848	809	782	764
2129.03	1	-7	748	726	704	689	682	680	680	681	682	681	675	668	667	674	685	696	703
2096.24	1	-7	707	720	745	782	824	855	868	873	876	866	841	810	783	765	754	751	757
2063.46	1	-7	770	792	826	873	937	1023	1136	1274	1428	1542	1568	1559	1572	1614	1664	1703	1727
2030.68	1	-7	1747	1775	1811	1849	1903	1994	2136	2361	2710	3246	4178	5601	7101	8413	8407	7252	6242
1997.89	1	-6	562	548	580	657	804	928	886	852	873	939	1046	1212	1442	1789	2318	3100	4205
1965.11	1	-6	5582	6978	7934	8046	7328	6162	4936	3861	3008	2361	1888	1556	1329	1172	1035	907	791
1932.33	1	-7	6874	6012	5277	4679	4214	3842	3572	3427	3358	3285	3083	2837	2702	2674	2780	2956	2828
1899.54	1	-7	2606	2486	2452	2510	2703	3053	3521	3943	4165	4252	4417	4695	5022	5141	5028	5001	5149
1866.76	1	-6	517	509	527	537	518	500	497	508	533	570	621	687	767	866	992	1148	1353
1833.97	1	-5	162	200	250	321	417	545	707	895	1080	1211	1236	1142	975	791	626	491	387
1801.19	1	-6	3105	2570	2180	1889	1652	1460	1268	1077	911	776	671	590	528	481	444	415	395
1768.41	1	-6	384	385	402	444	528	681	914	1119	1073	821	599	473	385	318	274	243	220
1735.62	1	-7	2038	1918	1832	1777	1751	1751	1771	1816	1937	2224	2855	4037	4436	3418	2863	2711	2712
1702.84	1	-6	269	271	281	300	327	357	377	379	384	414	477	570	649	698	807	979	1126
1670.05	1	-6	1126	983	807	663	564	501	466	441	422	409	405	409	421	454	469	457	464
1637.27	1	-6	482	511	550	609	697	834	1058	1448	2124	3047	3640	3330	2557	1965	1612	1424	1294
1604.49	1	-6	1173	1070	993	949	939	961	1001	1059	1130	1181	1180	1129	1055	985	931	892	857
1571.70	1	-6	851	844	796	759	742	742	761	797	849	933	1053	1199	1284	1341	1469	1698	2051
1538.92	1	-6	2555	3190	3947	4729	5396	5785	5804	5480	4935	4320	3737	3241	2848	2556	2349	2218	2157
1507.10	0	-6	2158	2167	2204	2253	2323	2421	2555	2688	2880	3061	3265	3530	3800	4168	4599	5098	5723
1490.71	0	-4	65	75	88	105	130	165	215	289	404	581	832	1102	1231	1131	909	682	499
1474.31	0	-5	3762	3039	2617	2207	1775	1420	1153	958	810	692	601	524	464	417	385	363	351
1457.92	0	-6	3509	3593	3711	3868	3984	3979	3853	3626	3353	3040	2725	2444	2193	1984	1805	1655	1521
1441.53	0	-6	1401	1289	1192	1106	1032	970	909	858	817	779	748	719	698	676	658	644	633
1424.17	1	-6	619	616	616	627	645	677	718	774	856	981	1151	1401	1789	2395	3269	4256	4796
1391.39	1	-6	4442	3707	2882	2165	1657	1284	1042	884	770	687	625	580	549	528	512	506	502
1359.57	0	-7	5057	5066	5143	5156	5260	5379	5580	5781	5996	6224	6481	6727	7027	7321	7728	8139	8695
1343.18	0	-6	942	1034	1147	1254	1368	1552	1824	2232	2827	3730	5072	6938	8942	9947	9419	8060	6601
1326.79	0	-6	5284	4196	3414	2919	2601	2294	1987	1739	1541	1394	1281	1201	1141	1099	1065	1035	1012
1309.43	1	-7	9663	9105	8472	7997	7526	7031	6589	6199	5922	5719	5596	5525	5419	5350	5271	5127	5057
1276.65	1	-6	506	505	504	508	521	540	568	605	660	733	843	985	1159	1328	1424	1393	1272
1243.86	1	-6	1139	1034	966	927	909	903	909	920	933	946	961	982	1003	1030	1062	1102	1148
1211.08	1	-6	1207	1277	1376	1501	1618	1671	1724	1812	1926	2078	2263	2499	2808	3203	3615	3987	4375
1178.29	1	-6	4697	4851	4776	4521	4256	4092	4088	4196	4214	4040	3778	3545	3365	3243	3168	3117	3037
1145.51	1	-6	2893	2683	2448	2219	2013	1835	1680	1549	1440	1344	1263	1190	1128	1073	1023	984	954
1112.73	1	-6	932	922	929	931	909	882	859	842	834	829	833	841	861	891	933	961	1016
1079.94	1	-6	1061	1119	1178	1246	1312	1396	1500	1627	1784	1975	2230	2529	2899	3374	3965	4786	5930
1047.16	1	-5	760	1026	1468	2237	3507	5007	5588	4898	3714	2644	1879	1374	1049	838	698	610	558
1014.37	1	-6	5386	5512	5757	5247	4495	3987	3687	3532	3464	3444	3509	3618	3610	3409	3212	3102	3042
981.59	1	-6	2967	2928	2938	2975	3019	3059	3048	2994	2879	2741	2577	2407	2258	2140	2062	2015	1965
948.81	1	-6	1884	1812	1768	1682	1554	1461	1383	1347	1351	1417	1431	1373	1353	1323	1277	1206	1154
916.02	1	-6	1111	1077	1069	1095	1113	1129	1133	1143	1154	1168	1188	1210	1244	1288	1345	1402	1473
883.24	1	-6	1548	1643	1751	1881	2029	2204	2387	2568	2739	2899	3060	3262	3518	3843	4196	4554	4856
850.46	1	-6	5039	5021	4811	4486	4132	3825	3576	3383	3235	3141	3109	3184	3338	3634	4139	4942	6455
817.67	1	-5	941	1545	2464	2628	1836	1153	773	566	444	362	315	282	259	239	229	221	223
784.89	1	-6	2316	2475	2828	3368	4215	5278	5253	4231	3397	2945	2696	2586	2192	2263	2342	2432	2536
752.10	1	-6	2664	2766	2876	3005	3151	3314	3493	3687	3896	4130	4388	4674	4991	5344	5738	6180	6678
719.32	1	-5	724	788	862	949	1053	1168	1293	1444	1627	1849	2121	2457	2881	3429	4170	5252	6982
686.54	1	-4	995	1511	2357	3613	5249	7091	8798	9598	8456	5773	3368	1979	1248	843	612	474	383
653.75	1	-5	3189	2699	2315	2007	1756	1550	1378	1233	1110	1005	914	836	767	707	654	607	566
620.97	1	-6	5293	4969	4688	4453	4451	4732	4558	4065	3663	3338	3019	2756	2556	2396	2321	2221	2113
588.18	1	-6	1992	1848	1750	1688	1633	1575	1609	1604	1594	1602	1563	1494	1372	1264	1142	987	937
555.40	1	-6	807	745	725	759	698	779	840	885	1024	1045	1212	1348	1700	2107	3039	4390	6745
522.62	1	-4	105	163	234	286	231	175	167	199	285	482	953	1878	2239	1690	1297	1027	680
489.83	1	-3	43	27	17	11	7	5	3	2	2	1	1	1	1	1	1538	1535	1534
457.05	1	-3	1532	1530	1528	1527	1532												

---

[a] See footnote a to Table IV.1.

[b] See footnote b to Table V.1.

Table VI.14. Real refractive indices between 6500 and 450 cm^{-1} of 79.34% liquid benzene-h_6 in liquid benzene-d_6 at 25 °C.[a,b]

cm^{-1}	*XE*	0	1	2	3	4	5	6	7	8	9	10	11	12	13	14	15	16
6499.90	3	14795	14795	14795	14795	14795	14795	14795	14795	14795	14795	14795	14795	14795	14795	14795	14794	14794
6368.76	3	14794	14794	14794	14794	14794	14794	14794	14794	14794	14794	14794	14794	14794	14794	14794	14794	14794
6237.63	3	14794	14794	14794	14794	14794	14794	14794	14794	14794	14794	14794	14794	14794	14794	14794	14794	14794
6106.49	3	14794	14794	14794	14794	14794	14794	14793	14793	14793	14793	14793	14793	14793	14792	14792	14792	14793
5975.36	3	14795	14795	14795	14795	14795	14794	14794	14794	14794	14795	14795	14795	14795	14795	14795	14795	14795
5844.22	3	14795	14795	14795	14795	14794	14794	14794	14794	14794	14794	14794	14794	14794	14794	14794	14794	14794
5713.09	3	14794	14794	14794	14794	14794	14794	14794	14794	14794	14794	14794	14794	14794	14794	14794	14794	14794
5581.95	3	14794	14794	14794	14793	14793	14793	14793	14793	14793	14793	14793	14793	14793	14793	14793	14793	14793
5450.81	3	14793	14793	14793	14793	14793	14793	14793	14793	14793	14793	14793	14793	14793	14793	14793	14793	14793
5319.68	3	14793	14793	14793	14793	14793	14793	14793	14793	14793	14793	14793	14793	14793	14793	14793	14792	14792
5188.54	3	14792	14792	14792	14792	14792	14792	14792	14792	14792	14792	14792	14792	14792	14792	14792	14792	14792
5057.41	3	14792	14792	14792	14792	14792	14792	14792	14792	14792	14792	14792	14792	14792	14791	14791	14791	14791
4926.27	3	14791	14791	14791	14791	14791	14791	14791	14791	14791	14791	14791	14791	14791	14791	14791	14791	14791
4798.99	2	14790	14790	14790	14790	14790	14790	14790	14790	14790	14790	14790	14790	14790	14790	14790	14790	14790
4733.42	2	14790	14790	14789	14789	14789	14789	14789	14789	14789	14789	14788	14788	14789	14789	14788	14788	14788
4667.86	2	14790	14791	14791	14790	14789	14789	14789	14790	14791	14791	14790	14790	14791	14791	14791	14791	14790
4602.29	2	14791	14790	14790	14789	14789	14791	14792	14792	14792	14792	14792	14791	14791	14791	14791	14791	14791
4536.72	2	14791	14791	14791	14791	14791	14790	14790	14790	14790	14790	14789	14789	14789	14790	14790	14790	14791
4471.15	2	14791	14791	14790	14790	14790	14790	14790	14790	14790	14790	14790	14790	14790	14790	14790	14790	14790
4405.58	2	14790	14790	14790	14790	14790	14789	14789	14789	14790	14790	14790	14790	14790	14790	14789	14789	14789
4340.02	2	14789	14789	14789	14789	14789	14789	14789	14789	14789	14789	14788	14788	14788	14788	14788	14788	14788
4274.45	2	14788	14788	14788	14788	14788	14788	14788	14788	14788	14788	14788	14788	14788	14787	14787	14787	14787
4208.88	2	14787	14787	14787	14787	14787	14787	14787	14787	14787	14787	14787	14787	14787	14787	14786	14786	14786
4143.31	2	14786	14786	14785	14785	14785	14785	14784	14784	14784	14783	14783	14782	14782	14782	14781	14780	14781
4077.75	2	14781	14780	14779	14777	14776	14782	14795	14801	14801	14800	14798	14796	14794	14794	14794	14794	14793
4014.11	1	14793	14793	14792	14792	14792	14792	14792	14791	14791	14791	14791	14791	14790	14790	14790	14790	14790
3981.32	1	14790	14790	14790	14790	14790	14789	14789	14789	14789	14788	14789	14789	14789	14789	14789	14789	14789
3948.54	1	14789	14789	14789	14789	14788	14788	14788	14789	14789	14790	14790	14790	14789	14789	14789	14789	14789
3915.75	1	14789	14789	14789	14789	14789	14789	14788	14788	14788	14788	14788	14788	14788	14788	14788	14788	14788
3882.97	1	14788	14788	14788	14788	14788	14788	14788	14788	14788	14788	14788	14788	14787	14787	14787	14787	14787
3850.19	1	14787	14787	14787	14787	14787	14787	14787	14787	14786	14786	14786	14787	14787	14787	14787	14787	14787
3817.40	1	14786	14786	14786	14786	14786	14786	14786	14786	14786	14787	14787	14787	14787	14786	14786	14786	14786
3784.62	1	14786	14786	14786	14786	14786	14786	14786	14786	14786	14786	14786	14786	14786	14785	14785	14785	14785
3751.83	1	14785	14785	14785	14785	14785	14785	14785	14785	14785	14785	14785	14785	14785	14785	14784	14784	14784
3719.05	1	14784	14784	14784	14784	14784	14783	14783	14783	14783	14782	14782	14782	14784	14786	14786	14786	14786
3686.27	1	14786	14787	14787	14786	14786	14786	14786	14785	14785	14785	14785	14785	14785	14784	14784	14784	14784
3653.48	1	14783	14783	14782	14781	14781	14782	14784	14787	14787	14787	14787	14786	14786	14786	14785	14785	14785
3620.70	1	14785	14784	14784	14784	14785	14785	14786	14786	14786	14786	14786	14786	14786	14785	14785	14785	14785
3587.91	1	14785	14785	14785	14784	14784	14784	14784	14784	14784	14784	14784	14784	14784	14784	14784	14783	14783
3555.13	1	14783	14783	14783	14783	14783	14783	14783	14783	14783	14783	14783	14783	14782	14782	14782	14782	14782
3522.35	1	14782	14782	14782	14782	14782	14782	14782	14782	14782	14782	14781	14781	14781	14781	14781	14781	14781
3489.56	1	14781	14781	14781	14781	14781	14781	14781	14781	14780	14780	14780	14780	14780	14780	14780	14780	14780
3456.78	1	14779	14779	14779	14779	14779	14780	14780	14780	14780	14780	14780	14780	14779	14779	14779	14779	14779
3423.99	1	14779	14779	14779	14779	14779	14779	14779	14778	14778	14778	14778	14778	14778	14778	14778	14778	14778
3391.21	1	14778	14778	14778	14777	14777	14777	14777	14777	14777	14777	14777	14776	14776	14776	14776	14776	14776
3358.43	1	14776	14776	14776	14775	14775	14775	14775	14775	14775	14775	14775	14774	14774	14774	14774	14774	14774
3325.64	1	14773	14773	14773	14773	14773	14773	14773	14773	14772	14772	14772	14772	14772	14772	14771	14771	14771
3292.86	1	14771	14771	14770	14770	14770	14770	14769	14769	14769	14769	14769	14769	14768	14768	14768	14768	14767
3260.07	1	14767	14767	14767	14766	14766	14766	14765	14765	14764	14764	14763	14763	14763	14764	14765	14766	14766
3227.29	1	14766	14766	14766	14765	14765	14764	14764	14763	14763	14762	14762	14761	14761	14760	14760	14760	14759
3194.51	1	14759	14758	14758	14757	14757	14756	14756	14755	14755	14754	14753	14753	14752	14752	14751	14750	14749
3161.72	1	14749	14748	14747	14746	14745	14744	14743	14742	14741	14740	14739	14737	14736	14735	14733	14731	14729
3128.94	1	14728	14725	14723	14720	14717	14714	14711	14708	14704	14700	14695	14689	14682	14673	14662	14648	14630
3096.16	1	14610	14600	14636	14732	14799	14813	14804	14791	14774	14753	14729	14704	14704	14777	14819	14819	14809
3063.37	1	14797	14786	14774	14765	14759	14749	14735	14719	14699	14673	14642	14609	14589	14625	14747	14882	14954
3030.59	1	14981	14986	14980	14968	14954	14940	14928	14918	14908	14900	14893	14887	14881	14877	14873	14870	14867
2997.80	1	14865	14862	14860	14857	14855	14853	14850	14848	14846	14845	14843	14841	14840	14838	14837	14836	14834
2965.02	1	14833	14832	14831	14829	14828	14827	14826	14826	14825	14825	14824	14823	14823	14822	14821	14820	14819
2932.24	1	14819	14818	14817	14817	14816	14815	14815	14814	14813	14812	14811	14810	14810	14810	14811	14812	14811
2899.45	1	14810	14809	14808	14807	14805	14805	14807	14813	14814	14813	14812	14811	14810	14810	14809	14808	14808
2866.67	1	14807	14806	14806	14805	14805	14805	14806	14806	14806	14805	14805	14805	14805	14804	14804	14804	14803
2833.88	1	14803	14802	14802	14802	14801	14801	14801	14801	14802	14804	14804	14804	14804	14803	14803	14803	14802
2801.10	1	14802	14802	14801	14801	14801	14800	14800	14800	14800	14799	14799	14799	14799	14799	14799	14798	14798
2768.32	1	14798	14798	14798	14798	14797	14797	14797	14797	14797	14797	14796	14796	14796	14796	14796	14796	14795
2735.53	1	14795	14795	14795	14795	14795	14795	14794	14794	14794	14794	14794	14794	14794	14793	14793	14793	14793
2702.75	1	14793	14793	14793	14792	14792	14792	14792	14792	14792	14791	14791	14791	14791	14791	14791	14790	14790
2669.96	1	14790	14790	14790	14789	14789	14788	14788	14787	14788	14790	14792	14792	14792	14792	14791	14791	14791
2637.18	1	14790	14790	14790	14789	14789	14789	14788	14788	14788	14787	14787	14787	14788	14789	14789	14789	14789
2604.40	1	14788	14787	14787	14786	14787	14789	14791	14791	14791	14790	14790	14789	14789	14789	14789	14788	14788
2571.61	1	14788	14788	14788	14788	14787	14787	14787	14787	14787	14787	14787	14787	14787	14787	14787	14786	14786
2539.79	0	14786	14786	14786	14786	14786	14786	14786	14786	14785	14785	14785	14785	14785	14785	14785	14785	14785
2523.40	0	14785	14785	14785	14785	14785	14785	14785	14785	14785	14785	14785	14785	14784	14784	14784	14784	14784
2507.01	0	14784	14784	14784	14784	14784	14784	14784	14784	14783	14783	14783	14783	14783	14783	14783	14783	14783
2489.65	1	14783	14783	14782	14783	14783	14783	14782	14782	14782	14782	14782	14782	14782	14781	14781	14781	14781
2456.87	1	14781	14780	14780	14780	14780	14780	14780	14780	14779	14779	14779	14779	14778	14778	14778	14778	14778
2424.08	1	14777	14777	14777	14776	14776	14776	14776	14775	14775	14775	14775	14775	14774	14774	14773	14772	14771
2391.30	1	14771	14772	14774	14775	14776	14777	14777	14776	14777	14779	14779	14778	14777	14776	14775	14776	14776
2358.52	1	14775	14775	14774	14773	14772	14772	14771	14770	14770	14769	14768	14767	14766	14764	14763	14761	14761

Table VI.14. Continued.

cm^{-1}	*XE*	0	1	2	3	4	5	6	7	8	9	10	11	12	13	14	15	16
2325.73	1	14765	14772	14776	14776	14775	14773	14771	14769	14767	14765	14763	14761	14759	14757	14755	14752	14748
2292.95	1	14744	14739	14733	14724	14716	14716	14738	14774	14797	14803	14800	14796	14802	14817	14824	14825	14823
2260.16	1	14820	14817	14814	14812	14809	14807	14806	14804	14803	14801	14800	14798	14797	14796	14795	14794	14793
2227.38	1	14792	14791	14790	14789	14788	14787	14785	14784	14785	14790	14793	14794	14793	14792	14791	14790	14790
2194.60	1	14789	14788	14788	14787	14787	14786	14786	14786	14785	14785	14785	14784	14784	14784	14783	14783	14783
2161.81	1	14782	14782	14782	14781	14781	14781	14781	14781	14781	14780	14780	14780	14780	14779	14779	14779	14779
2129.03	1	14778	14778	14778	14778	14777	14777	14777	14777	14776	14776	14776	14776	14776	14775	14775	14775	14775
2096.24	1	14774	14774	14774	14774	14773	14773	14773	14773	14773	14772	14772	14772	14772	14771	14771	14771	14770
2063.46	1	14770	14770	14769	14769	14769	14768	14768	14768	14767	14767	14767	14767	14766	14766	14766	14765	14765
2030.68	1	14764	14764	14763	14763	14762	14762	14761	14760	14759	14758	14757	14757	14757	14758	14759	14759	14759
1997.89	1	14758	14756	14755	14753	14752	14752	14752	14751	14749	14747	14744	14741	14738	14734	14730	14727	14725
1965.11	1	14728	14737	14753	14773	14790	14801	14806	14807	14805	14802	14799	14796	14794	14791	14790	14788	14786
1932.33	1	14785	14784	14782	14781	14779	14778	14777	14776	14775	14774	14773	14773	14772	14771	14770	14769	14769
1899.54	1	14768	14767	14766	14765	14764	14763	14763	14762	14762	14761	14760	14760	14759	14759	14759	14758	14757
1866.76	1	14757	14756	14755	14754	14753	14752	14751	14749	14747	14746	14744	14742	14739	14737	14734	14731	14728
1833.97	1	14724	14719	14715	14710	14705	14702	14702	14708	14723	14746	14773	14799	14816	14825	14828	14826	14823
1801.19	1	14818	14814	14810	14806	14804	14801	14799	14797	14795	14793	14791	14789	14787	14785	14783	14782	14780
1768.41	1	14779	14777	14776	14774	14773	14771	14771	14773	14776	14777	14777	14776	14774	14773	14772	14771	14770
1735.62	1	14769	14769	14768	14767	14766	14765	14765	14764	14763	14762	14761	14761	14762	14762	14761	14760	14759
1702.84	1	14759	14758	14757	14756	14756	14755	14755	14754	14753	14752	14751	14751	14750	14750	14749	14749	14751
1670.05	1	14753	14754	14755	14754	14753	14752	14751	14750	14749	14748	14747	14746	14745	14744	14743	14742	14741
1637.27	1	14740	14738	14737	14735	14733	14730	14728	14725	14723	14726	14736	14747	14751	14751	14749	14747	14746
1604.49	1	14744	14743	14741	14740	14738	14736	14735	14734	14733	14733	14733	14733	14732	14731	14730	14728	14727
1571.70	1	14725	14724	14723	14721	14718	14716	14714	14711	14709	14706	14703	14701	14699	14696	14692	14687	14683
1538.92	1	14679	14676	14675	14677	14681	14688	14695	14701	14704	14704	14702	14698	14692	14686	14678	14670	14661
1507.10	0	14656	14650	14645	14639	14633	14626	14619	14612	14604	14596	14587	14576	14565	14553	14539	14523	14506
1490.71	0	14486	14462	14435	14402	14363	14318	14265	14205	14144	14102	14134	14331	14694	15051	15261	15339	15331
1474.31	0	15282	15230	15196	15178	15156	15129	15101	15075	15052	15032	15013	14997	14981	14967	14955	14943	14932
1457.92	0	14923	14914	14908	14903	14900	14898	14897	14895	14893	14891	14888	14884	14881	14877	14873	14870	14866
1441.53	0	14863	14860	14857	14854	14851	14848	14845	14843	14840	14838	14836	14833	14831	14829	14827	14825	14823
1424.17	1	14819	14816	14813	14809	14806	14803	14800	14796	14793	14790	14786	14782	14778	14775	14774	14779	14791
1391.39	1	14802	14809	14811	14810	14808	14804	14801	14798	14795	14792	14790	14788	14786	14783	14781	14779	14777
1359.57	0	14776	14775	14774	14773	14772	14771	14770	14769	14768	14766	14765	14764	14763	14761	14760	14758	14757
1343.18	0	14755	14753	14751	14748	14746	14742	14738	14733	14728	14723	14720	14722	14736	14761	14786	14802	14810
1326.79	0	14813	14812	14808	14805	14802	14801	14799	14796	14794	14792	14790	14788	14786	14785	14783	14782	14781
1309.43	1	14780	14778	14777	14775	14774	14773	14771	14770	14768	14767	14766	14765	14764	14762	14761	14760	14759
1276.65	1	14758	14757	14756	14754	14753	14752	14751	14749	14748	14747	14745	14744	14744	14744	14746	14747	14748
1243.86	1	14747	14746	14745	14744	14743	14742	14740	14739	14738	14737	14736	14735	14734	14733	14731	14730	14729
1211.08	1	14727	14726	14724	14723	14723	14722	14721	14719	14717	14716	14714	14712	14711	14710	14711	14712	14714
1178.29	1	14718	14723	14728	14731	14732	14732	14732	14732	14735	14738	14739	14739	14738	14738	14737	14737	14738
1145.51	1	14739	14739	14739	14738	14737	14735	14733	14732	14730	14728	14726	14724	14722	14720	14718	14716	14714
1112.73	1	14712	14710	14708	14706	14704	14702	14700	14698	14696	14693	14690	14688	14685	14682	14679	14676	14673
1079.94	1	14669	14666	14662	14658	14653	14649	14643	14637	14631	14624	14616	14607	14597	14585	14571	14555	14535
1047.16	1	14510	14480	14444	14409	14406	14501	14695	14863	14948	14965	14949	14923	14897	14873	14853	14835	14820
1014.37	1	14807	14798	14795	14796	14792	14785	14778	14772	14766	14761	14757	14754	14754	14752	14749	14746	14744
981.59	1	14741	14738	14735	14733	14731	14730	14729	14729	14728	14727	14726	14724	14722	14719	14717	14715	14713
948.81	1	14711	14709	14707	14705	14703	14700	14697	14694	14692	14689	14688	14686	14683	14681	14679	14677	14674
916.02	1	14672	14669	14666	14663	14660	14658	14655	14652	14650	14647	14644	14641	14638	14634	14631	14628	14625
883.24	1	14622	14618	14615	14611	14608	14605	14602	14599	14596	14593	14590	14587	14584	14581	14579	14578	14579
850.46	1	14580	14582	14583	14582	14579	14575	14570	14564	14557	14550	14541	14532	14521	14510	14495	14479	14457
817.67	1	14433	14416	14458	14584	14652	14650	14630	14609	14590	14574	14559	14546	14534	14523	14511	14500	14489
784.89	1	14478	14466	14454	14443	14434	14433	14439	14438	14427	14415	14402	14389	14378	14361	14347	14332	14317
752.10	1	14302	14287	14271	14254	14236	14217	14198	14177	14155	14132	14107	14081	14053	14024	13992	13957	13920
719.32	1	13880	13837	13789	13737	13680	13618	13548	13469	13381	13280	13165	13032	12875	12688	12458	12168	11799
686.54	1	11336	10795	10264	09926	10040	10874	12697	15646	18852	20537	20403	19619	18873	18273	17807	17449	17170
653.75	1	16947	16765	16612	16481	16368	16269	16182	16105	16035	15973	15916	15865	15818	15774	15734	15697	15663
620.97	1	15631	15601	15572	15545	15518	15498	15481	15463	15444	15425	15407	15389	15372	15355	15339	15324	15310
588.18	1	15296	15282	15269	15256	15244	15231	15219	15208	15196	15185	15175	15164	15153	15142	15131	15119	15108
555.40	1	15095	15082	15069	15056	15042	15028	15014	14998	14982	14964	14945	14923	14899	14871	14838	14802	14760
522.62	1	14720	14690	14686	14742	14782	14719	14613	14479	14303	14069	13815	14030	15126	15816	15940	16096	16131
489.83	1	16048	15935	15822	15726	15647	15583	15530	15487	15451	15419	15392	15369	15349	15332	15375	15352	15335
457.05	1	15315	15296	15283	15272	15318												

[a,b] See footnotes a and b to Table IV.2.

Table VI.15. Imaginary refractive indices between 6500 and 450 cm^{-1} of 94.26% liquid benzene-h$_6$ in liquid benzene-d$_6$ at 25 °C.[a,b]

cm^{-1}	*XE*	*YE*	0	1	2	3	4	5	6	7	8	9	10	11	12	13	14	15	16
6499.90	3	-7	12	12	12	14	16	17	17	18	16	19	20	19	19	21	21	21	21
6368.76	3	-7	23	25	27	26	25	23	24	26	29	32	42	44	40	41	41	41	42
6237.63	3	-7	44	46	47	48	54	61	74	93	110	127	190	341	433	442	367	360	386
6106.49	3	-7	394	383	468	348	245	210	202	226	277	395	556	687	803	1162	1682	2355	3236
5975.36	3	-7	2831	2308	1897	1715	1451	1188	1596	1379	2136	1707	1122	776	798	807	789	718	547
5844.22	3	-7	374	238	176	129	120	152	164	167	197	234	252	180	163	177	160	134	160
5713.09	3	-7	265	296	397	416	331	226	195	198	196	145	118	113	130	209	237	189	150
5581.95	3	-7	157	165	157	152	178	236	269	227	232	248	170	131	101	85	74	62	63
5450.81	3	-7	69	78	104	134	131	109	126	112	97	118	146	135	132	147	156	128	121
5319.68	3	-7	110	106	89	80	80	77	86	111	163	186	177	125	103	86	83	75	75
5188.54	3	-7	83	83	73	75	108	112	104	105	107	88	81	100	115	107	103	111	107
5057.41	3	-7	108	116	110	95	89	92	107	120	125	107	109	103	107	100	90	96	106
4926.27	3	-7	106	105	114	128	121	112	125	163	180	188	194	190	166	138	122	124	117
4798.99	2	-7	120	126	133	149	166	171	163	158	158	163	166	169	171	177	188	199	214
4733.42	2	-7	239	260	288	324	367	412	466	564	719	889	1245	1764	1708	1583	1792	2645	4456
4667.86	2	-7	5095	3160	2087	1737	1947	2864	3834	3955	3040	2044	1935	2958	3626	2650	1945	1755	1919
4602.29	2	-7	1918	1693	1703	2243	3545	4480	3716	2693	1849	1356	1066	916	868	937	1227	1594	1397
4536.72	2	-7	1003	737	568	468	407	370	355	353	361	383	427	500	602	713	796	782	676
4471.15	2	-7	569	505	500	517	536	550	545	533	535	580	657	654	599	555	589	690	636
4405.58	2	-7	628	579	534	513	515	567	778	1140	1078	805	607	478	406	366	339	327	324
4340.02	2	-7	320	316	317	315	312	311	316	333	358	388	426	465	492	499	498	502	521
4274.45	2	-7	571	667	843	1148	1230	1063	944	928	978	958	910	886	890	987	1175	1196	1146
4208.88	2	-7	1154	1150	1251	1543	1614	1340	1146	1099	1194	1365	1275	1121	1046	1011	1014	999	981
4143.31	2	-7	985	1009	1020	1074	1178	1266	1362	1470	1662	1925	2333	2925	3601	4080	4698	6048	7692
4077.74	2	-6	786	787	926	1267	2038	3029	3028	2071	1314	843	566	422	371	407	412	319	254
4014.11	1	-7	2286	2093	1922	1786	1653	1572	1476	1426	1346	1294	1269	1271	1265	1316	1328	1339	1357
3981.32	1	-7	1321	1255	1179	1113	1071	1022	1033	1121	1371	1755	2004	2198	2497	2651	2442	2094	1805
3948.54	1	-7	1605	1479	1428	1477	1675	2123	2886	3212	2789	2359	2003	1727	1520	1379	1283	1221	1179
3915.75	1	-7	1138	1102	1079	1065	1058	1051	1038	1025	1014	1003	994	987	981	982	975	956	937
3882.97	1	-7	913	883	845	806	771	743	720	702	684	665	650	639	630	621	609	596	582
3850.19	1	-7	568	557	547	537	529	525	528	542	574	622	672	698	688	654	615	583	568
3817.40	1	-7	576	587	581	581	598	639	716	803	824	780	733	715	732	789	869	920	887
3784.62	1	-7	807	740	703	690	699	733	789	862	915	910	865	820	788	770	765	770	790
3751.83	1	-7	827	875	938	1015	1098	1169	1210	1223	1216	1198	1178	1160	1155	1166	1188	1219	1247
3719.05	1	-7	1274	1305	1352	1415	1512	1660	1884	2177	2547	3109	4124	5838	7123	6306	4940	4203	3977
3686.27	1	-7	3845	3427	2840	2330	1975	1735	1548	1408	1333	1310	1331	1326	1239	1135	1070	1055	1094
3653.48	1	-7	1206	1446	1909	2802	4468	6873	8277	7086	4957	3545	2771	2317	1987	1735	1569	1482	1474
3620.70	1	-7	1563	1775	2143	2659	3185	3450	3305	2866	2356	1904	1561	1323	1137	986	871	785	714
3587.91	1	-7	646	582	531	497	475	447	407	373	349	336	330	326	320	313	307	299	294
3555.13	1	-7	293	293	296	302	307	310	311	306	301	293	289	286	282	275	268	268	277
3522.35	1	-7	289	315	364	432	472	418	363	342	340	344	347	347	346	350	365	404	476
3489.56	1	-7	594	683	610	525	475	435	410	396	392	395	405	423	445	474	515	577	660
3456.78	1	-7	770	924	1130	1356	1520	1540	1419	1237	1062	916	797	706	646	622	656	743	718
3423.99	1	-7	686	694	713	713	700	682	661	640	628	629	643	668	693	707	698	664	612
3391.21	1	-7	557	504	458	420	389	363	344	328	315	307	300	293	287	284	284	288	297
3358.43	1	-7	309	320	323	322	326	334	338	329	315	306	304	309	323	340	348	364	398
3325.64	1	-7	439	448	430	408	392	382	374	369	365	365	368	374	380	389	399	410	424
3292.86	1	-7	439	456	477	502	534	571	613	654	696	737	778	806	817	823	834	857	892
3260.07	1	-7	938	992	1047	1100	1148	1199	1256	1328	1422	1552	1741	1999	2279	2465	2460	2306	2120
3227.29	1	-7	1975	1870	1784	1723	1684	1659	1528	1448	1586	1646	1698	1696	1611	1731	1819	1943	1963
3194.51	1	-7	2114	2166	2276	2468	2615	2470	2780	2700	2737	2766	2828	2895	2967	3006	3096	3398	3303
3161.72	1	-7	3471	3521	3652	3776	3961	4109	4173	4402	4582	4833	5075	5456	5659	5995	6196	6408	6672
3128.94	1	-6	695	758	803	865	978	1082	1218	1360	1517	1678	1863	2083	2364	2784	3422	4506	6461
3096.15	1	-5	1002	1636	2508	2809	2227	1586	1178	936	771	711	785	1066	1738	2101	1565	1137	893
3063.37	1	-5	758	672	631	638	622	577	564	586	652	792	1075	1606	2553	3862	4763	4524	3652
3030.59	1	-5	2828	2186	1680	1298	1025	834	694	593	512	452	407	374	347	324	301	281	258
2997.80	1	-6	2378	2190	1974	1819	1677	1548	1447	1338	1254	1173	1104	1028	949	888	811	767	722
2965.02	1	-7	7010	6808	6695	6442	6273	6184	6043	6082	6003	5585	5123	4754	4554	4354	4282	4220	4213
2932.23	1	-7	4246	4251	4183	4214	4107	4041	3788	3843	3801	3957	4399	5259	6581	7788	7665	6516	5462
2899.45	1	-6	479	446	453	525	709	1076	1510	1365	918	670	523	417	348	307	281	267	257
2866.67	1	-7	2447	2394	2450	2647	2989	3331	3610	3756	3649	3384	3118	2903	2690	2550	2456	2360	2262
2833.88	1	-7	2205	2221	2281	2464	2962	3969	5308	6502	6982	6128	4907	4045	3390	2797	2307	1948	1675
2801.10	1	-7	1455	1291	1181	1114	1069	1047	1048	1056	1071	1070	1054	1021	982	942	909	875	843
2768.32	1	-7	809	783	758	740	727	715	697	678	666	652	633	603	578	564	559	556	565
2735.53	1	-7	575	593	597	581	558	538	528	521	523	528	532	534	536	539	542	548	557
2702.75	1	-7	569	583	595	610	624	638	654	670	691	718	749	781	807	826	841	862	894
2669.96	1	-7	942	1013	1115	1264	1493	1876	2555	3806	5898	7273	5587	3716	2716	2131	1721	1464	1297
2637.18	1	-7	1166	1076	1027	1010	1023	1071	1159	1307	1574	2062	2764	3668	4313	3841	3053	2534	2278
2604.40	1	-7	2237	2448	3059	4350	6627	7792	5740	3861	2746	2080	1717	1534	1427	1395	1370	1401	1466
2571.61	1	-7	1412	1272	1171	1132	1141	1190	1278	1415	1608	1735	1598	1348	1151	1017	929	864	808
2539.79	0	-7	784	763	746	733	723	716	713	713	714	719	727	739	756	778	806	841	888
2523.40	0	-7	948	1009	1045	1062	1053	1025	1000	982	970	959	948	935	919	903	884	867	852
2507.01	0	-7	839	828	819	811	805	802	801	803	807	814	827	842	862	887	919	958	1007
2489.65	1	-7	1129	1279	1449	1532	1395	1219	1107	1056	1061	1132	1265	1301	1189	1090	1001	945	934
2456.87	1	-7	961	1021	1086	1088	1030	958	899	859	837	833	852	900	993	1145	1287	1299	1275
2424.08	1	-7	1282	1320	1391	1510	1700	1961	2254	2490	2610	2624	2582	2534	2511	2521	2566	2707	3053
2391.30	1	-7	3776	4716	5183	5608	6165	6254	5768	5316	5014	4260	3439	2871	2552	2441	2542	2628	2369
2358.52	1	-6	211	198	193	194	198	206	217	231	248	264	289	334	410	526	720	1053	1575

Table VI.15. Continued.

cm^{-1}	*XE*	*YE*	0	1	2	3	4	5	6	7	8	9	10	11	12	13	14	15	16
2325.73	1	-6	2123	2147	1617	1110	779	578	454	377	326	294	275	267	269	277	293	318	353
2292.95	1	-6	407	488	625	870	1306	1990	2632	2745	2364	1904	1637	1663	1848	1729	1385	1072	848
2260.16	1	-7	6886	5737	4869	4220	3739	3372	3060	2772	2509	2296	2137	2012	1908	1847	1814	1801	1802
2227.38	1	-6	182	187	195	212	248	326	482	783	1233	1358	1057	756	526	375	279	222	186
2194.60	1	-7	1599	1415	1300	1224	1160	1108	1061	1020	980	942	918	891	873	859	842	822	804
2161.81	1	-7	786	775	766	765	778	796	794	769	743	719	691	670	651	636	624	607	590
2129.03	1	-7	577	566	555	536	524	533	552	564	570	578	569	564	583	590	586	590	592
2096.24	1	-7	604	624	640	678	715	774	807	844	880	870	848	810	802	797	793	802	800
2063.46	1	-7	815	855	901	978	1062	1172	1329	1487	1673	1800	1843	1836	1850	1898	1945	1963	1998
2030.68	1	-7	2027	2077	2125	2170	2230	2304	2458	2692	3098	3756	4853	6498	8243	9734	9772	8471	7249
1997.89	1	-6	649	622	653	744	924	1076	1030	992	1018	1096	1224	1418	1695	2107	2727	3639	4909
1965.11	1	-6	6489	8112	9274	9501	8742	7397	5948	4667	3646	2871	2306	1905	1628	1430	1259	1097	951
1932.32	1	-7	8226	7151	6253	5533	4939	4483	4166	3967	3875	3777	3512	3177	2916	2776	2687	2661	2607
1899.54	1	-7	2543	2524	2573	2712	2968	3394	3934	4460	4744	4870	5051	5348	5664	5719	5443	5141	4971
1866.76	1	-6	486	479	486	496	505	517	534	560	595	643	705	784	881	999	1148	1335	1581
1833.97	1	-5	191	235	296	379	492	639	825	1040	1255	1420	1471	1378	1185	964	764	599	472
1801.19	1	-6	3766	3083	2601	2259	1983	1723	1468	1240	1043	885	763	669	596	542	498	466	437
1768.40	1	-6	423	443	462	512	614	799	1078	1315	1242	954	702	555	452	373	320	284	257
1735.62	1	-7	2385	2246	2137	2053	1993	1965	1963	1994	2119	2448	3172	4529	4985	3780	3099	2885	2839
1702.84	1	-6	274	269	269	276	285	297	309	317	330	356	401	469	554	658	821	1036	1214
1670.05	1	-6	1223	1073	881	718	598	516	464	431	411	403	405	413	431	469	483	460	459
1637.27	1	-6	467	486	506	542	601	683	818	1048	1434	1997	2369	2134	1712	1440	1298	1250	1227
1604.48	1	-6	1183	1114	1054	1022	1029	1075	1142	1231	1336	1444	1574	1582	1420	1245	1123	1039	965
1571.70	1	-6	905	862	818	793	772	758	766	782	812	868	943	1050	1166	1316	1535	1856	2304
1538.92	1	-6	2918	3673	4561	5475	6267	6751	6825	6500	5899	5192	4498	3901	3421	3059	2800	2633	2551
1507.10	0	-6	2488	2496	2565	2632	2738	2856	3010	3185	3378	3625	3906	4257	4613	5007	5478	6056	6770
1490.71	0	-4	77	88	104	124	153	193	251	337	468	668	953	1260	1426	1345	1102	832	608
1474.31	0	-5	4558	3669	3147	2652	2130	1700	1379	1142	962	817	703	607	528	465	413	371	339
1457.92	0	-6	3156	2993	2825	2734	2653	2561	2459	2351	2219	2101	1991	1947	1963	1912	1715	1523	1391
1441.53	0	-6	1277	1198	1121	1032	969	936	864	820	802	778	764	750	735	714	703	687	665
1424.17	1	-6	654	650	655	672	692	724	764	818	898	1017	1196	1471	1916	2610	3583	4635	5147
1391.39	1	-6	4760	3903	3020	2294	1766	1379	1125	950	824	732	664	617	580	546	527	512	496
1359.57	0	-7	4900	4894	4813	4814	4820	4849	4890	4943	5011	5099	5204	5310	5420	5520	5617	5726	5858
1343.18	0	-6	603	628	659	692	730	786	865	979	1146	1393	1761	2262	2783	3031	2891	2544	2169
1326.79	0	-6	1827	1546	1345	1221	1147	1078	1015	966	934	915	907	908	916	927	940	951	959
1309.43	1	-7	9561	9263	8800	8306	7802	7296	6836	6405	6046	5768	5550	5382	5255	5156	5085	5048	5050
1276.65	1	-6	509	520	532	544	562	589	621	666	730	819	943	1109	1313	1519	1646	1627	1495
1243.86	1	-6	1339	1213	1130	1081	1058	1050	1051	1059	1071	1084	1101	1124	1153	1188	1230	1280	1339
1211.08	1	-6	1408	1491	1598	1734	1853	1912	1989	2101	2243	2418	2635	2908	3257	3695	4140	4528	4956
1178.29	1	-6	5317	5501	5384	5022	4607	4246	3997	3830	3694	3548	3418	3337	3302	3308	3345	3375	3353
1145.51	1	-6	3243	3044	2801	2556	2332	2134	1966	1824	1705	1610	1537	1482	1421	1345	1281	1232	1189
1112.73	1	-6	1153	1134	1135	1134	1112	1086	1072	1067	1080	1088	1115	1165	1251	1391	1649	1906	1928
1079.94	1	-6	1773	1651	1607	1617	1666	1778	1956	2057	2191	2409	2676	3019	3450	4000	4711	5683	7033
1047.16	1	-5	902	1213	1736	2636	4110	5855	6626	5882	4479	3189	2269	1668	1304	1086	870	741	669
1014.37	1	-6	6385	6493	6764	6188	5313	4735	4472	4295	4143	4115	4174	4305	4292	4036	3787	3626	3535
981.59	1	-6	3445	3399	3397	3421	3467	3487	3469	3397	3265	3092	2900	2714	2524	2357	2215	2108	2013
948.81	1	-6	1897	1813	1733	1651	1570	1504	1448	1421	1384	1369	1342	1309	1296	1262	1239	1195	1172
916.02	1	-6	1154	1151	1150	1160	1178	1209	1248	1249	1228	1219	1223	1233	1250	1276	1311	1353	1405
883.24	1	-6	1466	1536	1618	1714	1828	1957	2102	2262	2439	2640	2872	3165	3511	3923	4366	4797	5156
850.45	1	-6	5366	5336	5084	4684	4240	3826	3476	3185	2937	2729	2563	2437	2349	2315	2352	2498	2837
817.67	1	-6	3571	5076	7254	7705	5781	3948	2907	2358	2040	1855	1738	1675	1647	1640	1659	1707	1794
784.89	1	-6	1958	2244	2751	3439	4448	5595	5617	4570	3660	3152	2899	2800	2786	2833	2915	3033	3191
752.10	1	-6	3396	3665	4096	4909	6320	6843	6145	5683	4452	4733	5044	5386	5765	6186	6656	7181	7772
719.32	1	-5	844	920	1006	1106	1223	1357	1511	1694	1913	2177	2500	2899	3402	4052	4932	6216	8271
686.53	1	-3	118	179	280	429	623	842	1045	1140	1004	685	399	234	147	99	72	56	45
653.75	1	-5	3737	3161	2710	2347	2052	1809	1607	1436	1291	1167	1060	967	886	815	752	696	646
620.97	1	-6	6018	5620	5265	4948	4657	4381	4132	3907	3703	3516	3344	3186	3038	2902	2776	2659	2552
588.18	1	-6	2454	2365	2283	2209	2139	2068	1996	1925	1859	1798	1741	1690	1643	1601	1562	1527	1495
555.40	1	-6	1467	1443	706	665	652	535	522	555	498	434	438	360	349	426	590	885	1528
522.61	1	-5	250	414	608	756	587	427	403	496	749	1354	2879	6242	6872	4235	3147	2457	1566
489.83	1	-6	9700	5739	3280	1847	1011	437	167										

---

[a] See footnote a to Table IV.1.

[b] See footnote b to Table V.1.

Table VI.16. Real refractive indices between 6500 and 450 cm^{-1} of 94.26% liquid benzene-h_6 in liquid benzene-d_6 at 25 °C.[a,b]

cm^{-1}	*XE*	0	1	2	3	4	5	6	7	8	9	10	11	12	13	14	15	16
6499.90	3	14798	14798	14798	14798	14798	14798	14798	14798	14798	14798	14798	14798	14798	14798	14798	14798	14798
6368.76	3	14798	14798	14798	14798	14798	14798	14798	14798	14798	14798	14798	14798	14798	14798	14798	14798	14798
6237.63	3	14798	14798	14798	14798	14798	14798	14798	14798	14797	14797	14797	14797	14797	14797	14797	14797	14797
6106.49	3	14797	14797	14797	14797	14797	14797	14797	14797	14797	14797	14797	14796	14796	14796	14796	14796	14797
5975.36	3	14798	14798	14798	14798	14798	14798	14798	14798	14798	14799	14799	14799	14798	14799	14798	14799	14799
5844.22	3	14799	14798	14798	14798	14798	14798	14798	14798	14798	14798	14798	14798	14798	14798	14798	14798	14797
5713.09	3	14797	14797	14797	14798	14798	14798	14798	14797	14798	14797	14797	14797	14797	14797	14797	14797	14797
5581.95	3	14797	14797	14797	14797	14797	14797	14797	14797	14797	14797	14797	14797	14797	14797	14797	14797	14797
5450.81	3	14797	14797	14797	14797	14797	14797	14797	14797	14797	14797	14797	14797	14797	14797	14797	14796	14796
5319.68	3	14796	14796	14796	14796	14796	14796	14796	14796	14796	14796	14796	14796	14796	14796	14796	14796	14796
5188.54	3	14796	14796	14796	14796	14796	14796	14796	14796	14796	14796	14796	14796	14796	14796	14796	14795	14795
5057.41	3	14795	14795	14795	14795	14795	14795	14795	14795	14795	14795	14795	14795	14795	14795	14795	14795	14795
4926.27	3	14795	14795	14795	14795	14795	14795	14794	14794	14794	14794	14794	14794	14794	14794	14794	14794	14794
4798.99	2	14794	14794	14794	14794	14794	14794	14794	14794	14794	14793	14793	14793	14793	14793	14793	14793	14793
4733.42	2	14793	14793	14793	14793	14793	14792	14792	14792	14792	14792	14791	14792	14792	14792	14791	14791	14791
4667.86	2	14794	14795	14794	14793	14793	14792	14793	14794	14795	14794	14794	14793	14794	14795	14795	14794	14794
4602.29	2	14794	14794	14793	14793	14793	14794	14796	14796	14796	14796	14795	14795	14795	14794	14794	14794	14795
4536.72	2	14795	14795	14795	14795	14794	14794	14794	14794	14794	14794	14794	14793	14793	14793	14793	14794	14794
4471.15	2	14794	14793	14793	14793	14793	14793	14793	14793	14793	14793	14793	14793	14793	14793	14793	14793	14793
4405.58	2	14793	14793	14793	14793	14792	14792	14792	14792	14793	14793	14793	14793	14793	14792	14792	14792	14792
4340.02	2	14792	14792	14792	14792	14792	14792	14792	14792	14791	14791	14791	14791	14791	14791	14791	14791	14791
4274.45	2	14791	14791	14790	14791	14791	14791	14791	14791	14791	14791	14791	14790	14790	14790	14790	14790	14790
4208.88	2	14790	14790	14790	14790	14790	14790	14790	14790	14790	14790	14790	14790	14789	14789	14789	14789	14789
4143.31	2	14788	14788	14788	14788	14787	14787	14787	14786	14786	14785	14785	14784	14784	14784	14783	14782	14783
4077.74	2	14783	14782	14780	14778	14777	14784	14799	14806	14807	14805	14803	14801	14799	14798	14798	14798	14797
4014.11	1	14797	14797	14796	14796	14796	14796	14795	14795	14795	14795	14795	14794	14794	14794	14794	14794	14794
3981.32	1	14794	14794	14793	14793	14793	14793	14793	14792	14792	14792	14792	14792	14792	14793	14793	14793	14793
3948.54	1	14793	14793	14792	14792	14792	14791	14792	14792	14793	14793	14793	14793	14793	14793	14793	14793	14792
3915.75	1	14792	14792	14792	14792	14792	14792	14792	14792	14792	14792	14792	14792	14792	14792	14792	14791	14791
3882.97	1	14791	14791	14791	14791	14791	14791	14791	14791	14791	14791	14791	14791	14791	14791	14791	14791	14791
3850.19	1	14790	14790	14790	14790	14790	14790	14790	14790	14790	14790	14790	14790	14790	14790	14790	14790	14790
3817.40	1	14790	14790	14789	14789	14789	14789	14789	14789	14789	14789	14789	14789	14789	14789	14789	14789	14789
3784.62	1	14789	14789	14789	14789	14789	14788	14788	14788	14788	14788	14788	14788	14788	14788	14788	14788	14788
3751.83	1	14788	14788	14788	14788	14787	14787	14787	14787	14787	14787	14787	14787	14787	14787	14787	14787	14787
3719.05	1	14787	14787	14786	14786	14786	14786	14785	14785	14785	14785	14784	14785	14787	14789	14789	14789	14789
3686.27	1	14789	14789	14790	14789	14789	14789	14789	14788	14788	14788	14788	14788	14787	14787	14787	14787	14786
3653.48	1	14786	14785	14784	14784	14783	14784	14787	14790	14791	14790	14790	14789	14789	14789	14788	14788	14788
3620.70	1	14787	14787	14787	14787	14787	14788	14788	14789	14789	14789	14789	14789	14788	14788	14788	14788	14788
3587.91	1	14788	14788	14787	14787	14787	14787	14787	14787	14787	14787	14787	14786	14786	14786	14786	14786	14786
3555.13	1	14786	14786	14786	14786	14786	14785	14785	14785	14785	14785	14785	14785	14785	14785	14785	14785	14785
3522.35	1	14784	14784	14784	14784	14784	14784	14784	14784	14784	14784	14784	14784	14784	14783	14783	14783	14783
3489.56	1	14783	14783	14783	14783	14783	14783	14783	14783	14783	14783	14782	14782	14782	14782	14782	14782	14782
3456.78	1	14782	14781	14781	14781	14782	14782	14782	14782	14782	14782	14782	14782	14782	14781	14781	14781	14781
3423.99	1	14781	14781	14781	14781	14781	14781	14781	14780	14780	14780	14780	14780	14780	14780	14780	14780	14780
3391.21	1	14780	14780	14779	14779	14779	14779	14779	14779	14779	14779	14778	14778	14778	14778	14778	14778	14778
3358.43	1	14777	14777	14777	14777	14777	14777	14777	14777	14776	14776	14776	14776	14776	14776	14775	14775	14775
3325.64	1	14775	14775	14775	14775	14774	14774	14774	14774	14774	14774	14773	14773	14773	14773	14773	14772	14772
3292.86	1	14772	14772	14772	14771	14771	14771	14771	14770	14770	14770	14770	14770	14769	14769	14769	14769	14768
3260.07	1	14768	14768	14768	14767	14767	14767	14766	14766	14766	14765	14765	14765	14765	14765	14765	14765	14764
3227.29	1	14764	14764	14763	14763	14763	14762	14762	14761	14761	14760	14760	14759	14759	14758	14758	14757	14757
3194.51	1	14756	14756	14755	14755	14754	14754	14753	14753	14752	14751	14751	14750	14749	14748	14747	14747	14746
3161.72	1	14745	14744	14743	14742	14741	14740	14738	14737	14736	14734	14733	14731	14730	14728	14727	14725	14722
3128.94	1	14720	14717	14715	14711	14708	14705	14701	14697	14693	14688	14682	14675	14666	14656	14642	14625	14604
3096.15	1	14582	14570	14612	14725	14804	14820	14810	14794	14774	14749	14721	14693	14692	14779	14829	14829	14816
3063.37	1	14803	14790	14776	14765	14759	14746	14730	14710	14686	14656	14620	14581	14557	14599	14740	14898	14987
3030.59	1	15019	15025	15019	15005	14989	14973	14959	14947	14936	14926	14918	14911	14905	14899	14895	14891	14888
2997.80	1	14884	14881	14878	14875	14872	14869	14867	14864	14862	14860	14858	14856	14854	14852	14851	14849	14847
2965.02	1	14845	14844	14842	14841	14840	14839	14838	14837	14836	14835	14834	14833	14832	14831	14830	14829	14828
2932.23	1	14827	14827	14826	14825	14825	14824	14823	14822	14821	14820	14819	14818	14818	14819	14820	14820	14820
2899.45	1	14819	14817	14816	14814	14813	14812	14815	14822	14823	14822	14821	14820	14819	14818	14817	14817	14816
2866.67	1	14815	14815	14814	14813	14813	14813	14813	14813	14813	14813	14812	14812	14812	14811	14811	14811	14810
2833.88	1	14810	14809	14809	14808	14807	14807	14807	14807	14809	14811	14811	14811	14811	14810	14810	14810	14809
2801.10	1	14809	14808	14808	14808	14807	14807	14807	14806	14806	14806	14806	14806	14805	14805	14805	14805	14805
2768.32	1	14804	14804	14804	14804	14804	14803	14803	14803	14803	14803	14803	14802	14802	14802	14802	14802	14801
2735.53	1	14801	14801	14801	14801	14801	14801	14800	14800	14800	14800	14800	14800	14799	14799	14799	14799	14799
2702.75	1	14799	14798	14798	14798	14798	14798	14798	14797	14797	14797	14797	14797	14797	14796	14796	14796	14796
2669.96	1	14796	14795	14795	14795	14794	14794	14793	14793	14793	14796	14798	14798	14798	14798	14797	14797	14796
2637.18	1	14796	14796	14795	14795	14795	14794	14794	14794	14793	14793	14793	14793	14794	14795	14795	14795	14794
2604.40	1	14793	14793	14792	14792	14792	14795	14797	14797	14797	14796	14796	14795	14795	14795	14795	14794	14794
2571.61	1	14794	14794	14794	14794	14793	14793	14793	14793	14793	14793	14793	14793	14793	14793	14793	14792	14792
2539.79	0	14792	14792	14792	14792	14792	14792	14792	14792	14792	14791	14791	14791	14791	14791	14791	14791	14791
2523.40	0	14791	14791	14791	14791	14791	14791	14791	14791	14791	14791	14791	14790	14790	14790	14790	14790	14790
2507.01	0	14790	14790	14790	14790	14790	14790	14790	14790	14790	14789	14789	14789	14789	14789	14789	14789	14789
2489.65	1	14789	14789	14789	14789	14789	14789	14789	14789	14788	14788	14788	14788	14788	14788	14788	14788	14788
2456.87	1	14787	14787	14787	14787	14787	14787	14787	14787	14786	14786	14786	14786	14785	14785	14785	14785	14785
2424.08	1	14785	14785	14784	14784	14784	14784	14784	14784	14784	14784	14784	14783	14783	14783	14783	14782	14782
2391.30	1	14781	14782	14782	14782	14783	14784	14785	14785	14785	14786	14785	14785	14784	14784	14783	14783	14783
2358.52	1	14783	14782	14782	14781	14781	14780	14780	14779	14779	14778	14777	14776	14775	14774	14772	14771	14772

Table VI.16. Continued.

cm^{-1}	*XE*	0	1	2	3	4	5	6	7	8	9	10	11	12	13	14	15	16
2325.73	1	14777	14785	14790	14791	14790	14789	14787	14786	14785	14784	14783	14782	14781	14780	14779	14778	14777
2292.95	1	14775	14774	14772	14769	14767	14768	14773	14782	14788	14789	14789	14787	14789	14793	14795	14795	14794
2260.16	1	14793	14792	14791	14791	14790	14789	14788	14788	14787	14787	14786	14786	14785	14785	14784	14784	14783
2227.38	1	14783	14782	14781	14781	14780	14778	14777	14776	14778	14784	14788	14788	14788	14787	14787	14786	14785
2194.60	1	14785	14784	14784	14783	14783	14782	14782	14782	14782	14781	14781	14781	14781	14780	14780	14780	14780
2161.81	1	14779	14779	14779	14779	14779	14778	14778	14778	14778	14778	14777	14777	14777	14777	14777	14776	14776
2129.03	1	14776	14776	14776	14775	14775	14775	14775	14775	14774	14774	14774	14774	14773	14773	14773	14773	14773
2096.24	1	14772	14772	14772	14772	14771	14771	14771	14771	14770	14770	14770	14770	14769	14769	14769	14769	14768
2063.46	1	14768	14768	14767	14767	14766	14766	14766	14765	14765	14765	14765	14764	14764	14764	14763	14763	14762
2030.68	1	14762	14761	14761	14760	14760	14759	14758	14757	14756	14755	14754	14753	14753	14754	14756	14757	14756
1997.89	1	14755	14753	14751	14749	14748	14748	14748	14747	14744	14742	14739	14736	14732	14727	14723	14719	14717
1965.11	1	14720	14730	14748	14771	14791	14805	14811	14813	14811	14808	14805	14801	14798	14796	14794	14792	14790
1932.32	1	14788	14786	14785	14783	14782	14780	14779	14778	14776	14775	14775	14774	14773	14772	14771	14770	14769
1899.54	1	14768	14767	14766	14765	14764	14763	14762	14761	14761	14760	14760	14759	14758	14758	14758	14757	14756
1866.76	1	14755	14754	14753	14751	14750	14749	14747	14745	14743	14741	14739	14737	14734	14731	14728	14725	14721
1833.97	1	14716	14711	14705	14699	14694	14691	14691	14698	14713	14739	14771	14802	14825	14836	14840	14839	14835
1801.19	1	14830	14824	14819	14815	14812	14809	14807	14804	14801	14799	14796	14794	14792	14790	14788	14786	14784
1768.40	1	14782	14780	14779	14777	14775	14774	14773	14776	14779	14781	14780	14779	14778	14776	14775	14774	14773
1735.62	1	14772	14771	14770	14769	14768	14767	14766	14765	14764	14763	14762	14762	14763	14763	14763	14762	14761
1702.84	1	14760	14759	14759	14758	14757	14756	14756	14755	14754	14753	14752	14751	14750	14749	14748	14749	14750
1670.05	1	14753	14755	14755	14754	14754	14752	14751	14750	14749	14748	14747	14746	14745	14744	14743	14743	14741
1637.27	1	14740	14739	14738	14736	14735	14733	14731	14729	14727	14728	14734	14740	14741	14740	14739	14737	14737
1604.48	1	14736	14735	14734	14732	14731	14729	14728	14727	14726	14726	14726	14727	14728	14727	14726	14724	14723
1571.70	1	14721	14719	14717	14715	14712	14710	14707	14704	14701	14698	14695	14691	14688	14683	14679	14674	14669
1538.92	1	14664	14661	14660	14662	14667	14675	14683	14690	14694	14695	14693	14688	14682	14674	14666	14656	14646
1507.10	0	14640	14633	14627	14620	14613	14605	14597	14588	14579	14569	14558	14546	14534	14520	14504	14486	14465
1490.71	0	14442	14414	14382	14344	14300	14248	14187	14119	14048	14000	14033	14244	14643	15058	15331	15443	15441
1474.31	0	15387	15326	15285	15264	15238	15206	15173	15143	15116	15092	15071	15052	15034	15019	15004	14991	14979
1457.92	0	14968	14958	14949	14941	14934	14928	14923	14917	14912	14907	14903	14898	14894	14892	14889	14886	14882
1441.53	0	14878	14875	14871	14868	14865	14862	14859	14856	14853	14851	14848	14846	14844	14842	14840	14837	14835
1424.17	1	14831	14827	14824	14820	14817	14813	14810	14806	14803	14799	14795	14791	14786	14783	14782	14788	14801
1391.39	1	14813	14820	14822	14821	14818	14815	14812	14809	14806	14803	14801	14799	14797	14795	14793	14791	14789
1359.57	0	14788	14788	14787	14786	14785	14784	14783	14783	14782	14781	14780	14779	14779	14778	14777	14776	14775
1343.18	0	14774	14773	14772	14771	14770	14769	14767	14766	14764	14762	14761	14762	14765	14771	14777	14781	14783
1326.79	0	14783	14782	14781	14780	14779	14778	14777	14776	14775	14774	14773	14773	14772	14772	14771	14771	14770
1309.43	1	14770	14770	14769	14768	14768	14767	14766	14765	14764	14763	14762	14761	14759	14758	14757	14756	14755
1276.65	1	14754	14753	14751	14750	14749	14748	14746	14745	14744	14742	14741	14740	14739	14740	14741	14743	14744
1243.86	1	14744	14743	14742	14741	14739	14738	14737	14736	14735	14733	14732	14731	14730	14728	14727	14726	14724
1211.08	1	14723	14721	14720	14719	14718	14717	14716	14714	14712	14711	14709	14707	14706	14705	14707	14708	14711
1178.29	1	14715	14721	14728	14732	14734	14735	14734	14734	14733	14733	14732	14731	14730	14729	14729	14729	14730
1145.51	1	14731	14732	14732	14732	14731	14729	14727	14725	14723	14721	14719	14717	14715	14713	14711	14709	14707
1112.73	1	14705	14702	14700	14698	14695	14693	14690	14687	14684	14682	14678	14675	14671	14667	14664	14663	14662
1079.94	1	14660	14656	14651	14646	14640	14634	14628	14621	14614	14605	14596	14585	14573	14559	14543	14523	14500
1047.16	1	14471	14435	14392	14352	14348	14454	14676	14882	14988	15009	14991	14960	14928	14906	14884	14862	14844
1014.37	1	14828	14816	14812	14813	14807	14799	14791	14785	14778	14773	14768	14765	14764	14763	14759	14756	14752
981.59	1	14749	14746	14743	14741	14739	14737	14736	14736	14735	14734	14732	14731	14728	14726	14723	14721	14718
948.81	1	14715	14713	14710	14708	14705	14702	14699	14696	14694	14691	14689	14686	14683	14681	14678	14675	14673
916.02	1	14670	14667	14664	14661	14658	14656	14653	14651	14648	14645	14642	14639	14636	14632	14629	14626	14622
883.24	1	14619	14615	14612	14608	14604	14601	14597	14594	14590	14586	14583	14579	14576	14573	14572	14572	14574
850.45	1	14576	14580	14582	14583	14581	14579	14575	14570	14565	14560	14554	14547	14541	14533	14525	14516	14506
817.67	1	14496	14487	14494	14519	14532	14527	14516	14505	14495	14485	14475	14465	14456	14446	14436	14426	14415
784.89	1	14404	14391	14379	14368	14359	14359	14366	14364	14353	14339	14324	14309	14294	14278	14262	14245	14228
752.10	1	14209	14190	14169	14147	14131	14126	14113	14091	14073	14034	14003	13970	13937	13901	13863	13822	13779
719.32	1	13731	13680	13624	13562	13495	13420	13338	13245	13140	13021	12885	12727	12542	12319	12047	11704	11266
686.53	1	10716	10074	09443	09042	09179	10170	12336	15840	19650	21652	21493	20560	19674	18961	18407	17981	17650
653.75	1	17386	17170	16989	16835	16701	16585	16482	16391	16310	16236	16170	16110	16055	16004	15958	15915	15875
620.97	1	15838	15804	15772	15742	15714	15688	15663	15639	15617	15596	15576	15557	15539	15522	15505	15489	15474
588.18	1	15460	15446	15433	15420	15408	15396	15385	15374	15364	15353	15343	15334	15324	15315	15306	15298	15290
555.40	1	15282	15276	15268	15257	15247	15238	15229	15220	15211	15201	15192	15182	15170	15158	15145	15130	15114
522.61	1	15099	15086	15081	15093	15100	15078	15042	14998	14940	14862	14771	14842	15298	15438	15421	15447	15439
489.83	1	15409	15374	15341	15312	15288	15268	15250										

[a,b] See footnotes a and b to Table IV.2.